Title

Synthesis and Enhancement of Process Intensification Networks for Hydrogen Production

Author

Lowd, John

Publication Date

2022

Peer reviewed|Thesis/dissertation

UNIVERSITY OF CALIFORNIA

Los Angeles

Synthesis and Enhancement of Process Intensification Networks for Hydrogen Production

A dissertation submitted in partial satisfaction of the requirements for the degree of Doctor of Philosophy in Chemical Engineering

by

John Edward Lowd

2022

ABSTRACT OF THE DISSERTATION

Synthesis and Enhancement of Process Intensification Networks for Hydrogen Productions

by

John Edward Lowd

Doctor of Philosophy in Chemical Engineering

University of California, Los Angeles, 2022

Professor Vasilios Manousiouthakis, Chair

Over the course of the last forty years, process intensification (PI) has continued to develop as an area of active chemical engineering research, incorporating numerous considerations, including process safety and process systems engineering. PI encompasses any process design strategy that leads to a smaller, cleaner, safer and or more energy-efficient technology. Additionally, PI also includes system designs which reduce the number of devices employed. To this end, chemical reactor design incorporating separation technologies continues to be an active area of PI research, with prominent examples membrane reactors (MR) carrying out steam methane reforming (SMR) based hydrogen production at lower temperatures, dividing-wall columns combining multiple distillation channels into a single unit, and compact catalytic plate reactors for Fischer-Tropsch synthesis. As advances in computational software continue, there has also been a substantial increase in the number of tools developed for identifying new PI methodologies at the theoretical level. Advanced mathematical formulation, such as the Infinite DimEnsionAl State-Space (IDEAS) framework and multi-objective optimization techniques, have helped introduce systematic approaches for developing and identifying PI pathways for various chemical systems. These advances have naturally led to the development of software for the

generation of sustainable design alternatives to be used for PI purposes, as well as for using thermodynamic analysis to assess the viability of proposed technologies. The objective of this work is to present novel process intensification methodologies for the creation of a potential intensified reaction networks. In chapter 1, the PI concept is reviewed. Then, the first PI methodology developed in this work, the Storage Reactor (SR) concept, is formulated and demonstrated in chapter 2. The SR process is shown to enhance methane conversion and hydrogen yield over traditional steady state processes by combining multiple operations within a single unit, a key component of process intensification methods. Then, the novel Lexicographic method for network synthesis is first formulated in chapter 3 and its ability to synthesize reaction networks is demonstrated in chapter 4. Discussion and Conclusions are presented in Chapter 5, the Appendix containing mathematical formulations is presented in Chapter 6, and references are provided in Chapter 7.

This dissertation of John Edward Lowd is approved.

Yunfeng Lu

Dante A. Simonetti

Robert Thomas M'Closkey

Vasilios Manousiouthakis, Committee Chair

University of California, Los Angeles

2022

Table of Contents

List of Figures

List of Tables

Chapter 1 - Introduction: Process intensification, reaction networks, reactor modeling

Over the course of the last four decades, process intensification (PI) has developed as an area of chemical engineering research. Having first appeared in the literature in the early 1970's, PI has continued to grow incorporating a variety of aspects in chemical engineering, including process safety [1] and process systems engineering [2]. While an exact definition has been difficult to pin down, most seem to agree that PI involves any strategy or chemical engineering development that leads to a substantially smaller, cleaner, safer and more energy-efficient technology or which combines multiple operations into fewer devices [3].

Historically, major advancements in PI have been the result of improvements based on iterative experimental design. Examples include membrane reactors for methane steam reforming (MSR) for hydrogen generation at lower temperatures [4], the so-called dividing-wall columns that combine multiple distillation columns into a single unit [5], and compact catalytic plate reactors for use in Fischer-Tropsch synthesis [6]. However, in recent years there have also been numerous advances in systematic approaches and analytical tools for identifying, at the theoretical level, new PI methodologies. Mathematical formulation advances, such as the IDEAS framework [7], as well as multi-objective optimization techniques [8] have helped to introduce a more systematic approach in developing and identifying PI pathways for various chemical systems. Additionally, software has been developed [9] based on the implementation of an extended systematic methodology for sustainable process design for use in PI.

To this end, a novel process, termed the storage reactor (SR), is presented), which aims to intensify traditional, steady-state, reactor designs, by carrying-out simultaneously reaction,

separation, and storage in a single unit, while avoiding the reliability shortcomings associated with high-temperature membrane tubes typically used in membrane reactors that also simultaneously carry-out reaction and separation. A SR consists of two physically distinct domains, designated as the reactor domain and the storage domain, which are allowed to communicate with each other through a semipermeable boundary. It is envisioned that the SR is operated in a dynamic (periodic) manner, that enables the loading and unloading of the storage domain. The mathematical framework for the SR process is first constructed for the general case, combining both reactor and pellet scale equations. After making some simplifying assumptions a 0-D first principle SR model is presented that quantifies SR dynamic behavior. The resulting governing equations are nondimensionalized, and two dimensionless groups are shown to uniquely determine SR performance, which is quantified through the use of several proposed metrics. An illustrative case study on Steam Methane Reforming (SMR) is then carried out, involving parametric studies on the two aforementioned dimensionless groups. Next, a dynamic 1-dimensional isobaric and isothermal first principles-based model is presented. The resulting governing equations are rendered dimensionless, and are again shown to feature two dimensionless groups that can be used to affect process performance. A number of metrics are then introduced and applied to a case study on Steam Methane Reforming, for which a parametric study is carried out which establishes the superior performance of the MSR when compared to a reactor operating at steady state (SSR). Following this analysis a more comprehensive 1-dimensional non-isobaric non-isothermal model is presented and made dimensionless. The model is then simulated and analyzed using the previously defined metrics.

While the increase in raw material consumption and in desirable product output our demonstrated to be beneficial, they can also potential increase the production of undesirable

byproducts. For example, in the case studies on SMR it is shown that there is also a significant increase the carbon dioxide production, a known pollutant and climate change bad boy. Even in the general sense, as the SR process is intended to be implemented, many industrial relevant reactions produce one or more undesirable species that must either be captured during the reaction, or separated and sequestered further down in the production line. Therefore, a novel methodology for the synthesis of closed reaction pathways (reaction clusters) with an emphasis on hydrogen production is subsequently presented. Briefly, this so-called lexicographic approach performs half reaction generation prior to the incorporation of thermodynamic feasibility and other constraints into the synthesis process. A half reaction lexicon is created to identify intermediate full reactions. Once the candidate intermediate reactions have been identified, their thermodynamic properties can be assessed and their eligibility for reaction cluster membership can be evaluated in detail. A cluster generation algorithm is finally devised, which employs intermediate elimination as its basis. The power of the proposed method is illustrated on the synthesis of a reaction cluster for five target reactions.

Chapter 2 – Storage Reactor Steam Methane Reforming Case Studies

In the following we go through several case studies. In these case studies, the derived SR model is applied to the design of a novel process intensification reactor for SMR based hydrogen production using a SR under PPSO. As mentioned earlier, it is envisioned that the proposed SR process is operated in a dynamic (periodic) manner. A possible implementation of the proposed "Partial Pressure Swing Operation" (PPSO) of the SR, which keeps the reactor pressure and temperature constant, involves three operating phases. In the first phase, the SR operates in a *Loading-Reaction* mode in the (g) domain (where the reactants are loaded into the SR and the desired reactions are carried out in (g)), and in a *Storage* mode in the (s) domain (where one or more desired species are preferentially transported from (g) to (s), where they are stored). In the second phase, the SR operates in a *Reactant-Flushing* mode in the (g) domain (where the reactants are removed from (g)), and in *Storage-Maintenance* mode in the (s) domain (where the desired species are maintained in storage within (s)). Finally, in the third phase, the SR operates in an *Emptying* mode in the (s) domain (where the desired chemicals are emptied from storage within (s) and transported into (g)), and in *Unloading-Production* mode in the (g) domain (where the desired species are removed from (g), to yield the main SR products).
It will be shown that the proposed 3 phase PPSO of the SMR SR outperforms a conventional SMR reactor operating at steady state. Steam reforming of natural gas (and of other light hydrocarbons) is a process that is used extensively in petroleum refineries today to generate the hydrogen needed for their operation, for example, in the hydroprocessing of crude oil for the production of gasoline and other fuels. Indeed, approximately 95% of the hydrogen produced in

the United States industrially was obtained via the SMR reaction[10]. These SMR reactors typically operate near chemical reaction equilibrium, and represent a significant component of a refinery's capital and operating costs. Membrane separation has attracted attention over the past three decades as a process intensification tool due to its low energy requirements compared to more conventional separation technologies like distillation. Polymeric membranes have been the most intensively investigated, and are now widely used commercially. Inorganic membranes on the other hand, which include metallic, carbon, and ceramic membranes, have received relatively less attention, despite the fact they also show good promise for broad applications[11]. There are presently several commercial liquid-phase separations employing such membranes, but commercial gas-phase applications are presently lacking. However, high-temperature and high-pressure gas-phase reactive separations are an area where inorganic membranes have, potentially, a distinct advantage over polymeric membranes, and thus such applications remain today key drivers for the continued development of inorganic membranes. The equations found in the following sections come from making simplifying assumptions to the general SR process derivation found in Appendix A.1.

2.1. 0-dimensional studies

In this first section, a composite 0-dimensional model for the intensified SR process is first derived that captures and highlights the basic characteristics of this novel reactor process. Following non-dimensionalization, it is established that two dimensionless groups govern SR behavior.

2.1.1 Mathematical Formulation

The SR is considered to be a composite thermodynamic system comprised of two simple subsystems, the reactor gas domain (g) and the storage pellet domain (s), which communicate

with one another through a permselective layer, but are spatially exclusive. Considering that each domain is spatially uniform, that the storage domain is uniformly dispersed within the gas domain, that no reaction occurs within the storage domain, and that the composite system is isothermal, gives rise to the following, species conservation based, 0-dimensional model for the SR.

$$\frac{dn_j^g(t)}{dt} = \dot{n}_j^{in}(t) - \dot{n}_j^{out}(t) + r_j\left(\left\{P_k^g(t)\right\}_{k=1}^{NC}, T\right)V\varepsilon_c\eta_j\rho_c - \dot{n}_j^{sg}(t), \;\; n_j^g(0) = n_j^{g0} \quad \forall j = 1,...,NC$$

(2.1.1)

$$\frac{dn_j^s(t)}{dt} = \dot{n}_j^{sg}(t), \;\; n_j^s(0) = n_j^{s0} \quad \forall j = 1,...,NC \qquad (2.1.2)$$

where the first and second terms on the right-hand side of (1) are the inlet and outlet molar flowrates respectively, the third term is the reaction based molar rate of generation of species j (with r_j the reaction based rate of generation of species j, V the total reactor volume, ε_c the volume fraction of the reactor occupied by the catalyst pellets, η_j the catalyst effectiveness factor of species j, and ρ_c the apparent mass density of the catalyst pellets, i.e. pellet mass over pellet volume), and the fourth term is the molar flowrate of species j, leaving the reactor gas domain through the permeable storage domain boundary and entering into the storage domain. The storage domain is isolated from the inlet and outlet flows, and thus species j can only enter from the reactor to the storage domain through its boundary. Thus, the right hand side of (2.1.2) only contains the molar flow rate of species j, entering the storage domain through the permeable storage domain boundary, having left the reactor gas domain (We assume here that the permselective layer is ideal allowing only species j to permeate through. A practical example of

that would be a storage medium coated by a then Pd-alloy layer that allows only hydrogen to permeate through during MSR).

Sieverts' Law is typically employed in quantifying the molar flow rate of a species j through a Pd membrane layer[11]. For such membranes, it has been shown, both theoretically[12] and experimentally[15], that the molar flow rate is proportional to the difference of the nth power of the partial pressures across the membrane, where 0.5<n<1. For very thin Pd membranes n is near 1, and this is the form of Sieverts' law that is employed in this work. A similar transport equation has been shown to hold true for high-temperature carbon molecular sieve (CMS) membranes[13]. The resulting equation is then:

$$\dot{n}_j^{sg} = \beta_j A^{gs}\left(P_j^g - P_j^s\right) \forall j = 1,...,NC \quad (2.1.3)$$

where β_j is the j^{th} species molar permeance through the permselective layer, A^{gs} is reactor gas-storage medium interfacial area, and P_j^g, P_j^s are the j_{th} species partial pressures in the reactor gas and storage mediums. Considering an ideal gas mixture, and the volume fractions of the catalyst pellet solid, catalyst pellet gas, catalyst pellet, reactor void unoccupied by either catalyst or storage pellets, reactor gas, storage pellet gas, storage pellet solid, and storage pellet to be $\varepsilon_{sc}, \varepsilon_{gc}, \varepsilon_c, \varepsilon_r, \varepsilon_g, \varepsilon_{gs}, \varepsilon_{ss}, \varepsilon_s$ respectively, yields:

$$\left\{\begin{array}{l} P_j^g V\varepsilon_g = n_j^g RT,\ \ P_j^{g0} V\varepsilon_g = n_j^{g0} RT \quad \forall j = 1,...,NC \\ P_j^s V\varepsilon_{gs} = n_j^s RT,\ \ P_j^{s0} V\varepsilon_{gs} = n_j^{s0} RT \quad \forall j = 1,...,NC \\ \varepsilon_{sc} + \varepsilon_{gc} = \varepsilon_c;\ \varepsilon_{gc} + \varepsilon_r = \varepsilon_g;\ \varepsilon_{gs} + \varepsilon_{ss} = \varepsilon_s;\ \varepsilon_c + \varepsilon_r + \varepsilon_s = 1 \end{array}\right\} \quad (2.1.4)$$

where R is the universal gas constant, and T is the common temperature in all considered domains. Incorporating (2.1.4) , into (2.1.1) and (2.1.2) then yields:

$$\frac{dP_j^g(t)}{dt} = \frac{RT}{V\varepsilon_g}\begin{bmatrix} \dot{n}_j^{in}(t) - \dot{n}^{out}(t)\dfrac{P_j^g(t)}{\sum_{k=1}^{NC} P_k^g(t)} + \varepsilon_c V \rho_c \eta_j r_j\left(\left\{P_k^g(t)\right\}_{k=1}^{NC}, T\right) \\ -A^{gs}\beta_j\left(P_j^g(t) - P_j^s(t)\right) \end{bmatrix} \quad P_j^{g0}(0) = P_j^{g0} \quad \forall j = 1,...,NC$$

(2.1.5)

$$\frac{dP_j^s(t)}{dt} = \frac{RT}{V\varepsilon_{gs}} A^{gs}\beta_j\left(P_j^g(t) - P_j^s(t)\right) \quad P_j^{s0}(0) = P_j^{s0} \quad \forall j = 1,...,NC \qquad (2.1.6)$$

Next, the above model is nondimensionalized, and dimensionless groups are identified governing the SR's behavior.

Introducing $\dot{n}^*, P^*, r^*, t^* \triangleq \dfrac{P^* V \varepsilon_g}{\dot{n}^* RT}$ as reference values of molar flowrate, pressure, reaction rate, and time, allows the definition of the following dimensionless variables:

$$\bar{t} \triangleq \frac{t}{t^*}, \bar{P}_j^g \triangleq \frac{P_j^g}{P^*}, \bar{P}_j^s \triangleq \frac{P_j^s}{P^*}, \bar{\dot{n}}_j^{in} \triangleq \frac{\dot{n}_j^{in}}{\dot{n}^*}, \bar{\dot{n}}^{out} \triangleq \frac{\dot{n}^{out}}{\dot{n}^*}, \bar{r}_j\left(\left\{\bar{P}_k^g(\bar{t})\right\}_{k=1}^{NC}, T\right) \triangleq \frac{r_j\left(\left\{\bar{P}_k^g(t)\cdot P^*\right\}_{k=1}^{NC}, T\right)}{r^*}$$

with values for the reference parameters $P^*, \dot{n}^*$, and r^* to be specified by the particulars of the considered problem, since the choice of reference parameters can vary widely[14] and can significantly affect the range of values of the resulting dimensionless groups[15], and therefore must be chosen such that the resulting dimensionless problem's solution is not adversely influenced[16].

Equations (2.1.5), and (2.1.6) can then be written in dimensionless form as follow

$$\frac{d\bar{P}_j^g(\bar{t})}{d\bar{t}} = \begin{bmatrix} \bar{\dot{n}}_j^{in}(\bar{t}) - \bar{\dot{n}}^{out}(\bar{t})\dfrac{\bar{P}_j^g(\bar{t})}{\sum_{k=1}^{NC}\bar{P}_k^g(\bar{t})} + \\ +\varepsilon_c\eta_j\dfrac{r^* V\rho_c}{\dot{n}^*}\bar{r}_j\left(\left\{\bar{P}_k^g(\bar{t})\right\}_{k=1}^{NC}, T\right) - \dfrac{A^{gs}\beta_1 P^*}{\dot{n}^*}\dfrac{\beta_j}{\beta_1}\left(\bar{P}_j^g(\bar{t}) - \bar{P}_j^s(\bar{t})\right) \end{bmatrix} \quad \bar{P}_j^{g0}(0) = \bar{P}_j^{g0} \quad \forall j = 1,...,NC$$

(2.1.7)

$$\frac{d\bar{P}_j^s\left(\bar{t}\right)}{d\bar{t}} = \frac{\varepsilon_g}{\varepsilon_{gs}} \frac{A^{gs}\beta_1 P^*}{\dot{n}^*} \frac{\beta_j}{\beta_1}\left(\bar{P}_j^g\left(\bar{t}\right) - \bar{P}_j^s\left(\bar{t}\right)\right) \;\; \bar{P}_j^{s0}\left(0\right) = \bar{P}_j^{s0} \;\; \forall j = 1,...,NC \tag{2.1.8}$$

where the first species and its molar permeance through the permselective layer, β_1 is employed in defining the dimensionless group that captures the effect of the storage domain on overall process performance.

The operation of the proposed SR process must necessarily be dynamic (periodic) in nature, since the species stored in the storage medium must at some point in time be removed, otherwise the storage medium will "fill-up" and no longer allow species permeation though its boundary. In this work, a "Partial Pressure Swing Operation" (PPSO) of the SR is envisioned, which keeps reactor pressure and temperature constant. Such operation, aims to reduce reactor heating/cooling and compression costs. To this end, and for the sequel of this work, it is thus considered that the reactor outlet flowrate is adjusted so that $\sum_{k=1}^{NC} P_k^g\left(t\right) = constant$. In turn, this suggests that, the following must hold at all times

$$\bar{\dot{n}}^{out}\left(\bar{t}\right) = \bar{\dot{n}}^{in}\left(\bar{t}\right) + \varepsilon_c \frac{r^* V \rho_c}{\dot{n}^*} \sum_{k=1}^{NC}\left(\eta_k \bar{r}_k\left(\left\{\bar{P}_l^g\left(\bar{t}\right)\right\}_{l=1}^{NC}, T\right)\right) - \frac{A^{gs}\beta_1 P^*}{\dot{n}^*} \sum_{k=1}^{NC}\left(\frac{\beta_k}{\beta_1}\left(\bar{P}_k^g\left(\bar{t}\right) - \bar{P}_k^s\left(\bar{t}\right)\right)\right) \geq 0 \;\; \forall \bar{t} \geq 0$$

(2.1.9)

To further simplify the above derived dimensionless model, the following reference value is selected, and dimensionless groups are introduced:

$$P^* \triangleq \sum_{k=1}^{NC} P_k^g\left(t\right) = constant \Rightarrow \sum_{k=1}^{NC} \bar{P}_k^g\left(\bar{t}\right) = 1 \tag{2.1.10}$$

$$\Theta \triangleq \frac{P^* A^{gs}\beta_1}{\dot{n}^*} = \frac{1}{Pe_{mem}}, \;\; D_a \triangleq \frac{r^* V \varepsilon_c \rho_c}{\dot{n}^*} = \frac{RT}{P^*}\frac{\varepsilon_c}{\varepsilon_g}\rho_c r^* t^* \tag{2.1.11}$$

The resulting dimensionless model, and outlet flowrate non-negativity constraint are

$$\frac{d\bar{P}_j^g(\bar{t})}{d\bar{t}} = \begin{bmatrix} \left(\bar{\dot{n}}_j^{in}(\bar{t}) - \bar{\dot{n}}^{in}(\bar{t})\bar{P}_j^g(\bar{t})\right) + \\ +D_a\left(\eta_j \bar{r}_j\left(\left\{\bar{P}_k^g(\bar{t})\right\}_{k=1}^{NC}, T\right) - \bar{P}_j^g(\bar{t})\sum_{k=1}^{NC}\left(\eta_k \bar{r}_k\left(\left\{\bar{P}_l^g(\bar{t})\right\}_{l=1}^{NC}, T\right)\right)\right) \\ -\Theta\left(\frac{\beta_j}{\beta_1}\left(\bar{P}_j^g(\bar{t}) - \bar{P}_j^s(\bar{t})\right) - \bar{P}_j^g(\bar{t})\sum_{k=1}^{NC}\left(\frac{\beta_k}{\beta_1}\left(\bar{P}_k^g(\bar{t}) - \bar{P}_k^s(\bar{t})\right)\right)\right) \end{bmatrix}, \; \bar{P}_j^{g0}(0) = \bar{P}_j^{g0} \;\; \forall j = 1,...,NC$$

(2.1.12)

$$\frac{d\bar{P}_j^s(\bar{t})}{d\bar{t}} = \frac{\varepsilon_g}{\varepsilon_{gs}}\Theta\frac{\beta_j}{\beta_1}\left(\bar{P}_j^g(\bar{t}) - \bar{P}_j^s(\bar{t})\right) \;\; \bar{P}_j^{s0}(0) = \bar{P}_j^{s0} \;\; \forall j = 1,...,NC \qquad (2.1.13)$$

$$\bar{\dot{n}}^{in}(\bar{t}) + D_a\sum_{k=1}^{NC}\left(\eta_k \bar{r}_k\left(\left\{\bar{P}_l^g(\bar{t})\right\}_{l=1}^{NC}, T\right)\right) - \Theta\sum_{k=1}^{NC}\left(\frac{\beta_k}{\beta_1}\left(\bar{P}_k^g(\bar{t}) - \bar{P}_k^s(\bar{t})\right)\right) \geq 0 \quad \forall \bar{t} \geq 0 \;\; (2.1.14)$$

The above equations suggest that two dimensionless numbers determine the PPSO SR's dynamic behavior. The first, $\Theta = \frac{1}{Pe_{mem}}$, provides a measure of how effectively the reference species is being extracted from the reaction domain into the storage domain, compared to the employed molar flowrate reference value. Pe_{mem} is a Peclet number commonly employed by other authors[17]–[20] for the analysis of membrane reactors. D_a is the commonly employed Damkohler number, which indicates the ratio of the reference reaction rate to the molar flowrate's reference value, and encapsulates the reactor's residence time. The performance of membrane reactor systems has been analyzed in terms of these dimensionless numbers[21], [22]. Comparing the performance of the PPSO SR, which is a periodic process, with that of a traditional reactor, which is a steady-state process, requires that a number of process

performance metrics be introduced. Since the PPSO SR is a periodic process that takes place over several phases, it is appropriate to define metrics over each phase separately and over all phases. When the inverse Peclet number Θ is set to zero, the second and third operating phases become obsolete, and as the duration of the first phase approaches infinity, its associated metrics must approach their steady-state counterparts. Thus, the following metrics are considered.

Limiting Reactant Conversion

A limiting reactant K will be typically fed in the SR, and will be removed from the SR in varying amounts during each phase. It is thus appropriate to define its conversion over all phases as follows:

$$X_K = \frac{\sum_{k=1}^{NP}\left[\int_0^{\tau_k} \dot{\bar{n}}_{K,k}^{in}(\bar{t})d\bar{t} - \int_0^{\tau_k} \dot{\bar{n}}_{K,k}^{out}(\bar{t})d\bar{t}\right]}{\sum_{k=1}^{NP}\left[\int_0^{\tau_k} \dot{\bar{n}}_{K,k}^{in}(\bar{t})d\bar{t}\right]} \tag{2.1.15}$$

Desired Product Ratio

Molar ratios of desired product over limiting reactant can also be introduced, for either a single phase, or all phases. The molar ratio, of j produced during phase i, over limiting reactant K fed over all phases, is:

$$\omega_{j,i} \triangleq \frac{\int_0^{\tau_i} \dot{\bar{n}}_{j,i}^{out}(\bar{t})d\bar{t} - \int_0^{\tau_i} \dot{\bar{n}}_{j,i}^{in}(\bar{t})d\bar{t}}{\sum_{k=1}^{NP}\left[\int_0^{\tau_k} \dot{\bar{n}}_{K,k}^{in}(\bar{t})d\bar{t}\right]} \tag{2.1.16}$$

The molar ratio, of j produced during all phases, over limiting reactant K fed over all phases, is:

$$\Omega_j \triangleq \frac{\sum_{k=1}^{NP}\left[\int_0^{\tau_k} \bar{\dot{n}}_{j,k}^{out}(\bar{t})d\bar{t} - \int_0^{\tau_k} \bar{\dot{n}}_{j,k}^{in}(\bar{t})d\bar{t}\right]}{\sum_{k=1}^{NP}\left[\int_0^{\tau_k} \bar{\dot{n}}_{K,k}^{in}(\bar{t})d\bar{t}\right]} \tag{2.1.17}$$

This is often referred to as product yield. It then holds

$$\Omega_j = \sum_{i=1}^{NP} \omega_{j,i} \tag{2.1.18}$$

Finally, the molar ratios defined below, can be considered as product recovery percentages over each PPSO phase, and are thus referred to as the Product Recovery percentages.

$$R_{j,i} \triangleq \frac{\omega_{j,i}}{\Omega_j} \quad \forall i = 1, NP \quad \forall j = 1, ..., NC \tag{2.1.19}$$

The above system of non-linear first order differential equations $(2.1.12),(2.1.13)$ can be used to simulate all three PPSO SR phases, and can be solved using a standard implicit multistep backward differentiation formulation (BDF) that can accurately capture the solution of stiff initial value problems. Simultaneously with the time evolution of $(2.1.12),(2.1.13)$, the algebraic inequality $(2.1.14)$ is monitored to ensure the positivity of the storage reactor's outlet flow rate. The above solution strategy was implemented within the COMSOL Multiphysics software platform. The storage reactor concept is next illustrated on a steam methane reforming (SMR) case study, in which the impact of both dimensionless parameters on the PPSO of an SMR SR is quantified.

2.1.2 Case Study

In the analysis that follows, the molar flowrate $\dot{n}^*$, and reaction generation rate r^* reference values are selected as $\dot{n}^* \triangleq \dot{n}^{in}(0)$, $r^* \triangleq \frac{k_1}{\left(P^*\right)^{0.5}}$. According to Xu and Froment[23], SMR is carried out through the following three reversible reactions $R1$, $R2$, and $R3$, with enthalpies of formation as shown below:

$$CH_4 + H_2O \rightleftarrows CO + 3H_2 \quad \Delta H_1^\circ : 206.1 \, {kJ}/{mol} \qquad (R1)$$

$$CO + H_2O \rightleftarrows CO_2 + H_2 \quad \Delta H_2^\circ : -41.15 \, {kJ}/{mol} \qquad (R2)$$

$$CH_4 + 2H_2O \rightleftarrows CO_2 + 4H_2 \quad \Delta H_3^\circ : 164.9 \, {kJ}/{mol} \qquad (R3)$$

Alternative SMR models employing only the first two of the above reactions have also been developed[24], which argue that the above three reactions are linearly dependent. Although this is true in a stoichiometric, and equilibrium sense, it is not true in a kinetic sense. Indeed, the kinetic rate expressions provided in [25], can be brought in dimensionless form, as suggested in [15]. The resulting dimensionless reaction rates for R1, R2, and R3 become:

$$\bar{R}_1 = \frac{\frac{\bar{k}_1}{\left(\bar{P}_{H_2}^g\right)^{2.5}}\left(\bar{P}_{CH_4}^g \bar{P}_{H_2O}^g - \frac{\left(\bar{P}_{H_2}^g\right)^3 \bar{P}_{CO}^g}{\bar{K}_1}\right)}{\left(\overline{\mathrm{DEN}}\right)^2} \qquad (2.1.20)$$

$$\bar{R}_2 = \frac{\frac{\bar{k}_2}{\bar{P}_{H_2}^g}\left(\bar{P}_{CO}^g \bar{P}_{H_2O}^g - \frac{\bar{P}_{H_2}^g \bar{P}_{CO_2}^g}{\bar{K}_2}\right)}{\left(\overline{\mathrm{DEN}}\right)^2} \qquad (2.1.21)$$

$$\bar{R}_3 = \frac{\frac{\bar{k}_3}{\left(\bar{P}_{H_2}^g\right)^{3.5}}\left(\bar{P}_{CH_4}^g \left(\bar{P}_{H_2O}^g\right)^2 - \frac{\left(\bar{P}_{H_2}^g\right)^4 \bar{P}_{CO}^g}{\bar{K}_3}\right)}{\left(\overline{\mathrm{DEN}}\right)^2} \qquad (2.1.22)$$

$$\overline{\mathrm{DEN}}=1+\bar{K}_{CO}\bar{P}_{CO}^{g}+\bar{K}_{H_2}\bar{P}_{H_2}^{g}+\bar{K}_{CH_4}\bar{P}_{CH_4}^{g}+\frac{\bar{K}_{H_2O}\bar{P}_{H_2O}^{g}}{\bar{P}_{H_2}^{g}} \tag{2.1.23}$$

where

$$\left\{\begin{array}{l}\bar{K}_1=\dfrac{K_1}{\left(P^*\right)^2},\ \bar{K}_2=K_2,\ \ \bar{K}_3=\dfrac{K_3}{\left(P^*\right)^2},\bar{k}_1=1,\ \bar{k}_2=\dfrac{\left(P^*\right)^{1.5}k_2}{k_1}=\left(P^*\right)^{1.5},\ \ \bar{k}_3=\dfrac{k_3}{k_1}\\ \bar{K}_{CO}=K_{CO}P^*,\ \bar{K}_{H_2}=K_{H_2}P^*,\ \bar{K}_{CH_4}=K_{CH_4}P^*,\ \bar{K}_{H_2O}=K_{H_2O}\end{array}\right\} \tag{2.1.24}$$

In the spirit of [26] considering the above reaction rate expressions as elements of the linear space of real valued functions of the five species' partial pressures, yields that the reactions R1, R2, and R3 are linearly independent in a kinetic rate sense. Indeed, it can be readily verified that the only real numbers $\lambda_1,\lambda_2,\lambda_3$ for which the equation $\lambda_1\bar{r}_1+\lambda_2\bar{r}_2+\lambda_3\bar{r}_3=0$ is satisfied for all possible partial pressures $\bar{P}_{CH_4}^{g},\bar{P}_{H_2O}^{g},\bar{P}_{H_2}^{g},\bar{P}_{CO}^{g},\bar{P}_{CO_2}^{g}$ must satisfy $\lambda_1=0,\lambda_2=0,\lambda_3=0$.

The PPSO of the SMR SR is carried out in three phases, each of which is described by the activity occuring in the (g) and (s) domains and is designated as follows:

Phase 1 (Loading-Reaction/Storage), Phase 2 (Decarbonization/Maintenance), and Phase 3 (Unloading-Production/Emptying). These three phases have a time duration designated as τ_1,τ_2, and τ_3, as illustrated in the figure below, and are described next.

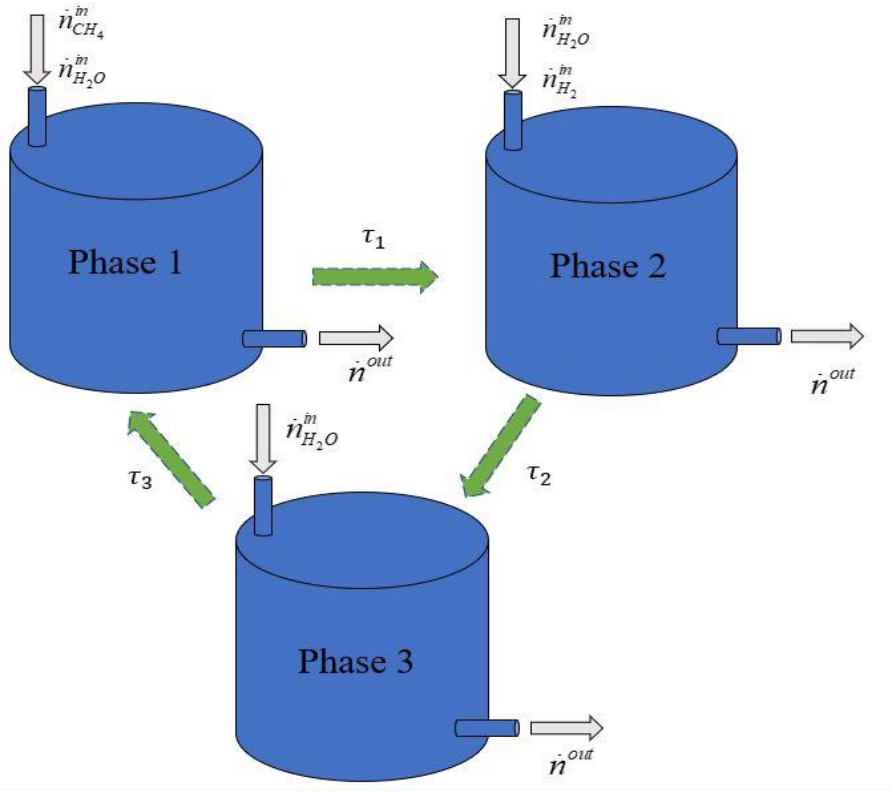

Figure 2-1: Proposed PPSO 3 phase SR operation

Phase 1: SR Loading-Reaction/Storage Phase

At the beginning of this phase, (g) is largely composed of steam and some hydrogen, while (s) only contains hydrogen at a pressure higher than the partial pressure of hydrogen in (g). A mixture of methane and steam is then fed into the SR at a constant flow rate, the SMR reactions are carried-out, and the generated hydrogen begins to permeate into (s) as its partial pressure in (g) exceeds the total pressure of (s). The outlet flowrate varies, as described by $(2.1.9)$, so as to maintain constant pressure in (g).

Phase 2: SR Decarbonization/Maintenance Phase

Phase 2 begins at the final conditions of phase 1, and the feed is switched to a mixture of steam and hydrogen, the composition of which is selected so that the partial pressure of hydrogen

in (g) is above the hydrogen pressure in (s) so as to maintain the stored hydrogen in (s). Thus (g) is decarbonized, until its contents essentially consist of steam and hydrogen.

Phase 3: SR Unloading-Production/Emptying Phase

Similarly, Phase 3 begins at the final conditions of phase 2, and (g) is fed pure steam. This action empties the contents of (s) into (g), and unloads the contents of (g) generating a mixture of hydrogen and steam as the MSR SR product, which is readily separable at high pressure, thus avoiding compression related operating costs.

Comparing the performance of the PPSO SMR SR, which is a periodic process, with that of a traditional, SMR reactor, which is a steady-state process, requires that the above defined process performance metrics be specialized to the SMR case study.

Designating methane as our limiting reactant, equation (2.1.15) becomes:

$$X_{CH_4} = \frac{\sum_{k=1}^{NP}\left[\int_0^{\tau_k} \bar{\dot{n}}_{CH_4,k}^{in}(\bar{t})d\bar{t} - \int_0^{\tau_k} \bar{\dot{n}}_{CH_4,k}^{out}(\bar{t})d\bar{t}\right]}{\sum_{k=1}^{NP}\left[\int_0^{\tau_k} \bar{\dot{n}}_{CH_4,k}^{in}(\bar{t})d\bar{t}\right]} \tag{2.1.25}$$

Similarly, equations (2.1.16)-(2.1.19) can be expressed for all products, CO, CO_2, H_2 , and are listed below for the species of interest.

$$\omega_{CO_2,1} \triangleq \frac{\int_0^{\tau_1} \bar{\dot{n}}_{CO_2,1}^{out}(\bar{t})d\bar{t} - \int_0^{\tau_1} \bar{\dot{n}}_{CO_2,1}^{in}(\bar{t})d\bar{t}}{\sum_{k=1}^{NP}\left[\int_0^{\tau_k} \bar{\dot{n}}_{CH_4,k}^{in}(\bar{t})d\bar{t}\right]} \tag{2.1.26}$$

$$Y_{H_2} \triangleq \frac{\sum_{k=1}^{NP}\left[\int_0^{\tau_k} \bar{\dot{n}}_{H_2,k}^{out}(\bar{t})d\bar{t} - \int_0^{\tau_k} \bar{\dot{n}}_{H_2,k}^{in}(\bar{t})d\bar{t}\right]}{\sum_{k=1}^{NP}\left[\int_0^{\tau_k} \bar{\dot{n}}_{CH_4,k}^{in}(\bar{t})d\bar{t}\right]} \tag{2.1.27}$$

$$\mathrm{R}_{H_2,rec} = \frac{\int_0^{\tau_i} \dot{\bar{n}}_{H_2,i}^{out}(\bar{t})d\bar{t} - \int_0^{\tau_i} \dot{\bar{n}}_{H_2,i}^{in}(\bar{t})d\bar{t}}{\sum_{k=1}^{NP}\left[\int_0^{\tau_k} \dot{\bar{n}}_{H_2,k}^{out}(\bar{t})d\bar{t} - \int_0^{\tau_k} \dot{\bar{n}}_{H_2,k}^{in}(\bar{t})d\bar{t}\right]} \tag{2.1.28}$$

Equation (2.1.26) captures the CO_2 molar production ratio in phase 1 over the total amount of CH_4 fed over all three phases. Equation (2.1.27) quantifies the molar ratio of total hydrogen produced over natural gas raw material, and represents the hydrogen yield over all three phases of operation Finally, of significance is the hydrogen recovery ratio quantified by equation (2.1.28) during the 3rd phase, $i = 3$, as it quantifies the molar ratio of readily purifiable (through water separation) hydrogen to total hydrogen produced.

To determine the time duration τ_1, τ_2, and τ_3 of the three PPSO phases, a stopping criterion for each phase must be selected. Two different stopping criteria are considered for phase 1, and the obtained results are compared in terms of the above listed performance metrics in the discussion section. The first selection for the duration of the first phase τ_1^* is the time at which the function $\omega_{\mathrm{CO}_2,1} : \tau_1 \to \omega_{\mathrm{CO}_2,1}(\tau_1)$ reaches its maximum value, i.e. $\tau_1^* \triangleq \arg\max_{\tau_1 \in [0,\infty)} \omega_{\mathrm{CO}_2,1}(\tau_1)$. The rationale for this decision is that for small values of τ_1, the value of $\omega_{\mathrm{CO}_2,1}(\tau_1)$ is close to zero, while for large values of τ_1, the value of $\omega_{\mathrm{CO}_2,1}(\tau_1)$ approaches the corresponding product ratio of the steady-state, no storage, reactor. The above τ_1 selection ensures that significant CO_2 product generation has occurred during the first phase, leading inevitably to significant H_2 hydrogen generation and storage, and also leaving the SR gas phase at the end of phase 1 in a CO_2 rich state, increasing the decarbonization efficiency of the second phase.

Our second selection for the duration of the first phase τ_1^* is the time at which the hydrogen partial pressure inside the storage medium reaches 90% of the hydrogen partial pressure attained in the reactor for operating times approaching infinity (which is equal to the hydrogen partial pressure at the exit of the corresponding steady-state reactor). Mathematically, $\tau_1^* : \bar{P}_{H_2}^s\left(\tau_1^*\right) = 0.9 \cdot \left(\bar{P}_{H_2}^g\right)_{ss} \triangleq 0.9 \cdot \lim_{\tau_1 \to +\infty} \bar{P}_{H_2}^s\left(\tau_1\right)$.

The duration of the second phase τ_2^* is selected as the time at which the function $\bar{P}_{\mathrm{C}}^g\left(\bar{t}\right) \triangleq \bar{P}_{\mathrm{CO}_2}^g\left(\bar{t}\right) + \bar{P}_{\mathrm{CH}_4}^g\left(\bar{t}\right) + \bar{P}_{\mathrm{CO}}^g\left(\bar{t}\right)$ is brought below a predefined decarbonization limit (e.g. 0.01). This selection determines the level of carbon impurities in the H_2 product generated during phase 3. Similarly, the duration of the third phase τ_3^* is selected as the time at which the function $\dfrac{\bar{P}_{\mathrm{H}_2}^s\left(\bar{t}\right)}{\bar{P}_{\mathrm{H}_2}^s\left(\tau_2^*\right)}$ is brought below a predefined depressurization limit (e.g. 0.05). This selection determines the pressure fluctuation experienced by the storage medium over the SR PPSO. Next, the time evolution of all SR state variables (species mole fractions in the gas and storage phases) are shown for the SR model parameter values and the summarized in the Tables below.

Table 2-1: Simulation Parameters

Description	Parameter	Value
Species k effectiveness factor	η_k	1
Species j permeance ratio	β_j / β_1	0 for all $j \neq 1$
Reactor gas void fraction to Storage gas void fraction ratio	$\varepsilon_g / \varepsilon_{gs}$	0.1
Membrane Permeation (Inverse Peclet) number	Θ	50

Damköhler number	D_a	7

Table 2-2: Reactor Dimensionless Inlet Flow Rates

Description	Parameter	Value
Inlet methane flow rate: phase 1	$\bar{\dot{n}}^{in}_{CH_4,1}$	0.25
Inlet water flow rate: phase 1	$\bar{\dot{n}}^{in}_{H_2O,1}$	0.75
Inlet flowrate of other species: phase 1	$\bar{\dot{n}}^{in}_{j,1} \quad j \neq H_2O, CH_4$	0
Inlet water flow rate: phase 2	$\bar{\dot{n}}^{in}_{H_2O,2}$	0.85
Inlet hydrogen flow rate: phase 2	$\bar{\dot{n}}^{in}_{H_2,2}$	0.15
Inlet flow rate of other species: phase 2	$\bar{\dot{n}}^{in}_{j,2} \quad j \neq H_2O, H_2$	0
Inlet water flowrate: phase 3	$\bar{\dot{n}}^{in}_{H_2O,3}$	6
Inlet flow rate of other species: phase 3	$\bar{\dot{n}}^{in}_{j,3} \quad j \neq H_2O$	0

Table 2-3: Reaction Kinetic Parameters for $P^* = 26 \cdot 10^5\, Pa,\ T = 900\, K$

Description	Parameter	Value
Dimensionless reaction rate constant 1	$\bar{k}_1$	1
Dimensionless reaction rate constant 2	$\bar{k}_2$	662.6
Dimensionless reaction rate constant 3	$\bar{k}_3$	0.143
Dimensionless equilibrium constant reaction 1	$\bar{K}_1$	0.002

Dimensionless equilibrium constant reaction 2	$\bar{K}_2$	2.35
Dimensionless equilibrium constant reaction 2	$\bar{K}_3$	0.005
Dimensionless adsorption coefficient CO	$\bar{K}_{CO}$	26.97
Dimensionless adsorption coefficient H_2	$\bar{K}_{H_2}$	0.01
Dimensionless adsorption coefficient CH_4	$\bar{K}_{CH_4}$	2.88
Dimensionless adsorption coefficient H_2O	$\bar{K}_{H_2O}$	1.26

Table 2-4: Reactor Initial Dimensionless Partial Pressure Conditions

Description	Value
$\bar{P}^g_{CH_4}$ Phase 1	0.0002
$\bar{P}^g_{H_2O}$ Phase 1	0.9992
$\bar{P}^g_{H_2}$ Phase 1	0.0002
$\bar{P}^g_{CO}$ Phase 1	0.0002
$\bar{P}^g_{CO_2}$ Phase 1	0.0002
$\bar{P}^s_{H_2}$ Phase 1	0.019

In Figure 2-2, the phase-1 time evolution of all species mole fractions in the gas domain is shown. It can be seen that the CO_2 mole fraction time function exhibits a maximum, while the CH_4, CO, and H_2 mole fractions increase with time, and the H_2O mole fraction decreases with time. This behavior is consistent with the reactor starting phase-1 in a completely decarbonized

state, and largely full of H_2O. Thus, despite the vigorous transformation of CH_4 into CO, and CO_2, the CH_4 mole fraction in the gas phase increases. Additionally, the phase-1 time evolution of H_2 in the storage domain is also captured, in the form of the ratio of the hydrogen storage pressure over the total reactor pressure, which is a monotonically increasing function of time whose limit for long times becomes equal to the H_2 mole fraction in the gas domain. Figure 2-3 illustrates the positivity of the outlet molar flowrate throughout the phase-1 time evolution, confirming the physical realizability of PPSO during phase 1. Figure 2-4 illustrates the time averaged metric $\omega_{\mathrm{CO}_2,1}$ as a function of the potential phase-1 operating time τ_1. Figure 2-4 also exhibits a maximum at $\tau_1^* = 3.89$, similar to the CO_2 mole fraction behavior shown in Figure 2-2, which according to the first stopping criterion $\tau_1^* \triangleq \underset{\tau_1 \in [0,\infty)}{\arg\max}\, \omega_{\mathrm{CO}_2,1}(\tau_1)$ is then chosen as the operating time for phase-1, since it ensures significant CO_2 product generation that is higher than that of an SSR. Figures 2-5 through 2-9, illustrate the performance of the SR PPSO operation under the aforementioned stopping criterion $\tau_1^* = 3.89$ for phase 1.

In Figure 2-5 the phase-2 time evolution of all species mole fractions in the gas domain is shown. Since the SR feed during phase-2 consists of only H_2 and H_2O the outlet mole fractions of all other species decrease over time. In Figure 2-5 the phase-2 ratio of the hydrogen storage pressure over the total reactor pressure, is also shown to be approximately constant, except at small times as the hydrogen partial pressure in the gas equilibrates to the lower total storage pressure. Figure 3-6 shows $\bar{P}_{\mathrm{C}}^{g}(\bar{t}) \triangleq \bar{P}_{\mathrm{CO}_2}^{g}(\bar{t}) + \bar{P}_{\mathrm{CH}_4}^{g}(\bar{t}) + \bar{P}_{\mathrm{CO}}^{g}(\bar{t})$ as a function of time, and illustrates that the sum of all carbon containing species mole fractions falls below 0.01 at

$\tau_2^* = 3.13$. As with phase 1, Figure 2-7 shows that the outlet molar flowrate positivity is maintained throughout phase 2.

Finally, Figures 2-8 and 2-9 show the SR behavior during the Unloading Phase (phase 3) of operation, depicting the partial pressure of each species in the gas and storage domains. Choosing a depressurization limit of 0.05, the phase 3 operating time is then determined to be $\tau_3^* = 4.42$. As with the other phases, Figure 2-9 shows the positivity of the outlet molar flow is maintained throughout phase 3 reactor operation.

With the operational times calculated, it is now possible to calculate the metrics as described in equations (2.1.25)-(2.1.28). Conversion of methane increased over 100% by implementing the SR over a SSR, going from 0.32 to 0.68. The hydrogen recovery ratio is 0.81, indicating a large amount of hydrogen is recovered in phase 3 of SR operation, exceeding values of comparable metrics recently obtained by membrane reactors operating at steady state [27]. The SR hydrogen yield of $Y_{H_2} = 1.92$ is also significantly higher than its SSR counterpart of $Y_{H_2} = 1.08$. These high SR metric values suggest that the SR outperforms the SSR based on the defined criteria, and that SR operation at the designated temperature $T = 900\,K$ (which is lower than traditionally used SMR temperatures [25], may be economically viable and realizable using alternative fuel sources that would reduce carbon dioxide emissions[28].

Next we investigate the effect of the inverse Peclet number on reactor performance. Figures 2-2 thru 2-4 (Figures 2-10 thru 2-12) summarize the results for reactor designs with $\Theta = 50$ ($\Theta = 1$), while keeping all other simulation parameters the same. In particular, Figure 2-4 (Figure 2-12) illustrate that the magnitude of $\omega_{\mathrm{CO}_2,1}$ has a peak value of 0.49 for $\Theta = 50$ (0.31 for $\Theta = 1$), indicating that less CO_2 is being generated and that less reaction is occurring in the

gas domain as Θ decreases. They are also used to identify $\tau_1^* = 3.89$ for $\Theta = 50$ ($\tau_1^* = 8.01$ for $\Theta = 1$) according to the first stopping criterion $\tau_1^* \triangleq \arg\max_{\tau_1 \in [0,\infty)} \omega_{CO_2,1}(\tau_1)$. Figures 2-5 thru 2-9 (Figures 2-13 thru 2-17) summarize the remaining results for reactor designs with $\Theta = 50$ ($\Theta = 1$), while keeping all other simulation parameters the same and using the first stopping criterion. Methane conversion is reduced from 0.68 for $\Theta = 50$ to 0.43 for $\Theta = 1$. As Θ is lowered, operational times increase in both phases one and three, from $\tau_1^* = 3.89$ and $\tau_3^* = 4.42$ for $\Theta = 50$ to $\tau_1^* = 8.01$ and $\tau_3^* = 25.01$ for $\Theta = 1$. The above suggest that a number of potential operational and energy savings can be attained by using storage medium material that can deliver large inverse Peclet numbers. The inverse Peclet number Θ has a minimal effect on τ_2^*, as during this phase there is minimal hydrogen permeation through the gas-storage domain boundary, since the reactor is being flushed of reactants and undesirable products. The hydrogen yield and hydrogen product recovery are also both reduced from $Y_{H_2} = 1.92$ and $R_{H_2,rec} = 0.81$ at $\Theta = 50$ to $Y_{H_2} = 1.35$ and $R_{H_2,rec} = 0.47$ at $\Theta = 1$, suggesting that the inverse Peclet number should be increased as much as physically possible, to obtain the best reactor performance.

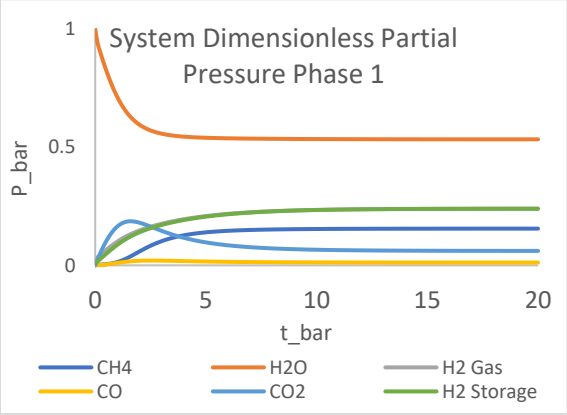

Figure 2-2: Dimensionless time evolution of species' partial pressure in composite reactor system Phase 1, Θ=50.

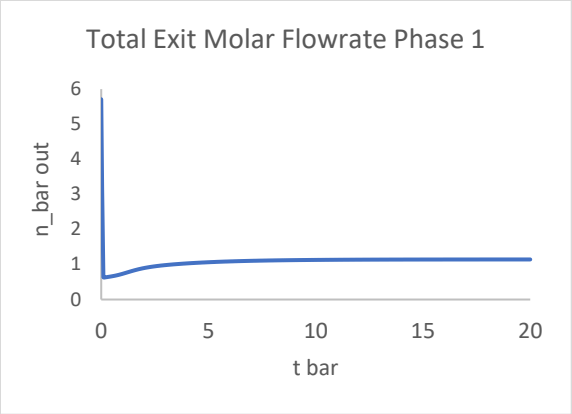

Figure 2-3:Total exit flowrate of reactor during operation of Phase 1, Θ=50.

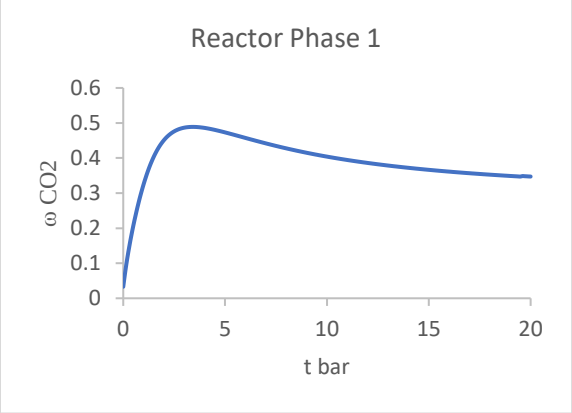

Figure 2-4: Evolution of parameters $\omega_{CO_2,1}$ during operation of Phase 1, Θ=50.

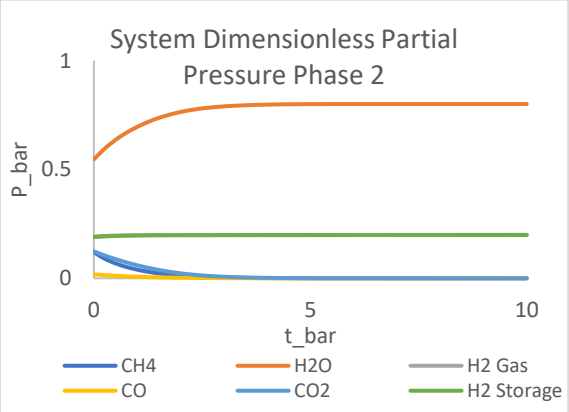

Figure 2-5: Dimensionless time evolution of species' partial pressure in composite reactor system Phase 2, Θ=50.

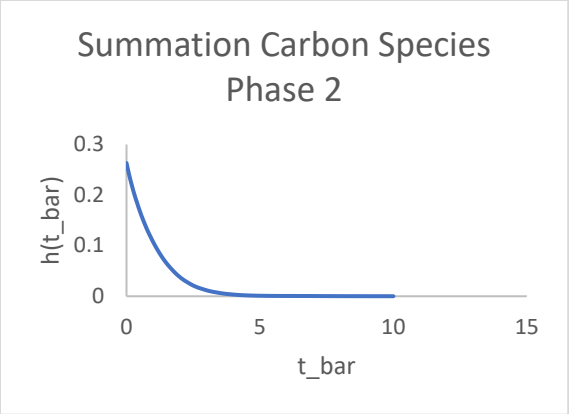

Figure 2-6: Sum of carbon containing species mol fraction in reactor gas during phase 2 of operation, Θ=50.

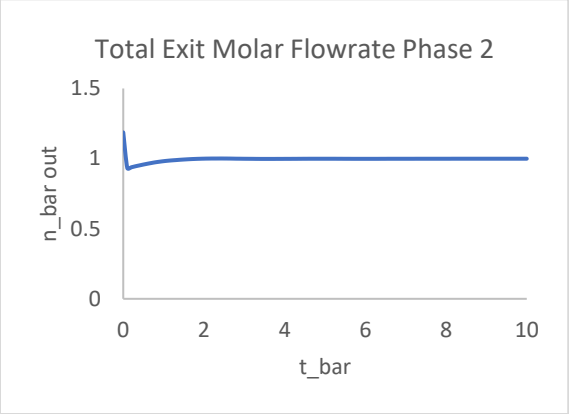

Figure 2-7: Total exit flowrate of reactor during operation of Phase 2, Θ=50.

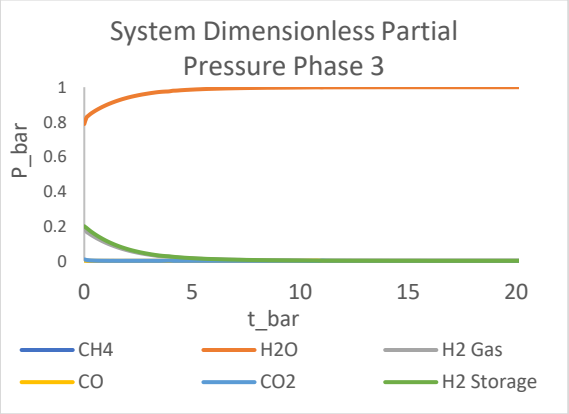

Figure 2-8: Dimensionless time evolution of species' partial pressure in composite reactor system Phase 3, Θ=50.

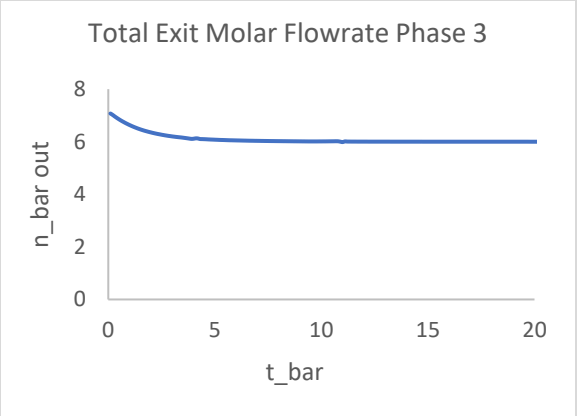

Figure 2-9: Total exit flowrate of reactor during operation of Phase 3, Θ=50.

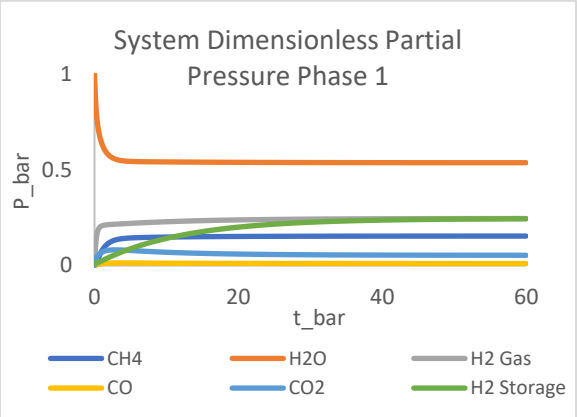

Figure 2-10: Dimensionless time evolution of species' partial pressure in composite reactor system Phase 1, Θ=1

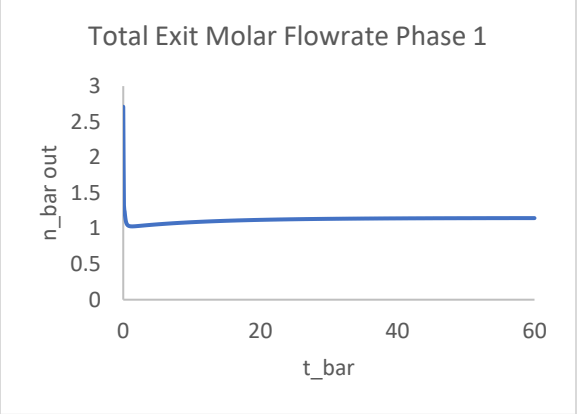

Figure 2-11: Total exit flowrate of reactor during operation of Phase 1, Θ=1.

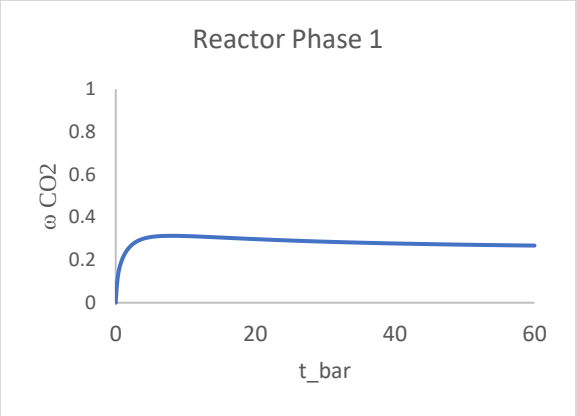

Figure 2-12: Evolution of parameters $\omega_{CO_2,1}$ during operation of Phase 1, Θ=1.

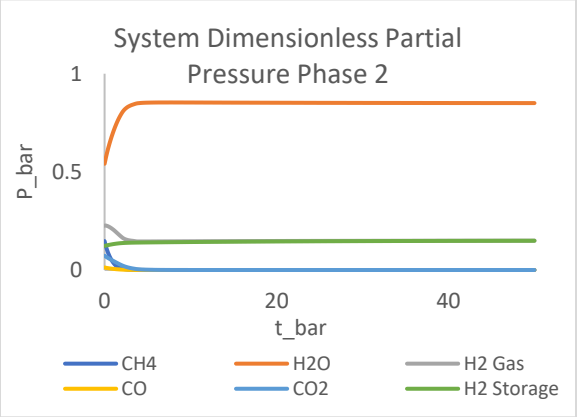

Figure 2-13: Dimensionless time evolution of species' partial pressure in composite reactor system Phase 2, Θ=1.

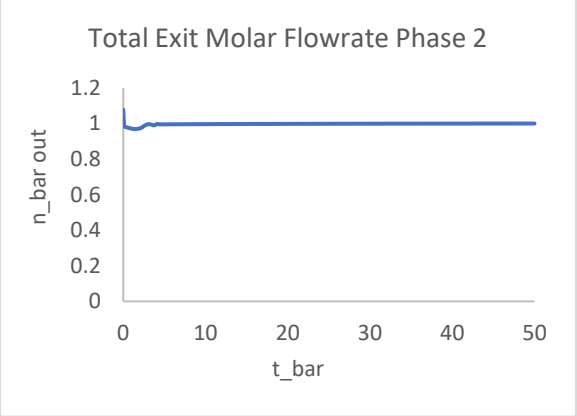

Figure 2-14: Total exit flowrate of reactor during operation of Phase 2, Θ=1.

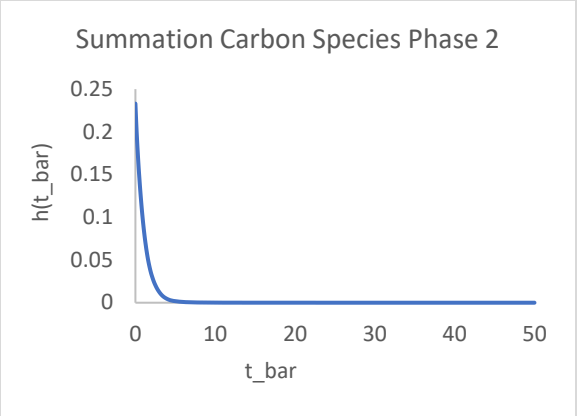

Figure 2-15: Sum of carbon containing species mol fraction in reactor gas during phase 2 of operation, Θ=1.

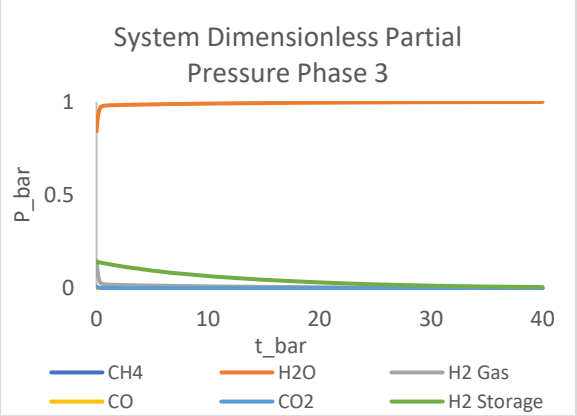

Figure 2-16: Dimensionless time evolution of species' partial pressure in composite reactor system Phase 3, Θ=1.

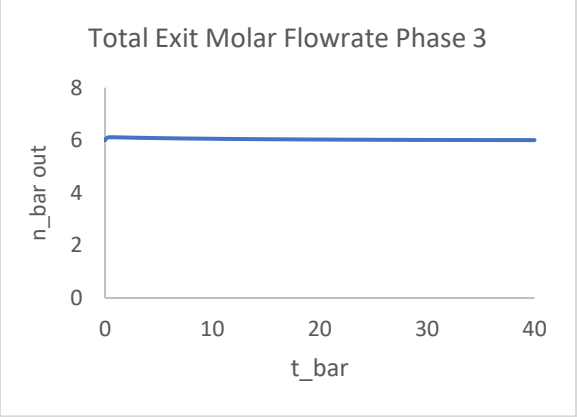

Figure 2-17: Total exit flowrate of reactor during operation of Phase 3, Θ=1.

There are several process design and operational parameters that can be adjusted to increase Θ. First, the inlet flowrate can be reduced, thus increasing reactant residence time, and allowing for additional reactant conversion to occur within the gas domain. Second, the gas-storage domain interfacial area can be increased, allowing for increased transport between the two domains. Third, increased preferential hydrogen permeance through the storage medium's permselective layer can be pursued, through appropriate selection of the layer's pore structure and material. Finally, high reactor operating pressure would also lead to higher Θ values.

Table 2-5: Comparison of performance metrics for SSR and SR.

Metric	SSR	SR: Θ=1, Da=7	SR: Θ=50, Da=7	SR: Θ=50, Da=0.1
X_{CH_4}	0.32	0.43	0.68	0.36
Y_{H_2}	1.08	1.35	1.92	0.74
$R_{H_2,rec}$	N/A	0.47	0.81	0.80

Table 2-6: SR Operating Times.

Metric	Θ=1, Da=7	Θ=50, Da=7	Θ=50, Da=0.1
τ_1^*	8.01	3.89	4.624
τ_2^*	3.19	3.13	3.053
τ_3^*	25.01	4.42	3.488

The above Tables 2-5 and 2-6 summarize the effects of varying Θ on SR performance. They also quantify the effect of varying Da on SR performance. As shown in Table 2-5, for $\Theta = 50$, methane conversion, hydrogen production ratio and hydrogen product recovery are all

reduced from $X_{CH_4} = 0.68$, and $R_{H_2,rec} = 0.81$ at $Da = 7$ to $X_{CH_4} = 0.36$ $Y_{H_2} = 0.74$ and $R_{H_2,rec} = 0.80$ at $Da = 0.1$. These reductions are significant, suggesting that SR's with high Θ, and low Da values may not be efficient, and reaffirming that both the reaction and separation characteristics of SR must be simultaneously considered to optimize SR performance. In regard to operating times, Table 2-6 illustrates that varying Da has a relatively small effect on operating times for each phase of the SR.

In comparing the proposed SR process to existing periodically-operated reforming reactors (e.g., sorption-enhanced), it should be emphasized that the SR does not employ sorption to enhance reactor performance. Rather, it employs a storage medium whose outer surface is permselective to the desired species, which are thus preferentially transported from the reacting phase into the storage medium. The transport across this permselective layer can be driven by a variety of driving forces, depending on the nature of the particular storage medium chosen, that affect the chemical potential difference of the preferentially-transported species across the aforementioned surface. This suggests, that the SR process can be applied to reactors in which the reaction and storage domains can be composed of any combination of gas-phase, liquid-phase and/or solid-phase media.

In comparing the proposed SR process to existing membrane-assisted reactors (MR), it is important to emphasize that the SR process does not suffer from any potentially severe performance degradation induced by structural imperfections, as commonly encountered with large-area membranes employed in such MR. Since the storage medium is likely to be in a pellet form, it is expected that it will be a straightforward task to prepare defect-free permselective coatings (e.g., via dip-coating of pre-ceramic precursors with subsequent pyrolysis to form ceramic surface films, see [29]). Indeed, any pinhole and/or crack that may form during

operation on a given pellet's surface coating is likely to have less of a detrimental effect on reactor performance than forming a similar size defect on a membrane tube. This means then that any reactor performance degradation that may occur, due to the storage medium's decline in permselectivity is likely to be gradual and incremental, and performance recovery may be easier to implement than in the MR case.

In comparing the effect of different stopping criteria for phase 1 on overall SR performance, it was found that stopping criterion one $\left(\tau_1^* \triangleq \arg\max_{\tau_1 \in [0,\infty)} \omega_{\mathrm{CO}_2,1}(\tau_1) \right)$ was superior to stopping criterion two $\tau_1^* : \bar{P}_{H_2}^s(\tau_1^*) = 0.9 \cdot \left(\bar{P}_{H_2}^g \right)_{ss} \triangleq 0.9 \cdot \lim_{\tau_1 \to +\infty} \bar{P}_{H_2}^s(\tau_1)$ across all metrics. Indeed as can be seen in Table 2-7, methane conversion, hyrogen yield, and hydrogen recovery are all lower when the second phase 1 stopping criterion is employed. This is consistent with the stopping criterion effect on the operational times of all three SR phases, summarized in Table 8. In the limit of long SR operational times, the SR performance metric values approach those of the SSR, thus negating the potential SR benefits. This further highlights the need for further studies aiming at identifying the optimal SR phase operational times for the optimization of various SR performance metrics.

Table 2-7: Comparison of SR performance metrics for both phase 1 stopping criteria.

Metric	CR1: Θ=1, Da=7	CR2: Θ=1, Da=7	CR1: Θ=50, Da=7	CR2: Θ=1, Da=7
X_{CH_4}	0.43	0.36	0.68	0.58
Y_{H_2}	1.35	1.23	1.92	1.69
$R_{H_2,rec}$	0.47	0.26	0.81	0.69

Table 2-8: SR Phase Operating Times for both phase 1 stopping criteria

Metric	CR1: Θ=1, Da=7	CR2: Θ=1, Da=7	CR1: Θ=50, Da=7	CR2: Θ=1, Da=7
τ_1^*	8.01	27.2	3.89	5.91
τ_2^*	3.19	3.01	3.13	2.97
τ_3^*	25.01	28.9	4.42	4.60

The long-term periodic behavior of the SR process is attained within a few operating cycles. Indeed, the reactor at the end of the regeneration phase is largely filled with water and low levels of desired species (hydrogen) in the storage medium. Using initial conditions of y_{CH4}=0.01, y_{H2O}=0.96, y_{H2}=0.01, y_{CO}=0.01, y_{CO2}=0.01, y_{H2S}=0.02, the process converges to its long-term behavior within 3 cycles. The associated evolution of stopping times for each phase for a reactor with Θ=50, Da=7 is shown in the table below.

Table 2-9: Convergence of operating times for each phase.

Metric	Cycle 1	Cycle 2	Cycle 3
τ_1^*	3.76	3.88	3.89
τ_2^*	3.09	3.13	3.13
τ_3^*	4.40	4.42	4.42

This quick convergence can be readily explained by the dominant presence of water in the reactor domain at the end of the regeneration phase.

2.1.3 Conclusions

A novel reactor process, termed the storage reactor (SR), was proposed, and a first principle based model capturing its behavior was presented. The SR process combines reaction

and separation, and can deliver high purity products, and potentially overcome equilibrium limitations. It is envisioned that the SR will find applications in the energy and other sectors, where there is a great demand for process intensification. To assess SR behavior, a 0-dimensional dynamical model was developed, whose dimensionless form highlights that two dimensionless parameters, Da (Damkohler number) and $\Theta = 1/Pe_{mem}$ (inverse Peclet number), determine SR behavior. A number of metrics were introduced for assessing SR behavior, which were easily amenable to comparison with conventional metrics of steady-state reactor (SSR) performance. A case study on hydrogen production through Steam Methane Reforming was carried out, and SR Conversion, Yield, and Hydrogen Recovery were all shown to be greater than their SSR counterparts. A parametric study was then carried out on the aforementioned , Da and $\Theta = 1/Pe_{mem}$ dimensionless groups, and it was shown that maximizing both groups led to improved SR performance. This work should be viewed as a proof of concept study, that introduces the SR process, and will be followed by modeling and optimization studies of increased complexity.

One of the many advantages of the SR process is its flexibility in accommodating any desired production scale. For example, in the presented case study for steam methane reforming, it is envisioned that the SR could be applied at the refinery level to meet hydrogen raw material needs; but it is also quite feasible to apply the SR technology at the hydrogen-fueling station level for decentralized hydrogen generation.

The SR is amenable to retrofit implementation in existing plants, since all it requires is the loading of the reactor with the storage media in addition to the catalyst, so no reactor rebuilding and/or replacement is required, as would be the case, for example, for industrial implementation of MR. Further, additional feed and effluent lines may need to be constructed in

order to appropriately direct material to and from the reactor at different times. Such construction is expected to be minimal, however, as the SR process does not require chemical components exogenous to the original process (e.g., extraction fluids). In addition, given the dynamic nature of the SR process, and since most conventional reactors operate at steady state conditions, there may be an increased need for additional dynamic control equipment. Thus, it appears that the SR may be more easily incorporated into existing units than many of the currently investigated process intensification technologies, such as those employing solid sorbents and/or membranes. The presented SR dynamic model considers the reactor and storage domains to be spatially uniform, and has been employed to demonstrate the novel SR concept. Future research will focus on the development of an SR model that can capture both spatiotemporal and multi-scale effects. Further, as the SR process is shown to offer significant advantages for equilibrium-limited reactions, often carried-out at high pressures and/or temperatures, the incorporation of gas compressibility factors and energy balance considerations in the SR model will also be pursued.

2.1.4 Notation

English Symbols

$A^{gs}\left(m^2\right)$: reactor gas-storage medium interfacial area

D_a: Damköhler number

$k_1\left(\frac{\text{kmol bar}^{0.5}}{\text{kg}_{\text{cat}}\,\text{hr}}\right), k_2\left(\frac{\text{kmol}}{\text{kg}_{\text{cat}}\,\text{hr bar}}\right), k_3\left(\frac{\text{kmol bar}^{0.5}}{\text{kg}_{\text{cat}}\,\text{hr}}\right)$: Rate coefficients for SMR reaction

$K_1\left(\text{bar}^2\right), K_2, K_3\left(\text{bar}^2\right)$: Equilibrium constants for SMR reaction

$K_{CH_4}\left(\text{bar}^{-1}\right), K_{H_2}\left(\text{bar}^{-1}\right), K_{CO}\left(\text{bar}^{-1}\right), K_{H_2O},$: Species adsorption constants for SMR reaction

$\bar{k}_j$: Dimensionless rate coefficient for reaction j

$\bar{K}_j \ \forall j = 1,2,3$: Dimensionless equilibrium constant for reaction j

$\bar{K}_j \ \forall j = CH_4, H_2O, H_2, CO, CO_2$: Dimensionless adsorption constant for species j

$n_j^g\left(mol\right), n_j^s\ \left(mol\right)$: j_{th} species moles in reactor gas and in storage medium

$n_j^{g0}\left(mol\right), n_j^{s0}\ \left(mol\right)$: j_{th} species initial moles in reactor gas and in storage medium

$\dot{n}_j^{in}\left(\frac{mol}{s}\right), \dot{n}_j^{out}\left(\frac{mol}{s}\right)$: j_{th} species inlet and outlet molar flowrates

$\bar{\dot{n}}_j^{in}$: j_{th} species dimensionless inlet molar flowrate

$\dot{n}^{in}\left(\frac{mol}{s}\right), \dot{n}^{out}\left(\frac{mol}{s}\right)$: total inlet and outlet molar flowrate

$\bar{\dot{n}}^{in}, \bar{\dot{n}}^{out}$: Total dimensionless inlet and outlet molar flowrates

$\dot{n}_j^{sg}\left(\frac{mol}{s}\right)$: j_{th} species molar flowrate from the reactor gas to the storage medium

$\dot{n}^{*}\left(\frac{mol}{s}\right)$: Reference molar flowrate

NC: Number of species

NP: Number of reactor operational phases

$P_j^g\left(Pa\right), P_j^s\left(Pa\right)$: j_{th} species partial pressure in gas and storage medium

$P_j^{g0}\left(Pa\right), P_j^{s0}\left(Pa\right)$: j_{th} species initial partial pressure in gas and storage medium

$\bar{P}_j^g, \bar{P}_j^s$: j_{th} species dimensionless partial pressure in gas and storage medium

$\bar{P}_j^{g0}, \bar{P}_j^{s0}$: j_{th} species dimensionless initial partial pressure in gas and storage medium

$P^{*}\left(Pa\right)$: Reference pressure

Pe_{mem}: Modified Peclet number for membranes

$r_j\left(\frac{mol\ j}{kg\ catalyst \cdot s}\right)$: j_{th} species reaction based generation rate

$\bar{r}_j$: j_{th} species dimensionless reaction based generation rate

$r^{*}\left(\frac{mol}{kg\ catalyst \cdot s}\right)$: Reference reaction generation rate

$R_{j,i}$: Dimensionless Recovery Ratio of jth species in ith phase

$\bar{R}_j$: Dimensionless rate for j_{th} reaction

$R\left(\frac{J}{mol \cdot K}\right) \triangleq 8.314462$: Universal Gas Constant

$t\left(s\right)$: Time

$\bar{t}$: Dimensionless time

$t^{*}\left(s\right)$: Reference time

$T\left(K\right)$: Temperature in all reactor domains

$V\left(m^3\right)$: Total reactor volume

X_K: Conversion of limiting reactant K

$Y_{j,i}$: Desired product yield in reactor operation phase i

Y_j : Desired product yield of species j

Greek Symbols

$\beta_j \left(\frac{mol\ j}{Pa \cdot m^2 \cdot s} \right) \forall j = 1, NC$: j_{th} species permeance through storage medium permselective layer

$\varepsilon_{sc}, \varepsilon_{gc}, \varepsilon_c, \varepsilon_r, \varepsilon_g, \varepsilon_{gs}, \varepsilon_{ss}, \varepsilon_s$: volume fractions of catalyst pellet solid, catalyst pellet gas, catalyst pellet, reactor void unoccupied by catalyst, reactor void unoccupied by storage pellet, reactor gas, storage pellet gas, storage pellet solid, and storage pellet.

η_j : j_{th} species catalyst effectiveness factor

Θ : dimensionless membrane permeation (inverse Peclet) number

$\rho_c \left(\frac{kg\ catalyst}{m^3\ catalyst} \right)$: catalyst density

$\omega_{j,k}$: molar ratio of species j produced during phase i, over limiting reactant K

Ω_j : summation of molar production ratio over all phases of operation

τ_k : operational time for reactor operating phase k.

τ_k^* : selected operational time for reactor operating phase k

2.2. 1-dimensional isobaric studies

The focus of this section is the continued development of the novel Membrane Storage Reactor (MSR) process, which aims to intensify traditional steady-state reactor designs. This work expands on our previous studies on the subject by incorporating spatial variation into the mathematical development of the MSR model, and demonstrating that the MSR process can intensify high temperature/pressure processes subjected to limitations stemming from either reaction equilibrium or kinetics [11]. In the current paper, the proposed process is shown to incorporate several PI features, such as simultaneously carrying out reaction, separation, and storage in a single unit, in addition to driving force maximization through dynamic operation, while avoiding reliability issues currently associated with high-temperature membranes.

2.2.1 Mathematical Formulation

In this study, a composite one-dimensional model for the intensified MSR process is derived which captures and highlights several attractive MSR characteristics. Following non-dimensionalization, dimensionless groups governing the MSR behavior are identified. The MSR is considered to be a composite thermodynamic system (r) comprised of three domains that are spatially distributed and exclusive of each other (reactor voids (v), catalyst pellet (c), and storage pellet (s)), and a maximum of two phases (gas (g), and solid (so)). The volume fractions of the voids (v), catalyst (c), and storage (s) domains are denoted as $\varepsilon_v, \varepsilon_c, \varepsilon_s$, respectively, while the volume fractions of the gas and solid phases in the storage domain are denoted as $\varepsilon_{gs}, \varepsilon_{sos}$, respectively. In the context of this study, the following are then considered to hold:

$$\varepsilon_v + \varepsilon_c + \varepsilon_s = 1,\ \varepsilon_{gs} + \varepsilon_{sos} = \varepsilon_s \tag{2.1.29}$$

The communication between the catalyst and reactor voids (gas phase) domains is quantified using an effectiveness factor approach, and the communication between the storage domain and reactor gas phase domains through a permselective layer on the storage domain's control surface is quantified using species transport equations obeying Sieverts' Law. The composite system (r) is considered to be isothermal, whereas the reactor voids domain (v) is also considered to be isobaric. The molar diffusion flux of gaseous species in the voids domain is considered to be negligible compared to the species convective molar flux. No reaction occurs within the storage domain. The reacting mixture is considered to be an ideal gas. The equation describing Mass Conservation (molar form) of species i in phase g within domain v on a system r volumetric basis is:

$$\left[\frac{\partial}{\partial t}\left(\varepsilon_v c_{i,gv}(t,z)\right)+\frac{\partial}{\partial z}\left(\varepsilon_v v_g(t,z)c_{i,gv}(t,z)\right)\right]=\left[\varepsilon_c\rho_c\eta r_i\left(\left\{c_{k,gv}(t,z)\right\}_{k=1}^{NC},T\right)+S_{i,gv,gs}(t,z)\right]\ i=1,NC \quad (2.1.30)$$

The Peclet number, $Pe'=\frac{v_{eff}L_{char}}{D_{eff}}$, is typically used to determine whether a process is dominated by convective or diffusive mass transport processes, where v_{eff} is a gas velocity, L_{char} is a characteristic length, and D_{eff} is the effective diffusion coefficient of the transferrable species. Although there is still considerable debate regarding the choice of these parameters, which depend on the structure and geometry of the system at hand [30], it is generally agreed that $Pe' \gg 1$ is sufficient to ignore diffusive effects. For example, the porosity of the system that is available for diffusion is generally smaller than the total porosity itself [31]. The parameter D_{eff} is evaluated as $D_{eff}=\varepsilon_v D_{AB}$ using the binary diffusion coefficient, D_{AB}, of the transferrable species, which in turn can be evaluated using the Chapman–Enskog solution to the Boltzmann Equation along with a Lennard-Jones potential for estimating the effects of intermolecular forces. Using the formulation established in our previous results [14], the values of D_{AB} for the species present in the considered case study fall in the range of $0.02 \le D_{AB} \le 0.15\left(cm^2/s\right)$.

Values for the characteristic length can be obtained by considering L_{char} to be equal either to the length or the radius of the reactor, which in turn yield Pe' values that satisfy $Pe' \ge 1\times10^5$ and $Pe' \ge 100$, respectively, and justify neglecting diffusion in the void domain."

The equation describing Mass Conservation (molar form) of species i in phase g within domain s on a system r volumetric basis is:

$$\frac{\partial}{\partial t}\left(\varepsilon_{gs}c_{i,gs}(t,z)\right)=S_{i,gs,gv}(t,z)\ i=1,NC \quad (2.1.31)$$

where the temporal and spatial dependence of all volume fractions, the effectiveness factor, and the catalyst pellet density are not shown, because they will next be considered constant. Sieverts' Law, as described in the previous section, is again employed to quantify the species' molar flux through the storage:

$$S_{i,gs,gv}(t,z) = -S_{i,gv,gs}(t,z) = \alpha_{s,v}\beta_i\left(P_{i,gv}(t,z) - P_{i,gs}(t,z)\right) \forall i = 1,...,NC \qquad (2.1.32)$$

where β_i is the i_{th} species molar permeance through the permselective layer, $\alpha_{s,v}$ is the storage-void interfacial area per unit reactor volume, and $P_{i,gv}, P_{i,gs}$ are the i_{th} species partial pressures in the gas phase of the reactor void and storage domains. Considering an ideal gas mixture, the following relations hold:

$$P_{i,gv}(t,z) = c_{i,gv}(t,z)RT, \quad P_{i,gs}(t,z) = c_{i,gs}(t,z)RT \quad \forall i = 1,...,NC \qquad (2.1.33)$$

where R is the universal gas constant, and T is the reactor temperature that is considered to be constant over both time and space. Combining the above equations yields:

$$\frac{\partial P_{i,gv}(t,z)}{\partial t} + \frac{\partial}{\partial z}\left(v_g(t,z)P_{i,gv}(t,z)\right) = \frac{RT}{\varepsilon_v}\left[\begin{array}{l}\varepsilon_c\rho_c\eta r_i\left(\left\{\dfrac{P_{k,gv}(t,z)}{RT}\right\}_{k=1}^{NC}, T\right) - \\ \beta_i\alpha_{s,v}\left(P_{i,gv}(t,z) - P_{i,gs}(t,z)\right)\end{array}\right] i = 1, NC \qquad (2.1.34)$$

$$\frac{\partial P_{i,gs}(t,z)}{\partial t} = \frac{RT}{\varepsilon_{gs}}\alpha_{s,v}\beta_i\left(P_{i,gv}(t,z) - P_{i,gs}(t,z)\right) i = 1, NC \qquad (2.1.35)$$

Summing the gas phase species conservation equations in the void domain and utilizing the isobaric void domain assumption yields:

$$\frac{\partial v_g(t,z)}{\partial z} = \frac{RT}{\varepsilon_v\sum_{k=1}^{NC}P_{k,gv}}\left[\varepsilon_c\rho_c\eta\sum_{l=1}^{NC}r_l\left(\left\{\frac{P_{k,gv}}{RT}\right\}_{k=1}^{NC}, T\right) - \alpha_{s,v}\sum_{l=1}^{NC}\left[\beta_l\left(P_{l,gv} - P_{l,gs}\right)\right]\right] \qquad (2.1.36)$$

Substitution of Equation (2.1.36) into Equations (2.1.34) and (2.1.35) then yields:

$$\frac{\partial P_{i,gv}(t,z)}{\partial t}+v_g(t,z)\frac{\partial P_{i,gv}(t,z)}{\partial z}=\frac{RT}{\varepsilon_v}\left[\begin{array}{l}\varepsilon_c\rho_c\eta\left[\begin{array}{l}r_i\left(\left\{\frac{P_{k,gv}(t,z)}{RT}\right\}_{k=1}^{NC},T\right)-\\ \frac{P_{i,gv}(t,z)}{\sum_{k=1}^{NC}P_{k,gv}}\sum_{l=1}^{NC}r_l\left(\left\{\frac{P_{k,gv}(t,z)}{RT}\right\}_{k=1}^{NC},T\right)\end{array}\right]-\\ \alpha_{s,v}\left[\begin{array}{l}\beta_i\left(P_{i,gv}(t,z)-P_{i,gs}(t,z)\right)-\\ \frac{P_{i,gv}(t,z)}{\sum_{k=1}^{NC}P_{k,gv}}\sum_{l=1}^{NC}\left[\beta_l\left(P_{l,gv}(t,z)-P_{l,gs}(t,z)\right)\right]\end{array}\right]\end{array}\right] i=1,NC$$

(2.1.37)

$$\frac{\partial P_{i,gs}(t,z)}{\partial t}=\frac{RT}{\varepsilon_{gs}}\alpha_{s,v}\beta_i\left(P_{i,gv}(t,z)-P_{i,gs}(t,z)\right) i=1,NC \quad (2.1.38)$$

$$\frac{\partial v_g(t,z)}{\partial z}=\frac{RT}{\varepsilon_v\sum_{k=1}^{NC}P_{k,gv}}\left[\varepsilon_c\rho_c\eta\sum_{l=1}^{NC}r_l\left(\left\{\frac{P_{k,gv}(t,z)}{RT}\right\}_{k=1}^{NC},T\right)-\alpha_{s,v}\sum_{l=1}^{NC}\left[\beta_l\left(P_{l,gv}(t,z)-P_{l,gs}(t,z)\right)\right]\right]$$

(2.1.39)

Next, dimensionless variables are introduced, and dimensionless groups are identified governing MSR behavior:

$$\left\{\begin{array}{l}\bar{z}\triangleq\frac{z}{L^*},\bar{v}_g\triangleq\frac{v_g}{v^*},t^*\triangleq\frac{L^*}{v^*},\bar{t}\triangleq\frac{t}{t^*},\bar{P}_{i,gv}\triangleq\frac{P_{i,gv}}{P^*},\bar{P}_{i,gs}\triangleq\frac{P_{i,gs}}{P^*},\Theta\triangleq\frac{t^*RT\alpha_{s,v}\beta_1}{\varepsilon_v}=\frac{1}{Pe}\\ \\ D_a\triangleq\frac{RT}{P^*}\rho_c r^*t^*,\bar{r}_i\left(\left\{\frac{\bar{P}_{k,gv}\cdot P^*}{RT}\right\}_{k=1}^{NC},T\right)\triangleq\frac{r_i\left(\left\{\frac{P_{k,gv}}{RT}\right\}_{k=1}^{NC},T\right)}{r^*}\end{array}\right\} \quad (2.1.40)$$

where P^* is the operating pressure of the reactor, L^* is the length of the reactor, v^* is the inlet velocity to the reactor at time zero, and $t^*=L^*/v^*$ is the reactor's residence time at time zero, and r* is defined later in this paper. Given that z is the reactor's axial coordinate, L^* is the length of

the reactor, and $\bar{z} \triangleq z/L^*$, the reactor inlet and outlet can be designated as $\bar{z}=0$, $\bar{z}=1$, respectively.

Given that the reactor voids domain (v) is considered isobaric, with operating pressure P^*, then $\sum_{k=1}^{NC} P_{k,gv} = P^*$, which implies that $\sum_{k=1}^{NC} \bar{P}_{k,gv} = 1$. Then, the resulting dimensionless equations for the MSR model are:

$$\begin{bmatrix} \dfrac{\partial \bar{P}_{i,gv}(\bar{t},\bar{z})}{\partial \bar{t}} + \\ +\bar{v}_g(\bar{t},\bar{z})\dfrac{\partial \bar{P}_{i,gv}(\bar{t},\bar{z})}{\partial \bar{z}} \end{bmatrix} = \begin{bmatrix} D_a \dfrac{\varepsilon_c}{\varepsilon_v}\eta \begin{bmatrix} \bar{r}_i\left(\left\{\dfrac{\bar{P}_{k,gv}(\bar{t},\bar{z})\cdot P^*}{RT}\right\}_{k=1}^{NC},T\right) - \\ \bar{P}_{i,gv}(\bar{t},\bar{z})\sum_{l=1}^{NC}\bar{r}_i\left(\left\{\dfrac{\bar{P}_{k,gv}(\bar{t},\bar{z})\cdot P^*}{RT}\right\}_{k=1}^{NC},T\right) \end{bmatrix} - \\ -\Theta\begin{bmatrix} \dfrac{\beta_i}{\beta_1}\left(\bar{P}_{i,gv}(\bar{t},\bar{z}) - \bar{P}_{i,gs}(\bar{t},\bar{z})\right) - \\ \bar{P}_{i,gv}(\bar{t},\bar{z})\sum_{l=1}^{NC}\left[\dfrac{\beta_l}{\beta_1}\left(\bar{P}_{l,gv}(\bar{t},\bar{z}) - \bar{P}_{l,gs}(\bar{t},\bar{z})\right)\right] \end{bmatrix} \end{bmatrix} \quad i=1,NC \tag{2.1.41}$$

$$\frac{\partial \bar{P}_{i,gs}(\bar{t},\bar{z})}{\partial \bar{t}} = \Theta\frac{\varepsilon_v}{\varepsilon_{gs}}\frac{\beta_i}{\beta_1}\left(\bar{P}_{i,gv}(\bar{t},\bar{z}) - \bar{P}_{i,gs}(\bar{t},\bar{z})\right) \; i=1,NC \tag{2.1.42}$$

$$\frac{\partial \bar{v}_g(\bar{t},\bar{z})}{\partial \bar{z}} = \begin{bmatrix} D_a\dfrac{\varepsilon_c}{\varepsilon_v}\eta\sum_{l=1}^{NC}\bar{r}_i\left(\left\{\dfrac{\bar{P}_{k,gv}(\bar{t},\bar{z})\cdot P^*}{RT}\right\}_{k=1}^{NC},T\right) - \\ \Theta\sum_{l=1}^{NC}\left[\dfrac{\beta_l}{\beta_1}\left(\bar{P}_{l,gv}(\bar{t},\bar{z}) - \bar{P}_{l,gs}(\bar{t},\bar{z})\right)\right] \end{bmatrix} \tag{2.1.43}$$

The above MSR dimensionless model suggests that two dimensionless numbers determine the MSR's dynamic behavior. The first dimensionless quantity, $\Theta = 1/Pe$, provides a measure of how effectively the desired product species is being extracted from the reactor void domain into the gas storage domain, as compared to its axial convective transport in the reactor void domain. In this context, the Peclet number, P_e, has a similar meaning as in the previous

section, and is a dimensionless group commonly used in the analysis of membrane reactors. The Damkohler number, D_a, captures the importance of the rate of convection compared to the reaction rate and can be thought as the ratio of the characteristic time for convective flow to the characteristic time for reaction.

Comparing the performance of a periodic process with that of a traditionally steady-state process necessitates the introduction of several performance metrics. These metrics can be defined for each OM and for the process as a whole, namely for the duration of all three aforementioned OMs. To this end, the axial molar flowrate of the i_{th} species $F_{i,gv}$ is expressed in terms of a reference molar flowrate F^* and a dimensionless molar flowrate $\bar{F}_{i,gv}$, as follows:

$$F^* \triangleq \frac{P^* v^* \varepsilon_v A_r}{RT},\ \bar{F}_{i,gv} \triangleq \frac{F_{i,gv}}{F^*} = \frac{c_{i,gv} v_g \varepsilon_v A_r}{F^*} = \frac{P^* \bar{P}_{i,gv} v^* \bar{v}_g \varepsilon_v A_r}{RTF^*} = \bar{P}_{i,gv} \bar{v}_g \tag{2.1.44}$$

Then, the following dimensionless metrics are defined and explained below:

Limiting Reactant Conversion

An important metric for the assessment of MSR performance is the conversion of a limiting reactant R_{LIM}. Typically, this reactant will be fed in the MSR during one OM, but may be removed from the MSR during multiple OMs. Thus, we define its conversion over all OM as follows:

$$X_{R_{LIM}} \triangleq \frac{\left[\int_0^{\sum_{k=1}^{NOM}\tau_k} F_{R_{LIM},gv}(t',0)dt' - \int_0^{\sum_{k=1}^{NOM}\tau_k} F_{R_{LIM},gv}(t',L^*)dt'\right]}{\int_0^{\sum_{k=1}^{NOM}\tau_k} F_{R_{LIM},gv}(t',0)dt'} = \frac{\left[\int_0^{\sum_{k=1}^{NOM}\bar{\tau}_k} \bar{F}_{R_{LIM},gv}(\bar{t}',0)d\bar{t}' - \int_0^{\sum_{k=1}^{NOM}\bar{\tau}_k} \bar{F}_{R_{LIM},gv}(\bar{t}',1)d\bar{t}'\right]}{\int_0^{\sum_{k=1}^{NOM}\bar{\tau}_k} \bar{F}_{R_{LIM},gv}(\bar{t}',0)d\bar{t}'} \tag{2.1.45}$$

Desired Product Ratio

Another important metric for the assessment of MSR performance is one that captures the extent to which the desired product is formed as the limiting reactant is converted. Thus, the following OM-dependent metric is introduced that is equal to the ratio of the i_{th} species amount generated during OM k over the limiting reactant's R_{LIM} amount fed throughout all OMs.

$$\omega_{i,k} \triangleq \frac{\left[\int_{\sum_{k'=0}^{k'=k-1}\tau_{k'}}^{\sum_{k'=0}^{k'=k}\tau_{k'}} F_{i,gv}\left(t',L^*\right)dt' - \int_{\sum_{k'=0}^{k'=k-1}\tau_{k'}}^{\sum_{k'=0}^{k'=k}\tau_{k'}} F_{i,gv}\left(t',0\right)dt'\right]}{\int_{0}^{\sum_{k=1}^{NOM}\tau_k} F_{R_{LIM},gv}\left(t',0\right)dt'} = \frac{\left[\int_{\sum_{k'=0}^{k'=k-1}\bar{\tau}_{k'}}^{\sum_{k'=0}^{k'=k}\bar{\tau}_{k'}} \bar{F}_{i,gv}\left(\bar{t}',1\right)d\bar{t}' - \int_{\sum_{k'=0}^{k'=k-1}\bar{\tau}_{k'}}^{\sum_{k'=0}^{k'=k}\bar{\tau}_{k'}} \bar{F}_{i,gv}\left(\bar{t}',0\right)d\bar{t}'\right]}{\int_{0}^{\sum_{k=1}^{NOM}\bar{\tau}_k} \bar{F}_{R_{LIM},gv}\left(\bar{t}',0\right)d\bar{t}'}$$

$$k = 1, NOM,\ i = 1, NC$$

(2.1.46)

where $\tau_0 = 0, \bar{\tau}_0 = 0$.

An overall OM-independent metric is also introduced that is equal to the ratio of the i_{th} species amount generated during all OMs over the limiting reactant's R_{LIM} amount fed throughout all OMs.

$$\Omega_i \triangleq \frac{\left[\int_{0}^{\sum_{k=1}^{NOM}\tau_k} F_{i,gv}\left(t',L^*\right)dt' - \int_{0}^{\sum_{k=1}^{NOM}\tau_k} F_{i,gv}\left(t',0\right)dt'\right]}{\int_{0}^{\sum_{k=1}^{NOM}\tau_k} F_{R_{LIM},gv}\left(t',0\right)dt'} = \frac{\left[\int_{0}^{\sum_{k=1}^{NOM}\bar{\tau}_k} \bar{F}_{i,gv}\left(\bar{t}',1\right)d\bar{t}' - \int_{0}^{\sum_{k=1}^{NOM}\bar{\tau}_k} \bar{F}_{i,gv}\left(\bar{t}',0\right)d\bar{t}'\right]}{\int_{0}^{\sum_{k=1}^{NOM}\bar{\tau}_k} \bar{F}_{R_{LIM},gv}\left(\bar{t}',0\right)d\bar{t}'}\Bigg| i = 1, NC$$

(2.1.47)

This is often referred to as product yield. It then holds:

$$\Omega_i = \sum_{k=1}^{NOM} \omega_{i,k} \tag{2.1.48}$$

Desired Product Recovery Fraction

Finally, we define the fraction of product generated during a given OM over the total product generated over the duration of all OMs as the Product Recovery fraction, defined as:

$$R_{i,k} \triangleq \frac{\omega_{i,k}}{\Omega_i} \quad \forall k = 1, NOM \quad \forall i = 1, ..., NC \tag{2.1.49}$$

The system of non-linear first-order partial differential equations described by Equations (2.1.41), (2.1.42), and (2.1.43) are used to simulate all three OMs of the MSR PPSO, and is solved using a direct finite element solver with implicit multistep free backward differentiation (BDF) with total time discretization consisting of $1x10^6$ time steps for each simulation. A fractional initial step for backward Euler consistent initialization was used, and linear first-order Lagrange shape functions were used for space discretization and consistent stabilization based on full calculation of the residual was employed. Because of the changing boundary conditions, a minimum non-linear damping factor of $1x10^{-9}$ was used during the Newton–Raphson iteration. The above solution strategy was coded and implemented using the COMSOL Multiphysics software platform. The MSR concept is next illustrated for the SMR process. We demonstrate, through parametric analysis, the impact of the previously identified dimensionless parameters D_a, Θ on the performance of an SMR-MSR process operating under PPSO.

2.2.2 Case Study

SMR is carried out through three reversible reactions $RX1$, $RX2$, and $RX3$, with enthalpies of formation and kinetic rates as shown below:

$$CH_4 + H_2O \leftrightarrow CO + 3H_2 \quad \Delta H_1^{\circ} : 206.1 \, {}^{kJ}\!/_{mol} \qquad (RX1)$$

$$CO + H_2O \leftrightarrow CO_2 + H_2 \quad \Delta H_2^{\circ} : -41.15 \, {}^{kJ}\!/_{mol} \qquad (RX2)$$

$$CH_4 + 2H_2O \leftrightarrow CO_2 + 4H_2 \quad \Delta H_3^{\circ} : 164.9 \, {}^{kJ}\!/_{mol} \qquad (RX3)$$

$$\{R_1, R_2, R_3\} = \left\{ \begin{array}{l} \dfrac{\dfrac{k_1}{\left(P_{H_2,gv}\right)^{2.5}}\left(P_{CH_4,gv}P_{H_2O,gv} - \dfrac{\left(P_{H_2,gv}\right)^3 P_{CO,gv}}{K_1}\right)}{\left(\mathrm{DEN}\right)^2}, \dfrac{\dfrac{k_2}{P_{H_2,gv}}\left(P_{CO,gv}P_{H_2O,gv} - \dfrac{P_{H_2,gv}P_{CO_2,gv}}{K_2}\right)}{\left(\mathrm{DEN}\right)^2} \\ , \dfrac{\dfrac{k_3}{\left(P_{H_2,gv}\right)^{3.5}}\left(P_{CH_4,gv}\left(P_{H_2O,gv}\right)^2 - \dfrac{\left(P_{H_2,gv}\right)^4 P_{CO,gv}}{K_3}\right)}{\left(\mathrm{DEN}\right)^2} \end{array} \right\}$$

(2.1.50)

With

$$\mathrm{DEN} = 1 + K_{CO}P_{CO,gv} + K_{H_2}P_{H_2,gv} + K_{CH_4}P_{CH_4,gv} + K_{H_2O}\frac{P_{H_2O,gv}}{P_{H_2,gv}} \qquad (2.1.51)$$

The kinetic and equilibrium constant values in the above expressions are listed in Tables 2-10 and 2-11.

Table 2-10: Rate coefficients and adsorption constants for use in Arrhenius or Van't Hoff Equations

Rate Coefficient or Adsorption Constant	**Pre-Exponential Factor**	**Unit Pre-Exponential Factor**	**Activation Energy or Adsorption Enthalpy** (kJ)
k_1	4.225×10^{15}	$\left(kmol\, bar^{0.5}\right)/\left(kg_{cat}\, hr\right)$	240.1
k_2	1.955×10^{6}	$\left(kmol\right)/\left(kg_{cat}\, hr\, bar\right)$	67.13

k_3	$1.020\text{x}10^{15}$	$\left(kmol\,bar^{0.5}\right)/\left(kg_{cat}\,hr\right)$	243.9
K_{CO}	$8.23\text{x}10^{-5}$	bar^{-1}	–70.65
K_{H_2}	$6.12\text{x}10^{-9}$	bar^{-1}	–82.90
K_{CH_4}	$6.65\text{x}10^{-4}$	bar^{-1}	–38.28
K_{H_2O}	$1.77\text{x}10^{-4}$	dimensionless	88.68

Table 2-11: SMR reaction equilibrium constants

Equilibrium Constant	**Units**
$K_1 = \exp\left(-26{,}830/T + 30.114\right)$	bar^2
$K_2 = \exp\left(4{,}400/T - 40.63\right)$	dimensionless
$K_3 = K_1 \cdot K_2$	bar^2

The above kinetic rates can be brought in dimensionless form, as suggested in [17,32]. In the definition of the Damkohler number, the reference reaction generation rate r^* is selected as the reaction rate for $RX1$ evaluated at the reactor entrance conditions during OM1:

$$r^* \triangleq r_1\left(\left\{\frac{\left(P_{i,gv}(0,0)\right)}{RT}\right\}_{i=1}^{NC}, T\right) = \frac{k_1\left(P_{CH_4,gv}(0,0)P_{H_2O,gv}(0,0) - \frac{\left(P_{H_2,gv}(0,0)\right)^3 P_{CO,gv}(0,0)}{K_1}\right)}{\left(P_{H_2,gv}(0,0)\right)^{2.5}} \Big/ \left(\begin{array}{l} 1 + K_{CO}P_{CO,gv}(0,0) + K_{H_2}P_{H_2,gv}(0,0) + \\ + K_{CH_4}P_{CH_4,gv}(0,0) + K_{H_2O}\dfrac{P_{H_2O,gv}(0,0)}{P_{H_2,gv}(0,0)} \end{array}\right)^2 \tag{2.1.52}$$

The resulting dimensionless reaction rates become:

$$\bar{R}_1 = \frac{\dfrac{k_1}{\left(P^*\right)^{0.5}\left(\bar{P}_{H_2,gv}\right)^{2.5}}\left(\bar{P}_{CH_4,gv}\bar{P}_{H_2O,gv} - \dfrac{\left(P^*\right)^2\left(\bar{P}_{H_2,gv}\right)^3\bar{P}_{CO,gv}}{K_1}\right)}{\left(1+K_{CO}P^*\bar{P}_{CO,gv}+K_{H_2}P^*\bar{P}_{H_2,gv}+K_{CH_4}P^*\bar{P}_{CH_4,gv}+\dfrac{K_{H_2O}\bar{P}_{H_2O,gv}}{\bar{P}_{H_2,gv}}\right)^2} \quad (2.1.53)$$

$$\bar{R}_2 = \frac{\dfrac{k_2P^*}{\bar{P}^g_{H_2,gv}}\left(\bar{P}_{CO,gv}\bar{P}_{H_2O,gv} - \dfrac{\bar{P}_{H_2,gv}\bar{P}_{CO_2,gv}}{K_2}\right)}{\left(1+K_{CO}P^*\bar{P}_{CO,gv}+K_{H_2}P^*\bar{P}_{H_2,gv}+K_{CH_4}P^*\bar{P}_{CH_4,gv}+\dfrac{K_{H_2O}\bar{P}_{H_2O,gv}}{\bar{P}_{H_2,gv}}\right)^2} \quad (2.1.54)$$

$$\bar{R}_3 = \frac{\dfrac{k_3}{\left(P^*\right)^{0.5}\left(\bar{P}_{H_2,gv}\right)^{3.5}}\left(\bar{P}_{CH_4,gv}\left(\bar{P}_{H_2O,gv}\right)^2 - \dfrac{\left(P^*\right)^2\left(\bar{P}_{H_2,gv}\right)^4\bar{P}_{CO,gv}}{K_3}\right)}{\left(1+K_{CO}P^*\bar{P}_{CO,gv}+K_{H_2}P^*\bar{P}_{H_2,gv}+K_{CH_4}P^*\bar{P}_{CH_4,gv}+\dfrac{K_{H_2O}\bar{P}_{H_2O,gv}}{\bar{P}_{H_2,gv}}\right)^2} \quad (2.1.55)$$

The PPSO of the SMR-MSR is carried out in three distinct operating modes: OM 1 (Loading-Reaction/Storage), OM 2 (Decarbonization/Maintenance), and OM 3 (Unloading-Production/Emptying) each of which is characterized by different processes occurring in the (v) and (s) domains. These three OMs have a time duration designated as τ_1, τ_2, and τ_3, as described next and shown in the Figure 3-18 below.

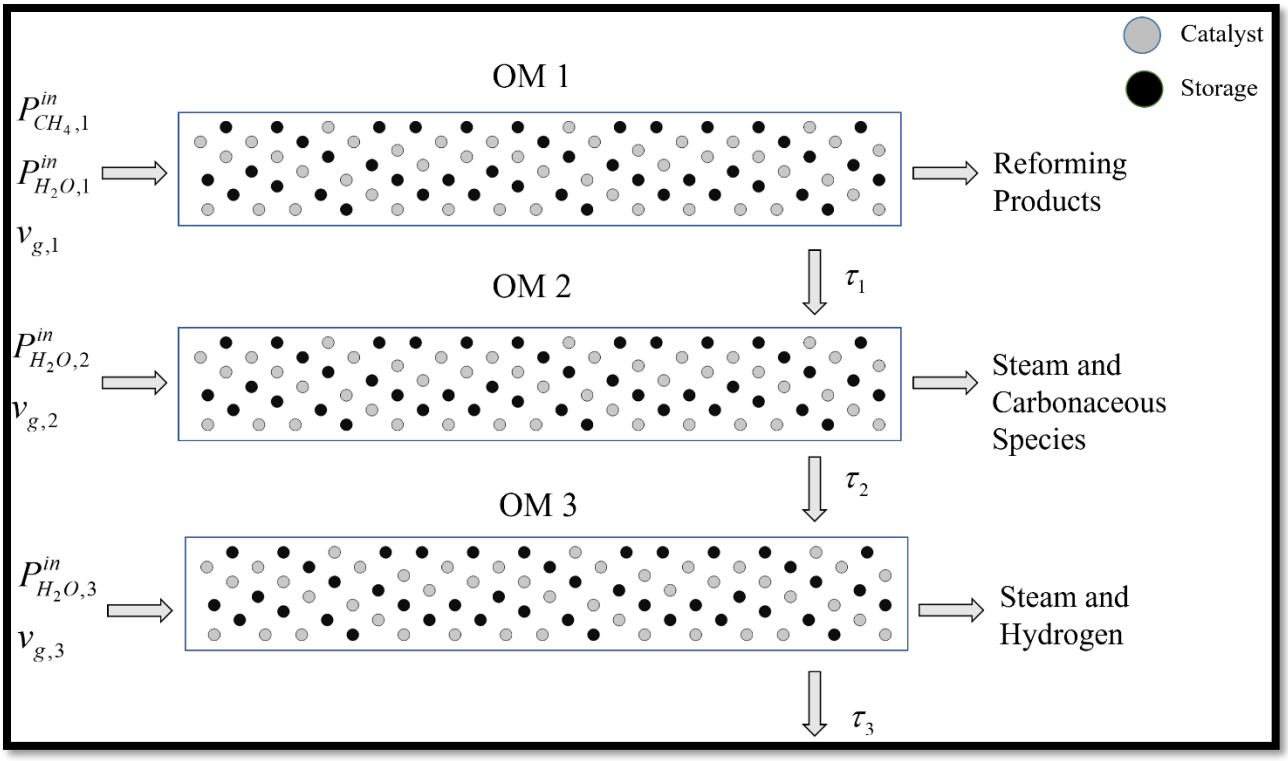

Figure 2-18: Proposed SMR-MSR process and its operating modes.

OM 1: MSR Loading-Reaction/Storage Phase

At the beginning of this OM, phase (g) in domain (v) is largely composed of steam and minute amounts of hydrogen, phase (g) in domain (s) only contains hydrogen at a pressure slightly above the partial pressure of hydrogen in (v), and a mixture of methane and steam at a constant flowrate is fed into the MSR. During this OM, the hydrogen that is produced from the SMR reactions taking place begins to permeate into (s) as its partial pressure in (v) increases above the total pressure of (s). Under isobaric conditions in (v), the outlet flowrate varies, as described in Equation (2.4.43). The duration τ_1 of OM 1 is chosen so that a desirable level of limiting reactant conversion is attained. Reactant conversion, as defined by Equation (2.1.45), is

defined over all three OMs. Typically, however, the limiting reactant is fed to the MSR only during OM 1, whereas any unreacted limiting reactant exits the MSR during OM 1 and OM 2. As discussed below, the duration of OM 2 is fixed and chosen to be equal to the reactor's OM 2 residence time. Thus, the duration τ_1 of OM 1 is the only degree of freedom that can be chosen so that the amount of unreacted limiting reactant that exits the MSR over $\tau_1 + \tau_2$ (i.e., over the duration of OM 1 and OM 2) is acceptably low, compared to the amount of limiting reactant fed to the MSR during OM 1, so that a desirable level of limiting reactant conversion can be attained.

OM 2: MSR Decarbonization/Maintenance Phase

OM 2 begins at the final conditions of OM 1, and the reactor is then fed pure steam at a constant flowrate. If the reactor is operating under plug flow conditions with no diffusional effects, as is the case here, a sharp steam front is formed that propagates through the reactor and reaches the reactor outlet in time equal to the reactor's OM 2 residence time. In the reactor section ahead of the steam front, the SMR reaction continues to occur in the void domain, and hydrogen is transported from the void to the storage domain. Behind the steam front hydrogen is transported from the storage to the void domain. Thus, under plug flow conditions, the duration τ_2 of OM 2 is chosen to be equal to the reactor's OM 2 residence time, because at that time complete reactor decarbonization has been attained. (If dispersion was to be present in the reactor, the steam front would not be as sharp. In that case, the duration τ_2 of OM 2 may need to be chosen to be greater than the reactor's OM 2 residence time for the desired level of reactor decarbonization to take place).

OM3 3: MSR Unloading-Production/Emptying Phase

Similarly, OM 3 begins at the final conditions of OM 2, and the reactor is again fed pure steam at a constant flowrate. This action empties the contents of (s) back into (v), generating a mixture of readily separable, high-pressure hydrogen and steam as the SMR-MSR product. The duration τ_3 of OM 3 is chosen so that the hydrogen in the domains (v), (s) is below a desirable low level.

To compare the performance of the SMR-MSR under PPSO with that of a traditional SMR-SSR, we utilized the process performance metrics defined by Equations (2.1.45)–(2.1.49) for the SMR case study. To this end, identifying methane as our limiting reactant, Equation (2.1.45) becomes:

$$X_{CH_4} = \frac{\left[\int_0^{\sum_{k=1}^{NOM}\bar{\tau}_k} \bar{F}_{CH_4,gv}(\bar{t}',0)d\bar{t}' - \int_0^{\sum_{k=1}^{NOM}\bar{\tau}_k} \bar{F}_{CH_4,gv}(\bar{t}',1)d\bar{t}'\right]}{\int_0^{\sum_{k=1}^{NOM}\bar{\tau}_k} \bar{F}_{CH_4,gv}(\bar{t}',0)d\bar{t}'} \tag{2.1.56}$$

Similarly, Equations (2.1.46)–(2.1.49) can be expressed for all products (carbon monoxide, carbon dioxide, and hydrogen), and are listed below for hydrogen.

$$\omega_{H_2,1} \triangleq \frac{\left[\int_0^{\bar{\tau}_1} \bar{F}_{H_2,gv}(\bar{t}',1)d\bar{t}' - \int_0^{\bar{\tau}_1} \bar{F}_{H_2,gv}(\bar{t}',0)d\bar{t}'\right]}{\int_0^{\sum_{k=1}^{NOM}\bar{\tau}_k} \bar{F}_{CH_4,gv}(\bar{t}',0)d\bar{t}'} \tag{2.1.57}$$

$$\Omega_{H_2} = \frac{\left[\int_0^{\sum_{k=1}^{NOM}\bar{\tau}_k} \bar{F}_{H_2,gv}(\bar{t}',1)d\bar{t}' - \int_0^{\sum_{k=1}^{NOM}\bar{\tau}_k} \bar{F}_{H_2,gv}(\bar{t}',0)d\bar{t}'\right]}{\int_0^{\sum_{k=1}^{NOM}\bar{\tau}_k} \bar{F}_{CH_4,gv}(\bar{t}',0)d\bar{t}'} \tag{2.1.58}$$

$$R_{H_2,3} = \frac{\omega_{H_2,3}}{\Omega_{H_2}} = \frac{\left[\int_{\bar{\tau}_1+\bar{\tau}_2}^{\bar{\tau}_1+\bar{\tau}_2+\bar{\tau}_3} \bar{F}_{H_2,gv}(\bar{t}',1)d\bar{t}' - \int_{\bar{\tau}_1+\bar{\tau}_2}^{\bar{\tau}_1+\bar{\tau}_2+\bar{\tau}_3} \bar{F}_{H_2,gv}(\bar{t}',0)d\bar{t}'\right]}{\left[\int_0^{\bar{\tau}_1+\bar{\tau}_2+\bar{\tau}_3} \bar{F}_{H_2,gv}(\bar{t}',1)d\bar{t}' - \int_0^{\bar{\tau}_1+\bar{\tau}_2+\bar{\tau}_3} \bar{F}_{H_2,gv}(\bar{t}',0)d\bar{t}'\right]} \tag{2.1.59}$$

Equation (2.1.57) captures the H_2 molar production ratio in OM 1 over the total amount of methane fed. Equation (2.1.58) describes the hydrogen yield over all three OMs, i.e., the total moles of hydrogen produced divided by the moles of methane fed to the reactor. Lastly, Equation (2.1.59) is used to calculate the hydrogen recovery ratio during the 3rd OM, which is of importance because it quantifies how much hydrogen is produced in readily purifiable form.

To determine the time duration $\bar{\tau}_1$, $\bar{\tau}_2$, and $\bar{\tau}_3$ for the three OMs, a criterion for terminating each OM must be selected. The reactor contents at the beginning of OM 1 consist largely of steam, while the reactor feed at that time switches to an appropriately chosen methane steam mixture, which in turn leads to a methane front propagating through the reactor. Thus, at each fixed reactor location, methane partial pressure initially increases, reaches a maximum value, and then decreases as the reactor feed is switched to steam at the beginning of OM2. The maximum methane partial pressure attained becomes ever lower at downstream reactor length locations. With this behavior in mind, our selection $\bar{\tau}_1$ for the duration of OM 1 will be related to the conversion (utilization) of the raw material (methane).

The duration $\bar{\tau}_2$ of OM 2 is selected to be equal to the OM 2 residence time, ensuring that the dimensionless pressure of all carbon-containing gas phase components in the domain will be zero, as will be the level of carbon impurities in the hydrogen product generated during OM 3. Similarly, the duration of OM 3 is selected as the time $\bar{\tau}_3$ at which the dimensionless partial pressure of hydrogen in domain (v) at the reactor exit falls below a set value, e.g., $\bar{P}_{H_2,gv}\left(\bar{\tau}_1 + \bar{\tau}_2 + \bar{\tau}_3, 1\right) \leq 0.01$, which ensures that most of the hydrogen in both domains (v) and (s) has been removed and thus the reactor is largely filled with unreacting steam.

Simulation of the dimensionless set of Equations (2.1.41)-(2.1.43) of the MSR model requires that a number of model parameters first be specified. It is considered that the reactor pressure and temperature are $P^* = 25 bar$ and $T = 900K$, respectively, and the MSR feed at the beginning of OM 1 contains steam and methane at a molar ratio of 3, and minute amounts of all other species. Knowledge of these parameters enables the computation of the reference reaction generation rate r^* using Equation (2.1.52), and expression of the dimensionless reaction rates $\bar{R}_1, \bar{R}_2, \bar{R}_3$ in terms of the dimensionless species pressures, using Equations (2.1.53)–(2.1.55). Selection of the storage domain, catalyst domain, and gas phase in storage domain volume fractions as $\varepsilon_s = 0.5,\ \varepsilon_c = 0.35,\ \varepsilon_{gs} = 0.495$, respectively, of the effectiveness factor as $\eta = 0.5$, and of the gas permeance ratios for all species (the first species being hydrogen) as $\beta_j / \beta_1 = \begin{Bmatrix} 0 & if\ j \neq 1 \\ 1 & if\ j = 1 \end{Bmatrix}$, enables the simulation of dimensionless set of Equations (2.1.41)-(2.1.43) of the MSR model as long as the values of the parameters $D_a, \Theta, \bar{\tau}_1, \bar{\tau}_2, \bar{\tau}_3$ are known.

In this work, assessment of SMR-MSR performance was performed by carrying out sixteen combinations (trials) of the above five parameters, as listed in Table 2-12 below. The values for D_a and Θ were chosen by selecting a range of reasonable values for the parameters shown in Equations (2.1.34)-(2.1.36). Fixing the operating pressure $P^* = 25(bar)$, temperature $T^* = 900(K)$, catalyst density $\rho_c = 2355.2\left(kg/m^3\right)$ [14], and reference reaction rate $r^* \triangleq r_1\left(\left\{\frac{\left(P_{i,gv}(0,0)\right)}{RT}\right\}_{i=1}^{NC}, T\right) = 13.606\left(mol/kg \cdot s\right)$, leaves residence time $t^*(s)$ as the only free parameter for calculation of D_a. Because of the rapid rate at which the SMR reactions attain equilibrium, the range of considered residence times was $0.01 \le t^*(s) \le 0.5$, so that the concentration profiles along the reactor do not immediately reach equilibrium. The resulting D_a range is $1 \le D_a \le 6$. Given the above range of residence times $0.01 \le t^*(s) \le 0.5$, and pressure $P^* = 25(bar)$, temperature $T^* = 900(K)$ values, evaluation of a range for Θ requires range information for the species membrane permeance $\beta_i\left(\frac{mol\,i}{Pa \cdot \left(m^2\,void - storage\,interface\right) \cdot s}\right)$ and the storage-void interfacial area per unit volume of reactor $\alpha_{s,v}\left(\frac{m^2\ storage - void\ interface}{m^3\ system\,r}\right)$.

The β_1 range is $1.05 \cdot 10^{-8} \le \beta_1 \le 1.21 \cdot 10^{-6}$ for hydrogen [23,33,], and the $\alpha_{s,v}$ range is selected so that the resulting Θ range is $1 \le \Theta \le 50$.

Table 2-12: MSR design parameters and OM dimensionless duration times

Trial	**Da**	**Θ**	$\bar{\tau}_1$	$\bar{\tau}_2$	$\bar{\tau}_3$
1	1	1	0.717543	1.00	0.674081
2	1	10	0.755321	1.00	2.261037
3	1	30	0.752953	1.00	2.049624
4	1	40	0.762492	1.00	1.941365
5	1	50	0.742631	1.00	1.814203
6	2	1	0.545116	1.00	0.367633
7	2	10	0.565994	1.00	2.509012
8	2	30	0.587789	1.00	1.998005
9	2	40	0.588387	1.00	1.8797
10	2	50	0.597422	1.00	1.754175
11	4	1	0.405848	1.00	0.24924
12	4	10	0.428648	1.00	2.455872
13	4	50	0.466553	1.00	1.713176
14	6	1	0.363228	1.00	0.222919
15	6	10	0.389041	1.00	2.457342
16	6	50	0.388379	1.00	1.76623

Each trial was simulated in COMSOL for three cycles of operation in order to ensure that dynamic operation had reached its long-term periodic behavior. COMSOL implementation of the alternating feed compositions for each OM was carried out by approximating for each OM an OM-specific Heaviside function h_k with an OM-specific Verhulst function, W_k, as shown in Equation (2.1.60) below:

$$h_k\left(\bar{t}\right)=\left\{\begin{matrix}0, & \text{if } \left(\bar{t}-\sum_{k'=0}^{k-1}\bar{\tau}_{k'}<0\right)\\ [0,1], & \text{if } \left(\bar{t}-\sum_{k'=0}^{k-1}\bar{\tau}_{k'}=0\right)\\ 1, & \text{if } \left(\bar{t}-\sum_{k'=0}^{k-1}\bar{\tau}_{k'}>0\right)\end{matrix}\right\}\approx W_k\left(\bar{t}\right)=-\frac{1}{1+\exp\left(-a\cdot\left(\bar{t}-\sum_{k'=0}^{k-1}\bar{\tau}_{k'}\right)+a\cdot c\right)},\ k=1,NOM$$

(2.1.60)

Figure 2 below illustrates the dynamic behavior of the methane inlet partial pressure at the reactor inlet as a function of dimensionless time, considering $\bar{\tau}_1=\bar{\tau}_2=\bar{\tau}_3=5,\ a=1$ and $c=8.5$.

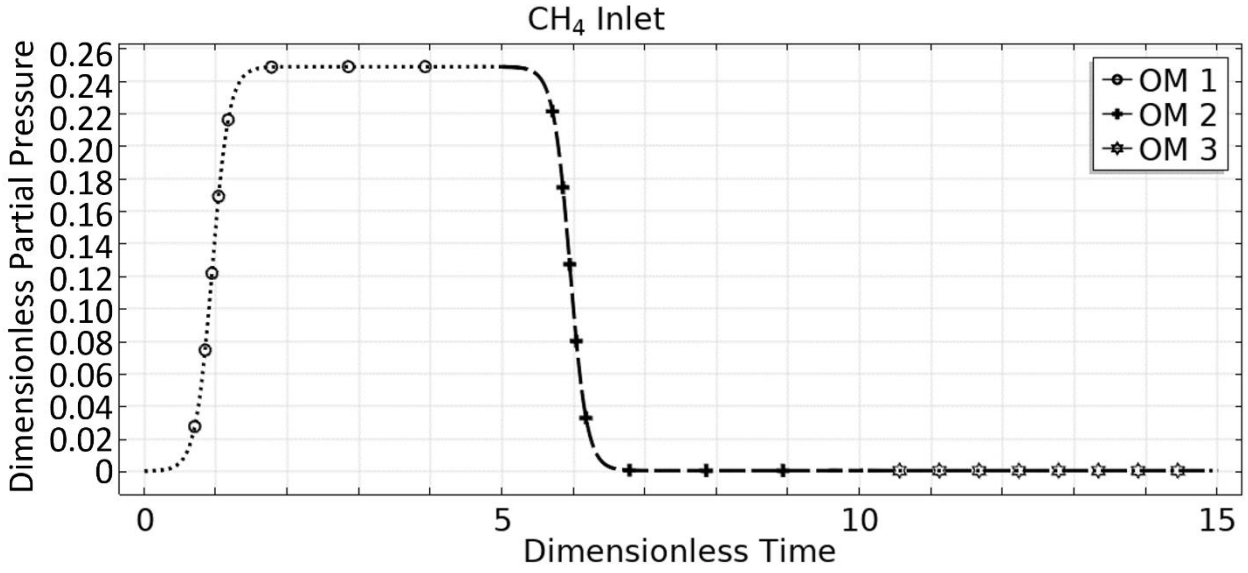

Figure 2-19: Methane dimensionless partial pressure at reactor inlet for $\bar{\tau}_1=\bar{\tau}_2=\bar{\tau}_3=5,\ a=1,\ c=8.5$

The resulting time evolution of SMR-MSR state variables for the seventh trial ($D_a=2,\Theta=10$) is displayed in the figures below. In Figure 3-20 the time evolution of all species' (except, of course, for the hydrogen in the storage domain) dimensionless partial pressures at the reactor inlet is shown, over three operating cycles. It is assumed that the conditions at the inlet of the reactor at the beginning of OM1 is the same as its condition at the end of OM3. During OM1, the reactor's feed consists mainly of steam and methane, at a 3:1

steam/methane ratio, and trace amounts of carbon monoxide and carbon dioxide. During OM2 and OM3 the reactor's feed consists only of steam. Similarly, Figure 2-21 shows the time evolution of species dimensionless partial pressures at the outlet of the reactor through the same three cycles of operation. Because the reactor's condition at the beginning of OM1 is the same as its condition at the end of OM3, at early operational times the reactor outlet consists mainly of steam. As the reaction proceeds, a mixture of methane, carbon dioxide, and carbon monoxide begins to exit the reactor. The hydrogen in the void domain continues to rise until it reaches its peak, which coincides with the end of OM2.

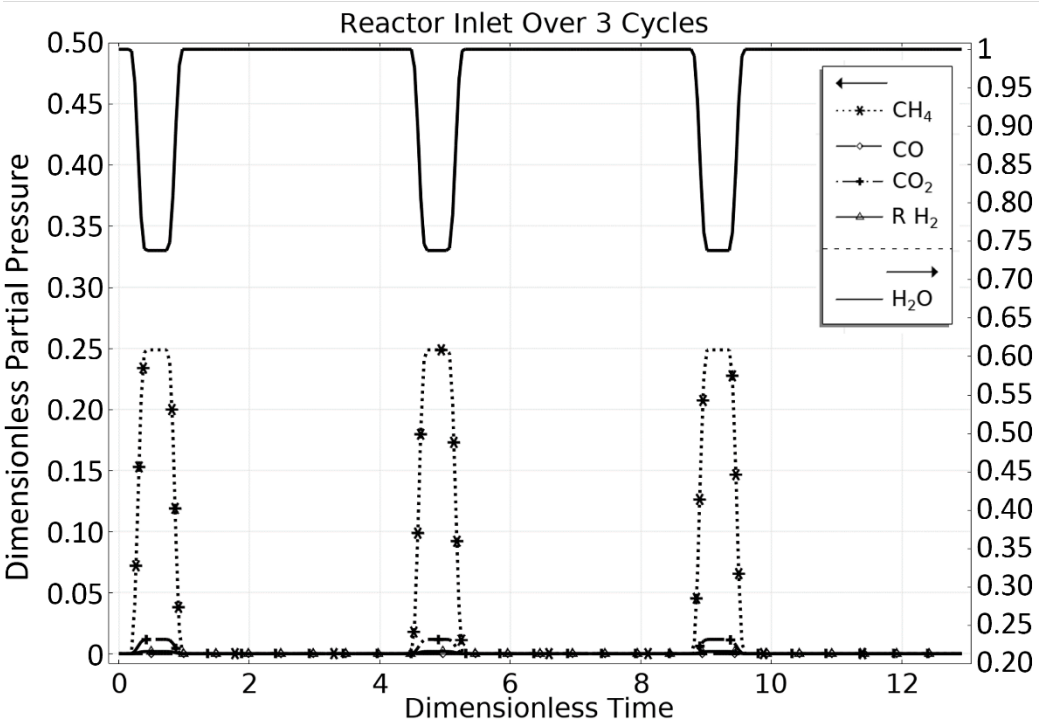

Figure 2-20: Dimensionless time evolution of species' dimensionless partial pressure at reactor inlet over 3 cycles of operation for Da = 2, Θ = 10.

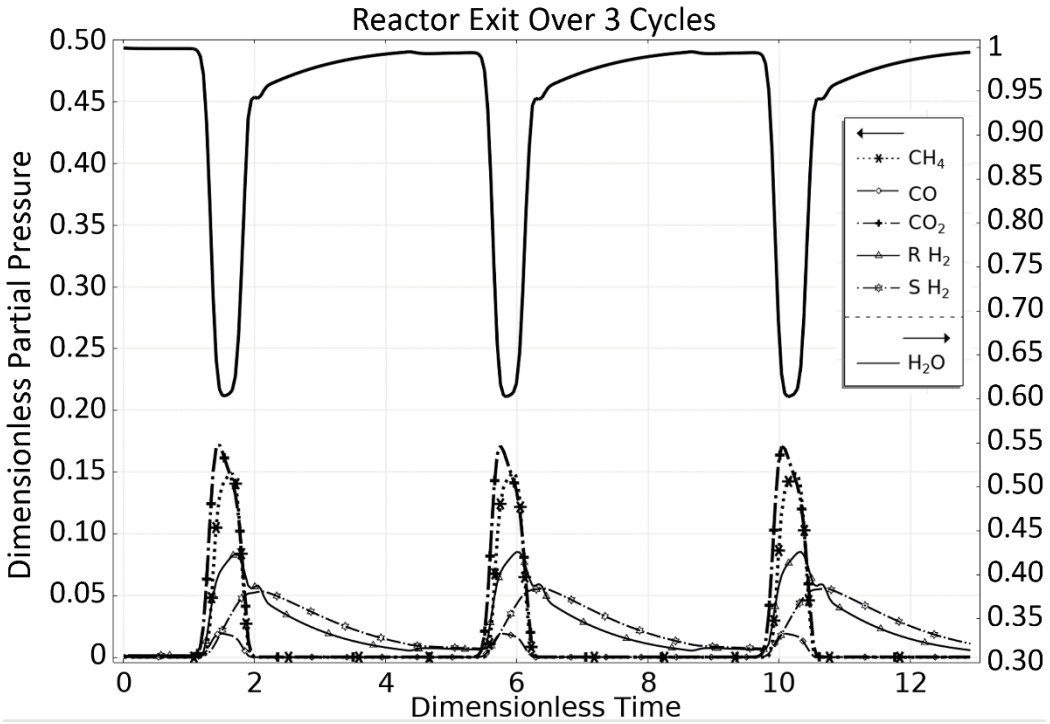

Figure 2-21: Dimensionless time evolution of species' dimensionless partial pressure at reactor outlet over 3 cycles of operation for Da = 2, Θ = 10.

Figure 3-22 shows the time evolution of the dimensionless partial pressure of hydrogen in the void and storage (represented by R H_2 and S H_2) domains, during the last cycle of operation, at four different reactor locations (25%, 50%, 75%, and 100% of the total reactor length), and Figure 2-23 shows the dimensionless partial pressures of methane and carbon dioxide in the void domain, during the last cycle of operation, at the same four reactor locations. In Figure 2-22 it can be seen that at the 25% length location the hydrogen concentration in the void domain is initially practically zero; then, as methane reacts to generate hydrogen, it increases, first rapidly and then less so as it begins to transport into the storage domain; finally, the concentration decreases as steam is fed into the reactor. The same behavior is observed at larger lengths.

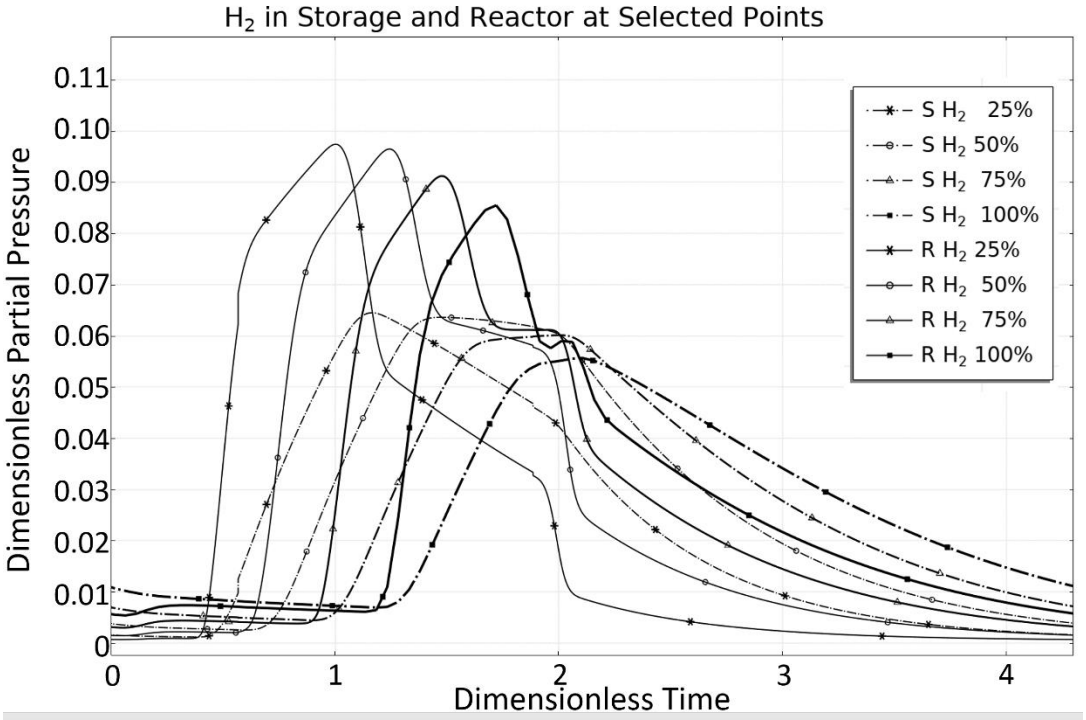

Figure 2-22: Dimensionless time evolution of H2 dimensionless partial pressure in void and storage domains at four reactor lengths for the last cycle of Da = 2, Θ = 10.

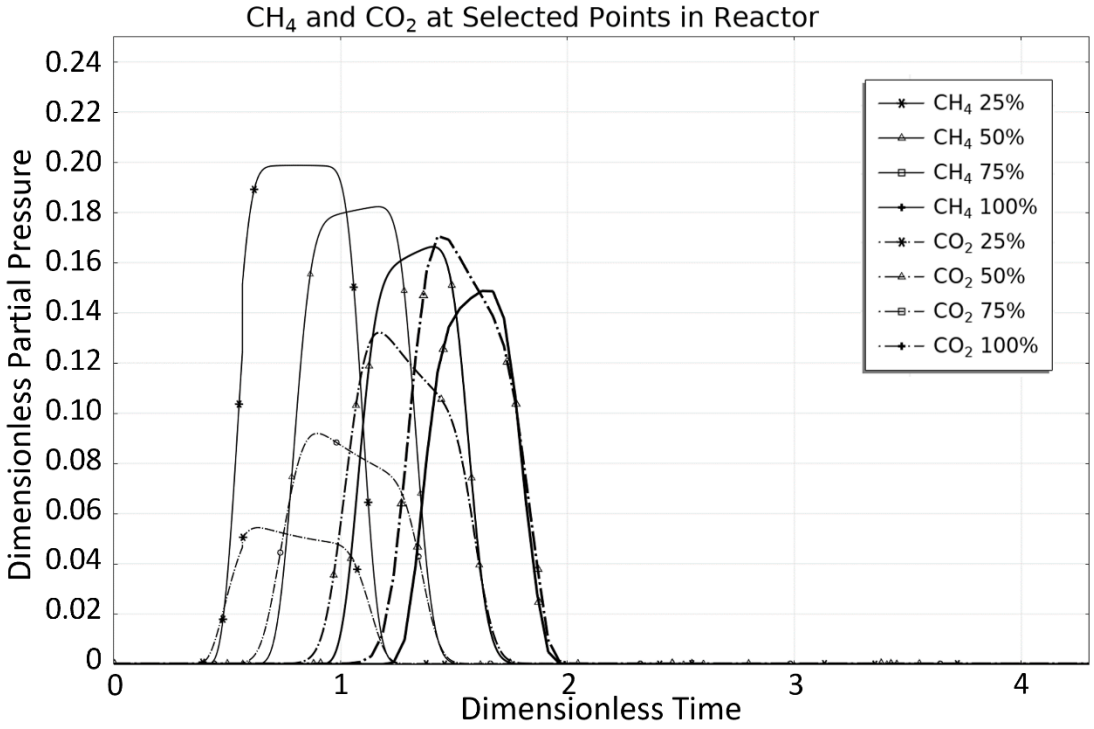

Figure 2-23: Dimensionless time evolution of CH4 and CO2 dimensionless partial pressures in void domain at four reactor lengths for the last cycle of Da = 2, Θ = 10.

In Figure 2-23, at the 25% reactor length location during the last cycle of operation, the methane and carbon dioxide concentrations are shown to first increase, reach a maximum, and then decrease, in correspondence with the composition changes at the inlet of the reactor shown in Figure 2-23. The methane (carbon dioxide) maximum occurs at the latter (earlier) part of a plateau-like region in time. At points further down the reactor (50%, 75%, and 100% of the reactor length), the methane (carbon dioxide) pulse exhibits a progressively lower (higher) maximum, which is indicative of its role as a reactant (product) in the reaction that takes place. The magnitude of the methane pulse remains larger than that of the carbon dioxide pulse until it reaches the end of the reactor.

Figures 2-24 thru 2-26 show the dimensionless partial pressure profiles for all species along the length of the reactor at the end of OM1, OM2, and OM3, respectively, for the 7th trial $D_a = 2, \Theta = 10$. In these simulations we selected the end of OM1 to be when $\bar{P}_{CH_4,gv}\Big|_{\bar{z}=0.3} = 0.05$ occurs for an operating time for the first OM of $\bar{\tau}_1 = 0.566$. From Figure 3-24 one observes that the contents of the reactor void domain up to point $\left(z^* = 0.3\right)$ contain a mixture of reforming products, whereas at larger reactor lengths there exists only water, validating that the reactor is operating in plug flow and that no species diffusion has occurred down the reactor. From the reactor inlet $\left(z^* = 0\right)$ to $\left(z^* = 0.3\right)$, the dimensionless partial pressure of the hydrogen in the storage shows a marked difference from the dimensionless partial pressure of hydrogen in the reactor void, which highlights the time-dependent nature of the process. As seen later in the analysis of the influence of the parameter Θ, reducing this difference during early operational times correlates to higher conversion and better overall reactor performance. Figures 2-25 and 2-26 show the corresponding profiles at the end of OM2 with $\bar{\tau}_2 = 1.00$, and at the end of OM3

with $\overline{\tau}_3 = 2.51$, respectively. From Figure 2-25 one sees that at the end of OM2 the reactor void contains a mixture of steam and hydrogen only, and that hydrogen has been successfully transferred to and stored in the storage domain. From Figure 2-26 one sees that, at the end of a cycle of operation, the reactor has returned to its initial state of operation, with the reactor void being filled with only steam and the contents of the storage medium having been emptied.

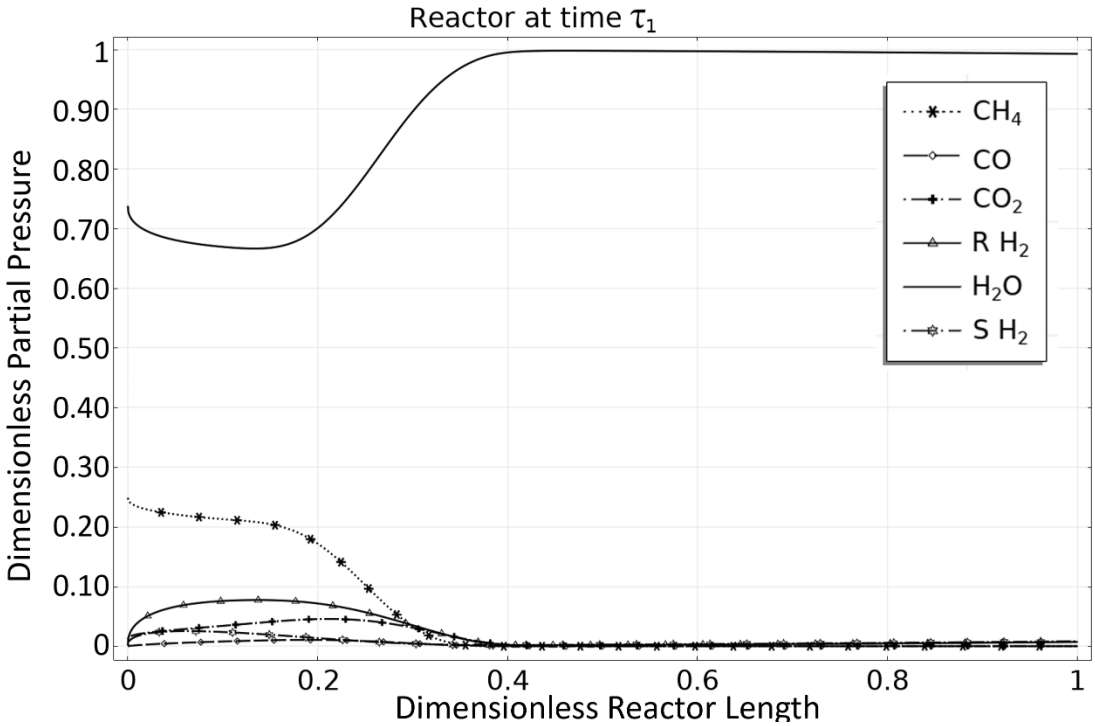

Figure 2-24: Species' dimensionless partial pressure axial length profile during cycle 3 at the end of OM1 for Da = 2, Θ = 10.

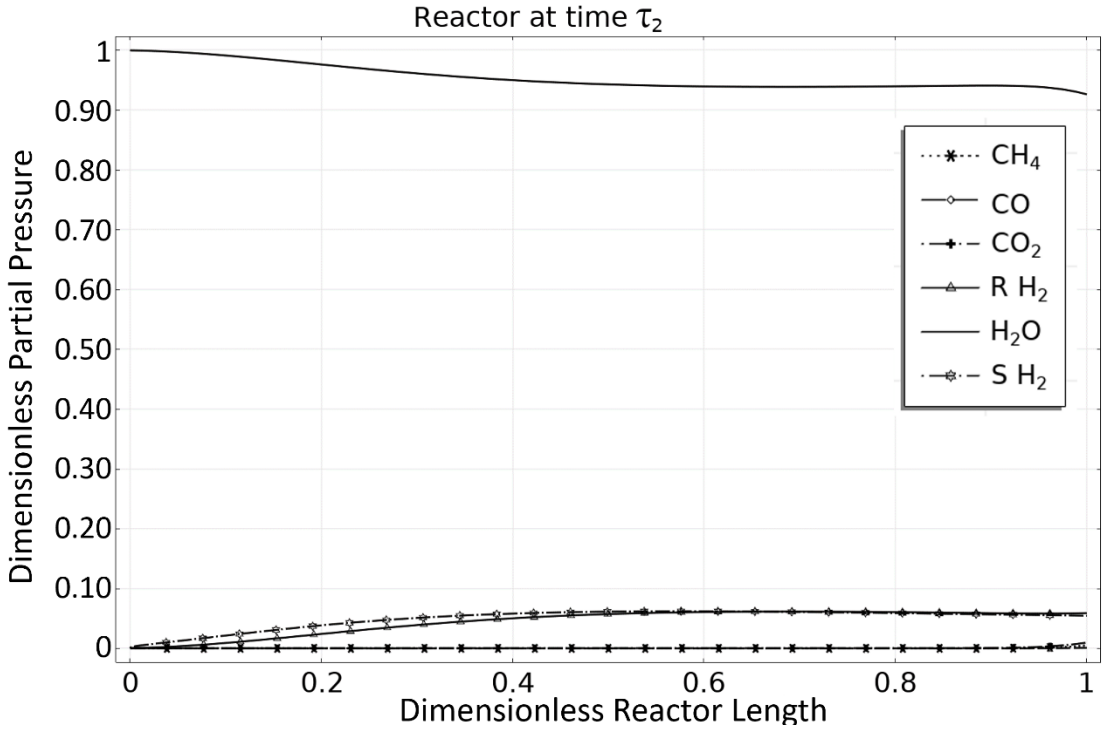

Figure 2-25: Species' dimensionless partial pressure axial length profile during cycle 3 at the end of OM2 for Da = 2, Θ = 10.

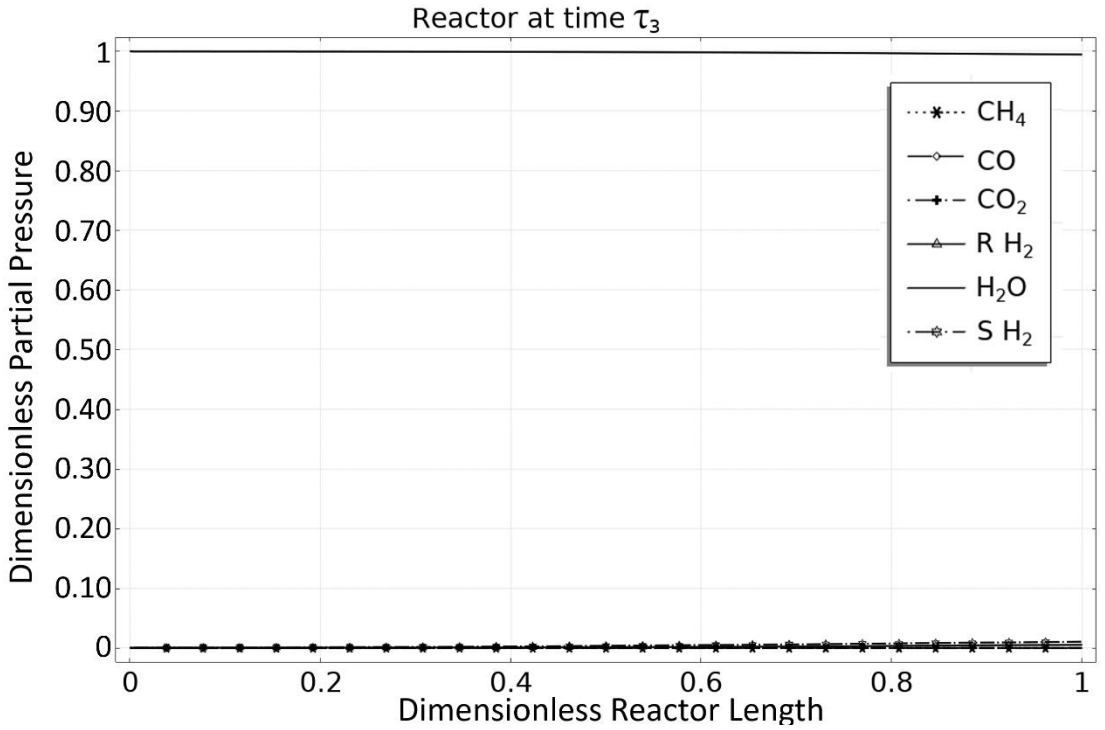

Figure 2-26: Species' dimensionless partial pressure axial length profile during cycle 3 at the end of OM3 for Da = 2, Θ = 10.

With the operating times for each OM set, it is now possible to calculate the metrics as described by Equations (2.1.56)–(2.1.59). These are shown for the different cases studied in Table 2-13. The SMR-MSR shows higher overall conversion than the traditional SMR-SSR for all cases studied. In addition, the SMR-MSR enables the in situ separation of the hydrogen product, which is a distinct advantage over the traditional SMR-SSR that requires an additional downstream separation step. For the design parameters employed in trial 7 (Da = 2, $\Theta = 10$) for which the SMR-MSR behavior has been described in detail above, the SMR-MSR exhibits a 116% increase in methane conversion over the SMR-SSR from 0.2564 to 0.5553. Additionally, the hydrogen recovery is 83%, indicating that a significant portion of the total generated hydrogen exits the reactor during OM3 in the form of ultra-high purity (UHP) hydrogen. For the case studies conducted here (see Table 2-13), a maximum increase in methane conversion of 235% was observed, indicating the significant benefit that can be gained by appropriately selecting design parameters. The substantial increases in conversion are accompanied by simultaneous significant gains in hydrogen yield. The hydrogen recovery ratios reported in Table 4 are comparatively higher than those by similar membrane reactors operating at steady state [27]. These high SMR-MSR metric values suggest that the SMR-MSR outperforms the SMR-SSR, and that the SMR-MSR operating at the selected temperature $T = 900\,K$ (which is lower than the temperatures traditionally used in SMR [25]), may be economically viable and realizable [28].

Table 2-13: Performance metric comparison for SMR-MSR and SMR-SSR for the sixteen considered trials.

Trial	**Da**	**Θ**	X_{CH_4} **MSR**	X_{CH_4} **SSR**	Y_{H_2} **MSR**	Y_{H_2} **SSR**	$R_{H_2,rec}$
1	1	1	0.268297	0.2205	0.925244	0.8505	0.133693
2	1	10	0.486804	0.2205	2.06218	0.8505	0.851397
3	1	30	0.51877	0.2205	2.172158	0.8505	0.874449
4	1	40	0.527766	0.2205	2.211969	0.8505	0.883636
5	1	50	0.557738	0.2205	2.317619	0.8505	0.895902
6	2	1	0.332334	0.2564	1.027561	0.9858	0.114506
7	2	10	0.555291	0.2564	2.311048	0.9858	0.828753
8	2	30	0.657883	0.2564	2.710915	0.9858	0.90206
9	2	40	0.683793	0.2564	2.797332	0.9858	0.917312
10	2	50	0.696967	0.2564	2.856135	0.9858	0.923089
11	4	1	0.406878	0. 2866	1.140335	1.102	0.122357
12	4	10	0.719437	0. 2866	2.918608	1.102	0.868964
13	4	50	0.900393	0. 2866	3.638564	1.102	0.958944
14	6	1	0.430822	0.2913	1.165753	1.131	0.122353
15	6	10	0.795136	0.2913	3.205293	1.131	0.884476
16	6	50	0.974497	0.2913	3.931581	1.131	0.972301

The effect of Θ (the inverse Peclet number) on reactor performance is also shown in Tables 2-12 (operational times) and 4 (performance metrics), with an increase in all metrics shown for increasing Θ. The cases with the lowest Θ value (Θ = 1) studied are characterized by minimal increases in methane conversion and hydrogen yield over their traditional reactor counterparts, and low recovery ratios, suggesting a lower limit threshold of Θ > 1 for desirable SMR-SSR performance. For a constant value of Da (and thus a constant value of the SMR-MSR dimensionless residence time), as Θ increases, the operating time $\bar{\tau}_1$ in OM1 can be increased, because reactor conversion then increases as Θ increases and it takes a longer time for the unreacted methane to reach the outlet of the reactor in substantial amounts. In contrast, operational times $\bar{\tau}_3$ in OM3 decrease upon increase in Θ for each fixed Da. These beneficial changes in OM duration times, coupled with the increase in the hydrogen recovery ratio as Θ increases (for fixed value of Da), suggest that Θ should be increased as much as possible in order to achieve desirable reactor performance.

Figures 2-27 thru 2-30 show corresponding results for the 13th trial (Da = 4 and Θ = 50). Figure 2-27 shows the time evolution of the dimensionless partial pressure for the various species at the outlet of the reactor through three cycles of operation. Figure 2-28 shows the time evolution of the dimensionless hydrogen partial pressure in the void and storage domains during the last cycle of operation at four locations in the reactor (25%, 50%, 75%, and 100% of the total reactor length). Figure 2-29 shows the time evolution of dimensionless partial pressures for methane and carbon dioxide in the void domain during the last cycle of operation at the same four reactor locations. Figure 2-30 shows the dimensionless partial pressure profiles for all species along the length of the reactor during cycle 3 at the end of OM1.

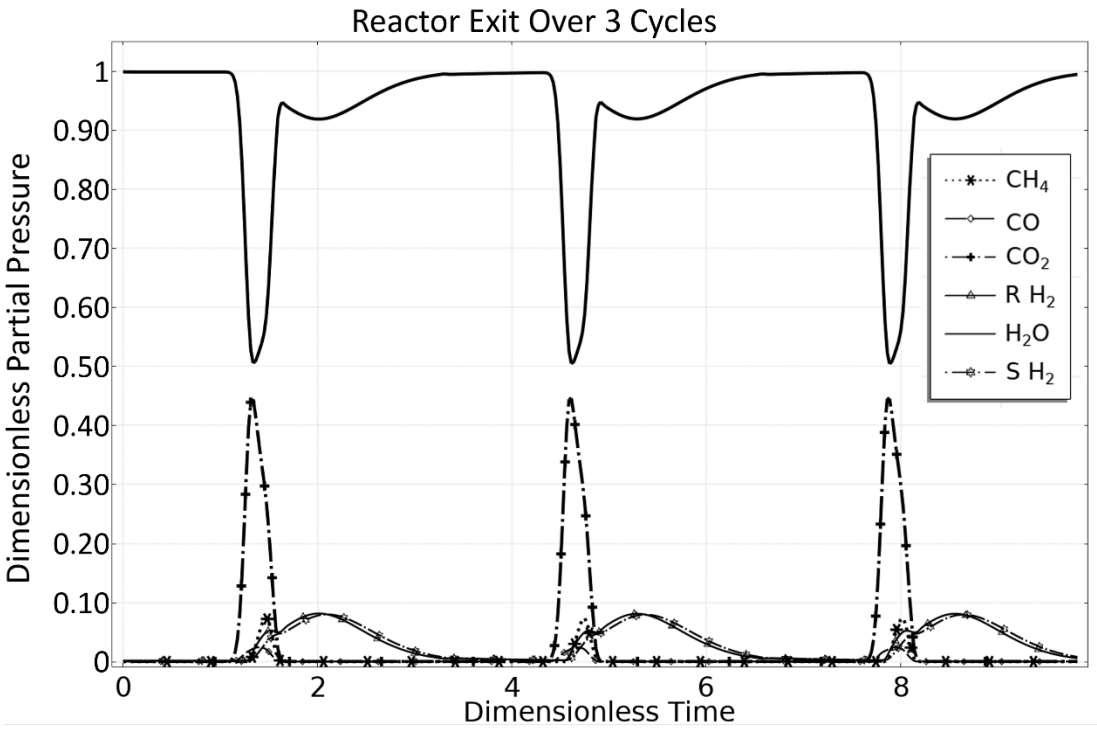

Figure 2-27: Dimensionless time evolution of dimensionless species' partial pressure at reactor outlet over 3 cycles of operation for Da = 4, Θ = 50

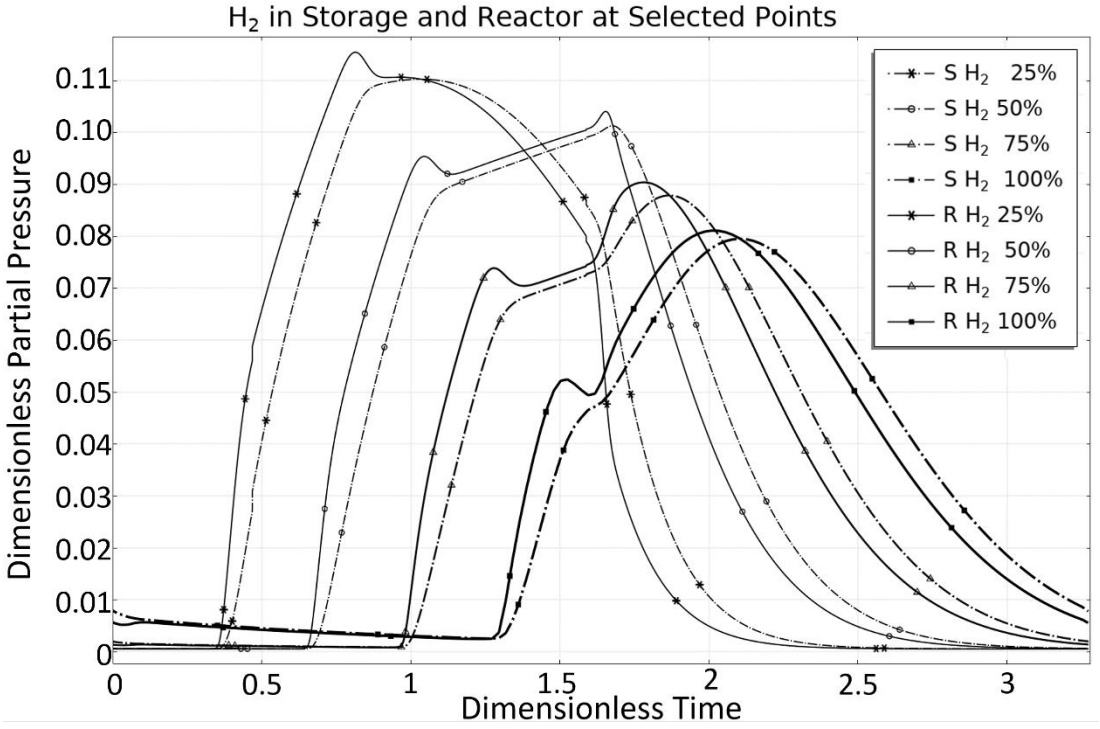

Figure 2-28: Dimensionless time evolution of H2 dimensionless partial pressure in void and storage domains at four reactor lengths for the last cycle for Da = 4, Θ = 50.

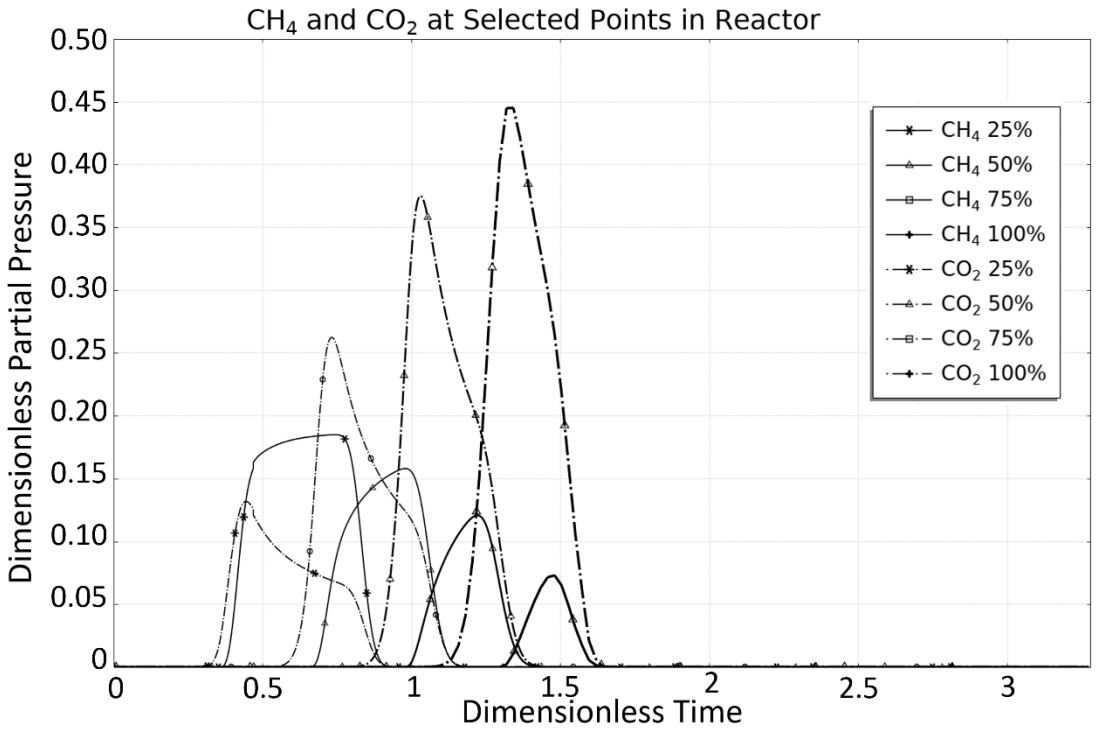

Figure 2-29: Dimensionless time evolution of CH4 and CO2 dimensionless partial pressure in void domain at four reactor lengths for the last cycle for Da = 4, Θ = 50.

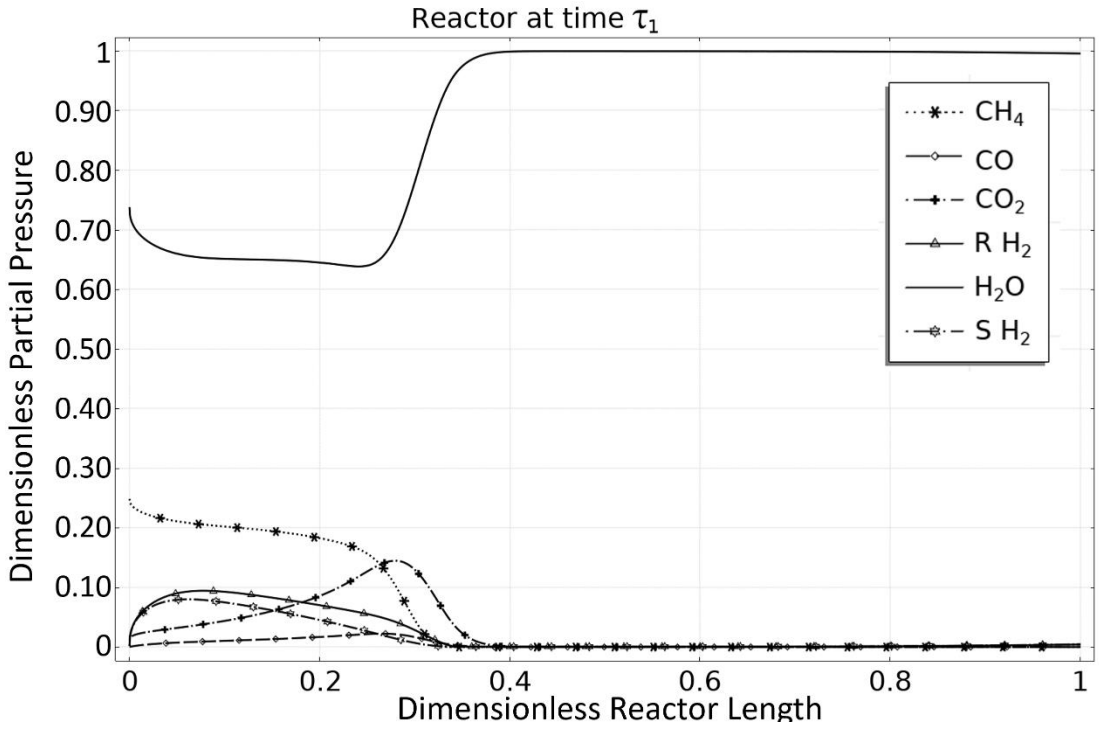

Figure 2-30: Species' dimensionless partial pressure axial length profile during cycle 3 at the end of OM1 for Da = 4, Θ = 50.

Comparing Figure 2-27 with Figure 2-21, we observe a large increase (decrease) in the amount of carbon dioxide (methane) exiting the reactor. Figures 2-22 and 2-28 show similar patterns of behavior for hydrogen in the reactor and storage void domains, with the hydrogen in the storage medium exhibiting a noticeably shorter response time in Figure 2-28. This is attributed to the higher Θ value, which allows the hydrogen to be more easily transferred between domains. Comparing Figures 2-23 and 2-29, we see a dramatic change in the behavior for both methane and carbon dioxide. In Figure 2-23, the methane waveform retains its three distinct phases through all measured points, and is also always greater in magnitude until the exit of the reactor. This is not the case for Da = 4 and Θ = 50, where the magnitude of the carbon dioxide pulse becomes greater than that of the methane pulse at the 50% location. This is particularly highlighted in Figure 3-30, which shows the species profiles in the reactor at the end of OM 1. When compared with Figure 2-24, it can also be seen in Figure 2-30 that the dimensionless partial pressures of hydrogen in the storage and reactor void are much closer in value, indicating a much higher rate of transfer of separated hydrogen.

From a process design and operational perspective, there are several parameters that can be adjusted to alter Da and Θ. For a fixed inlet composition at the beginning of OM1, the Da can be increased (decreased) by increasing (decreasing) the reactor's residence time, which in turn can be achieved by increasing (decreasing) the reactor's length and/or by decreasing (increasing) the reactor's residence time. The dimensionless parameter Θ can be increased (decreased) by increasing (decreasing) the residence time, storage-void domain interfacial area and hydrogen permeance, and/or by decreasing (increasing) the void domain volume fraction. Θ can be altered even while keeping the Da fixed, by altering the last three aforementioned design parameters. In particular, increasing the preferential hydrogen permeance through the storage medium's

permselective layer will increase Θ and can be accomplished through appropriate selection of the layer's pore structure and material properties.

2.2.3 Conclusions

In this work, a novel, first principle-based, spatially dependent model capturing the membrane storage reactor behavior was presented and simulated. This novel intensified process, termed the MSR, is capable of overcoming operational limitations of traditional reactor design by combining multiple mass transport processes into a single unit, and increases the production rate through dynamic operation. The resulting desired products are delivered at high pressure and in readily separable form, which leads to additional energetic and operational cost saving. The assessment of MSR behavior was described by a one-dimensional dynamic model which, when cast in dimensionless form, revealed two dimensionless parameters, Da (the Damkohler number) and $\Theta = 1/Pe_{mem}$ (the inverse Peclet number), that capture MSR behavior. Performance analysis of the MSR process was undertaken by introducing a number of metrics, and a case study on Steam Methane Reforming for the production of hydrogen was subsequently carried out. Numerous simulations of the developed spatially dependent dynamic model enabled parametric studies of the effect of the aforementioned Da and $\Theta = 1/Pe_{mem}$ dimensionless groups, and established that maximizing both groups leads to improved MSR performance. A comparative analysis between SMR-MSR and SSR showed that the SMR-MSR process obtained a higher methane conversion, X_{CH_4}, and a greater yield of hydrogen, Ω_{H_2}. It was also shown that the SMR-MSR hydrogen recovery ratio, $R_{H_2,3}$, was comparable to or above those obtained by currently investigated membrane technologies.

There are several notable advantages of the proposed MSR process, the first being its ability to be modularized and to accommodate a variety of economic production scales. Although the current case study emphasized application to hydrogen production for use at the level of a refinery or a large plant, smaller scales of production are also quite feasible. The MSR process can conceivably be applied to hydrogen-fueling stations so as to facilitate the creation of sustainable decentralized hydrogen generation. Additionally, implementation of the MSR process into existing plants would help reduce many of the economic barriers faced by industrial operations when converting to new technology. Using SMR as an example, retrofitting of an existing plant would consist mainly of reactor repacking with catalyst and storage media. Because of the need for the MSR process to direct material flow, it is imagined that additional fluid lines (for both feed and effluent) need to be constructed. This additional cost, however, is not expected to be large, especially when considering that no additional exogenous chemical components are required. Additional component cost from MSR implementation can also be expected from the need to incorporate dynamic control equipment because, as noted earlier, most industrial reactors operate at steady state. All of this suggests that the MSR process has the potential to overcome many of the barriers that hinder many potential process intensification technologies and be implemented at an industrial scale.

The presented one-dimensional dynamic model was used to demonstrate the novel MSR concept. Because the MSR process is shown to offer significant performance advantages, future work will attempt to rigorously quantify energetic savings by incorporating energy balances into the MSR model. Additionally, development of a MSR model that can capture multi-scale effects and help quantify storage media structural parameters will be investigated.

2.2.4 Notation

English Symbols

a	Verhulst function parameter.
$A_r\left(m^2\right)$	Reactor cross section area
c	Verhulst function parameter.
$c_{i,gv}\left(\frac{mol\,i\,in\,g\,of\,v}{m^3\,g\,of\,v}\right), c_{i,gs}\left(\frac{mol\,i\,in\,g\,of\,s}{m^3\,g\,of\,s}\right)$	i_{th} species concentration in gas phase of void and storage domains
$D_{eff}\left(\frac{cm^2}{s}\right)$	effective diffusivity
$D_{AB}\left(\frac{cm^2}{s}\right)$	binary diffusion coefficient
D_a	Reference Damköhler number
$d_{pel}\left(m\right)$	Pellet diameter
$F_{i,gv}\left(\frac{mol\,i}{s}\right)$	Axial molar flowrate of i_{th} species
$F^*\left(\frac{mol}{s}\right)$	Reference axial molar flowrate
$\bar{F}_{i,gv}$	Dimensionless axial molar flowrate of i_{th} species
h_k	operating mode (OM) specific Heaviside function.
$k_1\left(\frac{\text{kmol bar}^{0.5}}{\text{kg}_{\text{cat}}\,\text{hr}}\right), k_2\left(\frac{\text{kmol}}{\text{kg}_{\text{cat}}\,\text{hr bar}}\right), k_3\left(\frac{\text{kmol bar}^{0.5}}{\text{kg}_{\text{cat}}\,\text{hr}}\right)$	Rate coefficients for SMR reactions
$K_1\left(\text{bar}^2\right), K_2, K_3\left(\text{bar}^2\right)$	Equilibrium constants for SMR reactions
$K_{CH_4}\left(\text{bar}^{-1}\right), K_{H_2}\left(\text{bar}^{-1}\right), K_{CO}\left(\text{bar}^{-1}\right), K_{H_2O},$	Species adsorption constants for SMR reactions
$L^*\left(m\right)$	Reactor Length
$L_{char}\left(m\right)$	Characteristic length
NC	Number of species
NOM	Number of reactor operating modes
OM	Operating mode
$P_{i,gv}\left(Pa\right), P_{i,gs}\left(Pa\right)$	i_{th} species partial pressure in gas phase of void and storage domains
$\bar{P}_{i,gv}, \bar{P}_{i,gs}$	i_{th} species dimensionless partial pressure in gas phase of void and storage domains
$\left(\tilde{\bar{P}}_{i,gv}\right)_{in,k}$	Ratio of inlet partial pressure for species i for operating mode k-1, based on operating mode k = 1
$\left(\tilde{\bar{P}}_{i,gv}\right)_{out,k}$	Ratio of inlet partial pressure for species i for operating mode k, based on operating mode k = 1
$P^*\left(Pa\right)$	Reference pressure
Pe'	Peclet number for convective to diffusive mass transport

Pe	Peclet number for membrane to convective transport
$r_i\left(\frac{mol\,i}{kg\,catalyst\cdot s}\right)$	i_{th} species reaction-based generation rate
$\overline{r_i}$	i_{th} species dimensionless reaction-based generation rate
$r^*\left(\frac{mol}{kg\,catalyst\cdot s}\right)$	Reference reaction generation rate
$R_{i,k}$	Molar ratio of i_{th} species produced during OM k over i_{th} species produced during all OM's
R_i	Rate of i_{th} SMR reaction
$\overline{R_i}$	Dimensionless rate of i_{th} SMR reaction
$R\left(\frac{J}{mol\cdot K}\right)\triangleq 8.314462$	Universal Gas Constant
R_{LIM}	Limiting reactant used in performance metric calculations
$S_{i,gv,gs}\left(\frac{mol\,of\ species\,i\,in\,phase\,g\ \ from\,s\,to\,v}{\left(m^3\ system\,r\right)\cdot s}\right)$	Molar generation rate of i_{th} species into the gas phase of the voids domain due to transport from the gas phase in the storage domain
$S_{i,gs,gv}\left(\frac{mol\,of\ species\,i\,in\,phase\,g\ \ from\,v\,to\,s}{\left(m^3\ system\,r\right)\cdot s}\right)$	Molar generation rate of i_{th} species into the gas phase of the storage domain due to transport from the gas phase in the voids domain
$t(s)$	Time
$\overline{t}$	Dimensionless time
$t^*(s)$	Reference time, chosen as the residence time
$T(K)$	Temperature in all reactor domains
$V\left(m^3\right)$	Total reactor volume
$v_{eff}\left(\frac{m}{s}\right)$	effective velocity
$v_g\left(\frac{m}{s}\right)$	gas velocity in reactor void domain
$v^*\left(\frac{m}{s}\right)$	Reference velocity, chosen as gas inlet velocity during OM 1
$\overline{v}_g$	Dimensionless gas velocity in reactor void domain
$X_{R_{LIM}}$	Conversion of limiting reactant R_{LIM} over all OM's
W_k	Verhulst function for switching between inlet boundary conditions during OM change.

$z(m)$	Reactor axial coordinate
$\overline{z}$	Reactor dimensionless axial coordinate
Geek Symbols	
$\alpha_{s,v}\left(\frac{m^2\ storage-void\ interface}{m^3\ system\,r}\right)$	Storage-void domain interfacial area per unit volume of reactor system
$\beta_i\left(\frac{mol\,i}{Pa\cdot\left(m^2\ void-storage\,interface\right)\cdot s}\right)\forall i=1,NC$	i_{th} species permeance through storage medium permselective layer
$\varepsilon_v,\varepsilon_c,\varepsilon_s,\varepsilon_{gs},\varepsilon_{sos}$	Volume fractions of voids, catalyst, storage, gas phase in storage domain, and solid phase in storage domain
η	Catalyst effectiveness factor
Θ	Dimensionless number quantifying membrane permeation to convection (inverse Peclet)
$\rho_c\left(\frac{kg\,catalyst}{m^3\,catalyst\ pellet}\right)$	Catalyst pellet density
$\omega_{i,k}$	Molar ratio of i_{th} species produced during OM k over limiting reactant fed throughout all OM's
Ω_i	Overall molar ratio of i_{th} species produced during all OMs over limiting reactant fed throughout all OM's
Ω_i	Desired product yield of species i
τ_k	Duration of k_{th} operating mode
$\overline{\tau}_k$	Dimensionless duration of k_{th} operating mode

2.3 1-D non-isobaric non-isothermal

In this section, the non-isobaric non-isothermal SR process is presented. The equations in this section require the formulation and calculation of transport coefficients for multicomponent systems. While under certain conditions these can be approximated as constant or nearly constant, transport coefficients are very often functions of temperature, pressure, as well as other atomic factors. In this section we will be using Elementary Kinetic theory and Chapman-Enskog[32] theory of intermolecular force interactions and approximated solution to the Boltzmann equation to estimate their values. For calculating the viscosity of a pure component the following equation is used:

$$\mu_{i,gv} = \frac{26.69\left(M_i T\right)^{0.5}}{o_i^2 \Omega_{V,i}} \tag{2.1.61}$$

where M and T are molecular weight $\left(g/mol\right)$ and Temperature $\left(K\right)$, M is the molecular weight in $\left(kg/mol\right)$, σ_i is a characteristic dimension of the molecule $\left(m\right)$ and $\Omega_{v,i}$ is a dimensionless collision integral given by:

$$\Omega_{V,i} = \frac{L_A}{\left(T^{\mu}\right)^{L_B}} + \frac{L_C}{\exp\left(L_D T^{\mu}\right)} + \frac{L_E}{\exp\left(L_F T^{\mu}\right)} \tag{2.1.62}$$

with $T^{\mu} = \frac{kT}{\delta_i}$, δ_i is the minimum of the pair potential curve, and k is Boltzmann's constant. To estimate the viscosity of a gas mixture we use the simplification method of developed by Wilke[33], [34] of the rigorous kinetic theory model which neglects second-order effects :

$$\mu_{gv} = \sum_{i=1}^{NC} \left(\frac{x_{i,gv}\mu_{i,gv}}{\sum_{j=1}^{NC} x_{j,gv}\Phi_{ij,gv}^{\mu}} \right) \tag{2.1.63}$$

where Φ_{ij} is given by:

$$\Phi_{ij} = \frac{1}{\sqrt{8}}\left(1+\frac{M_i}{M_j}\right)^{-1/2}\left[1+\left(\frac{\mu_{i,gv}}{\mu_{j,gv}}\right)^{1/2}\left(\frac{M_j}{M_i}\right)^{1/4}\right]^2 \tag{2.1.64}$$

A polynomial approximation based on the group contribution method work of Roy and Thodos[35] is used to estimate the pure component thermal conductivity:

$$\lambda_{i,r} = \lambda_i \mathrm{E} = \left(\lambda \mathrm{E}\right)_{tr} + \left(\lambda \mathrm{E}\right)_{\mathrm{int}} \tag{2.1.65}$$

Where E is the reduced thermal conductivity and is given by:

$$\mathrm{E} = 210\left(\frac{T_c M_i}{P_c^4}\right)^{1/6} \tag{2.1.66}$$

$\left(\lambda \mathrm{E}\right)_{tr}$ is the contribution to thermal conductivity from translational energy only and is given by:

$$\left(\lambda \mathrm{E}\right)_{tr} = 8.757\left(\exp\left(0.0464T_r\right) - \exp\left(-0.2412T_r\right)\right) \tag{2.1.67}$$

And $\left(\lambda \mathrm{E}\right)_{\mathrm{int}}$ is the contribution from rotational energy and vibrational interchange and is given by:

$$\left(\lambda \mathrm{E}\right)_{\mathrm{int}} = Cf\left(T_r\right) \tag{2.1.68}$$

Where C is a material specific constant estimated by group contributions techniques and the form of $f\left(T_r\right)$ is dependent on the classification of the material. A comprehensive list of other group contribution methods and their comparative accuracy with experimental data can be found in Su et al.[36]. In order to estimate the gas mixture thermal conductivity, the method of Mason and Saxena[37] is employed which gives the same functional form as the multicomponent viscosity.

$$\lambda_{gv} = \sum_{i=1}^{NC}\left(\frac{x_{i,gv}\lambda_{i,gv}}{\sum_{j=1}^{NC} x_{j,gv}\Phi_{ij,gv}^{\lambda}}\right) \tag{2.1.69}$$

Pure component heat capacity is estimated using the Shomate Equation

$$\hat{C}_{P,i} = a + b\frac{T}{1000} + c\left(\frac{T}{1000}\right)^2 + d\left(\frac{T}{1000}\right)^3 + \frac{e}{\left(\frac{T}{1000}\right)^2} \tag{2.1.70}$$

Multi-component diffusion coefficients can often be estimated by knowledge of all the species Fickian binary diffusion coefficients which are shown below:

$$D_{ij} = \frac{0.00266T^{3/2}}{PM_{ij}^{0.5}\sigma_{ij}^2\Omega_D} \tag{2.1.71}$$

$$M_{ij} = 2\left[\frac{1}{M_i} + \frac{1}{M_j}\right]^{-1} \tag{2.1.72}$$

$$\sigma_{ij} = \frac{\sigma_i + \sigma_j}{2} \tag{2.1.73}$$

$$\Omega_D = \frac{L_A}{\left(T^D\right)^{L_B}} + \frac{L_C}{\exp\left(L_D T^D\right)} + \frac{L_E}{\exp\left(L_F T^D\right)} + \frac{L_G}{\exp\left(L_H T^D\right)} \tag{2.1.74}$$

$$T^D = \frac{kT}{\delta_{ij}} \tag{2.1.75}$$

$$\delta_{ij} = \left(\delta_i \delta_j\right)^{0.5} \tag{2.1.76}$$

Again, the results stem from Chapman-Enskgog theory as represented in Poling et al[38].

3.3.1 Mathematical Formulation

In this study, the composite 1-dimensional model for the intensified SR process is extended to include contributions from axial pressure gradients and axial temperature variation, which captures and highlights several attractive SR characteristics. The newly derived equations are then non-dimensionalized, and the dimensionless groups governing the SR behavior are identified. The SR is considered to be a composite thermodynamic system (r) comprised of three domains that are spatially distributed and exclusive of each other (reactor voids (v), catalyst pellet (c), and storage pellet (s)), and a maximum of two phases (gas (g), and solid (so)). The volume fractions of the voids (v), catalyst (c), and storage (s) domains are denoted as $\varepsilon_v, \varepsilon_c, \varepsilon_s$ respectively, while the volume fractions of the gas and solid phases in the storage domain are denoted as $\varepsilon_{gs}, \varepsilon_{sos}$ respectively. In the context of this study, the following are then considered to hold:

$$\left\{\varepsilon_v + \varepsilon_c + \varepsilon_s = 1,\ \varepsilon_{gs} + \varepsilon_{sos} = \varepsilon_s\right\} \tag{2.1.77}$$

The communication between the catalyst and reactor voids (gas phase) domains is quantified using an effectiveness factor approach, while the communication between the storage domain and reactor gas phase domains through a permselective layer on the storage domain's control surface, is quantified using species transport equations obeying Sieverts' Law. The

composite system (r) is considered to be non-isothermal, while the reactor voids domain (v) is also considered to be non-isobaric. No reaction occurs within the storage domain. The reacting mixture is considered to be an ideal gas. The equation describing Mass Conservation (molar form) of species *i* in phase *g* within domain *v* on a system *r* volumetric basis is:

$$\left\{\begin{array}{l}\frac{\partial}{\partial t}\left(\varepsilon_v c_{i,gv}(t,z)\right)+\frac{\partial}{\partial z}\left(\varepsilon_v v_g^{\dagger}(t,z)c_{i,gv}(t,z)\right)\\ +\frac{\partial}{\partial z}\left(\varepsilon_v \vec{j}_{i,gv}^{\dagger}(t,z)\right)\end{array}\right\}=\left\{\varepsilon_c\rho_c\eta r_i\left(\left\{c_{k,gv}(t,z)\right\}_{k=1}^{NC},T_g(t,z)\right)+S_{i,gv,gs}(t,z)\right\}\ i=1,NC \tag{2.1.78}$$

The equation describing Mass Conservation (molar form) of species *i* in phase *g* within domain *s* on a system *r* volumetric basis is:

$$\frac{\partial}{\partial t}\left(\varepsilon_{gs}c_{i,gs}(t,z)\right)=S_{i,gs,gv}(t,z)\ i=1,NC \tag{2.1.79}$$

where the temporal and spatial dependence of all volume fractions, the effectiveness factor, and the catalyst pellet density is not shown, as they will next be considered constant. Sieverts' Law has commonly been employed in quantifying species' molar fluxes through Pd membrane layers and again is used her to quantify the molar flux from the gas domain to the storage domain.

$$S_{i,gs,gv}(t,z)=-S_{i,gv,gs}(t,z)=\alpha_{s,v}\beta_i\left(P_{i,gv}(t,z)-P_{i,gs}(t,z)\right)\ \forall i=1,...,NC \tag{2.1.80}$$

where β_i is the i_{th} species molar permeance through the permselective layer, $\alpha_{s,v}$ is the storage-void interfacial area per unit reactor volume, and $P_{i,gv}, P_{i,gs}$ are the i_{th} species partial pressures in the gas phase of the reactor void and storage domains. Considering an ideal gas mixture, the following relations hold:

$$P_{i,gv}(t,z)=c_{i,gv}(t,z)RT_g(t,z),\ \ P_{i,gs}(t,z)=c_{i,gs}(t,z)RT_g(t,z)\ \ \forall i=1,...,NC \tag{2.1.81}$$

Momentum balance is captured through the use of the Ergun equation:

$$\frac{\partial P_{gv}(t,z)}{\partial z} = -\frac{\vec{v}_g(t,z)}{d_{eff}}\left(\frac{1-\varepsilon_v}{\varepsilon_v^{\,3}}\right)\left[1.75\left(\vec{v}_g(t,z)\rho_{gv}(t,z)\right)+150\frac{(1-\varepsilon_v)\mu_{gv}(t,z)}{d_{eff}}\right] \quad (2.1.82)$$

Because the Ergun equation uses average velocity in its formulation, and the velocities in the species balance are mol average velocities, the previously derived expression equating which maps between the two quantities is used.

$$\vec{v}_g(t,z) = \vec{v}_g^{\dagger}(t,z) + \frac{1}{c_{gv}(t,z)}\sum_{i=1}^{NC}\left(\frac{M_i}{\sum_{k=1}^{NC} x_{k,gv}M_k}\left(\vec{j}_{i,gv}^{\dagger}(t,z)\right)\right) \quad (2.1.83)$$

The temperature profile in the reactor is captured by assuming

$$\left\{\begin{array}{l}\left(\varepsilon_v\rho_{gv}\hat{C}_P^{gv}+\varepsilon_c\rho_c\hat{C}_P^{c}+\varepsilon_{sos}\rho_s\hat{C}_P^{s}\right)\frac{\partial T_g}{\partial t}+\left(\varepsilon_v\rho_{gv}\hat{C}_P^{gv}\vec{v}_v\right)\frac{\partial T_g}{\partial z}\\ +\sum_{i=1}^{NC}\left(\left(\varepsilon_v\hat{C}_{P,i}^{gv}\frac{\partial T_g}{\partial z}\right)\vec{j}_{i,gv}\right)+\frac{\partial}{\partial z}\left(\left(\varepsilon_v\lambda_{gv}^{h}+\varepsilon_c\lambda_c^{h}+\varepsilon_{sos}\lambda_s^{h}\right)\frac{\partial T_g}{\partial z}\right)\end{array}\right\} = \left\{\begin{array}{l}-\sum_{i=1}^{NC}\left(\hat{h}_{i,gv}\varepsilon_c\rho_c\eta r_i\right)\\ -\sum_{i=1}^{NC}\left(\tilde{h}_{i,gv}S_{i,gs,gv}\right)\\ +\frac{A_r h_r^{fur}}{V_r}\left(T_g-T^{fur}\right)\\ +\frac{\partial P_{gv}}{\partial z}+\vec{v}_v\frac{\partial P_{gv}}{\partial z}\end{array}\right\}$$

(2.1.84)

Additionally, the following parameters are in introduced.

In order to cast equations (1)-(7) in dimensionless form we first define the following dimensionless parameters,

$$\bar{t}=\frac{t}{t^*},\ \bar{z}=\frac{z}{z^*},\ \bar{\vec{v}}_g^{\dagger}=\frac{\vec{v}_g^{\dagger}}{\vec{v}^*},\ \bar{\vec{v}}_g=\frac{\vec{v}_g}{\vec{v}^*},\bar{P}_{i,gv}=\frac{P_{i,gv}}{P^*},\bar{P}_{i,gs}=\frac{P_{i,gs}}{P^*},\bar{c}_{i,fv}=\frac{c_{i,gv}}{c^*},\ \bar{\vec{j}}_{i,gv}^{\dagger}=\frac{\vec{j}_{i,gv}^{\dagger}}{\vec{j}^*},\bar{T}=\frac{T}{T^*},\bar{C}_P^{gv}=\frac{\tilde{C}_P^{gv}}{\tilde{C}_P^{*,gv}}$$

$$\bar{r}_{i,fv}\left(\left\{\bar{P}_k^g(\bar{t})\right\}_{k=1}^{NC},T\right)\triangleq\frac{r_{i,fv}\left(\left\{\bar{P}_k^g(t)\cdot P^*\right\}_{k=1}^{NC},T\right)}{r^*}$$

Where t^* , z^*, $\vec{v}^*$, P^* , c^*, $\vec{j}^*$ r^*, T^* are the reference values of time, axial length, molar velocity, pressure, concentration, species flux, reaction rate, and temperature. Substitution of the above into the SR governing equations yields

$$\frac{\partial \bar{c}_{i,gv}}{\partial \bar{t}} + \bar{\vec{v}}_g^{\dagger} \frac{\partial \bar{c}_{i,gv}}{\partial \bar{z}} + \bar{c}_{i,gv} \frac{\partial \bar{\vec{v}}_g^{\dagger}}{\partial \bar{z}} + \frac{\partial \bar{\vec{j}}_{i,gv}^{\dagger}}{\partial \bar{z}} = \frac{\varepsilon_c}{\varepsilon_v} D_a \bar{r}_{i,vr} + \Theta\left(\bar{P}_{i,vr} - \bar{P}_{i,vs}\right) \quad \forall i = 1,....,NC \tag{2.1.85}$$

$$\frac{\partial \bar{c}_{i,gs}}{\partial \bar{t}} = \Theta \frac{\varepsilon_v}{\varepsilon_{gs}} \frac{\beta_i}{\beta_1}\left(\bar{P}_{i,gv} - \bar{P}_{i,gs}\right) \quad \forall i = 1,....,NC \tag{2.1.86}$$

$$\left\{\begin{array}{l} \dfrac{\partial \bar{T}_g}{\partial \bar{t}} + \left(\dfrac{\varepsilon_c \Psi_1}{\varepsilon_v \bar{c}_{gv} \bar{C}_P^{gv}} + \dfrac{\varepsilon_{sos} \Psi_2}{\varepsilon_v \bar{c}_{gv} \bar{C}_P^{gv}}\right) \dfrac{\partial \bar{T}_g}{\partial \bar{t}} \\ + \bar{\vec{v}}_v \dfrac{\partial \bar{T}_g}{\partial \bar{z}} + \displaystyle\sum_{i=1}^{NC} \left(\dfrac{\Psi_{3,i}}{\bar{c}_{gv} \bar{C}_P^{gv}} \bar{\vec{j}}_i^{\dagger} \dfrac{\partial \bar{T}_g}{\partial \bar{z}}\right) \\ + \left(\dfrac{\bar{\lambda}_{gv}^h \Psi_4}{\bar{c}_{gv} \bar{C}_P^{gv}} + \dfrac{\varepsilon_c \Psi_5}{\varepsilon_v \bar{c}_{gv} \bar{C}_P^{gv}} + \dfrac{\varepsilon_{sos} \Psi_6}{\varepsilon_v \bar{c}_{gv} \bar{C}_P^{gv}}\right) \dfrac{\partial^2 \bar{T}_g}{\partial \bar{z}^2} \\ + \dfrac{\Psi_4}{\bar{c}_{gv} \bar{C}_P^{gv}} \dfrac{\partial \bar{T}_g}{\partial \bar{z}} \dfrac{\partial \bar{\lambda}_{gv}^h}{\partial \bar{z}} \end{array}\right\} = \left\{\begin{array}{l} -\displaystyle\sum_{i=1}^{NC} \left(\dfrac{\varepsilon_c Da \Psi_7}{\varepsilon_v \bar{C}_P^{gv} \bar{c}_{gv}} \bar{r}_i\right) + \dfrac{\Psi_8}{\varepsilon_v \bar{c}_{gv} \bar{C}_P^{gv}}\left(\bar{T}_g - \bar{T}^{fur}\right) \\ -\displaystyle\sum_{i=1}^{NC} \left(\dfrac{\Theta}{\bar{C}_P^{gv} \bar{c}_{gv}} \Psi_7 \left(\bar{P}_{i,gv} - \bar{P}_{i,gs}\right)\right) \\ + \dfrac{\Psi_9}{\bar{C}_P^{gv} \bar{c}_{gv}} \left(\dfrac{\partial \bar{P}_{gv}}{\partial \bar{t}} + \bar{\vec{v}}_v \dfrac{\partial \bar{P}_{gv}}{\partial \bar{z}}\right) \end{array}\right\} \tag{2.1.87}$$

$$\frac{\partial \bar{P}_{gv}(t,z)}{\partial \bar{z}} = -\left[1.75 \bar{v}_g \bar{v}_g \bar{c}_{gv} \varpi_1 \left(\frac{1-\varepsilon_v}{\varepsilon_v^3}\right) + 150 \bar{v}_g \left(\frac{(1-\varepsilon_v)^2}{\varepsilon_v^3}\right) \varpi_2\right] \tag{2.1.88}$$

Equations (2.1.85)-(2.1.88) are considered the governing equations which describe the SR reactor process for a transient, non-isothermal, 1 dimensional flow reactor. As noted in earlier sections, the values of the reference parameters are specified by the particulars of the considered problem, since the choice of reference parameters can vary widely[14], can significantly affect the range of values of the resulting dimensionless groups[15], and must be such that the resulting dimensionless problem's solution is not adversely influenced[16].

Defining $t^* = z^* \Big/ \vec{v}^*$, $\vec{\bar{j}}^* = \vec{v}^* c^*$, $\tilde{C}_P^{*,gv} = \tilde{C}_P^{gv}\left(T_{wall}\right)\Big|_{Eq}$, $\lambda_{gv}^{*,h} = \lambda_{gv}^{h}\left(T_{wall}\right)\Big|_{Eq}$ and gives rise to the following dimensionless parameters for the transport equations: $D_a = \dfrac{z^* RT^* \rho_c \eta r^*}{\vec{v}^* P^*}$,

$\Theta = \dfrac{z^* RT^* \alpha_{s,v} \beta_1}{v^* \varepsilon_v}$, $\Psi_4 = \dfrac{\lambda_{gv}^{*,h}}{\tilde{C}_P^{*,gv} c^* z^* v^*}$, and $\Psi_9 = \dfrac{R}{\tilde{C}_P^{*,gv}}$.

Where the first parameter is the Damkohler number and the second is the inverse Peclet number. The second two heat transfer parameters make use of $\tilde{C}_P^{*,gv}$ and $\lambda_{gv}^{*,h}$, which are the molar heat capacity and thermal conductivity at the equilibrium mixture values based on the inlet feed and pressure conditions and the wall temperature. Both of these parameters are a function of the mol fraction of the participating species and the methodology for calculating these values is outlined in Appendix A.4. The SR dimensionless energy equation has 7 additional dimensionless variables, and two dimensionless parameters in the momentum balance, shown in the tables below.

Table 2-14: Dimensionless heat parameters and variables.

$\Psi_1 = \dfrac{\rho_c \hat{C}_P^c}{\tilde{C}_P^{*,gv} c^*}$	Dimensionless heat variable 1.
$\Psi_2 = \dfrac{\rho_s \hat{C}_P^s}{\tilde{C}_P^{*,gv} c^*}$	Dimensionless heat variable 2.
$\Psi_{3,i} = \left(\dfrac{\tilde{C}_{P,i}^{gv}}{\tilde{C}_P^{*,gv}} \right)$	Dimensionless heat variable 3 for species i.
$\Psi_4 = \dfrac{\lambda_{gv}^{*,h}}{\tilde{C}_P^{*,gv} c^* z^* v^*}$	Dimensionless heat parameter 4.

$\Psi_5 = \frac{\lambda_c^h}{c^* \tilde{C}_P^{*,gv} v^* z^*}$	Dimensionless heat variable 5.
$\Psi_6 = \frac{\lambda_s^h}{c^* \tilde{C}_P^{*,gv} v^* z^*}$	Dimensionless heat variable 6.
$\Psi_{7,i} = \frac{\tilde{h}_{i,gv}}{T^* \tilde{C}_P^{*,gv}}$	Dimensionless heat variable 7 for species i.
$\Psi_8 = \frac{z^*}{\tilde{C}_P^{*,gv} c^* v^*} \frac{A_r h_r^{fur}}{V_r}$	Dimensionless heat variable 9.
$\Psi_9 = \frac{R}{\tilde{C}_P^{*,gv}}$	Dimensionless heat parameter 9.

Table 2-15: Dimensionless momentum parameters.

$\varpi_1 = \frac{z^* v^* v^* M}{R T^* d_{eff}}$	Dimensionless momentum variable 1.
$\varpi_2 = \frac{v^* \mu_{gv} z^*}{P^* \left(d_{eff}\right)^2}$	Dimensionless momentum variable 2.

Comparing the performance of the PPSO SR, which is a periodic process, with that of a traditional reactor, which is a steady-state process, requires that a number of process performance metrics be introduced. Since the PPSO SR is a periodic process that takes place over several phases, it is appropriate to define metrics over each phase separately and over all phases. When the inverse Peclet number Θ is set to zero, the second and third operating phases become obsolete, and as the duration of the first phase approaches infinity, its associated metrics must approach their steady-state counterparts. For reactor design it is preferable to use a metrics based on mols as this gives a better notion of reaction specific quantities. To this end, the axial molar flowrate of the i_{th}

species $F_{i,gv}$ is expressed in terms of a reference molar flowrate F^* and a dimensionless molar flowrate $\bar{F}_{i,gv}$, as follows:

$$F^* \triangleq \frac{P^* v^* \varepsilon_v A_r}{RT},\ \bar{F}_{i,gv} \triangleq \frac{F_{i,gv}}{F^*} = \frac{c_{i,gv} v_g \varepsilon_v A_r}{F^*} = \frac{P^* \bar{P}_{i,gv} v^* \bar{v}_g \varepsilon_v A_r}{RTF^*} = \bar{P}_{i,gv} \bar{v}_g \tag{2.1.89}$$

Limiting Reactant Conversion

An important metric for the assessment of MSR performance is the conversion of a limiting reactant R_{LIM}. Typically, this reactant will be fed in the MSR during one OM, but may be removed from the MSR during multiple OM. Thus, we define its conversion over all OM as follows:

$$X_{R_{LIM}} \triangleq \frac{\left[\int_0^{\sum_{k=1}^{NOM}\tau_k} F_{R_{LIM},gv}(t',0)dt' - \int_0^{\sum_{k=1}^{NOM}\tau_k} F_{R_{LIM},gv}(t',L^*)dt'\right]}{\int_0^{\sum_{k=1}^{NOM}\tau_k} F_{R_{LIM},gv}(t',0)dt'} = \frac{\left[\int_0^{\sum_{k=1}^{NOM}\bar{\tau}_k} \bar{F}_{R_{LIM},gv}(\bar{t}',0)d\bar{t}' - \int_0^{\sum_{k=1}^{NOM}\bar{\tau}_k} \bar{F}_{R_{LIM},gv}(\bar{t}',1)d\bar{t}'\right]}{\int_0^{\sum_{k=1}^{NOM}\bar{\tau}_k} \bar{F}_{R_{LIM},gv}(\bar{t}',0)d\bar{t}'} \tag{2.1.90}$$

Desired Product Ratio

Another important metric for the assessment of MSR performance is one that captures the extent to which the desired product is formed as the limiting reactant is converted. Thus, the following OM-dependent metric is introduced, that is equal to the ratio of the i_{th} species amount generated during OM k over the limiting reactant's R amount fed throughout all OM's.

$$\omega_{i,k} \triangleq \frac{\left[\int_{\sum_{k'=0}^{k'=k-1}\tau_{k'}}^{\sum_{k'=0}^{k'=k}\tau_{k'}} F_{i,gv}\left(t', L^*\right)dt' - \int_{\sum_{k'=0}^{k'=k-1}\tau_{k'}}^{\sum_{k'=0}^{k'=k}\tau_{k'}} F_{i,gv}\left(t',0\right)dt'\right]}{\int_0^{\sum_{k=1}^{NOM}\tau_k} F_{R_{LIM},gv}\left(t',0\right)dt'} = \frac{\left[\int_{\sum_{k'=0}^{k'=k-1}\bar{\tau}_{k'}}^{\sum_{k'=0}^{k'=k}\bar{\tau}_{k'}} \bar{F}_{i,gv}\left(\bar{t}',1\right)d\bar{t}' - \int_{\sum_{k'=0}^{k'=k-1}\bar{\tau}_{k'}}^{\sum_{k'=0}^{k'=k}\bar{\tau}_{k'}} \bar{F}_{i,gv}\left(\bar{t}',0\right)d\bar{t}'\right]}{\int_0^{\sum_{k=1}^{NOM}\bar{\tau}_k} \bar{F}_{R_{LIM},gv}\left(\bar{t}',0\right)d\bar{t}'}$$

$k = 1, NOM,\ i = 1, NC$

(2.1.91)

where $\tau_0 = 0,\ \bar{\tau}_0 = 0$.

An overall OM-independent metric is also introduced, that is equal to the ratio of the i_{th} species amount generated during all OMs over the limiting reactant's R_{LIM} amount fed throughout all OM's.

$$\Omega_i \triangleq \frac{\left[\int_0^{\sum_{k=1}^{NOM}\tau_k} F_{i,gv}\left(t', L^*\right)dt' - \int_0^{\sum_{k=1}^{NOM}\tau_k} F_{i,gv}\left(t',0\right)dt'\right]}{\int_0^{\sum_{k=1}^{NOM}\tau_k} F_{R_{LIM},gv}\left(t',0\right)dt'} = \frac{\left[\int_0^{\sum_{k=1}^{NOM}\bar{\tau}_k} \bar{F}_{i,gv}\left(\bar{t}',1\right)d\bar{t}' - \int_0^{\sum_{k=1}^{NOM}\bar{\tau}_k} \bar{F}_{i,gv}\left(\bar{t}',0\right)d\bar{t}'\right]}{\int_0^{\sum_{k=1}^{NOM}\bar{\tau}_k} \bar{F}_{R_{LIM},gv}\left(\bar{t}',0\right)d\bar{t}'}\Bigg|_{NC}^{i=1,}$$

(2.1.92)

This is often referred to as product yield. It then holds

$$\Omega_i = \sum_{k=1}^{NOM} \omega_{i,k} \tag{2.1.93}$$

Desired Product Recovery Fraction

Finally, we define the fraction of product generated during a given OM over the total product generated over the duration of all OM's, as the Product Recovery fraction, defined as:

$$R_{i,k} \triangleq \frac{\omega_{i,k}}{\Omega_i} \quad \forall k = 1, NOM \quad \forall i = 1, ..., NC \tag{2.1.94}$$

The system of non-linear first order partial differential equations described above are used to simulate all three OM's of the MSR PPSO, and is solved using a direct finite element solver with implicit multistep backward differentiation (BDF) time stepping. The above solution strategy was coded and implemented using the COMSOL Multiphysics software platform. The MSR concept is next illustrated for the case of the SMR reaction. We show, through a parametric analysis, the impact that the previously identified dimensionless parameters have on the performance of an SMR-MSR operating under PPSO.

3.3.3 Problem Specification and Thermodynamic Data

In the analysis that follows, the molar velocity $\vec{v}^{*\dagger}$, and reaction generation rate r^* reference values are selected as $\vec{v}^{*\dagger} \triangleq \vec{v}_{vr}^{\dagger}(0,0), r^* \triangleq \frac{k_1}{\left(P^*\right)^{0.5}}$. In order to account for diffusion, the molar form of the Stefan Maxwell equation is used as shown in Table 2-16 along with its dimensionless form.

Table 2-16: Dimensionless Stefan-Maxwell formulation.

$\vec{j}_{i,gv}^{\dagger} = \left(\sum_{\substack{j=1 \\ i\neq j}}^{NC} \frac{x_{j,gv}}{D_{ij}}\right)^{-1} \left(-c_{gv}\frac{\partial x_{i,gv}}{\partial z} + \sum_{\substack{j=1 \\ i\neq j}}^{NC} \frac{\vec{j}_{j,gv}^{\dagger} x_{j,gv}}{D_{ij}}\right)$	Molar Steffan-Maxwell diffusion.
$\bar{\vec{j}}_{i,gv}^{\dagger} = \bar{D}_{i,diff}\left(\Gamma_{1,i} + \Gamma_{2,i}\right)\frac{\partial \bar{c}_{i,gv}}{\partial \bar{z}}$	Dimensionless Steffan-Maxwell difussion.
$\Gamma_{1,i} = \left(x_{i,gv}\frac{\frac{\partial c_{gv}}{\partial z}}{\frac{\partial c_{i,gv}}{\partial z}} - 1\right)$	Variable 1 for dimensionless Steffan-Maxwell difussion for species i.
$\Gamma_{2,i} = \frac{1}{\frac{\partial c_{i,gv}}{\partial z}} \sum_{\substack{j=1 \\ i\neq 1}}^{NC} \frac{\vec{j}_{j,gv}^{\dagger} x_{j,gv}}{D_{ij}}$	Variable 2 for dimensionless Steffan-Maxwell difussion for species i.

$\bar{D}_{diff} = \dfrac{\left(\sum_{\substack{j=1 \\ i \neq 1}}^{NC} \dfrac{x_{j,gv}}{D_{ij}} \right)^{-1}}{\vec{v}^{*\dagger} z^{*}}$	Dimensionelss diffusion coefficient.

According to Xu and Froment SMR is carried out through three reversible reactions $RX1$, $RX2$, and $RX3$, with enthalpies of formation and kinetic rates as shown below:

$$CH_4 + H_2O \leftrightarrow CO + 3H_2 \quad \Delta H_1^{\circ}: 206.1 \, {kJ}/{mol} \qquad (RX1)$$

$$CO + H_2O \leftrightarrow CO_2 + H_2 \quad \Delta H_2^{\circ}: -41.15 \, {kJ}/{mol} \qquad (RX2)$$

$$CH_4 + 2H_2O \Leftrightarrow CO_2 + 4H_2 \quad \Delta H_3^{\circ}: 164.9 \, {kJ}/{mol} \qquad (RX3)$$

$$\{R_1, R_2, R_3\} = \left\{ \begin{array}{l} \dfrac{\dfrac{k_1}{\left(P_{H_2,gv}\right)^{2.5}} \left(P_{CH_4,gv} P_{H_2O,gv} - \dfrac{\left(P_{H_2,gv}\right)^3 P_{CO,gv}}{K_1} \right)}{\left(\mathrm{DEN}\right)^2}, \dfrac{\dfrac{k_2}{P_{H_2,gv}} \left(P_{CO,gv} P_{H_2O,gv} - \dfrac{P_{H_2,gv} P_{CO_2,gv}}{K_2} \right)}{\left(\mathrm{DEN}\right)^2} \\ \dfrac{\dfrac{k_3}{\left(P_{H_2,gv}\right)^{3.5}} \left(P_{CH_4,gv} \left(P_{H_2O,gv}\right)^2 - \dfrac{\left(P_{H_2,gv}\right)^4 P_{CO,gv}}{K_3} \right)}{\left(\mathrm{DEN}\right)^2} \end{array} \right\} \qquad (2.1.95)$$

$$\text{with } \mathrm{DEN} = 1 + K_{CO} P_{CO,gv} + K_{H_2} P_{H_2,gv} + K_{CH_4} P_{CH_4,gv} + K_{H_2O} \frac{P_{H_2O,gv}}{P_{H_2,gv}} \qquad (2.1.96)$$

The kinetic and equilibrium constant values in the above expressions are listed in the tables below.

Table 2-17: Rate coefficients and adsorption constants for use in Arrhenius or Van't Hoff Equations

Rate Coefficient or Adsorption Constant	Pre-exponential Factor	Unit Pre-exponential Factor	Activation energy or adsorption enthalpy (kJ)
k_1	4.225×10^{15}	$\left(kmol\, bar^{0.5}\right)/\left(kg_{cat}\, hr\right)$	240.1
k_2	1.955×10^{6}	$\left(kmol\right)/\left(kg_{cat}\, hr\, bar\right)$	67.13

k_3	$1.020\text{x}10^{15}$	$\left(kmol\,bar^{0.5}\right)/\left(kg_{cat}\,hr\right)$	243.9
K_{CO}	$8.23\text{x}10^{-5}$	bar^{-1}	–70.65
K_{H_2}	$6.12\text{x}10^{-9}$	bar^{-1}	–82.90
K_{CH_4}	$6.65\text{x}10^{-4}$	bar^{-1}	–38.28
K_{H_2O}	$1.77\text{x}10^{-4}$	dimensionless	88.68

Table 2-18: SMR Reaction Equilibrium Constants

Equilibrium Constant	Units
$K_1 = \exp\left(-26{,}830/T + 30.114\right)$	bar^2
$K_2 = \exp\left(4{,}400/T - 40.63\right)$	dimensionless
$K_3 = K_1 \cdot K_2$	bar^2

The above kinetic rates can be brought in dimensionless form, as suggested in noted earlier. In the definition of the Damkohler number the reference reaction generation rate r^* is selected as the reaction rate for $RX1$ evaluated at the reactor entrance conditions during OM1:

$$r^* \triangleq r_1\left(\left\{\frac{\left(P_{i,gv}(0,0)\right)}{RT}\right\}_{i=1}^{NC}, T\right) = \frac{k_1\left(P_{CH_4,gv}(0,0)P_{H_2O,gv}(0,0) - \frac{\left(P_{H_2,gv}(0,0)\right)^3 P_{CO,gv}(0,0)}{K_1}\right)}{\left(P_{H_2,gv}(0,0)\right)^{2.5}\left(\begin{array}{l}1 + K_{CO}P_{CO,gv}(0,0) + K_{H_2}P_{H_2,gv}(0,0) + \\ + K_{CH_4}P_{CH_4,gv}(0,0) + K_{H_2O}\dfrac{P_{H_2O,gv}(0,0)}{P_{H_2,gv}(0,0)}\end{array}\right)^2} \quad (2.1.97)$$

$$\bar{R}_1 = \frac{\dfrac{k_1}{\left(P^*\right)^{0.5}\left(\bar{P}_{H_2,gv}\right)^{2.5}}\left(\bar{P}_{CH_4,gv}\bar{P}_{H_2O,gv} - \dfrac{\left(P^*\right)^2\left(\bar{P}_{H_2,gv}\right)^3\bar{P}_{CO,gv}}{K_1}\right)}{\left(1+K_{CO}P^*\bar{P}_{CO,gv}+K_{H_2}P^*\bar{P}_{H_2,gv}+K_{CH_4}P^*\bar{P}_{CH_4,gv}+\dfrac{K_{H_2O}\bar{P}_{H_2O,gv}}{\bar{P}_{H_2,gv}}\right)^2} \Big/ r^* \tag{2.1.98}$$

$$\bar{R}_2 = \frac{\dfrac{k_2P^*}{\bar{P}^g_{H_2,gv}}\left(\bar{P}_{CO,gv}\bar{P}_{H_2O,gv} - \dfrac{\bar{P}_{H_2,gv}\bar{P}_{CO_2,gv}}{K_2}\right)}{\left(1+K_{CO}P^*\bar{P}_{CO,gv}+K_{H_2}P^*\bar{P}_{H_2,gv}+K_{CH_4}P^*\bar{P}_{CH_4,gv}+\dfrac{K_{H_2O}\bar{P}_{H_2O,gv}}{\bar{P}_{H_2,gv}}\right)^2} \Big/ r^* \tag{2.1.99}$$

$$\bar{R}_3 = \frac{\dfrac{k_3}{\left(P^*\right)^{0.5}\left(\bar{P}_{H_2,gv}\right)^{3.5}}\left(\bar{P}_{CH_4,gv}\left(\bar{P}_{H_2O,gv}\right)^2 - \dfrac{\left(P^*\right)^2\left(\bar{P}_{H_2,gv}\right)^4\bar{P}_{CO,gv}}{K_3}\right)}{\left(1+K_{CO}P^*\bar{P}_{CO,gv}+K_{H_2}P^*\bar{P}_{H_2,gv}+K_{CH_4}P^*\bar{P}_{CH_4,gv}+\dfrac{K_{H_2O}\bar{P}_{H_2O,gv}}{\bar{P}_{H_2,gv}}\right)^2} \Big/ r^* \tag{2.1.100}$$

$$\overline{\mathrm{DEN}} = 1+\bar{K}_{CO}\bar{P}_{CO,vr}+\bar{K}_{H_2}\bar{P}_{H_2,vr}+\bar{K}_{CH_4}\bar{P}_{CH_4,vr}+\frac{\bar{K}_{H_2O}\bar{P}_{H_2O,vr}}{\bar{P}_{H_2,vr}} \tag{2.1.101}$$

where

$$\left\{\begin{array}{l} \bar{K}_1 = \dfrac{K_1}{\left(P^*\right)^2},\ \bar{K}_2 = K_2,\ \bar{K}_3 = \dfrac{K_3}{\left(P^*\right)^2}, \bar{k}_1 = 1,\ \bar{k}_2 = \dfrac{\left(P^*\right)^{1.5}k_2}{k_1} = \left(P^*\right)^{1.5},\ \bar{k}_3 = \dfrac{k_3}{k_1} \\ \bar{K}_{CO} = K_{CO}P^*,\ \bar{K}_{H_2} = K_{H_2}P^*,\ \bar{K}_{CH_4} = K_{CH_4}P^*,\ \bar{K}_{H_2O} = K_{H_2O} \end{array}\right\} \tag{2.1.102}$$

Table 2-19 Parameters values used in simulations

Parameter	Value	Dimension
Density of catalyst	2355.2	$\frac{kg}{m^3}$
Density of storage medium	1220.1	$\frac{kg}{m^3}$
Thermal conductivity catalyst	25	$\frac{W}{mK}$
Thermal conductivity storage medium	25	$\frac{W}{m\,K}$
Heat capacity of catalyst	1050	$\frac{J}{kg\,K}$
Heat capacity of storage medium	1050	$\frac{J}{kg\,K}$

Table 2-20 Initial and boundary conditions

Initial Conditions	Boundary Conditions
$\left.\begin{aligned}\bar{c}_{i,vr} &= \left(\bar{c}_{i,vr}\right)_{in}\\ \bar{c}_{i,vs} &= \left(\bar{c}_{i,vs}\right)_{in}\\ \bar{T}_r &= \left(\bar{T}\right)_{in}\\ \bar{P}_{vr} &= \left(\bar{P}_{vr}\right)_{in}\end{aligned}\right\}$	$\left.\begin{aligned}\bar{c}_{i,vr} &= \left(\bar{c}_{i,vr}\right)_{in,k}\\ \bar{c}_{i,vs} &= \left(\bar{c}_{i,vs}\right)_{in,k}\\ \bar{T}_r &= \left(\bar{T}_r\right)_{in,k}\\ \bar{P}_{vr} &= \left(\bar{P}_{vr}\right)_{in,k}\end{aligned}\right\}$ for $z = 0$, OP=k, $\left.\begin{aligned}\vec{\bar{N}}^{\dagger}_{i,vr} &= 0\\ \nabla\bar{T}_r &= 0\end{aligned}\right\}$ for $z = h$

Table 2-21 Reactor Concentration Boundary Conditions by Phase

Description	Value	Description	Value	Description	Value
$\left(\bar{c}_{CH_4,vr}\right)_{in,1}$	0.25	$\left(\bar{c}_{CH_4,vr}\right)_{in,2}$	0.0	$\left(\bar{c}_{CH_4,vr}\right)_{in,3}$	0.0

$\left(\overline{c}_{CO,vr}\right)_{in,1}$	0.001	$\left(\overline{c}_{CO,vr}\right)_{in,2}$	0.0	$\left(\overline{c}_{CO,vr}\right)_{in,3}$	0.0
$\left(\overline{c}_{CO_2,vr}\right)_{in,1}$	0.001	$\left(\overline{c}_{CO_2,vr}\right)_{in,2}$	0.0	$\left(\overline{c}_{CO_2,vr}\right)_{in,3}$	0.0
$\left(\overline{c}_{H_2O,vr}\right)_{in,1}$	0.747	$\left(\overline{c}_{H_2O,vr}\right)_{in,2}$	0.70	$\left(\overline{c}_{H_2O,vr}\right)_{in,3}$	1
$\left(\overline{c}_{H_2,vr}\right)_{in,1}$	0.001	$\left(\overline{c}_{H_2,vr}\right)_{in,2}$	0.30	$\left(\overline{c}_{H_2,vr}\right)_{in,3}$	0.0

The PPSO of the SMR-MSR is carried out in three distinct operating modes: OM 1 (Loading-Reaction/Storage), OM 2 (Decarbonization/Maintenance), and OM 3 (Unloading-Production/Emptying) each of which is characterized by different processes occurring in the (v) and (s) domains. These three OMs have a time duration designated as τ_1, τ_2, and τ_3, as described next and shown in the Figure 1 below.

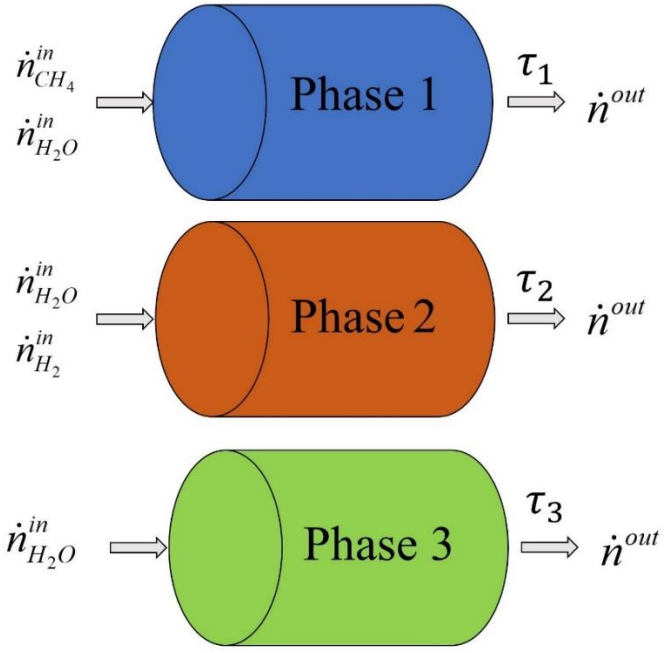

Figure 2-31: Conceptual sketch of the SR-MSR model.

OM 1: MSR Loading-Reaction/Storage Phase

At the beginning of this OM, phase (g) in domain (v) is largely composed of steam and minute amounts of hydrogen, phase (g) in domain (s) only contains hydrogen at a pressure slightly above the partial pressure of hydrogen in (v), and a mixture of methane and steam at a constant flowrate is fed into the MSR. During this OM, the hydrogen that is produced from the SMR reactions taking place begins to permeate into (s) as its partial pressure in (v) increases above the total pressure of (s).The duration τ_1 of OM 1 is chosen so that a desirable level of limiting reactant conversion is attained. Reactant conversion, as defined by Equation , is defined over all three OMs. Typically, however, the limiting reactant is fed to the MSR only during OM 1, whereas any unreacted limiting reactant exits the MSR during OM 1 and OM 2. Thus, the duration τ_1 of OM 1 is the only degree of freedom that can be chosen so that the amount of unreacted limiting reactant that exits the MSR over $\tau_1 + \tau_2$ (i.e., over the duration of OM 1 and OM 2) is acceptably low, compared to the amount of limiting reactant fed to the MSR during OM 1, so that a desirable level of limiting reactant conversion can be attained.

OM 2: MSR Decarbonization/Maintenance Phase

OM 2 begins at the final conditions of OM, and the feed is switched to a mixture of steam and hydrogen, the composition of which is selected so that the partial pressure of hydrogen in (g) is above the hydrogen pressure in (s) so as to maintain the stored hydrogen in (s). Thus (g) is decarbonized, until its contents essentially consist of steam and hydrogen. When a reactor is operating under packed bed flow conditions with diffusional effects, as is the case here, there

will no longer a sharp steam front propagating through the reactor, and thus the duration τ_2 of OM 2 is chosen to be the time at which the function:

$$\bar{P}_{C,gv}(\bar{t}) \triangleq \bar{P}_{\mathrm{CO}_2,gv}(\bar{t}) + \bar{P}^{g}_{\mathrm{CH}_4,gv}(\bar{t}) + \bar{P}^{g}_{\mathrm{CO},gv}(\bar{t}) \tag{2.1.103}$$

is brought below a predefined decarbonization limit (e.g. 0.01). This selection determines the level of carbon impurities in the H_2 product generated during phase 3.

OM 3: MSR Unloading-Production/Emptying Phase

Similarly, OM 3 begins at the final conditions of OM 2, and the reactor is fed pure steam at a constant flowrate. This action empties the contents of (s) back into (v), generating a mixture of readily separable, high-pressure hydrogen and steam as the SMR-MSR product. the duration of OM 3 is selected as the time $\bar{\tau}_3$ at which the dimensionless partial pressure of hydrogen in domain (v) at the reactor exit falls below a set value, e.g.,

$\bar{P}_{\mathrm{H}_2,gv}\left(\bar{\tau}_1 + \bar{\tau}_2 + \bar{\tau}_3, 1\right) \le 0.01$, which ensures that most of the hydrogen in both domains (v) and (s) has been removed and thus the reactor is largely filled with unreacted steam.

To compare the performance of the SMR-MSR under PPSO with that of a traditional SMR-SSR, we utilized the process performance metrics defined above, for the SMR case study. To this end, identifying methane as our limiting reactant, Equation (2.1.90) becomes:

$$X_{CH_4} = \frac{\left[\int_0^{\sum_{k=1}^{NOM}\bar{\tau}_k} \bar{F}_{CH_4,gv}(\bar{t}',0)d\bar{t}' - \int_0^{\sum_{k=1}^{NOM}\bar{\tau}_k} \bar{F}_{CH_4,gv}(\bar{t}',1)d\bar{t}'\right]}{\int_0^{\sum_{k=1}^{NOM}\bar{\tau}_k} \bar{F}_{CH_4,gv}(\bar{t}',0)d\bar{t}'} \tag{2.1.104}$$

Similarly, the equations for the rest of the metrics can be expressed for all products (carbon monoxide, carbon dioxide, and hydrogen), and are listed below for hydrogen.

$$\omega_{H_2,1} \triangleq \frac{\left[\int_0^{\bar{\tau}_1} \bar{F}_{H_2,gv}(\bar{t}',1)d\bar{t}' - \int_0^{\bar{\tau}_1} \bar{F}_{H_2,gv}(\bar{t}',0)d\bar{t}'\right]}{\int_0^{\sum_{k=1}^{NOM}\bar{\tau}_k} \bar{F}_{CH_4,gv}(\bar{t}',0)d\bar{t}'} \tag{2.1.105}$$

$$\Omega_{H_2} = \frac{\left[\int_0^{\sum_{k=1}^{NOM}\bar{\tau}_k} \bar{F}_{H_2,gv}(\bar{t}',1)d\bar{t}' - \int_0^{\sum_{k=1}^{NOM}\bar{\tau}_k} \bar{F}_{H_2,gv}(\bar{t}',0)d\bar{t}'\right]}{\int_0^{\sum_{k=1}^{NOM}\bar{\tau}_k} \bar{F}_{CH_4,gv}(\bar{t}',0)d\bar{t}'} \tag{2.1.106}$$

$$R_{H_2,3} = \frac{\omega_{H_2,3}}{\Omega_{H_2}} = \frac{\left[\int_{\bar{\tau}_1+\bar{\tau}_2}^{\bar{\tau}_1+\bar{\tau}_2+\bar{\tau}_3} \bar{F}_{H_2,gv}(\bar{t}',1)d\bar{t}' - \int_{\bar{\tau}_1+\bar{\tau}_2}^{\bar{\tau}_1+\bar{\tau}_2+\bar{\tau}_3} \bar{F}_{H_2,gv}(\bar{t}',0)d\bar{t}'\right]}{\left[\int_0^{\bar{\tau}_1+\bar{\tau}_2+\bar{\tau}_3} \bar{F}_{H_2,gv}(\bar{t}',1)d\bar{t}' - \int_0^{\bar{\tau}_1+\bar{\tau}_2+\bar{\tau}_3} \bar{F}_{H_2,gv}(\bar{t}',0)d\bar{t}'\right]} \tag{2.1.107}$$

Equation (2.1.105) captures the H_2 molar production ratio in OM 1 over the total amount of methane fed. Equation (2.1.106) describes the hydrogen yield over all three OM's, i.e, the total moles of hydrogen produced divided by the moles of methane fed to the reactor. Lastly, Equation (2.1.107) is used to calculate the hydrogen recovery ratio during the 3rd OM, which is of importance as it quantifies how much hydrogen is produced in readily purifiable form.

Simulation of the dimensionless equations () of the MSR model requires that a number of model parameters first be specified. It is considered that the inlet reactor temperature and wall temperature are $T_{in} = 800K$ and $T_w = 950$ respectively, and the MSR feed at the beginning of OM 1 contains steam and methane at a molar ratio of 3, and minute amounts of all other species.

Knowledge of these parameters enables the computation of the reference reaction generation rate r^* and expression of the dimensionless reaction rates $\bar{R}_1, \bar{R}_2, \bar{R}_3$ in terms of the dimensionless species pressures. We carry out a parametric study with three different selections of the storage domain, catalyst domain, and gas phase in storage domain volume fractions as $\{\varepsilon_v = 0.35, \varepsilon_c = 0.20, \varepsilon_s = 0.45\}$, $\{\varepsilon_v = 0.27, \varepsilon_c = 0.4, \varepsilon_s = 0.33\}$, and $\{\varepsilon_v = 0.25, \varepsilon_c = 0.30, \varepsilon_s = 0.45\}$, along with an effectiveness factor as $\eta = 0.5$, and a gas permeance ratios for all species (the first species being hydrogen) as $\beta_j / \beta_1 = \begin{Bmatrix} 0 & if\ j \neq 1 \\ 1 & if\ j = 1 \end{Bmatrix}$ enables the simulation of dimensionless equations of the MSR model as long as the values of the parameters $D_a, \Theta, \bar{\tau}_1, \bar{\tau}_2, \bar{\tau}_3$ are known.

In this work, assessment of SMR-MSR performance was performed by carrying out thirty two combinations (trials) of the above five parameters, as listed in Table 3- below. The values for D_a and Θ were chosen by selecting a range of reasonable values for the parameters shown in above. Letting the operating pressure obtain values in the range $P^* \in \left[10(bar), 26(bar)\right]$, inlet temperature $T^* = 800(K)$, catalyst density $\rho_c = 2355.2\left(kg/m^3\right)$, the resulting D_a range is $1 \leq D_a \leq 30$. Evaluation of a range for Θ requires range information for the species membrane permeance $\beta_i \left(\frac{mol\, i}{Pa \cdot \left(m^2\, void - storage\, interface\right) \cdot s} \right)$ and the storage-void interfacial area per unit volume of reactor $\alpha_{s,v} \left(\frac{m^2\ storage - void\ interface}{m^3\ system\, r} \right)$. The β_1 range is

$1.05\cdot10^{-8} \le \beta_1 \le 1.21\cdot10^{-6}$ for hydrogen, and the $\alpha_{s,v}$ range is selected so that the resulting Θ range is $1 \le \Theta \le 50$.

Each trial was simulated in COMSOL for 3 cycles of operation, in order to ensure that dynamic operation had reached its long term periodic behavior. COMSOL implementation of the alternating feed compositions for each OM was carried out by approximating for each OM an OM-specific Heaviside function h_k with an OM-specific Verhulst function, W_k,: as shown in the equation below:

$$h_k\left(\bar{t}\right) = \left\{ \begin{array}{ll} 0, & \text{if } \left(\bar{t} - \sum_{k'=0}^{k-1} \bar{\tau}_{k'} < 0\right) \\ [0,1], & \text{if } \left(\bar{t} - \sum_{k'=0}^{k-1} \bar{\tau}_{k'} = 0\right) \\ 1, & \text{if } \left(\bar{t} - \sum_{k'=0}^{k-1} \bar{\tau}_{k'} > 0\right) \end{array} \right\} \approx W_k\left(\bar{t}\right) = -\frac{1}{1+\exp\left(-a\cdot\left(\bar{t} - \sum_{k'=0}^{k-1} \bar{\tau}_{k'}\right) + a\cdot c\right)},\ k = 1, NOM$$

(2.1.108)

Fig. 1 below illustrates the dynamic behavior of the methane inlet partial pressure at the reactor inlet as a function of dimensionless time, considering $\bar{\tau}_1 = \bar{\tau}_2 = \bar{\tau}_3 = 5$, $a = 1$ and $c = 8.5$.

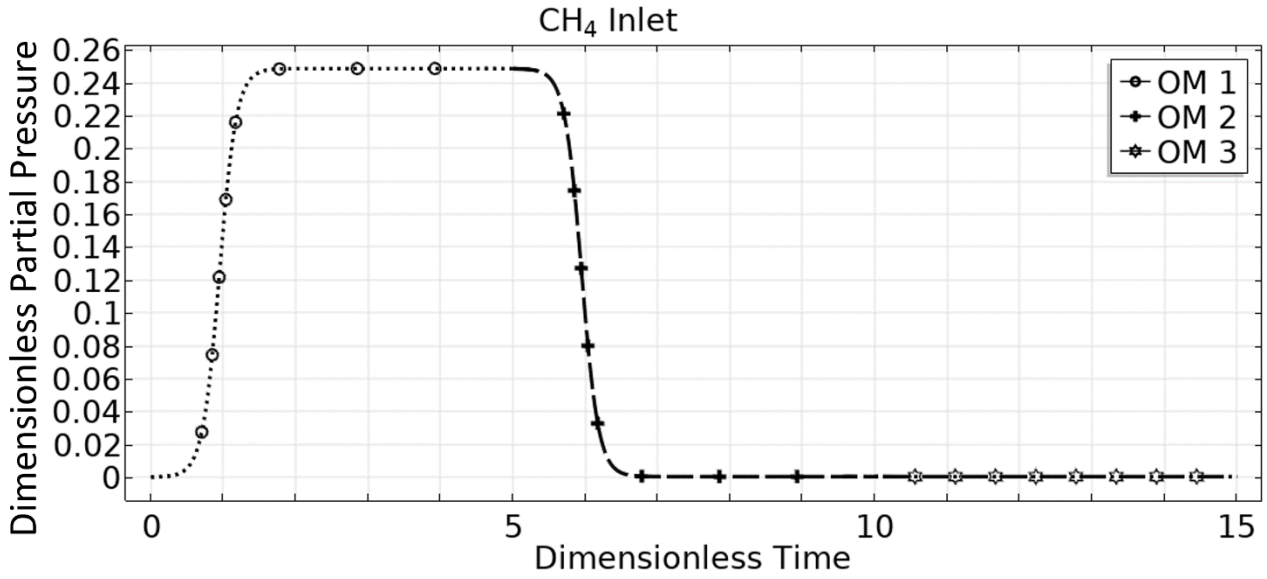

Figure 2-32 - Methane dimensionless partial pressure at reactor inlet for $\bar{\tau}_1 = \bar{\tau}_2 = \bar{\tau}_3 = 5, a = 1, c = 8.5$

Figure 2-33 shows the time evolution of all species', aside from hydrogen, dimensionless partial pressures at the reactor inlet over three operating cycles. It is assumed that the conditions at the inlet of the reactor at the beginning of OM 1 is the same as its condition at the end of OM 3. During OM 1, the reactor's feed consists mainly of steam and methane, at a 3:1 steam/methane ratio, and trace amounts of carbon monoxide and carbon dioxide. During OM 2 and OM 3 the reactor's feed consists only of steam. Similarly, Figure 3-34 shows the time evolution of species dimensionless partial pressures at the outlet of the reactor through the same three cycles of operation. Because the reactor's condition at the beginning of OM 1 is the same as its condition at the end of OM 3, at early operational times the reactor outlet consists mainly of steam. As the reaction proceeds, a mixture of methane, carbon dioxide, and carbon monoxide begins to exit the reactor. The hydrogen in the void domain continues to rise until it reaches its peak, which coincides with the end of OM 2.

Figures 2-35, 2-36, 2-37, and 2-38 show the time evolution of the dimensionless partial pressure of methane, carbon dioxide, carbon monoxide, hydrogen, and hydrogen in the storage at

three different reactor locations, 25%, 50%, 75%, and 100% respectively, during the last cycle of operation. Analyzing the behavior of hydrogen from these figures it can be seen that at the 25% length the hydrogen concentration in the void domain is initially practically zero at early cycle times. As methane reacts to generate hydrogen in the reactor domain it is transported into the storage and this is shown by a marked increase in hydrogen storage concentration. At the end of the reactor cycle when only steam is being fed, the hydrogen concentration in the storage decreases as it is evacuated back into the reactor domain. The figures also elucidate the behavior of methane and carbon dioxide, which are shown to first increase, reach a maximum, and then decrease, in correspondence with the composition changes at the inlet of the reactor shown in Figure 2-33. The methane (carbon dioxide) maximum occurs at the latter (earlier) part of a plateau-like region in time. At points further down the reactor (50%, 75%, and 100% of the reactor length), the methane (carbon dioxide) pulse exhibits a progressively lower (higher) maximum, which is indicative of its role as a reactant (product) in the reaction that takes place. The magnitude of the methane pulse remains larger than that of the carbon dioxide pulse until it reaches the end of the reactor, where it can be seen that the dimensionless partial pressure of carbon dioxide is slightly larger than that of methane.

Figures 2-39 , 2-40, and 2-41 show the dimensionless partial pressure profiles for all species along the length of the reactor at the end of OM 1, OM 2, and OM 3, respectively, for the nth trial $D_a =, \Theta =$. In these simulations we selected the end of OM 1 to be when $\overline{P}_{CH_4,gv}\big|_{\overline{z}=0.25} = 0.1$ occurs for an operating time for the first OM of $\overline{\tau}_1 = 0.141$. From Figure 2-39 one observes that the contents of the reactor void domain up to point $\left(z^* = 0.25\right)$ contain a mixture of reforming products, whereas at larger reactor lengths there exists only water. From

the reactor inlet $\left(z^* = 0\right)$ to $\left(z^* = 0.25\right)$, the dimensionless partial pressure of the hydrogen in the storage shows a marked difference from the dimensionless partial pressure of hydrogen in the reactor void, which highlights the time-dependent nature of the process. As seen later in the analysis of the influence of the parameter Θ, reducing this difference during early operational times correlates to higher conversion and better overall reactor performance. Figures 2-40 and 2-41 show the corresponding profiles at the end of OM 2 with $\overline{\tau}_2 = 0.309$, and at the end of OM 3 with $\overline{\tau}_3 = 1.758$, respectively. From Figure 2-40 one sees that at the end of OM 2 the reactor void contains a mixture of steam and hydrogen only, and that hydrogen has been successfully transferred to and stored in the storage domain. From Figure 2-41 one sees that, at the end of a cycle of operation, the reactor has returned to its initial state of operation, with the reactor void being filled with only steam and the contents of the storage medium having been emptied.

Figure 2-42 similarly shows the dimensionless temperature profile along the length of the reactor at the end of OM 1, OM 2, and OM 3, respectively, for the first trial $D_a = 1.33$, $\Theta = 5.39$. All three operating modes reach the same final temperature at the end of the reactor, but there can be seen some small differences at shorter reactor lengths, with OM1 having the highest temperature due to the endothermicity of the SMR reaction taking place. The temperature profile at the end of OM3 shows the greatest difference between the other two operating modes, with a noticeably lower temperature profile until about 70% down the reactor length. It is also apparent that the reactor gas never reaches the wall temperature.

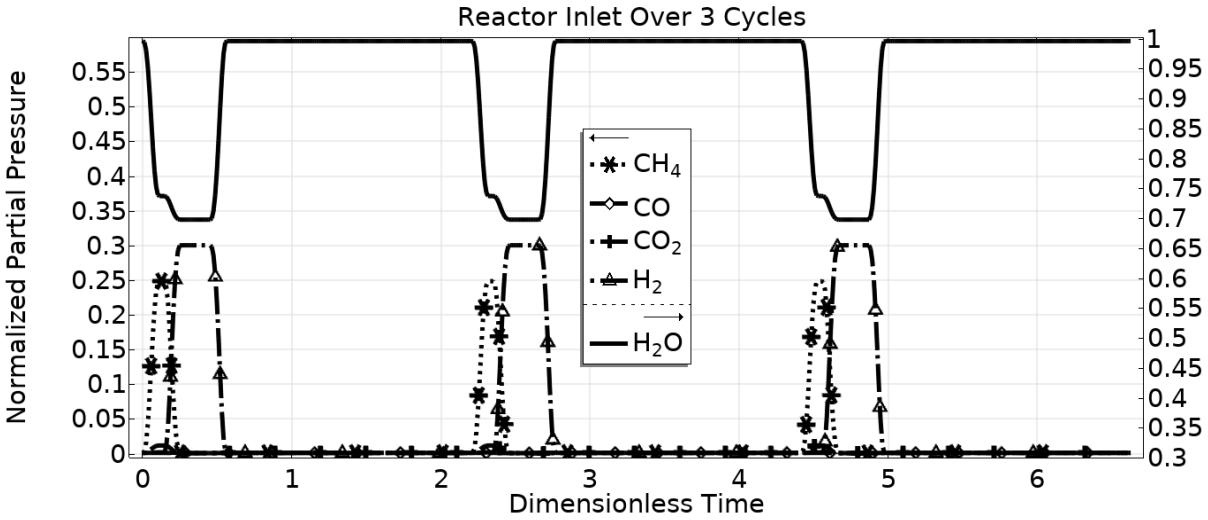

Figure 2-33 Dimensionless time evolution of species' dimensionless partial pressure at reactor inlet over 3 cycles of operation for Da =1.33 , Θ =5.39 .

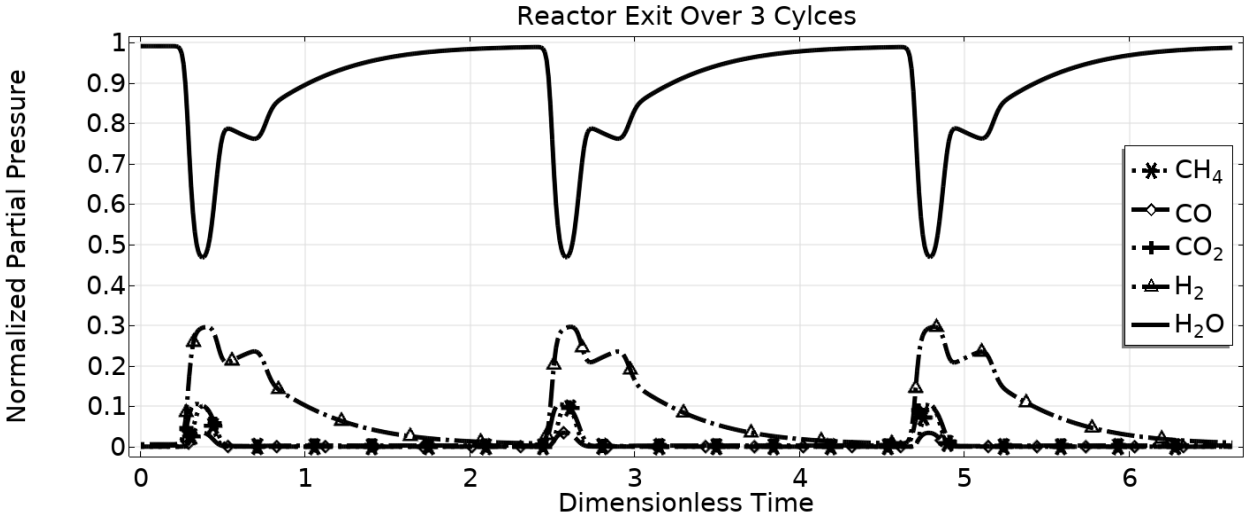

Figure 2-34 Dimensionless time evolution of species' dimensionless partial pressure at reactor outlet over 3 cycles of operation for Da =1.33 , Θ =5.39.

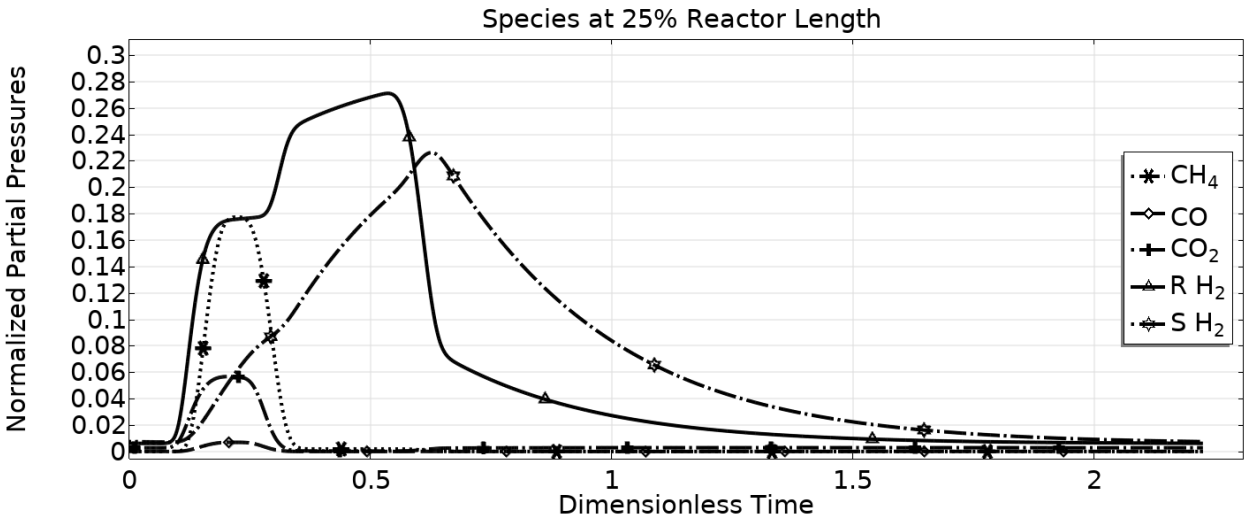

Figure 2-35 Dimensionless time evolution of species during the last cycle at 25% reactor length for Da =1.33 , Θ =5.39

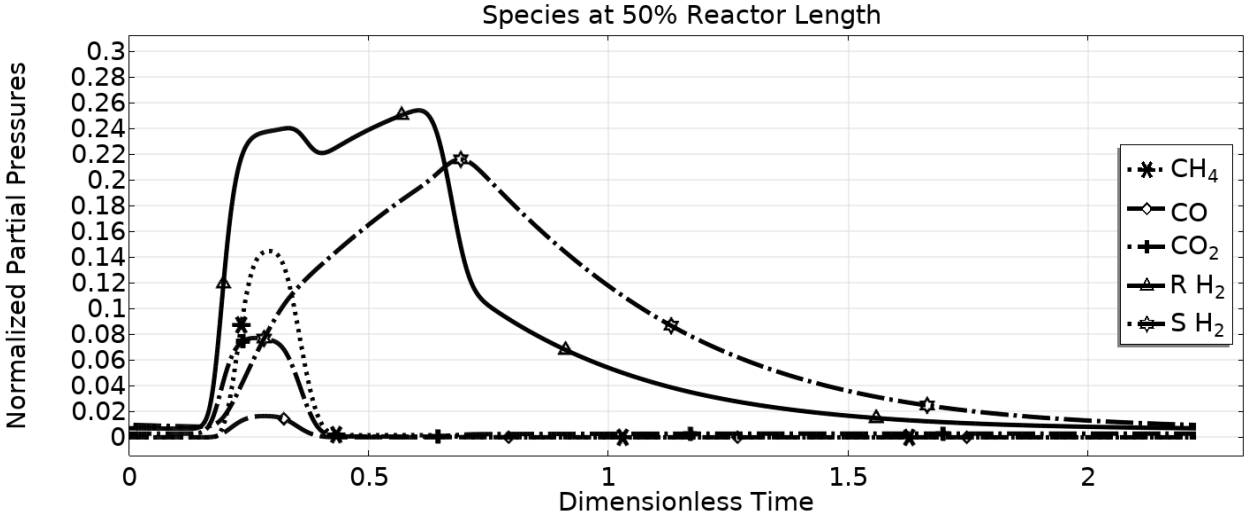

Figure 2-36 Dimensionless time evolution of species during the last cycle at 50% reactor length for Da =1.33 , Θ =5.39

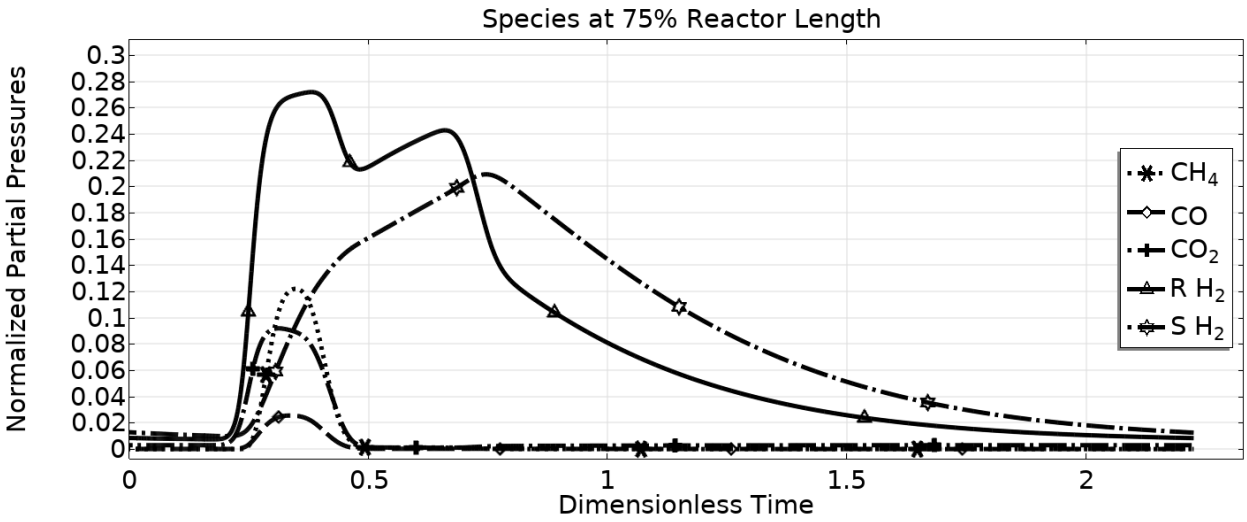

Figure 2-37 Dimensionless time evolution of species during the last cycle at 75% reactor length for Da =1.33 , Θ =5.39

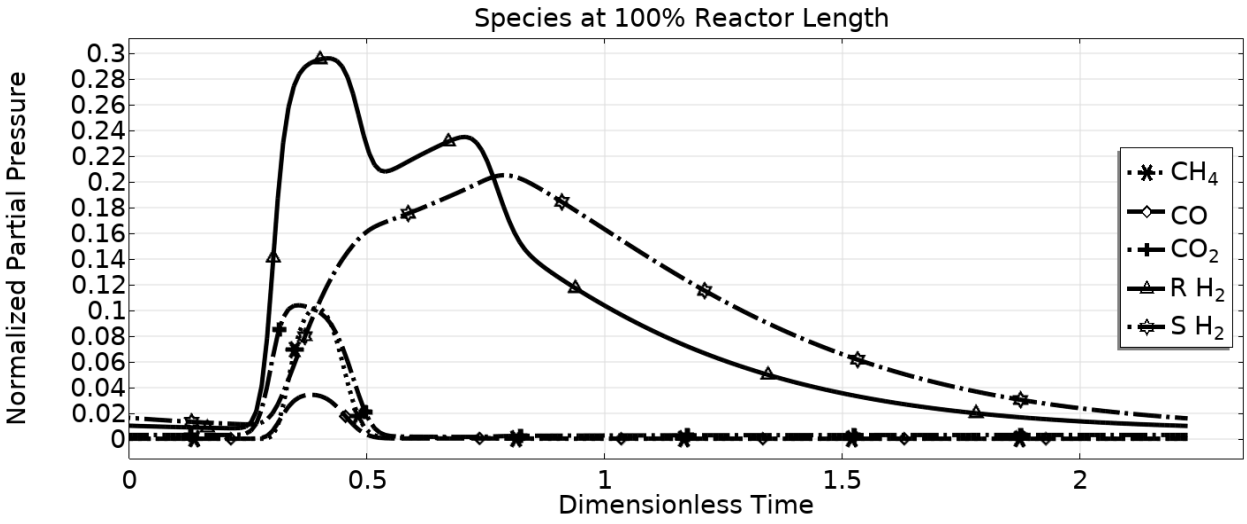

Figure 2-38 Dimensionless time evolution of species during the last cycle at 100% reactor length for Da =1.33 , Θ =5.39

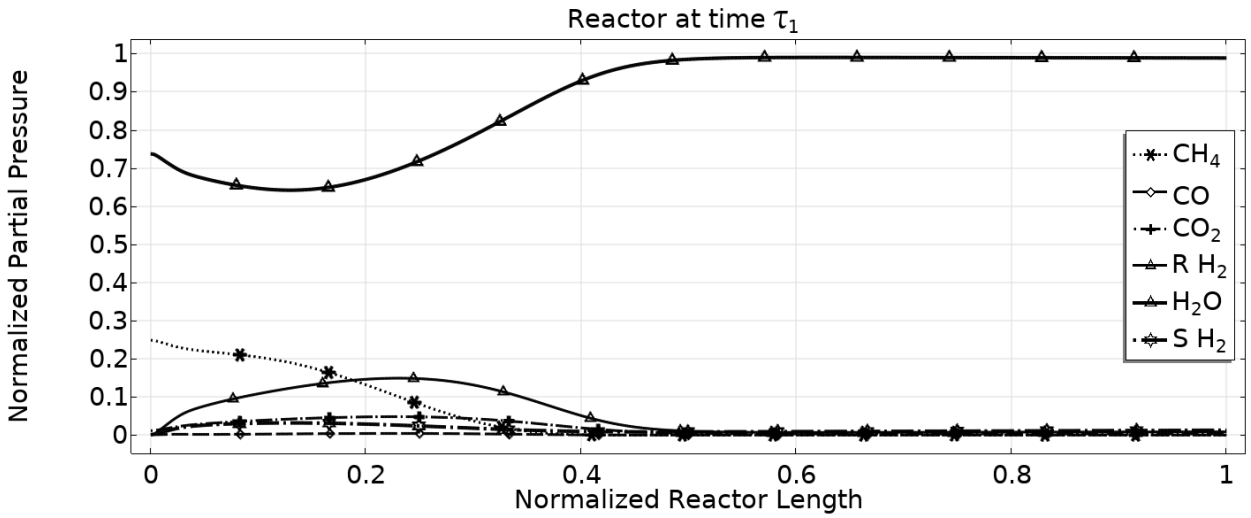

Figure 2-39 Species' dimensionless partial pressure axial length profile during cycle 3 at the end of OM 1 for Da =1.33 , Θ =5.39.

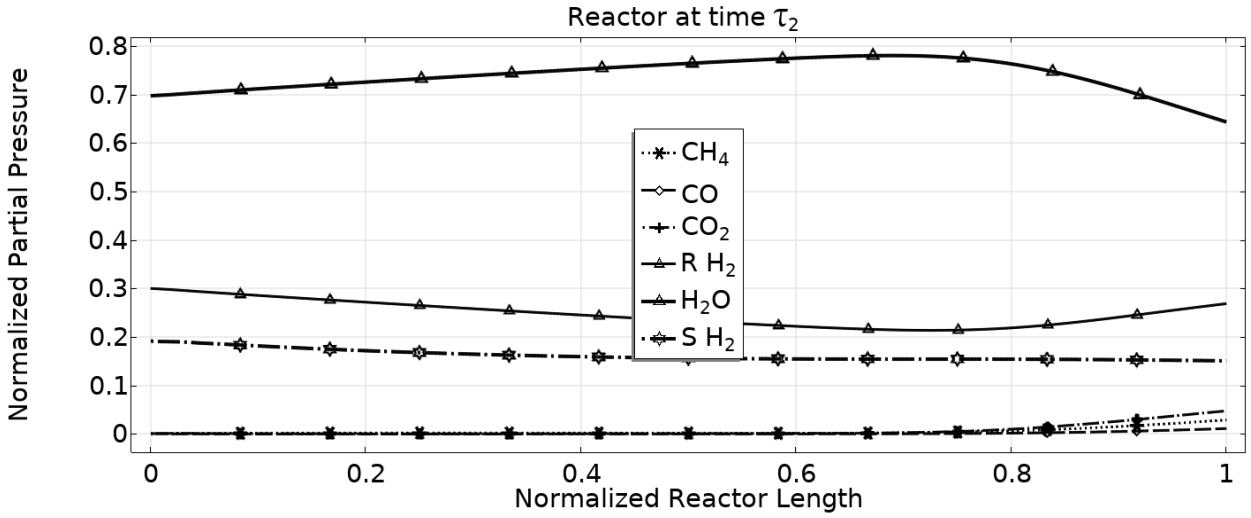

Figure 2-40 Species' dimensionless partial pressure axial length profile during cycle 3 at the end of OM 2 for Da =1.33 , Θ =5.39.

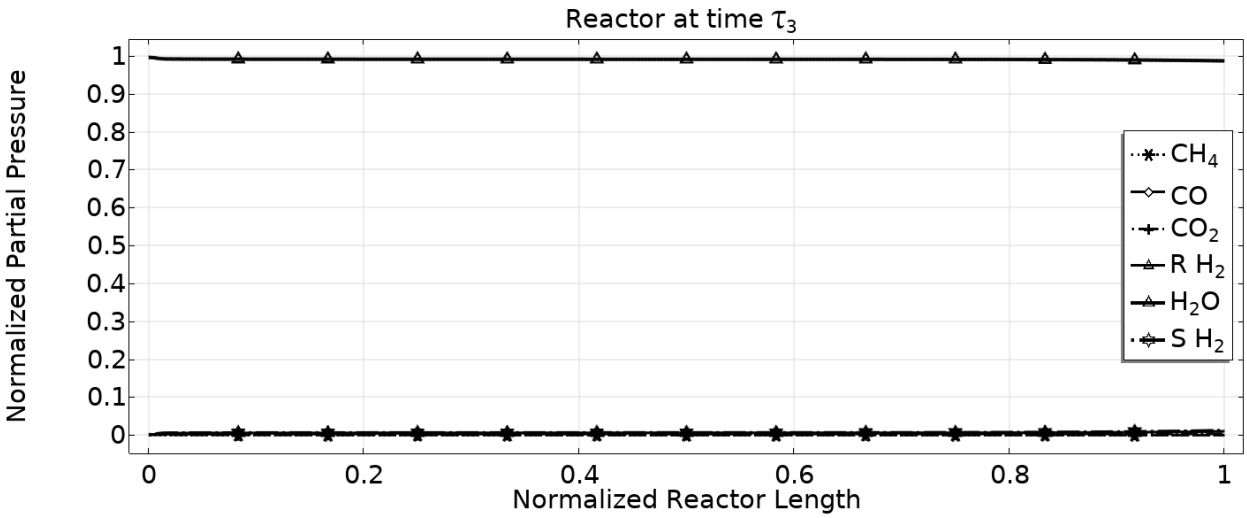

Figure 2-41 Species' dimensionless partial pressure axial length profile during cycle 3 at the end of OM 3 for Da =1.33 , Θ =5.39

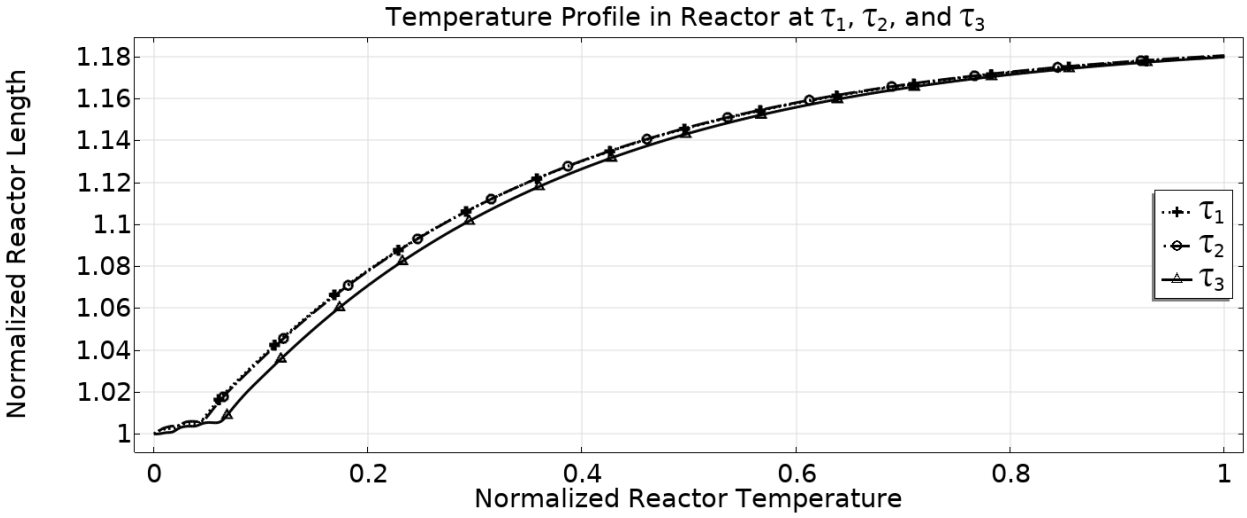

Figure 2-42 Species' dimensionless temperature profile in reactor at the end of OM1, OM2 and OM3 for Da =1.33 , Θ =5.39

With the operating times for each OM set, it is now possible to calculate the metrics as described above. These are shown for the different cases studied in Table 2-22. The SMR-MSR shows higher overall conversion than the traditional SMR-SSR for all cases studied. For the case studies conducted here a maximum increase in methane conversion of 120.5% was observed, indicating the significant benefit that can be gained by appropriately selecting design parameters. The substantial increases in conversion are accompanied by simultaneous significant gains in

hydrogen yield. In addition, the SMR-MSR enables the in situ separation of the hydrogen product, which is a distinct advantage over the traditional SMR-SSR that requires an additional downstream separation step.

Table 2-22 Performance metric comparison for SMR-MSR and SMR-SSR for 32 trials.

$\varepsilon_v = 0.35$, $\varepsilon_c = 0.20$, $\varepsilon_s = 0.45$, $\Theta \leq 50$								
Trial	D_a	Θ	Ψ_4	SR X_{CH_4}	SS X_{CH_4}	SR Y_{H_2}	SS Y_{H_2}	$R_{H_2,rec}$
1	1.330	5.392		0.640	0.387	2.513	1.450	0.646
2	1.333	49.405	0.355	0.752	0.397	2.893	1.483	0.701
3	1.476	16.057	0.382	0.754	0.407	2.904	1.519	0.669
4	1.541	39.963	0.413	0.769	0.407	2.964	1.519	0.719
5	1.552	44.577	0.401	0.769	0.397	2.974	1.483	0.741
6	1.686	20.311	0.523	0.746	0.397	2.906	1.483	0.756
7	1.797	29.658	0.484	0.785	0.419	3.031	1.558	0.730
8	2.220	24.150	0.761	0.788	0.407	3.076	1.519	0.795
9	2.437	9.935	1.065	0.714	0.387	2.828	1.450	0.794
10	5.236	29.779	1.869	0.896	0.478	3.503	1.764	0.841
11	5.314	35.258	2.212	0.901	0.460	3.537	1.704	0.862
12	5.549	5.392	1.232	0.852	0.550	3.245	2.008	0.624
13	5.617	14.984	3.057	0.840	0.431	3.301	1.602	0.849
14	5.677	9.935	2.073	0.827	0.478	3.237	1.764	0.795
15	5.939	24.212	5.315	0.853	0.387	3.366	1.450	0.893
16	6.002	20.088	4.374	0.853	0.407	3.358	1.519	0.877
17	6.153	49.880	1.901	0.924	0.498	3.608	1.834	0.851
18	9.333	49.880	3.087	0.929	0.550	3.596	2.008	0.838
19	9.841	20.088	6.546	0.904	0.460	3.553	1.704	0.881
20	10.153	30.467	10.517	0.912	0.419	3.601	1.558	0.910
21	10.166	14.984	5.077	0.898	0.498	3.510	1.834	0.850
22	10.224	9.935	3.945	0.873	0.550	3.372	2.008	0.777
23	10.314	24.212	8.311	0.912	0.445	3.590	1.650	0.896
24	14.759	25.826	11.437	0.929	0.478	3.646	1.764	0.894
25	14.925	30.467	15.405	0.935	0.460	3.679	1.704	0.907
26	15.420	14.984	10.905	0.869	0.550	3.339	2.008	0.800
27	15.420	48.697	9.724	0.932	0.550	3.629	2.008	0.870
28	17.664	17.164	14.327	0.876	0.550	3.368	2.008	0.812
29	19.943	24.212	18.941	0.917	0.522	3.569	1.914	0.870
30	22.051	21.427	19.270	0.889	0.550	3.430	2.008	0.832
31	24.917	24.212	27.430	0.900	0.550	3.473	2.008	0.844
32	26.578	25.826	27.206	0.903	0.550	3.491	2.008	0.850

Table 2-23: OM dimensionless duration times for 32 trials.

$\varepsilon_v = 0.35$, $\varepsilon_c = 0.20$, $\varepsilon_s = 0.45$, $\Theta \leq 50$						
Trial	D_a	Θ	Ψ_4	$\overline{\tau}_1$	$\overline{\tau}_2$	$\overline{\tau}_3$
1	1.330	5.392		0.141	0.309	1.758
2	1.333	49.405	0.355	0.149	0.298	0.905
3	1.476	16.057	0.382	0.149	0.298	1.192
4	1.541	39.963	0.413	0.148	0.302	0.961
5	1.552	44.577	0.401	0.141	0.297	0.936
6	1.686	20.311	0.523	0.137	0.317	1.194
7	1.797	29.658	0.484	0.146	0.305	1.042
8	2.220	24.150	0.761	0.131	0.320	1.164
9	2.437	9.935	1.065	0.118	0.322	1.529
10	5.236	29.779	1.869	0.133	0.317	1.115
11	5.314	35.258	2.212	0.125	0.318	1.082
12	5.549	5.392	1.232	0.166	0.295	1.736
13	5.617	14.984	3.057	0.110	0.316	1.354
14	5.677	9.935	2.073	0.126	0.317	1.524
15	5.939	24.212	5.315	0.099	0.312	1.187
16	6.002	20.088	4.374	0.103	0.313	1.248
17	6.153	49.880	1.901	0.139	0.312	0.986
18	9.333	49.880	3.087	0.167	0.309	0.983
19	9.841	20.088	6.546	0.108	0.312	1.248
20	10.153	30.467	10.517	0.100	0.309	1.121
21	10.166	14.984	5.077	0.119	0.315	1.357
22	10.224	9.935	3.945	0.153	0.315	1.528
23	10.314	24.212	8.311	0.104	0.311	1.188
24	14.759	25.826	11.437	0.116	0.309	1.168
25	14.925	30.467	15.405	0.110	0.309	1.122
26	15.420	14.984	10.905	0.189	0.312	1.362
27	15.420	48.697	9.724	0.170	0.312	1.018
28	17.664	17.164	14.327	0.190	0.311	1.310
29	19.943	24.212	18.941	0.148	0.309	1.192
30	22.051	21.427	19.270	0.187	0.308	1.230
31	24.917	24.212	27.430	0.183	0.309	1.193
32	26.578	25.826	27.206	0.182	0.307	1.172

In all experimental trials, only Ψ_4 is varied as the temperature of the reactor wall is not varied, and as such, we only report and comment on how its changing value affects reactor

performance. It should also be noted that for the trials in this study, Ψ_4 cannot be varied independently from D_a, and therefore its full impact is not quantified. The effect of Θ (the inverse Peclet number) on reactor performance can also be seen in the operational time and performance metrics shown in Table 2-22, with an increase in all metrics shown for increasing Θ. However, in contrast to our previous isobaric/isothermal model, it appears that conversion is much more sensitive to both D_a and Θ. The magnitude of Θ can be seen to have the largest impact on reducing $\bar{\tau}_3$ and increasing $R_{H_2,rec}$. The cases with the lowest Θ value studied are characterized by smaller increases in methane conversion and hydrogen yield over their traditional reactor counterparts, and lower recovery ratios, suggesting a lower limit threshold of $\Theta > 1$ for desirable SMR-SSR performance. For a values of $D_a \pm 0.1$, as Θ increases, operational times $\bar{\tau}_3$ in OM 3 decrease. These beneficial changes in OM duration times, coupled with the increase in the hydrogen recovery ratio as Θ increases (for fixed value of D_a), suggest that Θ should be increased as much as possible in order to achieve desirable reactor performance.

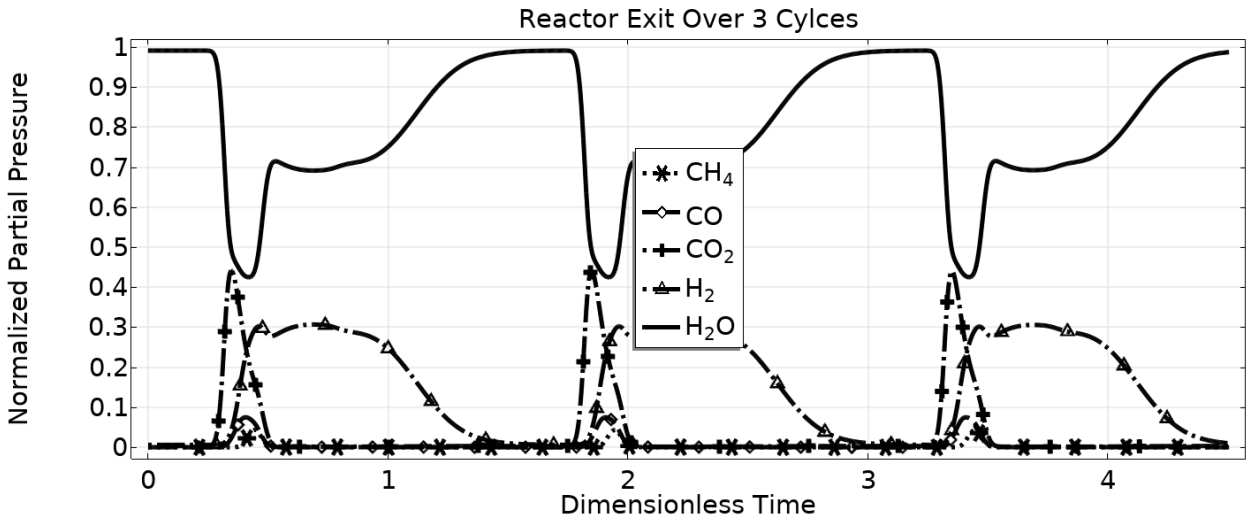

Figure 2-43 Dimensionless time evolution of species' dimensionless partial pressure at reactor outlet over 3 cycles of operation for Da =15.42 , Θ =48.70.

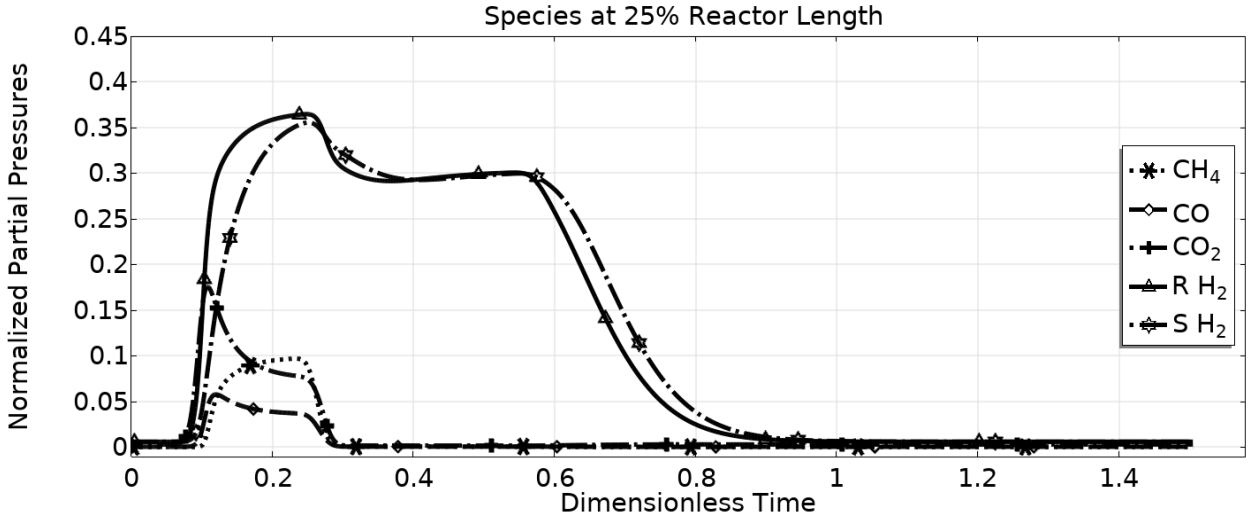

Figure 2-44 Dimensionless time evolution of species during the last cycle at 25% reactor length for Da =15.42 , Θ =48.70.

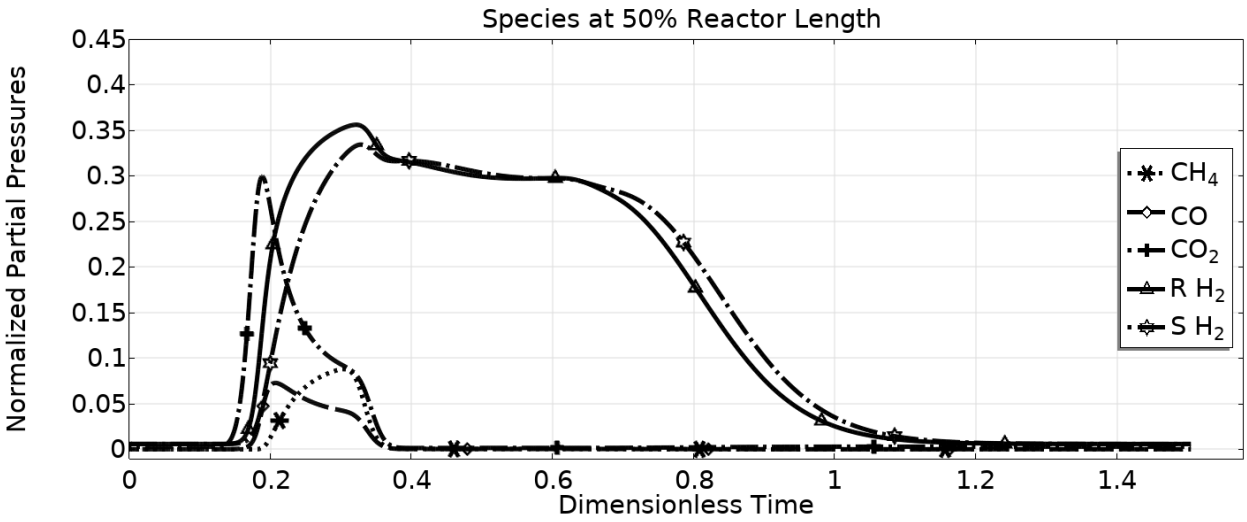

Figure 2-45 Dimensionless time evolution of species during the last cycle at 50% reactor length for Da =15.42 , Θ =48.70.

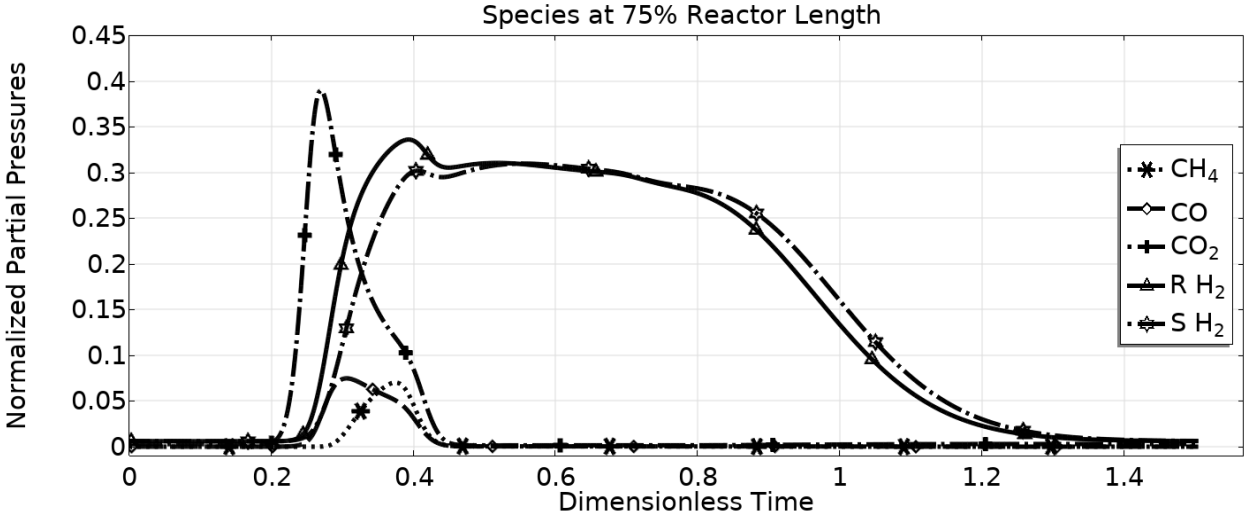

Figure 2-46 Dimensionless time evolution of species during the last cycle at 75% reactor length for Da =15.42 , Θ =48.70.

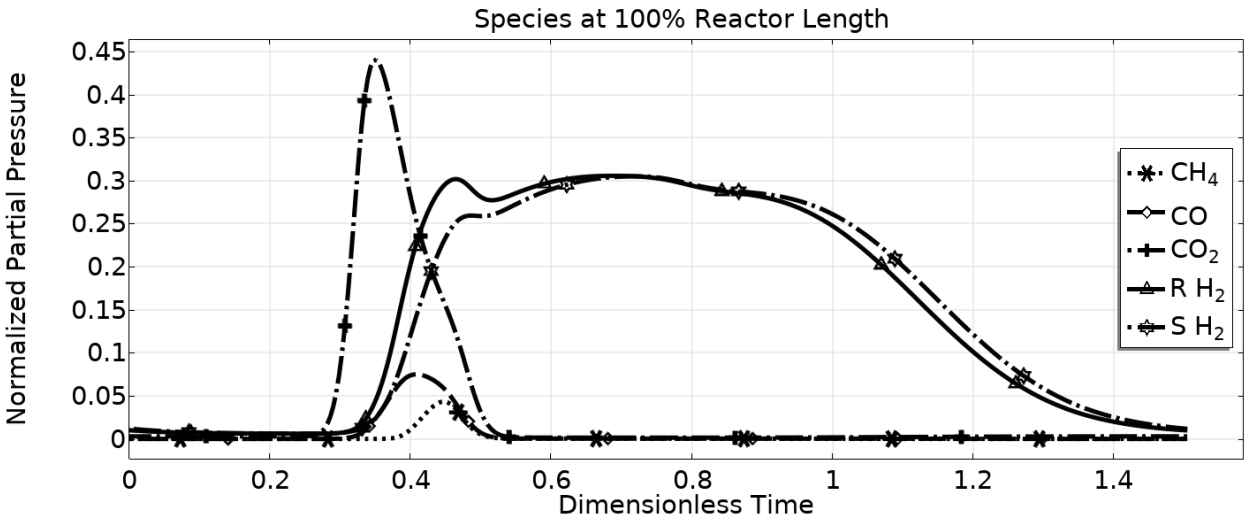

Figure 2-47 Dimensionless time evolution of species during the last cycle at 100% reactor length for Da =15.42 , Θ =48.70.

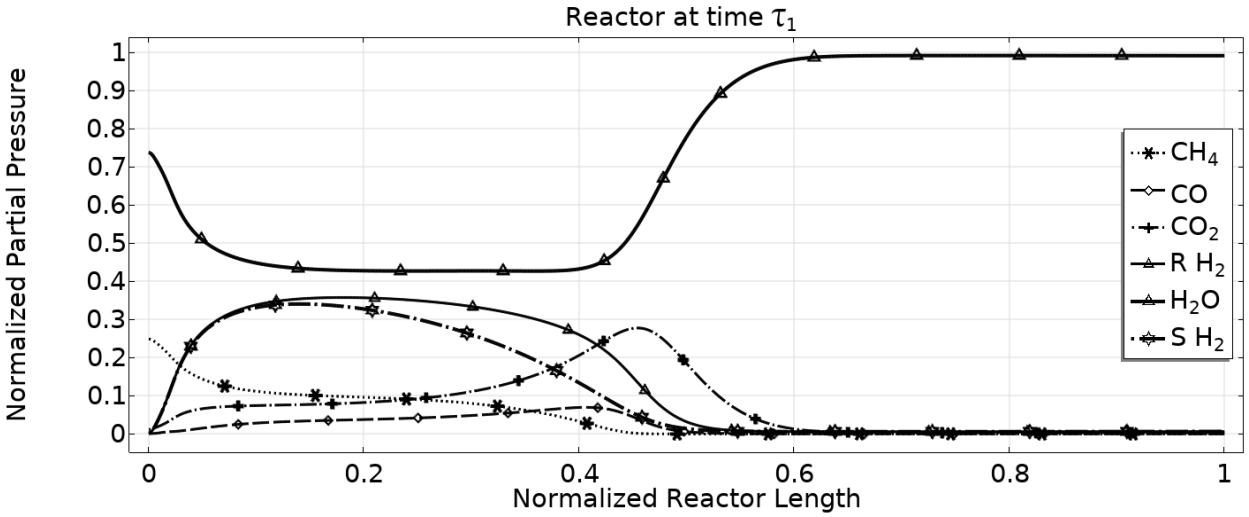

Figure 2-48 Species' dimensionless partial pressure axial length profile during cycle 3 at the end of OM 1 for Da =15.42 , Θ =48.70.

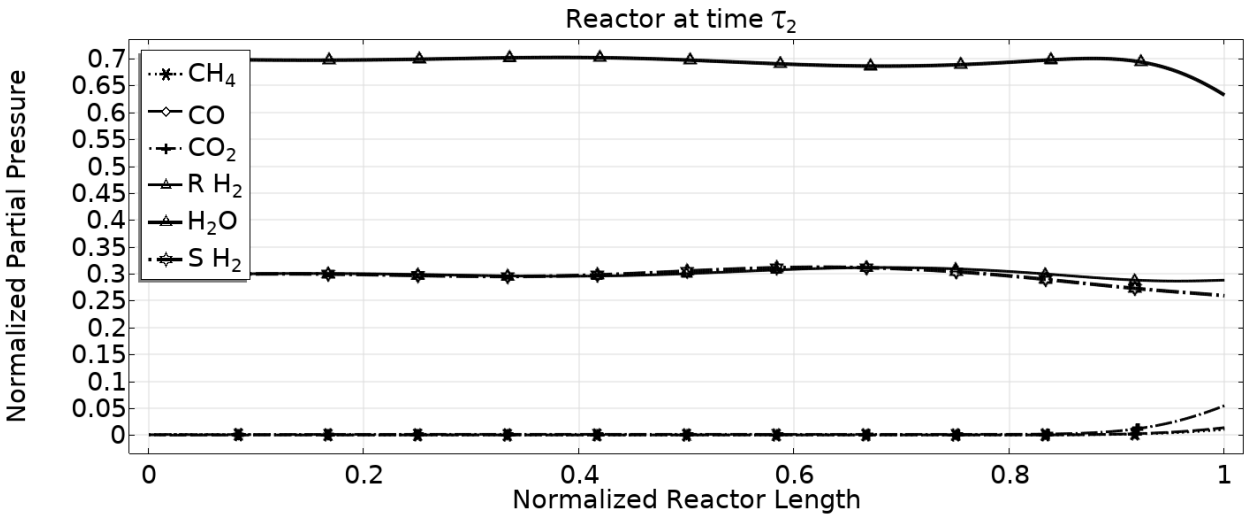

Figure 2-49 Species' dimensionless partial pressure axial length profile during cycle 3 at the end of OM 2 for Da =15.42 , Θ =48.70.

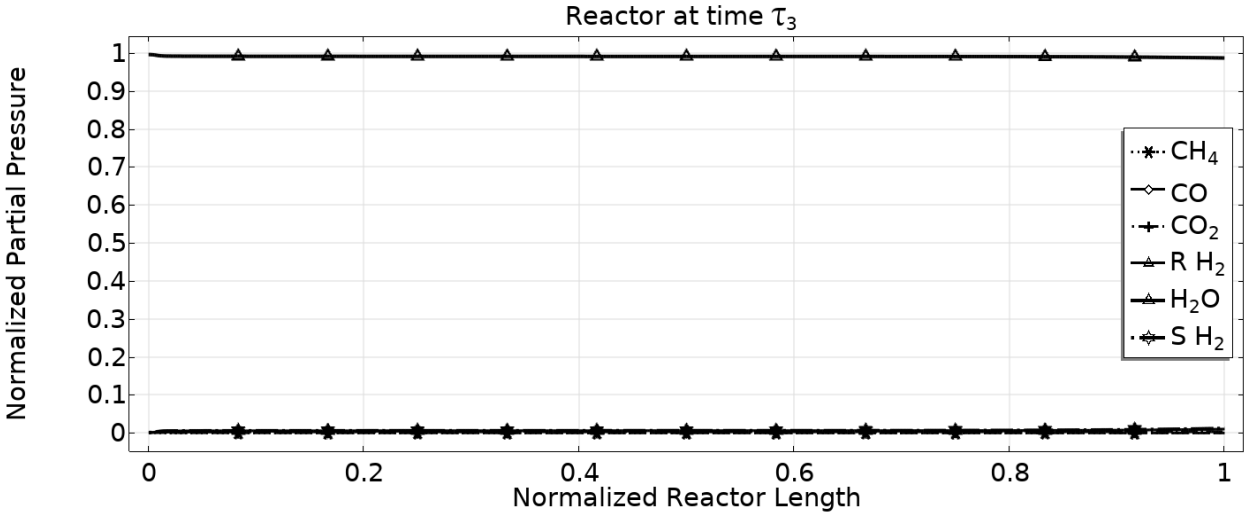

Figure 2-50 Species' dimensionless partial pressure axial length profile during cycle 3 at the end of OM 3 for Da =15.42 , Θ =48.70.

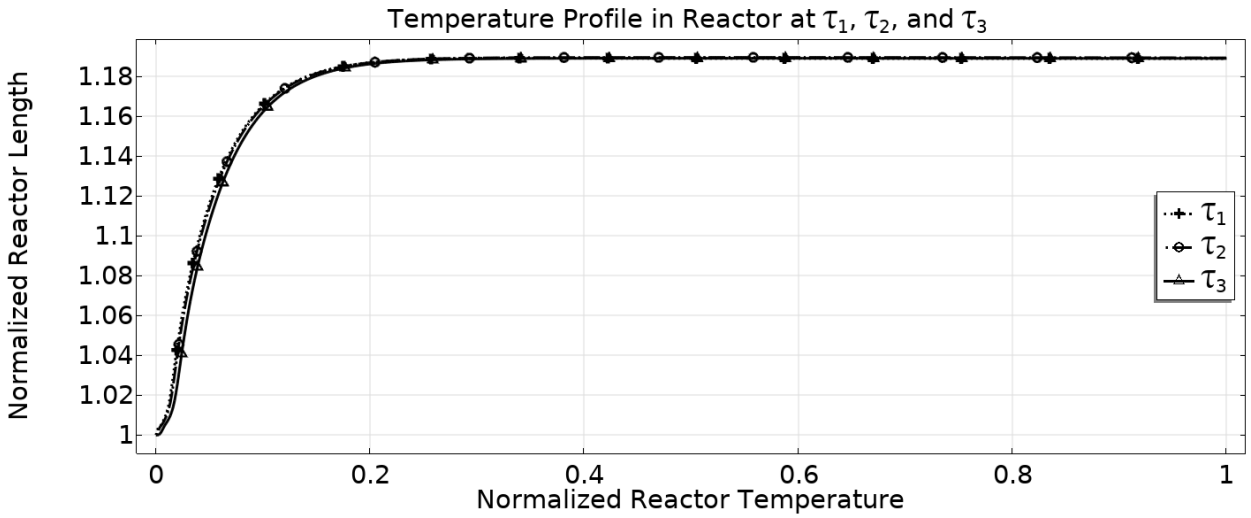

Figure 2-51 Species' dimensionless temperature profile in reactor at the end of OM1, OM2 and OM3 for Da =15.42 , Θ =48.70.

Figures 2–43 thru 2-51 show corresponding results for the 27th trial (*Da* = 15.42 and Θ = 48.70). Figure 2-43 shows the time evolution of the dimensionless partial pressure for the various species at the outlet of the reactor through three cycles of operation. Figures 2-44, 2-45, 2-46 , and 3-47 show the time evolution of the dimensionless partial pressure of methane, carbon dioxide, carbon monoxide, hydrogen, and hydrogen in the storage at four different reactor locations, 25%, 50%, 75% , and 100% respectively, during the last cycle of operation for the 27th trial (*Da* =15.42 and Θ =48.70). Figures 3-48, 3-49, and 3-50 show the dimensionless partial pressure profiles for all species along the length of the reactor at the end of OM 1, OM 2, and OM 3, respectively, for the 27th trial(*Da* =15.42 and Θ =48.70). Figure 3-51 similarly shows the dimensionless temperature profile along the length of the reactor at the end of OM 1, OM 2, and OM 3, respectively, for the nth trial(*Da* =15.42 and Θ =48.70).

Comparing Figures 2-35 thru 2-38 with Figures 2-44 thru 2-47, we observe a large increase (decrease) in the amount of carbon dioxide (methane) exiting the reactor. These figures also show similar patterns of behavior for hydrogen in the reactor and storage void domains, with

the hydrogen in the storage medium exhibiting a noticeably shorter response time. This is attributed to the higher Θ value, which allows the hydrogen to be more easily transferred between domains. The figures also highlight a dramatic change in the behavior for both methane and carbon dioxide. The methane waveform retains its three distinct phases through all measured points, and is also always greater in magnitude until the exit of the reactor. This is not the case for *Da* = 1.33 and Θ =5.39 , where the magnitude of the carbon dioxide pulse becomes greater than that of the methane pulse at the 50% location. This is particularly highlighted in Figure 2-48, which shows the species profiles in the reactor at the end of OM 1. When compared with Figure 2-39, it can also be seen in Figure 2-48 that the dimensionless partial pressures of hydrogen in the storage and reactor void are much closer in value, indicating a much higher rate of transfer of separated hydrogen.

When comparing figures 2-42 with 2-51, it can be seen that the increase in Ψ_4 and D_a reduces the variation in temperature profiles between end of phases as the fluid is able to reach the wall temperature before exiting the reactor. Because they SMR reaction is endothermic and the equilibrium concentration are strongly dependent on temperature, it is unsurprising to see corresponding increases X_{CH_4} with increases in Ψ_4.

In addition to the above experiments, we also investigated the effect when not restricting $\Theta \leq 50$, as well as two other sets of values for ε_v , ε_c, and ε_s. The result from these experiments is shown in the tables below.

Table 2-24 Performance metric comparison for SMR-MSR and SMR-SSR, and OM dimensionless duration times for 17 trials

$\varepsilon_v = 0.35$, $\varepsilon_c = 0.20$, $\varepsilon_s = 0.45$											
Trial	D_a	Θ	Ψ_5	SR X_{CH_4}	SS X_{CH_4}	SR Y_{H_2}	SS Y_{H_2}	$R_{H_2,rec}$	$\bar{\tau}_1$	$\bar{\tau}_2$	$\bar{\tau}_3$
1	1.323	5.392	0.377	0.642	0.387	2.522	1.450	0.645	0.141	0.309	1.757
2	1.866	33906.78	0.399	0.833	0.419	3.186	1.558	0.714	0.144	0.267	0.592

3	3.439	95581.81	1.636	0.891	0.397	3.550	1.483	0.912	0.117	0.314	0.708
4	3.439	67969.29	1.636	0.891	0.397	3.550	1.483	0.912	0.117	0.314	0.709
5	5.549	5.392	1.232	0.852	0.550	3.246	2.008	0.623	0.166	0.295	1.736
6	5.585	170747.4	4.005	0.935	0.387	3.750	1.450	0.947	0.108	0.309	0.703
7	5.762	33906.78	1.027	0.960	0.550	3.658	2.008	0.734	0.165	0.257	0.575
8	5.782	67852.58	4.346	0.942	0.397	3.776	1.483	0.947	0.110	0.310	0.706
9	6.570	200879.3	3.958	0.944	0.387	3.683	1.450	1.100	0.107	0.305	0.696
10	10.041	200879.3	5.577	0.975	0.431	3.920	1.602	0.965	0.111	0.306	0.698
11	10.497	67852.58	7.068	0.980	0.460	3.944	1.704	0.961	0.117	0.311	0.708
12	13.115	12.744	6.793	0.864	0.550	3.318	2.008	0.783	0.184	0.311	1.419
13	14.538	67852.58	9.280	0.987	0.498	3.971	1.834	0.963	0.122	0.311	0.709
14	22.051	67852.58	13.341	0.991	0.550	3.991	2.008	0.965	0.130	0.311	0.712
15	22.051	21.427	19.270	0.890	0.550	3.430	2.008	0.832	0.187	0.308	1.230
16	26.186	135705.1	13.102	0.991	0.550	3.990	2.008	0.968	0.127	0.307	0.706
17	27.564	200879.3	13.028	0.991	0.550	3.990	2.008	0.969	0.127	0.306	0.703

Table 2-25 Performance metric comparison for SMR-MSR and SMR-SSR, and OM dimensionless duration times for 13 trials

$\varepsilon_v = 0.27$, $\varepsilon_c = 0.4$, $\varepsilon_s = 0.33$											
Trial	D_a	Θ	Ψ_5	SR X_{CH_4}	SS X_{CH_4}	SR Y_{H_2}	SS Y_{H_2}	$R_{H_2,rec}$	$\bar{\tau}_1$	$\bar{\tau}_2$	$\bar{\tau}_3$
1	3.439	64612.782	1.348	0.853	0.397	3.389	1.483	0.879	0.097	0.232	0.515
2	3.439	90861.725	1.348	0.853	0.397	3.389	1.483	0.879	0.097	0.232	0.515
3	5.585	162315.48	3.215	0.910	0.387	3.645	1.450	0.933	0.087	0.235	0.526
4	5.617	96540.583	2.661	0.918	0.431	3.664	1.602	0.913	0.096	0.237	0.530
5	5.782	64501.840	3.494	0.917	0.397	3.671	1.483	0.932	0.088	0.237	0.529
6	5.969	128720.77	2.114	0.916	0.407	3.662	1.519	0.924	0.089	0.227	0.507
7	6.570	190959.39	3.153	0.921	0.387	3.697	1.450	0.940	0.085	0.231	0.518
8	7.919	230162.98	4.506	0.935	0.387	3.756	1.450	0.951	0.084	0.232	0.522
9	8.162	7.5389609	2.120	0.892	0.550	3.359	2.008	0.609	0.132	0.209	1.229
10	9.787	128720.77	3.139	0.963	0.460	3.857	1.704	0.939	0.093	0.225	0.507
11	10.166	96540.583	4.303	0.968	0.498	3.874	1.834	0.930	0.102	0.236	0.530
12	10.497	64501.840	5.623	0.972	0.460	3.904	1.704	0.950	0.093	0.236	0.530
13	11.083	32419.674	2.150	0.968	0.550	3.755	2.008	0.793	0.117	0.183	0.418

Table 2-26 Performance metric comparison for SMR-MSR and SMR-SSR, and OM dimensionless duration times for 7 trials

$\varepsilon_v = 0.25$, $\varepsilon_c = 0.30$, $\varepsilon_s = 0.45$											
Trial	D_a	Θ	Ψ_5	SR X_{CH_4}	SS X_{CH_4}	SR Y_{H_2}	SS Y_{H_2}	$R_{H_2,rec}$	$\bar{\tau}_1$	$\bar{\tau}_2$	$\bar{\tau}_3$
1	3.44	95157.01	1.32	0.96	0.40	3.85	1.48	0.92	0.09	0.21	0.56

2	3.44	133814.54	1.32	0.96	0.40	3.85	1.48	0.92	0.09	0.21	0.56
3	5.62	142177.95	2.66	0.98	0.43	3.96	1.60	0.95	0.10	0.22	0.59
4	5.97	189570.60	2.12	0.98	0.41	3.96	1.52	0.96	0.09	0.21	0.56
5	10.17	142177.95	4.42	0.99	0.50	3.99	1.83	0.95	0.10	0.22	0.59
6	13.12	17.84	7.10	0.87	0.55	3.28	2.01	0.71	0.19	0.21	1.23
7	14.14	47027.01	3.46	1.00	0.55	4.00	2.01	0.94	0.12	0.19	0.51

Looking at things from the point of view of process design and systems operations, there are several parameters that can be adjusted to alter *Da* and Θ. For a fixed inlet composition at the beginning of OM 1, *Da* can be increased (decreased) by increasing (decreasing) the reactor's residence time, which in turn can be achieved by increasing (decreasing) the reactor's length and/or by decreasing (increasing) the reactor's residence time. The dimensionless parameter Θ can be increased (decreased) by increasing (decreasing) the residence time, storage-void domain interfacial area and hydrogen permeance, and/or by decreasing (increasing) the void domain volume fraction. Θ can be altered even while keeping the Da fixed, by altering the last three aforementioned design parameters. In particular, increasing the preferential hydrogen permeance through the storage medium's permselective layer will increase Θ and can be accomplished through appropriate selection of the layer's pore structure and material properties.

3.3.3 Conclusion

In this work, a novel, first principle-based, spatially dependent model capturing the membrane storage reactor behavior was presented and simulated. This novel intensified process, termed the MSR, is capable of overcoming operational limitations of traditional reactor design by combining multiple mass transport processes into a single unit, and increases the production rate through dynamic operation. The resulting desired products are delivered at high pressure and in readily separable form, which leads to additional energetic and operational cost saving. The

assessment of MSR behavior was described by a one-dimensional non-isobaric non-isothermal dynamic model which, when cast in dimensionless form, revealed two dimensionless parameters, Da (the Damkohler number) and $\Theta = 1/Pe_{mem}$ (the inverse Peclet number), that capture MSR behavior. Performance analysis of the MSR process was undertaken by introducing a number of metrics, and a case study on Steam Methane Reforming for the production of hydrogen was subsequently carried out. Numerous simulations of the developed spatially dependent dynamic model enabled parametric studies of the effect of the aforementioned Da and $\Theta = 1/Pe_{mem}$ dimensionless groups, and established that maximizing both groups leads to improved MSR performance. A comparative analysis between SMR-MSR and SSR showed that the SMR-MSR process obtained a higher methane conversion, X_{CH_4}, and a greater yield of hydrogen, Ω_{H_2}. It was also shown that the SMR-MSR hydrogen recovery ratio, $R_{H_2,3}$, was comparable to or above those obtained by currently investigated membrane technologies.

There are several notable advantages of the proposed MSR process, the first being its ability to be modularized and to accommodate a variety of economic production scales. Although the current case study emphasized application to hydrogen production for use at the level of a refinery or a large plant, smaller scales of production are also quite feasible. The MSR process can conceivably be applied to hydrogen-fueling stations so as to facilitate the creation of sustainable decentralized hydrogen generation. Additionally, implementation of the MSR process into existing plants would help reduce many of the economic barriers faced by industrial operations when converting to new technology. Using SMR as an example, retrofitting of an existing plant would consist mainly of reactor repacking with catalyst and storage media. Because of the need for the MSR process to direct material flow, it is imagined that additional fluid lines (for both feed and effluent) need to be constructed. This additional cost, however, is

not expected to be large, especially when considering that no additional exogenous chemical components are required. Additional component cost from MSR implementation can also be expected from the need to incorporate dynamic control equipment because, as noted earlier, most industrial reactors operate at steady state. All of this suggests that the MSR process has the potential to overcome many of the barriers that hinder many potential process intensification technologies and be implemented at an industrial scale. The presented one-dimensional non-isobaric/non-isothermal dynamic model was used to demonstrate the novel SR-MSR concept. Because the SR-MSR process is shown to offer significant performance advantages, future work will attempt to study in more detail the thermal behavior of the process by examining the space of the Ψ parameters.

3.3.4 Notation

English Symbols

a : Verhulst function parameter.

$A_r\left(m^2\right)$: Reactor cross section area

c : Verhulst function parameter.

$c_{i,gv}\left(\frac{mol\,i\,in\,g\,of\,v}{m^3\,g\,of\,v}\right), c_{i,gs}\left(\frac{mol\,i\,in\,g\,of\,s}{m^3\,g\,of\,s}\right)$: i_{th} species concentration in gas phase of void and storage domains

$c_{gv}\left(\frac{mol\,in\,g\,of\,v}{m^3\,g\,of\,v}\right)$: total concentration

$\hat{C}_P^{gv}, \hat{C}_P^{s}, \hat{C}_P^{c}\left(\frac{J}{(g\cdot K)}\right)$: mass heat capacity

$\bar{C}_{P,i}^{gv}\left(\frac{J}{(mol\cdot K)}\right)$: molar heat capcity

D_a : Reference Damköhler number

$d_{eff}\,(m)$:effective pellet diameter

$F_{i,gv}\left(\frac{mol\,i}{s}\right)$: Axial molar flowrate of i_{th} species

$F^*\left(\frac{mol}{s}\right)$: Reference axial molar flowrate

$\bar{F}_{i,gv}$: Dimensionless axial molar flowrate of i_{th} species

$h_k(\ )$: OM specific Heaviside function.

$\tilde{h}_{i,gv}\left(\frac{J}{mol}\right)$: molar enthalpy of species i.

$h_r^{furr}\left(\frac{J}{m^2 \cdot K}\right)$: heat transfer coefficient between reactor wall

$\vec{j}_{i,gv}\left(\frac{kg}{m^2 s}\right)$: mass flux

$\vec{j}_{i,gv}^{\dagger}\left(\frac{mol}{m^2 s}\right)$: molar flux

$k_1\left(\frac{\text{kmol bar}^{0.5}}{\text{kg}_{\text{cat}}\ \text{hr}}\right), k_2\left(\frac{\text{kmol}}{\text{kg}_{\text{cat}}\ \text{hr bar}}\right), k_3\left(\frac{\text{kmol bar}^{0.5}}{\text{kg}_{\text{cat}}\ \text{hr}}\right)$: Rate coefficients for SMR reactions

$K_1\left(\text{bar}^2\right), K_2, K_3\left(\text{bar}^2\right)$: Equilibrium constants for SMR reactions

$K_{CH_4}\left(\text{bar}^{-1}\right), K_{H_2}\left(\text{bar}^{-1}\right), K_{CO}\left(\text{bar}^{-1}\right), K_{H_2O},$: Species adsorption constants for SMR reactions

$L^*(m)$: Reactor Length

$M_i\left(\frac{kg}{mol}\right)$: molar mass

NC: Number of species

NOM: Number of reactor operating modes

OM: Operating mode

$P_{i,gv}(Pa), P_{i,gs}(Pa) : i_{th}$ species partial pressure in gas phase of void and storage domains

$\bar{P}_{i,gv}, \bar{P}_{i,gs} : i_{th}$ species dimensionless partial pressure in gas phase of void and storage domains

$\left(\tilde{\bar{P}}_{i,gv}\right)_{in,k}$: Ratio of inlet partial pressure for species i for operating mode k-1, based on operating mode k=1

$\left(\tilde{\bar{P}}_{i,gv}\right)_{out,k}$: Ratio of inlet partial pressure for species i for operating mode k, based on operating mode k=1

$P^*(Pa)$: Reference pressure

Pe: Peclet number for membrane to convective transport

$r_i\left(\frac{mol\, i}{kg\, catalyst \cdot s}\right)$: i_{th} species reaction based generation rate

$\bar{r}_i$: i_{th} species dimensionless reaction based generation rate

$r^*\left(\frac{mol}{kg\,catalyst\cdot s}\right)$: Reference reaction generation rate

$R_{i,k}$: Molar ratio of i_{th} species produced during OM k over i_{th} species produced during all OM's

R_i: Rate of i_{th} SMR reaction

$\overline{R}_i$: Dimensionless rate of i_{th} SMR reaction

$R\left(\frac{J}{mol\cdot K}\right)\hat{=}8.314462$: Universal Gas Constant

R_{LIM}: Limiting reactant used in performance metric calculations

$S_{i,gv,gs}\left(\frac{mol\ of\ species\ i\ in\ phase\ g\ from\ s\ to\ v}{\left(m^3\ system\ r\right)\cdot s}\right)$: Molar generation rate of i_{th} species into the gas phase of the voids domain due to transport from the gas phase in the storage domain

$S_{i,gs,gv}\left(\frac{mol\ of\ species\ i\ in\ phase\ g\ from\ v\ to\ s}{\left(m^3\ system\ r\right)\cdot s}\right)$: Molar generation rate of i_{th} species into the gas phase of the storage domain due to transport from the gas phase in the voids domain

$t(s)$: Time

$\overline{t}$: Dimensionless time

$t^*(s)$: Reference time, chosen as the residence time

$T_g(K)$: Temperature in all reactor domains

$T^{fur}(K)$: furnace wall temp

$V\left(m^3\right)$: Total reactor volume

$v_g\left(\frac{m}{s}\right)$: gas mass velocity in reactor void domain

$\vec{v}_g^{\dagger}\left(\frac{m}{s}\right)$: gas molar velocity in reactor void domain

$v^*\left(\frac{m}{s}\right)$: Reference velocity, chosen as gas inlet velocity during OM 1

$\overline{v}_g$: Dimensionless gas velocity in reactor void domain

$X_{R_{LIM}}$:Conversion of limiting reactant R_{LIM} over all OM's

W_k: Verhulst function for switching between inlet boundary conditions during OM change.

$x_{k,gv}$: mol fraction of gas in void

$z(m)$: Reactor axial coordinate

$\overline{z}$: Reactor dimensionless axial coordinate

Greek Symbols

$\alpha_{s,v}\left(\frac{m^2\ storage-void\ interface}{m^3\ system\,r}\right)$: Storage-void domain interfacial area per unit volume of reactor system

$\beta_i\left(\frac{mol\,i}{Pa\cdot\left(m^2\ void-storage\,interface\right)\cdot s}\right)\forall i=1,NC$: i_{th} species permeance through storage medium permselective layer

$\varepsilon_v,\varepsilon_c,\varepsilon_s,\varepsilon_{gs},\varepsilon_{sos}$: Volume fractions of voids, catalyst, storage, gas phase in storage domain, and solid phase in storage domain

η: Catalyst effectiveness factor

Θ: Dimensionless number quantifying membrane permeation to convection (inverse Peclet)

$\rho_c\left(\frac{kg\,catalyst}{m^3\,catalyst\ pellet}\right)$: Catalyst pellet density

$\rho_{gv}\left(\frac{kg}{m^3}\right)$: mass density of gas

$\mu_{gv}\left(\frac{kg}{m\cdot s}\right)$: viscosity of gas

$\omega_{i,k}$: Molar ratio of i_{th} species produced during OM k over limiting reactant fed throughout all OM's

Ω_i: Overall molar ratio of i_{th} species produced during all OM's over limiting reactant fed throughout all OM's

Ω_i: Desired product yield of species i

τ_k: Duration of k_{th} operating mode

$\overline{\tau}_k$: Dimensionless duration of k_{th} operating mode

$\lambda_s^h,\lambda_c^h,\lambda_{gv}^h\left(\frac{J}{m\cdot K}\right)$: thermal conductivity

Φ_{ij}: collision integral

Ψ_j: Dimensinless heat variable or parameter j.

ω_j: Dimensionless momentum variable j.

Chapter 3 - Lexicographic approach network synthesis

3.1. Lexicographic Introduction

We begin by identifying the attributes of the aforementioned clusters that make them feasible. First, every reaction within the reaction cluster must obey atom balance requirements and the reactions must sum to the target reaction. If this primary requirement is not satisfied, the group of reactions does not constitute a reaction cluster. Unfortunately, this is a necessary, but not sufficient, condition on the reactions that comprise a cluster: Many reaction clusters that satisfy this requirement are still unacceptable as a result of thermodynamic infeasibility.

We therefore consider a thermodynamically feasible reaction to be a reaction whose equilibrium yield, as dictated by thermodynamic considerations, is sufficient to ensure economic feasibility. In a reaction cluster, this implies that each reaction comprising the cluster must be thermodynamically feasible at some operating temperature (although each reaction in the cluster may occur at a different temperature). Thermodynamic yield of a reaction is related to the Gibbs free energy of formation for that reaction. For the reaction of general form for a chemical reaction amongst species of various phases:

$$\sum_{i\in R}\left(-\nu_i\right)S_{i_{(\alpha_i)}} \rightleftarrows \sum_{j\in P}\nu_i S_{i_{(\alpha_j)}}$$

with NC participating species with stoichiometric coefficients $\nu_i \quad i\in\{1,\cdots,NC\}$, where

$\left.\begin{matrix}\nu_j>0 \text{ if } j\in P\triangleq\{\text{index of product species}\}\\ \nu_i<0 \text{ if } i\in R\triangleq\{\text{index of reactant species}\}\end{matrix}\right\}, P\cup R=\{1,\cdots,NC\}$. The reaction's extent satisfies the relation:

$$\left\{\begin{array}{l} n_i = n_{i,o} + \nu_i \xi \quad \forall i \in \{1,\cdots,NC\} \\ \xi \in \left[0, \min_{i \in R}\left(\frac{n_{i,o}}{-\nu_i}\right)\right] \end{array}\right\} \qquad (3.1.1)$$

Let G, L, S be the index sets of the species that are in the ideal gas, ideal liquid, and ideal solid states respectively, at the considered temperature and pressure conditions T, P. It then holds: $G \cup L \cup S = \{1,\cdots,NC\}$. Using the above ideal assumptions the fugacities for gas, liquid, and solid phase species are given by the following equations:

Gas Fugacity: $$\left\{\frac{\hat{f}_i^{(g)}}{f_i^{o(g)}} = y_i \frac{P}{P^o} = \frac{n_i}{\sum_{i \in G} n_i}\frac{P}{P^o} = \frac{n_{i,o} + \nu_i \xi}{\sum_{i \in G} n_{i,o} + \xi \sum_{i \in G} \nu_i}\frac{P}{P^o} \quad \forall i \in G\right\} \qquad (3.1.2)$$

Liquid Fugacity: $$\left\{\frac{\hat{f}_i^{(l)}}{f_i^{o(l)}} = x_i = \frac{n_i}{\sum_{i \in L} n_i} = \frac{n_{i,o} + \nu_i \xi}{\sum_{i \in L} n_{i,o} + \xi \sum_{i \in L} \nu_i} \quad \forall i \in L\right\} \qquad (3.1.3)$$

Solid Fugacity: $$\left\{\frac{\hat{f}_i^{(s)}}{f_i^{o(s)}} = 1 \quad \forall i \in S\right\} \qquad (3.1.4)$$

It then holds:

$$\prod_{i \in G}\left(\frac{\hat{f}_i^{(g)}}{f_i^{o(g)}}\right)^{\nu_i} \prod_{i \in L}\left(\frac{\hat{f}_i^{(l)}}{f_i^{o(l)}}\right)^{\nu_i} \prod_{i \in S}\left(\frac{\hat{f}_i^{(s)}}{f_i^{o(s)}}\right)^{\nu_i} = \exp\left[\frac{-\Delta G^o(T)}{RT}\right] \Leftrightarrow \qquad (3.1.5)$$

$$\prod_{i \in G}\left(\frac{n_{i,o} + \nu_i \xi}{\sum_{i \in G} n_{i,o} + \xi \sum_{i \in G} \nu_i}\frac{P}{P^o}\right)^{\nu_i} \prod_{i \in L}\left(\frac{n_{i,o} + \nu_i \xi}{\sum_{i \in L} n_{i,o} + \xi \sum_{i \in L} \nu_i}\right)^{\nu_i} \prod_{i \in S}(1)^{\nu_i} = \exp\left[\frac{-\Delta G^o(T)}{RT}\right] \Leftrightarrow \qquad (3.1.6)$$

$$\prod_{i \in G}\left(\frac{n_{i,o} + \nu_i \xi}{\sum_{i \in G} n_{i,o} + \xi \sum_{i \in G} \nu_i}\right)^{\nu_i} \prod_{i \in L}\left(\frac{n_{i,o} + \nu_i \xi}{\sum_{i \in L} n_{i,o} + \xi \sum_{i \in L} \nu_i}\right)^{\nu_i} = \left(\frac{P}{P^o}\right)^{-\left(\sum_{i \in G} \nu_i\right)} \exp\left[\frac{-\Delta G^o(T)}{RT}\right] \qquad (3.1.7)$$

Define

$$f_i : \left[0, \min_{i \in R}\left(\frac{n_{i,o}}{-\nu_i}\right)\right] \to \mathbb{R},\ f_i : \xi \to f_i(\xi) \triangleq \left(\frac{n_{i,o} + \nu_i \xi}{\sum_{i \in G} n_{i,o} + \xi \sum_{i \in G} \nu_i}\right)^{\nu_i} \quad \forall i \in G \tag{3.1.8}$$

$$g_i : \left[0, \min_{i \in R}\left(\frac{n_{i,o}}{-\nu_i}\right)\right] \to \mathbb{R},\ g_i : \xi \to g_i(\xi) \triangleq \left(\frac{n_{i,o} + \nu_i \xi}{\sum_{i \in L} n_{i,o} + \xi \sum_{i \in L} \nu_i}\right)^{\nu_i} \quad \forall i \in L \tag{3.1.9}$$

Then, the above equilibrium relation becomes:

$$\left\{\prod_{i \in G}\left(\frac{n_{i,o} + \nu_i \xi}{\sum_{i \in G} n_{i,o} + \xi \sum_{i \in G} \nu_i}\right)^{\nu_i} \prod_{i \in L}\left(\frac{n_{i,o} + \nu_i \xi}{\sum_{i \in L} n_{i,o} + \xi \sum_{i \in L} \nu_i}\right)^{\nu_i} = \left(\frac{P}{P^o}\right)^{-\left(\sum_{i \in G} \nu_i\right)} \exp\left[\frac{-\Delta G^o(T)}{RT}\right]\right\} \Leftrightarrow \tag{3.1.10}$$

$$\left\{\prod_{i \in G} f_i(\xi) \prod_{i \in L} g_i(\xi) = \left(\frac{P}{P^o}\right)^{-\left(\sum_{i \in G} \nu_i\right)} \exp\left[\frac{-\Delta G^o(T)}{RT}\right]\right\} \tag{3.1.11}$$

where ΔG^o is the standard Gibbs of formation for the reaction and can be calculated from:

$$\Delta G^o \triangleq \sum_{i \in NC} \nu_i \Delta G_i^o(T) \tag{3.1.12}$$

where ν_i is the stoichiometric coefficient and ΔG_i^o is the standard Gibbs of formation for species i. Note that $\Delta G^o(T)$ is only a function of temperature, and in many cases, it can be reasonably assumed that $\Delta G^o(T)$ varies linearly with temperature, a consequence of the compensation effect. The compensation effect describes how the enthalpy change in a reaction ΔH^o is generally associated with a corresponding change in entropy ΔS^o. Specifically, both

ΔH^o and ΔS^o tend to react to temperature in a similar manner (i.e., they either both increase or they both decrease with a change in temperature). Exothermic reactions $\Delta H^o < 0$ generally proceed through tighter transition states, so the products of the reaction possess less entropy than do the reactants $\Delta S^o < 0$. The fundamental thermodynamic relation $\Delta G^o \triangleq \Delta H^o - T\Delta S^o$ shows that these differences cancel to a large extent. As a result, ΔG^o values have much smaller variations with temperature than either ΔH^o or ΔS^o, which implies that good accuracy can be obtained by a linear model[39]. Nevertheless, we will present in this work a way to determine the temperature which maximizes $(3.1.11)$ over a temperature range without assuming that $\Delta G^o(T)$ possesses a linear dependence upon temperature.

In order for a reaction to be physically meaningful, it must occur at a temperature below the decomposition temperatures of the reaction products. A decomposition reaction (containing a single reactant) can take place either above (thermal) or below (catalytic) the reactant's decomposition temperature. Unlike single species decomposition reactions, general reactions must occur at temperatures below the decomposition temperature of the reactants as well. Another attribute of realizable reaction clusters is the minimization of side reactions. Potential side reactions might occur between products and/or reactants. Consider the general reaction:

$$\nu_A A_{(\alpha_A)} + \nu_B B_{(\alpha_B)} \rightleftarrows + \nu_C C_{(\alpha_C)} + \nu_D D_{(\alpha_D)}$$

In order for this to proceed as written, the reaction must have higher yield (as determined by thermodynamic considerations) than other reactions that could occur between the same reactants and products. Although there exists a rigorous detailed framework to accurately assess the impact of side reactions on the equilibrium conversion of a reaction, for the purposes of this study we will simply require that the following side reactions should have significantly smaller

value (perhaps by an order of magnitude or some other user defined amount) of the equilibrium constant

$$K_{eq}(T) = \exp\left[\frac{-\Delta G^{o}(T)}{RT}\right] \tag{1.13}$$

than the desired reaction:

$$\nu_{A_1} A_{(\alpha_A)} + \nu_{B_1} B_{(\alpha_B)} \rightleftarrows \nu_{z_1} Z_{(\alpha_{Z_1})} + \nu_{y_1} Y_{(\alpha_{Y_1})}, \nu_{A_2} A_{(\alpha_A)} + \nu_{D_2} D_{(\alpha_D)} \rightleftarrows \nu_{z_2} Z_{(\alpha_{Z_2})} + \nu_{y_2} Y_{(\alpha_{Y_2})}$$

$$\nu_{B_3} B_{(\alpha_B)} + \nu_{D_3} D_{(\alpha_D)} \rightleftarrows \nu_{z_3} Z_{(\alpha_{Z_3})} + \nu_{y_3} Y_{(\alpha_{Y_3})}, \nu_{A_4} A_{(\alpha_A)} + \nu_{C_4} C_{(\alpha_C)} \rightleftarrows \nu_{z_4} Z_{(\alpha_{Z_4})} + \nu_{y_4} Y_{(\alpha_{Y_4})}$$

$$\nu_{B_5} A_{(\alpha_B)} + \nu_{C_5} C_{(\alpha_C)} \rightleftarrows \nu_{z_5} Z_{(\alpha_{Z_5})} + \nu_{y_5} Y_{(\alpha_{Y_5})}, \nu_{C_6} C_{(\alpha_C)} + \nu_{D_6} D_{(\alpha_D)} + \rightleftarrows \nu_{z_6} Z_{(\alpha_{Z_6})} + \nu_{y_6} Y_{(\alpha_{Y_6})}$$

where Z and Y are any combination of chemical species other than $\nu_C C_{(\alpha_C)} + \nu_D D_{(\alpha_D)}$. However, with the widespread usage of catalysts in industry, even reactions that are not selective (e.g. $A_{(\alpha_A)} + B_{(\alpha_B)} \rightleftarrows C_{(\alpha_C)} + D_{(\alpha_D)}$ competes with $\nu_A A_{(\alpha_A)} + \nu_B B_{(\alpha_B)} \rightleftarrows \nu_z Z_{(\alpha_Z)} + \nu_y Y_{(\alpha_Y)}$) should not be immediately discarded. Certainly, some of these thermodynamically feasible reactions will exhibit increased selectivity with the use of appropriate catalysts. As such, this criterion may or may not be used in the initial screening.

The lexicographic technique presented here offers flexibility and superior computational properties to these other search methods. A variety of considerations can be incorporated in the methodology during intermediate stages, so as to accelerate and customize the overall search. Consequently, this method has the advantage of finding all potential clusters in an efficient manner.

3.2. Algorithm description

Before explaining the lexicographic approach, we briefly review some terminology that will prove useful in this discussion. Algorithms can be characterized by their time complexity

and/or their space complexity. Time complexity refers to the running time of an algorithm, whereas space complexity denotes the memory requirements of an algorithm. Although exact running times and memory requirements can sometimes be determined, complexity is typically expressed as an order estimate that neglects lower-order and constant terms. This is referred to as the asymptotic complexity of an algorithm, which is a bound as the input size grows large. Asymptotic complexity is generally denoted by the Θ-notation. This notation gives an order estimate of either the running time or memory requirements of an algorithm as a function of the input size. The definition of asymptotic complexity is as follows[40], where we say that $f(x)$ is of the order $g(x)$:

$$f(x) = \Theta(g(x)) \Leftrightarrow \exists c_1, c_2, x_o \geq 0 \ \ s.t. \ 0 \leq c_1 \cdot g(x) \leq f(x) \leq c_2 \cdot g(x) \quad \forall x \geq x_o \qquad (3.1.14)$$

where $f(x)$ and $g(x)$ are functions, and c_1, c_2, x_o are positive constants. For example, if the running time of an algorithm is $\Theta(x^2)$,this statement implies that the running time increases as the square of the input size x. In most cases, the input parameter x will be the number of elements (i.e., the number of elements to be sorted in a sorting algorithm). Algorithms that perform the same function can have different time and space complexities. Unless otherwise stated, complexity refers to the worst case. For example, if x elements are to be sorted, two simple sorting algorithms that are often employed are insertion sort and merge sort. The time complexity of insertion sort is $\Theta(x^2)$, whereas the time complexity of merge sort is $\Theta(x\log(x))$. For large values of x, the running time of merge sort is faster than insertion sort because the function $x\log(x)$ does not grow as quickly as x^2 with increasing x. Heapsort is another sorting algorithm that has time complexity $\Theta(x\log(x))$, which is optimal for a

comparison based sort algorithm[40].

The proposed cluster synthesis formulation allows the user to define a number of parameters that can help shape the attributes of the intermediate reactions and presupposes basic knowledge of atoms, elements, molecules, and chemical reactions, and set theory. The user designates the size of the species database which creates the set of Species N_S of useable species. Once this is specified, the set N_A is generated, which is defined as the set of distinct atomic elements used to create N_S. Informally, if the set $N_S \triangleq \{CH_4, CO, CO_2, H_2, H_2O, O_2\}$ then: $N_A \triangleq \{C, H, O\}$. While it is true that $\{C, H, O\} = \{H, O, C\} = \{O, H, C\}$, an ordering of elements can be established by the creation of a function which maps the elements alphabetical lettering to its position in the alphabet and arranging by ascending order. Similarly, the user defines the characteristics of intermediate reactions: there are a maximum of S_{sp} species per half reaction, and each species attains integer coefficients up to a maximum value of $\nu^{\max}$. The user also specifies the lower and upper limits of the temperature operating window, T_L and T_U, and the operating window for pressure P_L and P_U. The program sorts the input species list and then creates an index mapping between the species and its numerical position in the sorted list defined by the function $h : N_s \to E \subseteq \mathbb{N}$. During this sorting procedure the atoms used are collected into a list, then converted into a set, and then a sorted list. This maintains the same order of species and atoms when running the same input parameters multiple times for consistency and validation checks as set operations do not preserve order.

The program then creates two sets of mapping pairs. The first is between a species at the input temperatures and its standard Gibbs energy of formation, and the second is between a

species at the input temperatures and its phase. The program then takes the input species list and creates $\#(N_A)\times\#(N_S)$ matrix S. Using the above example this would be:

$$\begin{array}{c} \\ C \\ H \\ O \end{array}\begin{array}{c} \begin{array}{cccccc} CH_4 & CO & CO_2 & H_2O & H_2 & O_2 \end{array} \\ \begin{bmatrix} 1 & 1 & 1 & 0 & 0 & 0 \\ 4 & 0 & 0 & 2 & 2 & 0 \\ 0 & 1 & 2 & 1 & 0 & 2 \end{bmatrix} \end{array}$$

The maximum half reactions formula:

$$HR_{\max} = \sum_{i=1}^{S_{sp}} \left[\binom{N_s}{i} \left(\nu^{\max}\right)^i \right] \tag{1.15}$$

is then used to pre-allocate the size and create the set of Half Reactions, HR, which is a sequence quintuple:

$(w,q,p,u,d) = \left(\{w(j)\}_{j=1}^{HR_{\max}}, \{q(j)\}_{j=1}^{HR_{\max}}, \{p(j)\}_{j=1}^{HR_{\max}}, \{u(j)\}_{j=1}^{HR_{\max}}, \{d(j)\}_{j=1}^{HR_{\max}} \right)$. The first element, w, is a sequence of $\#(N_A)\times\#(N_S)$ matrices whose jth term corresponds to a half reaction which satisfies stochiometric coefficient and the maximum number of species restraints. The second element, q, is a sequence of $1\times S_{sp}$ vectors whose jth term correspond to the stochiometric coefficient of each species participating in the jth half reaction. The third element, p, is a sequence of $1\times N_A$ vectors whose jth term corresponds to the total number of each atom present in the jth half reaction and is used to create the lexicon for matching half reactions. The fourth element, u, is a sequence of integers whose jth term designates how many species are participating in the jth half reaction. The fifth element, d, is a sequence of $1\times\#(N_S)$ vectors whose jth term has entries that are either 0 or 1, corresponding to whether a species from the input list is present in the jth half reaction. To illustrate, we continue with the same example

from above. Consider the half reaction $CH_4 + CO_2$, which would be represented by the tuple

$$\left(\begin{bmatrix} 1 & 0 & 1 & 0 & 0 & 0 \\ 4 & 0 & 0 & 0 & 0 & 0 \\ 0 & 0 & 2 & 0 & 0 & 0 \end{bmatrix}, [1,1,0], [2,4,2], 2, [1,0,1,0,0,0]\right)$$

Similarly, the half reaction $2(CO) + 2(H_2)$ would be represented by:

$$\left(\begin{bmatrix} 0 & 2 & 0 & 0 & 0 & 0 \\ 0 & 0 & 0 & 0 & 4 & 0 \\ 0 & 2 & 0 & 0 & 0 & 0 \end{bmatrix}, [2,2,0], [2,4,2], 2, [0,1,0,01,0]\right)$$ The creation of the entries for each

tuple is done sequentially, with half reactions containing one species created first, followed by half reactions containing two species, repeated up to S_{sp}. We also note that the set generated by the combinatorial function $\left\{\binom{Z}{n}: \ n \in \mathbb{N}\right\}$ with cardinality $\#\left(\left\{\binom{Z}{n}\right\}\right) = m$ is a collection of disjoint sets where each set within has cardinality $\#(x_i) = n \forall x_i \in \left\{\binom{Z}{n}\right\} \forall i = 1....m$. In general, the enumeration of two and three combination of half reactions can be accomplished with the following recursive formulas:

2 Combinations: $\left\{\left\{h(N_s)_i\right\}_{i=1}^{i=\#(N_s)-1} \times \left\{h(N_s)_{i+j}\right\}_{j=i+1}^{j=\#(N_s)-i}\right\}$

3 combinations: $\left\{\left\{h(N_s)_i\right\}_{i=1}^{i=\#(N_s)-2} \times \left\{h(N_s)_{i+j}\right\}_{j=i+1}^{j=\#(N_s)-i} \times \left\{h(N_s)_{i+j+k}\right\}_{k=i+j+1}^{k=\#(N_s)-i-j}\right\}$

and taking the n-cartesian product with the set(s) generated by incrementing from 1 to $\nu^{\max}$:

$$ST \triangleq \left\{x : x \le \nu^{\max} \ \forall x \in \mathbb{N} \setminus 0\right\}$$

to generate the stoichiometric vector for each half reaction.

The information from this quintuple sequence is then used to generate a sequence sextuple containing the information for the set of all Full Reactions (FR):

$$\left(\bar{w},\bar{q},\bar{o},\bar{p},\bar{u},\bar{d}\right)=\left(\left\{\bar{w}(j)\right\}_{j=1}^{\#(FR)},\left\{\bar{q}(j)\right\}_{j=1}^{\#(FR)},\left\{\bar{o}(j)\right\}_{j=1}^{\#(FR)},\left\{p(j)\right\}_{j=1}^{\#(FR)},\left\{\bar{u}(j)\right\}_{j=1}^{\#(FR)},\left\{\bar{d}(j)\right\}_{j=1}^{\#(FR)}\right)$$

The tuple sequence is generated by matching half reactions with the same lexicon (p vector), and therefore the first element $\bar{w}$ is a sequence of $\#(N_A)\times\#(N_S)$ matrices whose jth term corresponds to the subtraction of two half reaction matrices, $w(\alpha)-w(\beta)$ that have the same p , where $w(\alpha)$ is considered to be the products and $w(\beta)$ is considered to be the reactants. The second (third) element, $\bar{q}$ $(\bar{o})$, is a sequence of $1\times S_{sp}$ vectors whose jth term correspond to the stochiometric coefficients of each reactant (product) participating in the jth full reaction. The fourth element is the p vector that identifies the matching between jth full reaction. The fifth (sixth) element, $\bar{u}$ $(\bar{d})$, is a sequence of integers whose jth term denotes the minimum (maximum) coefficient of the jth full reaction. Combining the two half reactions from above, the reaction:

$$CH_4+CO_2\rightleftarrows 2(CO)+2(H_2)$$

would then be represented by the tuple:

$$\left(\begin{bmatrix}-1&2&-1&0&0&0\\-4&0&0&0&4&0\\0&2&-2&0&0&0\end{bmatrix},[1,1,0],[2,2,0],[2,4,2],1,2\right)$$

In the next step, the algorithm creates the set off Gibbs Feasible Reactions, GFR, which is a sequence of sextuples that contains the full reaction sextuple along with relevant thermodynamic information:

$$\left(F_R, T, P, G, K_{eq}, X_{eq}\right) = \begin{pmatrix} \left\{F_R(j)\right\}_{j=1}^{\#(GFR)}, \left\{T(j)\right\}_{j=1}^{\#(GFR)}, \left\{P(j)\right\}_{j=1}^{\#(GFR)}, \\ \left\{G(j)\right\}_{j=1}^{\#(GFR)}, \left\{K_{eq}(j)\right\}_{j=1}^{\#(GFR)}, \left\{X_{eq}(j)\right\}_{j=1}^{\#(GFR)} \end{pmatrix}$$

The first element, F_R, is the full reaction sextuple as mentioned above. The second element, T, is a sequence of real numbers whose jth term denotes the temperature that the jth Gibbs Full Reaction occurs at. The third element, P, is a sequence of real numbers whose jth term denotes the pressure that the jth Gibbs Full Reaction occurs at. The fourth element, G, is a sequence of real numbers whose jth term denotes the standard Gibbs energy of formation for the jth Gibbs Full Reaction. The fifth element, K_{eq}, is a sequence of real numbers whose jth term denotes the equilibrium constant for the jth Gibbs Full Reaction. The sixth element, X_{eq}, is a sequence of real numbers, $X_{\min} \le X_{eq} \le 1$, whose jth term denotes the equilibrium conversion for the jth Gibbs Feasible Reaction. Because the set FR is generated without knowledge of any thermodynamic information and is based solely on atom balance, the program calculates thermodynamic properties for the forward and reverse direction, and therefore $2 \cdot \#(FR)$ tuples are generated.

Creating the set GFR necessitates solving equations (3.1.10)-(3.1.12) for each reaction. the standard molar Gibbs of formation for each species, which is accomplished through the use of the NASA Glenn coefficients[41]:

$$\Delta G_i^o(T) = \left\{ \begin{array}{l} RT\left(\begin{array}{l} -a_{1,i}(T)T^{-2} + a_{2,i}(T)\dfrac{\ln T}{T} + a_{3,i}(T) + a_{4,i}(T)\dfrac{T}{2} + \\ +a_{5,i}(T)\dfrac{T^2}{3} + a_{6,i}(T)\dfrac{T^3}{4} + a_{7,i}(T)\dfrac{T^4}{5} + \dfrac{b_{1,i(T)}}{T} \end{array} \right) \\ -R\left(\begin{array}{l} -a_{1,i}(T)\dfrac{T^{-2}}{2} + a_{2,i}(T)T^{-2} + a_{3,i}(T)\ln(T) + a_{4,i}(T)T \\ +a_{5,i}(T)\dfrac{T^2}{2} + a_{6,i}(T)\dfrac{T^3}{3} + a_{7,i}(T)\dfrac{T^4}{4} + b_{2,i(T)} \end{array} \right) \\ -\left(\sum_{j \in A_E \cap i} \dfrac{\psi_j}{\psi_{jm}} \lambda_j \right) \end{array} \right\} \qquad (3.1.16)$$

For more detailed information on the calculating of thermodynamic properties see Appendix A.3.

Theorem 1: *For a stoichiometric feed containing only reactants, Equation 3.1.12 is monotonically increasing in* ξ.

Proof: See Appendix A.4

The results from Theorem 1 give a necessary and sufficient condition on the feasibility of a reaction over the temperature range and show that for stoichiometric feed conditions that maximizing extent of reaction correlates to maximizing the right-hand side of (3.1.12). The advantage of this method is that the linearization of the Gibbs free energy data is not required to estimate whether a reaction is feasible over a given temperature range. Additionally, this allows for the use of the Brent-Dekker hybrid root finding algorithm when solving the rational function obtained in (3.1.12). The thermodynamic criterion utilized in this lexicographic method is that ξ must be greater than a value specified by the user (e.g., $\xi > 0.2$), and that this must occur within the feasible range of operating temperatures and pressures, which is initially given as $[T_L, T_U]$ and $[P_L, P_U]$ respectively. For the pressure window, Theorem 1 allows the algorithm to pick either the

minimum or maximum value of the pressure window depending on whether the products or reactants side has a greater number of moles. -In our formulation temperature dependent phase or other chemical change for many species is considered, and as such, the conclusions from Theorem 1 do not apply to a reaction if one of the species involved undergoes a transition, which changes the form of the left-hand side of (3.1.11). The algorithm therefore identifies the temperatures at which these changes occur for all species in the initial input and creates a subset of intervals to use as test points for every reaction that contains a species undergoing a phase change within the original interval. Thus, the actual upper temperature $\bar{T}_U$ of the operating window is defined for each individual reaction as, $\bar{T}_U = \min\left(T_U, T_{PC}^i\right)$ where T_{PC}^i is the temperature of a phase change for species i. The following theorem is then used to find the minimum value of $\frac{-\Delta G^o(T)}{RT}$ on each interval.

Theorem 2:*For all reactions, the function* $\frac{-\Delta G^o(T)}{RT}$ *is Lipschitz continuous on every interval in which the polynomial coefficients of the species participating do not change.*

Proof: See Appendix A.5

Since $\frac{-\Delta G^o(T)}{RT}$ is Lipschitz continuous on each given domain, this allows for the use of a larger class of covering methods for finding the minimizing temperature[42]. In this work a simplicial partitioning algorithm is used in conjunction with Lipschitz optimization, a technique that is based on making assumptions about the bounded of the slope of the objective function[43] and is used to identify the optimum temperature which maximizes ξ. The so-called simplicial homology global optimization (SHGO) algorithm has been shown to have promising

performance properties[44], and in our experiments was comparable to or outperformed other global optimization algorithms such as DIRECT-L1[45], basinhopping[46], and differential evolution[47].

The general cluster synthesizing algorithm is as follows. The target reaction $T_{\arg}^{*}$ is identified as: $T_{\arg}^{*} = aA_{(\beta_1)} + bB_{(\beta_2)} + cC_{(\beta_3)} \rightleftarrows dD_{(\beta_4)} + eE_{(\beta_5)} + fF_{(\beta_6)}$ and the lexicon of feasible whole reactions GFR. Clearly, if the target reaction is to contain a reactant, that reactant must be present as a reactant in at least one of the reactions comprising the cluster. Likewise, if the target reaction is to contain a certain product, at least one of the reactions comprising the cluster must contain that product. If the target reaction contains a single reactant or a single product, there is no choice but to employ reactions containing that species, but there is more freedom when the target reaction contains two (or more) Reactants and Products. Thus from GFR set two sets are constructed, the first $L_{tot} \triangleq \{L_i\}_{i=1}^{n}$ is a tuple whose ith element contains a set of reactions in GFR that have the ith species of the target reaction $T_{\arg}^{*}$ on the LHS. Similarly, the set $\mathrm{R}_{tot} \triangleq \{R_i\}_{i=1}^{n}$ is a tuple whose ith element contains a set of reactions in GFR that have the ith species of the target reaction $T_{\arg}^{*}$ on the RHS. Specifically, L_1 is the set of reactions whose left half reaction contains the first reactant of the target reaction (for the reaction above, this is species A), whereas L_2 is the corresponding set for the second reactant (if present) and so on. In order to ensure we capture all possible feasible reactions we take the union of all sets in L_{tot} and R_{tot}.

The formal creation of the sets for searching requires some work to remain consistent with established Set Theory, so we therefore start with the accepted notion of an ordered pair as:

$(x,y) \triangleq \{\{x\},\{x,y\}\}$, and the cross product of two sets A and B as:

$A \times B \triangleq \{(x,y) : x \in A \wedge y \in B\}$, noting that the set $A \times B$ is different from the set $B \times A$, $A \times B \neq B \times A$. However, in the context of reaction clusters we wish to establish that the cluster containing reactions (l_1, r_1) is equivalent to the cluster (r_1, l_1). We then define the transformation on a set of ordered pairs, Ψ, to a set of elements with cardinality 2, $\aleph$, as $g : \Psi \to \aleph$,

$g : \{\{x\},\{x,y\}\} \to \{x,y\}$

$$g(\Psi) \triangleq \left\{ \{x,y\} : \begin{pmatrix} \forall \alpha \in \psi \subseteq \Psi : x \in \alpha \\ (\exists \alpha \in \psi \subseteq \Psi : y \in \alpha) \wedge (\forall \alpha_1, \alpha_2 \in \psi \subseteq \Psi : \alpha_1 \neq \alpha_2 \Rightarrow (y \notin \alpha_1 \vee y \notin \alpha_2)) \end{pmatrix} \right\}.$$

The union of the following three sets is then used for searching 2/3 clusters:

$$(1)\, LR_1 \triangleq \left\{ \{l_1, r_1\} : g\left(\left(L \setminus R \right) \times R \right) \forall l_1 \in L, r_1 \in R \right\}$$

$$(2)\, LR_2 \triangleq \left\{ \{l_1, r_1\} : g\left(\left(L \bigcap R \right) \times \left(R \setminus L \right) \right) \forall l_1 \in L, r_1 \in R \right\}$$

$$(3)\, LR_3 \triangleq \left\{ \{l_1, r_1\} : g\left(\left\{ \begin{pmatrix} L \bigcap R \\ 2 \end{pmatrix} \right\} \right) \forall l_1 \in L, r_1 \in R \right\}$$

$LR \triangleq LR_1 \cup LR_2 \cup LR_3$

Theorem 3: *The three sets* LR_1, LR_2, LR_3 *are disjoint.*

Proof: See Appendix A.6

For all reaction combinations of $\{l,r\} \in LR$, let $T_{\arg} = T_{\arg}^{\,*} - l - r$. If $T_{\arg} = 0$, then l and r form a two-reaction cluster whose overall reaction is the target reaction $T_{\arg}^{\,*}$. If $T_{\arg} \in GFR$, then l, r, and $T_{\arg}$ form a three-reaction cluster. If $T_{\arg} \notin GFR$, then recurse using $T_{\arg}$ as the target instead of $T_{\arg}^{*}$ to find four- and five-reaction clusters. This recursive process can be repeated up to

$\left(N_R/2\right)$ times to find clusters that contain up to N_R reactions. The value $\left(N_R/2\right)$ is a result of the fact that in each loop of the algorithm, the even clusters are found automatically when searching for odd clusters. For example, when searching for 3-reaction clusters, all feasible 2-reaction clusters are found. Similarly, when searching for 5-reaction clusters, 4- reaction clusters are automatically found, and so on.

The number of elements in the set GFR depends the size of HR, depends on the size of the species database, the number of species allowed for each half reaction, and the maximum stoichiometric coefficient. The maximum half reaction formula can equivalently be recast as:

$$HR_{\max} = \sum_{i=1}^{S_{sp}} \left(\frac{\left(\nu^{\max}\right)^i}{i!} \cdot \prod_{k=0}^{i-1} \left[\#\left(N_S\right) - k \right] \right) \qquad (3.1.17)$$

Theorem 4: *The complexity of* $HR_{\max}$ *is of order* $\Theta\left(\#\left(N_S\right)^{S_{sp}}\right)$

Proof: See Appendix A.7

Given $HR_{\max}$ half reactions, there are at most $\Theta\left(\left(HR_{\max}\right)^{\nu^{\max}}\right)$ whole reactions. However, considering mass balances and employing thermodynamic feasibility constraints greatly reduces this number. A closer inspection of the relationship between the size of the lexicon and the size of the sets HR, FR, and N_A reveal insight into the size of FR. For $S_{sp} = 2$, experiments have shown that FR is bounded by the size of the lexicon, which is in turn bounded by the size of HR. Designating the lexicon set as Λ_L this observation suggests that $\#\left(HR\right) > \#\left(\Lambda_L\right) > \#\left(FR\right)$ and indicates that mass balance constraints alone yield a considerable constraint on the size of FR. However, for $S_{sp} = 3$ this is no longer the case. From

experimental trials we see that size of the lexicon is still bounded by the size of HR, but that the size of FR quickly outgrows them as N_S increases. In the figures below the sizes of HR, FR, and N_A are plotted against the size of N_S for $S_{sp} = 3$ and $\nu^{\max} = 8$.

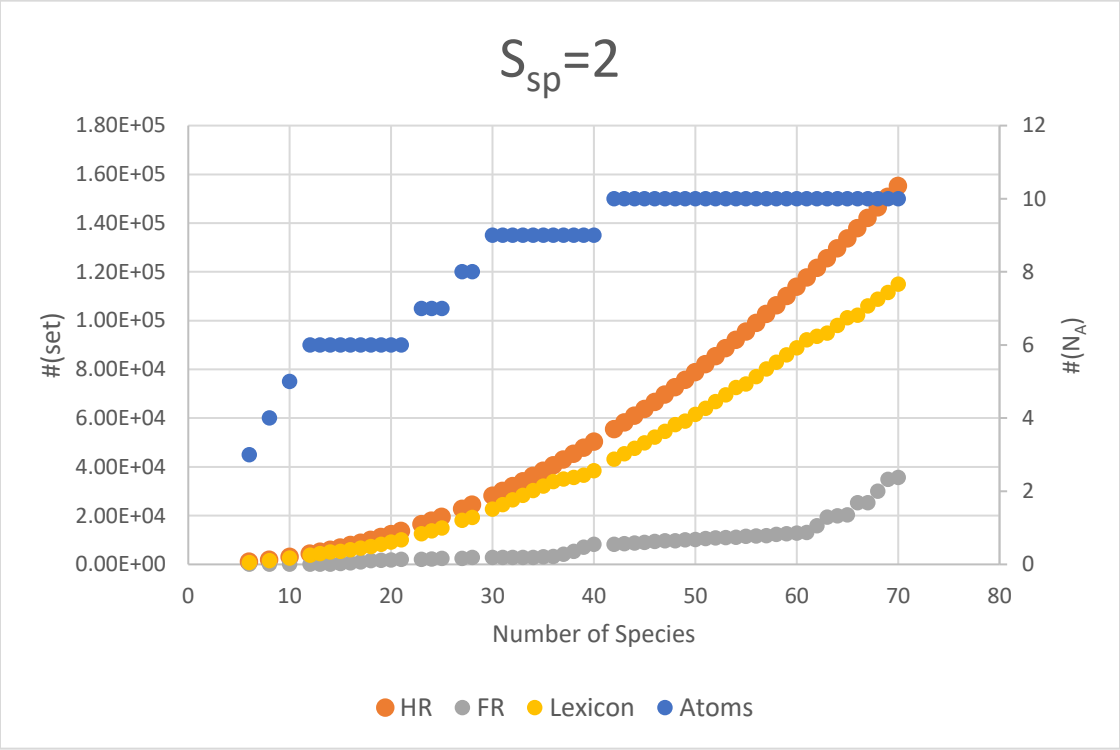

Figure 3-1 Size of HR, FR, Lexicon and NA as for increasing size of NS, max species per HR=2, experiment 1.

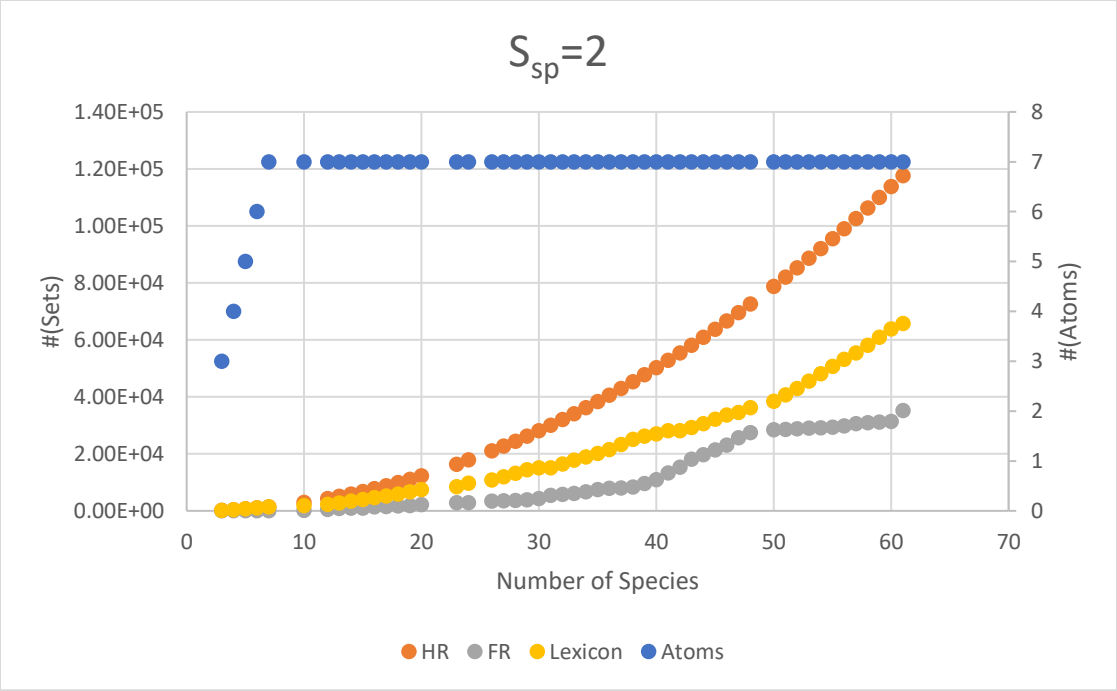

Figure 3-2 - Size of HR, FR, Lexicon and N_A as for increasing size of N_S, max species per HR=2, experiment 2

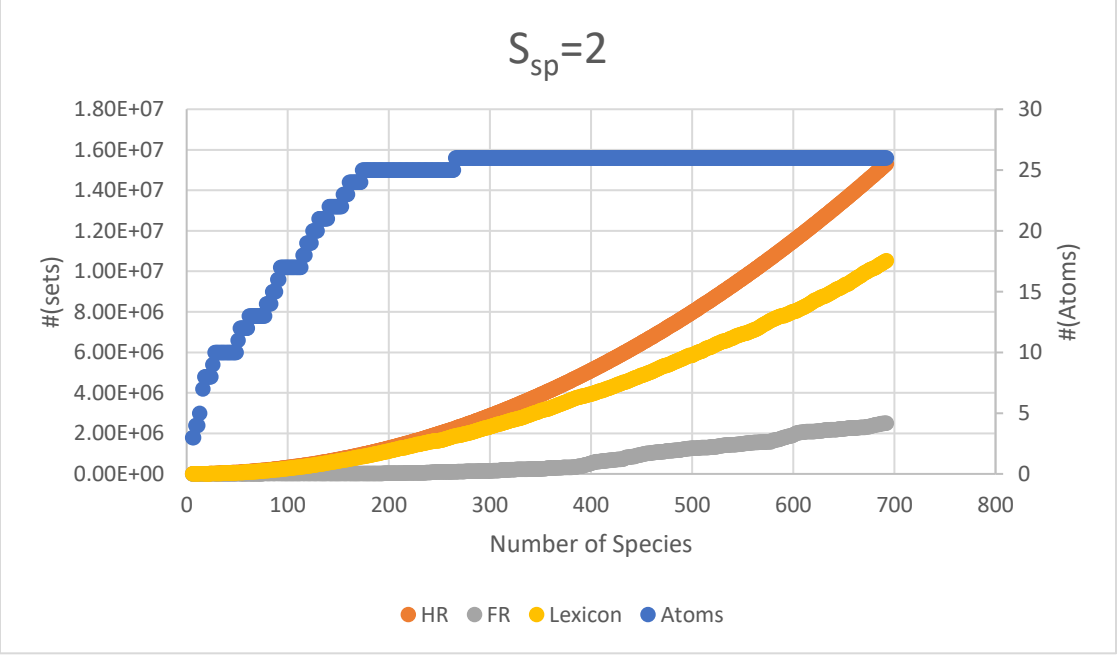

Figure 3-3 Size of HR, FR, Lexicon and N_A as for increasing size of N_S, max species per HR=2, experiment 3.

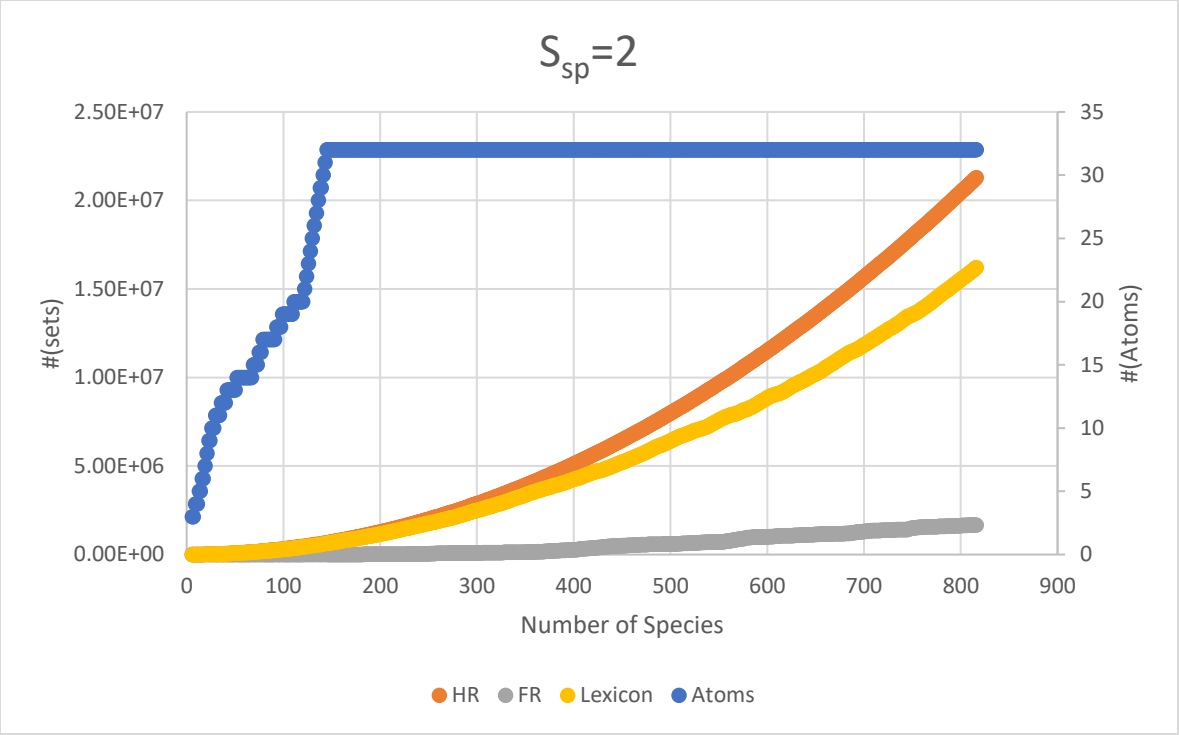

Figure 3-4 Figure 3 3 Size of HR, FR, Lexicon and NA as for increasing size of NS, max species per HR=2, experiment 4.

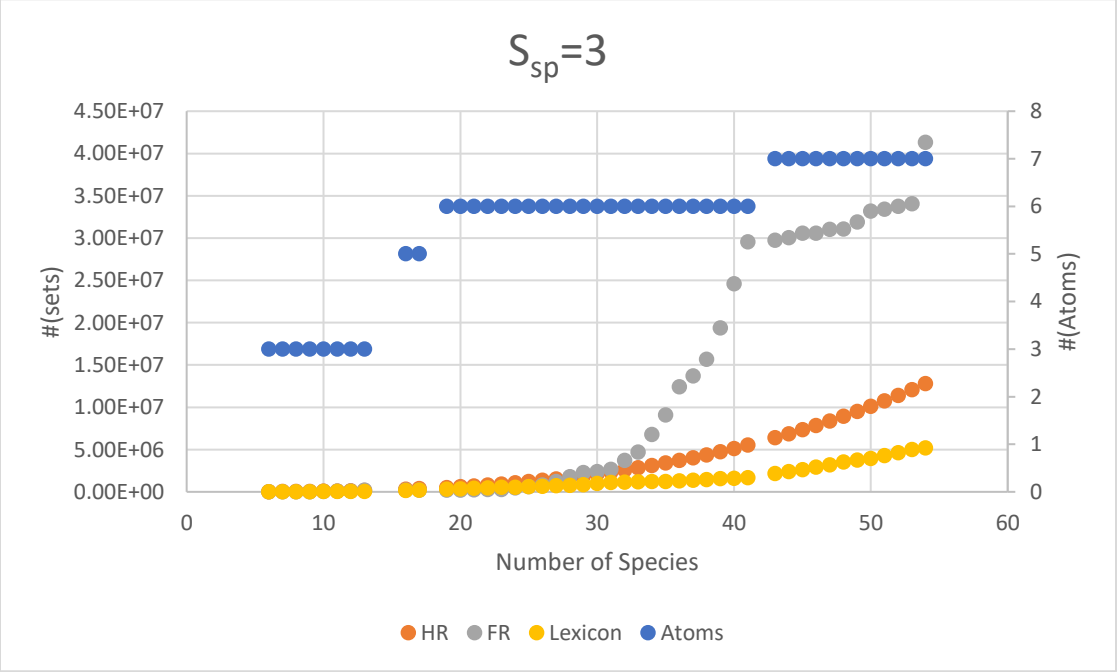

Figure 3-5 Size of HR, FR, Lexicon and N_A as for increasing size of N_S, max species per HR=3, experiment 1

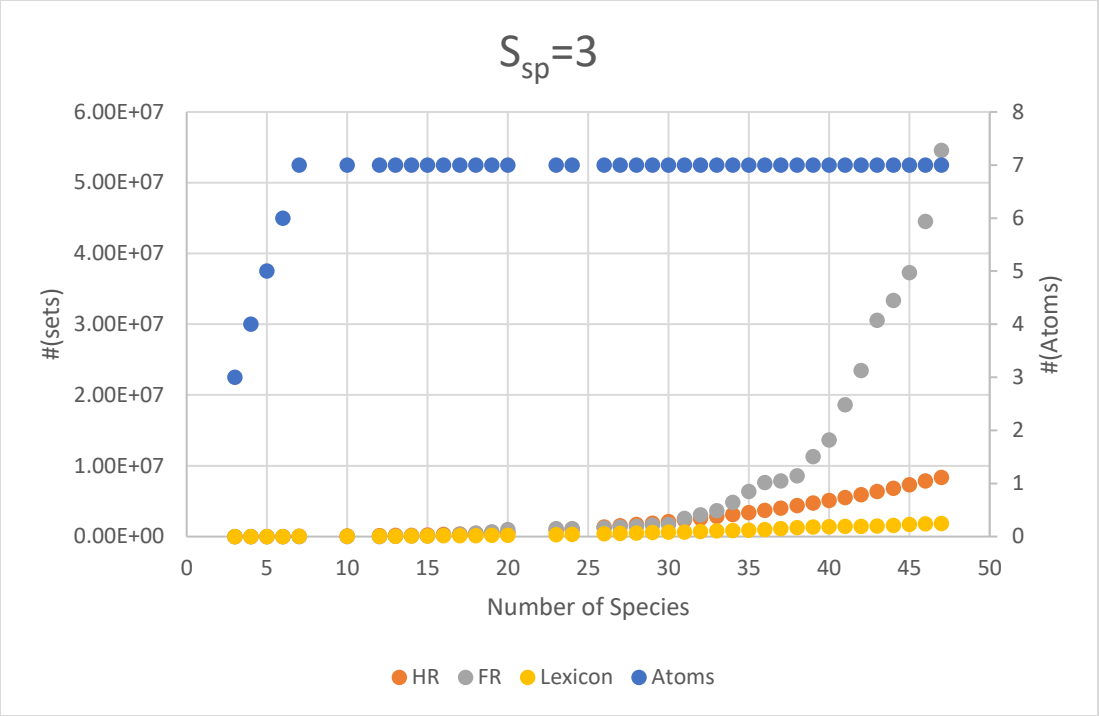

Figure 3-6 Size of HR, FR, Lexicon and N_A as for increasing size of N_S, max species per HR=3, experiment 2

However, the overwhelming majority of industrial relevant reactions have at most one half reaction with 3 species while the other half reaction will have at most 2 species. This observation can easily be implemented into the algorithm to generate reactions that are more feasible from that perspective. The results that indicate that in this scenario the inequality for $S_{sp} = 2$ still holds, namely that $\#(HR) > \#(\Lambda_L) > \#(FR)$.

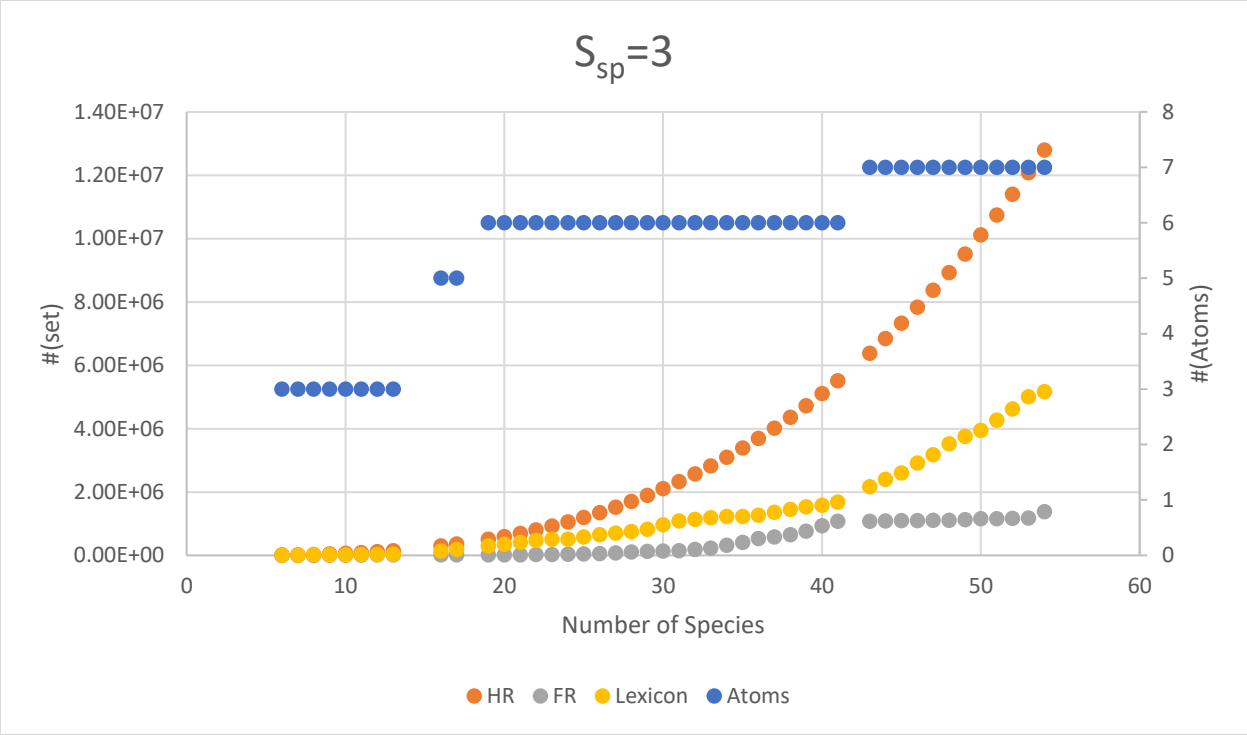

Figure 3-7 Size of HR, FR, Lexicon and N_A as for increasing size of N_S, max species per FR=5, experiment 1

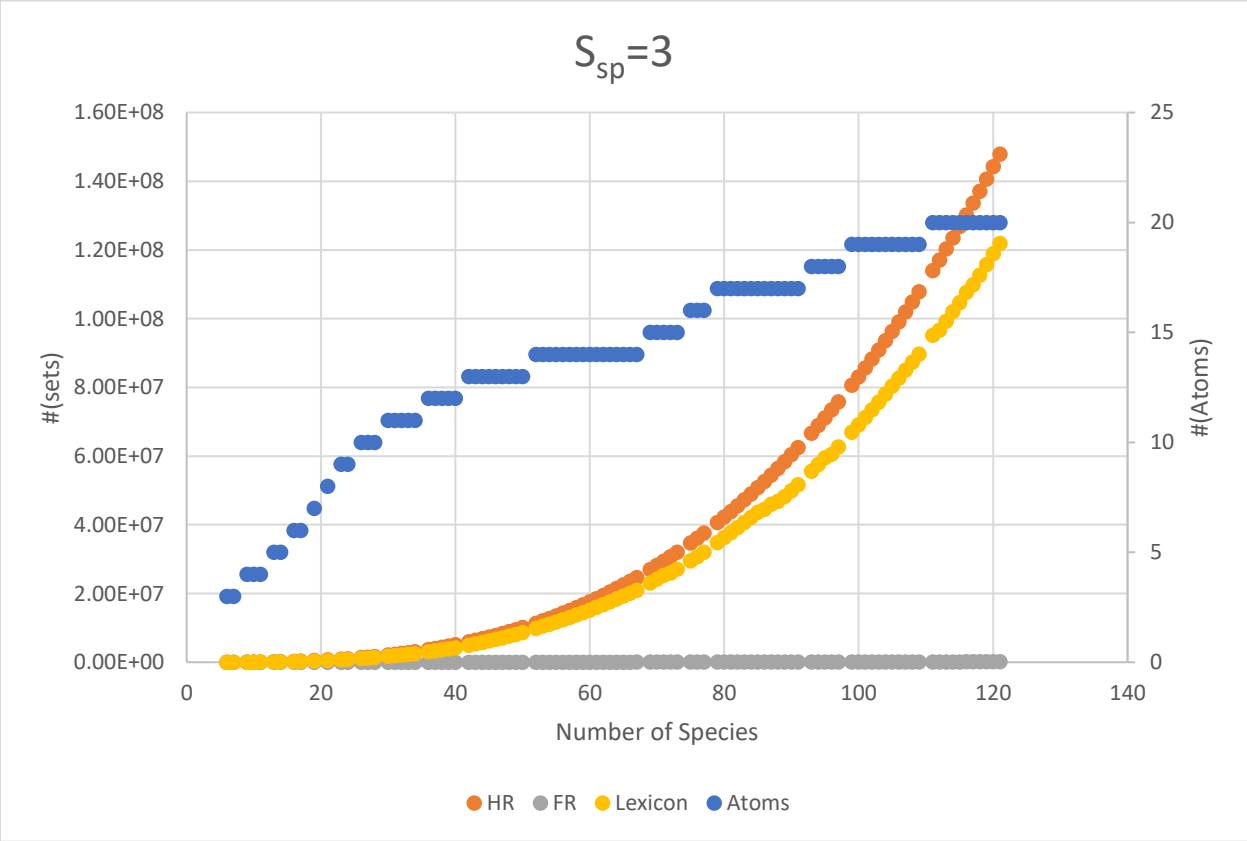

Figure 3-8 Size of HR, FR, Lexicon and N_A as for increasing size of N_S, max species per FR=5, experiment 2

For a set of feasible whole reactions, GFR, the worst-case time complexity of this algorithm can be calculated in the following manner. Scan the set N_S times and keep track of how many times each species occurs on the left and right side of the feasible reactions and let $L_{\max}$ be the set containing the maximum number of occurrences (over all N_S species) of any species occurring on the left side of the reaction. Similarly, let $R_{\max}$ be the maximum number of occurrences on the right side. That means that in the worst case, $L = L_{\max}$ and $R = R_{\max}$ for each recurrence. Thus, for $N_R = 2$, there are at most $\#(L_{\max}) \cdot \#(R_{\max})$ possible combinations of clusters that must be considered. For $N_R = 3$, the set GFR must be scanned for each combination of L and R, so the complexity is $\Theta(\#(GFR) \cdot \#(L_{\max}) \cdot \#(R_{\max}))$. If a cluster is not found and the algorithm recurses, each combination leads to another set of L and R lists, and there are again $\#(L_{\max}) \cdot \#(R_{\max})$ combinations for each of the $\#(GFR) \cdot \#(L_{\max}) \cdot \#(R_{\max})$ potential clusters, yielding complexity $\Theta\left(\#(GFR) \cdot (\#(L_{\max}))^2 \cdot (\#(R_{\max}))^2\right)$ for $N_R = 5$.

In general, the algorithm generates clusters in rounds: the first round searches for 2/3-reaction clusters, the second call searches for 4/5-reaction clusters, the third call searches for 6/7-reaction clusters, and so on. Therefore the complexity is $\Theta\left(\#(GFR) \cdot (\#(L_{\max}) \cdot \#(R_{\max}))^{\frac{N_R}{2}}\right)$.

The advantage of using the strategy above is that it can reduce the order of complexity by several orders of magnitude over our previous formulation. In an experimental trial with a database of $N_S = 30$ species that results in 7759 feasible whole reactions, where $\#(L_{\max}) = 275$ and $\#(R_{\max}) = 744$, the total number of possibilities for reaction clusters containing up to 5

reactions per cluster (N_R = 5), would be $3.248E^{14}$ using the original formula. If every possible combination of reactions were considered there would be approximately $\binom{7759}{5} \approx 2.35E^{17}$ such combinations to consider in this case. Using the sets defined about it was found that there were $7.969E^{9}$ combinations, constituting a reduction of 5 orders of magnitude. Additionally, through the use of indexing and combinatorial function set construction, the sequence for each cluster search can be determined before sending to the cluster finding algorithm, which can allow for the full use of multiprocessing capabilities. Create the set $\mathrm{A}_{idx} \triangleq \left\{ n \in \mathbb{N} \setminus \{0\} : n \le \#(GFR) \right\}$ of natural numbers and define an indexing function $f_1 \triangleq GFR \to \mathrm{A}_{idx}$ which maps each element in GFR to a unique natural number. Thus f_1 is bijective and its forward image:

$$f_1(S) \triangleq \left\{ f_1(x) : x \in S \subseteq GFR \right\}$$

and reverse image:

$$f_1^{-1}(U) \triangleq \left\{ x : f_1^{-1}(x) \in U \subseteq \mathbb{N} \ \forall x \in S \subseteq GFR \right\}$$

are well defined. Applying this function to the creation of the previously defined disjoint sets by first creating the two sets:

$$A_L \triangleq \left\{ x : f_1^{-1}(x) \in L \, \forall x \in A_{idx} \right\}$$

$$A_R \triangleq \left\{ y : f_1^{-1}(y) \in R \, \forall y \in A_{idx} \right\}$$

$$(1) LR_{1,idx} \triangleq \left\{ \left\{ l_{n,1}, r_{n,1} \right\} : g\left(\left(A_L \setminus A_R \right) \times A_R \right) \forall l_{n,1} \in A_L, r_{n,1} \in A_R \right\}$$

$$(2) LR_{2,idx} \triangleq \left\{ \left\{ l_{n,1}, r_{n,1} \right\} : g\left(\left(A_L \bigcap A_R \right) \times \left(A_R \setminus A_L \right) \right) \forall l_{n,1} \in A_L, r_{n,1} \in A_R \right\}$$

$$(3)\, LR_{3,idx} \triangleq \left\{ \left\{ l_{n,1}, r_{n,1} \right\} : g\left(\left\{ \binom{A_L \bigcap A_R}{2} \right\} \right) \forall l_{n,1} \in A_L, r_{n,1} \in A_R \right\}$$

This saves memory during multithreaded function call because only the feasible set and the index is sent to each thread, as opposed to sending each thread the whole feasible set in addition to all of sets L and R. This also allows the cluster finding algorithm to be split into separate functions for each set of n/m-clusters.

3.3 Algorithm Implementation and Database Creation/Maintenance

The above algorithm is implemented in Python and utilizes just-in-time (JIT) parallel processing functions for increase computational speed and features the use of the multiprocessing module for certain operations during the process (such as calculating ξ for each reaction). The information for calculating all the thermodynamic properties for the species in the input data set is taken from the NASA Glenn coefficients, as noted above. However, for use in our program it is advantageous to be able to augment or change the information contained within the original file in order to better reflect and stay current with any experimental results, or to compute other thermodynamic functions such as non-ideal gas equation of state properties. Additionally, it is desirable to include species data not included in the original data set, whether by data fitting known values from another database or validated experimental results. Therefore, the original NASA Glenn file is converted to SQL database, which the algorithm initiates upon execution. In this way information can be changed or added when needed.

To demonstrate, the species Co_3O_4, $CoCl_2$, CoO, KBF_4, BFO, and $Cu(OH)_2$ are not in the original NASA Glenn file but thermodynamic properties are readily found on NIST or JANAF. We therefore applied least squares minimization on heat capacity, entropy, enthalpy,

and Gibbs of formation data over the set of 9 parameters for each species at the temperatures and phases listed. The results of this process are shown in the figure below and show excellent agreement against published data, with a maximum difference of 1.15% across all species' thermodynamic properties.

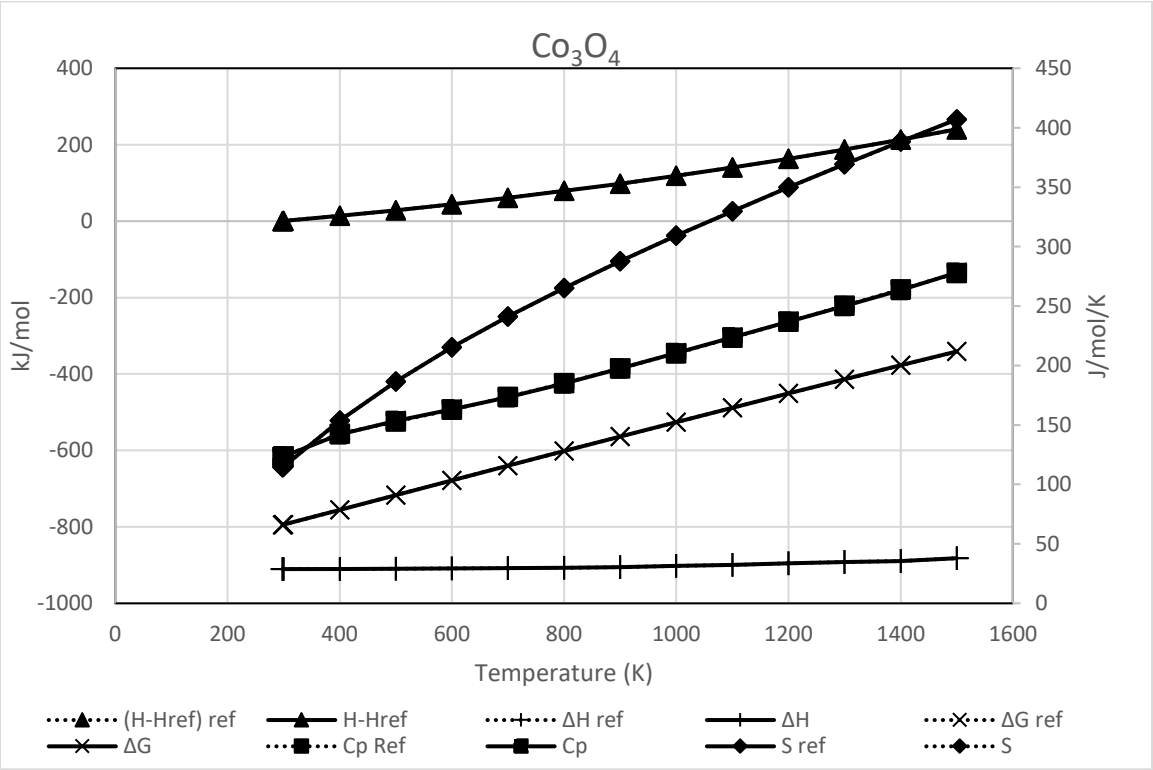

Figure 3-9 Calculated values of thermodynamic properties for cobalt (II,III) oxide against values obtained from NIST.

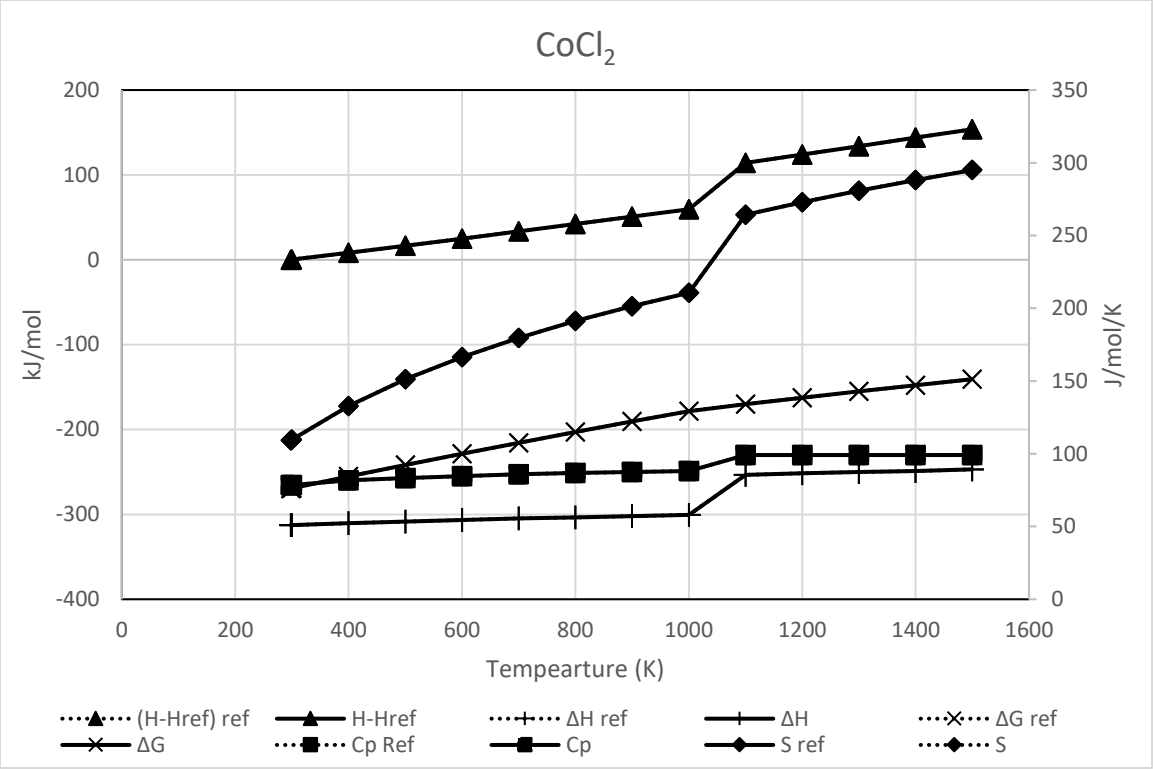

Figure 3-10 Calculated values of thermodynamic properties for cobalt chloride against values obtained from NIST.

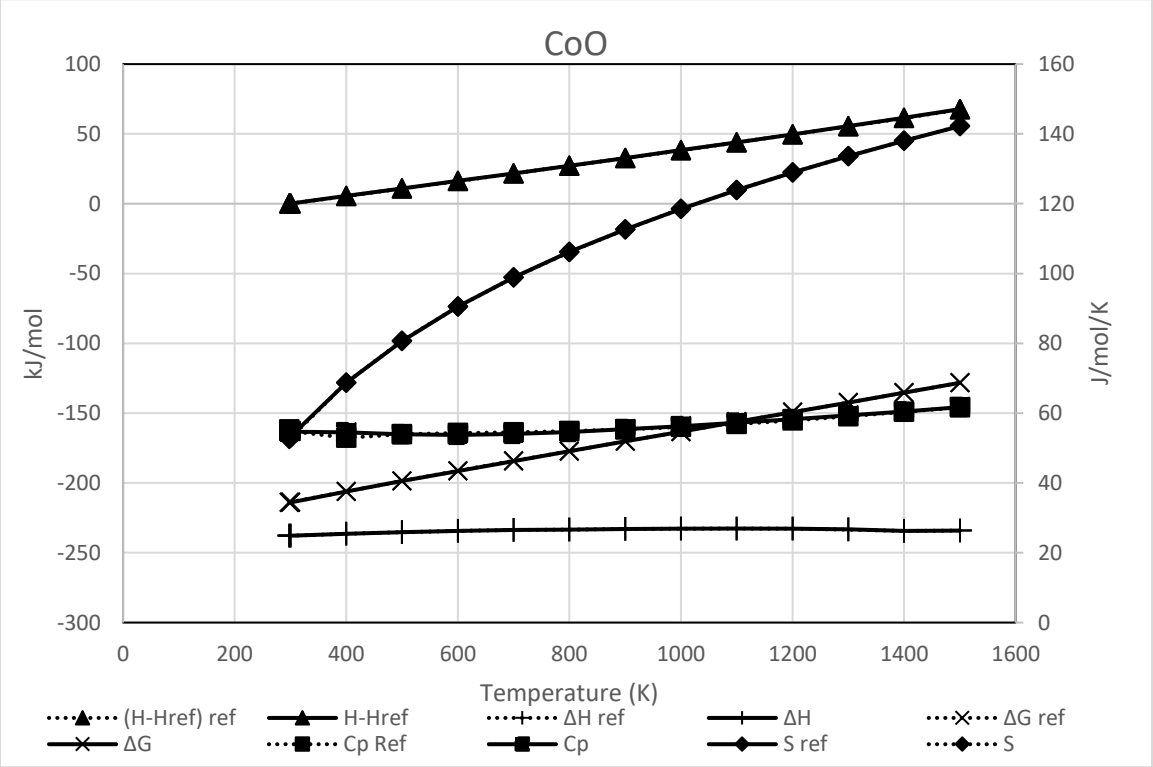

Figure 3-11 Calculated values of thermodynamic properties for cobalt (II) oxide against values obtained from NIST.

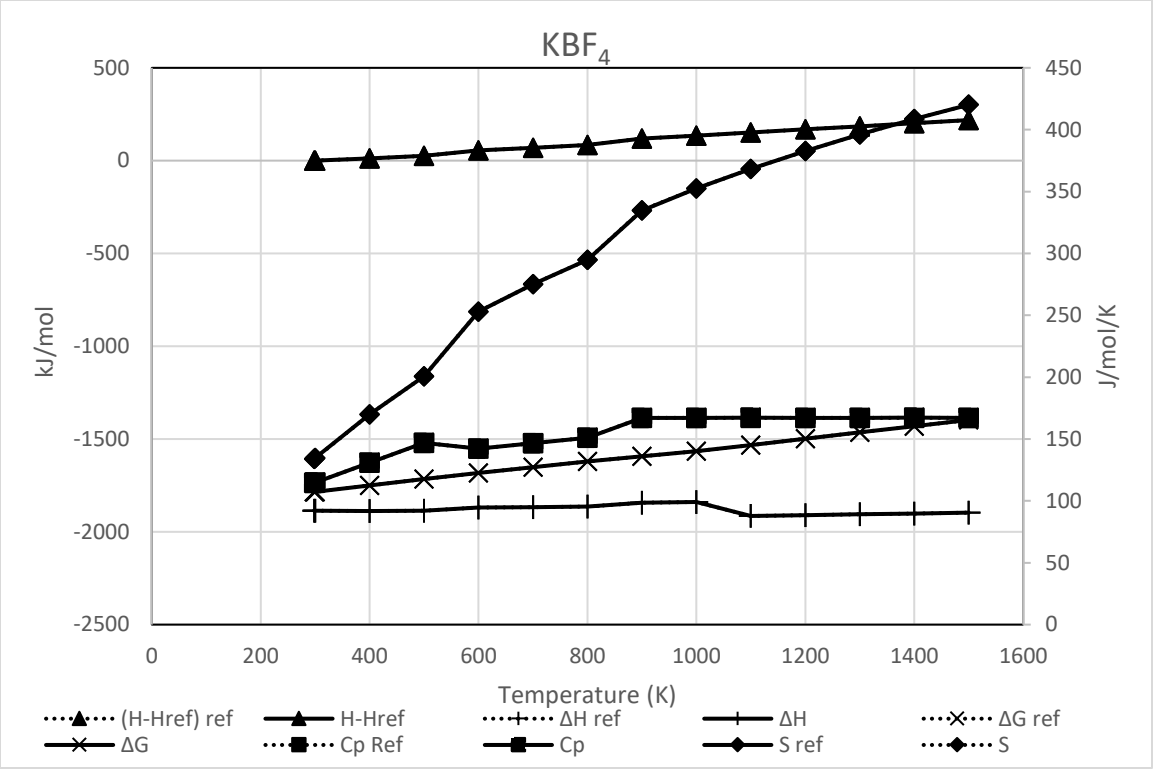

Figure 3-12 Calculated values of thermodynamic properties for potassium tetrafluroborate against values obtained from NIST.

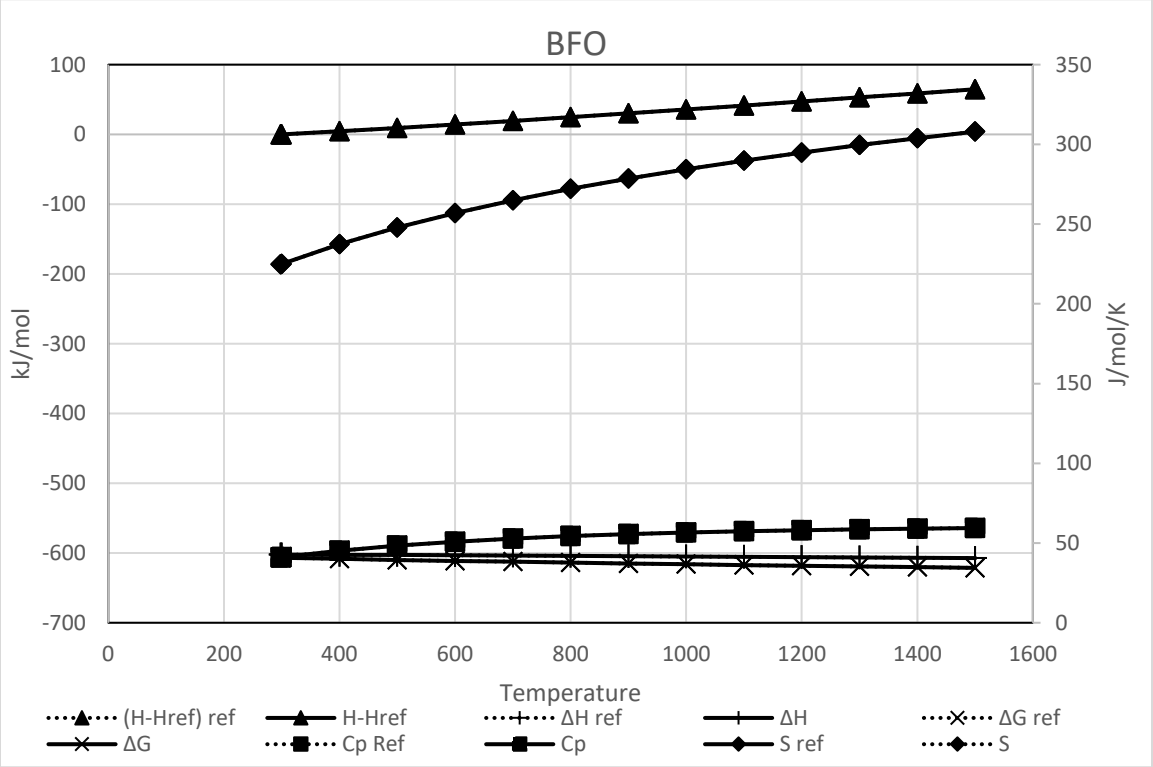

Figure 3-13 Calculated values of thermodynamic properties for boron monofluoride monoxide against values obtained from NIST.

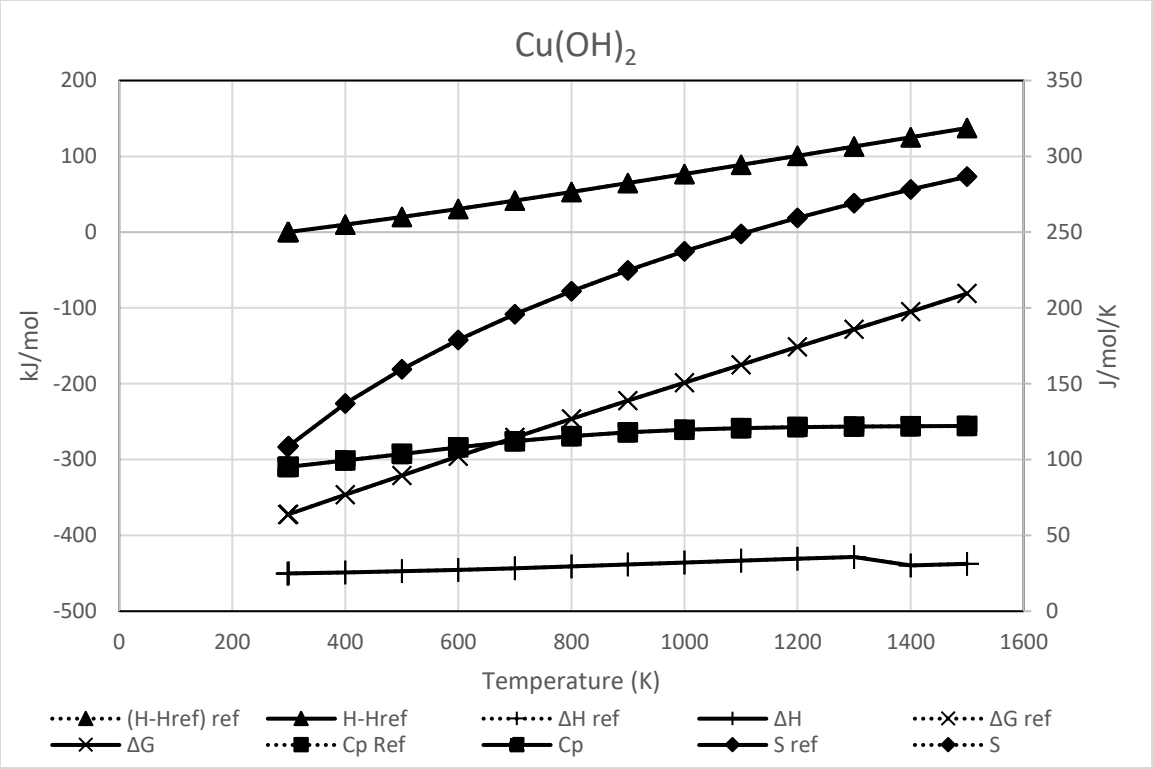

Figure 3-14 Calculated values of thermodynamic properties for copper(II) hydroxide against values obtained from NIST.

3.4 Notation

English Symbols

A_E : Set of atomic elements.

$a_{1,i}, a_{2,i}, a_{3,i}, a_{4,i}, a_{5,i}, a_{6,i}, a_{7,i}, b_{1,i}, b_{2,i}$: Nasa Glenn thermodynamic coefficients for species i.

$C_{p,i}^{o}\left(\frac{J}{mol\ K}\right)$: standard molar heat capacity for species i in phase.

d^{*} : Target reaction for reaction cluster synthesis.

$\hat{f}_i^{(\alpha)}$: Species i fugacity in solution in phase α.

$f_i^{o(\alpha)}$: Pure species i fugacity at standard conditions in phase .

FHR : full reaction sequence quintuple.

G : Set of species that are gas.

$\Delta G^o\left(\frac{J}{mol}\right)$: Standard Gibbs energy of formation for a chemical reaction.

GHR: Gibbs feasible reaction sequence sextuple.

$\Delta H^o\left(\frac{J}{mol}\right)$: Standard Enthalpy of formation for a chemical reaction.

HR: half reaction sequence quintuple.

K_{eq} : equilibrium constant.

L : set of species that are liquid.

L_x : a tuple where each entry contains a set of reactions containing a species on the reactant side found in the target reaction.

$n_{i,o}\left(mol\right)$: initial amount of species i present in a chemical reaction.

N_S: The number species present used in reaction cluster screening.

N_A : The number of different kind of atoms present in reaction cluster screening.

N_R : maximum number of reaction clusters.

NC: number of species participating in a chemical reaction.

$P\left(Pa\right)$: Pressure

$P_L\left(Pa\right)$: Lower pressure bound.

$P_U\left(Pa\right)$: Upper pressure bound.

$R\left(\frac{J}{mol\,K}\right)$: Gas constant.

R_χ : a tuple where each entry contains a set of reactions containing a species on the product side found in the target reaction.

$T_i^{fus}\left(K\right)$: fusion temperature

$T_i^{vap}\left(K\right)$: vaporization temperature.

$T\left(K\right)$: Temperature.

T_{PC}^{i} : phase change temperature of species i.

$T_L\left(K\right)$: Lower temperature bound.

$T_U\left(K\right)$: Upper temperature bound.

$\overline{T}_U\left(K\right)$: Augmented upper temperature bound.

$T_{\arg}^{\ *}$: Target reaction for cluster synthesis.

$P^o\left(Pa\right)$: Reference pressure.

S_{sp} : maximum number of species present in each half reaction.

$\Delta S^o\left(\frac{J}{mol}\right)$: standard Entropy of formation for a chemical reaction.

W : set of feasible reactions.

Greek Symbols

α_i : flag variable for denoting phase of species i.

ν_i : stochiometric coefficient of species i.

ν_{im}: Stoichiometric coefficient quantifying number of atoms of element m in species i in the most thermodynamically stable state (molecular form, and phase) of element m at 298.15 K and 1 bar.

ν^{max} : maximum allowable stochiometric coefficient.

ξ: extent of reaction/ conversion.

ξ_{min} : minimum allowable extent of reaction.

Θ : complexity function.

ψ_j : Number of occurrences of atomic element j in a chemical species.

ψ_{jm} : Number of atoms of atomic element j that form a stable molecule at STP.

λ_j : Atomic element j in a chemical species.

Chapter 4 - Lexicographic case studies:

In this chapter we present some of the results of the Lexicographic approach to cluster synthesis with five different target reactions. The first target reaction is water splitting, the second target reaction is formic acid production with hydrogen generation from natural gas, the third target reaction is acetic acid production with hydrogen generation from natural gas, the fourth target reaction is dimethyl ether (DME) production with hydrogen generation from natural gas, and the last target reaction is water splitting cycle that has imbedded in it steam methane reforming (SMR). In the last section we present some potential features for further screening and enhancement of found clusters. Importantly, none of the cycles release harmful carbon containing byproducts and use natural gas as a raw material. As seen in the figure below[48], U.S. natural gas production has been steadily increasing since 2010:

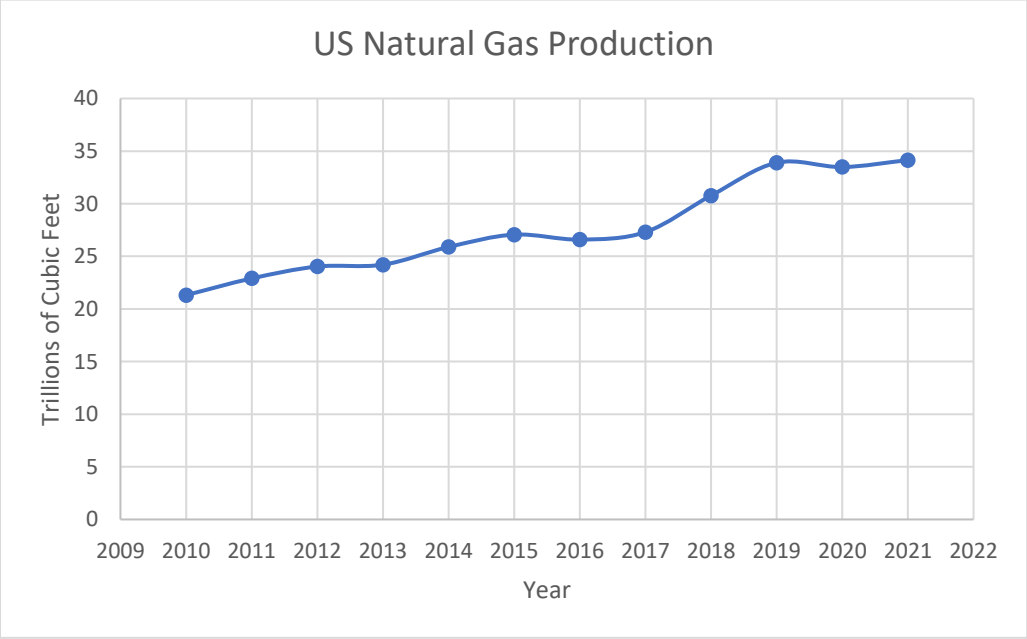

Figure 4-1- US Natural gas production by year.

4.1 Water Splitting Cycles

In this section we present clusters that sum to water splitting $2(H_2O) \Leftrightarrow O_2 + 2(H_2)$. Direct thermolysis of this reaction yields very poor conversion even at elevated temperatures, with an estimated conversion of ~4% for temperatures at 2273K. Finding alternative pathways for hydrogen generation using a variety of raw materials would have a major impact on disadvantaged communities, enabling them to become energy self-sufficient, to minimize their carbon footprint, and improve the air quality of their environment

The lexicographic algorithm was applied to a database with 120 species (see Appendix 3) and 20 atoms. A maximum of 3 reactants or 3 products were allowed for each candidate $(S_{sp} = 3)$, an enforcement that was put in at the mass balance generated reaction step and reflects the specialization capabilities of our proposed methodology. Clusters of up to three reactions were generated $(N_R = 3)$ at a temperature range between 298 K and 1500 K $(T_L = 298, T_U = 1500)$ and a pressure range of 1 and 25 bar $(P_L = 1, P_U = 25)$. The minimum extent of reaction was set to 0.6 $(\xi_{\min} = 0.6)$. The input parameters for the simulation are listed in Table 4-1 and the algorithm generated clusters are listed in table 2.

Table 4-1: Problem Parameters

Parameter	T_L	T_U	P_L	P_U	$\#(N_S)$	N_R	S_{sp}	$\nu^{\max}$	$\xi_{\min}$
Value	298	1500	1	25	120	3	3	8	0.6

The results from the simulation are shown in table 4-2. Nine reaction clusters were generated, with two 2-cluster cycles and seven 3-cluster cycles. The clusters generated occur at temperatures that are generally attainable for industrial processes, which is an important consideration in the automatic synthesis of reaction clusters. Additionally, the incorporation of

the thermodynamic criterion improves the possibility of synthesizing reaction clusters that can be successfully implemented on an industrial level. Examining the temperature and pressures shows that every reaction cluster generated contains reactions that occur at two or more different temperatures, and only 1 reaction cluster, cycle 2, contains reactions that occur all at the same pressure.

Table 4-2: Water splitting cycles

	Reactions	$T(K)$	$P(bar)$	$\Delta G^o\left(\frac{kJ}{mol}\right)$	ξ
1	$4H_2O_{(l)} + 6CO_{(g)} \Leftrightarrow CH_{4(g)} + 2H_{2(g)} + 5CO_{2(g)}$	298	1	-252.07	0.99
	$4GeO_{(g)} + 6CO_{2(g)} \Leftrightarrow O_{2(g)} + 4GeO_{2(s)} + 6CO_{(g)}$	298	25	-284.81	0.99
	$CH_{4(g)} + 4GeO_{2(l)} \Leftrightarrow CO_{(g)} + 2H_2O_{(g)} + 4GeO_{(g)}$	1500	1	-252.67	0.99
2	$2H_2O_{(l)} + 3Ga_2I_{2(g)} \Leftrightarrow Ga_2I_{6(g)} + 2Ga_2O_{(g)} + 2H_{2(g)}$	373	1	-25.17	0.98
	$2Ga_2O_{(g)} + 3I_{2(s)} \Leftrightarrow Ga_2I_{6(g)} + O_{2(g)} + 2Ga_{(s)}$	298	1	-114.55	0.99
	$2Ga_2I_{6(g)} + 2Ga_{(l)} \Leftrightarrow 3Ga_2I_{2(g)} + 3I_{2(g)}$	1500	1	-23.25	0.88
3	$3H_2O_{(g)} + 5K_2O_{(l)} \Leftrightarrow O_{2(g)} + 3K_2O_2H_{2(g)} + 4K_{(g)}$	1500	1	-19.73	0.90
	$4K_2O_2H_{2(g)} + 6K_{(s)} \Leftrightarrow H_2O_{(l)} + 3H_{2(g)} + 7K_2O_{(s)}$	298	25	-36.13	0.99
	$H_{2(g)} + 2K_2O_{(l)} \Leftrightarrow K_2O_2H_{2(g)} + 2K_{(g)}$	1500	1	-138.82	0.99
4	$3H_2O_{(g)} + 5K_2O_{(l)} \Leftrightarrow O_{2(g)} + 3K_2O_2H_{2(g)} + 4K_{(g)}$	1500	1	-19.73	0.90
	$3K_2O_2H_{2(g)} + 4K_{(s)} \Leftrightarrow H_2O_{(l)} + 2H_{2(g)} + 5K_2O_{(s)}$	298	25	-5.907	0.90
5	$4K_2O_{(s)} + 6H_2O_{(g)} \Leftrightarrow O_{2(g)} + 2H_{2(g)} + 4K_2O_2H_{2(g)}$	1500	1	45.47	0.60

	$Cu_{2(g)} + 4K_2O_2H_{2(g)} \Leftrightarrow \begin{pmatrix} 2Cu(OH)_{2(s)} + 2H_{2(g)} \\ + 4K_2O_{(s)} \end{pmatrix}$	298	25	-11.19	0.96
	$2Cu(OH)_{2(s)} + 2H_{2(g)} \Leftrightarrow Cu_{2(g)} + 4H_2O_{(g)}$	1500	1	-252.3	0.99
6	$Cu_{2(g)} + 4H_2O_{(l)} \Leftrightarrow 2Cu(OH)_{2(s)} + 2H_{2(g)}$	298	1	-229.91	0.99
	$2Cl_{2(g)} + 2Cu(OH)_{2(s)} \Leftrightarrow Cu_{2(g)} + 2O_{2(g)} + 4HCl_{(g)}$	1500	1	-10.14	0.92
	$4HCl_{(g)} + O_{2(g)} \Leftrightarrow 2Cl_{2(g)} + 2H_2O_{(l)}$	298	25	-93.13	0.99
7	$2Cl_{2(g)} + 2H_2O_{(g)} \Leftrightarrow O_{2(g)} + 4HCl_{(g)}$	1500	1	-86.53	0.81
	$2CaH_{2(l)} + 4HCl_{(g)} \Leftrightarrow Cl_{2(g)} + 2CaCl_{(g)} + 4H_{2(g)}$	1500	1	-74.86	0.93
	$2CaCl_{(g)} + 2H_{2(g)} \Leftrightarrow Cl_{2(g)} + 2CaH_{2(s)}$	298	25	-15.94	0.99
8	$5H_2O_{(l)} + 7SO_{3(g)} \Leftrightarrow O_{2(g)} + 2SO_{2(g)} + 5H_2SO_{4(l)}$	298	25	-266.7	0.99
	$2SO_{2(g)} + 5H_2SO_{4(g)} \Leftrightarrow 2H_{2(g)} + 3H_2O_{(g)} + 7SO_{3(g)}$	1500	1	-143.6	0.90
9	$2H_2O_{(g)} + 3Li_2Cl_{2(g)} \Leftrightarrow O_{2(g)} + 2H_{2(g)} + 6LiCl_{(s)}$	298	N/A	-28.62	0.98
	$2SO_{3(g)} + 6LiCl_{(l)} \Leftrightarrow O_{2(g)} + 2SO_{2(g)} + 3Li_2Cl_{2(g)}$	1500	1	-7.56	0.90
	$O_{2(g)} + 2SO_{2(g)} \Leftrightarrow 2SO_{3(g)}$	298	25	-141.86	0.99

The first reaction cluster in Table 4-2 is a Germanium based cycle. Germanium has found recent attention in the context of forming reaction clusters for water splitting using concentrated solar power [49], [50] and several proposed reaction clusters have been investigated. It also features the use of methane which could be enhanced with natural gas pipelines that are already in existence. The second reaction cluster is a Gallium oxide/iodide based cycle. Application of these species has been found recently in a number of fields, including hybrid car production, electrical components for power generating systems, and

ultraviolet radiation sensors[51]. Current limitations for widespread implementation into industry stem from inadequate synthesis technology and poor scalability, however research into these drawbacks is ongoing.

The third and fourth reaction clusters are Potassium oxide based clusters. Metal oxide reaction clusters have been the subject of investigation for numerous years[52] and remain an area of active research[53]. Cluster 3 is one of four clusters found that contains a reaction with a target reaction product (hydrogen) used as reactant. The fifth reaction cluster is Potassium and Copper based cycle, while the sixth is a Copper-Chlorine based cluster. Copper Chlorine based cycles have also been extensively researched[54], [55], usually in combination with electrolysis. Both of these clusters use target reaction products in one of their reactions, with cluster five using Hydrogen in its third reaction, and cluster six using Oxygen in its third reaction as well.

The seventh reaction cluster is a Calcium based cluster. There has been recent interest in Calcium based reaction clusters[56], albeit in the context of thermal reduction of Calcium oxide. However, the use of Calcium chloride and Calcium hydride in thermochemical energy storage has been investigated and research continues into these promising materials[57], [58]. The eighth reaction cluster is a Sulfuric acid based cluster. There has been extensive investigation into these types of clusters [59], [60]. The last reaction cluster is a Lithium based cluster that used Sulfur trioxide. It also uses Oxygen as a reactant in the third reaction.

Several of these reactions may not be feasible as written due to the presence of side reactions or other chemical mechanistic interferences, however this does not necessarily preclude their feasibility. For the second reaction cluster, in the last reaction, the synthesis of dinuclear Gallium (II) iodide has been reported to come from treating Tetragallium (I) $\left(Ga_4\left(C\left(SiMe_3\right)_3\right)_4\right)$ with Aluminum iodide $\left(AlI_3\right)$ and Iodine monochloride $\left(ICl\right)$ [61]–[63]. Additionally, it's

reactivity with water to produce Gallium (I) oxide in the first reaction is unclear as conventional synthesis routes for this product is to react Gallium with Silicon dioxide (SiO_2) and either Lanthanum (III) oxide (La_2O_3) or Strontium peroxide (SrO_2) [64]. The first reaction in cluster five would also not be likely to occur due to competing side reactions. Indeed, at a 2:3 feed ratio of $K_2O : H_2O$ at a temperature of 1500(K) the production of potassium hydroxide with hydrogen and oxygen is more likely to occur:

$$2K_2O_{(s)} + 3H_2O_{(g)} \Leftrightarrow 5KOH_{(l)} + 2H_{2(g)} + 2O_{2(g)}$$

This reaction has an equilibrium constant of $K_{eq} = 4.014E^{12}$ and a calculated equilibrium conversion of 0.99. Had reactions been eliminated from consideration in the case when any of the competing reactions possessed an equilibrium constant of the same order as the original reaction, then reaction cluster five would not be found due to the elimination of the first reaction from the feasible set. The hydrolyzation of chlorine gas in water from cluster 7 is also unlikely to proceed as listed as more realistic reaction products are hypochlorous acid with various amounts of H^+ and Cl^- or CLO^- [65], [66]. However, as noted when we first discussed side reactions, catalysts can be utilized to increase the selectivity of reactions. As such, we find it more useful to generate reaction clusters without regard to potential side reactions. At that point, the behavior of each reaction with respect to side reactions can be further analyzed.

Also of note, although almost the operating temperature of all identified cluster reactions occurs at the boundary of the original temperature window, reaction 1 in the second cluster occurs at 373(K), indicating that the cluster algorithm is able to identify maximum extent of reaction conditions whose temperature component lies inside the temperature window. The figures below show the standard Gibbs energy and extent of reaction at different points within the original temperature window for every reaction found in a cluster.

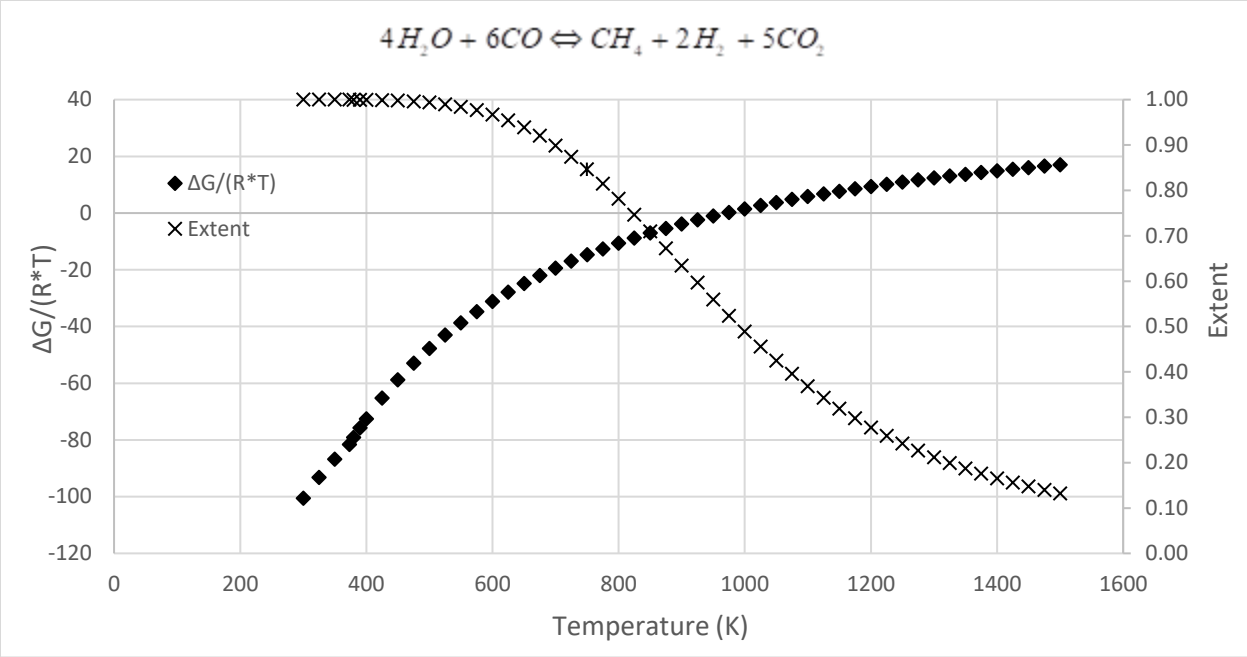

Figure 4-2 $\frac{\Delta G^o}{RT}$ and ξ vs temperature for Water Splitting cycle 1 reaction 1.

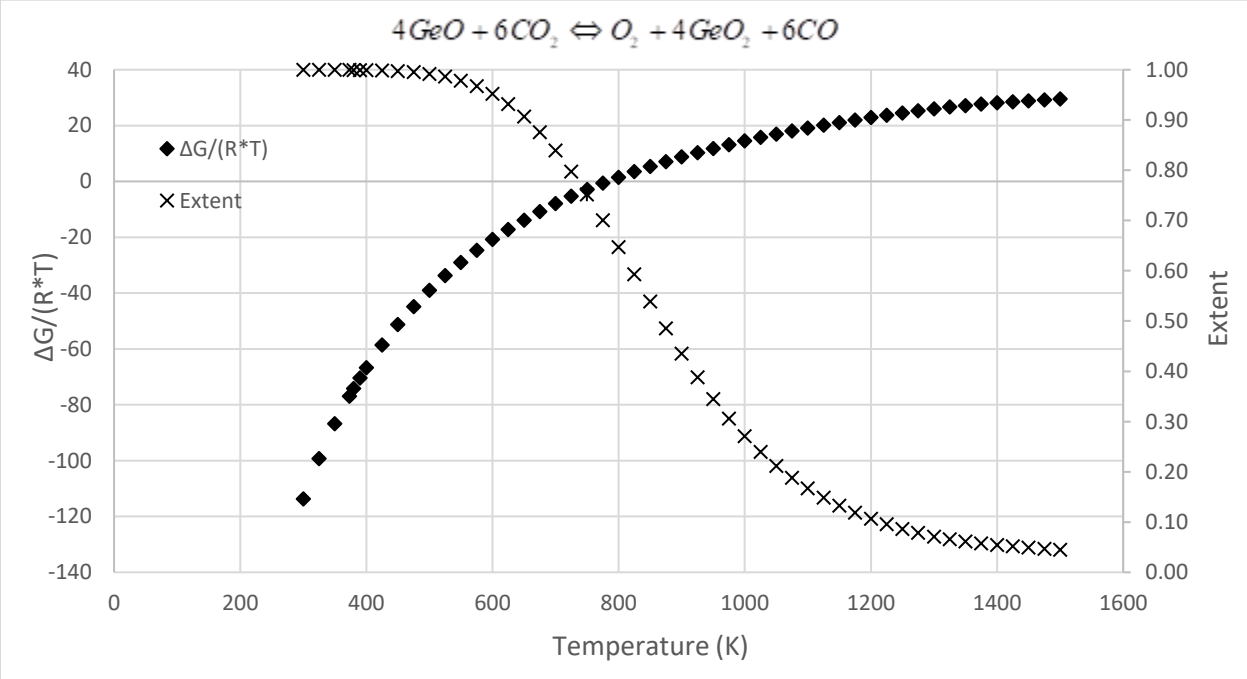

Figure 4-3 $\frac{\Delta G^o}{RT}$ and ξ vs temperature for Water Splitting cycle 1 reaction 2.

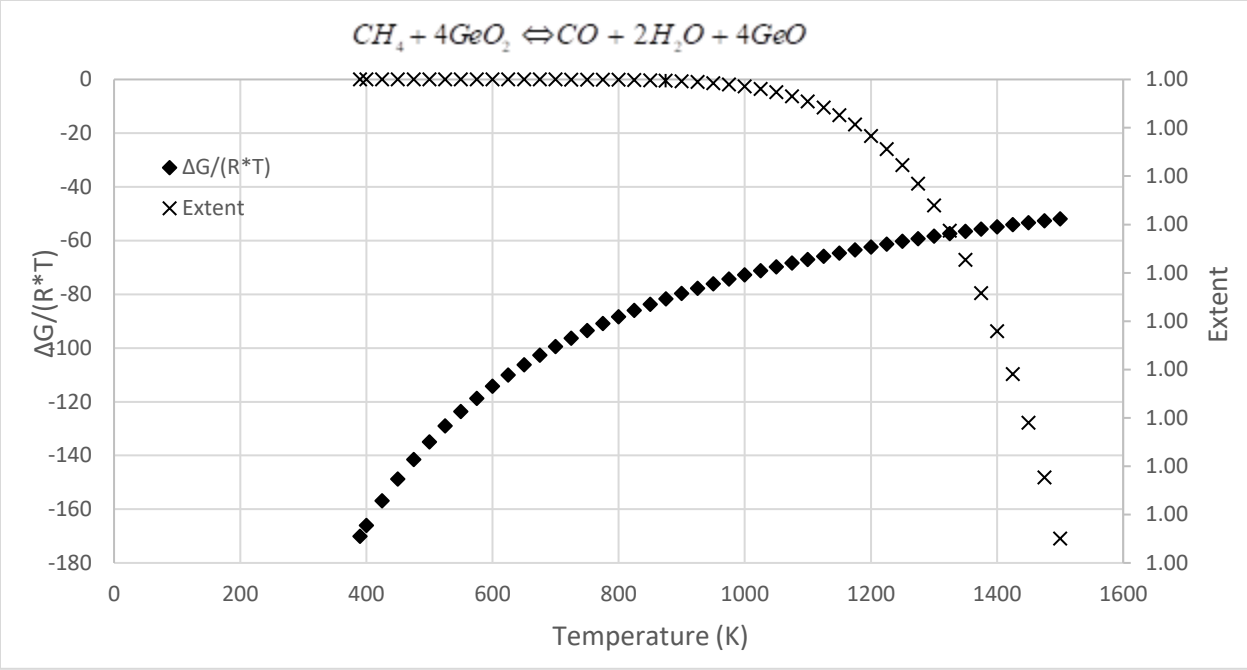

Figure 4-4 $\frac{\Delta G^o}{RT}$ and ξ vs temperature for Water Splitting cycle 1 reaction 3.

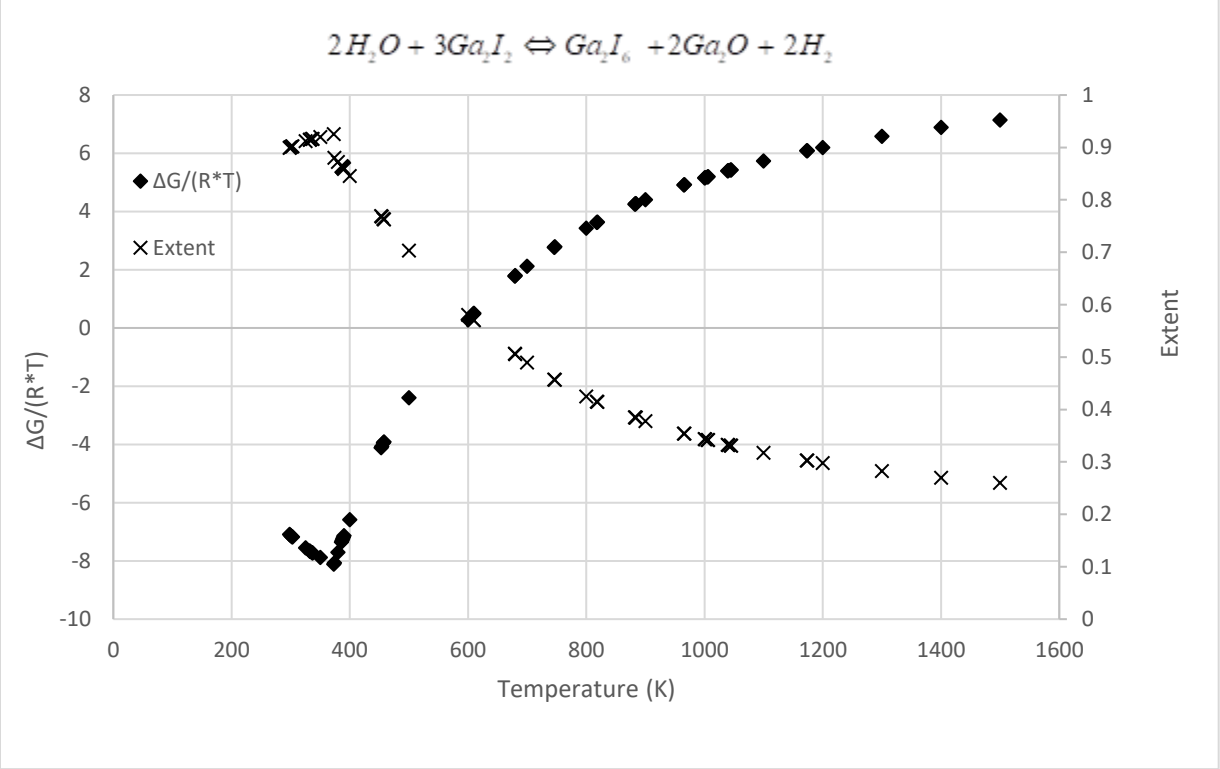

Figure 4-5 $\frac{\Delta G^o}{RT}$ and ξ vs temperature for Water Splitting cycle 2 reaction 1.

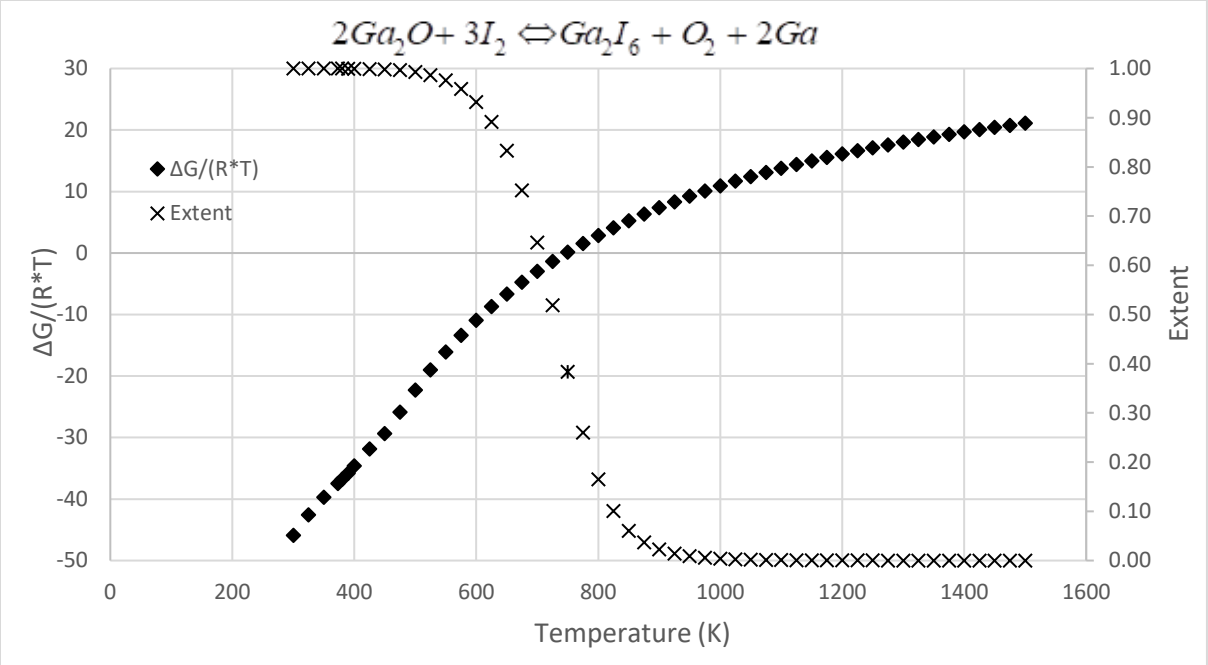

Figure 4-6 $\frac{\Delta G^o}{RT}$ and ξ vs temperature for Water Splitting cycle 2 reaction 2.

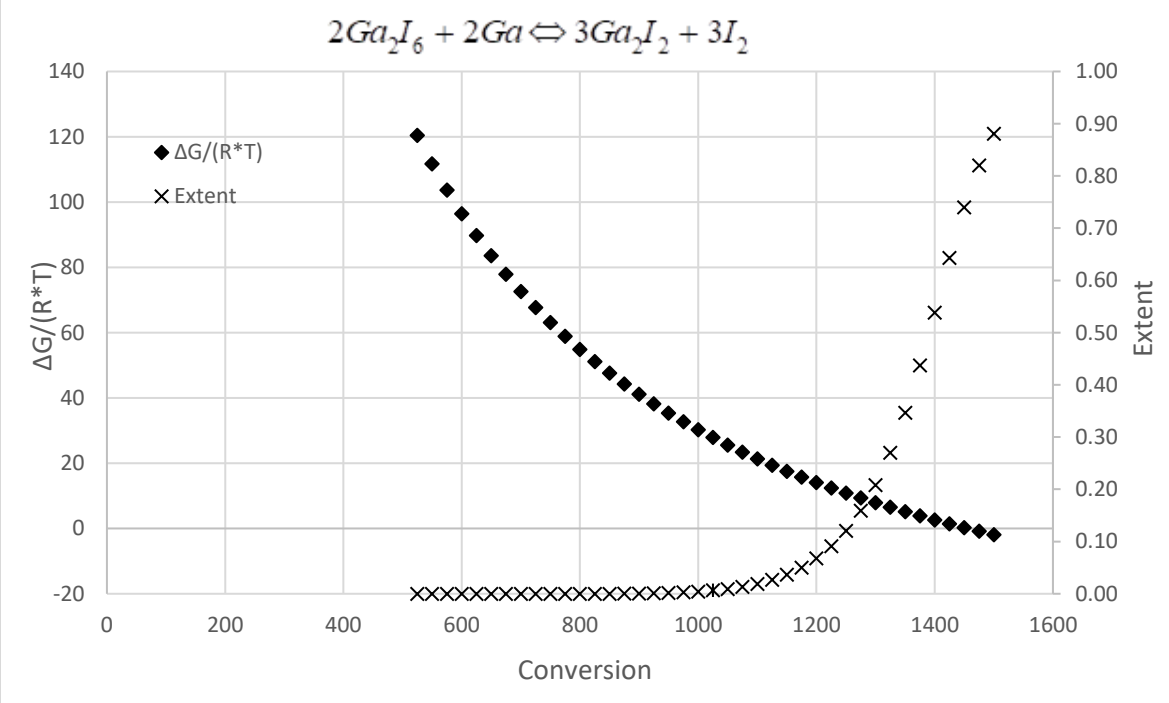

Figure 4-7 $\frac{\Delta G^o}{RT}$ and ξ vs temperature for Water Splitting cycle 2 reaction 3.

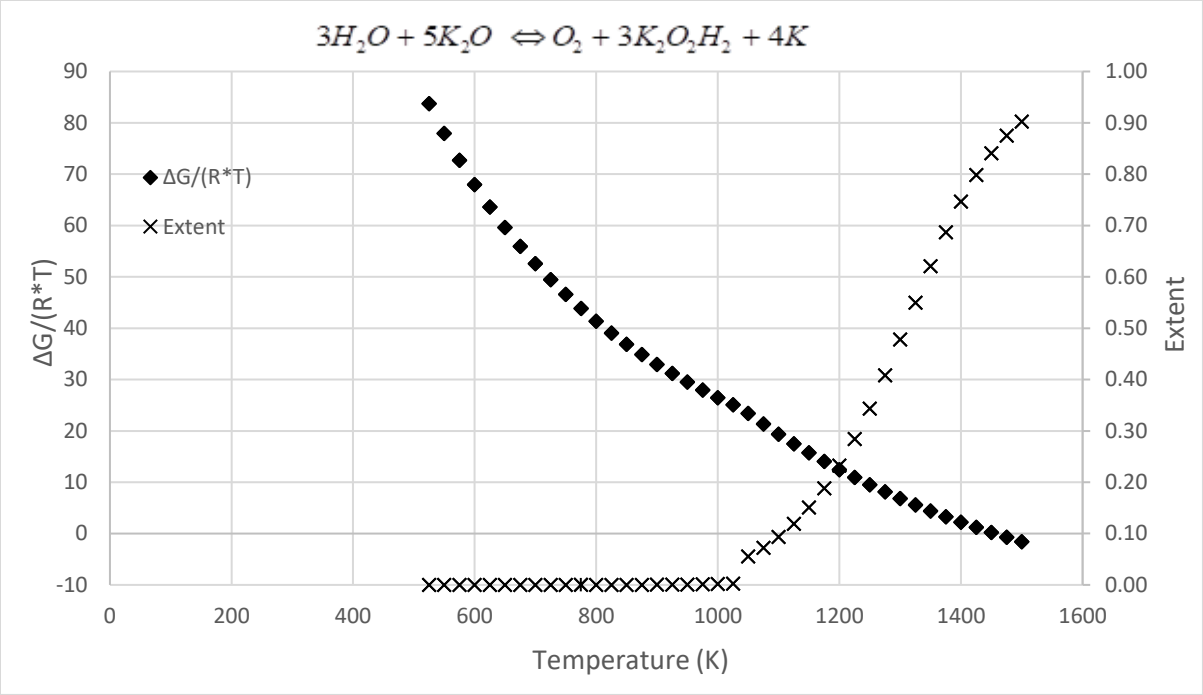

Figure 4-8 $\frac{\Delta G^o}{RT}$ and ξ vs temperature for Water Splitting cycle 3/4 reaction 1.

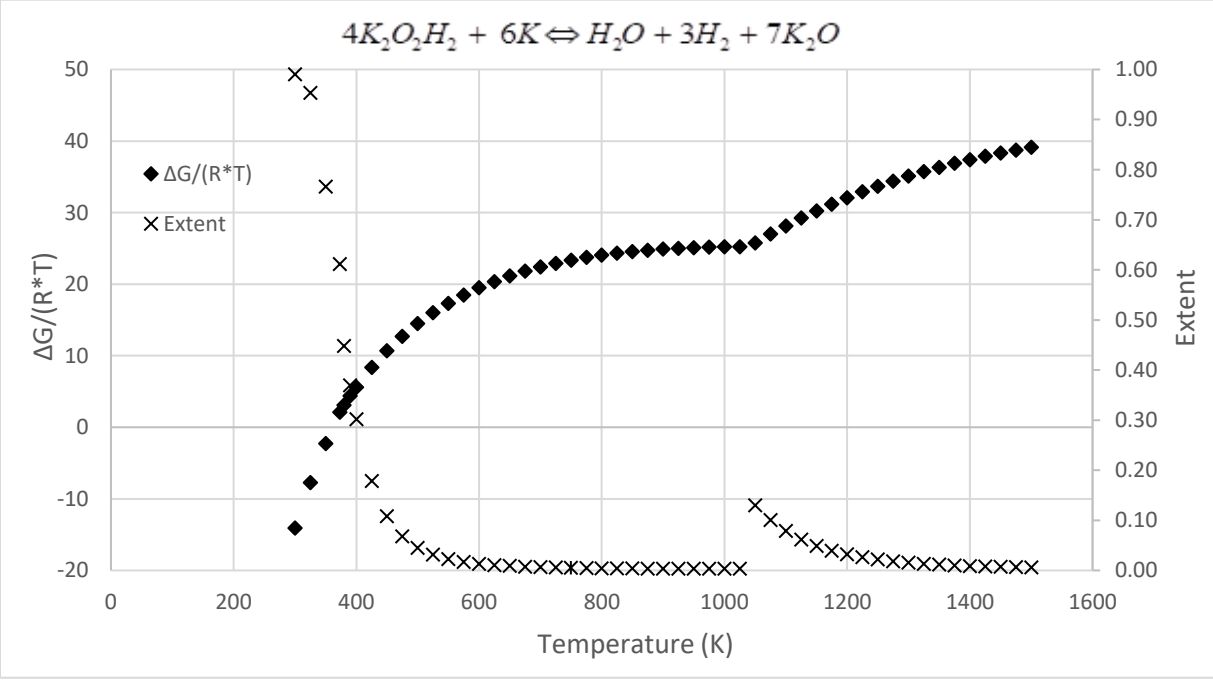

Figure 4-9 $\frac{\Delta G^o}{RT}$ and ξ vs temperature for Water Splitting cycle 3 reaction 2.

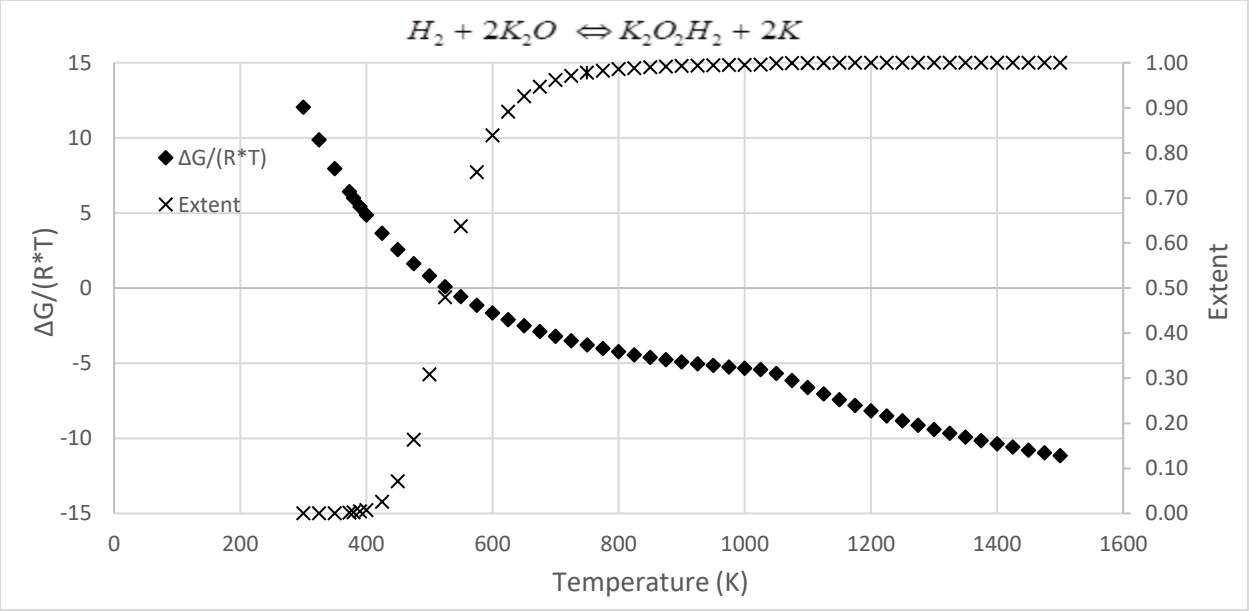

Figure 4-10 $\frac{\Delta G^o}{RT}$ and ξ vs temperature for Water Splitting cycle 3 reaction 3.

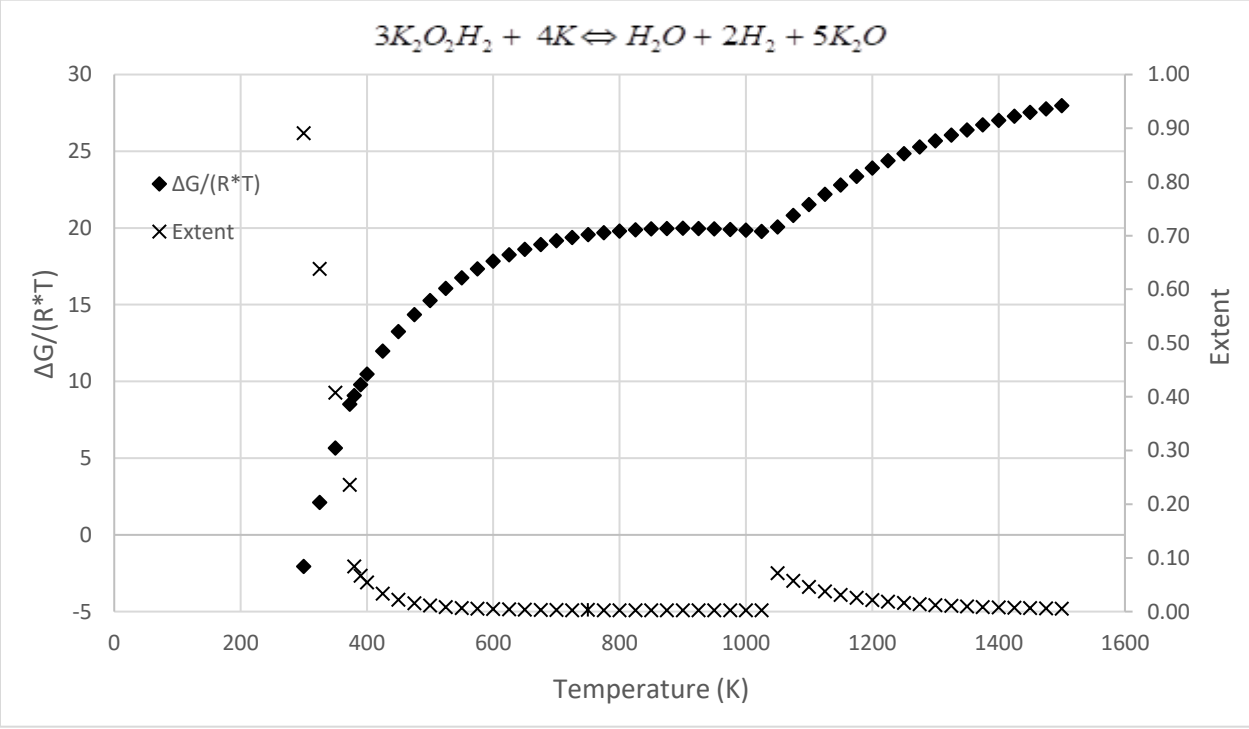

Figure 4-11 $\frac{\Delta G^o}{RT}$ and ξ vs temperature for Water Splitting cycle 4 reaction 2.

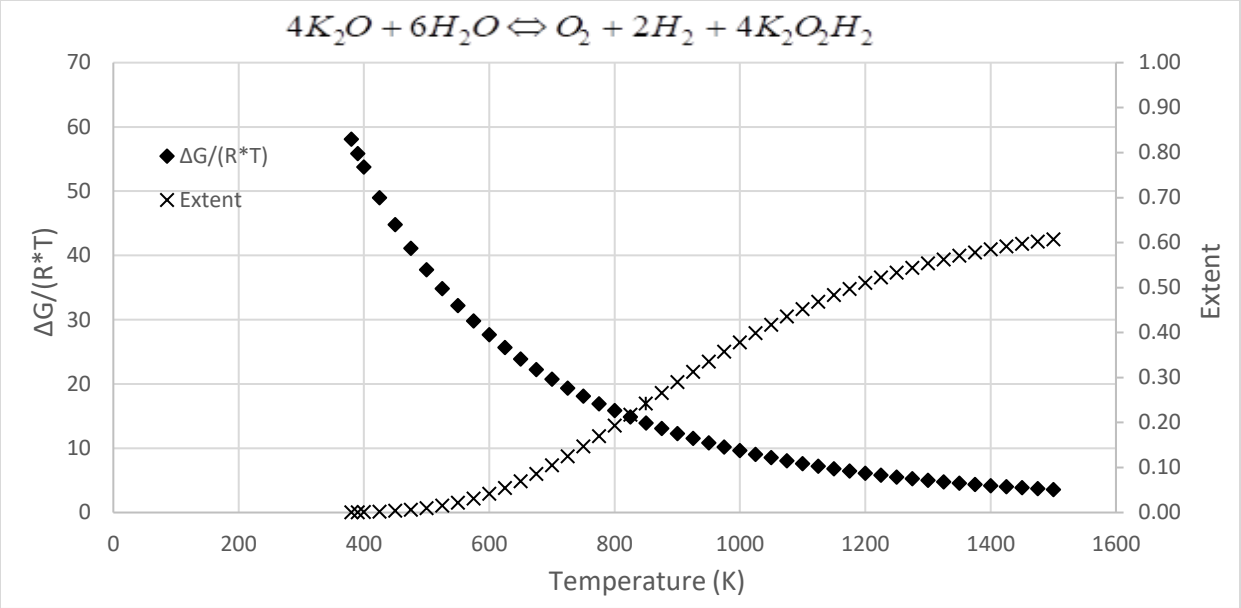

Figure 4-12 $\frac{\Delta G^o}{RT}$ and ξ vs temperature for Water Splitting cycle 5 reaction12.

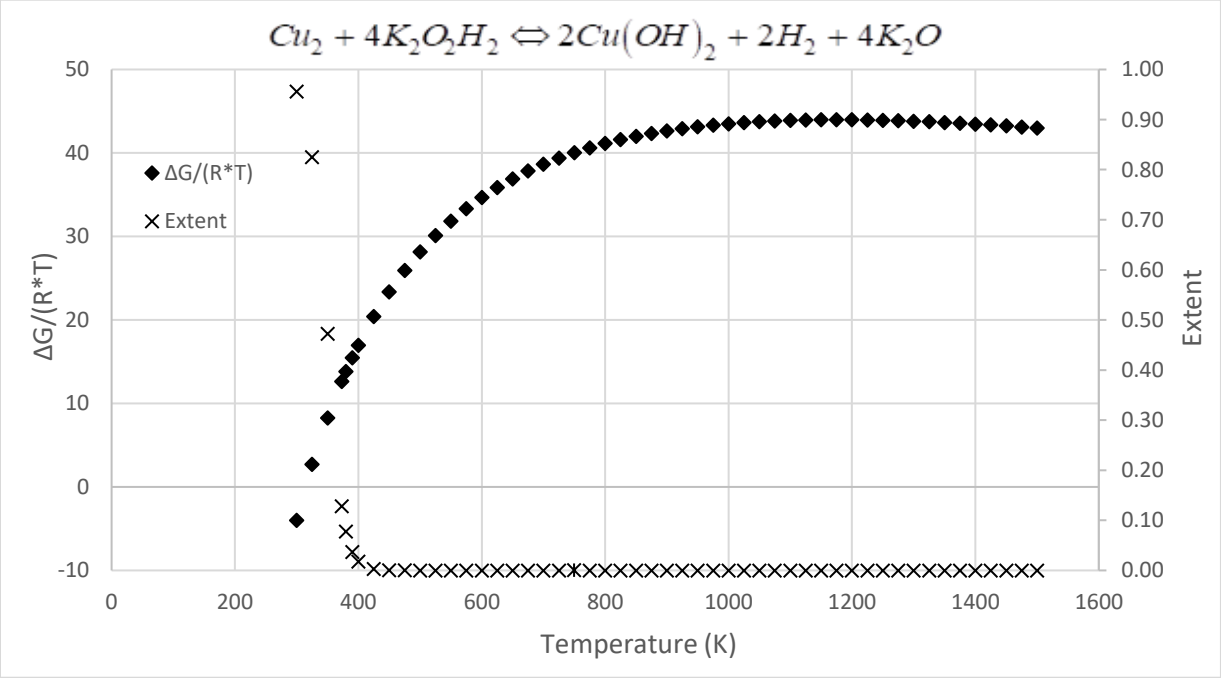

Figure 4-13 $\frac{\Delta G^o}{RT}$ and ξ vs temperature for Water Splitting cycle 5 reaction 2.

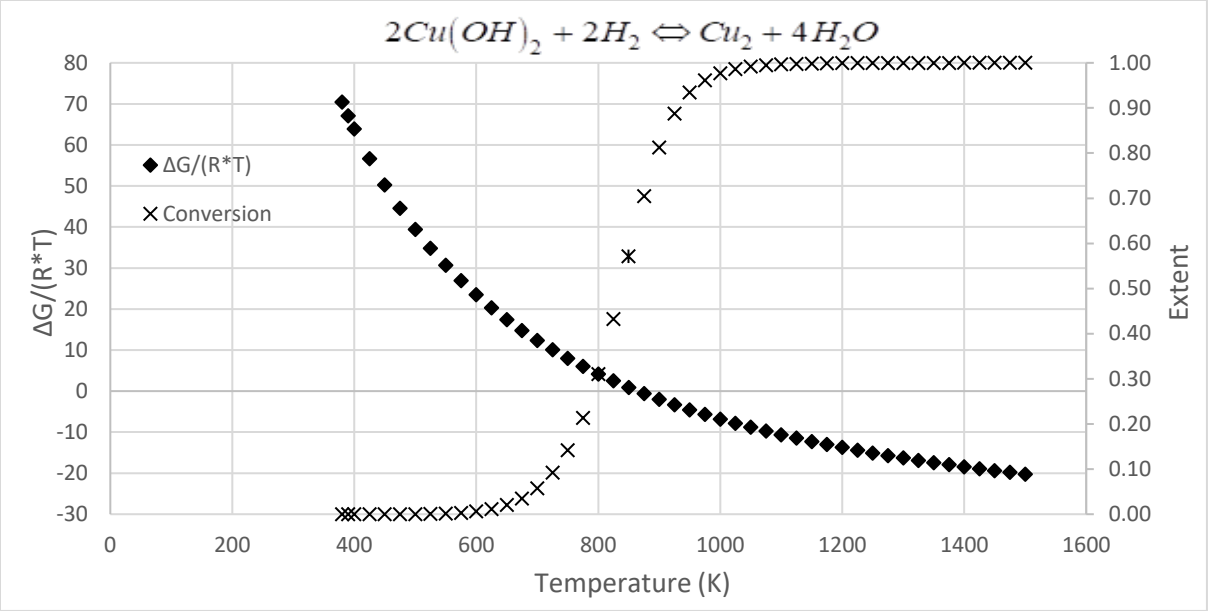

Figure 4-14 $\frac{\Delta G^o}{RT}$ and ξ vs temperature for Water Splitting cycle 5 reaction 3.

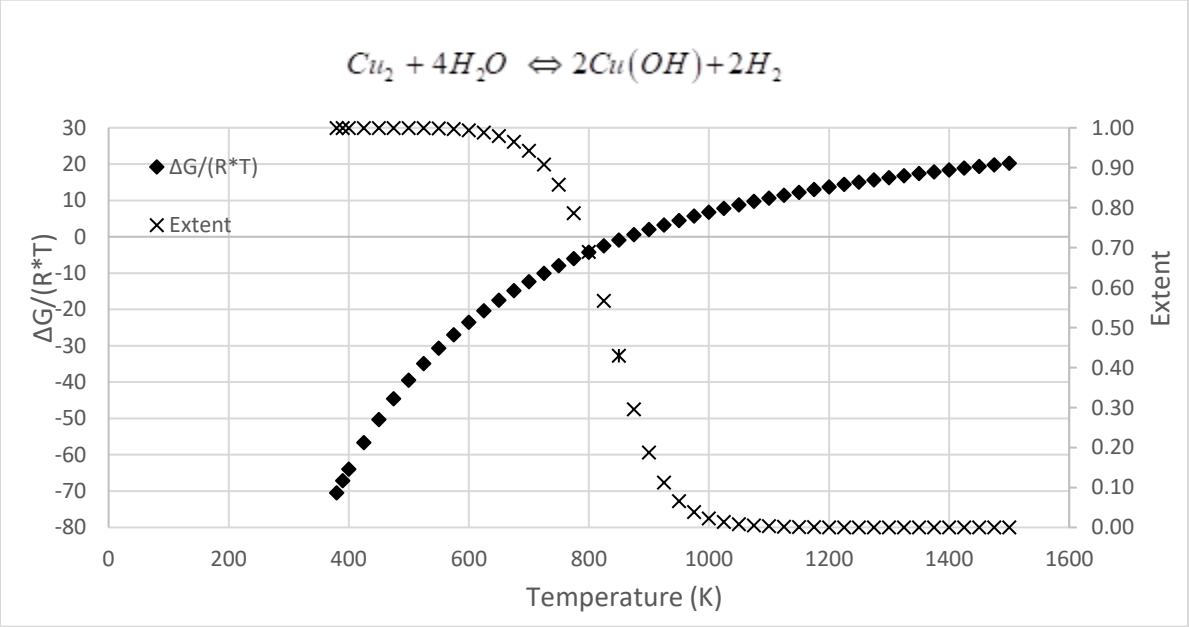

Figure 4-15 $\frac{\Delta G^o}{RT}$ and ξ vs temperature for Water Splitting cycle 6 reaction 1.

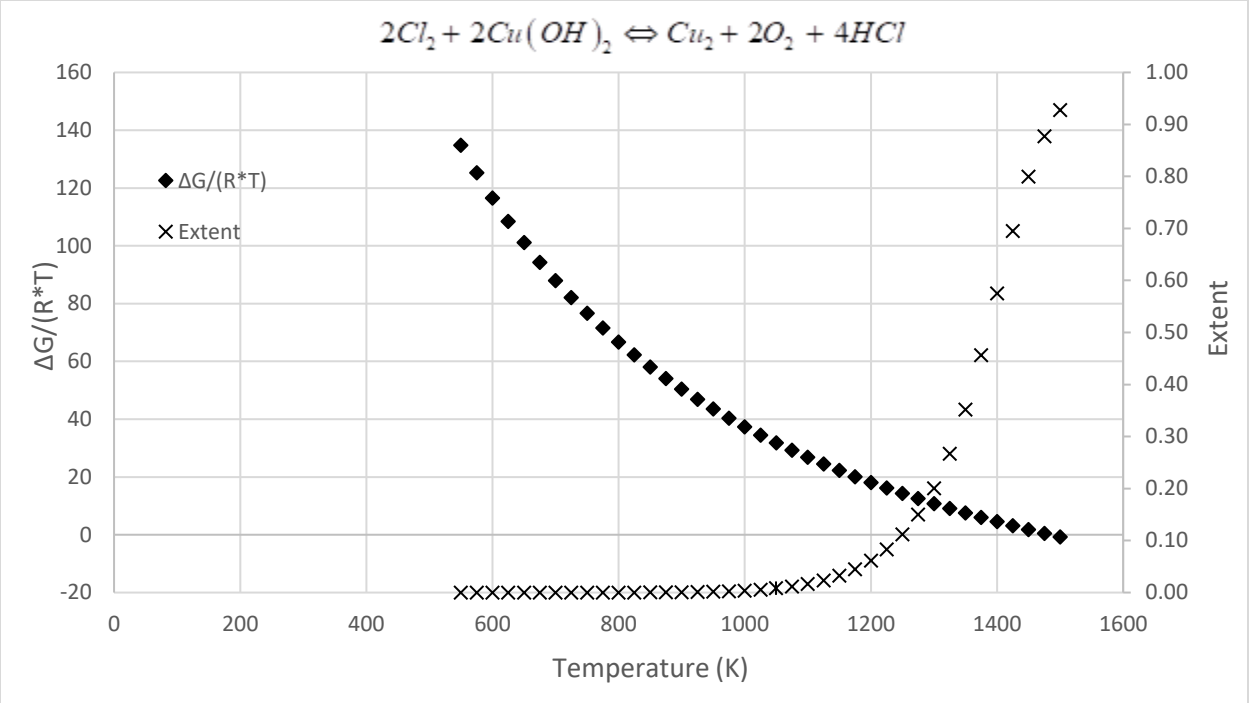

Figure 4-16 $\frac{\Delta G^o}{RT}$ and ξ vs temperature for Water Splitting cycle 6 reaction 2.

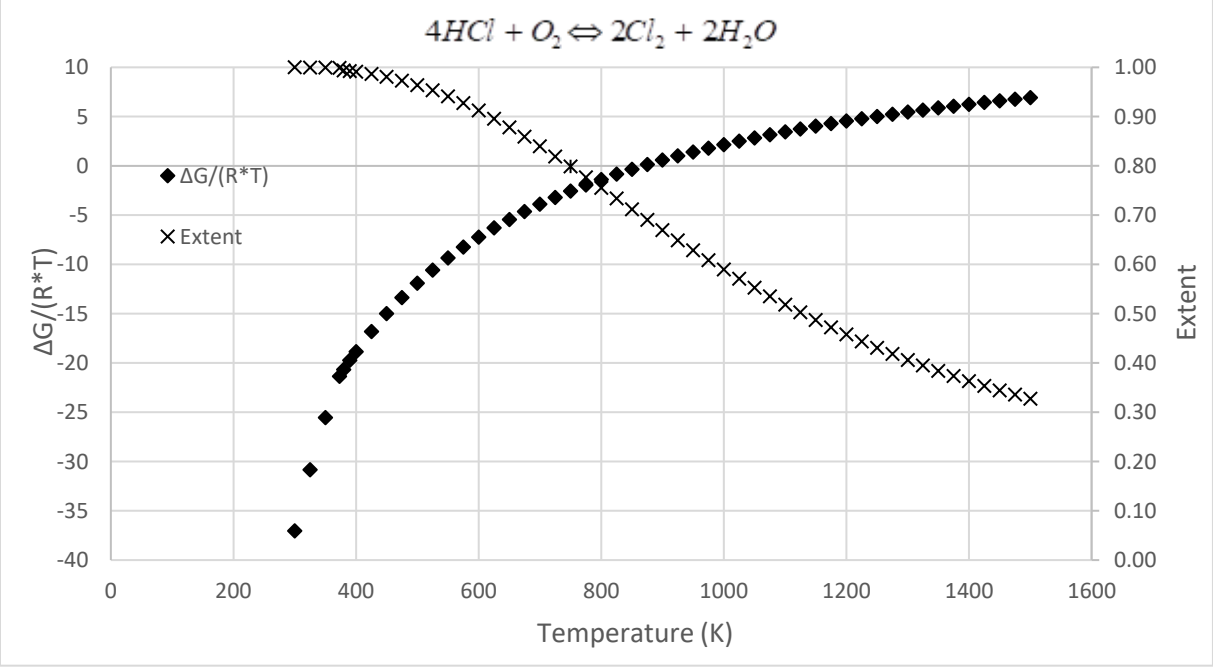

Figure 4-17 $\frac{\Delta G^o}{RT}$ and ξ vs temperature for Water Splitting cycle 6 reaction 3.

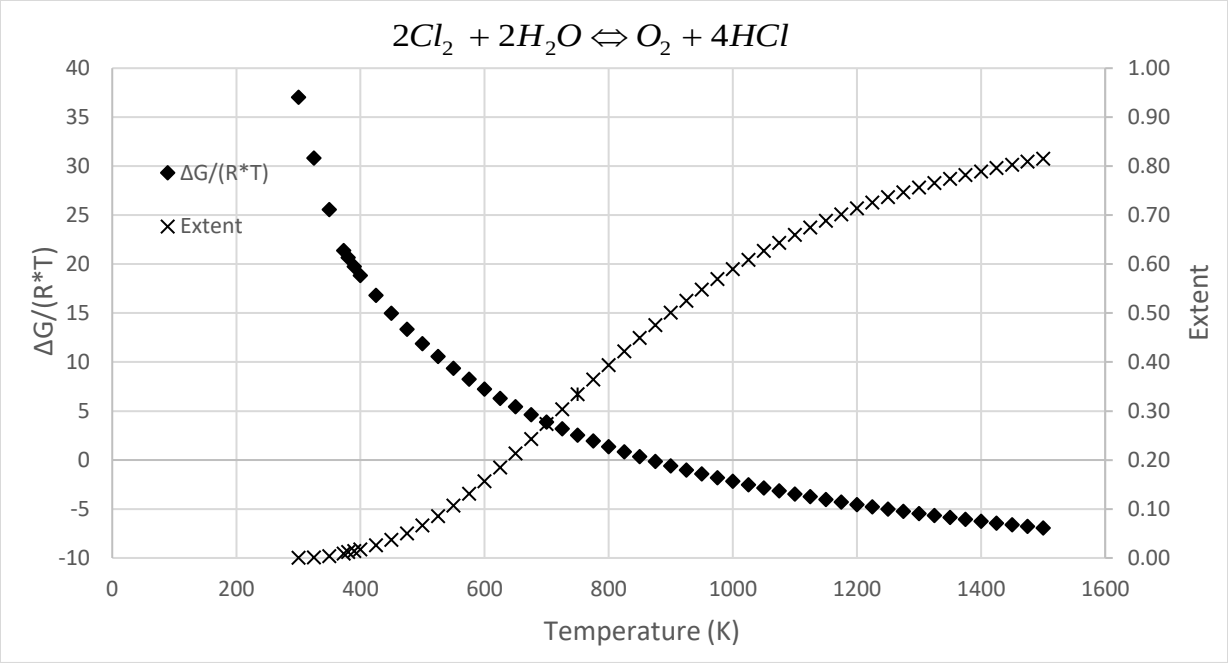

Figure 4-18 $\frac{\Delta G^o}{RT}$ and ξ vs temperature for Water Splitting cycle 7 reaction 1.

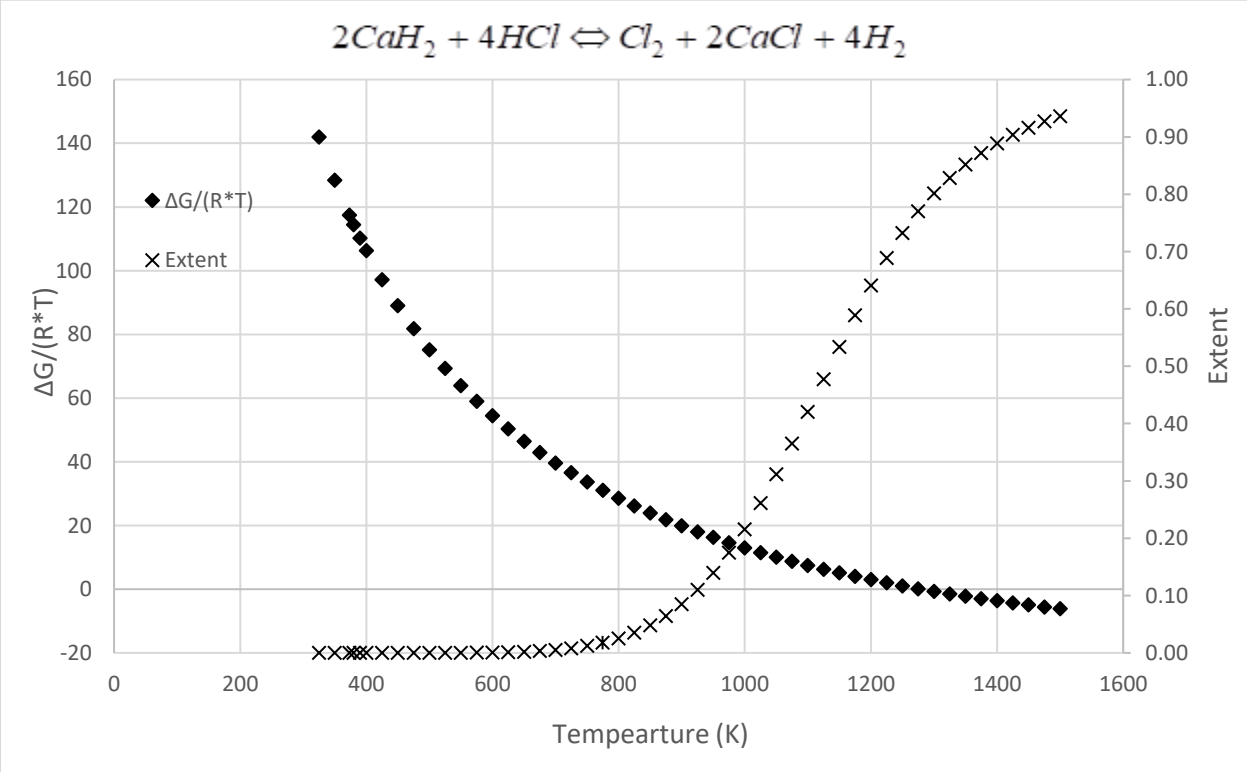

Figure 4-19 $\frac{\Delta G^o}{RT}$ and ξ vs temperature for Water Splitting cycle 7 reaction 2.

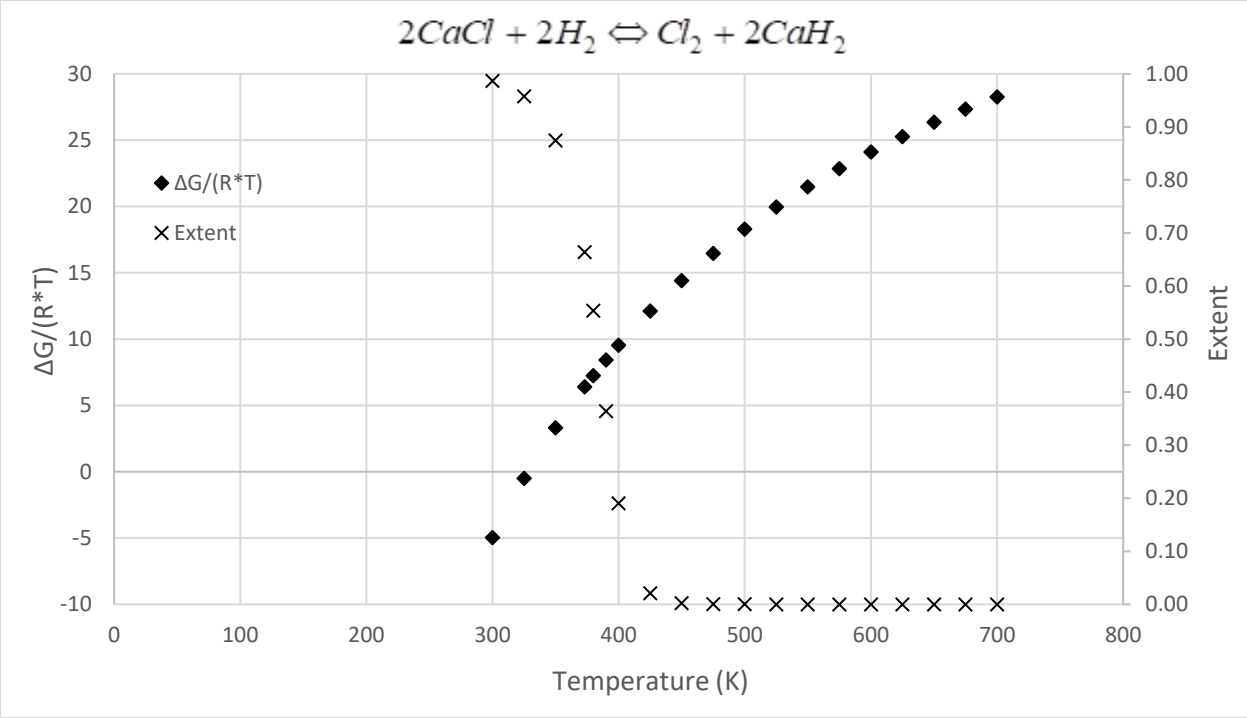

Figure 4-20 $\frac{\Delta G^o}{RT}$ and ξ vs temperature for Water Splitting cycle 7 reaction 3.

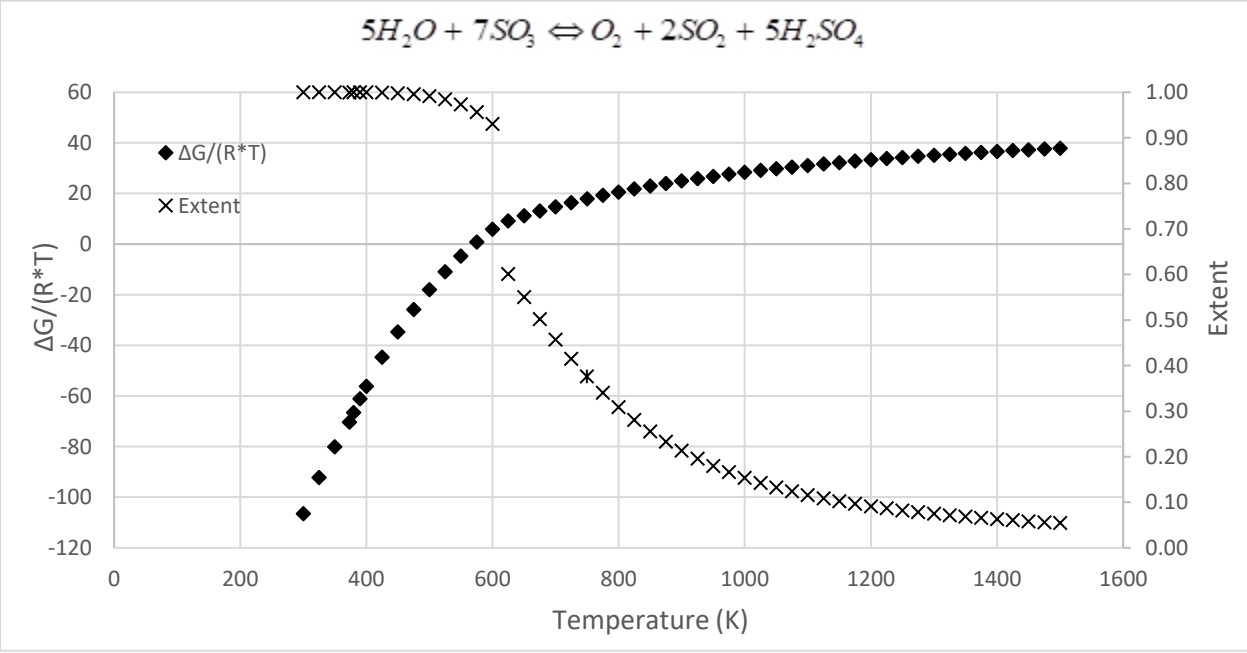

Figure 4-21 $\frac{\Delta G^o}{RT}$ and ξ vs temperature for Water Splitting cycle 8 reaction 1.

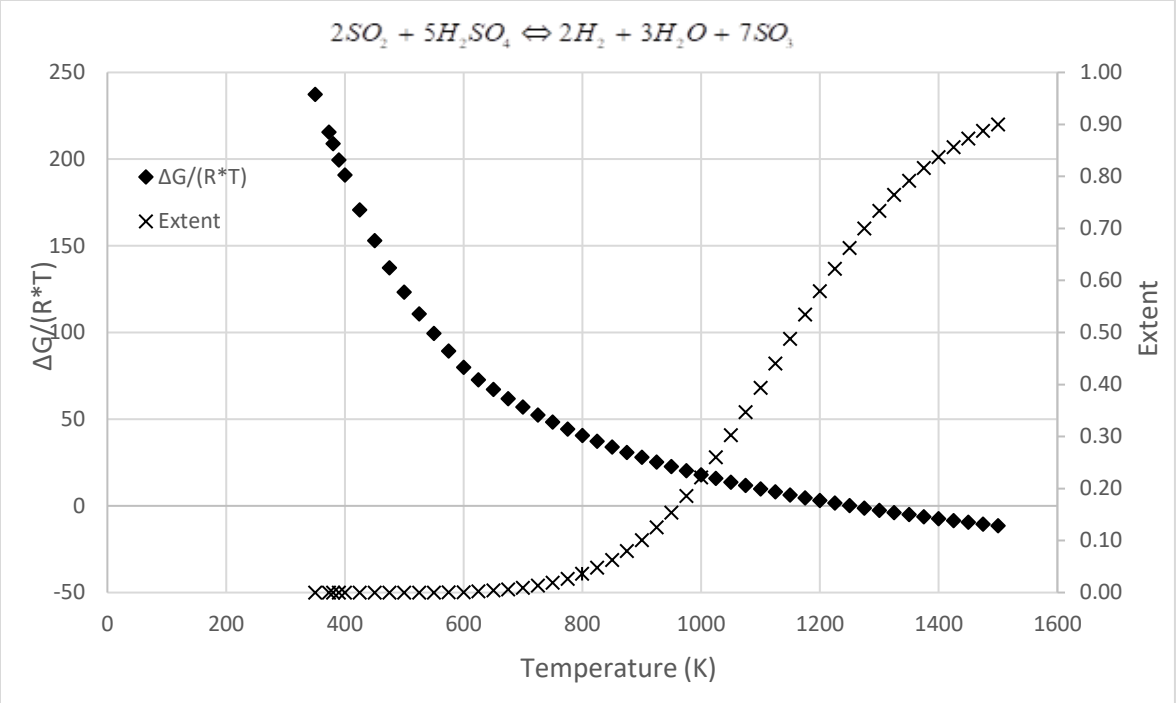

Figure 4-22 $\frac{\Delta G^o}{RT}$ and ξ vs temperature for Water Splitting cycle 8 reaction 2.

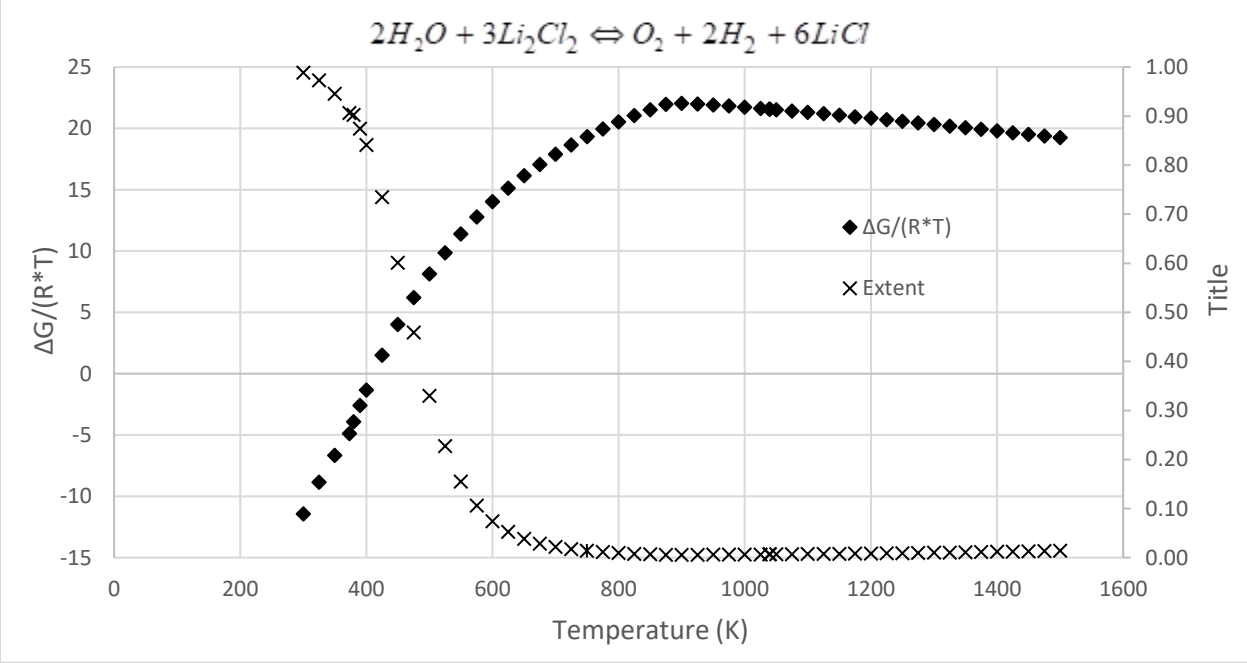

Figure 4-23 $\frac{\Delta G^o}{RT}$ and ξ vs temperature for Water Splitting cycle 9 reaction 1.

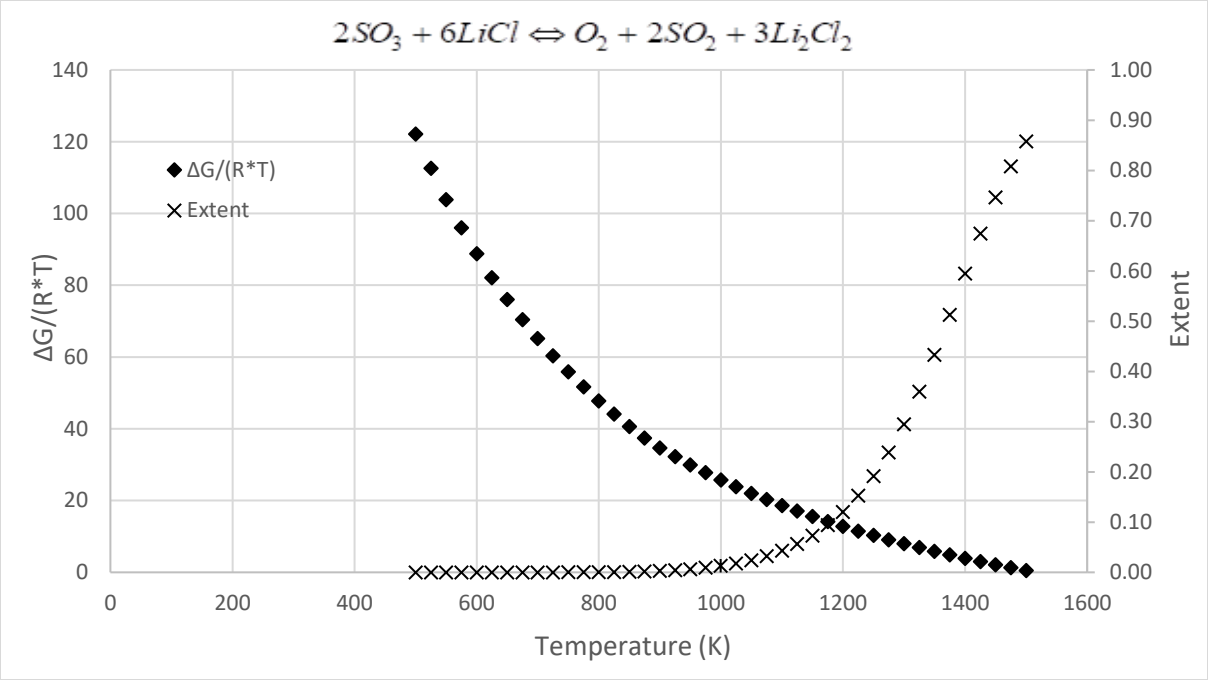

Figure 4-24 $\frac{\Delta G^o}{RT}$ and ξ vs temperature for Water Splitting cycle 9 reaction 2.

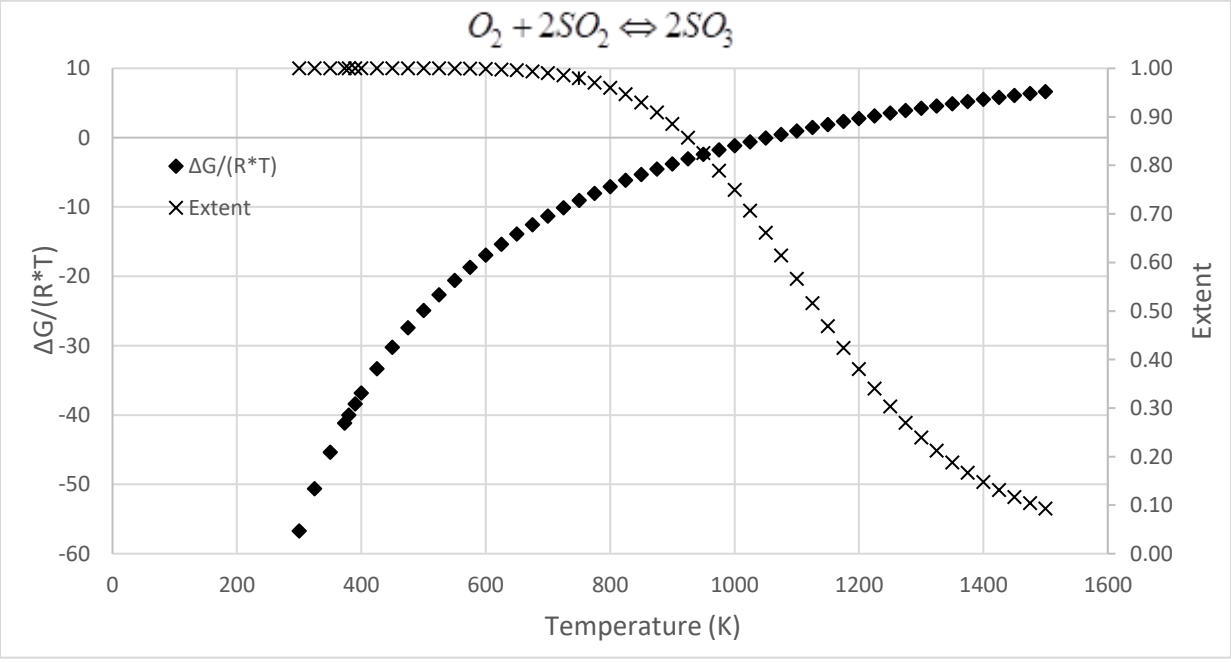

Figure 4-25 $\frac{\Delta G^o}{RT}$ and ξ vs temperature for Water Splitting cycle 9 reaction 3.

As can be seen, $\frac{\Delta G^o}{RT}$ is clearly non-linear over this temperature range and appears to hit a minimum at a temperature of 373. This point also corresponds to the maximum $\xi_{\min}$. The temperature of 373(K) is the upper bound for liquid water in the database before changing phases to gas, and so it appears that while a reaction may not have its maximum $\xi_{\min}$ at the original boundary, it is likely to occur at one of the boundaries of a species involved in the reaction.

4.2 Formic Acid, Acetic Acid, and Dimethyl Ether Production With Hydrogen Generation Cycles

In this section we present clusters that amount to formic acid production:

$$CH_4 + 2H_2O \Leftrightarrow HCOOH + 3H_2$$

acetic acid production:

$$2CH_4 + 2H_2O \Leftrightarrow CH_3COOH + 4H_2$$

or DME production:

$$2CH_4 + H_2O \Leftrightarrow CH_3OCH_3 + 2H_2$$

with hydrogen generation using methane and water as feed.

Formic acid can substitute some inorganic acids in chemical processes and it is less corrosive than many of them. It also does not result in loading of nitrate, phosphate, or sulfate into wastewater. According to the data of the European Chemical Agency, formic acid and the formate ion are readily biodegradable. Furthermore, formic acid and the formate ion are readily biodegradable in seawater. The worldwide production capacity of formic acid was estimated to be up to 950 thousand tons per year. The demand for formic acid is growing because of its

relatively nontoxic and non corrosive properties and this allows easy handling. It has been estimated that the market for this chemical will increase to 5.6% per year through.

The uses of acetic acid are numerous. It can be used as a chemical intermediate for the synthesis of many other desirable chemicals, such as vinyl acetate, acetic anhydride, or cellulose acetate. These chemicals are used as the raw materials for the manufacturing of a variety of productions such as of adhesives, coatings, textile finishes, cement additives, coatings, cellulose plastics, aspirin, and acetaminophen. Additionally, acetic acid can directly be used when producing terephthalic acid. Because of its wide range of applications, the global demand of acetic acid was valued at 12.1 million metric tons in 2014 and it is expected to reach 16.2 million metric tons/year by 2020 with a compound annual growth rate of 4.9%[67]. The global market is also expected to reach USD 12.2 billion per year by 2020[68].

In 2020, the global DME market size was estimated to lie between $4 – $7.72 billion, and is expected to grow with a Compound Annual Growth Rate (CAGR) of between 9.6% and 16.8% from 2021 to 2031[68]–[70]. While DME is a carbon containing chemical, it also has a number of attractive qualities from a manufacturing and production perspective because it is nontoxic, noncarcinogenic, and environmentally friendly[71]. It has many potential uses, such as a replacement fuel for diesel engines. There are a number of qualities that make DME a strong candidate for use as a fuel replacement, such a relatively short ignition delay time for complete combustion. It is safe to handle as a liquid, and it also burns clean, as there are very low particulate, carbon dioxide, or other toxic gas emissions[72]. Another attractive quality is that the existing liquid petroleum gas infrastructure can be used because DME share similar chemical and physical properties, reducing cost for wide-spread implementation[73]. DME can also be used as a raw material in the synthesis of a number of useful chemicals, such as dimethyl sulfate,

and can be used as a pesticide or antitrust agent[74]. Research has also shown DME could be used for enhanced petroleum production when used as an oil recovery agent in specialized procedures, such as water flood techniques[75], [76]. Given all that, it is not surprising that DME production demand has be increasing in the past 10 years.

Table 4-3: Formic acid cycles.

	Reactions	$T(K)$	$P(bar)$	$\Delta G^o\left(\frac{kJ}{mol}\right)$	ξ
1	$2CH_{4(g)} + 4CO_{2(g)} \Leftrightarrow CH_3OH_{(g)} + 2H_2O_{(g)} + 5CO_{(g)}$	1500	1	-85.75	0.81
	$2CH_3OH_{(g)} \Leftrightarrow CH_{4(g)} + H_{2(g)} + HCOOH_{(g)}$	298	1	-77.01	0.99
	$4H_2O_{(l)} + 5CO_{(g)} \Leftrightarrow CH_3OH_{(g)} + 2H_{2(g)} + 4CO_{2(g)}$	298	1	-105.45	0.99
2	$2CaH_{2(l)} + 2H_2O_{(g)} \Leftrightarrow 2CaOH_{(g)} + 3H_{2(g)}$	1500	1	-156.41	0.99
	$2CH_{4(g)} + 2CaOH_{(g)} \Leftrightarrow \begin{Bmatrix} CH_3COOH_{(g)} + H_{2(g)} \\ + 2CaH_{2(s)} \end{Bmatrix}$	298	25	-145.45	0.99
	$CH_3COOH_{(g)} + H_{2(g)} \Leftrightarrow CH_{4(g)} + HCOOH_{(g)}$	298	N/A	-27.28	0.99

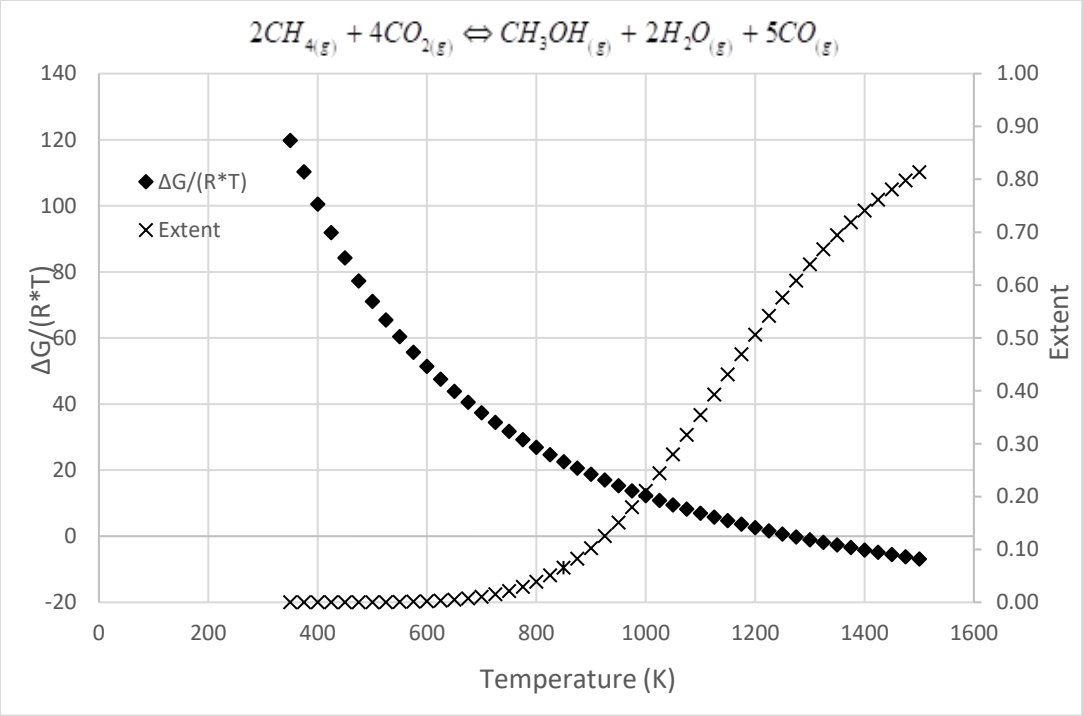

Figure 4-26 $\frac{\Delta G^o}{RT}$ and ξ vs temperature for Formic acid cycle 1 reaction 1.

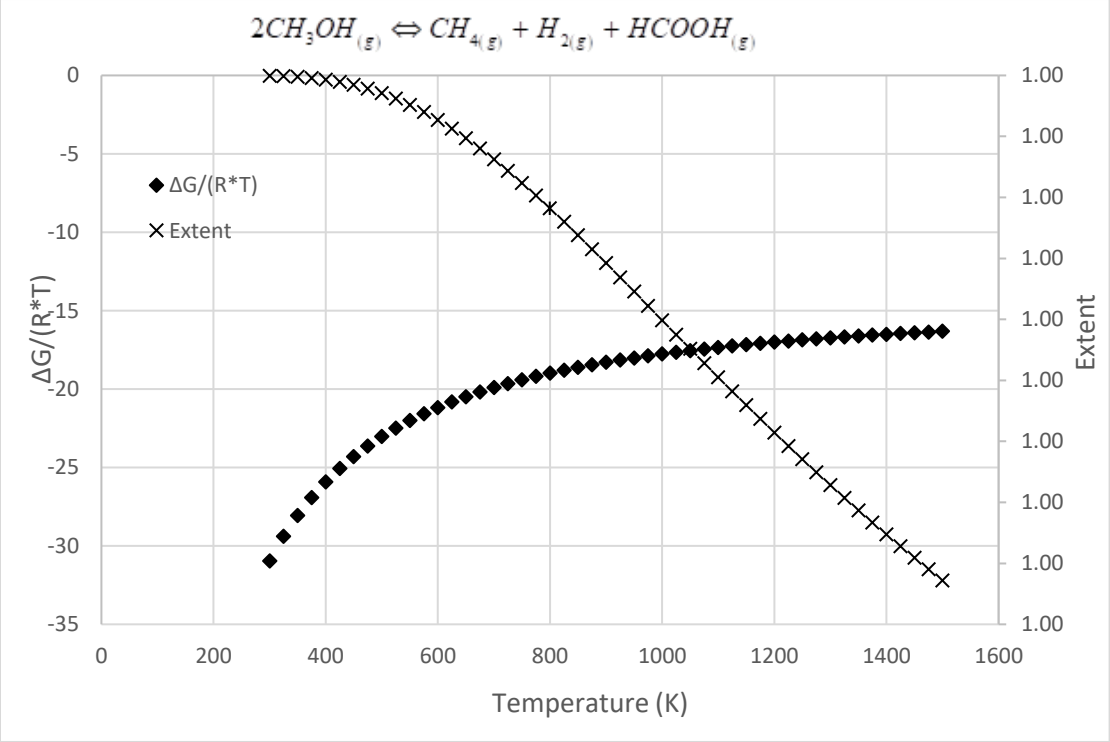

Figure 4-27 $\frac{\Delta G^o}{RT}$ and ξ vs temperature for Formic acid cycle 1 reaction 2.

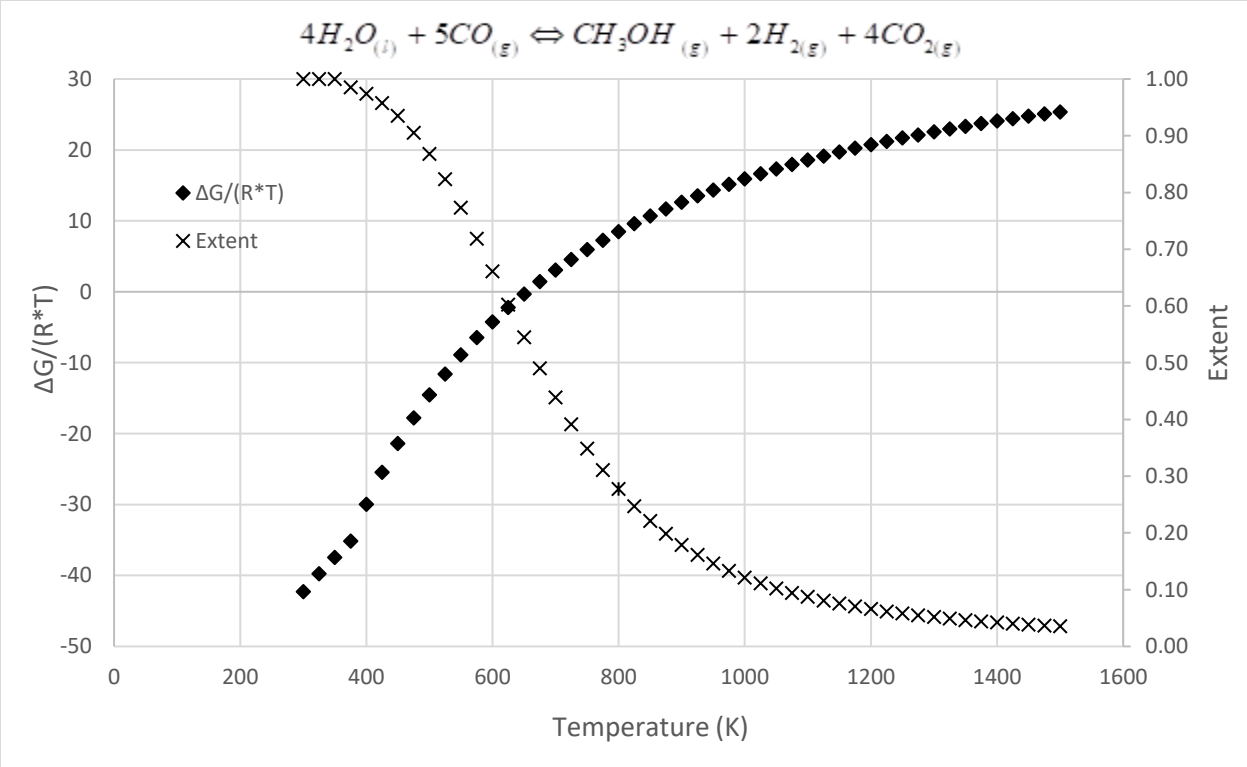

Figure 4-28 $\frac{\Delta G^o}{RT}$ and ξ vs temperature for Formic acid cycle 1 reaction 3.

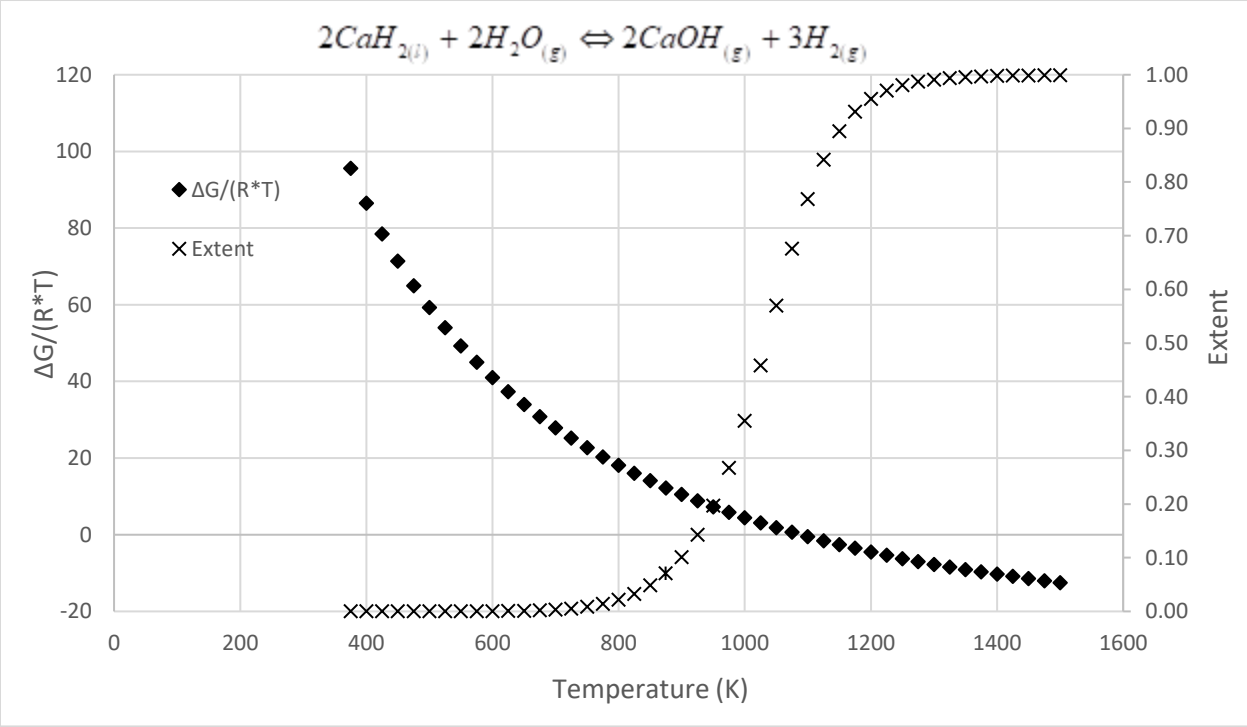

Figure 4-29 $\frac{\Delta G^o}{RT}$ and ξ vs temperature for Formic acid cycle 2 reaction 1.

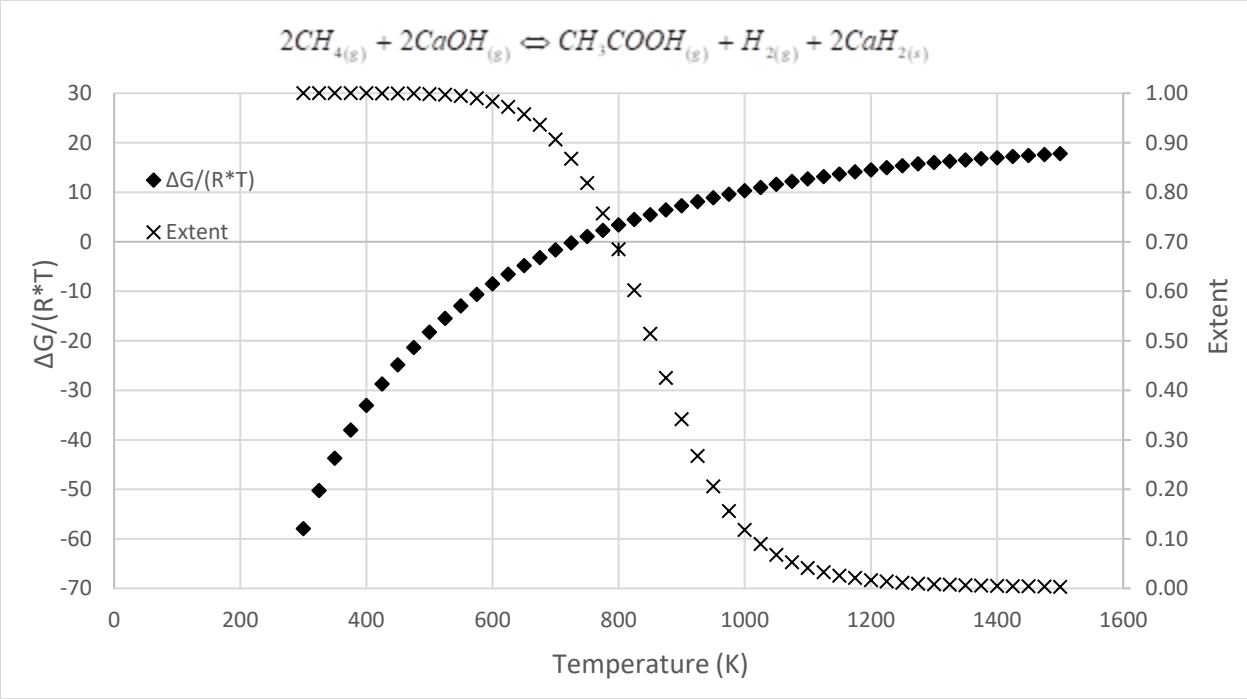

Figure 4-30 $\frac{\Delta G^o}{RT}$ and ξ vs temperature for Formic acid cycle 2 reaction 2.

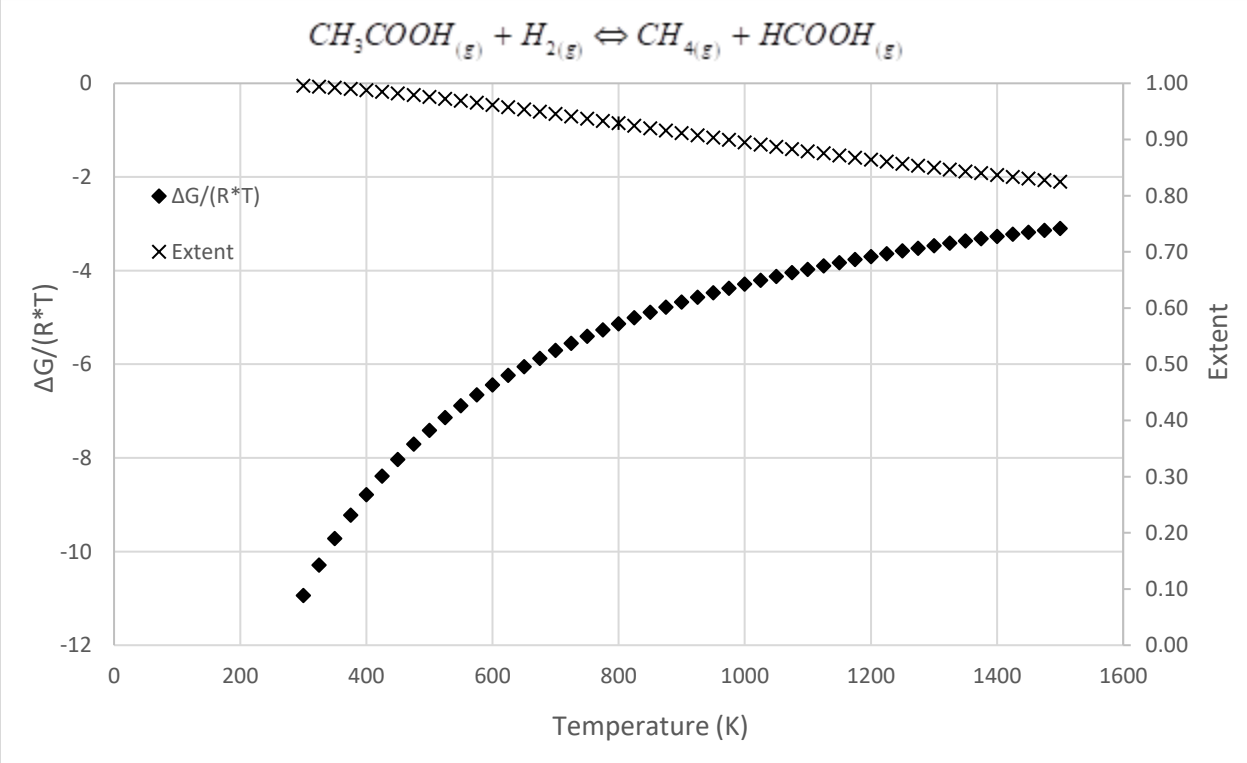

Figure 4-31 $\frac{\Delta G^o}{RT}$ and ξ vs temperature for Formic acid cycle 2 reaction 3.

Table 4-4:Acetic acid cycles

	Reactions	$T(K)$	$P(bar)$	$\Delta G^{o}\left(\frac{kJ}{mol}\right)$	ξ
1	$3CH_{4(g)} + H_2O_{(g)} \Leftrightarrow CH_3COOH_{(g)} + CO_{(g)} + 7H_{2(g)}$	1500	1	-848.6	0.77
	$CO_{(g)} + NaOH_{(s)} \Leftrightarrow H_{2(g)} + Na_2CO_{3(s)}$	298	N/A	-151.6	0.99
	$Na_2CO_{3(s)} + 4H_{2(g)} \Leftrightarrow CH_{4(g)} + H_2O_{(l)} + 2NaOH_{(s)}$	298	25	1.082	0.97
2	$2H_2O_{(l)} + 4CO_{(g)} \Leftrightarrow CH_3COOH_{(g)} + 2CO_{2(g)}$	298	25	-140.32	0.99
	$CaCO_{3(s)} + 2CH_{4(g)} \Leftrightarrow CaH_{2(l)} + 3CO_{(g)} + 3H_{2(g)}$	1500	1	-30.04	0.91
	$CaH_{2(s)} + 2CO_{2(g)} \Leftrightarrow CO_{(g)} + CaCO_{3(s)} + H_{2(g)}$	298	N/A	-338.11	0.99

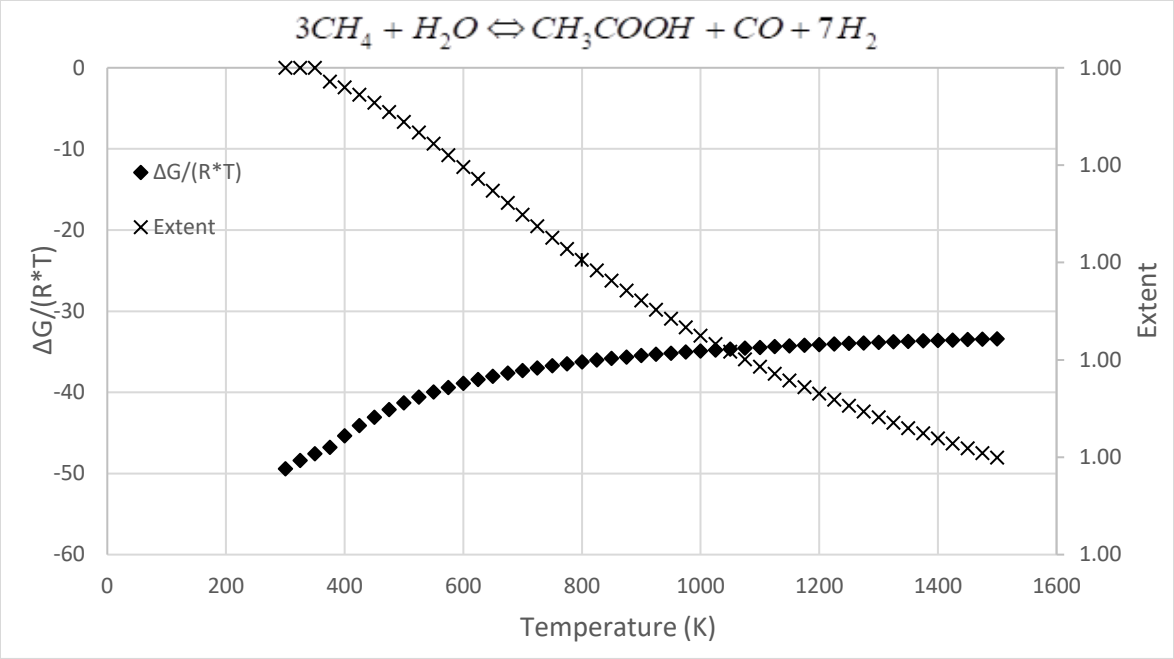

Figure 4-32 $\frac{\Delta G^o}{RT}$ and ξ vs temperature for Acetic acid cycle 1 reaction 1.

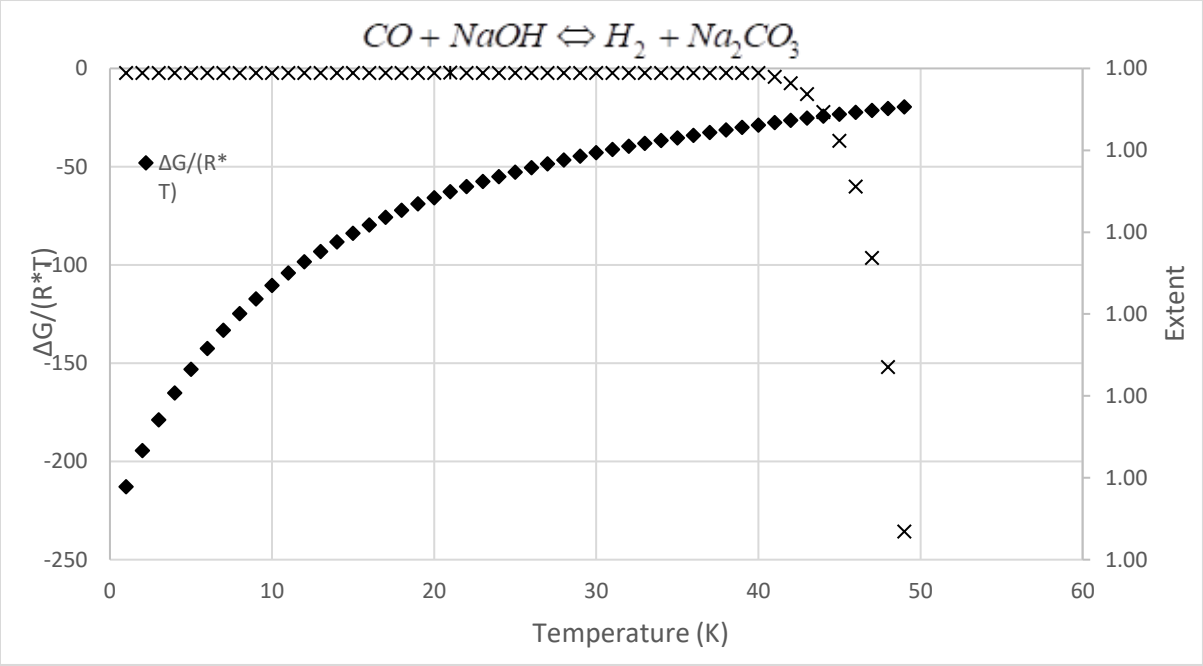

Figure 4-33 $\frac{\Delta G^o}{RT}$ and ξ vs temperature for Acetic acid cycle 1 reaction 2.

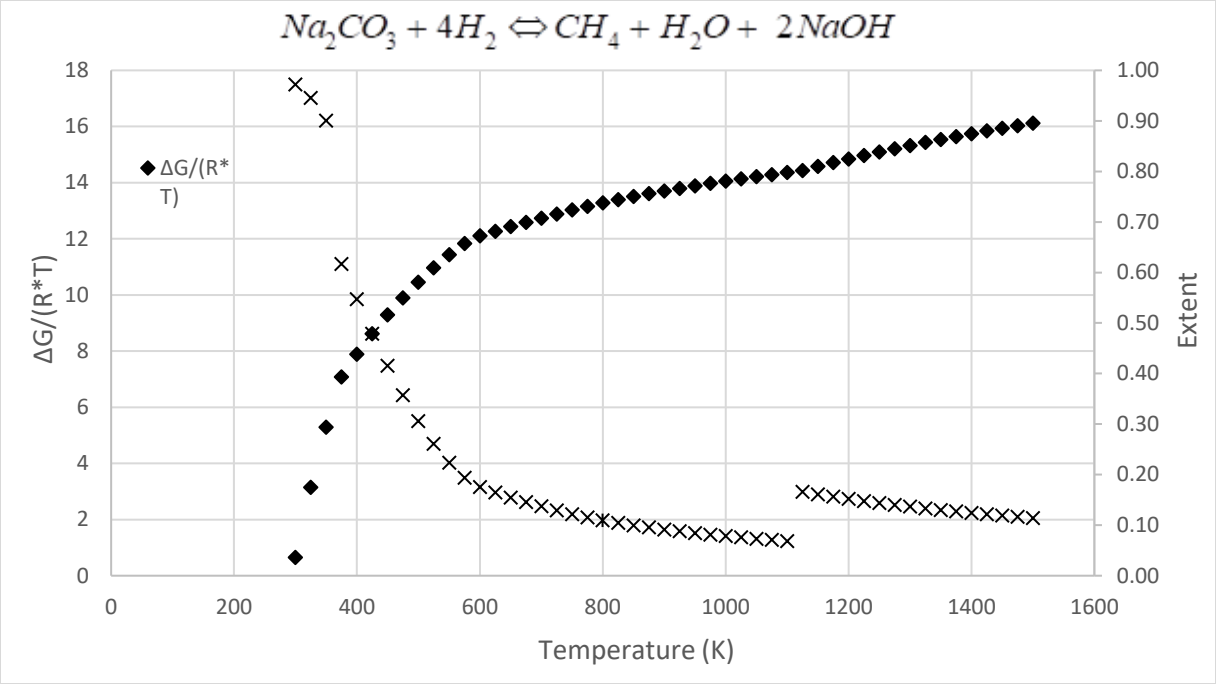

Figure 4-34 $\frac{\Delta G^o}{RT}$ and ξ vs temperature for Acetic acid cycle 1 reaction 3.

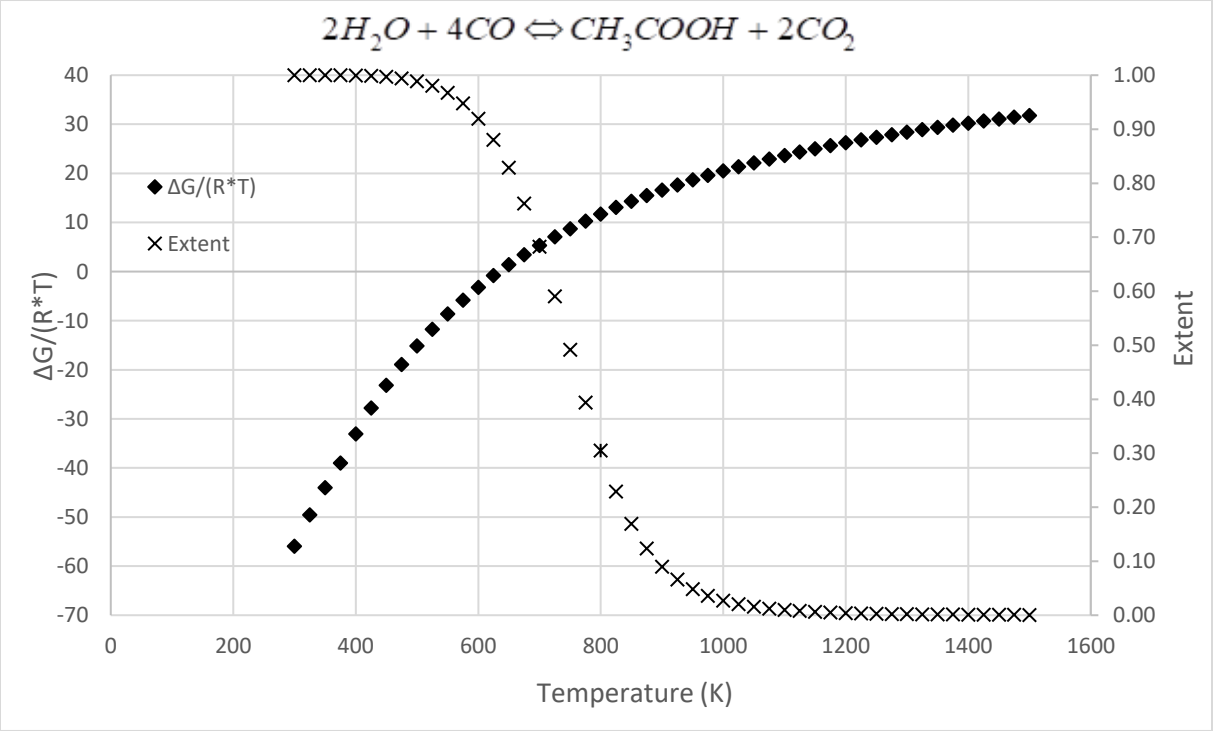

Figure 4-35 $\frac{\Delta G^o}{RT}$ and ξ vs temperature for Acetic acid cycle 2 reaction 1.

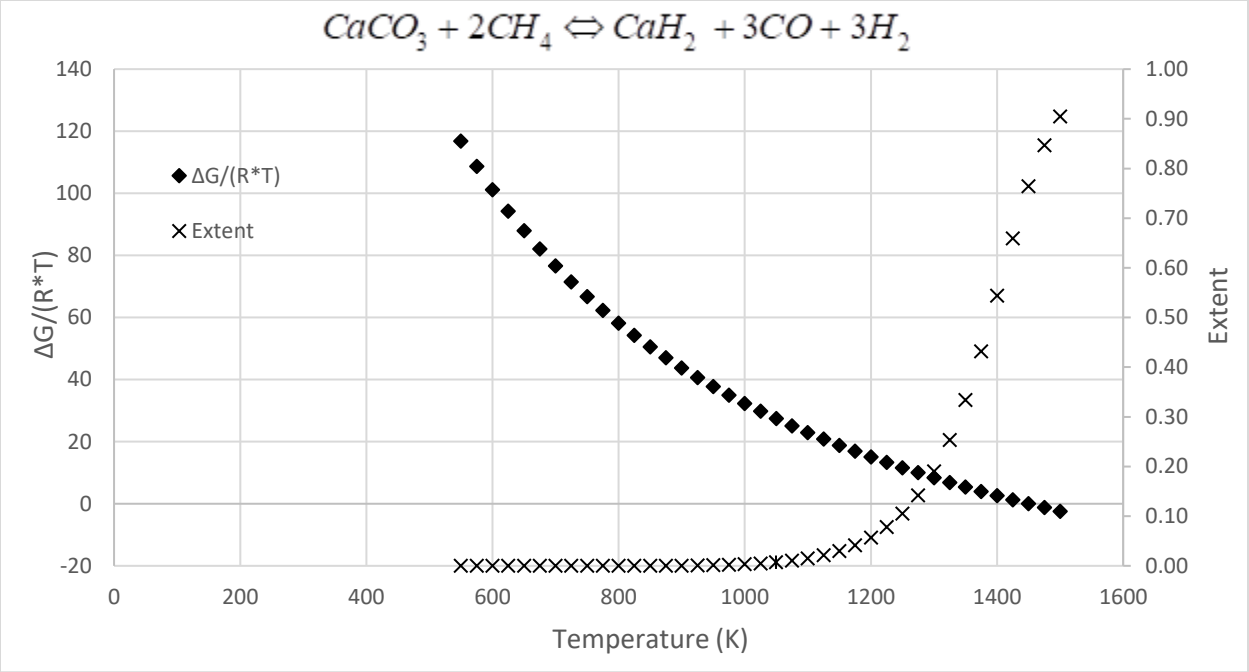

Figure 4-36 $\frac{\Delta G^o}{RT}$ and ξ vs temperature for Acetic acid cycle 2 reaction 2.

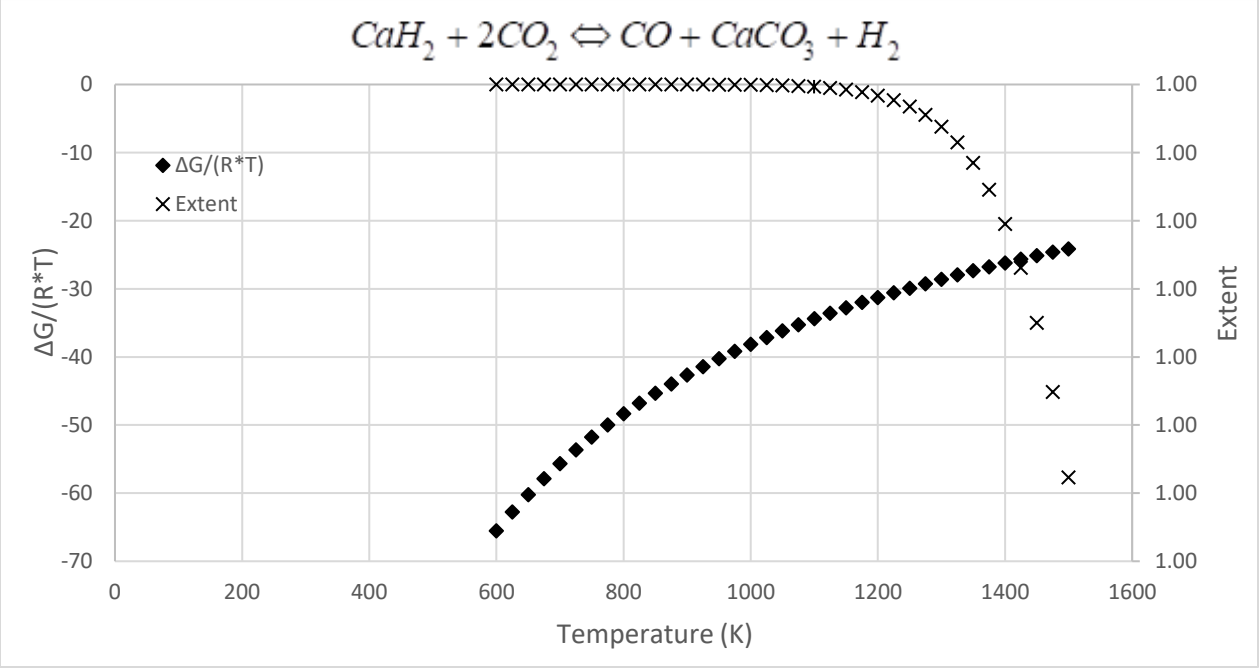

Figure 4-37 $\frac{\Delta G^o}{RT}$ and ξ vs temperature for Acetic acid cycle 2 reaction 3.

Table 4-5: DME acid cycles.

	Reactions	$T(K)$	$P(bar)$	$\Delta G^o\left(\frac{kJ}{mol}\right)$	ξ
1	$2CH_{4(g)} + 3CO_{2(g)} \Leftrightarrow H_2O_{(g)} + 3H_{2(g)} + 5CO_{(g)}$	1500	1	-342.71	0.99
	$CH_3OCH_{3(g)} + 3H_2O_{(g)} \Leftrightarrow 2CO_{2(g)} + 6H_{2(g)}$	1500	1	-515.56	0.99
	$5CO_{(g)} + 7H_{2(g)} \Leftrightarrow CO_{2(g)} + H_2O_{(l)} + 2CH_3OCH_{3(g)}$	298	25	-171.44	0.99
2	$2H_2O_{(l)}\ 2K_{(s)} \Leftrightarrow H_{2(g)} + K_2O_2H_{2(g)}$	298	1	-139.92	0.99
	$2CO_{(g)} + 4H_{2(g)} \Leftrightarrow CH_3OCH_{3(g)} + H_2O_{(l)}$	298	25	-75.04	0.99
	$K_2O_2H_{2(g)} + 2CH_{4(g)} \Leftrightarrow 2CO_{(g)} + 2K_{(g)} + 5H_{2(g)}$	1500	1	-304.64	0.99

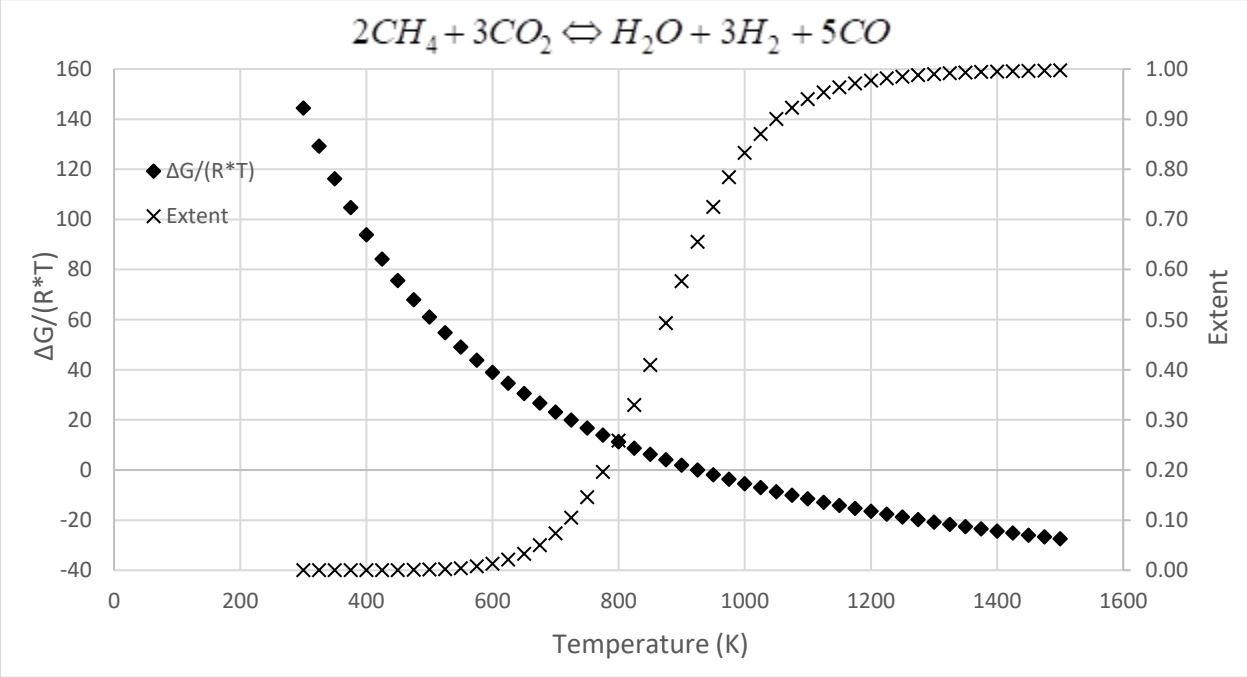

Figure 4-38 $\frac{\Delta G^o}{RT}$ and ξ vs temperature for DME acid cycle 1 reaction 1.

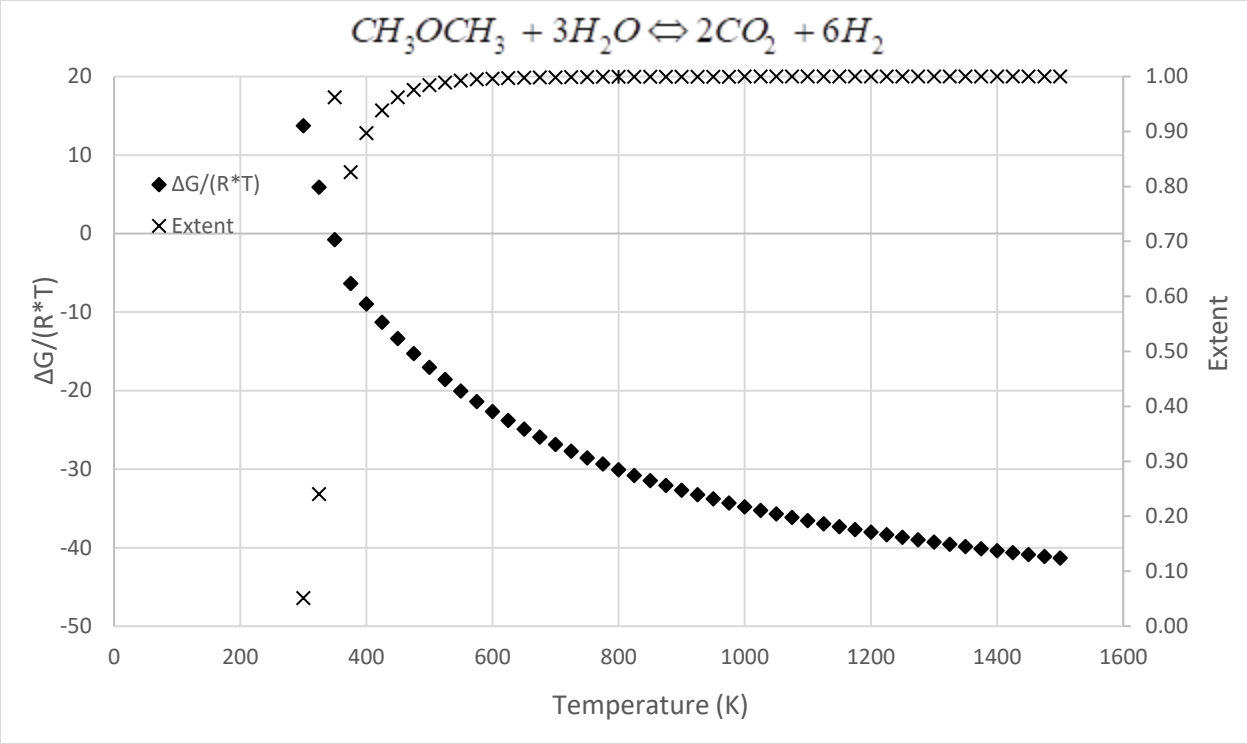

Figure 4-39 $\frac{\Delta G^o}{RT}$ and ξ vs temperature for DME acid cycle 1 reaction 2.

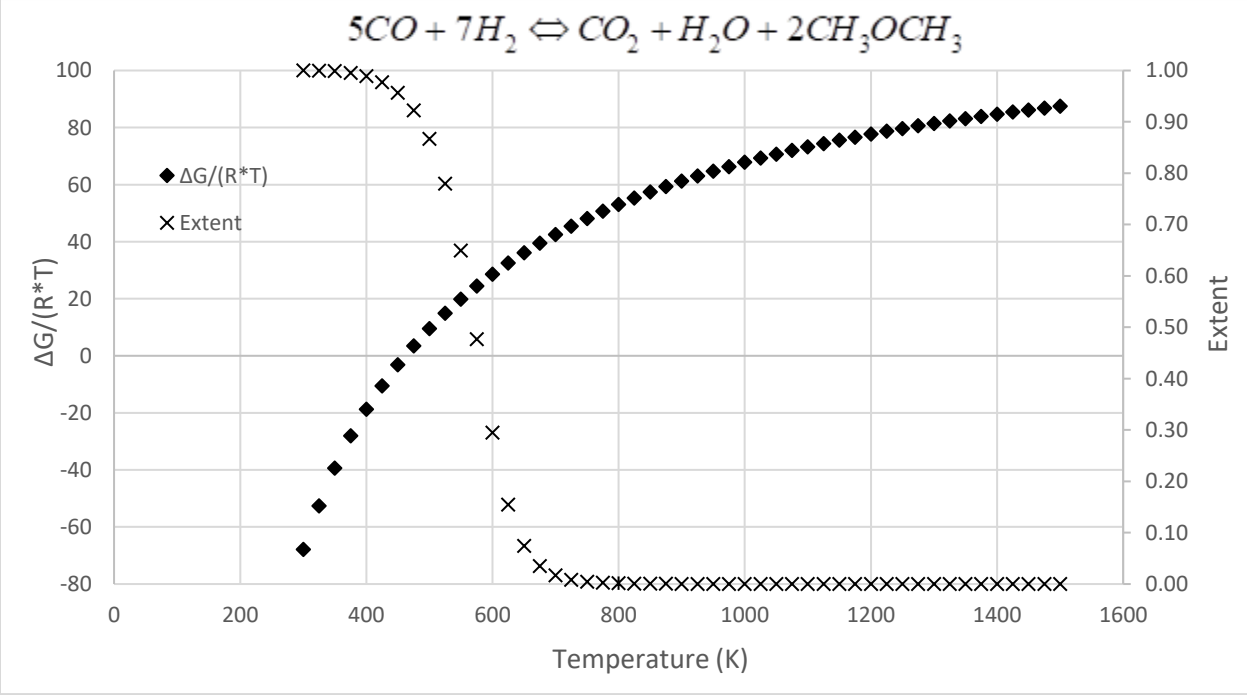

Figure 4-40 $\frac{\Delta G^o}{RT}$ and ξ vs temperature for DME acid cycle 1 reaction 3.

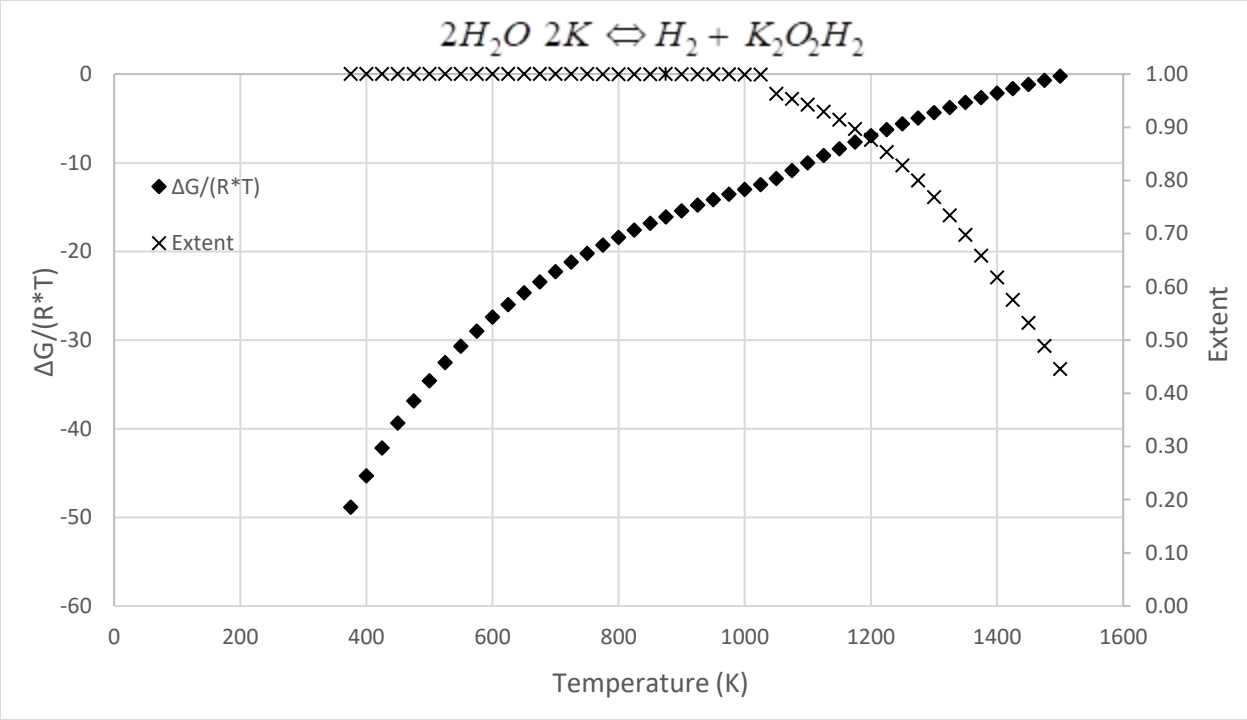

Figure 4-41 $\frac{\Delta G^o}{RT}$ and ξ vs temperature for DME acid cycle 2 reaction 1.

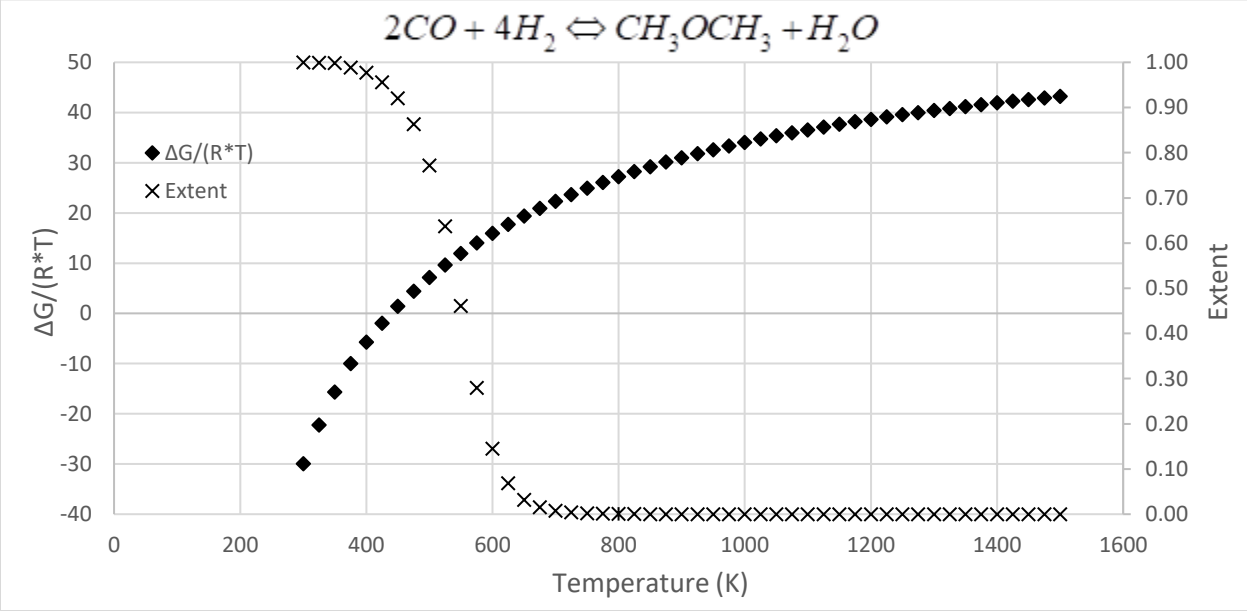

Figure 4-42 $\frac{\Delta G^o}{RT}$ and ξ vs temperature for DME acid cycle 2 reaction 2.

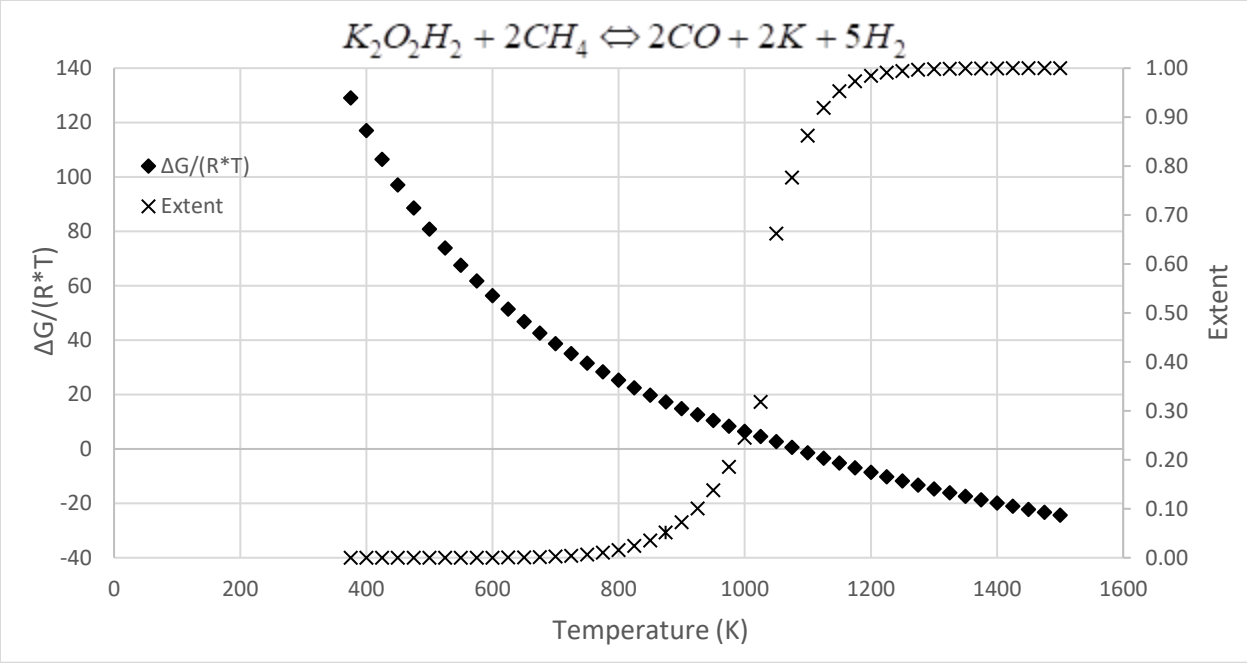

Figure 4-43 $\frac{\Delta G^o}{RT}$ and ξ vs temperature for DME acid cycle 2 reaction 3.

The reactions in Tables 4-3 thru 4-5 are all feasible within the original operating window and have an extent $\xi \geq 0.70$. Similar to the clusters found using water splitting as the target, the highest ξ is found at one of the edges of a temperature interval, and in fact for these cases were found on the boundary of the original temperature window. The first reaction cluster in the formic acid cycles in Table4-3 is an all low pressure cycle while the second cycle features a reaction that favors low pressure, a reaction that favors high pressure, and one that where pressure effects are negligible on the value for ξ under the current assumptions. It should be noted however that in the first reaction of cycle 1, methanol is likely to decompose at this temperature[77] and thus reaction would not proceed as written, even though there is thermodynamic data readily available for methanol up to 1500 K. This highlights the need for additional scrutiny when analyzing presented clusters, but also demonstrates the benefit of being able to amend the database as discussed in the previous section. Additionally, in reaction 1 of the

second cluster, the more stable from of calcium hydroxide is $Ca(OH)_2$ and would likely be formed over $CaOH$ even if there is thermodynamic data supporting the molar Gibbs energy of formation at that temperature[78]. For the acetic acid cycles in Table 4-4, both clusters shown feature a reaction that favors high pressure, one that favors low pressure, and one where pressure effects are negligible. Both the formic and acetic acid cycles have 2 low temperature reactions and 1 high temperature reaction, in contrast to the DME cycles shown in Table 4-5, in which the first cycle features 2 high temperature reactions and 1 low temperature reaction. All cycles found follow the trend of high temperature reactions be more favorable at low pressures, while low temperature reactions can be favored at low, high pressures, or have no pressure dependence.

4.3 Code Augmentations and Future Work

Having presented the results of lexicographic approach to network synthesis, we briefly discuss some possible further advancements that could be implemented within the algorithm to enhance its search process and refine search results. Some of these additions have already been incorporated, but there remains to perform rigorous validation testing against the previous stable version of the code.

Firstly, if it is desirable that an industrial prevalent reaction be included in the cluster, this can easily be formulated into the target reaction as described below.

$$CH_4 + H_2O \Leftrightarrow CO + 3H_2$$

$$CO + H_2O \Leftrightarrow CO_2 + H_2$$

$$CH_4 + 2H_2O \Leftrightarrow CO_2 + 4H_2$$

Which overall sum to:

$$2CH_4 + 4H_2O \Leftrightarrow 2CO_2 + 8H_2$$

When subtracted from water splitting and used as the target reaction:

$$2CO_2 + 6H_2 \Leftrightarrow 2CH_4 + 2H_2O + O_2$$

the same cluster generating algorithm can then be used to generate clusters, with each search yielding (n)/(n+1) results.

Additionally, we discuss is the ability to find clusters with non-irreducible reactions that is both computationally efficient and does not significantly increase the algorithms time complexity. Reaction clusters containing non-irreducible reactions have been presented numerous times in the literature[79] and can be thought of as approximate reactor sizing or relative flowrate ratios that need to occur in order the cycle to be a closed loop. As an example, a simple computationally effective way to include these reactions in the cluster search is iterate through the GFR list and use the information in the embedded FR's q vector to create incremented copies which are then added to the GFR until $\max(q) > \nu^{\max}$. This approach however significantly raises the time complexity of the algorithm by greatly increasing the number of elements in GFR, L, and R that have to be searched. In an experimental trial, a preliminary implementation of the above procedure was applied with $\nu^{\max} = 7$ and the size of GFR increased by %, while the sets L, and R both increased by % and % respectively. If it was desired to search for 5-clusters the increase in $\Theta\left(\#(GFR)\cdot\left(\#(L_{\max})\right)^2\cdot\left(\#(R_{\max})\right)^2\right)$ would be .

In a separate experiment with $\nu^{\max} = 12$ the increase in time complexity was

For certain reactions the extent of reaction can cancel out on the LHS side of (2.1.13). To preserve extent, it suffices to add an inert gas to the reactant side of the equation (2.1.13). Consider the two reactions shown below:

$$\left\{\begin{array}{ll} Rx1: & 2Na_2CO_{3(l)} \Leftrightarrow 4Na_{(g)} + 2CO_{2(g)} + O_{2(g)} \\ Rx2: & 4Na_{(g)} + 2CO_{2(g)} + O_{2(g)} \Leftrightarrow 2Na_2CO_{3(l)} \end{array}\right\}$$

Using the formulation in the last chapter to find the extent of reaction:

$$\left\{\begin{array}{l} K_{Rx1}(T)=\dfrac{\left(\dfrac{\hat{f}_{Na}^{(g)}}{f_{Na}^{o(g)}}\right)^4\left(\dfrac{\hat{f}_{CO_2}^{(g)}}{f_{CO_2}^{o(g)}}\right)^2\left(\dfrac{\hat{f}_{O_2}^{(g)}}{f_{O_2}^{o(g)}}\right)}{\left(\dfrac{\hat{f}_{Na_2CO_3}^{(l)}}{f_{Na_2CO_3}^{o(l)}}\right)^2}=\dfrac{\left(\dfrac{y_{Na}P}{P^\circ}\right)^4\left(\dfrac{y_{CO_2}P}{P^\circ}\right)^2\left(\dfrac{y_{O_2}P}{P^\circ}\right)}{\left(x_{Na_2CO_3}\right)^2} \\ K_{Rx2}(T)=\dfrac{\left(\dfrac{\hat{f}_{Na_2CO_3}^{(l)}}{f_{Na_2CO_3}^{o(l)}}\right)^2}{\left(\dfrac{\hat{f}_{Na}^{(g)}}{f_{Na}^{o(g)}}\right)^4\left(\dfrac{\hat{f}_{CO_2}^{(g)}}{f_{CO_2}^{o(g)}}\right)^2\left(\dfrac{\hat{f}_{O_2}^{(g)}}{f_{O_2}^{o(g)}}\right)}=\dfrac{\left(x_{Na_2CO_3}\right)^2}{\left(\dfrac{y_{Na}P}{P^\circ}\right)^4\left(\dfrac{y_{CO_2}P}{P^\circ}\right)^2\left(\dfrac{y_{O_2}P}{P^\circ}\right)}= \end{array}\right\}\Leftrightarrow$$

$$\left\{\begin{array}{l} K_{Rx1}(T)=\dfrac{\left(\dfrac{y_{Na}P}{P^\circ}\right)^4\left(\dfrac{y_{CO_2}P}{P^\circ}\right)^2\left(\dfrac{y_{O_2}P}{P^\circ}\right)}{\left(x_{Na_2CO_3}\right)^2}=\dfrac{\left(\dfrac{4\xi_1}{7\xi_1}\right)^4\left(\dfrac{2\xi_1}{7\xi_1}\right)^2\left(\dfrac{\xi_1}{7\xi_1}\right)}{1}\left(\dfrac{P}{P^\circ}\right)^7 \\ K_{Rx2}(T)=\dfrac{1}{\left(\dfrac{4-4\xi_2}{7-7\xi_2}\right)^4\left(\dfrac{2-2\xi_2}{7-7\xi_2}\right)^2\left(\dfrac{1-\xi_2}{7-7\xi_2}\right)}\left(\dfrac{P}{P^\circ}\right)^{-7}=\dfrac{1}{\left(\dfrac{4(1-\xi_1)}{7(1-\xi_1)}\right)^4\left(\dfrac{2(1-\xi_1)}{7(1-\xi_1)}\right)^2\left(\dfrac{1-\xi_1}{7(1-\xi_1)}\right)}\left(\dfrac{P}{P^\circ}\right)^{-7} \end{array}\right\}$$

Which both lead to obvious cancellations of the extent of reaction. In order to remedy this, an inert gas species is added to the reactant side and prescribed ratio relative to the species with the smallest coefficient. For the example reactions at hand this would yield:

$$\left\{\begin{array}{l} \alpha_{R1}=n_I^{(g)}\big/n_{Na_2CO_3}^{0(l)} \\ \alpha_{R2}=n_I^{(g)}\big/n_{O_2}^{0(g)} \end{array}\right\}\Rightarrow\left\{\begin{array}{l} n_{R1}{}^{(g)}=\alpha_{R1}n_{Na_2CO_3}^{0(l)}+7\xi_1 \\ n_{R2}{}^{(g)}=7+\alpha_{R2}n_{O_2}^{0(g)}-7\xi \end{array}\right\}$$

$$\left\{\begin{array}{l} K_{Rx1}(T)=\left(\dfrac{4\xi_1}{\alpha_1 n_{Na_2CO_3}^{0(l)}+7\xi_1}\right)^4\left(\dfrac{2\xi_1}{\alpha_1 n_{Na_2CO_3}^{0(l)}+7\xi_1}\right)^2\left(\dfrac{\xi_1}{\alpha_1 n_{Na_2CO_3}^{0(l)}+7\xi_1}\right)\left(\dfrac{P}{P^\circ}\right)^7 \\ K_{Rx2}(T)=\dfrac{1}{\left(\dfrac{4-4\xi_1}{7+\alpha_{R2}n_{O_2}^{0(g)}-7\xi}\right)^4\left(\dfrac{2-2\xi_1}{7+\alpha_{R2}n_{O_2}^{0(g)}-7\xi}\right)^2\left(\dfrac{1-\xi_1}{7+\alpha_{R2}n_{O_2}^{0(g)}-7\xi}\right)}\left(\dfrac{P}{P^\circ}\right)^{-7} \end{array}\right\}$$

which allows for the calculation of ξ. These augmentations were incorporated into the code and in an experimental trial generated the clusters shown in the table below:

Table 4-6: Problem parameters for augmented code trials

Parameter	T_L	T_U	P_L	P_U	$\#(N_S)$	N_R	S_{sp}	$\nu^{\max}$	$\xi_{\min}$
Value	298	1500	1	50	70	5	3	8	0.5

Table 4-7 Water cycles with implementation of inert ratio, non-irreducible reactions, and augmented target into the algorithm

	Reactions	$T(K)$	$P(bar)$	$\Delta G^o\left(\frac{kJ}{mol}\right)$	ξ	Dilution
1	$H_2O_{(g)} + SO_{3(g)} \Leftrightarrow H_2SO_{4(l)}$	374	50	-68.92	0.99	1.5
	$CO_{(g)} + 3GeO_{(g)} \Leftrightarrow CO_{2(g)} + O_{2(g)} + 3Ge_{(s)}$	300	50	-62.75	0.99	-
	$H_2O_{(g)} + O_{2(g)} + 3Ge_{(l)} \Leftrightarrow H_{2(g)} + 3GeO_{(g)}$	1415.57	1	-284.92	0.99	-
	$H_2SO_{4(g)} + 4SO_{3(g)} \Leftrightarrow H_{2(g)} + 3O_{2(g)} + 5SO_{2(g)}$	1500	1	-152.97	0.95	-
	$CO_{2(g)} + 2O_{2(g)} + 5SO_{2(g)} \Leftrightarrow CO_{(g)} + 5SO_{3(g)}$	300	50	-96.76	0.99	-
2	$O_{2(g)} + 2H_2O_{(g)} + 2Mg_{(s)} \Leftrightarrow 2Mg(OH)_{2(s)}$	374	50	-117.0	0.99	0.01
	$O_{2(g)} + 8HBr_{(g)} \Leftrightarrow 2H_2O_{(l)} + 2H_{2(g)} + 4Br_{2(l)}$	300	50	-45.94	0.99	-
	$4Br_{2(g)} + 8Fe(OH)_{2(s)} + 8H_2O_{(g)} \Leftrightarrow 8Fe(OH)_{3(s)} + 8HBr_{(g)}$	374	50	-64.8	0.99	-
	$O_{2(g)} + 2Mg(OH)_{2(l)} + 4H_{2(g)} \Leftrightarrow 2Mg_{(s)} + 6H_2O_{(g)}$	1500	1	-64.03	0.75	-
	$8Fe(OH)_{3(s)} \Leftrightarrow 4H_{2(g)} + 4O_{2(g)} + 4Fe(OH)_{2(s)}$	1500	1	48.92	0.59	1.5
4	$3CO_{2(g)} + 3Fe_{(s)} + 3H_2O_{(g)} \Leftrightarrow 3CO_{(g)} + 3Fe(OH)_{2(s)}$	374	50	4.499	0.72	-
	$H_{2(g)} + 3Fe(OH)_{2(s)} \Leftrightarrow O_{2(g)} + 3Fe_{(s)} + 4H_2O_{(g)}$	1500	1	-117.8	0.99	-
	$3CO_{(g)} + 5H_{2(g)} \Leftrightarrow CO_{2(g)} + H_2O_{(l)} + 2CH_{4(g)}$	300	50	-319.9	0.99	-

	$2CH_4 + 4H_2O \Leftrightarrow 2CO_2 + 8H_2$	N/A	N/A	N/A	N/A	N/A

The first reaction cluster in table 4-6 is a Germanium and Sulfuric acid combined cycle, each of which was discussed in the previous section on water splitting cycles. The cycle features to reactions which utilize the presence of an inert, and is the only cycle discovered thus far to feature a reaction whose maximum ξ occurs at a temperature that is not at one of the endpoints of the temperature intervals. Figures 4-44, 4-45, 4-46 below show the $\frac{\Delta G^o}{RT}$ and ξ vs temperature the reaction on the whole temperature window, on the discretized interval $[1300,1500]$ in steps of 5(K), and on the discretized interval $[1415,1416]$ in steps of 0.01 (K) respectively. It can be seen from Figure 4-46 that the temperature identified by the algorithm, $T = 1415.57(K)$, is at least within ± 0.1 of the true optimum, and that the difference in values for the objective function is at the 10th significant digit. It should also be noted that while the difference in the calculated value for ξ is less than 0.0000001 for all values within the temperature range of Figure 4-46, this example is used to illustrate the algorithms effectiveness at finding interior points within the original temperature window, even when their affect on ξ is negligible from an industrial perspective. The second reaction cluster in table 4-6 is an Iron, Magnesium, and Bromine cycle that features two non-irreducible reactions, reactions 3 and 5, and two reactions that feature the use of an inert gas, reactions 1 and 5. The 5th reactions of the second cycle features a reaction who's equilibrium can be shifted above $\xi_{\min}$ by adjusting the

pressure, as can be seen by the positive $\frac{\Delta G^o}{RT}$. The last reaction cluster features the use of the supplemental target which is listed as the fourth reaction.

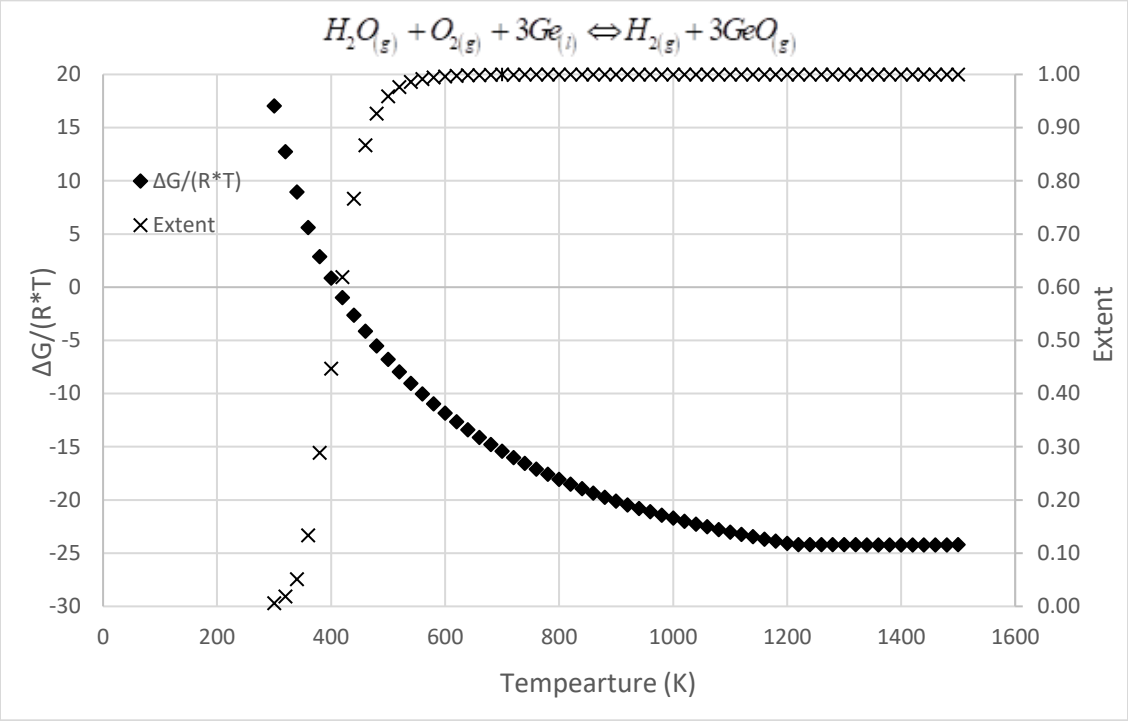

Figure 4-44 $\frac{\Delta G^o}{RT}$ and ξ vs temperature for augmented water splitting cycle 1 reaction 3, whole interval.

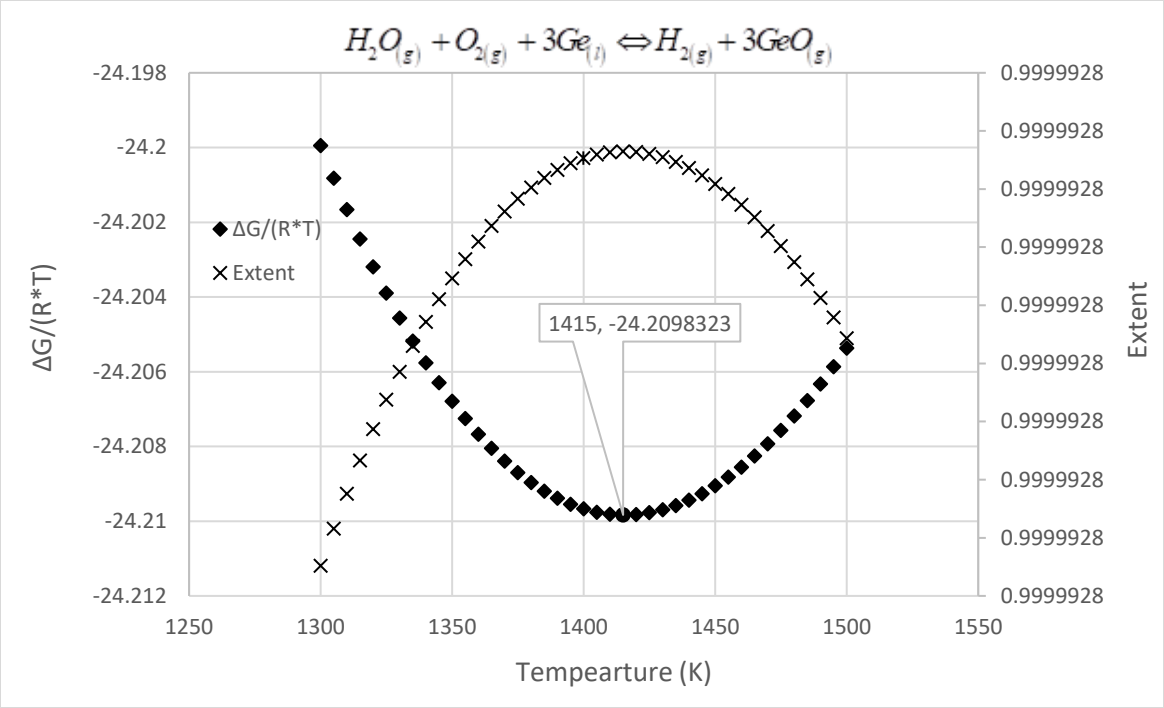

Figure 4-45 $\frac{\Delta G^o}{RT}$ and ξ vs temperature for augmented water splitting cycle 1 reaction 3, reduced interval 1.

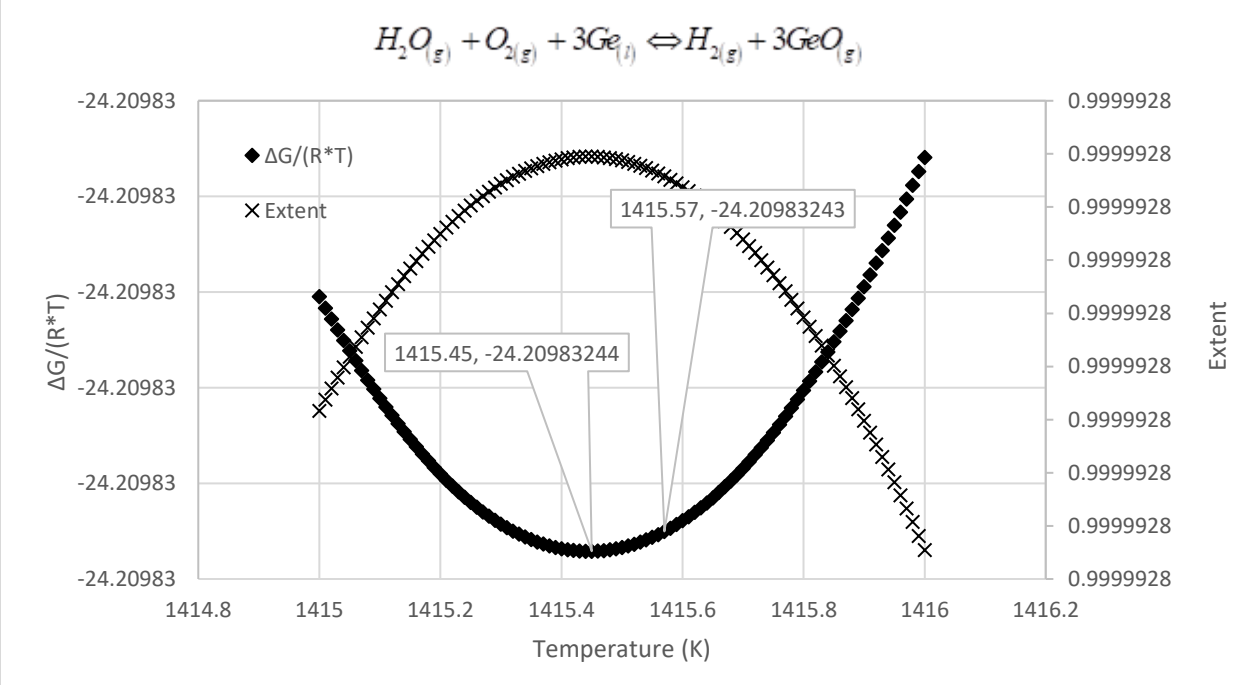

Figure 4-46 $\frac{\Delta G^o}{RT}$ and ξ vs temperature for augmented water splitting cycle 1 reaction 3, reduced interval 2.

Improvements to memory management and efficiency could also facilitate and expand the number of reaction clusters that can be found. For example, the information stored in the set HR, defined in the previous chapter as the sequence quintuple:

$$(w,q,p,u,d)=\left(\left\{w(j)\right\}_{j=1}^{HR_{\max}},\left\{q(j)\right\}_{j=1}^{HR_{\max}},\left\{p(j)\right\}_{j=1}^{HR_{\max}},\left\{u(j)\right\}_{j=1}^{HR_{\max}},\left\{d(j)\right\}_{j=1}^{HR_{\max}}\right)$$

can be reformulated, with proper augmentation to the FR generating function, as a sequence triplet:

$$(q,p,d)=\left(\left\{q(j)\right\}_{j=1}^{HR_{\max}},\left\{p(j)\right\}_{j=1}^{HR_{\max}},\left\{d(j)\right\}_{j=1}^{HR_{\max}}\right)$$

where the sequence of $\#(N_A)\times\#(N_S)$ matrices representing the half reaction and sequence of integers designating the number of species participating in the reaction have been removed, and the sequence of $1\times\#(N_S)$ vectors has been replaced by the sequence d' of $1\times S_{Sp}$ vectors whose entries consist of the species present from the input list that are present or -1. Since the number of half reactions is significantly larger (by several orders of magnitude) than the number of full reactions, the delaying the construction of the sequence of $\#(N_A)\times\#(N_S)$ matrices until the full reaction step saves a considerable amount of memory and greatly expands that search capabilities of the algorithm to include larger sets of N_S. For the FR generating function, each full reaction is made by creating linear combinations of the original $\#(N_A)\times\#(N_S)$ matrix S from the input data and subtracting them. This eliminates the need for both the sequence w and u during set generation and reduces the size of the last sequence as $\#(N_S)$ is going to be much larger than S_{Sp} for any trial of interest. Since at this time the size of the FR cannot be calculated from knowledge of the input data and thus cannot be pre-allocated, the advantage to

the described method is the reduction in memory cost during set creation. The table below shows the size (in gigabytes) for the sequences w, q, p, and d' for increasing species database.

Table 4-8 Memory size of for sequences w, q, p, and d as N_S and N_A increase.

$\#(N_s)$	$\#(N_A)$	w (Gb)	q (Gb)	p (Gb)	d' (Gb)
6	3	0.000404928	3.37E-05	6.75E-05	3.37E-05
7	3	0.00081144	5.80E-05	0.000116	5.80E-05
9	4	0.003267648	0.00018154	0.000272	0.000136
10	4	0.005152	0.0002576	0.000386	0.000193
11	4	0.007751744	0.00035235	0.000529	0.000264
13	5	0.01969864	0.00075764	0.000909	0.000455
14	5	0.02692256	0.00096152	0.001154	0.000577
16	6	0.056549376	0.00176717	0.001767	0.000884
17	6	0.072828	0.002142	0.002142	0.001071
18	6	0.092389248	0.00256637	0.002566	0.001283
21	8	0.233374848	0.00555654	0.004167	0.002084
22	8	0.28281088	0.00642752	0.004821	0.00241
23	8	0.339711104	0.00738502	0.005539	0.002769
24	8	0.404791296	0.00843315	0.006325	0.003162
25	8	0.4788	0.009576	0.007182	0.003591
26	8	0.562518528	0.01081766	0.008113	0.004057
28	9	0.857670912	0.01531555	0.01021	0.005105
30	10	1.26408	0.021068	0.012641	0.00632
31	10	1.44549776	0.02331448	0.013989	0.006994
33	11	2.052785328	0.03110281	0.016965	0.008483
34	11	2.318788032	0.03409982	0.0186	0.0093
35	11	2.609838	0.0372834	0.020336	0.010168
37	12	3.57079008	0.04825392	0.024127	0.012063
38	12	3.980449536	0.05237434	0.026187	0.013094
39	12	4.424382144	0.05672285	0.028361	0.014181
40	12	4.904448	0.0613056	0.030653	0.015326
41	12	5.422556352	0.06612874	0.033064	0.016532
43	13	7.129181904	0.08289746	0.03826	0.01913
44	13	7.827046656	0.08894371	0.041051	0.020525
45	13	8.57493	0.095277	0.043974	0.021987
46	13	9.375166528	0.10190398	0.047033	0.023516
47	13	10.23014408	0.10883132	0.05023	0.025115
49	14	13.04599677	0.13312242	0.057052	0.028526
50	14	14.1596	0.141596	0.060684	0.030342

51	14	15.34301462	0.15042171	0.064466	0.032233
52	14	16.59909888	0.15960672	0.068403	0.034201
53	14	17.93076835	0.16915819	0.072496	0.036248
54	14	19.34099597	0.1790833	0.07675	0.038375
55	14	20.832812	0.1893892	0.081167	0.040583
56	14	22.40930406	0.20008307	0.08575	0.042875
57	14	24.07361712	0.21117208	0.090502	0.045251

It can clearly be seen that the size of W is two to three orders of magnitude larger than the other sequences and its removal from the set creation process greatly improves memory efficiency and output performance.

Chapter 5 - Discussion and Conclusions

In this document we have presented the SR process for enhanced hydrogen production and raw material conversion. After defining several metrics with which to quantify reactor performance, 3 different dimensional case studies on SMR were carried out and the SR process was shown to be superior than conventional reactors by combining multiple processes within a single unit and operating in a dynamic manner. In the 0-dimensional isothermal CSTR case it was shown that conversion of methane increased by upwards of 100% through appropriate selection of Da and Θ, and that the use of hydrogen during the second mode of operation could increase the recovery during the final operation. While it is unlikely that SMR reaction to operate in CSTR fashion, the methodology demonstrated in the SR process is envisioned to be applicable in a general to enhance any reactive process. The 1-dimensional isobaric/isothermal studies revealed similar insights with methane conversion increased to over 200% for higher values Da and Θ. Reactors operating in this manner do not need to use hydrogen to increase recovery as the reactor is operating in plug flow. It is conceivable to operate SMR in isobaric plug flow through the use of microreactors or monolith reactor with catalyst support, as both of the reactors by design feature very low pressure drops. The 1-dimensional non-isobaric/non-isothermal study revealed two new dimensionless parameters associated with energy transfer. The parameter space of Ψ_9 was not investigated and Ψ_4 as not varied independently in the current studies, but the experimental trials show methane conversion increased to over 120% for higher values Da and Θ. Future studies on heat and momentum affects on conversion and hydrogen separation and recovery should be undertaken in the future to fully appreciate their impact on reactor design and performance.

During the course of the SR studies, it becomes apparent that the increase in conversion and hydrogen production comes at the cost of higher production of carbon dioxide as well. To reduce the negative environmental impact associated with increasing greenhouse gas emissions, the lexicographic approach to network synthesis was developed and applied to creating closed pathways of hydrogen production with no harmful emissions. The algorithm developed is an efficient and flexible tool that can tremendously impact the early process development stages by generating alternative reaction pathways. One of the novel aspects of the approach concerns the free energy data. Whereas this has typically been assumed to have a strictly linear dependence upon temperature, the new model showed that this assumption need not be invoked to take advantage of computational savings. It is important to note that kinetics have not yet been considered. Thus, although the resulting reactions are thermodynamically feasible, they may not be kinetically favorable. Moreover, although heat capacity data exists for each of the species at these temperatures, the pressure dependence is unclear. Consequently, some of these species may actually decompose at the given temperature and pressure, or they may react violently upon heating. In light of these points, a more detailed investigation of the clusters synthesized by the lexicographic method is should be undertaken. The above limitations notwithstanding, this lexicographic approach is useful in generating alternative cluster candidates. It identifies all potential clusters obtainable from a given set of chemical species, ensuring that the reactions are thermodynamically feasible and satisfy mass balance considerations. At that point, the list of clusters can be more thoroughly evaluated for things such as potential side reactions and competing byproducts, kinetics and potential catalyst cost, hazards like toxicity, flammability or corrosiveness, and reliability of reactions. Moreover, process synthesis considerations can then be addressed such cost of separations, energy requirements, process flexibility, and capital

investment. It is hoped that this methodology will eventually lead to clusters that can be implemented in an economically viable manner.

Chapter 6 - Appendix

Appendix A.1- Storage reactor formulation

Having briefly described the storage reactor concept in the introduction, we now formalize the process mathematically by explicitly deriving the governing equations. The first section goes through Reynolds transport theorem, then mass momentum and energy equations are derived for the reactor, the catalyst pellet, and storage pellet domains. Some underlying assumptions: solid phase is stationary, ideal gas law, etc.

A.1.1 Preliminary Information

The following terms are defined:

$\varepsilon^{V}_{\alpha\beta}\left(\frac{m^3\ of\ \ phase\ \alpha}{m^3\ of\ domain\ \beta}\right)$, $\beta \in \{c,s,v,w,r\}, \alpha \in \{s,\ f\}$: control volume fraction of phase α in domain β, where $\alpha \in \{s,\ f\}$ with $s,\ f$ denoting the solid and gas phases respectively; $\beta \in \{c,s,v,w,r\}$ with c,s,v,w,r denoting the catalyst pellet, storage pellet, reactor void unoccupied by either catalyst or storage pellets, reactor wall, and total reactor domains.

$\varepsilon^{A}_{\alpha\beta}\left(\frac{m^2\ of\ \ phase\ \alpha}{m^2\ of\ domain\ \beta}\right), \beta \in \{c,s,v,w,r\}, \alpha \in \{s,\ f\}$: control surface fraction of phase α in domain β, where $\alpha \in \{s,\ f\}$ with $s,\ f$ denoting the solid and gas phases respectively; $\beta \in \{c,s,v,w,r\}$ with c,s,v,w,r denoting the catalyst pellet, storage pellet, reactor void unoccupied by either catalyst or storage pellets, reactor wall, and total reactor domains.

It has been established[80], [81] that for a multi-component, multi-phase system, repeated application and summation of the Reynolds Transport Theorem (RTT):

$$\frac{dM_{CSys}(t)}{dt} = \frac{\partial}{\partial t}\left(\iiint_{CV} M \rho dV_t \right) + \iint_{CS} M \rho \vec{v} \cdot \vec{n} dA_t \tag{A.1.1}$$

to each sub system will yield the total rate of change for an extensive property. Additionally, assuming certain structural and geometric parameters can be established, an extensive properties rate of change can be expressed as the summation of contributions from various volumes elements within its phase and or domain:

$$\frac{dM_{\alpha\beta,CSys}(t)}{dt} = \frac{\partial}{\partial t}\left(\iiint_{CV} \varepsilon^V_{\beta r}\varepsilon^V_{\alpha\beta} M \rho dV_t \right) + \iint_{CS} \varepsilon^A_{\beta r}\varepsilon^A_{\alpha\beta} M \rho \vec{v} \cdot \vec{n} dA_t \tag{A.1.2}$$

Applying Gauss Divergence theorem on the control surface and Leibniz's Theorem for a fixed control volume yields:

$$\frac{dM_{\alpha\beta,CSys}(t)}{dt} = \iiint_{CV} \frac{\partial}{\partial t}\left(\varepsilon^V_{\beta r}\varepsilon^V_{\alpha\beta} M \rho dV \right)_t + \iiint_{CV} \vec{\nabla} \cdot \left(\varepsilon^A_{\beta r}\varepsilon^A_{\alpha\beta} M \rho \vec{v} \right) dV_t \tag{A.1.3}$$

with the total system given by:

$$\frac{dM_{CSys}(t)}{dt} = \sum_{j=\alpha}^{NP_\alpha} \sum_{k=\beta}^{NP_\beta} \frac{dM_{jk,CSys}(t)}{dt} \tag{A.1.4}$$

Therefore, in order to establish governing equations and gain insight into reactor performance it remains to apply this methodology to the extensive properties of choice and establish connections between different zones through physical/mathematical descriptions.

First, some assumptions are presented and assumed to hold true. The first being that the quasi-equilibrium postulate holds:

$$d\hat{U}_{\alpha\beta} = T_{\alpha\beta} d\hat{S}_{\alpha\beta} - P_{\alpha\beta} d\hat{V}_{\alpha\beta} + \sum_{i=1}^{NS} \frac{\hat{G}_{i,\alpha\beta}}{M_i} dw_{i,\alpha\beta} \tag{A.1.5}$$

Using the assumptions above, the linearity postulate is assumed to be valid:

$$\vec{Q}_{\alpha\beta} = -a_{00,\alpha\beta} \nabla \left(\ln T_{\alpha\beta} \right) - \sum_{i=1}^{NS} \frac{a_{0i,\alpha\beta} c_{\alpha\beta} R T_{\alpha\beta}}{\rho_{i,\alpha\beta}} \vec{d}_{i,\alpha\beta} \qquad \forall i = 1,...., NC \tag{A.1.6}$$

$$\vec{N}_{i,\alpha\beta} = -a_{i0,\alpha\beta}\nabla\left(\ln T_{\alpha\beta}\right) - \rho_{i,\alpha\beta}\sum_{k=1}^{NS}\left(\frac{a_{ki,\alpha\beta}c_{\alpha\beta}RT_{\alpha\beta}}{\rho_{i,\alpha\beta}\rho_{k,\alpha\beta}}\vec{d}_{k,\alpha\beta}\right) \qquad \forall i = 1,....,NC \qquad \text{(A.1.7)}$$

Which give rise to the Stefan Maxwel diffusional driving force relation

$$\vec{d}_{i,\alpha\beta} = \nabla x_{i,\alpha\beta} + \frac{1}{c_{\alpha\beta}RT_{\alpha\beta}}\left(\left(c_{i,\alpha\beta}\bar{V}_{i,\alpha\beta} - w_{i,\alpha\beta}\right)\nabla P_{\alpha\beta} - \rho_{i,\alpha\beta}\vec{g}_i + w_{i,\alpha\beta}\sum_{k=1}^{NS}\rho_{k,\alpha\beta}\vec{g}_k\right) \quad \forall i = 1,....,NC$$

(A.1.8)

Which will be used as a basis to model mass flux in the SR.

A.1.2. Mass Derivation

For an arbitrary system in one domain, selecting total mass

$$\left\{M = 1 \wedge \frac{dM_{Csys}(t)}{dt} = \frac{d(m)_{Csys}(t)}{dt} = 0\right\} \qquad \text{(A.1.9)}$$

yields total the total mass conservation equation

$$\frac{\partial}{\partial t}(\rho) + \vec{\nabla}\cdot(\rho\vec{v}) = 0 \qquad \text{(A.1.10)}$$

Using the summability property therefore gives:

$$\left\{\begin{array}{l} M = 1 \wedge \dfrac{dM_{Csys}(t)}{dt} = \dfrac{d(m)_{Csys}(t)}{dt} = 0 \\ \dfrac{dM_{CSys}(t)}{dt} = \displaystyle\sum_{j=\alpha}^{NP_\alpha}\sum_{k=\beta}^{NP_\beta}\frac{dM_{jk,CSys}(t)}{dt} \end{array}\right\} \Rightarrow \qquad \text{(A.1.11)}$$

$$\left\{\frac{\partial}{\partial t}(\rho) + \vec{\nabla}\cdot(\rho\vec{v}) = 0\right\} \Leftrightarrow \left\{\sum_{j=\alpha}^{NP_\alpha}\sum_{k=\beta}^{NP_\beta}\frac{\partial}{\partial t}\left(\varepsilon_{kr}^{V}\varepsilon_{jk}^{V}\rho_{\alpha\beta}\right) + \vec{\nabla}\cdot\left(\varepsilon_{kr}^{A}\varepsilon_{jk}^{A}\vec{N}_{jk}\right) = 0\right\} \qquad \text{(A.1.12)}$$

Which when generally applied to phase α within domain β on a domain r volumetric basis gives general mass balance equation:

$$\frac{\partial}{\partial t}\left(\varepsilon_{\beta r}^{V}\varepsilon_{\alpha\beta}^{V}\rho_{\alpha\beta}\right) + \vec{\nabla}\cdot\left(\varepsilon_{\beta r}^{A}\varepsilon_{\alpha\beta}^{A}\vec{N}_{\alpha\beta}\right) = 0 \qquad \text{(A.1.13)}$$

Similarly, selecting component mass

$$\left\{ M = w_i \wedge \frac{dM(t)}{dt} = \iiint_{CV} R_i \, dV_t - \iint_{CS} \overrightarrow{j_i} \cdot \overrightarrow{n} dA_t \right\} \tag{A.1.14}$$

yields component conservation equation. Utilizing summability property

$$\left\{ \begin{array}{l} \dfrac{dM_{CSys}(t)}{dt} \wedge M = w_i \triangleq \left\{ \dfrac{\partial}{\partial t}\left(\rho_i\right) + \vec{\nabla} \cdot \left(\rho_i \vec{v}_i\right) = \hat{R}_i \right\} \\ \dfrac{dM_{CSys}(t)}{dt} = \sum_{j=\alpha}^{NP_\alpha} \sum_{k=\beta}^{NP_\beta} \dfrac{dM_{jk,CSys}(t)}{dt} \end{array} \right\} \Rightarrow \tag{A.1.15}$$

$$\left\{ \left\{ \frac{\partial}{\partial t}\left(\rho_i\right) + \vec{\nabla} \cdot \left(\rho_i \vec{v}_i\right) - \hat{R}_i = 0 \right\} \Leftrightarrow \left\{ \sum_{j=\alpha}^{NP_\alpha} \sum_{k=\beta}^{NP\beta} \left(\frac{\partial}{\partial t}\left(\varepsilon_{kr}^V \varepsilon_{jk}^V \rho_{i,jk}\right) + \vec{\nabla} \cdot \left(\varepsilon_{kr}^A \varepsilon_{jk}^A \overrightarrow{N}_{i,jk}\right) = \varepsilon_{kr}^V \varepsilon_{jk}^V \hat{R}_{i,jk} \right) \right\} \right\} \tag{A.1.16}$$

Which when generally applied to phase α within domain β on a domain r volumetric basis gives general species mass balance equation:

$$\frac{\partial}{\partial t}\left(\varepsilon_{\beta r}^V \varepsilon_{\alpha\beta}^V \rho_{i,\alpha\beta}\right) + \vec{\nabla} \cdot \left(\varepsilon_{\beta r}^A \varepsilon_{\alpha\beta}^A \vec{N}_{i,\alpha\beta}\right) = \varepsilon_{\beta r}^V \varepsilon_{\alpha\beta}^V \hat{R}_{i,\alpha\beta} \tag{A.1.17}$$

With the following defined as:

Mass fraction - density of species i relations:

$$\rho_{i,\alpha\beta} = w_{i,\alpha\beta} \rho_{\alpha\beta} \qquad \forall i = 1,....,NC$$

Total Mass Flux of species q relations:

$$\overrightarrow{N}_{i,\alpha\beta} = \rho_{i,\alpha\beta} \vec{v}_{i,\alpha\beta} \qquad \forall i = 1,....,NC$$

Mass average velocity definition

$$\vec{v}_{\alpha\beta} = \sum_{i=1}^{NC} w_{i,\alpha\beta} \vec{v}_{i,\alpha\beta} = \sum_{i=1}^{NC} \frac{\rho_{i,\alpha\beta}}{\rho_{\alpha\beta}} \vec{v}_{i,\alpha\beta}$$

Total Mass Flux relations:

$$\overrightarrow{N}_{\alpha\beta} = \sum_{i=1}^{NC} \overrightarrow{N}_{i,\alpha\beta} = \sum_{i=1}^{NC} \rho_{i,\alpha\beta} \vec{v}_{i,\alpha\beta} = \rho_{\alpha\beta} \vec{v}_{\alpha\beta}$$

Diffusive Mass Flux of species i definitions:

$$\vec{j}_{i,\alpha\beta} = \overrightarrow{N}_{i,\alpha\beta} - \rho_{i,\alpha\beta} \vec{v}_{\alpha\beta} \quad \forall i = 1,....,NC$$

Diffusive Mass Flux relation:

$$\sum_{i=1}^{NC} \vec{j}_{i,\alpha\beta} = \sum_{i=1}^{NC} \vec{N}_{i,\alpha\beta} - \sum_{i=1}^{NC} \rho_{i,\alpha\beta} \vec{v}_{\alpha\beta} = \rho_{\alpha\beta} \vec{v}_{\alpha\beta} - \rho_{\alpha\beta} \vec{v}_{\alpha\beta} = 0$$

Because chemical engineering typically deals with mols, the above total and component mass balances can be converted to mols.

$$\frac{\partial}{\partial t}\left(\varepsilon_{\beta r}^{V} \varepsilon_{\alpha\beta}^{V} c_{\alpha\beta}\right) + \vec{\nabla} \cdot \left(\varepsilon_{\beta r}^{A} \varepsilon_{\alpha\beta}^{A} \vec{N}_{\alpha\beta}^{\dagger}\right) = \varepsilon_{\beta r}^{V} \varepsilon_{\alpha\beta}^{V} \left(\sum_{i=1}^{NC} \hat{R}_{i,\alpha\beta}\right)$$

$$\frac{\partial}{\partial t}\left(\varepsilon_{\beta r}^{V} \varepsilon_{\alpha\beta}^{V} c_{i,\alpha\beta}\right) + \vec{\nabla} \cdot \left(\varepsilon_{\beta r}^{A} \varepsilon_{\alpha\beta}^{A} \vec{N}_{i,\alpha\beta}^{\dagger}\right) = \varepsilon_{\beta r}^{V} \varepsilon_{\alpha\beta}^{V} \hat{R}_{i,\alpha\beta}$$

With similarly defined relations:

Mol fraction - molar density of species i relations:

$$c_{i,\alpha\beta} = x_{i,\alpha\beta} c_{\alpha\beta} \quad \forall i = 1,....,NC$$

Total Mol Flux of species i relations:

$$\vec{N}_{i,\alpha\beta}^{\dagger} = c_{i,\alpha\beta} \vec{v}_{i,\alpha\beta} \qquad \forall i = 1,....,NC$$

Mol average velocity definition

$$\vec{v}_{\alpha\beta}^{\dagger} = \sum_{i=1}^{NC} x_{i,\alpha\beta} \vec{v}_{i,\alpha\beta} = \sum_{i=1}^{NC} \frac{c_{i,\alpha\beta}}{c_{\alpha\beta}} \vec{v}_{i,\alpha\beta}$$

Total Mol Flux relations:

$$\vec{N}_{\alpha\beta}^{\dagger} = \sum_{i=1}^{NC} \vec{N}_{i,\alpha\beta}^{\dagger} = \sum_{i=1}^{NC} c_{i,\alpha\beta} \vec{v}_{i,\alpha\beta} = c_{\alpha\beta} \vec{v}_{\alpha\beta}^{\dagger}$$

Diffusive Molar Flux of species i definitions:

$$\vec{j}_{i,\alpha\beta}^{\dagger} = \vec{N}_{i,\alpha\beta}^{\dagger} - c_{i,\alpha\beta} \vec{v}_{\alpha\beta}^{\dagger} \quad \forall i = 1,....,NC$$

Diffusive Mol Flux relation:

$$\sum_{i=1}^{NC} \vec{j}_{i,\alpha\beta}^{\dagger} = \sum_{i=1}^{NC} \vec{N}_{i,\alpha\beta}^{\dagger} - \sum_{i=1}^{NC} c_{i,\alpha\beta} \vec{v}_{\alpha\beta}^{\dagger} = c_{\alpha\beta} \vec{v}_{\alpha\beta}^{\dagger} - c_{\alpha\beta} \vec{v}_{\alpha\beta}^{\dagger} = 0$$

Because mixed mass and mol velocities a relation is derived to convert between mass averaged and mol averaged velocities:

$$\left.\begin{aligned}\vec{v}_{\alpha\beta}-\vec{v}^{\dagger}_{\alpha\beta}&=\sum_{i=1}^{NC}w_{i,\alpha\beta}\left(\vec{v}_{i,\alpha\beta}-\vec{v}^{\dagger}_{\alpha\beta}\right)\\ \vec{v}^{\dagger}_{\alpha\beta}-\vec{v}_{\alpha\beta}&=\sum_{i=1}^{NC}x_{i,\alpha\beta}\left(\vec{v}_{i,\alpha\beta}-\vec{v}_{\alpha\beta}\right)\end{aligned}\right\}\Rightarrow\left\{\vec{v}_{\alpha\beta}=\vec{v}^{\dagger}_{\alpha\beta}+\sum_{i=1}^{NC}w_{i,\alpha\beta}\left(\vec{v}_{i,\alpha\beta}-\vec{v}^{\dagger}_{\alpha\beta}\right)\right\}\Rightarrow$$

$$\left\{\vec{v}_{\alpha\beta}=\vec{v}^{\dagger}_{\alpha\beta}+\sum_{i=1}^{NC}\left(\frac{x_{i,\alpha\beta}M_i}{\sum_{j=1}^{NC}x_{j,\alpha\beta}M_j}\left(\vec{v}_{i,\alpha\beta}-\vec{v}^{\dagger}_{\alpha\beta}\right)\right)\right\}\Rightarrow\left\{\vec{v}_{\alpha\beta}=\vec{v}^{\dagger}_{\alpha\beta}+\sum_{i=1}^{NC}\left(\frac{x_{i,\alpha\beta}M_i c_{\alpha\beta}}{\rho_{\alpha\beta}}\left(\vec{v}_{i,\alpha\beta}-\vec{v}^{\dagger}_{\alpha\beta}\right)\right)\right\}\Rightarrow$$

$$\left\{\vec{v}_{\alpha\beta}=\vec{v}^{\dagger}_{\alpha\beta}+\sum_{i=1}^{NC}\left(\frac{x_{i,\alpha\beta}M_i c_{\alpha\beta}}{\rho_{\alpha\beta}}\left(\vec{v}_{i,\alpha\beta}-\vec{v}^{\dagger}_{\alpha\beta}\right)\right)\right\}\Rightarrow$$

$$\left\{\vec{v}_{\alpha\beta}=\vec{v}^{\dagger}_{\alpha\beta}+\sum_{i=1}^{NC}\left(\frac{M_i c_{i,\alpha\beta}}{\rho_{\alpha\beta}}\left(\vec{v}_{i,\alpha\beta}-\vec{v}^{\dagger}_{\alpha\beta}\right)\right)\right\}\Rightarrow$$

$$\left\{\vec{v}_{\alpha\beta}=\vec{v}^{\dagger}_{\alpha\beta}+\sum_{i=1}^{NC}\left(\frac{M_i}{\rho_{\alpha\beta}}\left(c_{i,\alpha\beta}\vec{v}_{i,\alpha\beta}-c_{i,\alpha\beta}\vec{v}^{\dagger}_{\alpha\beta}\right)\right)\right\}\Rightarrow$$

$$\boxed{\left\{\vec{v}_{\alpha\beta}=\vec{v}^{\dagger}_{\alpha\beta}+\frac{1}{c_{\alpha\beta}}\sum_{i=1}^{NC}\left(\frac{M_i}{\sum_{j=1}^{NC}x_{j,\alpha\beta}M_j}\left(\vec{j}^{\dagger}_{i,\alpha\beta}\right)\right)\right\}} \qquad \text{(A.1.18)}$$

In this work it is considered that mass flow only occurs in the reactor void, catalyst void, and storage void, while other solid phases are stagnant. Using these assumptions and the relations amongst mass fluxes leads to the following component equations:

$$\left\{\begin{array}{l} \dfrac{\partial}{\partial t}\left(\varepsilon_{vr}^{V}\varepsilon_{fv}^{V}\rho_{fv}\right)+\vec{\nabla}\cdot\left(\varepsilon_{vr}^{A}\varepsilon_{fv}^{A}\rho_{fv}\vec{v}_{fv}\right)=0 \ \text{ on } \Omega_{fv} \\ \vec{N}_{f-f}^{c\to v}=\sum_{i=1}^{NC}\vec{N}_{i,f-f}^{c\to v}=\sum_{i=1}^{NC}\vec{N}_{i,f-f}^{c\to v}\Big|^{CS_c} \text{ on } \partial\Omega_{f,cv} \\ \vec{N}_{f-f}^{s\to v}=\sum_{i=1}^{NC}\vec{N}_{i,f-f}^{s\to v}=\sum_{i=1}^{NC}\vec{N}_{i,f-f}^{s\to v}\Big|^{CS_s} \text{ on } \partial\Omega_{f,sv} \end{array}\right\} \qquad \text{(A.1.19)}$$

Total Reactor Mass

$$\left\{\begin{array}{l} \dfrac{\partial}{\partial t}\left(\varepsilon_{cr}^{V}\varepsilon_{fc}^{V}\rho_{fc}\right)+\vec{\nabla}\cdot\left(\varepsilon_{cr}^{A}\varepsilon_{fc}^{A}\rho_{fc}\vec{v}_{fc}\right)=0 \text{ on } \Omega_{fc} \\ \vec{N}_{f-f}^{v\to c}=\sum_{i=1}^{NC}\vec{N}_{i,f-f}^{v\to c}=\sum_{i=1}^{NC}\vec{N}_{i,f-f}^{v\to c}\Big|^{CS_v} \text{ on } \partial\Omega_{f,vc} \end{array}\right\} \qquad \text{(A.1.20)}$$

Total Catalyst Mass

$$\left\{\begin{array}{l} \dfrac{\partial}{\partial t}\left(\varepsilon_{sr}^{V}\varepsilon_{fs}^{V}\rho_{fs}\right)+\vec{\nabla}\cdot\left(\varepsilon_{sr}^{A}\varepsilon_{fs}^{A}\rho_{fs}\vec{v}_{fs}\right)=0 \text{ on } \Omega_{fs} \\ \vec{N}_{f-f}^{v\to c}=\sum_{i=1}^{NC}\vec{N}_{i,f-f}^{v\to s}=\sum_{i=1}^{NC}\vec{N}_{i,f-f}^{v\to s}\Big|^{CS_v} \text{ on } \partial\Omega_{f,vs} \end{array}\right\} \qquad \text{(A.1.21)}$$

Total Storage Mass

Where boundary conditions have been listed in order to emphasize that in $\mathbb{R}^n, n \geq 2$, species source terms for multi domain systems appear as flux boundary conditions between domains. Upon reduction of problem dimensionality, these will be represented by source terms in the governing PDE. For the subsequent derivations of Momentum and Energy conservation, the above general balance form will be used. The species mol balances for the domains of interest are presented below.

$$\left\{\begin{array}{l} \dfrac{\partial}{\partial t}\left(\varepsilon_{vr}^{V}\varepsilon_{fv}^{V}c_{i,fv}\right)+\vec{\nabla}\cdot\left(\varepsilon_{\beta r}^{A}\varepsilon_{\alpha\beta}^{A}\left(c_{i,fv}\vec{v}_{fv}^{\dagger}+\vec{j}_{i,fv}^{\dagger}\right)\right)=\varepsilon_{vr}^{V}\varepsilon_{fv}^{V}\bar{R}_{i,fv} \text{ on } \Omega_{fv} \\ \vec{N}_{i,f-f}^{\dagger c\to v}=\vec{N}_{i,f-f}^{\dagger c\to v}\Big|^{CS_c} \text{ on } \partial\Omega_{f,cv} \\ \vec{N}_{i,f-f}^{\dagger s\to v}=\vec{N}_{i,f-f}^{\dagger s\to v}\Big|^{CS_s} \text{ on } \partial\Omega_{f,sv} \end{array}\right\} \qquad \text{(A.1.22)}$$

Species Reactor Mol

$$\left\{\begin{array}{l}\dfrac{\partial}{\partial t}\left(\varepsilon_{cr}^{V}\varepsilon_{fc}^{V}c_{i,\,fc}\right)+\vec{\nabla}\cdot\left(\varepsilon_{cr}^{A}\varepsilon_{fc}^{A}\left(c_{q,\,fc}\vec{v}_{fc}^{\,\dagger}+\vec{j}_{i,\,fc}^{\,\dagger}\right)\right)=\varepsilon_{cr}^{V}\varepsilon_{fc}^{V}\bar{R}_{i,\,fc}\ \text{ on }\Omega_{fc}\\ \vec{N}_{i,\,f-f}^{\dagger\,v\to c}=\vec{N}_{i,\,f-f}^{\dagger\,v\to c}\Big|^{CS_v}\ \text{ on }\partial\Omega_{f,\,vc}\end{array}\right\} \qquad \text{(A.1.23)}$$

Species Catalyst

$$\left\{\begin{array}{l}\dfrac{\partial}{\partial t}\left(\varepsilon_{sr}^{V}\varepsilon_{fs}^{V}c_{i,\,fs}\right)+\vec{\nabla}\cdot\left(\varepsilon_{sr}^{A}\varepsilon_{fs}^{A}\left(c_{i,sf}\vec{v}_{fs}^{\,\dagger}+\vec{j}_{i,\,fs}^{\,\dagger}\right)\right)=\varepsilon_{sr}^{V}\varepsilon_{fs}^{V}\bar{R}_{i,\,fs}\ \text{ on }\Omega_{fs}\\ \vec{N}_{i,\,f-f}^{\dagger\,v\to s}=\vec{N}_{i,\,f-f}^{\dagger\,v\to s}\Big|^{CS_v}\ \text{ on }\partial\Omega_{f,\,vs}\end{array}\right\} \qquad \text{(A.1.24)}$$

Species Storage

A.1.3. Momentum Derivation

Selecting momentum

$$\left\{\begin{array}{l}M\ =\vec{v}\wedge\dfrac{dM_{CSys}^{t}(t)}{dt}=\dfrac{d\left(\delta m\ \vec{v}\right)(t)}{dt}=\sum\vec{F}_{external}\\ \dfrac{dM_{CSys}(t)}{dt}=\sum_{j=\alpha}\sum_{k=\beta}\dfrac{dM_{jk\,sys}(t)}{dt}\end{array}\right\} \qquad \text{(A.1.25)}$$

Leads to:

$$\left\{\frac{\partial}{\partial t}\left(\rho\vec{v}\right)+\vec{\nabla}\cdot\left(\rho\vec{v}\vec{v}\right)=\rho\vec{g}+\vec{\nabla}\cdot\vec{\vec{T}}\right\} \qquad \text{(1.1.26)}$$

Using summability

$$\left\{\left\{\begin{array}{l}\dfrac{\partial}{\partial t}\left(\rho\vec{v}\right)+\vec{\nabla}\cdot\left(\rho\vec{v}\vec{v}\right)\\ -\rho\vec{g}-\vec{\nabla}\cdot\vec{\vec{T}}=0\end{array}\right\}\Leftrightarrow\left\{\sum_{j=\alpha}^{NP_\alpha}\sum_{k=\beta}^{NP_\beta}\left(\left(\begin{array}{l}\dfrac{\partial}{\partial t}\left(\varepsilon_{kr}^{V}\varepsilon_{jk}^{V}\rho_{jk}\vec{v}_{jk}\right)+\vec{\nabla}\cdot\left(\varepsilon_{kr}^{A}\varepsilon_{jk}^{A}\rho_{jk}\vec{v}_{jk}\vec{v}_{jk}\right)-\rho_{jk}\vec{g}\\ -\vec{\nabla}\cdot\left(\varepsilon_{kr}^{A}\varepsilon_{jk}^{A}\vec{\vec{T}}_{jk}\right)\end{array}\right)=0\right)\right\}\right\}$$

(A.1.27)

Generalizing for phase α within domain β on a domain r volumetric basis, mass and momentum balances are given by:

$$\left\{ \frac{\partial}{\partial t}\left(\varepsilon_{\beta \mathrm{r}}^{V} \varepsilon_{\alpha\beta}^{V} \rho_{\alpha\beta} \vec{v}_{\alpha\beta} \right) + \vec{\nabla} \cdot \left(\varepsilon_{\beta \mathrm{r}}^{A} \varepsilon_{\alpha\beta}^{A} \rho_{\alpha\beta} \vec{v}_{\alpha\beta} \vec{v}_{\alpha\beta} \right) - \rho_{\alpha\beta} \vec{g} - \vec{\nabla} \cdot \left(\varepsilon_{\beta \mathrm{r}}^{A} \varepsilon_{\alpha\beta}^{A} \vec{\vec{T}}_{\alpha\beta} \right) = 0 \right\}$$

Expanding terms in momentum balance gives:

$$\varepsilon_{\beta \mathrm{r}}^{V} \varepsilon_{\alpha\beta}^{V} \vec{v}_{\alpha\beta} \frac{\partial \rho_{\alpha\beta}}{\partial t} + \varepsilon_{\beta \mathrm{r}}^{V} \varepsilon_{\alpha\beta}^{V} \rho_{\alpha\beta} \frac{\partial \vec{v}_{\alpha\beta}}{\partial t} + \vec{\nabla} \cdot \left(\varepsilon_{\beta \mathrm{r}}^{A} \varepsilon_{\alpha\beta}^{A} \rho_{\alpha\beta} \vec{v}_{\alpha\beta} \vec{v}_{\alpha\beta} \right) - \rho_{\alpha\beta} \vec{g} - \vec{\nabla} \cdot \left(\varepsilon_{\beta \mathrm{r}}^{A} \varepsilon_{\alpha\beta}^{A} \vec{\vec{T}}_{\alpha\beta} \right) = 0$$

Using:

$$\vec{\nabla} \cdot \left(\varepsilon_{\beta \mathrm{r}}^{A} \varepsilon_{\alpha\beta}^{A} \rho_{\alpha\beta} \vec{v}_{\alpha\beta} \vec{v}_{\alpha\beta} \right) = \varepsilon_{\beta \mathrm{r}}^{A} \varepsilon_{\alpha\beta}^{A} \vec{\nabla} \cdot \left(\rho_{\alpha\beta} \vec{v}_{\alpha\beta} \vec{v}_{\alpha\beta} \right) = \varepsilon_{\beta \mathrm{r}}^{A} \varepsilon_{\alpha\beta}^{A} \left(\sum_{\varpi_1=1}^{3} \vec{e}_{\varpi_1} \frac{\partial}{\partial x_{\varpi_1}} \right) \cdot \left(\rho_{\alpha\beta} \sum_{\varpi_2=1}^{3} \vec{e}_{\varpi_2} v_{\varpi_2,\alpha\beta} \sum_{\varpi_3=1}^{3} \vec{e}_{\varpi_3} v_{\varpi_3,\alpha\beta} \right) =$$

$$\varepsilon_{\beta \mathrm{r}}^{A} \varepsilon_{\alpha\beta}^{A} \left(\sum_{\varpi_1=1}^{3} \sum_{\varpi_2=1}^{3} \sum_{\varpi_3=1}^{3} \vec{e}_{\varpi_1} \cdot \vec{e}_{\varpi_2} \vec{e}_{\varpi_3} \frac{\partial \rho_{\alpha\beta} v_{\varpi_2,\alpha\beta} v_{\varpi_3,\alpha\beta}}{\partial x_{\varpi_1}} \right) =$$

$$\varepsilon_{\beta \mathrm{r}}^{A} \varepsilon_{\alpha\beta}^{A} \left(\sum_{\varpi_1=1}^{3} \sum_{\varpi_2=1}^{3} \sum_{\varpi_3=1}^{3} \vec{e}_{\varpi_1} \cdot \vec{e}_{\varpi_2} \vec{e}_{\varpi_3} \left(\frac{\partial \rho_{\alpha\beta}}{\partial x_{\varpi_1}} v_{\varpi_2,\alpha\beta} v_{\varpi_3,\alpha\beta} + \rho_{\alpha\beta} \frac{\partial v_{\varpi_2,\alpha\beta}}{\partial x_{\varpi_1}} v_{\varpi_3,\alpha\beta} + \rho_{\alpha\beta} v_{\varpi_2,\alpha\beta} \frac{\partial v_{\varpi_3,\alpha\beta}}{\partial x_{\varpi_1}} \right) \right) =$$

$$\varepsilon_{\beta \mathrm{r}}^{A} \varepsilon_{\alpha\beta}^{A} \left(\sum_{\varpi_1=1}^{3} \sum_{\varpi_2=1}^{3} \sum_{\varpi_3=1}^{3} \delta_{\varpi_1\varpi_2} \vec{e}_{\varpi_3} \left(\frac{\partial \rho_{\alpha\beta}}{\partial x_{\varpi_1}} v_{\varpi_2,\alpha\beta} v_{\varpi_3,\alpha\beta} + \rho_{\alpha\beta} \frac{\partial v_{\varpi_2,\alpha\beta}}{\partial x_{\varpi_1}} v_{\varpi_3,\alpha\beta} + \rho_{\alpha\beta} v_{\varpi_2,\alpha\beta} \frac{\partial v_{\varpi_3,\alpha\beta}}{\partial x_{\varpi_1}} \right) \right) =$$

$$\varepsilon_{\beta \mathrm{r}}^{A} \varepsilon_{\alpha\beta}^{A} \left(\sum_{\varpi_1=1}^{3} \sum_{\varpi_3=1}^{3} \vec{e}_{\varpi_3} \left(\frac{\partial \rho_{\alpha\beta}}{\partial x_{\varpi_1}} v_{\varpi_1,\alpha\beta} v_{\varpi_3,\alpha\beta} + \rho_{\alpha\beta} \frac{\partial v_{\varpi_1,\alpha\beta}}{\partial x_{\varpi_1}} v_{\varpi_3,\alpha\beta} + \rho_{\alpha\beta} v_{\varpi_1,\alpha\beta} \frac{\partial v_{\varpi_3,\alpha\beta}}{\partial x_{\varpi_1}} \right) \right) =$$

$$\varepsilon_{\beta \mathrm{r}}^{A} \varepsilon_{\alpha\beta}^{A} \left(\begin{array}{l} \sum_{\varpi_1=1}^{3} \sum_{\varpi_3=1}^{3} \vec{e}_{\varpi_3} \frac{\partial \rho_{\alpha\beta}}{\partial x_{\varpi_1}} v_{\varpi_1,\alpha\beta} v_{\varpi_3,\alpha\beta} + \sum_{\varpi_1=1}^{3} \sum_{\varpi_3=1}^{3} \vec{e}_{\varpi_3} \rho_{\alpha\beta} \frac{\partial v_{\varpi_1,\alpha\beta}}{\partial x_{\varpi_1}} v_{\varpi_3,\alpha\beta} \\ + \sum_{\varpi_1=1}^{3} \sum_{\varpi_3=1}^{3} \vec{e}_{\varpi_3} \rho_{\alpha\beta} v_{\varpi_1,\alpha\beta} \frac{\partial v_{\varpi_3,\alpha\beta}}{\partial x_{\varpi_1}} \end{array} \right) =$$

$$\varepsilon_{\beta \mathrm{r}}^{A} \varepsilon_{\alpha\beta}^{A} \left(\begin{array}{l} \sum_{\varpi_1=1}^{3} \sum_{\varpi_3=1}^{3} \vec{e}_{\varpi_3} \frac{\partial \rho_{\alpha\beta}}{\partial x_{\varpi_1}} v_{\varpi_1,\alpha\beta} v_{\varpi_3,\alpha\beta} + \sum_{\varpi_1=1}^{3} \sum_{\varpi_3=1}^{3} \vec{e}_{\varpi_3} \rho_{\alpha\beta} v_{\varpi_3,\alpha\beta} \frac{\partial v_{\varpi_1,\alpha\beta}}{\partial x_{\varpi_1}} \\ + \sum_{\varpi_1=1}^{3} \sum_{\varpi_3=1}^{3} \vec{e}_{\varpi_3} \rho_{\alpha\beta} v_{\varpi_1,\alpha\beta} \frac{\partial v_{\varpi_3,\alpha\beta}}{\partial x_{\varpi_1}} \end{array} \right) =$$

$$\varepsilon_{\beta r}^{A}\varepsilon_{\alpha\beta}^{A}\left(\begin{array}{l}\sum_{\varpi_1=1}^{3}\sum_{\varpi_3=1}^{3}\vec{e}_{\varpi_3}\rho_{\alpha\beta}v_{\varpi_3,\alpha\beta}\dfrac{\partial v_{\varpi_1,\alpha\beta}}{\partial x_{\varpi_1}} \\ +\sum_{\varpi_1=1}^{3}\sum_{\varpi_3=1}^{3}\vec{e}_{\varpi_3}\left(\rho_{\alpha\beta}v_{\varpi_1,\alpha\beta}\dfrac{\partial v_{\varpi_3,\alpha\beta}}{\partial x_{\varpi_1}}+\dfrac{\partial \rho_{\alpha\beta}}{\partial x_{\varpi_1}}v_{\varpi_1,\alpha\beta}v_{\varpi_3,\alpha\beta}\right)\end{array}\right)=$$

$$\varepsilon_{\beta r}^{A}\varepsilon_{\alpha\beta}^{A}\left(\begin{array}{l}\sum_{\varpi_1=1}^{3}\sum_{\varpi_3=1}^{3}\vec{e}_{\varpi_3}\rho_{\alpha\beta}v_{\varpi_3,\alpha\beta}\dfrac{\partial v_{\varpi_1,\alpha\beta}}{\partial x_{\varpi_1}} \\ +\sum_{\varpi_1=1}^{3}\sum_{\varpi_3=1}^{3}\vec{e}_{\varpi_3}\left(v_{\varpi_1,\alpha\beta}\dfrac{\partial\left(\rho_{\alpha\beta}v_{\varpi_3,\alpha\beta}\right)}{\partial x_{\varpi_1}}\right)\end{array}\right)=$$

$$\varepsilon_{\beta r}^{A}\varepsilon_{\alpha\beta}^{A}\sum_{\varpi_1=1}^{3}\sum_{\varpi_2=1}^{3}\sum_{\varpi_3=1}^{3}\left(\delta_{\varpi_1\varpi_2}\vec{e}_{\varpi_3}v_{\varpi_3,\alpha\beta}\frac{\partial\left(\rho_{\alpha\beta}v_{\varpi_2,\alpha\beta}\right)}{\partial x_{\varpi_1}}\right)+\varepsilon_{\beta r}^{A}\varepsilon_{\alpha\beta}^{A}\sum_{\varpi_1=1}^{3}\sum_{\varpi_2=1}^{3}\sum_{\varpi_3=1}^{3}\left(\delta_{\varpi_2\varpi_1}\vec{e}_{\varpi_3}\rho_{\alpha\beta}v_{\varpi_2,\alpha\beta}\frac{\partial v_{\varpi_3,\alpha\beta}}{\partial x_{\varpi_1}}\right)=$$

$$\varepsilon_{\beta r}^{A}\varepsilon_{\alpha\beta}^{A}\sum_{\varpi_1=1}^{3}\sum_{\varpi_2=1}^{3}\sum_{\varpi_3=1}^{3}\left(\vec{e}_{\varpi_1}\cdot\vec{e}_{\varpi_2}\vec{e}_{\varpi_3}v_{\varpi_3,\alpha\beta}\frac{\partial\left(\rho_{\alpha\beta}v_{\varpi_2,\alpha\beta}\right)}{\partial x_{\varpi_1}}\right)+\varepsilon_{\beta r}^{A}\varepsilon_{\alpha\beta}^{A}\sum_{\varpi_1=1}^{3}\sum_{\varpi_2=1}^{3}\sum_{\varpi_3=1}^{3}\left(\vec{e}_{\varpi_1}\cdot\vec{e}_{\varpi_2}\vec{e}_{\varpi_3}\rho_{\alpha\beta}v_{\varpi_2,\alpha\beta}\frac{\partial v_{\varpi_3,\alpha\beta}}{\partial x_{\varpi_1}}\right)=$$

$$\vec{v}_{\alpha\beta}\left(\vec{\nabla}\cdot\left(\varepsilon_{\beta r}^{A}\varepsilon_{\alpha\beta}^{A}\rho_{\alpha\beta}\vec{v}_{\alpha\beta}\right)\right)+\varepsilon_{\beta r}^{A}\varepsilon_{\alpha\beta}^{A}\rho_{\alpha\beta}\vec{v}_{\alpha\beta}\cdot\left(\vec{\nabla}\vec{v}_{\alpha\beta}\right)$$

Vector product with mass balance:

$$\vec{v}_{\alpha\beta}\left(\frac{\partial}{\partial t}\left(\varepsilon_{\beta r}^{V}\varepsilon_{\alpha\beta}^{V}\rho_{\alpha\beta}\right)+\vec{\nabla}\cdot\left(\varepsilon_{\beta r}^{A}\varepsilon_{\alpha\beta}^{A}\rho_{\alpha\beta}\vec{v}_{\alpha\beta}\right)=0\right)$$

$$\vec{v}_{\alpha\beta}\frac{\partial}{\partial t}\left(\varepsilon_{\beta r}^{V}\varepsilon_{\alpha\beta}^{V}\rho_{\alpha\beta}\right)+\vec{v}_{\alpha\beta}\vec{\nabla}\cdot\left(\varepsilon_{\beta r}^{A}\varepsilon_{\alpha\beta}^{A}\rho_{\alpha\beta}\vec{v}_{\alpha\beta}\right)=0$$

$$\left\{\begin{array}{l}\varepsilon_{\beta r}^{V}\varepsilon_{\alpha\beta}^{V}\vec{v}_{\alpha\beta}\dfrac{\partial\rho_{\alpha\beta}}{\partial t}+\vec{v}_{\alpha\beta}\vec{\nabla}\cdot\left(\varepsilon_{\beta r}^{A}\varepsilon_{\alpha\beta}^{A}\rho_{\alpha\beta}\vec{v}_{\alpha\beta}\right)=0 \\ \left\{\begin{array}{l}\varepsilon_{\beta r}^{V}\varepsilon_{\alpha\beta}^{V}\vec{v}_{\alpha\beta}\dfrac{\partial\rho_{\alpha\beta}}{\partial t}+\varepsilon_{\beta r}^{V}\varepsilon_{\alpha\beta}^{V}\rho_{\alpha\beta}\dfrac{\partial\vec{v}_{\alpha\beta}}{\partial t} \\ +\vec{v}_{\alpha\beta}\left(\vec{\nabla}\cdot\left(\varepsilon_{\beta r}^{A}\varepsilon_{\alpha\beta}^{A}\rho_{\alpha\beta}\vec{v}_{\alpha\beta}\right)\right)+\varepsilon_{\beta r}^{A}\varepsilon_{\alpha\beta}^{A}\rho_{\alpha\beta}\vec{v}_{\alpha\beta}\cdot\left(\vec{\nabla}\vec{v}_{\alpha\beta}\right)\end{array}\right\}=\rho_{\alpha\beta}\vec{g}+\vec{\nabla}\cdot\left(\varepsilon_{\beta r}^{A}\varepsilon_{\alpha\beta}^{A}\vec{\vec{T}}_{\alpha\beta}\right)\end{array}\right\}$$

Subtracting equations

$$\varepsilon_{\beta r}^{V}\varepsilon_{\alpha\beta}^{V}\rho_{\alpha\beta}\frac{\partial\vec{v}_{\alpha\beta}}{\partial t}+\varepsilon_{\beta r}^{A}\varepsilon_{\alpha\beta}^{A}\rho_{\alpha\beta}\vec{v}_{\alpha\beta}\cdot\left(\vec{\nabla}\vec{v}_{\alpha\beta}\right)=\rho_{\alpha\beta}\vec{g}+\vec{\nabla}\cdot\left(\varepsilon_{\beta r}^{A}\varepsilon_{\alpha\beta}^{A}\vec{\vec{T}}_{\alpha\beta}\right)$$

In this work, gravity is not considered to impact momentum, and:

$$\frac{\sum\vec{F}_{external}}{\delta V^{t}}=\vec{\nabla}\cdot\left(\varepsilon_{\beta r}^{A}\varepsilon_{\alpha\beta}^{A}\vec{\vec{T}}_{\alpha\beta}\right)=-\nabla\left(\varepsilon_{\beta r}^{A}\varepsilon_{\alpha\beta}^{A}P_{\alpha\beta}\right)-\varepsilon_{\beta r}^{A}\varepsilon_{\alpha\beta}^{A}\left(K_{D}\vec{v}_{\alpha\beta}+K_{V}\vec{v}_{\alpha\beta}\vec{v}_{\alpha\beta}\right)$$

Where K_D and K_V are constants for the viscous and kinetic pressure drop. Neglecting the gravitational forces, the pressure drop constants are given as:

$$K_{D}=150\frac{\left(1-\varepsilon_{\beta r}^{V}\varepsilon_{\alpha\beta}^{V}\right)^{2}\mu_{\alpha\beta}}{d_{pellet}^{2}\left(\varepsilon_{\beta r}^{V}\varepsilon_{\alpha\beta}^{V}\right)^{3}},K_{V}=\frac{1.75\left(1-\varepsilon_{\beta r}^{V}\varepsilon_{\alpha\beta}^{V}\right)\rho_{\alpha\beta}}{d_{pellet}\left(\varepsilon_{\beta r}^{V}\varepsilon_{\alpha\beta}^{V}\right)^{3}}$$

Incorporating in momentum balance gives:

$$\left\{\varepsilon_{\beta r}^{V}\varepsilon_{\alpha\beta}^{V}\rho_{\alpha\beta}\frac{\partial\vec{v}_{\alpha\beta}}{\partial t}+\varepsilon_{\beta r}^{A}\varepsilon_{\alpha\beta}^{A}\rho_{\alpha\beta}\vec{v}_{\alpha\beta}\cdot\left(\vec{\nabla}\vec{v}_{\alpha\beta}\right)=\begin{pmatrix}-\varepsilon_{\beta r}^{A}\varepsilon_{\alpha\beta}^{A}\begin{pmatrix}150\frac{\left(1-\varepsilon_{\beta r}^{V}\varepsilon_{\alpha\beta}^{V}\right)^{2}\mu_{\alpha\beta}}{d_{pellet}^{2}\left(\varepsilon_{\beta r}^{V}\varepsilon_{\alpha\beta}^{V}\right)^{3}}\vec{v}_{\alpha\beta}\\+\frac{1.75\left(1-\varepsilon_{\beta r}^{V}\varepsilon_{\alpha\beta}^{V}\right)\rho_{\alpha\beta}}{d_{pellet}\left(\varepsilon_{\beta r}^{V}\varepsilon_{\alpha\beta}^{V}\right)^{3}}\vec{v}_{\alpha\beta}\vec{v}_{\alpha\beta}\end{pmatrix}\\-\nabla\left(\varepsilon_{\beta r}^{A}\varepsilon_{\alpha\beta}^{A}P_{\alpha\beta}\right)\end{pmatrix}\text{on }\Omega_{fv}\right\}$$

(A.1.28)

Velocity not considered in the pellet, therfore above equation applies only to reactor and there is no corresponding equations for the storage or catalyst. It is assumed the ergun equation captures the momentum transferred due to fluid storage or fluid pellet interactions, and therefore general boundary conditions are not given between phases.

A.1.4 Energy Balance

$$\left\{\begin{matrix}M_{CSys}^{t}=E^{t}\\\frac{dM_{CSys}(t)}{dt}=\sum_{j=\alpha}\sum_{k=\beta}\frac{dM_{jk\,sys}(t)}{dt}\end{matrix}\right\}\Rightarrow\left\{M=\frac{E^{t}}{m}=U+\frac{1}{2}\vec{v}\cdot\vec{v}-\vec{g}\cdot\vec{r}\wedge\frac{dM^{t}(t)}{dt}=\frac{dE^{t}(t)}{dt}=\frac{dQ}{dt}+\frac{dW}{dt}\right\}$$

(A.1.29)

Energy Balance:

$$\left\{ M_{\alpha\beta} = \frac{E^t_{\alpha\beta}}{m_{\alpha\beta}} = U_{\alpha\beta} + \frac{1}{2}\vec{v}_{\alpha\beta} \cdot \vec{v}_{\alpha\beta} - \vec{g} \cdot \vec{r} \wedge \frac{dM^t_{\alpha\beta}(t)}{dt} = \frac{dE^t_{\alpha\beta}(t)}{dt} = \frac{dQ_{\alpha\beta}}{dt} + \frac{dW_{\alpha\beta}}{dt} \right\}$$

(A.1.30)

Heat:

$$\left[\frac{dQ_{\alpha\beta}}{dt} = -\iiint_{CV} \sum_{\alpha_1=1}^{NP_\alpha} \sum_{\substack{\beta_1=1 \\ \beta_1 \neq \beta}}^{NP_\beta} q^{\beta_1 \to \beta}_{\alpha_1 - \alpha} \varepsilon^I_{\alpha\beta} dV^t - \iint_{CS} \overrightarrow{Q_{\alpha\beta}} \cdot \vec{n} \varepsilon^A_{\beta r} \varepsilon^A_{\alpha\beta} dA^t - \iint_{CS} \sum_{i=1}^{NC} \frac{1}{M_i} \bar{h}_{f,i} \vec{j}_i \cdot \vec{n} \varepsilon^A_{\beta r} \varepsilon^A_{\alpha\beta} dA^t \right]$$

Work:

$$\frac{dW_{\alpha\beta}}{dt} = \iint_{CS} \left[\vec{o}_{\alpha\beta}\left(\vec{n}\right) \cdot \vec{v}_{\alpha\beta} \right] \cdot \varepsilon^A_{\beta r} \varepsilon^A_{\alpha\beta} dA^t_{\alpha\beta} - \iiint_{CV} W_{ext} \varepsilon^I_{\alpha\beta} dV^t$$

Vector/Tensor Relations for fluid stress, work on the control surface of a fluid:

$$\left\{ \begin{array}{l} \vec{o}_{\alpha\beta}\left(\vec{n}\right) = \vec{n} \cdot \vec{\vec{T}}_{\alpha\beta} \\ \left(\vec{\vec{T}}_{\alpha\beta}\right) = \left(\vec{\vec{T}}_{\alpha\beta}\right)^T \\ \vec{\vec{T}}_{\alpha\beta} = -P_{\alpha\beta}\vec{\vec{I}} + \vec{\tau}_{\alpha\beta} \\ \vec{\tau}_{\alpha\beta} = \mu_{\alpha\beta}\left(\vec{\nabla}\vec{v}_{\alpha\beta} + \left(\vec{\nabla}\vec{v}_{\alpha\beta}\right)^T\right) + \chi_{\alpha\beta}\left(\vec{\nabla} \cdot \vec{v}_{\alpha\beta}\right)\vec{\vec{I}} \\ \chi_{\alpha\beta} = \frac{2}{3}\left(\kappa_{\alpha\beta} - \mu_{\alpha\beta}\right) \\ \vec{o}_{\alpha\beta}\left(\vec{n}\right) \cdot \vec{v}_{\alpha\beta} = \vec{v}_{\alpha\beta} \cdot \vec{o}_{\alpha\beta}\left(\vec{n}\right) \\ \vec{v}_{\alpha\beta} \cdot \left(\vec{n} \cdot \vec{\vec{T}}_{\alpha\beta}\right) = \vec{n} \cdot \left(\vec{v}_{\alpha\beta} \cdot \left(\vec{\vec{T}}\right)^T\right) \end{array} \right\} \Rightarrow \left\{ \begin{array}{l} \iint_{CS} \left[\vec{o}_{\alpha\beta}\left(\vec{n}\right) \cdot \vec{v}_{\alpha\beta} \right] \cdot \varepsilon^A_{\beta r} \varepsilon^A_{\alpha\beta} dA^t_{\alpha\beta} \Leftrightarrow \\ \iint_{CS} \left[\vec{v}_{\alpha\beta} \cdot \vec{o}_{\alpha\beta}\left(\vec{n}\right) \right] \cdot \varepsilon^A_{\beta r} \varepsilon^A_{\alpha\beta} dA^t_{\alpha\beta} \Leftrightarrow \\ \iint_{CS} \vec{n} \cdot \left[\vec{v}_{\alpha\beta} \cdot \vec{\vec{T}}_{\alpha\beta} \right] \cdot \varepsilon^A_{\beta r} \varepsilon^A_{\alpha\beta} dA^t_{\alpha\beta} \Leftrightarrow \\ \iint_{CS} \left[\vec{v}_{\alpha\beta} \cdot \vec{\vec{T}}_{\alpha\beta} \right] \cdot \vec{n} \cdot \varepsilon^A_{\beta r} \varepsilon^A_{\alpha\beta} dA^t_{\alpha\beta} \Leftrightarrow \\ \iiint_{CV} \nabla \cdot \left[\vec{v}_{\alpha\beta} \cdot \vec{\vec{T}}_{\alpha\beta} \right] \cdot \varepsilon^A_{\beta r} \varepsilon^A_{\alpha\beta} dV^t_{\alpha\beta} \end{array} \right\}$$

Using the following thermodynamic relations,

$$\left\{\begin{array}{l} U_{\alpha\beta}^{m} = h_{\alpha\beta}^{m} - \dfrac{P_{\alpha\beta}}{\rho_{\alpha\beta}} \quad h_{\alpha\beta}^{m} \\ h_{\alpha\beta}^{a} = \sum_{i=1}^{NC} x_{i,\alpha\beta} \bar{h}_{i,\alpha\beta} \wedge h_{i,\alpha\beta}^{m} = \dfrac{h_{i,\alpha\beta}^{a}}{M_i} \\ dh_{\alpha\beta}^{a} = \bar{C}_{P}^{\alpha\beta} dT_{\alpha\beta} + \left(V_{\alpha\beta}^{a} - T_{\alpha\beta} \left(\dfrac{\partial V_{\alpha\beta}^{a}}{\partial T_{\alpha\beta}} \right)_{P} \right) dP_{\alpha\beta} + \sum_{i=1}^{NC} \left(\left[\dfrac{\partial n_{\alpha\beta} h_{\alpha\beta}^{a}}{\partial n_{i,\alpha\beta}} \right]_{P,T,n_j} dx_{i,\alpha\beta} \right) \\ h_{i,\alpha\beta}^{a} = h_{i,\alpha\beta}^{a,0} + \int_{T^0}^{T} C_{P,i}^{\alpha\beta}(T_{\alpha\beta}) dT_{i,\alpha\beta} + \int_{P^0}^{P} \left(V_{i,\alpha\beta}^{a} - T_{\alpha\beta} \left(\dfrac{\partial V_{i,\alpha\beta}^{a}}{\partial T_{\alpha\beta}} \right) \right) dP_{i,\alpha\beta} \end{array}\right\}$$

And assuming ideal solution model $\left\{\begin{array}{l} \hat{h}_{\alpha\beta}^{id} = h_{\alpha\beta}^{m} \\ \bar{h}_{\alpha\beta}^{id} = h_{\alpha\beta}^{a} \end{array}\right\} \Rightarrow \left\{\begin{array}{l} h_{\alpha\beta}^{a} = \sum_{i=1}^{NC} x_{i,\alpha\beta} h_{i,\alpha\beta}^{a} \\ h_{\alpha\beta}^{m} = \dfrac{h_{\alpha\beta}^{a}}{\sum_{j=1}^{NC} x_{j,\alpha\beta} M_j} \\ h_{i,\alpha\beta}^{a} = M_i h_{i,\alpha\beta}^{m} \end{array}\right\} \Leftrightarrow$

$$\left\{ h_{\alpha\beta}^{m} = \frac{\sum_{i=1}^{NC} x_{i,\alpha\beta} M_i h_{i,\alpha\beta}^{m}}{\sum_{j=1}^{NC} x_{j,\alpha\beta} M_j} \right\} \Leftrightarrow \left\{ h_{\alpha\beta}^{m} = \sum_{i=1}^{NC} \left(\frac{x_{i,\alpha\beta} M_i h_{i,\alpha\beta}^{m}}{\sum_{j=1}^{NC} x_{j,\alpha\beta} M_j} \right) \right\} \Leftrightarrow \left\{ h_{\alpha\beta}^{m} = \sum_{i=1}^{NC} w_{i,\alpha\beta} h_{i,\alpha\beta}^{m} \right\}$$

General multi-component energy balance.

$$\left\{\begin{array}{l}\dfrac{\partial}{\partial t}\left[\left(\hat{U}\ +\dfrac{1}{2}\vec{v}\cdot\vec{v}-\vec{g}\cdot\vec{r}\right)\rho\right]+\vec{\nabla}\cdot\left[\rho\vec{v}\left(\hat{U}\ +\dfrac{1}{2}\vec{v}\cdot\vec{v}-\vec{g}\cdot\vec{r}\right)\right]= \\ =-q_{ext}-\vec{\nabla}\cdot\left(\overrightarrow{Q}\right)-\vec{\nabla}\cdot\left(\sum_{i=1}^{NC}\hat{h}_i\vec{j}_i\right)-W_{ext}+\vec{\nabla}\cdot\left[\left(\vec{v}\cdot\vec{\vec{T}}\right)\right]\end{array}\right\}\Leftrightarrow$$

$$\left\{\sum_{j=\alpha}^{NP_\alpha}\sum_{k=\beta}^{NP_\beta}\left\{\begin{array}{l}\dfrac{\partial}{\partial t}\left[\varepsilon_{kr}^{V}\varepsilon_{jk}^{V}\rho_{jk}\left(\hat{U}_{jk}+\dfrac{1}{2}\vec{v}_{jk}\cdot\vec{v}_{jk}-\vec{g}\cdot\vec{r}\right)\right] \\ +\vec{\nabla}\cdot\left[\varepsilon_{kr}^{A}\varepsilon_{jk}^{A}\rho_{jk}\vec{v}_{jk}\left(\hat{U}_{jk}+\dfrac{1}{2}\vec{v}_{jk}\cdot\vec{v}_{jk}-\vec{g}\cdot\vec{r}\right)\right]\end{array}\right\}=\left\{\begin{array}{l}-\vec{\nabla}\cdot\left(\varepsilon_{kr}^{A}\varepsilon_{jk}^{A}\overrightarrow{Q_{jk}}\right) \\ -\left(\sum_{i=1}^{NC}\vec{\nabla}\cdot\dfrac{1}{M_i}\overline{h}_{i,jk}\varepsilon_{kr}^{A}\varepsilon_{jk}^{A}\vec{j}_{i,jk}\right) \\ -W_{ext}+\vec{\nabla}\cdot\left[\varepsilon_{kr}^{A}\varepsilon_{jk}^{A}\left(\vec{v}_{jk}\cdot\vec{\vec{T}}_{jk}\right)\right]\end{array}\right\}\right\}$$

$$\left\{\begin{array}{l}\dfrac{\partial}{\partial t}\left[\varepsilon_{\beta r}^{V}\varepsilon_{\alpha\beta}^{V}\rho_{\alpha\beta}\left(U_{\alpha\beta}^{m}+\dfrac{1}{2}\vec{v}_{\alpha\beta}\cdot\vec{v}_{\alpha\beta}-\vec{g}\cdot\vec{r}\right)\right] \\ +\vec{\nabla}\cdot\left[\varepsilon_{\beta r}^{A}\varepsilon_{\alpha\beta}^{A}\rho_{\alpha\beta}\vec{v}_{\alpha\beta}\left(U_{\alpha\beta}^{m}+\dfrac{1}{2}\vec{v}_{\alpha\beta}\cdot\vec{v}_{\alpha\beta}-\vec{g}\cdot\vec{r}\right)\right]\end{array}\right\}=\left\{\begin{array}{l}-\vec{\nabla}\cdot\left(\varepsilon_{\beta r}^{A}\varepsilon_{\alpha\beta}^{A}\overrightarrow{Q_{\alpha\beta}}\right) \\ -\left(\sum_{i=1}^{NC}\vec{\nabla}\cdot\dfrac{1}{M_i}h_{i,\alpha\beta}^{a}\varepsilon_{\beta r}^{A}\varepsilon_{\alpha\beta}^{A}\vec{j}_{i,\alpha\beta}\right) \\ -W_{ext}\varepsilon_{\alpha\beta}^{I}+\vec{\nabla}\cdot\left[\varepsilon_{\beta r}^{A}\varepsilon_{\alpha\beta}^{A}\left(\vec{v}_{\alpha\beta}\cdot\vec{\vec{T}}_{\alpha\beta}\right)\right]\end{array}\right\}$$

No work or gravity effects, no external/shaft work, $\vec{v}_{\alpha\beta}\cdot\vec{v}_{\alpha\beta}=\left|\vec{v}_{\alpha\beta}\right|^2$

$$\left\{\begin{array}{l}\dfrac{\partial}{\partial t}\left[\varepsilon_{\beta r}^{V}\varepsilon_{\alpha\beta}^{V}\rho_{\alpha\beta}\left(U_{\alpha\beta}^{m}+\dfrac{1}{2}\left|\vec{v}_{\alpha\beta}\right|^2\right)\right] \\ +\vec{\nabla}\cdot\left[\varepsilon_{\beta r}^{A}\varepsilon_{\alpha\beta}^{A}\rho_{\alpha\beta}\vec{v}_{\alpha\beta}\left(U_{\alpha\beta}^{m}+\dfrac{1}{2}\left|\vec{v}_{\alpha\beta}\right|^2\right)\right]\end{array}\right\}=\left\{\begin{array}{l}-\vec{\nabla}\cdot\left(\varepsilon_{\beta r}^{A}\varepsilon_{\alpha\beta}^{A}\overrightarrow{Q_{\alpha\beta}}\right)-\left(\sum_{i=1}^{NC}\vec{\nabla}\cdot\dfrac{1}{M_i}h_{i,\alpha\beta}^{a}\varepsilon_{\beta r}^{A}\varepsilon_{\alpha\beta}^{A}\vec{j}_{i,\alpha\beta}\right) \\ +\vec{\nabla}\cdot\left[\varepsilon_{\beta r}^{A}\varepsilon_{\alpha\beta}^{A}\left(\vec{v}_{\alpha\beta}\cdot\vec{\vec{T}}_{\alpha\beta}\right)\right]\end{array}\right\}$$

Vector/ symmetric tensor gradient expansion

$$\vec{\nabla}\cdot\left(\vec{v}_{\alpha\beta}\cdot\vec{\vec{T}}_{\alpha\beta}\right)=\vec{\nabla}\cdot\left(\vec{\vec{T}}_{\alpha\beta}\cdot\vec{v}_{\alpha\beta}\right)=\left(\sum_{\varpi_1=1}^{3}\vec{e}_{\varpi_1}\frac{\partial}{\partial x_{\varpi_1}}\right)\cdot\left(\left(\sum_{\varpi_2=1}^{3}\sum_{\varpi_3=1}^{3}\vec{e}_{\varpi_2}\vec{e}_{\varpi_3}T_{\varpi_2\varpi_3,\alpha\beta}^{s}\right)\cdot\left(\sum_{\varpi_4=1}^{3}\vec{e}_{\varpi_4}v_{\varpi_4,\alpha\beta}\right)\right)=$$

$$\left(\sum_{\varpi_1=1}^{3}\vec{e}_{\varpi_1}\frac{\partial}{\partial x_{\varpi_1}}\right)\cdot\left(\left(\sum_{\varpi_2=1}^{3}\sum_{\varpi_3=1}^{3}\sum_{\varpi_4=1}^{3}\vec{e}_{\varpi_2}\vec{e}_{\varpi_3}\cdot\vec{e}_{\varpi_4}T_{\varpi_2\varpi_3,\alpha\beta}^{s}v_{\varpi_4,\alpha\beta}\right)\right)=\left(\sum_{\varpi_1=1}^{3}\sum_{\varpi_2=1}^{3}\sum_{\varpi_3=1}^{3}\sum_{\varpi_4=1}^{3}\vec{e}_{\varpi_1}\cdot\vec{e}_{\varpi_2}\vec{e}_{\varpi_3}\cdot\vec{e}_{\varpi_4}\frac{\partial}{\partial x_i}\left(T_{\varpi_2\varpi_3,\alpha\beta}^{s}v_{\varpi_4,\alpha\beta}\right)\right)=$$

$$\left(\sum_{\varpi_1=1}^{3}\sum_{\varpi_2=1}^{3}\sum_{\varpi_3=1}^{3}\sum_{\varpi_4=1}^{3}\vec{e}_{\varpi_1}\cdot\vec{e}_{\varpi_2}\vec{e}_{\varpi_3}\cdot\vec{e}_{\varpi_4}\left(\frac{\partial T^{s}_{\varpi_2\varpi_3,\alpha\beta}}{\partial x_{\varpi_1}}v_{\varpi_4,\alpha\beta}+T^{s}_{\varpi_2\varpi_3,\alpha\beta}\frac{\partial v_{\varpi_4,\alpha\beta}}{\partial x_{\varpi_1}}\right)\right)=$$

$$\left(\sum_{\varpi_1=1}^{3}\sum_{\varpi_2=1}^{3}\sum_{\varpi_3=1}^{3}\sum_{\varpi_4=1}^{3}\vec{e}_{\varpi_1}\cdot\vec{e}_{\varpi_2}\vec{e}_{\varpi_3}\cdot\vec{e}_{\varpi_4}\left(\frac{\partial T^{s}_{\varpi_2\varpi_3,\alpha\beta}}{\partial x_{\varpi_1}}v_{\varpi_4,\alpha\beta}\right)\right)+\left(\sum_{\varpi_1=1}^{3}\sum_{\varpi_2=1}^{3}\sum_{\varpi_3=1}^{3}\sum_{\varpi_4=1}^{3}\vec{e}_{\varpi_1}\cdot\vec{e}_{\varpi_2}\vec{e}_{\varpi_3}\cdot\vec{e}_{\varpi_4}\left(T^{s}_{\varpi_2\varpi_3,\alpha\beta}\frac{\partial v_{\varpi_4,\alpha\beta}}{\partial x_{\varpi_1}}\right)\right)=$$

Term 1:

$$\sum_{\varpi_1=1}^{3}\sum_{\varpi_2=1}^{3}\sum_{\varpi_3=1}^{3}\sum_{\varpi_4=1}^{3}\vec{e}_{\varpi_1}\cdot\vec{e}_{\varpi_2}\vec{e}_{\varpi_3}\cdot\vec{e}_{\varpi_4}\left(\frac{\partial T^{s}_{\varpi_2\varpi_3,\alpha\beta}}{\partial x_{\varpi_1}}v_{\varpi_4,\alpha\beta}\right)=\sum_{\varpi_1=1}^{3}\sum_{\varpi_2=1}^{3}\sum_{\varpi_3=1}^{3}\sum_{\varpi_4=1}^{3}\delta_{\varpi_1\varpi_2}\delta_{\varpi_3\varpi_4}\left(\frac{\partial T^{s}_{\varpi_2\varpi_3,\alpha\beta}}{\partial x_{\varpi_1}}v_{\varpi_4,\alpha\beta}\right)=$$

$$\sum_{\varpi_1=1}^{3}\sum_{\varpi_3=1}^{3}\left(\frac{\partial T^{s}_{\varpi_1\varpi_3,\alpha\beta}}{\partial x_{\varpi_1}}v_{\varpi_3,\alpha\beta}\right)=\sum_{\varpi_3=1}^{3}\sum_{\varpi_1=1}^{3}\left(v_{\varpi_3,\alpha\beta}\frac{\partial T^{s}_{\varpi_1\varpi_3,\alpha\beta}}{\partial x_{\varpi_1}}\right)=\sum_{\varpi_3=1}^{3}\sum_{\varpi_4=1}^{3}\sum_{\varpi_1=1}^{3}\left(\delta_{\varpi_3\varpi_4}v_{\varpi_3,\alpha\beta}\frac{\partial T^{s}_{\varpi_1\varpi_4,\alpha\beta}}{\partial x_{\varpi_1}}\right)=$$

$$\sum_{\varpi_3=1}^{3}\sum_{\varpi_4=1}^{3}\sum_{\varpi_1=1}^{3}\left(\vec{e}_{\varpi_3}\cdot\vec{e}_{\varpi_4}v_{\varpi_3,\alpha\beta}\frac{\partial T^{s}_{\varpi_1\varpi_4,\alpha\beta}}{\partial x_{\varpi_1}}\right)=\left(\sum_{\varpi_3=1}^{3}\vec{e}_{\varpi_3}v_{\varpi_3,\alpha\beta}\right)\cdot\left(\sum_{\varpi_4=1}^{3}\sum_{\varpi_1=1}^{3}\vec{e}_{\varpi_4}\frac{\partial T^{s}_{\varpi_1\varpi_4,\alpha\beta}}{\partial x_{\varpi_1}}\right)=$$

$$\left(\sum_{\varpi_3=1}^{3}\vec{e}_{\varpi_3}v_{\varpi_3,\alpha\beta}\right)\cdot\left(\sum_{\varpi_1=1}^{3}\sum_{\varpi_2=1}^{3}\sum_{\varpi_4=1}^{3}\delta_{\varpi_1\varpi_2}\vec{e}_{\varpi_4}\frac{\partial T^{s}_{\varpi_2\varpi_4,\alpha\beta}}{\partial x_{\varpi_1}}\right)=\left(\sum_{\varpi_3=1}^{3}\vec{e}_{\varpi_3}v_{\varpi_3,\alpha\beta}\right)\cdot\left(\sum_{\varpi_1=1}^{3}\sum_{\varpi_2=1}^{3}\sum_{\varpi_4=1}^{3}\vec{e}_{\varpi_1}\cdot\vec{e}_{\varpi_2}\vec{e}_{\varpi_4}\frac{\partial T^{s}_{\varpi_2\varpi_4,\alpha\beta}}{\partial x_{\varpi_1}}\right)=$$

$$\left(\sum_{\varpi_3=1}^{3}\vec{e}_{\varpi_3}v_{\varpi_3,\alpha\beta}\right)\cdot\left(\sum_{\varpi_1=1}^{3}\vec{e}_{\varpi_1}\frac{\partial}{\partial x_{\varpi_1}}\right)\cdot\left(\sum_{\varpi_2=1}^{3}\sum_{\varpi_4=1}^{3}\vec{e}_{\varpi_2}\vec{e}_{\varpi_4}T^{s}_{\varpi_2\varpi_4,\alpha\beta}\right)=\vec{v}_{\alpha\beta}\cdot\left(\vec{\nabla}\cdot\vec{\vec{T}}_{\alpha\beta}\right)$$

Term 2:

$$\left(\sum_{\varpi_1=1}^{3}\sum_{\varpi_2=1}^{3}\sum_{\varpi_3=1}^{3}\sum_{\varpi_4=1}^{3}\vec{e}_{\varpi_1}\cdot\vec{e}_{\varpi_2}\vec{e}_{\varpi_3}\cdot\vec{e}_{\varpi_4}\left(T^{s}_{\varpi_2\varpi_3,\alpha\beta}\frac{\partial v_{\varpi_4,\alpha\beta}}{\partial x_{\varpi_1}}\right)\right)=\sum_{\varpi_1=1}^{3}\sum_{\varpi_2=1}^{3}\sum_{\varpi_3=1}^{3}\sum_{\varpi_4=1}^{3}\delta_{\varpi_1\varpi_2}\delta_{\varpi_3\varpi_4}\left(T^{s}_{\varpi_2\varpi_3,\alpha\beta}\frac{\partial v_{\varpi_4,\alpha\beta}}{\partial x_{\varpi_1}}\right)=$$

$$\left(\sum_{\varpi_1=1}^{3}\sum_{\varpi_3=1}^{3}\left(T^{s}_{\varpi_1\varpi_3,\alpha\beta}\frac{\partial v_{\varpi_3,\alpha\beta}}{\partial x_{\varpi_1}}\right)\right)=\left(\sum_{\varpi_3=1}^{3}\sum_{\varpi_1=1}^{3}\left(T^{s}_{\varpi_3\varpi_1,\alpha\beta}\frac{\partial v_{\varpi_3,\alpha\beta}}{\partial x_{\varpi_1}}\right)\right)=\left(\sum_{\varpi_3=1}^{3}\sum_{\varpi_1=1}^{3}\sum_{\varpi_2=1}^{3}\sum_{\varpi_4=1}^{3}\left(\delta_{\varpi_1\varpi_2}\delta_{\varpi_3\varpi_4}T^{s}_{\varpi_3\varpi_1,\alpha\beta}\frac{\partial v_{\varpi_3,\alpha\beta}}{\partial x_{\varpi_1}}\right)\right)=$$

$$\left(\sum_{\varpi_3=1}^{3}\sum_{\varpi_1=1}^{3}\vec{e}_{\varpi_3}\vec{e}_{\varpi_1}T^{s}_{\varpi_3\varpi_1,\alpha\beta}\right):\left(\sum_{\varpi_2=1}^{3}\sum_{\varpi_3=1}^{3}\vec{e}_{\varpi_2}\vec{e}_{\varpi_3}\frac{\partial v_{\varpi_3,\alpha\beta}}{\partial x_{\varpi_2}}\right)=\vec{\vec{T}}_{\alpha\beta}:\vec{\nabla}\vec{v}_{\alpha\beta}$$

Therefore:

$$\vec{\nabla}\cdot\left(\vec{v}_{\alpha\beta}\cdot\vec{\vec{T}}_{\alpha\beta}\right)=\vec{v}_{\alpha\beta}\cdot\left(\vec{\nabla}\cdot\vec{\vec{T}}_{\alpha\beta}\right)+\vec{\vec{T}}_{\alpha\beta}:\vec{\nabla}\vec{v}_{\alpha\beta}$$

Incorporate into energy balance

$$\left\{\begin{array}{l}\dfrac{\partial}{\partial t}\left(\varepsilon_{\beta\mathrm{r}}^{V}\varepsilon_{\alpha\beta}^{V}\rho_{\alpha\beta}U_{\alpha\beta}^{m}\right)\\+\dfrac{\partial}{\partial t}\left(\varepsilon_{\beta\mathrm{r}}^{V}\varepsilon_{\alpha\beta}^{V}\rho_{\alpha\beta}\dfrac{1}{2}\left|\vec{v}_{\alpha\beta}\right|^{2}\right)\\+\vec{\nabla}\cdot\left[\varepsilon_{\beta\mathrm{r}}^{A}\varepsilon_{\alpha\beta}^{A}\rho_{\alpha\beta}\vec{v}_{\alpha\beta}U_{\alpha\beta}^{m}\right]\\+\vec{\nabla}\cdot\left[\varepsilon_{\beta\mathrm{r}}^{A}\varepsilon_{\alpha\beta}^{A}\rho_{\alpha\beta}\vec{v}_{\alpha\beta}\dfrac{1}{2}\left|\vec{v}_{\alpha\beta}\right|^{2}\right]\\\\\end{array}\right\}=\left\{\begin{array}{l}-\vec{\nabla}\cdot\left(\varepsilon_{\beta\mathrm{r}}^{A}\varepsilon_{\alpha\beta}^{A}\overrightarrow{Q_{\alpha\beta}}\right)-\left(\sum_{i=1}^{NC}\vec{\nabla}\cdot\left(\dfrac{1}{M_{i}}h_{\mathrm{i},\alpha\beta}^{a}\varepsilon_{\beta\mathrm{r}}^{A}\varepsilon_{\alpha\beta}^{A}\vec{j}_{\mathrm{i},\alpha\beta}\right)\right)\\+\varepsilon_{\beta\mathrm{r}}^{A}\varepsilon_{\alpha\beta}^{A}\left(\vec{v}_{\alpha\beta}\cdot\left(\vec{\nabla}\cdot\vec{\vec{T}}_{\alpha\beta}\right)\right)+\varepsilon_{\beta\mathrm{r}}^{A}\varepsilon_{\alpha\beta}^{A}\left(\vec{\vec{T}}_{\alpha\beta}:\vec{\nabla}\vec{v}_{\alpha\beta}\right)\end{array}\right\}$$

(A.1.31)

An expression for $\vec{v}_{\alpha\beta}\cdot\left(\vec{\nabla}\cdot\vec{\vec{T}}_{\alpha\beta}\right)$ can be obtained from momentum and continuity, re-printed and arranged below:

$$\frac{\partial}{\partial t}\left(\varepsilon_{\beta\mathrm{r}}^{V}\varepsilon_{\alpha\beta}^{V}\rho_{\alpha\beta}\right)+\varepsilon_{\beta\mathrm{r}}^{A}\varepsilon_{\alpha\beta}^{A}\left(\vec{\nabla}\rho_{\alpha\beta}\right)\cdot\vec{v}_{\alpha\beta}+\varepsilon_{\beta\mathrm{r}}^{A}\varepsilon_{\alpha\beta}^{A}\rho_{\alpha\beta}\left(\vec{\nabla}\cdot\vec{v}_{\alpha\beta}\right)=0$$

$$\vec{\nabla}\cdot\left(\varepsilon_{\beta\mathrm{r}}^{A}\varepsilon_{\alpha\beta}^{A}\vec{\vec{T}}_{\alpha\beta}\right)=\frac{\partial}{\partial t}\left(\varepsilon_{\beta\mathrm{r}}^{V}\varepsilon_{\alpha\beta}^{V}\rho_{\alpha\beta}\vec{v}_{\alpha\beta}\right)+\vec{\nabla}\cdot\left(\varepsilon_{\beta\mathrm{r}}^{A}\varepsilon_{\alpha\beta}^{A}\rho_{\alpha\beta}\left(\vec{v}_{\alpha\beta}\vec{v}_{\alpha\beta}\right)\right)$$

Taking dot product of $\vec{v}_{\alpha\beta}$ with re-arranged momentum balance:

$$\vec{v}_{\alpha\beta}\cdot\left(\vec{\nabla}\cdot\left(\varepsilon_{\beta\mathrm{r}}^{A}\varepsilon_{\alpha\beta}^{A}\vec{\vec{T}}_{\alpha\beta}\right)\right)=\vec{v}_{\alpha\beta}\cdot\left(\frac{\partial}{\partial t}\left(\varepsilon_{\beta\mathrm{r}}^{V}\varepsilon_{\alpha\beta}^{V}\rho_{\alpha\beta}\vec{v}_{\alpha\beta}\right)+\vec{\nabla}\cdot\left(\varepsilon_{\beta\mathrm{r}}^{A}\varepsilon_{\alpha\beta}^{A}\rho_{\alpha\beta}\left(\vec{v}_{\alpha\beta}\vec{v}_{\alpha\beta}\right)\right)\right)$$

Momentum time differential:

$$\vec{v}_{\alpha\beta}\cdot\left(\varepsilon_{\beta\mathrm{r}}^{V}\varepsilon_{\alpha\beta}^{V}\frac{\partial\rho_{\alpha\beta}}{\partial t}\vec{v}_{\alpha\beta}+\varepsilon_{\beta\mathrm{r}}^{V}\varepsilon_{\alpha\beta}^{V}\rho_{\alpha\beta}\frac{\partial\vec{v}_{\alpha\beta}}{\partial t}\right)$$

First term: $\vec{v}_{\alpha\beta}\cdot\left(\varepsilon_{\beta\mathrm{r}}^{V}\varepsilon_{\alpha\beta}^{V}\dfrac{\partial\rho_{\alpha\beta}}{\partial t}\vec{v}_{\alpha\beta}\right)=$

$$\left(\sum_{\varpi_1=1}^{3}\vec{e}_{\varpi_1}v_{\varpi_1,\alpha\beta}\right)\cdot\left(\varepsilon_{\beta r}^{V}\varepsilon_{\alpha\beta}^{V}\frac{\partial\rho_{\alpha\beta}}{\partial t}\sum_{\varpi_2=1}^{3}\vec{e}_{\varpi_2}v_{\varpi_2,\alpha\beta}\right)=\sum_{\varpi_1=1}^{3}\sum_{\varpi_2=1}^{3}\varepsilon_{\beta r}^{V}\varepsilon_{\alpha\beta}^{V}\delta_{\varpi_1\varpi_2}v_{\varpi_1,\alpha\beta}v_{\varpi_2,\alpha\beta}\frac{\partial\rho_{\alpha\beta}}{\partial t}=\boxed{\varepsilon_{\beta r}^{V}\varepsilon_{\alpha\beta}^{V}\left|\vec{v}_{\alpha\beta}\right|^2\frac{\partial\rho_{\alpha\beta}}{\partial t}}$$

Second Term: $\vec{v}_{\alpha\beta}\cdot\left(\varepsilon_{\beta r}^{V}\varepsilon_{\alpha\beta}^{V}\rho_{\alpha\beta}\frac{\partial\vec{v}_{\alpha\beta}}{\partial t}\right)=$

$$\left(\sum_{\varpi_1=1}^{3}\vec{e}_{\varpi_1}v_{\varpi_1,\alpha\beta}\right)\cdot\left(\varepsilon_{\beta r}^{V}\varepsilon_{\alpha\beta}^{V}\rho_{\alpha\beta}\sum_{\varpi_2=1}^{3}\vec{e}_{\varpi_2}\frac{\partial v_{\varpi_2,\alpha\beta}}{\partial t}\right)=\sum_{\varpi_1=1}^{3}\sum_{\varpi_2=1}^{3}\varepsilon_{\beta r}^{V}\varepsilon_{\alpha\beta}^{V}\delta_{\varpi_1\varpi_2}v_{\varpi_1,\alpha\beta}\rho_{\alpha\beta}\frac{\partial v_{\varpi_2,\alpha\beta}}{\partial t}=\boxed{\varepsilon_{\beta r}^{V}\varepsilon_{\alpha\beta}^{V}\vec{v}_{\alpha\beta}\rho_{\alpha\beta}\frac{\partial\vec{v}_{\alpha\beta}}{\partial t}}$$

Combining first and second term:

$$\varepsilon_{\beta r}^{V}\varepsilon_{\alpha\beta}^{V}\left|\vec{v}_{\alpha\beta}\right|^2\frac{\partial\rho_{\alpha\beta}}{\partial t}+\varepsilon_{\beta r}^{V}\varepsilon_{\alpha\beta}^{V}\vec{v}_{\alpha\beta}\rho_{\alpha\beta}\frac{\partial\vec{v}_{\alpha\beta}}{\partial t}=\frac{\varepsilon_{\beta r}^{V}\varepsilon_{\alpha\beta}^{V}\left|\vec{v}_{\alpha\beta}\right|^2}{2}\frac{\partial\rho_{\alpha\beta}}{\partial t}+\frac{\varepsilon_{\beta r}^{V}\varepsilon_{\alpha\beta}^{V}\left|\vec{v}_{\alpha\beta}\right|^2}{2}\frac{\partial\rho_{\alpha\beta}}{\partial t}+\frac{\varepsilon_{\beta r}^{V}\varepsilon_{\alpha\beta}^{V}\rho_{\alpha\beta}}{2}\frac{\partial\left|\vec{v}_{\alpha\beta}\right|^2}{\partial t}=$$

$$\boxed{\varepsilon_{\beta r}^{V}\varepsilon_{\alpha\beta}^{V}\frac{\partial\,{}^{1}\!/\!_{2}\,\rho_{\alpha\beta}\left|\vec{v}_{\alpha\beta}\right|^2}{\partial t}+\varepsilon_{\beta r}^{V}\varepsilon_{\alpha\beta}^{V}\frac{\left|\vec{v}_{\alpha\beta}\right|^2}{2}\frac{\partial\rho_{\alpha\beta}}{\partial t}}$$

Where: $\left(\vec{v}_{\alpha\beta}\cdot\vec{v}_{\alpha\beta}\right)=\left|\vec{v}_{\alpha\beta}\right|^2$

Incorporated into momentum balance:

$$\left\{\begin{array}{l}\varepsilon_{\beta r}^{V}\varepsilon_{\alpha\beta}^{V}\frac{\partial\,{}^{1}\!/\!_{2}\,\rho_{\alpha\beta}\left|\vec{v}_{\alpha\beta}\right|^2}{\partial t}+\varepsilon_{\beta r}^{V}\varepsilon_{\alpha\beta}^{V}\frac{\vec{v}_{\alpha\beta}\cdot\vec{v}_{\alpha\beta}}{2}\frac{\partial\rho_{\alpha\beta}}{\partial t}\\ +\vec{v}_{\alpha\beta}\cdot\vec{\nabla}\cdot\left(\varepsilon_{\beta r}^{A}\varepsilon_{\alpha\beta}^{A}\rho_{\alpha\beta}\vec{v}_{\alpha\beta}\vec{v}_{\alpha\beta}\right)-\vec{v}_{\alpha\beta}\cdot\vec{\nabla}\cdot\left(\varepsilon_{\beta r}^{A}\varepsilon_{\alpha\beta}^{A}\vec{\vec{T}}_{\alpha\beta}\right)\end{array}\right\}=0$$

From continuity equation:

$$\frac{\vec{v}_{\alpha\beta}\cdot\vec{v}_{\alpha\beta}}{2}\frac{\partial}{\partial t}\left(\varepsilon_{\beta r}^{V}\varepsilon_{\alpha\beta}^{V}\rho_{\alpha\beta}\right)=\frac{\vec{v}_{\alpha\beta}\cdot\vec{v}_{\alpha\beta}}{2}\left(-\vec{\nabla}\cdot\left(\varepsilon_{\beta r}^{A}\varepsilon_{\alpha\beta}^{A}\rho_{\alpha\beta}\vec{v}_{\alpha\beta}\right)\right)$$

$$\left\{\begin{array}{l}\varepsilon_{\beta r}^{V}\varepsilon_{\alpha\beta}^{V}\frac{\partial\,{}^{1}\!/\!_{2}\,\rho_{\alpha\beta}\left|\vec{v}_{\alpha\beta}\right|^2}{\partial t}+\frac{\vec{v}_{\alpha\beta}\cdot\vec{v}_{\alpha\beta}}{2}\left(-\vec{\nabla}\cdot\left(\varepsilon_{\beta r}^{A}\varepsilon_{\alpha\beta}^{A}\rho_{\alpha\beta}\vec{v}_{\alpha\beta}\right)\right)\\ +\vec{v}_{\alpha\beta}\cdot\vec{\nabla}\cdot\left(\varepsilon_{\beta r}^{A}\varepsilon_{\alpha\beta}^{A}\rho_{\alpha\beta}\vec{v}_{\alpha\beta}\vec{v}_{\alpha\beta}\right)-\vec{v}_{\alpha\beta}\cdot\vec{\nabla}\cdot\left(\varepsilon_{\beta r}^{A}\varepsilon_{\alpha\beta}^{A}\vec{\vec{T}}_{\alpha\beta}\right)\end{array}\right\}=0$$

Term1: $\frac{\vec{v}_{\alpha\beta}\cdot\vec{v}_{\alpha\beta}}{2}\left(-\vec{\nabla}\cdot\left(\varepsilon_{\beta r}^{A}\varepsilon_{\alpha\beta}^{A}\rho_{\alpha\beta}\vec{v}_{\alpha\beta}\right)\right)$

Term2: $\vec{v}_{\alpha\beta}\cdot\vec{\nabla}\cdot\left(\varepsilon_{\beta r}^{A}\varepsilon_{\alpha\beta}^{A}\rho_{\alpha\beta}\vec{v}_{\alpha\beta}\vec{v}_{\alpha\beta}\right)$

Expansion of Term1:

$$\frac{\vec{v}_{\alpha\beta}\cdot\vec{v}_{\alpha\beta}}{2}\left(-\vec{\nabla}\cdot\left(\varepsilon_{\beta r}^{A}\varepsilon_{\alpha\beta}^{A}\rho_{\alpha\beta}\vec{v}_{\alpha\beta}\right)\right)=-\frac{\vec{v}_{\alpha\beta}\cdot\vec{v}_{\alpha\beta}}{2}\left(\vec{\nabla}\cdot\left(\varepsilon_{\beta r}^{A}\varepsilon_{\alpha\beta}^{A}\rho_{\alpha\beta}\vec{v}_{\alpha\beta}\right)\right)=$$

$$-\left(\sum_{\varpi_1=1}^{3}\frac{v_{\varpi_1,\alpha\beta}v_{\varpi_1,\alpha\beta}}{2}\right)\left(\sum_{\varpi_2=1}^{3}\vec{e}_{\varpi_2}\frac{\partial}{\partial x_{\varpi_2}}\cdot\varepsilon_{\beta r}^{A}\varepsilon_{\alpha\beta}^{A}\rho_{\alpha\beta}\sum_{\varpi_3=1}^{3}\vec{e}_{\varpi_3}v_{\varpi_3,\alpha\beta}\right)=$$

$$-\left(\sum_{\varpi_1=1}^{3}\frac{v_{\varpi_1,\alpha\beta}v_{\varpi_1,\alpha\beta}}{2}\right)\left(\sum_{\varpi_2=1}^{3}\sum_{\varpi_3=1}^{3}\delta_{\varpi_2\varpi_3}\varepsilon_{\beta r}^{A}\varepsilon_{\alpha\beta}^{A}\frac{\partial\rho_{\alpha\beta}v_{\varpi_3,\alpha\beta}}{\partial x_{\varpi_2}}\right)=-\left(\sum_{\varpi_1=1}^{3}\sum_{\varpi_2=1}^{3}\varepsilon_{\beta r}^{A}\varepsilon_{\alpha\beta}^{A}\frac{v_{\varpi_1,\alpha\beta}v_{\varpi_1,\alpha\beta}}{2}\frac{\partial\rho_{\alpha\beta}v_{\varpi_2,\alpha\beta}}{\partial x_{\varpi_2}}\right)=$$

$$\boxed{-\left(\sum_{\varpi_1=1}^{3}\sum_{\varpi_2=1}^{3}\varepsilon_{\beta r}^{A}\varepsilon_{\alpha\beta}^{A}\frac{v_{\varpi_1,\alpha\beta}v_{\varpi_1,\alpha\beta}}{2}\frac{\partial\rho_{\alpha\beta}}{\partial x_{\varpi_2}}v_{\varpi_2,\alpha\beta}+\sum_{\varpi_1=1}^{3}\sum_{\varpi_2=1}^{3}\varepsilon_{\beta r}^{A}\varepsilon_{\alpha\beta}^{A}\frac{v_{\varpi_1,\alpha\beta}v_{\varpi_1,\alpha\beta}\rho_{\alpha\beta}}{2}\frac{\partial v_{\varpi_2,\alpha\beta}}{\partial x_{\varpi_2}}\right)}$$

Expansion of Term2

$$\begin{pmatrix}\vec{v}_{\alpha\beta}\cdot\left(\vec{\nabla}\cdot\left(\varepsilon_{\beta r}^{A}\varepsilon_{\alpha\beta}^{A}\rho_{\alpha\beta}\vec{v}_{\alpha\beta}\vec{v}_{\alpha\beta}\right)\right)\\ \vec{\vec{v}}_{\alpha\beta}\triangleq\vec{v}_{\alpha\beta}\vec{v}_{\alpha\beta}\end{pmatrix}\Rightarrow\vec{v}_{\alpha\beta}\cdot\left(\vec{\nabla}\cdot\left(\varepsilon_{\beta r}^{A}\varepsilon_{\alpha\beta}^{A}\rho_{\alpha\beta}\vec{\vec{v}}_{\alpha\beta}\right)\right)=\left(\vec{v}_{\alpha\beta}\cdot\begin{pmatrix}\left(\vec{\nabla}\varepsilon_{\beta r}^{A}\varepsilon_{\alpha\beta}^{A}\rho_{\alpha\beta}\right)\cdot\vec{\vec{v}}_{\alpha\beta}\\ +\rho_{\alpha\beta}\left(\vec{\nabla}\cdot\varepsilon_{\beta r}^{A}\varepsilon_{\alpha\beta}^{A}\vec{\vec{v}}_{\alpha\beta}\right)\end{pmatrix}\right)=$$

$$\vec{v}_{\alpha\beta}\cdot\left(\vec{\nabla}\varepsilon_{\beta r}^{A}\varepsilon_{\alpha\beta}^{A}\rho_{\alpha\beta}\right)\cdot\vec{v}_{\alpha\beta}\vec{v}_{\alpha\beta}+\vec{v}_{\alpha\beta}\cdot\rho_{\alpha\beta}\left(\vec{\nabla}\cdot\varepsilon_{\beta r}^{A}\varepsilon_{\alpha\beta}^{A}\vec{v}_{\alpha\beta}\vec{v}_{\alpha\beta}\right)$$

Term 3: $\vec{v}_{\alpha\beta}\cdot\left(\vec{\nabla}\varepsilon_{\beta r}^{A}\varepsilon_{\alpha\beta}^{A}\rho_{\alpha\beta}\right)\cdot\vec{v}_{\alpha\beta}\vec{v}_{\alpha\beta}$

Term 4: $\vec{v}_{\alpha\beta}\cdot\rho_{\alpha\beta}\left(\vec{\nabla}\cdot\varepsilon_{\beta r}^{A}\varepsilon_{\alpha\beta}^{A}\vec{v}_{\alpha\beta}\vec{v}_{\alpha\beta}\right)$

Expansion on Term3:

$$\vec{v}_{\alpha\beta}\cdot\left(\vec{\nabla}\varepsilon_{\beta r}^{A}\varepsilon_{\alpha\beta}^{A}\rho_{\alpha\beta}\right)\cdot\vec{v}_{\alpha\beta}\vec{v}_{\alpha\beta}=\left(\sum_{\varpi_1=1}^{3}\vec{e}_{\varpi_1}v_{\varpi_1,\alpha\beta}\right)\cdot\left(\sum_{\varpi_2=1}^{3}\vec{e}_{\varpi_2}\frac{\partial\left(\varepsilon_{\beta r}^{A}\varepsilon_{\alpha\beta}^{A}\rho_{\alpha\beta}\right)}{\partial x_{\varpi_2}}\cdot\sum_{\varpi_3=1}^{3}\sum_{\varpi_4=1}^{3}\vec{e}_{\varpi_3}\vec{e}_{\varpi_4}v_{\varpi_3,\alpha\beta}v_{\varpi_4,\alpha\beta}\right)=$$

$$\left(\sum_{\varpi_1=1}^{3}\vec{e}_{\varpi_1}v_{\varpi_1,\alpha\beta}\right)\cdot\left(\sum_{\varpi_2=1}^{3}\sum_{\varpi_3=1}^{3}\sum_{\varpi_4=1}^{3}\delta_{\varpi_2\varpi_3}\vec{e}_{\varpi_4}\frac{\partial\left(\varepsilon_{\beta r}^{A}\varepsilon_{\alpha\beta}^{A}\rho_{\alpha\beta}\right)}{\partial x_{\varpi_2}}v_{\varpi_3,\alpha\beta}v_{\varpi_4,\alpha\beta}\right)=$$

$$\left(\sum_{\varpi_1=1}^{3}\vec{e}_{\varpi_1}v_{\varpi_1,\alpha\beta}\right)\cdot\left(\sum_{\varpi_4=1}^{3}\vec{e}_{\varpi_4}\sum_{\varpi_2=1}^{3}\frac{\partial\left(\varepsilon_{\beta\mathrm{r}}^{A}\varepsilon_{\alpha\beta}^{A}\rho_{\alpha\beta}\right)}{\partial x_{\varpi_2}}v_{\varpi_2,\alpha\beta}v_{\varpi_4,\alpha\beta}\right)=\sum_{\varpi_1=1}^{3}\sum_{\varpi_4=1}^{3}\delta_{\varpi_1\varpi_4}v_{\varpi_1,\alpha\beta}\sum_{\varpi_2=1}^{3}\frac{\partial\left(\varepsilon_{\beta\mathrm{r}}^{A}\varepsilon_{\alpha\beta}^{A}\rho_{\alpha\beta}\right)}{\partial x_{\varpi_2}}v_{\varpi_2,\alpha\beta}v_{\varpi_4,\alpha\beta}=$$

$$\boxed{\sum_{\varpi_1=1}^{3}\sum_{\varpi_2=1}^{3}v_{\varpi_1,\alpha\beta}v_{\varpi_1,\alpha\beta}v_{\varpi_2,\alpha\beta}\frac{\partial\left(\varepsilon_{\beta\mathrm{r}}^{A}\varepsilon_{\alpha\beta}^{A}\rho_{\alpha\beta}\right)}{\partial x_{\varpi_2}}}$$

Expansion on Term4:

$$\vec{v}_{\alpha\beta}\cdot\rho_{\alpha\beta}\left(\vec{\nabla}\cdot\varepsilon_{\beta\mathrm{r}}^{A}\varepsilon_{\alpha\beta}^{A}\vec{v}_{\alpha\beta}\vec{v}_{\alpha\beta}\right)=\left(\sum_{\varpi_1=1}^{3}\vec{e}_{\varpi_1}v_{\varpi_1,\alpha\beta}\right)\cdot\left(\rho_{\alpha\beta}\sum_{\varpi_2=1}^{3}\vec{e}_{\varpi_2}\frac{\partial}{\partial x_{\varpi_2}}\cdot\sum_{\varpi_3=1}^{3}\sum_{\varpi_4=1}^{3}\varepsilon_{\beta\mathrm{r}}^{A}\varepsilon_{\alpha\beta}^{A}\vec{e}_{\varpi_3}\vec{e}_{\varpi_4}v_{\varpi_3,\alpha\beta}v_{\varpi_4,\alpha\beta}\right)=$$

$$\left(\sum_{\varpi_1=1}^{3}\vec{e}_{\varpi_1}v_{\varpi_1,\alpha\beta}\right)\cdot\left(\sum_{\varpi_2=1}^{3}\sum_{\varpi_3=1}^{3}\sum_{\varpi_4=1}^{3}\delta_{\varpi_2\varpi_3}\vec{e}_{\varpi_4}\rho_{\alpha\beta}\frac{\partial\left(\varepsilon_{\beta\mathrm{r}}^{A}\varepsilon_{\alpha\beta}^{A}v_{\varpi_3,\alpha\beta}v_{\varpi_4,\alpha\beta}\right)}{\partial x_{\varpi_2}}\right)=$$

$$\left(\sum_{\varpi_1=1}^{3}\vec{e}_{\varpi_1}v_{\varpi_1,\alpha\beta}\right)\cdot\left(\sum_{\varpi_4=1}^{3}\vec{e}_{\varpi_4}\sum_{\varpi_2=1}^{3}\rho_{\alpha\beta}\frac{\partial\left(\varepsilon_{\beta\mathrm{r}}^{A}\varepsilon_{\alpha\beta}^{A}v_{\varpi_2,\alpha\beta}v_{\varpi_4,\alpha\beta}\right)}{\partial x_{\varpi_2}}\right)=\sum_{\varpi_1=1}^{3}\sum_{\varpi_4=1}^{3}\delta_{\varpi_1\varpi_4}v_{\varpi_1,\alpha\beta}\sum_{\varpi_2=1}^{3}\rho_{\alpha\beta}\frac{\partial\left(\varepsilon_{\beta\mathrm{r}}^{A}\varepsilon_{\alpha\beta}^{A}v_{\varpi_2,\alpha\beta}v_{\varpi_4,\alpha\beta}\right)}{\partial x_{\varpi_2}}=$$

$$\boxed{\sum_{\varpi_1=1}^{3}\sum_{\varpi_2=1}^{3}v_{\varpi_1,\alpha\beta}\rho_{\alpha\beta}\frac{\partial\left(\varepsilon_{\beta\mathrm{r}}^{A}\varepsilon_{\alpha\beta}^{A}v_{\varpi_2,\alpha\beta}v_{\varpi_1,\alpha\beta}\right)}{\partial x_{\varpi_2}}}$$

Re-write, and incorporate previous expansions:

$$\left[\begin{array}{l}\varepsilon_{\beta\mathrm{r}}^{V}\varepsilon_{\alpha\beta}^{V}\dfrac{\partial\,{}^{1}\!/_{2}\,\rho_{\alpha\beta}\left|\vec{v}_{\alpha\beta}\right|^{2}}{\partial t}+\\ -\left(\begin{array}{l}\displaystyle\sum_{\varpi_1=1}^{3}\sum_{\varpi_2=1}^{3}\varepsilon_{\beta\mathrm{r}}^{A}\varepsilon_{\alpha\beta}^{A}\frac{v_{\varpi_1,\alpha\beta}v_{\varpi_1,\alpha\beta}}{2}\frac{\partial\rho_{\alpha\beta}}{\partial x_{\varpi_2}}v_{\varpi_2,\alpha\beta}\\ \displaystyle+\sum_{\varpi_1=1}^{3}\sum_{\varpi_2=1}^{3}\varepsilon_{\beta\mathrm{r}}^{A}\varepsilon_{\alpha\beta}^{A}\frac{v_{\varpi_1,\alpha\beta}v_{\varpi_1,\alpha\beta}\rho_{\alpha\beta}}{2}\frac{\partial v_{\varpi_2,\alpha\beta}}{\partial x_{\varpi_2}}\end{array}\right)\\ +\displaystyle\sum_{\varpi_1=1}^{3}\sum_{\varpi_2=1}^{3}v_{\varpi_1,\alpha\beta}v_{\varpi_1,\alpha\beta}v_{\varpi_2,\alpha\beta}\frac{\partial\left(\varepsilon_{\beta\mathrm{r}}^{A}\varepsilon_{\alpha\beta}^{A}\rho_{\alpha\beta}\right)}{\partial x_{\varpi_2}}\\ +\displaystyle\sum_{\varpi_1=1}^{3}\sum_{\varpi_2=1}^{3}v_{\varpi_1,\alpha\beta}\rho_{\alpha\beta}\frac{\partial\left(\varepsilon_{\beta\mathrm{r}}^{A}\varepsilon_{\alpha\beta}^{A}v_{\varpi_2,\alpha\beta}v_{\varpi_1,\alpha\beta}\right)}{\partial x_{\varpi_2}}\end{array}\right]=\left[\vec{v}_{\alpha\beta}\cdot\vec{\nabla}\cdot\left(\varepsilon_{\beta\mathrm{r}}^{A}\varepsilon_{\alpha\beta}^{A}\vec{\vec{T}}_{\alpha\beta}\right)\right]$$

$$\left[\begin{array}{l}
\varepsilon_{\beta r}^{V}\varepsilon_{\alpha\beta}^{V}\dfrac{\partial\, 1/2\,\rho_{\alpha\beta}\left|\vec{v}_{\alpha\beta}\right|^{2}}{\partial t}+\\
-\left(\displaystyle\sum_{\varpi_1=1}^{3}\sum_{\varpi_2=1}^{3}\varepsilon_{\beta r}^{A}\varepsilon_{\alpha\beta}^{A}\frac{v_{\varpi_1,\alpha\beta}v_{\varpi_1,\alpha\beta}}{2}\frac{\partial\rho_{\alpha\beta}}{\partial x_{\varpi_2}}v_{\varpi_2,\alpha\beta}\right)\\
-\left(\displaystyle\sum_{\varpi_1=1}^{3}\sum_{\varpi_2=1}^{3}\varepsilon_{\beta r}^{A}\varepsilon_{\alpha\beta}^{A}\frac{v_{\varpi_1,\alpha\beta}v_{\varpi_1,\alpha\beta}\rho_{\alpha\beta}}{2}\frac{\partial v_{\varpi_2,\alpha\beta}}{\partial x_{\varpi_2}}\right)\\
+\left(\displaystyle\sum_{\varpi_1=1}^{3}\sum_{\varpi_2=1}^{3}v_{\varpi_1,\alpha\beta}v_{\varpi_1,\alpha\beta}v_{\varpi_2,\alpha\beta}\frac{\partial\left(\varepsilon_{\beta r}^{A}\varepsilon_{\alpha\beta}^{A}\rho_{\alpha\beta}\right)}{\partial x_{\varpi_2}}\right)\\
+\left(\displaystyle\sum_{\varpi_1=1}^{3}\sum_{\varpi_2=1}^{3}v_{\varpi_1,\alpha\beta}\rho_{\alpha\beta}\frac{\partial\left(\varepsilon_{\beta r}^{A}\varepsilon_{\alpha\beta}^{A}v_{\varpi_2,\alpha\beta}v_{\varpi_1,\alpha\beta}\right)}{\partial x_{\varpi_2}}\right)
\end{array}\right]=\left[\vec{v}_{\alpha\beta}\cdot\vec{\nabla}\cdot\left(\varepsilon_{\beta r}^{A}\varepsilon_{\alpha\beta}^{A}\vec{\vec{T}}_{\alpha\beta}\right)\right]$$

The LHS spatial derivative terms in the equation above is equivalent to RHS:

$$\vec{\nabla}\cdot\left(\varepsilon_{\beta r}^{A}\varepsilon_{\alpha\beta}^{A}\frac{\rho_{\alpha\beta}}{2}\left|\vec{v}_{\alpha\beta}\right|^{2}\vec{v}_{\alpha\beta}\right)$$

Proof: See Appendix A.3

This gives an expression containing $\vec{v}_{\alpha\beta}\cdot\left(\vec{\nabla}\cdot\left(\varepsilon_{\beta r}^{A}\varepsilon_{\alpha\beta}^{A}\vec{\vec{T}}_{\alpha\beta}\right)\right)$:

$$\left[\begin{array}{l}
\varepsilon_{\beta r}^{V}\varepsilon_{\alpha\beta}^{V}\dfrac{\partial}{\partial t}\left(\dfrac{\rho_{\alpha\beta}\left|\vec{v}_{\alpha\beta}\right|^{2}}{2}\right)+\\
\vec{\nabla}\cdot\left(\varepsilon_{\beta r}^{A}\varepsilon_{\alpha\beta}^{A}\dfrac{\rho_{\alpha\beta}\left|\vec{v}_{\alpha\beta}\right|^{2}\vec{v}_{\alpha\beta}}{2}\right)
\end{array}\right]=\left[\begin{array}{l}
\vec{v}_{\alpha\beta}\cdot\vec{\nabla}\cdot\left(\varepsilon_{\beta r}^{A}\varepsilon_{\alpha\beta}^{A}\vec{\vec{T}}_{\alpha\beta}\right)\\
+\vec{v}_{\alpha\beta}\cdot\varepsilon_{\beta r}^{V}\varepsilon_{\alpha\beta}^{V}\displaystyle\sum_{\substack{\alpha_1=1\\ \alpha_1\neq\alpha}}^{NP_\alpha}\sum_{\substack{\beta_1=1\\ \beta_1\neq\beta}}^{NP_\beta}F_{m,\alpha_1-\alpha}^{\beta_1-\beta}
\end{array}\right]$$

used to cancel kinetic energy terms in energy balance.

$$\left\{\begin{array}{l}
\dfrac{\partial}{\partial t}\left(\varepsilon_{\beta r}^{V}\varepsilon_{\alpha\beta}^{V}\rho_{\alpha\beta}U_{\alpha\beta}^{m}\right)\\
+\vec{\nabla}\cdot\left[\varepsilon_{\beta r}^{A}\varepsilon_{\alpha\beta}^{A}\rho_{\alpha\beta}\vec{v}_{\alpha\beta}U_{\alpha\beta}^{m}\right]
\end{array}\right\}=\left\{\begin{array}{l}
-\vec{\nabla}\cdot\left(\varepsilon_{\beta r}^{A}\varepsilon_{\alpha\beta}^{A}\overrightarrow{Q_{\alpha\beta}}\right)-\left(\displaystyle\sum_{i=1}^{NC}\vec{\nabla}\cdot\left(\frac{1}{M_i}h_{i,\alpha\beta}^{a}\varepsilon_{\beta r}^{A}\varepsilon_{\alpha\beta}^{A}\vec{j}_{i,\alpha\beta}\right)\right)\\
+\varepsilon_{\beta r}^{A}\varepsilon_{\alpha\beta}^{A}\left(\vec{\vec{T}}_{\alpha\beta}:\vec{\nabla}\vec{v}_{\alpha\beta}\right)
\end{array}\right\}$$

$$\left(\vec{\vec{T}}_{\alpha\beta} : \vec{\nabla}\vec{v}_{\alpha\beta}\right) = \vec{\tau}_{\alpha\beta} : \vec{\nabla}\vec{v}_{\alpha\beta} - P_{\alpha\beta}\vec{\nabla}\cdot\vec{v}_{\alpha\beta}$$

Where: $\left(P_{\alpha\beta}\vec{I}\right) : \vec{\nabla}\vec{v}_{\alpha\beta} = P_{\alpha\beta}\vec{\nabla}\cdot\left(\vec{v}_{\alpha\beta}\cdot\vec{I}\right) - P_{\alpha\beta}\vec{v}_{\alpha\beta}\cdot\left(\vec{\nabla}\cdot\vec{I}\right) = P_{\alpha\beta}\left(\vec{\nabla}\cdot\vec{v}_{\alpha\beta}\right)$

$$\left\{\begin{array}{l}\dfrac{\partial}{\partial t}\left(\varepsilon_{\beta r}^{V}\varepsilon_{\alpha\beta}^{V}\rho_{\alpha\beta}U_{\alpha\beta}^{m}\right) \\ +\vec{\nabla}\cdot\left[\varepsilon_{\beta r}^{A}\varepsilon_{\alpha\beta}^{A}\rho_{\alpha\beta}\vec{v}_{\alpha\beta}U_{\alpha\beta}^{m}\right] \\ \\ \\ \end{array}\right\} = \left\{\begin{array}{l}-\vec{\nabla}\cdot\left(\varepsilon_{\beta r}^{A}\varepsilon_{\alpha\beta}^{A}\overrightarrow{Q_{\alpha\beta}}\right) - \left(\sum_{i=1}^{NC}\vec{\nabla}\cdot\left(\dfrac{1}{M_i}h_{i,\alpha\beta}^{a}\varepsilon_{\beta r}^{A}\varepsilon_{\alpha\beta}^{A}\vec{j}_{i,\alpha\beta}\right)\right) \\ +\varepsilon_{\beta r}^{A}\varepsilon_{\alpha\beta}^{A}\left(\vec{\tau}_{\alpha\beta} : \vec{\nabla}\vec{v}_{\alpha\beta}\right) - \varepsilon_{\beta r}^{A}\varepsilon_{\alpha\beta}^{A}P_{\alpha\beta}\vec{\nabla}\cdot\vec{v}_{\alpha\beta}\end{array}\right\}$$ Recalling total

balance.

$$\frac{\partial}{\partial t}\left(\varepsilon_{\beta r}^{V}\varepsilon_{\alpha\beta}^{V}\rho_{\alpha\beta}\right) + \vec{\nabla}\cdot\left(\varepsilon_{\beta r}^{A}\varepsilon_{\alpha\beta}^{A}\rho_{\alpha\beta}\vec{v}_{\alpha\beta}\right) = 0$$

$$\left(\varepsilon_{\beta r}^{A}\varepsilon_{\alpha\beta}^{A}\right)\left(\vec{\nabla}\cdot\vec{v}_{\alpha\beta}\right) = -\frac{\varepsilon_{\beta r}^{V}\varepsilon_{\alpha\beta}^{V}}{\rho_{\alpha\beta}}\frac{\partial}{\partial t}\left(\rho_{\alpha\beta}\right) - \frac{\varepsilon_{\beta r}^{A}\varepsilon_{\alpha\beta}^{A}}{\rho_{\alpha\beta}}\left(\vec{\nabla}\rho_{\alpha\beta}\right)\cdot\left(\vec{v}_{\alpha\beta}\right)$$

$$\left(\varepsilon_{\beta r}^{A}\varepsilon_{\alpha\beta}^{A}\right)P_{\alpha\beta}\left(\vec{\nabla}\cdot\vec{v}_{\alpha\beta}\right) = -P_{\alpha\beta}\frac{\varepsilon_{\beta r}^{V}\varepsilon_{\alpha\beta}^{V}}{\rho_{\alpha\beta}}\frac{\partial}{\partial t}\left(\rho_{\alpha\beta}\right) - P_{\alpha\beta}\frac{\varepsilon_{\beta r}^{A}\varepsilon_{\alpha\beta}^{A}}{\rho_{\alpha\beta}}\left(\vec{\nabla}\rho_{\alpha\beta}\right)\cdot\left(\vec{v}_{\alpha\beta}\right)$$

Using following relationships:

$$\left\{-\frac{P_{\alpha\beta}}{\rho_{\alpha\beta}}\frac{\partial}{\partial t}\left(\rho_{\alpha\beta}\right) = \rho_{\alpha\beta}\frac{\partial}{\partial t}\left(\frac{P_{\alpha\beta}}{\rho_{\alpha\beta}}\right) - \frac{\partial P_{\alpha\beta}}{\partial t}\right\} \text{ and } \left\{-\frac{P_{\alpha\beta}}{\rho_{\alpha\beta}}\left(\vec{\nabla}\rho_{\alpha\beta}\right) = \rho_{\alpha\beta}\left(\vec{\nabla}\frac{P_{\alpha\beta}}{\rho_{\alpha\beta}}\right) - \vec{\nabla}\left(P_{\alpha\beta}\right)\right\}$$

Gives: $\left(\varepsilon_{\beta r}^{A}\varepsilon_{\alpha\beta}^{A}\right)P_{\alpha\beta}\left(\vec{\nabla}\cdot\vec{v}_{\alpha\beta}\right) = \left\{\begin{array}{l}\varepsilon_{\beta r}^{V}\varepsilon_{\alpha\beta}^{V}\rho_{\alpha\beta}\dfrac{\partial}{\partial t}\left(\dfrac{P_{\alpha\beta}}{\rho_{\alpha\beta}}\right) - \varepsilon_{\beta r}^{V}\varepsilon_{\alpha\beta}^{V}\dfrac{\partial P_{\alpha\beta}}{\partial t} \\ +\varepsilon_{\beta r}^{A}\varepsilon_{\alpha\beta}^{A}\rho_{\alpha\beta}\left(\vec{\nabla}\dfrac{P_{\alpha\beta}}{\rho_{\alpha\beta}}\right)\cdot\left(\vec{v}_{\alpha\beta}\right) - \varepsilon_{\beta r}^{A}\varepsilon_{\alpha\beta}^{A}\vec{\nabla}\left(P_{\alpha\beta}\right)\cdot\left(\vec{v}_{\alpha\beta}\right)\end{array}\right\}$

$$\left\{\begin{array}{l}\dfrac{\partial}{\partial t}\left(\varepsilon_{\beta r}^{V}\varepsilon_{\alpha\beta}^{V}\rho_{\alpha\beta}U_{\alpha\beta}^{m}\right)\\ +\vec{\nabla}\cdot\left[\varepsilon_{\beta r}^{A}\varepsilon_{\alpha\beta}^{A}\rho_{\alpha\beta}\vec{v}_{\alpha\beta}U_{\alpha\beta}^{m}\right]\\ +\varepsilon_{\beta r}^{A}\varepsilon_{\alpha\beta}^{A}P_{\alpha\beta}\vec{\nabla}\cdot\vec{v}_{\alpha\beta}\end{array}\right\}=\left\{\begin{array}{l}-\vec{\nabla}\cdot\left(\varepsilon_{\beta r}^{A}\varepsilon_{\alpha\beta}^{A}\overrightarrow{Q_{\alpha\beta}}\right)-\left(\sum_{i=1}^{NC}\vec{\nabla}\cdot\left(\dfrac{1}{M_i}h_{i,\alpha\beta}^{a}\varepsilon_{\beta r}^{A}\varepsilon_{\alpha\beta}^{A}\vec{j}_{i,\alpha\beta}\right)\right)\\ +\varepsilon_{\beta r}^{A}\varepsilon_{\alpha\beta}^{A}\left(\vec{\tau}_{\alpha\beta}:\vec{\nabla}\vec{v}_{\alpha\beta}\right)\end{array}\right\}$$

Incorporate to make enthalpies:

$$\left\{\begin{array}{l}\varepsilon_{\beta r}^{V}\varepsilon_{\alpha\beta}^{V}U_{\alpha\beta}^{m}\dfrac{\partial}{\partial t}\left(\rho_{\alpha\beta}\right)+\varepsilon_{\beta r}^{A}\varepsilon_{\alpha\beta}^{A}U_{\alpha\beta}^{m}\rho_{\alpha\beta}\left(\vec{\nabla}\cdot\vec{v}_{\alpha\beta}\right)\\ +\varepsilon_{\beta r}^{V}\varepsilon_{\alpha\beta}^{V}\rho_{\alpha\beta}\dfrac{\partial}{\partial t}U_{\alpha\beta}^{m}+\left(\vec{\nabla}\left(\varepsilon_{\beta r}^{A}\varepsilon_{\alpha\beta}^{A}U_{\alpha\beta}^{m}\rho_{\alpha\beta}\right)\right)\cdot\vec{v}_{\alpha\beta}\\ \varepsilon_{\beta r}^{V}\varepsilon_{\alpha\beta}^{V}\rho_{\alpha\beta}\dfrac{\partial}{\partial t}\left(\dfrac{P_{\alpha\beta}}{\rho_{\alpha\beta}}\right)+\varepsilon_{\beta r}^{A}\varepsilon_{\alpha\beta}^{A}\rho_{\alpha\beta}\left(\vec{\nabla}\dfrac{P_{\alpha\beta}}{\rho_{\alpha\beta}}\right)\cdot\left(\vec{v}_{\alpha\beta}\right)\end{array}\right\}=\left\{\begin{array}{l}-\vec{\nabla}\cdot\left(\varepsilon_{\beta r}^{A}\varepsilon_{\alpha\beta}^{A}\overrightarrow{Q_{\alpha\beta}}\right)\\ -\left(\sum_{i=1}^{NC}\vec{\nabla}\cdot\left(\dfrac{1}{M_i}h_{i,\alpha\beta}^{a}\varepsilon_{\beta r}^{A}\varepsilon_{\alpha\beta}^{A}\vec{j}_{i,\alpha\beta}\right)\right)\\ +\varepsilon_{\beta r}^{A}\varepsilon_{\alpha\beta}^{A}\left(\vec{\tau}_{\alpha\beta}:\vec{\nabla}\vec{v}_{\alpha\beta}\right)\\ +\varepsilon_{\beta r}^{V}\varepsilon_{\alpha\beta}^{V}\dfrac{\partial P_{\alpha\beta}}{\partial t}+\varepsilon_{\beta r}^{A}\varepsilon_{\alpha\beta}^{A}\vec{\nabla}\left(P_{\alpha\beta}\right)\cdot\left(\vec{v}_{\alpha\beta}\right)\end{array}\right\}$$

$$\left\{\begin{array}{l}\varepsilon_{\beta r}^{V}\varepsilon_{\alpha\beta}^{V}U_{\alpha\beta}^{m}\dfrac{\partial}{\partial t}\left(\rho_{\alpha\beta}\right)+\varepsilon_{\beta r}^{A}\varepsilon_{\alpha\beta}^{A}U_{\alpha\beta}^{m}\left(\vec{\nabla}\cdot\left(\rho_{\alpha\beta}\vec{v}_{\alpha\beta}\right)\right)\\ +\varepsilon_{\beta r}^{V}\varepsilon_{\alpha\beta}^{V}\rho_{\alpha\beta}\dfrac{\partial h_{\alpha\beta}^{m}}{\partial t}+\varepsilon_{\beta r}^{A}\varepsilon_{\alpha\beta}^{A}\rho_{\alpha\beta}\left(\vec{\nabla}h_{\alpha\beta}^{m}\right)\cdot\vec{v}_{\alpha\beta}\end{array}\right\}=\left\{\begin{array}{l}-\vec{\nabla}\cdot\left(\varepsilon_{\beta r}^{A}\varepsilon_{\alpha\beta}^{A}\overrightarrow{Q_{\alpha\beta}}\right)\\ -\left(\sum_{i=1}^{NC}\vec{\nabla}\cdot\left(\dfrac{1}{M_i}h_{i,\alpha\beta}^{a}\varepsilon_{\beta r}^{A}\varepsilon_{\alpha\beta}^{A}\vec{j}_{i,\alpha\beta}\right)\right)\\ +\varepsilon_{\beta r}^{A}\varepsilon_{\alpha\beta}^{A}\left(\vec{\tau}_{\alpha\beta}:\vec{\nabla}\vec{v}_{\alpha\beta}\right)\\ +\varepsilon_{\beta r}^{V}\varepsilon_{\alpha\beta}^{V}\dfrac{\partial P_{\alpha\beta}}{\partial t}+\varepsilon_{\beta r}^{A}\varepsilon_{\alpha\beta}^{A}\vec{\nabla}\left(P_{\alpha\beta}\right)\cdot\left(\vec{v}_{\alpha\beta}\right)\end{array}\right\}$$

$$\left\{\begin{array}{l}\varepsilon_{\beta r}^{V}\varepsilon_{\alpha\beta}^{V}U_{\alpha\beta}^{m}\dfrac{\partial}{\partial t}\left(\rho_{\alpha\beta}\right)\\ +\varepsilon_{\beta r}^{A}\varepsilon_{\alpha\beta}^{A}U_{\alpha\beta}^{m}\left(\vec{\nabla}\cdot\left(\rho_{\alpha\beta}\vec{v}_{\alpha\beta}\right)\right)\\ +\varepsilon_{\beta r}^{V}\varepsilon_{\alpha\beta}^{V}\rho_{\alpha\beta}\dfrac{\partial h_{\alpha\beta}^{m}}{\partial t}\\ +\varepsilon_{\beta r}^{A}\varepsilon_{\alpha\beta}^{A}\rho_{\alpha\beta}\left(\vec{\nabla}h_{\alpha\beta}^{m}\right)\cdot\vec{v}_{\alpha\beta}\end{array}\right\}=\left\{\begin{array}{l}-\vec{\nabla}\cdot\left(\varepsilon_{\beta r}^{A}\varepsilon_{\alpha\beta}^{A}\overrightarrow{Q_{\alpha\beta}}\right)-\left(\sum_{i=1}^{NC}\vec{\nabla}\cdot\left(\dfrac{1}{M_i}h_{i,\alpha\beta}^{a}\varepsilon_{\beta r}^{A}\varepsilon_{\alpha\beta}^{A}\vec{j}_{i,\alpha\beta}\right)\right)\\ +\varepsilon_{\beta r}^{V}\varepsilon_{\alpha\beta}^{V}\dfrac{\partial P_{\alpha\beta}}{\partial t}+\varepsilon_{\beta r}^{A}\varepsilon_{\alpha\beta}^{A}\vec{\nabla}\left(P_{\alpha\beta}\right)\cdot\left(\vec{v}_{\alpha\beta}\right)+\varepsilon_{\beta r}^{A}\varepsilon_{\alpha\beta}^{A}\left(\vec{\tau}_{\alpha\beta}:\vec{\nabla}\vec{v}_{\alpha\beta}\right)\end{array}\right\}$$

$$\left\{\begin{array}{l}\varepsilon_{\beta r}^{V}\varepsilon_{\alpha\beta}^{V}U_{\alpha\beta}^{m}\dfrac{\partial}{\partial t}\left(\rho_{\alpha\beta}\right)+\varepsilon_{\beta r}^{A}\varepsilon_{\alpha\beta}^{A}U_{\alpha\beta}^{m}\left(\vec{\nabla}\cdot\left(\rho_{\alpha\beta}\vec{v}_{\alpha\beta}\right)\right)\\ +\varepsilon_{\beta r}^{V}\varepsilon_{\alpha\beta}^{V}\rho_{\alpha\beta}\dfrac{\partial h_{\alpha\beta}^{m}}{\partial t}+\varepsilon_{\beta r}^{A}\varepsilon_{\alpha\beta}^{A}\rho_{\alpha\beta}\left(\vec{\nabla}h_{\alpha\beta}^{m}\right)\cdot\vec{v}_{\alpha\beta}\end{array}\right\}=\left\{\begin{array}{l}-\vec{\nabla}\cdot\left(\varepsilon_{\beta r}^{A}\varepsilon_{\alpha\beta}^{A}\overrightarrow{Q_{\alpha\beta}}\right)\\ -\left(\sum_{i=1}^{NC}\left(\vec{\nabla}\dfrac{1}{M_i}h_{i,\alpha\beta}^{a}\varepsilon_{\beta r}^{A}\varepsilon_{\alpha\beta}^{A}\right)\cdot\vec{j}_{i,\alpha\beta}\right)\\ -\left(\sum_{i=1}^{NC}\dfrac{1}{M_i}h_{i,\alpha\beta}^{a}\varepsilon_{\beta r}^{A}\varepsilon_{\alpha\beta}^{A}\left(\vec{\nabla}\cdot\vec{j}_{i,\alpha\beta}\right)\right)\\ +\varepsilon_{\beta r}^{V}\varepsilon_{\alpha\beta}^{V}\dfrac{\partial P_{\alpha\beta}}{\partial t}+\varepsilon_{\beta r}^{A}\varepsilon_{\alpha\beta}^{A}\vec{\nabla}\left(P_{\alpha\beta}\right)\cdot\left(\vec{v}_{\alpha\beta}\right)\\ +\varepsilon_{\beta r}^{A}\varepsilon_{\alpha\beta}^{A}\left(\vec{\tau}_{\alpha\beta}:\vec{\nabla}\vec{v}_{\alpha\beta}\right)\end{array}\right\}$$

From component mass balance:

$$\varepsilon_{\beta r}^{A}\varepsilon_{\alpha\beta}^{A}\vec{\nabla}\cdot\left(\left(\vec{j}_{i,\alpha\beta}\right)\right)=\varepsilon_{\beta r}^{V}\varepsilon_{\alpha\beta}^{V}\hat{R}_{i,\alpha\beta}-\frac{\partial}{\partial t}\left(\varepsilon_{\beta r}^{V}\varepsilon_{\alpha\beta}^{V}\rho_{\alpha\beta}w_{i,\alpha\beta}\right)-\vec{\nabla}\cdot\left(\varepsilon_{\beta r}^{A}\varepsilon_{\alpha\beta}^{A}\left(\rho_{i,\alpha\beta}\vec{v}_{\alpha\beta}\right)\right)$$

$$\left\{\begin{array}{l}\varepsilon_{\beta r}^{V}\varepsilon_{\alpha\beta}^{V}U_{\alpha\beta}^{m}\dfrac{\partial}{\partial t}\left(\rho_{\alpha\beta}\right)\\ +\varepsilon_{\beta r}^{A}\varepsilon_{\alpha\beta}^{A}U_{\alpha\beta}^{m}\left(\vec{\nabla}\cdot\left(\rho_{\alpha\beta}\vec{v}_{\alpha\beta}\right)\right)\\ +\varepsilon_{\beta r}^{V}\varepsilon_{\alpha\beta}^{V}\rho_{\alpha\beta}\dfrac{\partial h_{\alpha\beta}^{m}}{\partial t}\\ +\varepsilon_{\beta r}^{A}\varepsilon_{\alpha\beta}^{A}\rho_{\alpha\beta}\left(\vec{\nabla}h_{\alpha\beta}^{m}\right)\cdot\vec{v}_{\alpha\beta}\end{array}\right\}=\left\{\begin{array}{l}-\vec{\nabla}\cdot\left(\varepsilon_{\beta r}^{A}\varepsilon_{\alpha\beta}^{A}\overrightarrow{Q_{\alpha\beta}}\right)-\left(\sum_{i=1}^{NC}\left(\vec{\nabla}\dfrac{1}{M_i}h_{i,\alpha\beta}^{a}\varepsilon_{\beta r}^{A}\varepsilon_{\alpha\beta}^{A}\right)\cdot\vec{j}_{i,\alpha\beta}\right)\\ -\left(\sum_{i=1}^{NC}\dfrac{1}{M_i}h_{i,\alpha\beta}^{a}\left(\begin{array}{l}\varepsilon_{\beta r}^{V}\varepsilon_{\alpha\beta}^{V}\hat{R}_{i,\alpha\beta}-\dfrac{\partial}{\partial t}\left(\varepsilon_{\beta r}^{V}\varepsilon_{\alpha\beta}^{V}\rho_{\alpha\beta}w_{i,\alpha\beta}\right)\\ -\vec{\nabla}\cdot\left(\varepsilon_{\beta r}^{A}\varepsilon_{\alpha\beta}^{A}\left(\rho_{i,\alpha\beta}\vec{v}_{\alpha\beta}\right)\right)\end{array}\right)\right)\\ +\varepsilon_{\beta r}^{V}\varepsilon_{\alpha\beta}^{V}\dfrac{\partial P_{\alpha\beta}}{\partial t}+\varepsilon_{\beta r}^{A}\varepsilon_{\alpha\beta}^{A}\vec{\nabla}\left(P_{\alpha\beta}\right)\cdot\left(\vec{v}_{\alpha\beta}\right)+\varepsilon_{\beta r}^{A}\varepsilon_{\alpha\beta}^{A}\left(\vec{\tau}_{\alpha\beta}:\vec{\nabla}\vec{v}_{\alpha\beta}\right)\end{array}\right\}$$

$$\left\{\begin{array}{l}\varepsilon_{\beta r}^{V}\varepsilon_{\alpha\beta}^{V}U_{\alpha\beta}^{m}\dfrac{\partial}{\partial t}\left(\rho_{\alpha\beta}\right)\\ +\varepsilon_{\beta r}^{A}\varepsilon_{\alpha\beta}^{A}U_{\alpha\beta}^{m}\left(\vec{\nabla}\cdot\left(\rho_{\alpha\beta}\vec{v}_{\alpha\beta}\right)\right)\\ +\varepsilon_{\beta r}^{V}\varepsilon_{\alpha\beta}^{V}\rho_{\alpha\beta}\dfrac{\partial h_{\alpha\beta}^{m}}{\partial t}\\ +\varepsilon_{\beta r}^{A}\varepsilon_{\alpha\beta}^{A}\rho_{\alpha\beta}\left(\vec{\nabla}h_{\alpha\beta}^{m}\right)\cdot\vec{v}_{\alpha\beta}\end{array}\right\}=\left\{\begin{array}{l}-\vec{\nabla}\cdot\left(\varepsilon_{\beta r}^{A}\varepsilon_{\alpha\beta}^{A}\overrightarrow{Q_{\alpha\beta}}\right)\\ -\left(\sum_{i=1}^{NC}\left(\vec{\nabla}\dfrac{1}{M_i}h_{i,\alpha\beta}^{a}\varepsilon_{\beta r}^{A}\varepsilon_{\alpha\beta}^{A}\right)\cdot\vec{j}_{i,\alpha\beta}\right)-\sum_{i=1}^{NC}\left(\dfrac{1}{M_i}h_{i,\alpha\beta}^{a}\varepsilon_{\beta r}^{V}\varepsilon_{\alpha\beta}^{V}\hat{R}_{i,\alpha\beta}\right)\\ +\sum_{i=1}^{NC}\left(\dfrac{1}{M_i}h_{i,\alpha\beta}^{a}\dfrac{\partial}{\partial t}\left(\varepsilon_{\beta r}^{V}\varepsilon_{\alpha\beta}^{V}\rho_{\alpha\beta}w_{i,\alpha\beta}\right)\right)\\ +\sum_{i=1}^{NC}\left(\dfrac{1}{M_i}h_{i,\alpha\beta}^{a}\vec{\nabla}\cdot\left(\varepsilon_{\beta r}^{A}\varepsilon_{\alpha\beta}^{A}\left(\rho_{i,\alpha\beta}\vec{v}_{\alpha\beta}\right)\right)\right)\\ +\varepsilon_{\beta r}^{V}\varepsilon_{\alpha\beta}^{V}\dfrac{\partial P_{\alpha\beta}}{\partial t}+\varepsilon_{\beta r}^{A}\varepsilon_{\alpha\beta}^{A}\vec{\nabla}\left(P_{\alpha\beta}\right)\cdot\left(\vec{v}_{\alpha\beta}\right)\\ +\varepsilon_{\beta r}^{A}\varepsilon_{\alpha\beta}^{A}\left(\vec{\tau}_{\alpha\beta}:\vec{\nabla}\vec{v}_{\alpha\beta}\right)\end{array}\right\}$$

$$\begin{Bmatrix} \varepsilon_{\beta r}^{V}\varepsilon_{\alpha\beta}^{V}U_{\alpha\beta}^{m}\dfrac{\partial}{\partial t}\left(\rho_{\alpha\beta}\right) \\ +\varepsilon_{\beta r}^{A}\varepsilon_{\alpha\beta}^{A}U_{\alpha\beta}^{m}\left(\vec{\nabla}\cdot\left(\rho_{\alpha\beta}\vec{v}_{\alpha\beta}\right)\right) \\ +\varepsilon_{\beta r}^{V}\varepsilon_{\alpha\beta}^{V}\rho_{\alpha\beta}\dfrac{\partial h_{\alpha\beta}^{m}}{\partial t} \\ +\varepsilon_{\beta r}^{A}\varepsilon_{\alpha\beta}^{A}\rho_{\alpha\beta}\left(\vec{\nabla}h_{\alpha\beta}^{m}\right)\cdot\vec{v}_{\alpha\beta} \end{Bmatrix} = \begin{Bmatrix} -\sum\limits_{\substack{\alpha_1=1\\ \alpha_1\neq\alpha}}^{NP_\alpha}\sum\limits_{\substack{\beta_1=1\\ \beta_1\neq\beta}}^{NP_\beta} q_{\alpha_1-\alpha}^{\beta_1\to\beta}\varepsilon_{\alpha\beta}^{I} - \vec{\nabla}\cdot\left(\varepsilon_{\beta r}^{A}\varepsilon_{\alpha\beta}^{A}\overrightarrow{Q_{\alpha\beta}}\right) + \varepsilon_{\beta r}^{A}\varepsilon_{\alpha\beta}^{A}\left(\vec{\tau}_{\alpha\beta}:\vec{\nabla}\vec{v}_{\alpha\beta}\right) \\ -\left(\sum_{i=1}^{NC}\left(\vec{\nabla}\dfrac{1}{M_i}h_{i,\alpha\beta}^{a}\varepsilon_{\beta r}^{A}\varepsilon_{\alpha\beta}^{A}\right)\cdot\vec{j}_{i,\alpha\beta}\right) \\ -\sum_{i=1}^{NC}\left(\dfrac{1}{M_i}h_{i,\alpha\beta}^{a}\varepsilon_{\beta r}^{V}\varepsilon_{\alpha\beta}^{V}\hat{R}_{i,\alpha\beta}\right) + \sum_{i=1}^{NC}\left(\dfrac{1}{M_i}h_{i,\alpha\beta}^{a}\dfrac{\partial}{\partial t}\left(\varepsilon_{\beta r}^{V}\varepsilon_{\alpha\beta}^{V}\rho_{\alpha\beta}w_{i,\alpha\beta}\right)\right) \\ +\sum_{i=1}^{NC}\left(\dfrac{1}{M_i}h_{i,\alpha\beta}^{a}\vec{\nabla}\cdot\left(\varepsilon_{\beta r}^{A}\varepsilon_{\alpha\beta}^{A}\left(\rho_{i,\alpha\beta}\vec{v}_{\alpha\beta}\right)\right)\right) + \varepsilon_{\beta r}^{V}\varepsilon_{\alpha\beta}^{V}\dfrac{\partial P_{\alpha\beta}}{\partial t} \\ +\varepsilon_{\beta r}^{A}\varepsilon_{\alpha\beta}^{A}\vec{\nabla}\left(P_{\alpha\beta}\right)\cdot\left(\vec{v}_{\alpha\beta}\right) \end{Bmatrix}$$

$$\begin{Bmatrix} \varepsilon_{\beta r}^{V}\varepsilon_{\alpha\beta}^{V}U_{\alpha\beta}^{m}\dfrac{\partial}{\partial t}\left(\rho_{\alpha\beta}\right) \\ +\varepsilon_{\beta r}^{A}\varepsilon_{\alpha\beta}^{A}U_{\alpha\beta}^{m}\left(\vec{\nabla}\cdot\left(\rho_{\alpha\beta}\vec{v}_{\alpha\beta}\right)\right) \\ +\varepsilon_{\beta r}^{V}\varepsilon_{\alpha\beta}^{V}\rho_{\alpha\beta}\dfrac{\partial h_{\alpha\beta}^{m}}{\partial t} \\ +\varepsilon_{\beta r}^{A}\varepsilon_{\alpha\beta}^{A}\rho_{\alpha\beta}\left(\vec{\nabla}h_{\alpha\beta}^{m}\right)\cdot\vec{v}_{\alpha\beta} \end{Bmatrix} = \begin{Bmatrix} -\vec{\nabla}\cdot\left(\varepsilon_{\beta r}^{A}\varepsilon_{\alpha\beta}^{A}\overrightarrow{Q_{\alpha\beta}}\right) + \varepsilon_{\beta r}^{A}\varepsilon_{\alpha\beta}^{A}\left(\vec{\tau}_{\alpha\beta}:\vec{\nabla}\vec{v}_{\alpha\beta}\right) \\ -\left(\sum_{i=1}^{NC}\left(\vec{\nabla}\dfrac{1}{M_i}h_{i,\alpha\beta}^{a}\varepsilon_{\beta r}^{A}\varepsilon_{\alpha\beta}^{A}\right)\cdot\vec{j}_{i,\alpha\beta}\right) \\ -\sum_{i=1}^{NC}\left(\dfrac{1}{M_i}h_{i,\alpha\beta}^{a}\varepsilon_{\beta r}^{V}\varepsilon_{\alpha\beta}^{V}\hat{R}_{i,\alpha\beta}\right) + \sum_{i=1}^{NC}\left(\dfrac{1}{M_i}h_{i,\alpha\beta}^{a}\varepsilon_{\beta r}^{V}\varepsilon_{\alpha\beta}^{V}\dfrac{\partial}{\partial t}\left(\rho_{\alpha\beta}w_{i,\alpha\beta}\right)\right) \\ +\sum_{i=1}^{NC}\left(\varepsilon_{\beta r}^{A}\varepsilon_{\alpha\beta}^{A}\dfrac{1}{M_i}h_{i,\alpha\beta}^{a}\vec{\nabla}\cdot\left(\left(\rho_{i,\alpha\beta}\vec{v}_{\alpha\beta}\right)\right)\right) + \varepsilon_{\beta r}^{V}\varepsilon_{\alpha\beta}^{V}\dfrac{\partial P_{\alpha\beta}}{\partial t} \\ +\varepsilon_{\beta r}^{A}\varepsilon_{\alpha\beta}^{A}\vec{\nabla}\left(P_{\alpha\beta}\right)\cdot\left(\vec{v}_{\alpha\beta}\right) \end{Bmatrix}$$

Expansion 1:

$$\left(\sum_{i=1}^{NC}\frac{h_{i,\alpha\beta}^{a}\varepsilon_{\beta r}^{V}\varepsilon_{\alpha\beta}^{V}}{M_i}\frac{\partial\rho_{i,\alpha\beta}}{\partial t}\right) = \sum_{i=1}^{NC}\frac{h_{i,\alpha\beta}^{a}\varepsilon_{\beta r}^{V}\varepsilon_{\alpha\beta}^{V}}{M_i}\frac{\partial\left(w_{i,\alpha\beta}\rho_{\alpha\beta}\right)}{\partial t} = \sum_{i=1}^{NC}\frac{h_{i,\alpha\beta}^{a}\varepsilon_{\beta r}^{V}\varepsilon_{\alpha\beta}^{V}}{M_i}\left(\frac{w_{i,\alpha\beta}\partial\left(\rho_{\alpha\beta}\right)}{\partial t} + \frac{\rho_{\alpha\beta}\partial\left(w_{i,\alpha\beta}\right)}{\partial t}\right)$$

$$\left(\sum_{i=1}^{NC}\frac{h_{i,\alpha\beta}^{a}\varepsilon_{\beta r}^{V}\varepsilon_{\alpha\beta}^{V}}{M_i}\frac{\partial\rho_{i,\alpha\beta}}{\partial t}\right) = \sum_{i=1}^{NC}\left(\frac{h_{i,\alpha\beta}^{a}\varepsilon_{\beta r}^{V}\varepsilon_{\alpha\beta}^{V}}{M_i}\frac{w_{i,\alpha\beta}\partial\left(\rho_{\alpha\beta}\right)}{\partial t} + \frac{h_{i,\alpha\beta}^{a}\varepsilon_{\beta r}^{V}\varepsilon_{\alpha\beta}^{V}}{M_i}\frac{\rho_{\alpha\beta}\partial\left(w_{i,\alpha\beta}\right)}{\partial t}\right)$$

$$\boxed{\left(\sum_{i=1}^{NC}\frac{h_{i,\alpha\beta}^{a}\varepsilon_{\beta r}^{V}\varepsilon_{\alpha\beta}^{V}}{M_i}\frac{\partial\rho_{i,\alpha\beta}}{\partial t}\right) = h_{\alpha\beta}^{m}\varepsilon_{\beta r}^{V}\varepsilon_{\alpha\beta}^{V}\frac{\partial\rho_{\alpha\beta}}{\partial t} + \sum_{i=1}^{NC}\left(\frac{h_{i,\alpha\beta}^{a}\varepsilon_{\beta r}^{V}\varepsilon_{\alpha\beta}^{V}\rho_{\alpha\beta}}{M_i}\frac{\partial w_{i,\alpha\beta}}{\partial t}\right)}$$

Expansion 2:

$$\sum_{i=1}^{NC}\left(\varepsilon_{\beta r}^{A}\varepsilon_{\alpha\beta}^{A}h_{i,\alpha\beta}^{m}\left(\vec{\nabla}\cdot\left(\rho_{i,\alpha\beta}\vec{v}_{\alpha\beta}\right)\right)\right)=\sum_{i=1}^{NC}\left(\varepsilon_{\beta r}^{A}\varepsilon_{\alpha\beta}^{A}h_{i,\alpha\beta}^{m}\left(\left(\vec{\nabla}\rho_{i,\alpha\beta}\right)\cdot\vec{v}_{\alpha\beta}+\rho_{i,\alpha\beta}\left(\vec{\nabla}\cdot\vec{v}_{\alpha\beta}\right)\right)\right)=$$

$$\sum_{i=1}^{NC}\left(\varepsilon_{\beta r}^{A}\varepsilon_{\alpha\beta}^{A}h_{i,\alpha\beta}^{m}\left(w_{i,\alpha\beta}\vec{\nabla}\left(\rho_{\alpha\beta}\right)\cdot\vec{v}_{\alpha\beta}+\rho_{\alpha\beta}\vec{\nabla}\left(w_{i,\alpha\beta}\right)\cdot\vec{v}_{\alpha\beta}+\rho_{i,\alpha\beta}\left(\vec{\nabla}\cdot\vec{v}_{\alpha\beta}\right)\right)\right)=$$

$$\sum_{i=1}^{NC}\left(\varepsilon_{\beta r}^{A}\varepsilon_{\alpha\beta}^{A}h_{i,\alpha\beta}^{m}w_{i,\alpha\beta}\vec{\nabla}\left(\rho_{\alpha\beta}\right)\cdot\vec{v}_{\alpha\beta}+\varepsilon_{\beta r}^{A}\varepsilon_{\alpha\beta}^{A}h_{i,\alpha\beta}^{m}\rho_{\alpha\beta}\vec{\nabla}\left(w_{i,\alpha\beta}\right)\cdot\vec{v}_{\alpha\beta}+\varepsilon_{\beta r}^{A}\varepsilon_{\alpha\beta}^{A}h_{i,\alpha\beta}^{m}w_{i,\alpha\beta}\rho_{\alpha\beta}\left(\vec{\nabla}\cdot\vec{v}_{\alpha\beta}\right)\right)=$$

$$\sum_{i=1}^{NC}\left(\varepsilon_{\beta r}^{A}\varepsilon_{\alpha\beta}^{A}h_{i,\alpha\beta}^{m}w_{i,\alpha\beta}\vec{\nabla}\left(\rho_{\alpha\beta}\right)\cdot\vec{v}_{\alpha\beta}\right)+\sum_{i=1}^{NC}\varepsilon_{\beta r}^{A}\varepsilon_{\alpha\beta}^{A}h_{i,\alpha\beta}^{m}\rho_{\alpha\beta}\vec{\nabla}\left(w_{i,\alpha\beta}\right)\cdot\vec{v}_{\alpha\beta}+\sum_{i=1}^{NC}\varepsilon_{\beta r}^{A}\varepsilon_{\alpha\beta}^{A}h_{i,\alpha\beta}^{m}w_{i,\alpha\beta}\rho_{\alpha\beta}\left(\vec{\nabla}\cdot\vec{v}_{\alpha\beta}\right)=$$

$$\sum_{i=1}^{NC}\varepsilon_{\beta r}^{A}\varepsilon_{\alpha\beta}^{A}h_{i,\alpha\beta}^{m}\rho_{\alpha\beta}\vec{\nabla}\left(w_{i,\alpha\beta}\right)\cdot\vec{v}_{\alpha\beta}+\varepsilon_{\beta r}^{A}\varepsilon_{\alpha\beta}^{A}h_{i,\alpha\beta}^{m}\rho_{\alpha\beta}\left(\vec{\nabla}\cdot\vec{v}_{\alpha\beta}\right)+\varepsilon_{\beta r}^{A}\varepsilon_{\alpha\beta}^{A}h_{i\alpha\beta}^{m}\vec{\nabla}\left(\rho_{\alpha\beta}\right)\cdot\vec{v}_{\alpha\beta}=$$

$$\boxed{\sum_{i=1}^{NC}\left(\varepsilon_{\beta r}^{A}\varepsilon_{\alpha\beta}^{A}h_{i,\alpha\beta}^{m}\left(\vec{\nabla}\cdot\left(\rho_{i,\alpha\beta}\vec{v}_{\alpha\beta}\right)\right)\right)=\varepsilon_{\beta r}^{A}\varepsilon_{\alpha\beta}^{A}h_{\alpha\beta}^{m}\left(\vec{\nabla}\cdot\left(\rho_{\alpha\beta}\vec{v}_{\alpha\beta}\right)\right)+\sum_{i=1}^{NC}\left(\varepsilon_{\beta r}^{A}\varepsilon_{\alpha\beta}^{A}h_{i,\alpha\beta}^{m}\rho_{\alpha\beta}\vec{\nabla}\left(w_{i,\alpha\beta}\right)\cdot\vec{v}_{\alpha\beta}\right)}$$

$$\left\{\begin{array}{l}+\varepsilon_{\beta r}^{V}\varepsilon_{\alpha\beta}^{V}\rho_{\alpha\beta}\dfrac{\partial h_{\alpha\beta}^{m}}{\partial t}\\+\varepsilon_{\beta r}^{A}\varepsilon_{\alpha\beta}^{A}\rho_{\alpha\beta}\left(\vec{\nabla}h_{\alpha\beta}^{m}\right)\cdot\vec{v}_{\alpha\beta}\\\left(U_{\alpha\beta}^{m}-h_{\alpha\beta}^{m}\right)\left(\begin{array}{l}\varepsilon_{\beta r}^{V}\varepsilon_{\alpha\beta}^{V}\dfrac{\partial}{\partial t}\left(\rho_{\alpha\beta}\right)\\+\varepsilon_{\beta r}^{A}\varepsilon_{\alpha\beta}^{A}\left(\vec{\nabla}\cdot\left(\rho_{\alpha\beta}\vec{v}_{\alpha\beta}\right)\right)\end{array}\right)\end{array}\right\}=\left\{\begin{array}{l}-\vec{\nabla}\cdot\left(\varepsilon_{\beta r}^{A}\varepsilon_{\alpha\beta}^{A}\overrightarrow{Q_{\alpha\beta}}\right)+\varepsilon_{\beta r}^{A}\varepsilon_{\alpha\beta}^{A}\left(\vec{\tau}_{\alpha\beta}:\vec{\nabla}\vec{v}_{\alpha\beta}\right)\\-\left(\sum_{i=1}^{NC}\left(\vec{\nabla}\dfrac{1}{M_{i}}h_{i,\alpha\beta}^{a}\varepsilon_{\beta r}^{A}\varepsilon_{\alpha\beta}^{A}\right)\cdot\vec{j}_{i,\alpha\beta}\right)\\-\sum_{i=1}^{NC}\left(h_{i,\alpha\beta}^{m}\varepsilon_{\beta r}^{V}\varepsilon_{\alpha\beta}^{V}\hat{R}_{i,\alpha\beta}\right)+\sum_{i=1}^{NC}\left(\dfrac{h_{i,\alpha\beta}^{a}\varepsilon_{\beta r}^{V}\varepsilon_{\alpha\beta}^{V}\rho_{\alpha\beta}}{M_{i}}\dfrac{\partial w_{i,\alpha\beta}}{\partial t}\right)\\+\sum_{i=1}^{NC}\left(\varepsilon_{\beta r}^{A}\varepsilon_{\alpha\beta}^{A}h_{i,\alpha\beta}^{m}\rho_{\alpha\beta}\vec{\nabla}\left(w_{i,\alpha\beta}\right)\cdot\vec{v}_{\alpha\beta}\right)\\+\varepsilon_{\beta r}^{V}\varepsilon_{\alpha\beta}^{V}\dfrac{\partial P_{\alpha\beta}}{\partial t}+\varepsilon_{\beta r}^{A}\varepsilon_{\alpha\beta}^{A}\vec{\nabla}\left(P_{\alpha\beta}\right)\cdot\left(\vec{v}_{\alpha\beta}\right)\end{array}\right\}$$

$$\left\{\begin{array}{l}+\varepsilon_{\beta r}^{V}\varepsilon_{\alpha\beta}^{V}\rho_{\alpha\beta}\dfrac{\partial h_{\alpha\beta}^{m}}{\partial t}\\ +\varepsilon_{\beta r}^{A}\varepsilon_{\alpha\beta}^{A}\rho_{\alpha\beta}\left(\vec{\nabla}h_{\alpha\beta}^{m}\right)\cdot\vec{v}_{\alpha\beta}\\ \left(-\dfrac{P_{\alpha\beta}}{\rho_{\alpha\beta}}\right)\left(\begin{array}{l}\varepsilon_{\beta r}^{V}\varepsilon_{\alpha\beta}^{V}\dfrac{\partial}{\partial t}\left(\rho_{\alpha\beta}\right)\\ +\varepsilon_{\beta r}^{A}\varepsilon_{\alpha\beta}^{A}\left(\vec{\nabla}\cdot\left(\rho_{\alpha\beta}\vec{v}_{\alpha\beta}\right)\right)\end{array}\right)\end{array}\right\}=\left\{\begin{array}{l}-\vec{\nabla}\cdot\left(\varepsilon_{\beta r}^{A}\varepsilon_{\alpha\beta}^{A}\overrightarrow{Q_{\alpha\beta}}\right)+\varepsilon_{\beta r}^{A}\varepsilon_{\alpha\beta}^{A}\left(\vec{\tau}_{\alpha\beta}:\vec{\nabla}\vec{v}_{\alpha\beta}\right)\\ -\left(\sum_{i=1}^{NC}\left(\vec{\nabla}\dfrac{1}{M_i}h_{i,\alpha\beta}^{a}\varepsilon_{\beta r}^{A}\varepsilon_{\alpha\beta}^{A}\right)\cdot\vec{j}_{i,\alpha\beta}\right)\\ -\sum_{i=1}^{NC}\left(h_{i,\alpha\beta}^{m}\varepsilon_{\beta r}^{V}\varepsilon_{\alpha\beta}^{V}\hat{R}_{i,\alpha\beta}\right)+\sum_{i=1}^{NC}\left(\dfrac{h_{i,\alpha\beta}^{a}\varepsilon_{\beta r}^{V}\varepsilon_{\alpha\beta}^{V}\rho_{\alpha\beta}}{M_i}\dfrac{\partial w_{i,\alpha\beta}}{\partial t}\right)\\ +\sum_{i=1}^{NC}\left(\varepsilon_{\beta r}^{A}\varepsilon_{\alpha\beta}^{A}h_{i,\alpha\beta}^{m}\rho_{\alpha\beta}\vec{\nabla}\left(w_{i,\alpha\beta}\right)\cdot\vec{v}_{\alpha\beta}\right)\\ +\varepsilon_{\beta r}^{V}\varepsilon_{\alpha\beta}^{V}\dfrac{\partial P_{\alpha\beta}}{\partial t}+\varepsilon_{\beta r}^{A}\varepsilon_{\alpha\beta}^{A}\vec{\nabla}\left(P_{\alpha\beta}\right)\cdot\left(\vec{v}_{\alpha\beta}\right)\end{array}\right\}$$

Using total balance:

$\dfrac{\partial}{\partial t}\left(\varepsilon_{\beta r}^{V}\varepsilon_{\alpha\beta}^{V}\rho_{\alpha\beta}\right)+\vec{\nabla}\cdot\left(\varepsilon_{\beta r}^{A}\varepsilon_{\alpha\beta}^{A}\rho_{\alpha\beta}\vec{v}_{\alpha\beta}\right)=0$ to cancel out terms.

$$\left\{\begin{array}{l}+\varepsilon_{\beta r}^{V}\varepsilon_{\alpha\beta}^{V}\rho_{\alpha\beta}\dfrac{\partial h_{\alpha\beta}^{m}}{\partial t}+\varepsilon_{\beta r}^{A}\varepsilon_{\alpha\beta}^{A}\rho_{\alpha\beta}\left(\vec{\nabla}h_{\alpha\beta}^{m}\right)\cdot\vec{v}_{\alpha\beta}\\ +\vec{\nabla}\cdot\left(\varepsilon_{\beta r}^{A}\varepsilon_{\alpha\beta}^{A}\overrightarrow{Q_{\alpha\beta}}\right)+\left(\sum_{i=1}^{NC}\left(\vec{\nabla}\dfrac{1}{M_i}\bar{h}_{i,\alpha\beta}\varepsilon_{\beta r}^{A}\varepsilon_{\alpha\beta}^{A}\right)\cdot\vec{j}_{i,\alpha\beta}\right)\end{array}\right\}=\left\{\begin{array}{l}+\varepsilon_{\beta r}^{A}\varepsilon_{\alpha\beta}^{A}\left(\vec{\tau}_{\alpha\beta}:\vec{\nabla}\vec{v}_{\alpha\beta}\right)-\sum_{i=1}^{NC}\left(\hat{h}_{i,\alpha\beta}\varepsilon_{\beta r}^{V}\varepsilon_{\alpha\beta}^{V}\hat{R}_{i,\alpha\beta}\right)\\ +\sum_{i=1}^{NC}\left(\dfrac{h_{i,\alpha\beta}^{a}\varepsilon_{\beta r}^{V}\varepsilon_{\alpha\beta}^{V}\rho_{\alpha\beta}}{M_i}\dfrac{\partial w_{i,\alpha\beta}}{\partial t}\right)\\ +\sum_{i=1}^{NC}\left(\varepsilon_{\beta r}^{A}\varepsilon_{\alpha\beta}^{A}h_{i,\alpha\beta}^{m}\rho_{\alpha\beta}\vec{\nabla}\left(w_{i,\alpha\beta}\right)\cdot\vec{v}_{\alpha\beta}\right)\\ +\varepsilon_{\beta r}^{V}\varepsilon_{\alpha\beta}^{V}\dfrac{\partial P_{\alpha\beta}}{\partial t}+\varepsilon_{\beta r}^{A}\varepsilon_{\alpha\beta}^{A}\vec{\nabla}\left(P_{\alpha\beta}\right)\cdot\left(\vec{v}_{\alpha\beta}\right)\end{array}\right\}$$

Recalling:

$$\partial h_{i,\alpha\beta}^{m}\left(T_{\alpha\beta},P_{\alpha\beta}\right)=\hat{C}_{P,i}^{\alpha\beta}dT_{\alpha\beta}+\left(V_{i,\alpha\beta}^{m}-T_{\alpha\beta}\left(\frac{\partial V_{i,\alpha\beta}^{m}}{\partial T_{\alpha\beta}}\right)_{P}\right)dP_{i,\alpha\beta}$$

Expansion 3/4:

$$\rho_{\alpha\beta}\frac{\partial h_{\alpha\beta}^{m}}{\partial t}=\rho_{\alpha\beta}\frac{\partial}{\partial t}\left(\sum_{i=1}^{NC}w_{i,\alpha\beta}h_{i,\alpha\beta}^{m}\right)=\left(\sum_{i=1}^{NC}\rho_{\alpha\beta}w_{i,\alpha\beta}\frac{\partial h_{i,\alpha\beta}^{m}}{\partial t}+\rho_{\alpha\beta}h_{i,\alpha\beta}^{m}\frac{\partial w_{i,\alpha\beta}}{\partial t}\right)$$

$$\hat{C}_P^{\alpha\beta} = \sum_{i=1}^{NC} w_{i,\alpha\beta} \hat{C}_{P,i}^{\alpha\beta}$$

$$\sum_{i=1}^{NC} \rho_{\alpha\beta} w_{i,\alpha\beta} \frac{\partial h_{i,\alpha\beta}^m}{\partial t} = \sum_{i=1}^{NC} \rho_{i,\alpha\beta} \left(\hat{C}_{P,i}^{\alpha\beta} \frac{\partial T_{i,\alpha\beta}}{\partial t} + \left(V_{i,\alpha\beta}^m - T_{\alpha\beta} \left(\frac{\partial V_{i,\alpha\beta}^m}{\partial T_{\alpha\beta}} \right)_p \right) \frac{\partial P_{i,\alpha\beta}}{\partial t} \right) =$$

$$\sum_{i=1}^{NC} \left(\rho_{i,\alpha\beta} \hat{C}_{P,i}^{\alpha\beta} \frac{\partial T_{\alpha\beta}}{\partial t} + \left(1 - \rho_{i,\alpha\beta} T_{i,\alpha\beta} \left(\frac{\partial \frac{1}{\rho_{i,\alpha\beta}}}{\partial T_{\alpha\beta}} \right)_p \right) \frac{\partial P_{i,\alpha\beta}}{\partial t} \right) = \sum_{i=1}^{NC} \left(\begin{array}{l} \rho_{i,\alpha\beta} \hat{C}_{P,i}^{\alpha\beta} \frac{\partial T_{\alpha\beta}}{\partial t} \\ + \left(1 + \frac{T_{\alpha\beta}}{\rho_{i,\alpha\beta}} \left(\frac{\partial \rho_{i,\alpha\beta}}{\partial T_{\alpha\beta}} \right)_p \right) \frac{\partial P_{i,\alpha\beta}}{\partial t} \end{array} \right) =$$

$$\sum_{i=1}^{NC} \left(\rho_{i,\alpha\beta} \hat{C}_{P,i}^{\alpha\beta} \frac{\partial T_{\alpha\beta}}{\partial t} + \left(1 + \left(\frac{\partial \left(\ln\left(\rho_{i,\alpha\beta} \right) \right)}{\partial \left(\ln\left(T_{\alpha\beta} \right) \right)} \right)_p \right) \frac{\partial P_{i,\alpha\beta}}{\partial t} \right) = \left(\begin{array}{l} \sum_{i=1}^{NC} \left(\rho_{\alpha\beta} w_{i,\alpha\beta} \hat{C}_{P,i}^{\alpha\beta} \frac{\partial T_{\alpha\beta}}{\partial t} \right) \\ + \sum_{i=1}^{NC} \left(\left(1 + \left(\frac{\partial \left(\ln\left(\rho_{i,\alpha\beta} \right) \right)}{\partial \left(\ln\left(T_{\alpha\beta} \right) \right)} \right)_p \right) \frac{\partial P_{i,\alpha\beta}}{\partial t} \right) \end{array} \right) =$$

$$\rho_{\alpha\beta} \hat{C}_P^{\alpha\beta} \frac{\partial T_{\alpha\beta}}{\partial t} + \sum_{i=1}^{NC} \left(\left(1 + \left(\frac{\partial \left(\ln\left(\rho_{i,\alpha\beta} \right) \right)}{\partial \left(\ln\left(T_{\alpha\beta} \right) \right)} \right)_p \right) \frac{\partial P_{i,\alpha\beta}}{\partial t} \right)$$

$$\sum_{i=1}^{NC} \left(\left(1 + \left(\frac{\partial \left(\ln\left(\rho_{i,\alpha\beta} \right) \right)}{\partial \left(\ln\left(T_{\alpha\beta} \right) \right)} \right)_p \right) \frac{\partial P_{i,\alpha\beta}}{\partial t} \right) = \sum_{i=1}^{NC} \left(\left(\frac{\partial \left(\ln\left(\rho_{i,\alpha\beta} \right) \right)}{\partial \left(\ln\left(T_{\alpha\beta} \right) \right)} \right)_p \frac{\partial P_{i,\alpha\beta}}{\partial t} \right) + \frac{\partial P_{\alpha\beta}}{\partial t}$$

$$\boxed{\rho_{\alpha\beta} \frac{\partial h_{\alpha\beta}^m}{\partial t} = \rho_{\alpha\beta} \hat{C}_P^{\alpha\beta} \frac{\partial T_{\alpha\beta}}{\partial t} + \frac{\partial P_{\alpha\beta}}{\partial t} + \sum_{i=1}^{NC} \left(\rho_{\alpha\beta} h_{i,\alpha\beta}^m \frac{\partial w_{i,\alpha\beta}}{\partial t} \right) + \sum_{i=1}^{NC} \left(\left(\left(\frac{\partial \left(\ln\left(\rho_{i,\alpha\beta} \right) \right)}{\partial \left(\ln\left(T_{\alpha\beta} \right) \right)} \right)_p \right) \frac{\partial P_{i,\alpha\beta}}{\partial t} \right)}$$

Similarly:

$$\boxed{\rho_{\alpha\beta} \vec{\nabla} h_{\alpha\beta}^m = \rho_{\alpha\beta} \hat{C}_P^{\alpha\beta} \vec{\nabla} T_{\alpha\beta} + \vec{\nabla} P_{\alpha\beta} + \sum_{i=1}^{NC} \left(\rho_{\alpha\beta} h_{i,\alpha\beta}^m \vec{\nabla} w_{i,\alpha\beta} \right) + \sum_{i=1}^{NC} \left(\left(\left(\frac{\partial \left(\ln\left(\rho_{i,\alpha\beta} \right) \right)}{\partial \left(\ln\left(T_{\alpha\beta} \right) \right)} \right)_p \right) \vec{\nabla} P_{i,\alpha\beta} \right)}$$

And using Fourier's law from conduction: $\vec{\nabla} \cdot \left(\varepsilon_{\beta r}^A \varepsilon_{\alpha\beta}^A \overrightarrow{Q_{\alpha\beta}} \right) = \vec{\nabla} \cdot \left(\varepsilon_{\beta r}^A \varepsilon_{\alpha\beta}^A \lambda_{\alpha\beta}^h \vec{\nabla} \left(T_{\alpha\beta} \right) \right)$

Incorporating expansions, cancelling terms on each side, gives general thermal equation for phase α within domain β on a domain r volumetric.

$$\left\{\begin{array}{l}\varepsilon_{\beta r}^{V}\varepsilon_{\alpha\beta}^{V}\rho_{\alpha\beta}\hat{C}_{\mathrm{P}}^{\alpha\beta}\dfrac{\partial T_{\alpha\beta}}{\partial t} \\ +\varepsilon_{\beta r}^{A}\varepsilon_{\alpha\beta}^{A}\rho_{\alpha\beta}\left(\hat{C}_{\mathrm{P}}^{\alpha\beta}\nabla T_{\alpha\beta}\right)\cdot\vec{v}_{\alpha\beta} \\ +\varepsilon_{\beta r}^{A}\varepsilon_{\alpha\beta}^{A}\sum_{i=1}^{NC}\left(\left(\vec{\nabla}h_{\mathrm{i},\alpha\beta}^{m}\right)\cdot\vec{j}_{i,\alpha\beta}\right) \\ +\vec{\nabla}\cdot\left(\varepsilon_{\beta r}^{A}\varepsilon_{\alpha\beta}^{A}\lambda_{\alpha\beta}^{h}\vec{\nabla}\left(T_{\alpha\beta}\right)\right)\end{array}\right\}=\left\{\begin{array}{l}+\varepsilon_{\beta r}^{A}\varepsilon_{\alpha\beta}^{A}\left(\vec{\tau}_{\alpha\beta}:\vec{\nabla}\vec{v}_{\alpha\beta}\right) \\ -\sum_{i=1}^{NC}\left(h_{\mathrm{i},\alpha\beta}^{m}\varepsilon_{\beta r}^{V}\varepsilon_{\alpha\beta}^{V}\hat{R}_{\mathrm{i},\alpha\beta}\right) \\ -\varepsilon_{\beta r}^{V}\varepsilon_{\alpha\beta}^{V}\sum_{i=1}^{NC}\left(\left(\left(\dfrac{\partial\left(\ln\left(\rho_{i,\alpha\beta}\right)\right)}{\partial\left(\ln\left(T_{\alpha\beta}\right)\right)}\right)_{p}\right)\dfrac{\partial P_{i,\alpha\beta}}{\partial t}\right) \\ -\varepsilon_{\beta r}^{A}\varepsilon_{\alpha\beta}^{A}\sum_{i=1}^{NC}\left(\left(\left(\dfrac{\partial\left(\ln\left(\rho_{i,\alpha\beta}\right)\right)}{\partial\left(\ln\left(T_{\alpha\beta}\right)\right)}\right)_{p}\right)\vec{\nabla}P_{i,\alpha\beta}\right)\cdot\left(\vec{v}_{\alpha\beta}\right)\end{array}\right\}$$

As before with the mass balance, it is considered that energy flow occurs in the reactor void, catalyst void, storage void, and from the reactor vessel wall to the reactor void. Due to the proximity of phases within each domain the following assumptions are made.

$$T_{fv}=T_{sv}=T_{g}$$
$$T_{fc}=T_{sc}=T_{c}$$
$$T_{fs}=T_{ss}=T_{s}$$

Leading to a composite temperature equation in each domain. The thermal energy balance then yields for the reactor void, catalyst, and storage domains. Using these assumptions and the relations amongst mass fluxes leads to the following component equations:

$$
\begin{cases}
\left\{\begin{array}{l}
\varepsilon_{vr}^{V}\varepsilon_{fv}^{V}\rho_{fv}\hat{C}_{P}^{fv}\dfrac{\partial T_g}{\partial t} \\
+\varepsilon_{vr}^{A}\varepsilon_{fv}^{A}\rho_{fv}\left(\hat{C}_{P}^{fv}\nabla T_{fv}\right)\cdot\vec{v}_{fv} \\
+\varepsilon_{vr}^{A}\varepsilon_{fv}^{A}\sum\limits_{i=1}^{NC}\left(\left(\vec{\nabla}h_{i,fv}^{m}\right)\cdot\vec{j}_{i,fv}\right) \\
+\vec{\nabla}\cdot\left(\varepsilon_{vr}^{A}\varepsilon_{fv}^{A}\lambda_{fv}^{h}\vec{\nabla}\left(T_{fv}\right)\right)
\end{array}\right\} = \left\{\begin{array}{l}
+\varepsilon_{vr}^{A}\varepsilon_{fv}^{A}\left(\vec{\tau}_{fv}:\vec{\nabla}\vec{v}_{fv}\right)-\sum\limits_{i=1}^{NC}\left(h_{i,fv}^{m}\varepsilon_{vr}^{V}\varepsilon_{fv}^{V}\hat{R}_{i,fv}\right) \\
-\varepsilon_{vr}^{V}\varepsilon_{fv}^{V}\sum\limits_{i=1}^{NC}\left(\left(\left(\dfrac{\partial\left(\ln\left(\rho_{i,fv}\right)\right)}{\partial\left(\ln\left(T_g\right)\right)}\right)_{p}\right)\dfrac{\partial P_{i,fv}}{\partial t}\right) \\
-\varepsilon_{vr}^{A}\varepsilon_{fv}^{A}\sum\limits_{i=1}^{NC}\left(\left(\left(\dfrac{\partial\left(\ln\left(\rho_{i,fv}\right)\right)}{\partial\left(\ln\left(T_g\right)\right)}\right)_{p}\right)\vec{\nabla}P_{i,fv}\right)\cdot\left(\vec{v}_{fv}\right)
\end{array}\right\} & \text{on } \Omega_{fv} \\
q_{f-f}^{c\to v}=\varepsilon_{cr}^{I}\sum\limits_{i=1}^{NS}\left(\dfrac{\varepsilon_{fc}^{A}\tilde{h}_{i,fc}\vec{N}_{i,fc}}{M_i}\right)\Bigg|^{CS_c} & \text{on } \partial\Omega_{f,cv} \\
q_{s-f}^{c\to v}=\varepsilon_{cr}^{I}\left(\varepsilon_{sc}^{A}h_{r}^{f}\left(T_g-T_c\Big|^{CS_c}\right)\right) & \text{on } \partial\Omega_{f,cv} \\
q_{f-f}^{s\to v}=\varepsilon_{sr}^{I}\sum\limits_{i=1}^{NS}\left(\dfrac{\varepsilon_{fs}^{A}\tilde{h}_{i,fs}\vec{N}_{i,fs}}{M_i}\right)\Bigg|^{CS_s} & \text{on } \partial\Omega_{f,sv} \\
q_{s-f}^{s\to v}=\varepsilon_{sr}^{I}\left(\varepsilon_{ss}^{A}h_{r}^{f}\left(T_g-T_s\Big|^{CS_s}\right)\right) & \text{on } \partial\Omega_{f,sv} \\
q_{s-f}^{w\to v}=\dfrac{A_r h_r^{fur}}{V_r}\left(T_g-T^{fur}\right) & \text{on } \partial\Omega_{f,wv}
\end{cases}
$$

(A.1.32)

Total Reactor Thermal Energy

$$
\begin{cases}
\left\{\begin{array}{l}
\varepsilon_{cr}^{V}\varepsilon_{fc}^{V}\rho_{fc}\hat{C}_{P}^{fc}\dfrac{\partial T_c}{\partial t} \\
+\varepsilon_{cr}^{A}\varepsilon_{fc}^{A}\sum\limits_{i=1}^{NC}\left(\left(\vec{\nabla}h_{i,fc}^{m}\right)\cdot\vec{j}_{i,fc}\right) \\
+\vec{\nabla}\cdot\left(\varepsilon_{cr}^{A}\varepsilon_{fc}^{A}\lambda_{fc}^{h}\vec{\nabla}\left(T_c\right)\right)
\end{array}\right\} = \left\{\begin{array}{l}
-\sum\limits_{i=1}^{NC}\left(h_{i,fc}^{m}\varepsilon_{cr}^{V}\varepsilon_{fc}^{V}\hat{R}_{i,fc}\right) \\
-\varepsilon_{cr}^{V}\varepsilon_{fc}^{V}\sum\limits_{i=1}^{NC}\left(\left(\left(\dfrac{\partial\left(\ln\left(\rho_{i,fc}\right)\right)}{\partial\left(\ln\left(T_c\right)\right)}\right)_{p}\right)\dfrac{\partial P_{i,fc}}{\partial t}\right)
\end{array}\right\} & \text{on } \Omega_{fc} \\
q_{f-f}^{v\to c}=\varepsilon_{cr}^{I}\sum\limits_{i=1}^{NS}\left(\dfrac{\varepsilon_{fv}^{A}\tilde{h}_{i,fv}\vec{N}_{i,fv}}{M_i}\right)\Bigg|^{CS_c} & \text{on } \partial\Omega_{f,cv} \\
q_{s-f}^{v\to c}=\varepsilon_{cr}^{I}\left(\varepsilon_{sc}^{A}h_{gv}^{f}\left(T_c-T_g\Big|^{CS_c}\right)\right) & \text{on } \partial\Omega_{f,cv}
\end{cases}
$$

(A.1.33)

Total Catalyst Thermal Energy

$$\begin{Bmatrix} \begin{Bmatrix} \varepsilon_{sr}^{V}\varepsilon_{fs}^{V}\rho_{fs}\hat{C}_{P}^{fs}\dfrac{\partial T_s}{\partial t} \\ +\varepsilon_{sr}^{A}\varepsilon_{fs}^{A}\displaystyle\sum_{i=1}^{NC}\left(\left(\vec{\nabla}h_{i,fs}^{m}\right)\cdot\vec{j}_{i,fs}\right) \\ +\vec{\nabla}\cdot\left(\varepsilon_{sr}^{A}\varepsilon_{fs}^{A}\lambda_{fs}^{h}\vec{\nabla}\left(T_s\right)\right) \end{Bmatrix} = \begin{Bmatrix} -\displaystyle\sum_{i=1}^{NC}\left(h_{i,fs}^{m}\varepsilon_{sr}^{V}\varepsilon_{fs}^{V}\hat{R}_{i,fs}\right) \\ -\varepsilon_{sr}^{V}\varepsilon_{fs}^{V}\displaystyle\sum_{i=1}^{NC}\left(\left(\left(\frac{\partial\left(\ln\left(\rho_{i,sf}\right)\right)}{\partial\left(\ln\left(T_s\right)\right)}\right)_{p}\right)\frac{\partial P_{i,fs}}{\partial t}\right) \end{Bmatrix} \text{ on } \Omega_{fs} \\ q_{f-f}^{v\to s} = \varepsilon_{cr}^{I}\displaystyle\sum_{i=1}^{NS}\left(\frac{\varepsilon_{fv}^{A}\tilde{h}_{i,fv}\vec{N}_{i,fv}}{M_i}\right)\Bigg|^{CS_v} \quad \text{on } \partial\Omega_{f,vs} \\ q_{s-f}^{v\to s} = \varepsilon_{cr}^{I}\left(\varepsilon_{ss}^{A}h_{gv}^{f}\left(T_s - T_g\Big|^{CS_v}\right)\right) \quad \text{on } \partial\Omega_{f,vs} \end{Bmatrix}$$

(A.1.34)

Total Storage Thermal Energy

The equations derived in this chapter will be applied to the SR process.

A.1.5 Solution Approach

In the next chapter, the above equations will be simplified using various assumptions. In all but the first section the resultant set of equations comprise a set of non-linear partial differential equations (PDE) or partial differential algebraic equation (PDAE), where in the first section the equations are reduced to a set of non-linear ordinary differential equations (ODE). Numerical solution methods for systems of ODE's are quite plentiful and robust and an implicit backward differentiation method is used in this work. A more detailed description is given in the relevant chapter section. Numerical solutions to PDE's and PDAE's remains an area of active research and there are several approaches that can be taken[]. In this work we choose the Finite Element Method (FEM) which is based on recasting the system of PDE's in their so-called weak form and discretizing.

A.1.6 Notation

English Symbols

$a_{00,\alpha\beta}$, $a_{i0,\alpha\beta}$, $a_{0i,\alpha\beta}(\ )$: phenomenological transport coefficient.

$A_\beta\left(m^2\ domain\ \beta\right)$: area

$c_{i,\alpha\beta}\left(\frac{mol\ of\ species\ i\ in\ phase\ \alpha\ within\ domain\ \beta}{m^3\ of\ phase\ \alpha\ within\ domain\ \beta}\right)$: Concentration species i

$c_{\alpha\beta}\left(\frac{mol\ of\ phase\ \alpha\ within\ domain\ \beta}{m^3\ of\ phase\ \alpha\ within\ domain\ \beta}\right)$: Total concentration

$\bar{C}_P^{\alpha\beta}\left(\frac{J\ of\ phase\ \alpha\ within\ domain\ \beta}{(mol\cdot K)of\ phase\ \alpha\ within\ domain\ \beta}\right)$: Constant pressure heat capacity moles.

$\hat{C}_P^{\alpha\beta}\left(\frac{J\ of\ phase\ \alpha\ within\ domain\ \beta}{(g\cdot K)of\ phase\ \alpha\ within\ domain\ \beta}\right)$: Constant pressure heat capacity mass.

$\bar{C}_V^{\alpha\beta}\left(\frac{J\ of\ phase\ \alpha\ within\ domain\ \beta}{(mol\cdot K)of\ phase\ \alpha\ within\ domain\ \beta}\right)$: Constant volume heat capacity moles.

$\hat{C}_V^{\alpha\beta}\left(\frac{J\ of\ phase\ \alpha\ within\ domain\ \beta}{(g\cdot K)of\ phase\ \alpha\ within\ domain\ \beta}\right)$: Constant volume heat capacity mass.

$\hat{C}_{P,i}^{\alpha\beta}\left(\frac{J\ of\ species\ i\ in\ phase\ \alpha\ within\ domain\ \beta}{(kg\cdot K)of\ phase\ \alpha\ within\ domain\ \beta}\right)$ Constant pressure heat capacity species i

mass.

$\bar{C}_{P,i}^{\alpha\beta}\left(\frac{J\ of\ species\ i\ in\ phase\ \alpha\ within\ domain\ \beta}{(mol\cdot K)of\ phase\ \alpha\ within\ domain\ \beta}\right)$: Constant pressure heat capacity species i

mol.

$CS^\alpha\left(m^2\ of\ domain\ \alpha\right)$: control surface

$CV^{\alpha}\left(m^3\ of\ domain\ \alpha\right)$: control volume

$\vec{d}_{i,\alpha\beta}(\ )$: diffusional driving force

$d_p\ \left(m^2\right)$: Effective pore diameter

$d_{pellet}\left(m\right)$: diameter of catalyst/storage pellet.

$\vec{e}_i(\ )$: unit vector in i direction

$\vec{F}_{external}(\ )$: external forces acting in momentum balance

$F_{m,\alpha_1-\alpha}^{\beta_1-\beta}(\ )$: momentum force between domains and phases

$\hat{G}_{i,\alpha\beta}(\ )$: mass gibbs species i

$\bar{G}_{i,\alpha\beta}(\ )$: molar gibbs species i

$\vec{g}(\ )$: gravity force

$h_r^{furr}\left(\frac{J}{m^2\cdot K}\right)$: heat transfer coefficient between reactor wall

$\hat{h}_{\alpha\beta}\left(\frac{J\ \ in\ phase\ \alpha\ within\ domain\ \beta}{kg\ of\ \ phase\ \alpha\ within\ domain\ \beta}\right)$: total enthalpy mass

$\bar{h}_{\alpha\beta}\left(\frac{J\ in\ phase\ \alpha\ within\ domain\ \beta}{mol\ of\ \ phase\ \alpha\ within\ domain\ \beta}\right)$: total enthalpy moles

$\hat{h}_{i,\alpha\beta}\left(\frac{J\ of\ \ species\ i\ in\ phase\ \alpha\ within\ domain\ \beta}{kg\ of\ \ phase\ \alpha\ within\ domain\ \beta}\right)$: partial mass enthalpy species i

$\bar{h}_{i,\alpha\beta}\left(\frac{J\ of\ \ species\ i\ in\ phase\ \alpha\ within\ domain\ \beta}{mol\ of\ \ phase\ \alpha\ within\ domain\ \beta}\right)$: partial mol enthalpy species i

$\hat{h}^{IG}_{i,\alpha\beta}\left(\frac{J\ of\ \ species\ i\ in\ phase\ \alpha\ \ within\ domain\ \beta}{kg\ \ of\ \ phase\ \alpha\ \ within\ domain\ \beta}\right)$: species ideal gas partial mass enthalpy.

$\hat{h}^{R}_{i,\alpha\beta}\left(\frac{J\ of\ \ species\ i\ in\ phase\ \alpha\ \ within\ domain\ \beta}{kg\ \ of\ \ phase\ \alpha\ \ within\ domain\ \beta}\right)$: species partial residual mass enthalpy.

$\bar{h}^{0}_{i,\alpha\beta}\left(\frac{J\ of\ \ species\ i\ in\ phase\ \alpha\ \ within\ domain\ \beta}{mol\ \ of\ \ phase\ \alpha\ \ within\ domain\ \beta}\right)$: reference species enthalpy moles

$\bar{h}^{F}_{i,\alpha\beta}\left(\frac{J\ of\ \ species\ i\ in\ phase\ \alpha\ \ within\ domain\ \beta}{mol\ \ of\ \ phase\ \alpha\ \ within\ domain\ \beta}\right)$: species enthalpy of formation

$\vec{\mathrm{I}}$: Identity matrix

$\vec{j}_{i,\alpha\beta}\left(\frac{kg\ of\ \ species\ i\ in\ phase\ \alpha\ \ within\ domain\ \beta}{\left(m^2\ \ of\ \ phase\ \alpha\ \ within\ domain\ \beta\right)\cdot s}\right)$: diffusive mass flux of species i in phase

α within domain β

$K_D(\ )$: ergun equation

$K_V(\ )$: ergun equation

$M_i\left(\frac{kg}{mol}\right)$:Molar mass species i

$\vec{N}_{\alpha\beta}\left(\frac{kg\ \ of\ \ phase\ \alpha\ \ within\ domain\ \beta}{\left(m^2\ \ of\ \ phase\ \alpha\ \ within\ domain\ \beta\right)\cdot s}\right)$: total mass flux of phase α within domain β

$\vec{N}^{\dagger}_{\alpha\beta}\left(\frac{mol\ of\ \ phase\ \alpha\ \ within\ domain\ \beta}{\left(m^2\ \ of\ \ phase\ \alpha\ \ within\ domain\ \beta\right)\cdot s}\right)$: total molar flux of phase α within domain β

$\vec{N}_{\alpha,\beta_1\beta_2}(\ )$: boundary flux between domains mass

$\vec{N}^{\dagger}_{\alpha,\beta_1\beta_2}(\ )$: boundary flux between domains mol

$\overrightarrow{N}_{i,\alpha\beta}\left(\frac{kg\ of\ \ species\ i\ in\ phase\ \alpha\ \ within\ domain\ \beta}{\left(m^2\ \ of\ \ phase\ \alpha\ \ within\ domain\ \beta\right)\cdot s}\right)$: total mass flux of species i in phase α within domain β

$\overrightarrow{N}^{\dagger}_{i,\alpha\beta}\left(\frac{mol\ of\ \ species\ i\ in\ phase\ \alpha\ \ within\ domain\ \beta}{\left(m^2\ \ of\ \ phase\ \alpha\ \ within\ domain\ \beta\right)\cdot s}\right)$: total molar flux of species i in phase α within domain β

$\overrightarrow{N}^{\beta_1-\beta_2\ \dagger}_{\alpha,i}\left(\frac{mol}{m^2\cdot s}\right)$: molar flux between domains

$n_{\alpha\beta}(\ )$: moles

$\vec{n}(\ )$: normal vector

$P_{\alpha\beta}\left(Pa\ in\ phase\ \alpha\ \ within\ domain\ \beta\right)$: Pressure

$P_{i,\alpha\beta}\left(Pa\ of\ \ species\ i\ in\ phase\ \alpha\ \ within\ domain\ \beta\right)$: partial pressure species i

$P_{i,perm}\left(\frac{mol\ i}{Pa\cdot m^2\cdot s}\right)$: i_{th} species permeance through storage medium permselective layer

$\overrightarrow{Q_{\alpha\beta}}\left(\frac{J\ \ in\ phase\ \alpha\ \ within\ domain\ \beta}{\left(m^3\ \ of\ \ phase\ \alpha\ \ within\ domain\ \beta\right)\cdot s}\right)$: heat conduction

$q^{\beta_1\rightarrow\beta}_{\alpha_1-\alpha}\left(\frac{J}{m^3\cdot s}\right)$: heat transfer between phases

$q^{n}_{\alpha\beta}\left(\frac{J\ \ in\ phase\ \alpha\ \ within\ domain\ \beta}{\left(m^3\ \ of\ \ phase\ \alpha\ \ within\ domain\ \beta\right)\cdot s}\right)$: heat transfer modes

$r_c(m)$: catalyst radius

$r_s(m)$: storage radius

$R\left(\frac{J}{mol \cdot K}\right)$: Gas Constant

$\hat{R}_{i,\alpha\beta}\left(\frac{kg\ of\ \ species\ i\ in\ phase\ \alpha\ within\ domain\ \beta}{\left(m^3\ \ of\ \ phase\ \alpha\ within\ domain\ \beta\right)\cdot s}\right)$: species i generation rate by mass

$\bar{R}_{i,\alpha\beta}\left(\frac{mol\ of\ \ species\ i\ in\ phase\ \alpha\ within\ domain\ \beta}{\left(m^3\ \ of\ \ phase\ \alpha\ within\ domain\ \beta\right)\cdot s}\right)$: species i generation rate by mol

$\hat{S}_{\alpha\beta}(\ )$: mass entropy

$\vec{\vec{T}}_{\alpha\beta}\left(\frac{N\ of\ \ phase\ \alpha\ within\ domain\ \beta}{m^2\ of\ \ phase\ \alpha\ within\ domain\ \beta}\right)$: Fluid momentum stress tensor

$T^{fur}(K)$: Wall temperature

$T_{\alpha\beta}\left(K\ of\ \ phase\ \alpha\ within\ domain\ \beta\right)$: Temperature

$t(s)$: time

$\bar{U}_{\alpha\beta}\left(\frac{J\ \ in\ phase\ \alpha\ within\ domain\ \beta}{mol\ of\ \ phase\ \alpha\ within\ domain\ \beta}\right)$: total internal energy mass

$\hat{U}_{\alpha\beta}\left(\frac{J\ \ in\ phase\ \alpha\ within\ domain\ \beta}{kg\ of\ \ phase\ \alpha\ within\ domain\ \beta}\right)$: total internal energy mol.

$\vec{v}_{i,\alpha\beta}\left(\frac{m\ of\ species\ i\ in\ phase\ \alpha\ within\ domain\ \beta}{s}\right)$: velocity of species i in phase α within domain β

$\vec{v}_{\alpha\beta}\left(\frac{m\ of\ \ phase\ \alpha\ within\ domain\ \beta}{s}\right)$: mass average velocity of phase α within domain β

$\vec{v}^{\dagger}_{\alpha\beta}\left(\frac{m\ of\ \ phase\ \alpha\ within\ domain\ \beta}{s}\right)$: molar average velocity of phase α within domain β

$\hat{V}_{\alpha\beta}(\ )$: mass volume

$\bar{V}_{\alpha\beta}(\ )$: molar volume

$V_{\beta}\left(m^3\ domain\ \beta\right)$: volume

$W_{\alpha\beta}(\ )$: work done on

W_{ext}

$w_{i,\alpha\beta}\left(\frac{kg\ of\ \ species\ i\ in\ \ phase\ \alpha\ \ within\ domain\ \beta}{kg\ of\ \ phase\ \alpha\ \ within\ domain\ \beta}\right)$ mass fraction of species i in phase α within domain β

$x_{i,\alpha\beta}\left(\frac{mol\ of\ \ species\ i\ in\ \ phase\ \alpha\ \ within\ domain\ \beta}{mol\ of\ \ phase\ \alpha\ \ within\ domain\ \beta}\right)$ mol fraction of species i in phase α within domain β

x_i, $i=1,2,3$: cartesian component for vector operations

$z(m)$: axial length of reactor

Greek Symbols

$\alpha \in \{s, f\}$: phase α, where $\{s, f\}$ denote the solid and fluid phases respectively;

$\beta \in \{c,s,v,w,r\}$: domain β, where $\{c,s,v,w,r\}$ denote the catalyst pellet, storage pellet, reactor void unoccupied by either catalyst or storage pellets, reactor wall, and total reactor domains.

$\varepsilon_{\alpha\beta}^{A}\left(\frac{m^2\ of\ \ phase\ \alpha}{m^2\ of\ \ domain\ \beta}\right)$: control surface fraction of phase α in domain β

$\varepsilon_{\alpha\beta}^{V}\left(\frac{m^3\ of\ \ phase\ \alpha\ within\ domain\ \beta}{m^3\ of\ \ domain\ \beta}\right)$: control volume fraction of phase α in domain β

$\varepsilon_{\beta r}^{A}\left(\frac{m^2\ of\ \ domain\ \beta}{m^2\ of\ \ domain\ r}\right)$: control surface fraction of domain β in domain r

$\varepsilon_{\beta r}^{V}\left(\frac{m^3\ of\ \ domain\ \beta}{m^3\ of\ \ domain\ r}\right)$: control volume fraction of domain β in domain r

$\varepsilon_{\alpha\beta}^{I}$: Interfacial area

$\rho_{i,\alpha\beta}\left(\frac{kg\ of\ \ species\ i\ in\ \ phase\ \alpha\ within\ domain\ \beta}{m^3\ of\ \ phase\ \alpha\ within\ domain\ \beta}\right)$ mass density of species i in phase α within domain β

$\rho_{\alpha\beta}\left(\frac{kg\ of\ \ phase\ \alpha\ within\ domain\ \beta}{m^3\ of\ \ phase\ \alpha\ within\ domain\ \beta}\right)$ mass density of phase α within domain β

$\kappa_{\alpha\beta}\left(\frac{kg\ of\ \ phase\ \alpha\ within\ domain\ \beta}{(m\ of\ \ phase\ \alpha\ within\ domain\ \beta)\cdot s}\right)$: Dilatational viscosity

$\mu_{i,\alpha\beta}\left(\frac{kg\ species\ i\ in\ phase\ \alpha\ within\ domain\ \beta}{(m\ of\ \ phase\ \alpha\ within\ domain\ \beta)\cdot s}\right)$: viscosity of

$\mu_{\alpha\beta}\left(\frac{kg\ of\ \ phase\ \alpha\ within\ domain\ \beta}{(m\ of\ \ phase\ \alpha\ within\ domain\ \beta)\cdot s}\right)$: viscosity

$\lambda_{jk}^{h}\left(\frac{J}{m\cdot K}\right)$: thermal conductivity

$\lambda_{r}^{fur}\left(\frac{J}{m\cdot K}\right)$: thermal conductivity between reactor and wall

$\vec{\tau}_{\alpha\beta}\left(\frac{(N\cdot m)of\ \ phase\ \alpha\ within\ domain\ \beta}{m\ of\ \ phase\ \alpha\ within\ domain\ \beta}\right)$: fluid viscous stress tensor

$\chi_{\alpha\beta}(\ )$:combined viscosity and dilatational viscosity

$\vec{\varpi}_{\alpha\beta}(\ )$: normal stress on surface of fluid

$\Omega_{\alpha\beta}(\ )$: domain

$\partial\Omega_{\alpha,\beta_1\beta_2}(\ )$: boundary for phase α between domains β_1 and β_2

Appendix A.2 – Energy Balance Gradient

Expand kinetic energy gradient term:

$$\vec{\nabla}\cdot\left(\varepsilon_{\beta r}^{A}\varepsilon_{\alpha\beta}^{A}\frac{\rho_{\alpha\beta}}{2}\left|\vec{v}_{\alpha\beta}\right|^{2}\vec{v}_{\alpha\beta}\right)=\vec{\nabla}\cdot\left(\varepsilon_{\beta r}^{A}\varepsilon_{\alpha\beta}^{A}\frac{\rho_{\alpha\beta}}{2}\vec{v}_{\alpha\beta}\left|v_{\alpha\beta}\right|^{2}\right)=$$

$$\left(\sum_{\varpi_1=1}^{3}\vec{e}_{\varpi_1}\frac{\partial}{\partial x_{\varpi_1}}\right)\cdot\left(\varepsilon_{\beta r}^{A}\varepsilon_{\alpha\beta}^{A}\frac{\rho_{\alpha\beta}}{2}\sum_{\varpi_3=1}^{3}\vec{e}_{\varpi_3}v_{\varpi_3,\alpha\beta}\right)\left(\sum_{\varpi_2=1}^{3}\sum_{\varpi_4=1}^{3}e_{\varpi_2}\cdot e_{\varpi_4}v_{\varpi_2,\alpha\beta}v_{\varpi_4,\alpha\beta}\right)=$$

$$\sum_{\varpi_1=1}^{3}\sum_{\varpi_3=1}^{3}\sum_{\varpi_2=1}^{3}\sum_{\varpi_4=1}^{3}\left(\vec{e}_{\varpi_1}\cdot\vec{e}_{\varpi_3}\right)\left(\vec{e}_{\varpi_2}\cdot\vec{e}_{\varpi_4}\right)\frac{\partial}{\partial x_{\varpi_1}}\left(\varepsilon_{\beta r}^{A}\varepsilon_{\alpha\beta}^{A}\frac{\rho_{\alpha\beta}}{2}v_{\varpi_3,\alpha\beta}v_{\varpi_2,\alpha\beta}v_{\varpi_4,\alpha\beta}\right)=$$

$$\frac{\varepsilon_{\beta r}^{A}\varepsilon_{\alpha\beta}^{A}}{2}\sum_{\varpi_1=1}^{3}\sum_{\varpi_3=1}^{3}\sum_{\varpi_2=1}^{3}\sum_{\varpi_4=1}^{3}\delta_{\varpi_1\varpi_3}\delta_{\varpi_2\varpi_4}\left(\begin{array}{l}\rho_{\alpha\beta}v_{\varpi_3,\alpha\beta}v_{\varpi_2,\alpha\beta}\dfrac{\partial v_{\varpi_4,\alpha\beta}}{\partial x_{\varpi_1}}+\rho_{\alpha\beta}v_{\varpi_4,\alpha\beta}v_{\varpi_2,\alpha\beta}\dfrac{\partial v_{\varpi_3,\alpha\beta}}{\partial x_{\varpi_1}}\\ +\rho_{\alpha\beta}v_{\varpi_4,\alpha\beta}v_{\varpi_3,\alpha\beta}\dfrac{\partial v_{\varpi_2,\alpha\beta}}{\partial x_{\varpi_1}}+v_{\varpi_3,\alpha\beta}v_{\varpi_2,\alpha\beta}v_{\varpi_4,\alpha\beta}\dfrac{\partial\rho_{\alpha\beta}}{\partial x_{\varpi_1}}\end{array}\right)=$$

$$\frac{\varepsilon_{\beta r}^{A}\varepsilon_{\alpha\beta}^{A}}{2}\sum_{\varpi_1=1}^{3}\sum_{\varpi_2=1}^{3}\left(\begin{array}{l}\rho_{\alpha\beta}v_{\varpi_1,\alpha\beta}v_{\varpi_2,\alpha\beta}\dfrac{\partial v_{\varpi_2,\alpha\beta}}{\partial x_{\varpi_1}}+\rho_{\alpha\beta}v_{\varpi_2,\alpha\beta}v_{\varpi_2,\alpha\beta}\dfrac{\partial v_{\varpi_1,\alpha\beta}}{\partial x_{\varpi_1}}\\ +\rho_{\alpha\beta}v_{\varpi_2,\alpha\beta}v_{\varpi_1,\alpha\beta}\dfrac{\partial v_{\varpi_2,\alpha\beta}}{\partial x_{\varpi_1}}+v_{\varpi_1,\alpha\beta}v_{\varpi_2,\alpha\beta}v_{\varpi_2,\alpha\beta}\dfrac{\partial\rho_{\alpha\beta}}{\partial x_{\varpi_1}}\end{array}\right)\qquad\text{(A.2.1)}$$

Therefore, need to show that:

$$\left\{\begin{array}{l}\left(\sum_{\varpi_1=1}^{3}\sum_{\varpi_2=1}^{3} v_{\varpi_1,\alpha\beta}v_{\varpi_1,\alpha\beta}v_{\varpi_2,\alpha\beta}\dfrac{\partial\left(\varepsilon_{\beta r}^{A}\varepsilon_{\alpha\beta}^{A}\rho_{\alpha\beta}\right)}{\partial x_{\varpi_2}}\right)\\ +\left(\sum_{\varpi_1=1}^{3}\sum_{\varpi_2=1}^{3} v_{\varpi_1,\alpha\beta}\rho_{\alpha\beta}\dfrac{\partial\left(\varepsilon_{\beta r}^{A}\varepsilon_{\alpha\beta}^{A}v_{\varpi_2,\alpha\beta}v_{\varpi_1,\alpha\beta}\right)}{\partial x_{\varpi_2}}\right)\\ -\left(\sum_{\varpi_1=1}^{3}\sum_{\varpi_2=1}^{3}\varepsilon_{\beta r}^{A}\varepsilon_{\alpha\beta}^{A}\dfrac{v_{\varpi_1,\alpha\beta}v_{\varpi_1,\alpha\beta}}{2}\dfrac{\partial\rho_{\alpha\beta}}{\partial x_{\varpi_2}}v_{\varpi_2,\alpha\beta}\right)\\ -\left(\sum_{\varpi_1=1}^{3}\sum_{\varpi_2=1}^{3}\varepsilon_{\beta r}^{A}\varepsilon_{\alpha\beta}^{A}\dfrac{v_{\varpi_1,\alpha\beta}v_{\varpi_1,\alpha\beta}\rho_{\alpha\beta}}{2}\dfrac{\partial v_{\varpi_2,\alpha\beta}}{\partial x_{\varpi_2}}\right)\end{array}\right\}=\frac{\varepsilon_{\beta r}^{A}\varepsilon_{\alpha\beta}^{A}}{2}\sum_{\varpi_1=1}^{3}\sum_{\varpi_2=1}^{3}\left(\begin{array}{l}\rho_{\alpha\beta}v_{\varpi_1,\alpha\beta}v_{\varpi_2,\alpha\beta}\dfrac{\partial v_{\varpi_2,\alpha\beta}}{\partial x_{\varpi_1}}\\ +\rho_{\alpha\beta}v_{\varpi_2,\alpha\beta}v_{\varpi_2,\alpha\beta}\dfrac{\partial v_{\varpi_1,\alpha\beta}}{\partial x_{\varpi_1}}\\ +\rho_{\alpha\beta}v_{\varpi_2,\alpha\beta}v_{\varpi_1,\alpha\beta}\dfrac{\partial v_{\varpi_2,\alpha\beta}}{\partial x_{\varpi_1}}\\ +v_{\varpi_1,\alpha\beta}v_{\varpi_2,\alpha\beta}v_{\varpi_2,\alpha\beta}\dfrac{\partial\rho_{\alpha\beta}}{\partial x_{\varpi_1}}\end{array}\right)$$

$$\left\{\begin{array}{l}\left(\sum_{\varpi_1=1}^{3}\sum_{\varpi_2=1}^{3} v_{\varpi_1,\alpha\beta}v_{\varpi_1,\alpha\beta}v_{\varpi_2,\alpha\beta}\dfrac{\partial\left(\varepsilon_{\beta r}^{A}\varepsilon_{\alpha\beta}^{A}\rho_{\alpha\beta}\right)}{\partial x_{\varpi_2}}\right)\\ +\left(\sum_{\varpi_1=1}^{3}\sum_{\varpi_2=1}^{3} v_{\varpi_1,\alpha\beta}v_{\varpi_1,\alpha\beta}\rho_{\alpha\beta}\dfrac{\partial\left(\varepsilon_{\beta r}^{A}\varepsilon_{\alpha\beta}^{A}v_{\varpi_2,\alpha\beta}\right)}{\partial x_{\varpi_2}}\right)\\ +\left(\sum_{\varpi_1=1}^{3}\sum_{\varpi_2=1}^{3} v_{\varpi_1,\alpha\beta}v_{\varpi_2,\alpha\beta}\rho_{\alpha\beta}\dfrac{\partial\left(\varepsilon_{\beta r}^{A}\varepsilon_{\alpha\beta}^{A}v_{\varpi_1,\alpha\beta}\right)}{\partial x_{\varpi_2}}\right)\\ -\left(\sum_{\varpi_1=1}^{3}\sum_{\varpi_2=1}^{3}\varepsilon_{\beta r}^{A}\varepsilon_{\alpha\beta}^{A}\dfrac{v_{\varpi_1,\alpha\beta}v_{\varpi_1,\alpha\beta}}{2}\dfrac{\partial\rho_{\alpha\beta}}{\partial x_{\varpi_2}}v_{\varpi_2,\alpha\beta}\right)\\ -\left(\sum_{\varpi_1=1}^{3}\sum_{\varpi_2=1}^{3}\varepsilon_{\beta r}^{A}\varepsilon_{\alpha\beta}^{A}\dfrac{v_{\varpi_1,\alpha\beta}v_{\varpi_1,\alpha\beta}\rho_{\alpha\beta}}{2}\dfrac{\partial v_{\varpi_2,\alpha\beta}}{\partial x_{\varpi_2}}\right)\end{array}\right\}=\frac{\varepsilon_{\beta r}^{A}\varepsilon_{\alpha\beta}^{A}}{2}\sum_{\varpi_1=1}^{3}\sum_{\varpi_2=1}^{3}\left(\begin{array}{l}\rho_{\alpha\beta}v_{\varpi_1,\alpha\beta}v_{\varpi_2,\alpha\beta}\dfrac{\partial v_{\varpi_2,\alpha\beta}}{\partial x_{\varpi_1}}\\ +\rho_{\alpha\beta}v_{\varpi_2,\alpha\beta}v_{\varpi_2,\alpha\beta}\dfrac{\partial v_{\varpi_1,\alpha\beta}}{\partial x_{\varpi_1}}\\ +\rho_{\alpha\beta}v_{\varpi_2,\alpha\beta}v_{\varpi_1,\alpha\beta}\dfrac{\partial v_{\varpi_2,\alpha\beta}}{\partial x_{\varpi_1}}\\ +v_{\varpi_1,\alpha\beta}v_{\varpi_2,\alpha\beta}v_{\varpi_2,\alpha\beta}\dfrac{\partial\rho_{\alpha\beta}}{\partial x_{\varpi_1}}\end{array}\right)$$

$$\left\{\begin{array}{l}\left(\sum_{\varpi_1=1}^{3}\sum_{\varpi_2=1}^{3}\varepsilon_{\beta r}^{A}\varepsilon_{\alpha\beta}^{A}v_{\varpi_1,\alpha\beta}v_{\varpi_1,\alpha\beta}v_{\varpi_2,\alpha\beta}\frac{\partial\rho_{\alpha\beta}}{\partial x_{\varpi_2}}\right)\\ -\left(\sum_{\varpi_1=1}^{3}\sum_{\varpi_2=1}^{3}\varepsilon_{\beta r}^{A}\varepsilon_{\alpha\beta}^{A}\frac{v_{\varpi_1,\alpha\beta}v_{\varpi_1,\alpha\beta}v_{\varpi_2,\alpha\beta}}{2}\frac{\partial\rho_{\alpha\beta}}{\partial x_{\varpi_2}}\right)\\ +\left(\sum_{\varpi_1=1}^{3}\sum_{\varpi_2=1}^{3}\varepsilon_{\beta r}^{A}\varepsilon_{\alpha\beta}^{A}v_{\varpi_1,\alpha\beta}v_{\varpi_1,\alpha\beta}\rho_{\alpha\beta}\frac{\partial v_{\varpi_2,\alpha\beta}}{\partial x_{\varpi_2}}\right)\\ +\left(\sum_{\varpi_1=1}^{3}\sum_{\varpi_2=1}^{3}\varepsilon_{\beta r}^{A}\varepsilon_{\alpha\beta}^{A}v_{\varpi_1,\alpha\beta}v_{\varpi_2,\alpha\beta}\rho_{\alpha\beta}\frac{\partial v_{\varpi_1,\alpha\beta}}{\partial x_{\varpi_2}}\right)\\ -\left(\sum_{\varpi_1=1}^{3}\sum_{\varpi_2=1}^{3}\varepsilon_{\beta r}^{A}\varepsilon_{\alpha\beta}^{A}\frac{v_{\varpi_1,\alpha\beta}v_{\varpi_1,\alpha\beta}\rho_{\alpha\beta}}{2}\frac{\partial v_{\varpi_2,\alpha\beta}}{\partial x_{\varpi_2}}\right)\end{array}\right\}=\frac{\varepsilon_{\beta r}^{A}\varepsilon_{\alpha\beta}^{A}}{2}\sum_{\varpi_1=1}^{3}\sum_{\varpi_2=1}^{3}\left(\begin{array}{l}\rho_{\alpha\beta}v_{\varpi_1,\alpha\beta}v_{\varpi_2,\alpha\beta}\frac{\partial v_{\varpi_2,\alpha\beta}}{\partial x_{\varpi_1}}\\ +\rho_{\alpha\beta}v_{\varpi_2,\alpha\beta}v_{\varpi_2,\alpha\beta}\frac{\partial v_{\varpi_1,\alpha\beta}}{\partial x_{\varpi_1}}\\ +\rho_{\alpha\beta}v_{\varpi_2,\alpha\beta}v_{\varpi_1,\alpha\beta}\frac{\partial v_{\varpi_2,\alpha\beta}}{\partial x_{\varpi_1}}\\ +v_{\varpi_1,\alpha\beta}v_{\varpi_2,\alpha\beta}v_{\varpi_2,\alpha\beta}\frac{\partial\rho_{\alpha\beta}}{\partial x_{\varpi_1}}\end{array}\right)$$

$$\left\{\begin{array}{l}\left(\sum_{\varpi_1=1}^{3}\sum_{\varpi_2=1}^{3}\varepsilon_{\beta r}^{A}\varepsilon_{\alpha\beta}^{A}\frac{v_{\varpi_1,\alpha\beta}v_{\varpi_1,\alpha\beta}v_{\varpi_2,\alpha\beta}}{2}\frac{\partial\rho_{\alpha\beta}}{\partial x_{\varpi_2}}\right)+\\ \left(\sum_{\varpi_1=1}^{3}\sum_{\varpi_2=1}^{3}\varepsilon_{\beta r}^{A}\varepsilon_{\alpha\beta}^{A}v_{\varpi_1,\alpha\beta}v_{\varpi_2,\alpha\beta}\rho_{\alpha\beta}\frac{\partial v_{\varpi_1,\alpha\beta}}{\partial x_{\varpi_2}}\right)+\\ \left(\sum_{\varpi_1=1}^{3}\sum_{\varpi_2=1}^{3}\varepsilon_{\beta r}^{A}\varepsilon_{\alpha\beta}^{A}\frac{v_{\varpi_1,\alpha\beta}v_{\varpi_1,\alpha\beta}\rho_{\alpha\beta}}{2}\frac{\partial v_{\varpi_2,\alpha\beta}}{\partial x_{\varpi_2}}\right)\end{array}\right\}=\frac{\varepsilon_{\beta r}^{A}\varepsilon_{\alpha\beta}^{A}}{2}\sum_{\varpi_1=1}^{3}\sum_{\varpi_2=1}^{3}\left(\begin{array}{l}v_{\varpi_1,\alpha\beta}v_{\varpi_2,\alpha\beta}v_{\varpi_2,\alpha\beta}\frac{\partial\rho_{\alpha\beta}}{\partial x_{\varpi_1}}+\\ 2\rho_{\alpha\beta}v_{\varpi_2,\alpha\beta}v_{\varpi_1,\alpha\beta}\frac{\partial v_{\varpi_2,\alpha\beta}}{\partial x_{\varpi_1}}+\\ \rho_{\alpha\beta}v_{\varpi_2,\alpha\beta}v_{\varpi_2,\alpha\beta}\frac{\partial v_{\varpi_1,\alpha\beta}}{\partial x_{\varpi_1}}\end{array}\right)$$

$$\boxed{\frac{\varepsilon_{\beta r}^{A}\varepsilon_{\alpha\beta}^{A}}{2}\sum_{\varpi_1=1}^{3}\sum_{\varpi_2=1}^{3}\left(\begin{array}{l}v_{\varpi_1,\alpha\beta}v_{\varpi_1,\alpha\beta}v_{\varpi_2,\alpha\beta}\frac{\partial\rho_{\alpha\beta}}{\partial x_{\varpi_2}}+\\ 2\rho_{\alpha\beta}v_{\varpi_1,\alpha\beta}v_{\varpi_2,\alpha\beta}\frac{\partial v_{\varpi_1,\alpha\beta}}{\partial x_{\varpi_2}}+\\ \rho_{\alpha\beta}v_{\varpi_1,\alpha\beta}v_{\varpi_1,\alpha\beta}\frac{\partial v_{\varpi_2,\alpha\beta}}{\partial x_{\varpi_2}}\end{array}\right)=\frac{\varepsilon_{\beta r}^{A}\varepsilon_{\alpha\beta}^{A}}{2}\sum_{\varpi_1=1}^{3}\sum_{\varpi_2=1}^{3}\left(\begin{array}{l}v_{\varpi_1,\alpha\beta}v_{\varpi_2,\alpha\beta}v_{\varpi_2,\alpha\beta}\frac{\partial\rho_{\alpha\beta}}{\partial x_{\varpi_1}}+\\ 2\rho_{\alpha\beta}v_{\varpi_2,\alpha\beta}v_{\varpi_1,\alpha\beta}\frac{\partial v_{\varpi_2,\alpha\beta}}{\partial x_{\varpi_1}}+\\ \rho_{\alpha\beta}v_{\varpi_2,\alpha\beta}v_{\varpi_2,\alpha\beta}\frac{\partial v_{\varpi_1,\alpha\beta}}{\partial x_{\varpi_1}}\end{array}\right)}$$

Appendix A.3 Thermodynamic definitions and calculations

Using the following definitions:

$$\Delta G^o \triangleq \sum_{i \in NC} \nu_i \Delta G_i^o(T) \tag{A.3.1}$$

$$\sum_{i \in NC} \nu_i \Delta G_i^o(T) = \sum_{j \in P} \nu_j \left(\Delta G_j^o(T)\right) + \sum_{j \in R} \nu_j \left(\Delta G_j^o(T)\right) \tag{A.3.2}$$

$$\Delta G_i^o \triangleq \Delta H_i^o - T\Delta S_i^o \tag{A.3.3}$$

It is assumed that knowledge of ΔG_i^o can be obtained from the following:

$$\Delta H_i^0(T) = \begin{Bmatrix} 0 & \forall i \in A_E \\ H_i^0(T) - \sum_{j \in A_E \cap \Xi(i)} \frac{\psi_j}{\psi_{jm}} H_j^0(T) & \forall i \in N_S \end{Bmatrix} \tag{A.3.4}$$

$$\Delta S_i^0(T) = \begin{Bmatrix} 0 & \forall i \in A_E \\ S_i^0(T) - \sum_{j \in A_E \cap \Xi(i)} \frac{\psi_j}{\psi_{jm}} S_j^0(T) & \forall i \in N_S \end{Bmatrix} \tag{A.3.5}$$

Where A_E denotes the set of Atomic Elements, the function $\Xi(i)$ maps elements of N_S and creates the set of constituent atomic elements, ψ_j is the amount of atoms j in species i, and ψ_{jm} is the amount of atoms present for this element in its standard state. Enthalpy and entropy are calculated using:

$$\begin{Bmatrix} H_i^0(T) - H_i^0(T_o) = \int_{T_0}^{T} C_{p,i}^o(T)\,dT & \forall i \in N_S \\ S_i^0(T) - S_i^0(T_o) = \int_{T_0}^{T} \frac{C_{p,i}^o(T)}{T}\,dT & \forall i \in N_S \end{Bmatrix} \tag{A.3.6}$$

where $C_{p,i}^o(T)$ is defined as:

$$C_{p,i}^o(T)/R = \begin{pmatrix} a_{1,i}(T)T^{-2} + a_{2,i}(T)T^{-1} + a_{3,i}(T) \\ +a_{4,i}(T)T + a_{5,i}(T)T^2 + a_{6,i}(T)T^3 + a_{7,i}(T)T^4 \end{pmatrix} \quad \forall i \in N_S \tag{A.3.7}$$

And carrying out integration

$$\frac{H_i^0(T)}{RT}-\frac{H_i^0(T_o)}{RT}=\left(\begin{array}{l}-a_{1,i}(T)T^{-2}+a_{2,i}(T)\dfrac{\ln T}{T}+a_{3,i}(T)+a_{4,i}(T)\dfrac{T}{2}+\\ +a_{5,i}(T)\dfrac{T^2}{3}+a_{6,i}(T)\dfrac{T^3}{4}+a_{7,i}(T)\dfrac{T^4}{5}+\dfrac{b_{1,i(T)}}{T}\end{array}\right) \tag{A.3.8}$$

$$\frac{S_i^0(T)}{R}-\frac{S_i^0(T_o)}{R}=\left(\begin{array}{l}-a_{1,i}(T)\dfrac{T^{-2}}{2}+a_{2,i}(T)T^{-1}+a_{3,i}(T)\ln(T)+a_{4,i}(T)T\\ +a_{5,i}(T)\dfrac{T^2}{2}+a_{6,i}(T)\dfrac{T^3}{3}+a_{7,i}(T)\dfrac{T^4}{4}+b_{2,i(T)}\end{array}\right) \tag{A.3.9}$$

Where integration constants $b_{1,i}(T)$ and $b_{2,i}(T)$ have been added for increased accuracy over a range of temperatures. Embedded in these formulations on the heats of vaporization and fusion. The equation for calculating ΔG_i^o for each species is then:

$$\Delta G_i^o(T)=\left\{\begin{array}{l}RT\left(\begin{array}{l}-a_{1,i}(T)T^{-2}+a_{2,i}(T)\dfrac{\ln T}{T}+a_{3,i}(T)+a_{4,i}(T)\dfrac{T}{2}+\\ +a_{5,i}(T)\dfrac{T^2}{3}+a_{6,i}(T)\dfrac{T^3}{4}+a_{7,i}(T)\dfrac{T^4}{5}+\dfrac{b_{1,i(T)}}{T}\end{array}\right)\\ -RT\left(\begin{array}{l}-a_{1,i}(T)\dfrac{T^{-2}}{2}+a_{2,i}(T)T^{-1}+a_{3,i}(T)\ln(T)+a_{4,i}(T)T\\ +a_{5,i}(T)\dfrac{T^2}{2}+a_{6,i}(T)\dfrac{T^3}{3}+a_{7,i}(T)\dfrac{T^4}{4}+b_{2,i(T)}\end{array}\right)\\ -\left(\displaystyle\sum_{j\in A_E\cap i}\frac{\psi_j}{\psi_{jm}}\lambda_j\right)\end{array}\right\}\ \forall i\in NS \tag{A.3.10}$$

$$\lambda_j = \begin{bmatrix} RT\left(\begin{array}{l} -a_{1,j}(T)T^{-2} + a_{2,j}(T)\dfrac{\ln T}{T} + a_{3,j}(T) + a_{4,j}(T)\dfrac{T}{2} + \\ +a_{5,j}(T)\dfrac{T^2}{3} + a_{6,j}(T)\dfrac{T^3}{4} + a_{7,j}(T)\dfrac{T^4}{5} + \dfrac{b_{1,j(T)}}{T} \end{array}\right) \\ -RT\left(\begin{array}{l} -a_{1,j}(T)\dfrac{T^{-2}}{2} + a_{2,j}(T)T^{-1} + a_{3,j}(T)\ln(T) + a_{4,j}(T)T \\ +a_{5,j}(T)\dfrac{T^2}{2} + a_{6,j}(T)\dfrac{T^3}{3} + a_{7,j}(T)\dfrac{T^4}{4} + b_{2,j(T)} \end{array}\right) \end{bmatrix} \quad \forall j \in \Xi(i),\ \forall i \in NS$$

(A.3.11)

Appendix A.4 – Equilibrium Calculation Methodology Validation

For a fixed temperature and pressure, the total Gibbs Free energy, $G^t\left(\{n_i\}_{i=1}^{NC}\right)_{T,P}$, at equilibrium takes on its minimum value. To calculate conversion and by proxy the mol fraction of each species in the mixture, the Gibbs/Duhem relation is used, along with the definition of partial molar property and extent of reaction:

$$\left\{\begin{array}{l} d\left(nG^t\right) = \left(n\bar{V}\right)dP - \left(nT\right)dS + \sum_{i=1}^{NC}\mu_i dn_i \\ \mu_i \triangleq \left[\dfrac{\partial\left(nG^t\right)}{\partial n_i}\right]_{T,P,n_j} \end{array}\right\} \tag{A.4.1}$$

where NC is the number of chemical species and μ_i is the chemical potential of species i. The total moles may not be conserved in a chemical reaction, but total number of atoms always are, thus the atomic mass balance constraint based on initial conditions can be formulated as:

$$\sum_{i=1}^{NC}\left(n_i a_{i,k}\right) - A_{E_k} = 0 \quad \forall k = 1,...,\#\left(A_E\right) \tag{A.4.2}$$

Where A_E denotes the set of atomic elements that make up all species present, A_{E_k} is the kth element of the set A_E, n_i is the amount of moles present for species i, and $a_{i,k}$ is the amount of k atoms present in species i. As an illustrative example, for a mixture containing CO, CO_2, H_2 and H_2O, where initially 1 mol of H_2O and 1 mol of CO are present: $A_E \triangleq \{C, H, O\}$

$$\left\{\begin{array}{ll} n_{CO}+n_{CO_2}-1=0 & \text{carbon balance} \\ 2n_{H_2}+2n_{H_2O}-2= & \text{hydrogen balance} \\ n_{CO}+2n_{CO_2}+n_{H_2O}-2=0 & \text{oxygen balance} \end{array}\right\}$$

The minimization problem is then formulated as:

$$\left\{\begin{array}{l} \min\limits_{n_i}\left(G^t\left(\{n_i\}_{i=1}^{NC}\right)_{T,P}\right) \\ st. \\ \sum\limits_{i=1}^{NC}\left(n_i a_{i,k}\right)-A_{E_k}=0 \quad \forall k=1,...,\#\left(A_E\right) \\ n_i \geq 0 \qquad\qquad \forall i=1,...,NC \end{array}\right\} \tag{A.4.3}$$

The non-linear program (NLP) is set up and solved using Interior Point OPTimizer (IPOPT) minimization algorithm. Three test cases are presented below and taken from[82]. In the tables, "J" refers to the results generated by a python code.

Test Case 1:

A bed of coal (pure carbon) is fed a steam and air, with a water, oxygen, and nitrogen at a molar ratio of 1:0.5:1.88. Calculate the equilibrium composition of the gas at a pressure of 20 bar and for feed temperatures of 1000,1100,1200,1300,1400, and 1500 (K).

Table 6-1: Equilibrium mol fraction calculation for test case 1

Temperature (K)	x_{CO_2} [1]	x_{CO_2} J	x_{CO} [1]	x_{CO} J	x_{H_2O} [1]	x_{H_2O} J	x_{H_2} [1]	x_{H_2} J	x_{N_2} [1]	x_{N_2} J
1000	0.143	0.142	0.112	0.112	0.121	0.122	0.138	0.137	0.486	0.487
1100	0.090	0.090	0.226	0.226	0.068	0.068	0.169	0.169	0.447	0.446
1200	0.040	0.040	0.327	0.327	0.032	0.032	0.188	0.188	0.413	0.413
1300	0.015	0.015	0.378	0.378	0.014	0.014	0.197	0.197	0.396	0.396
1400	0.005	0.005	0.398	0.398	0.006	0.006	0.201	0.201	0.390	0.390
1500	0.002	0.002	0.405	0.405	0.003	0.003	0.203	0.203	0.387	0.387

Test Case 2:

Calculate the equilibrium compositions at 1000K and 1 bar of a gas-phase system containing CH_4, H_2O, CO, CO_2,and H_2 if initially in the unreacted state 2 mol CH_4 of and 3 mol of H_2O are present.

Table 6-2: Equilibrium mol fraction calculation for test case 2

Temperature (K)	x_{CO_2} [1]	x_{CO_2} J	x_{CO} [1]	x_{CO} J	x_{H_2O} [1]	x_{H_2O} J	x_{H_2} [1]	x_{H_2} J	x_{CH_4} [1]	x_{CH_4} J
1000	0.037	0.0369	0.1743	0.174	0.0980	0.0989	0.6710	0.6699	0.0196	0.020

Test Case 3: Water gas shift at the following 7 trials $CO_{(g)} + H_2O_{(g)} \Leftrightarrow CO_{2(g)} + H_{2(g)}$:

1. Reactants 1 mol of H_2O and 1 mol of CO at a temperature of 1100 (K) and pressure of 1 bar.
2. Reactants 1 mol of H_2O and 1 mol of CO at a temperature of 1100 (K) and pressure of 10 bar.
3. Reactants 1 mol of H_2O, 1 mol of CO, and 1 mol of N_2 at a temperature of 1100 (K) and pressure of 1 bar.
4. Reactants 2 mol of H_2O and 1 mol of CO at a temperature of 1100 (K) and pressure of 1 bar.
5. Reactants 1 mol of H_2O and 2 mol of CO at a temperature of 1100 (K) and pressure of 1 bar.
6. Reactants 1 mol of H_2O, 1 mol of CO, and 1 mol of CO_2 at a temperature of 1100 (K) and pressure of 1 bar.
7. Reactants 1 mol of H_2O and 1 mol of CO at a temperature of 1650 (K) and pressure of 1 bar.

Table 6-3: Equilibrium mol fraction calculation for test case 3

Trial	x_{CO_2} [1]	x_{CO_2} J	x_{CO} [1]	x_{CO} J	x_{H_2O} [1]	x_{H_2O} J	x_{H_2} [1]	x_{H_2} J
1	0.250	0.249	0.250	0.251	0.250	0.251	0.250	0.249
2	0.250	0.249	0.250	0.251	0.250	0.251	0.250	0.249
3	0.125	0.125	0.125	0.125	0.125	0.125	0.125	0.125
4	0.222	0.222	0.111	0.112	0.444	0.445	0.222	0.222
5	0.222	0.222	0.444	0.445	0.111	0.112	0.222	0.222
6	0.444	0.444	0.222	0.223	0.222	0.223	0.111	0.110

7	0.180	0.179	0.320	0.321	0.320	0.321	0.180	0.179

Test Case 4: Gas phase oxidation of SO_2 to SO_3 is carried out at a Pressure of 1 bar and temperature of 855.7 [K] with 20% excess air. Determine equilibrium concentration based on 1 mol of SO_2.

Table 6-4: Equilibrium mol fraction calculation for test case 4

Temperature (K)	x_{SO_2} [1]	x_{SO_2} J	x_{SO_3} [1]	x_{SO_3} J	x_{N_2} [1]	x_{N_2} J	x_{O_2} [1]	x_{O_2} J
855.7	0.066	0.0675	0.222	0.220	0.650	0.650	0.062	0.063

Test Case 5: In a laboratory acetylene is hydrogenated to ethylene at 1393.15 K and 1 bar. If the feed is equimolar mixture of acetylene and hydrogen, what is the final product stream at equilibrium?

Table 6-5: Equilibrium mol fraction calculation for test case 5

Temperature (K)	$x_{C_2H_2}$ [1]	$x_{C_2H_2}$ J	x_{H_2} [1]	x_{H_2} J	$x_{C_2H_4}$ [1]	$x_{C_2H_4}$ J
1393.15	0.414	0.420	0.414	0.420	0.172	0.160

It should be noted that in [1] values for ln(K) for each species formation reactions were approximated from reading off a graph and assumed to be equal and opposite in sign, giving K_eq=1 for the overall reaction.

Test Case 6: Calculate the equilibrium mol fractions for the reaction of $I_{2(g)} \rightleftarrows I_{(g)}$ if initial 1 mol of $I_{2(g)}$ is present at 1 bar and 1073.15 K.

Table 6-6: Equilibrium mol fraction calculation for test case 6

Temperature (K)	x_{I_2} [2]	x_{I_2} J	x_I [2]	x_I J
1393.15	0.9029	0.9009	0.0971	0.0991

Appendix A.5- Theorem 1

Consider a reaction with NC participating species with stoichiometric coefficients

$\nu_i \quad i \in \{1,\cdots,NC\}$, where $\left\{\begin{matrix}\nu_i > 0 \text{ if } i \in P \triangleq \{index of \ product species\} \\ \nu_i < 0 \text{ if } i \in R \triangleq \{index of \ reactant species\}\end{matrix}\right\}, P \cup R = \{1,\cdots,NC\}$. The reaction's extent satisfies the relations:

$$\left\{\begin{matrix} n_i = n_{i,o} + \nu_i \xi \quad \forall i \in \{1,\cdots,NC\} \\ \xi \in \left[0, \min_{i \in R}\left(\frac{n_{i,o}}{-\nu_i}\right)\right] \end{matrix}\right\} \tag{A.5.1}$$

Let G, L, S be the index sets of the species that are in the ideal gas, ideal liquid, and ideal solid states respectively, at the considered temperature and pressure conditions T, P. It then holds:

$G \cup L \cup S = \{1,\cdots,NC\}$.

Fugacity for Gas:

$$\left\{\frac{\hat{f}_i^{(g)}}{f_i^{o(g)}} = y_i \frac{P}{P^o} = \frac{n_i}{\sum_{i \in G} n_i}\frac{P}{P^o} = \frac{n_{i,o} + \nu_i \xi}{\sum_{i \in G} n_{i,o} + \xi \sum_{i \in G} \nu_i}\frac{P}{P^o} \quad \forall i \in G\right\} \tag{A.5.2}$$

Fugacity for Liquid:

$$\left\{\frac{\hat{f}_i^{(l)}}{f_i^{o(l)}} = x_i = \frac{n_i}{\sum_{i \in L} n_i} = \frac{n_{i,o} + \nu_i \xi}{\sum_{i \in L} n_{i,o} + \xi \sum_{i \in L} \nu_i} \quad \forall i \in L\right\} \tag{A.5.3}$$

Fugacity for Solid:

$$\left\{\frac{\hat{f}_i^{(s)}}{f_i^{o(s)}} = 1 \quad \forall i \in S\right\} \tag{A.5.4}$$

It then holds:

$$\prod_{i\in G}\left(\frac{\hat{f}_i^{(g)}}{f_i^{o(g)}}\right)^{\nu_i}\prod_{i\in L}\left(\frac{\hat{f}_i^{(l)}}{f_i^{o(l)}}\right)^{\nu_i}\prod_{i\in S}\left(\frac{\hat{f}_i^{(s)}}{f_i^{o(s)}}\right)^{\nu_i}=\exp\left[\frac{-\Delta G^o(T)}{RT}\right]\Leftrightarrow \tag{A.5.5}$$

$$\prod_{i\in G}\left(\frac{n_{i,o}+\nu_i\xi}{\sum_{i\in G}n_{i,o}+\xi\sum_{i\in G}\nu_i}\frac{P}{P^o}\right)^{\nu_i}\prod_{i\in L}\left(\frac{n_{i,o}+\nu_i\xi}{\sum_{i\in L}n_{i,o}+\xi\sum_{i\in L}\nu_i}\right)^{\nu_i}\prod_{i\in S}(1)^{\nu_i}=\exp\left[\frac{-\Delta G^o(T)}{RT}\right]\Leftrightarrow \tag{A.5.6}$$

$$\prod_{i\in G}\left(\frac{n_{i,o}+\nu_i\xi}{\sum_{i\in G}n_{i,o}+\xi\sum_{i\in G}\nu_i}\right)^{\nu_i}\prod_{i\in L}\left(\frac{n_{i,o}+\nu_i\xi}{\sum_{i\in L}n_{i,o}+\xi\sum_{i\in L}\nu_i}\right)^{\nu_i}=\prod_{i\in G}\left(\frac{P}{P^o}\right)^{-\nu_i}\exp\left[\frac{-\Delta G^o(T)}{RT}\right]\Leftrightarrow \tag{A.5.7}$$

$$\prod_{i\in G}\left(\frac{n_{i,o}+\nu_i\xi}{\sum_{i\in G}n_{i,o}+\xi\sum_{i\in G}\nu_i}\right)^{\nu_i}\prod_{i\in L}\left(\frac{n_{i,o}+\nu_i\xi}{\sum_{i\in L}n_{i,o}+\xi\sum_{i\in L}\nu_i}\right)^{\nu_i}=\left(\frac{P}{P^o}\right)^{-\left(\sum_{i\in G}\nu_i\right)}\exp\left[\frac{-\Delta G^o(T)}{RT}\right] \tag{A.5.8}$$

Define

$$f_i:\left[0,\min_{i\in R}\left(\frac{n_{i,o}}{-\nu_i}\right)\right]\to\mathbb{R},\ f_i:\xi\to f_i(\xi)\triangleq\left(\frac{n_{i,o}+\nu_i\xi}{\sum_{i\in G}n_{i,o}+\xi\sum_{i\in G}\nu_i}\right)^{\nu_i}\ \forall i\in G \tag{A.5.9}$$

$$g_i:\left[0,\min_{i\in R}\left(\frac{n_{i,o}}{-\nu_i}\right)\right]\to\mathbb{R},\ g_i:\xi\to g_i(\xi)\triangleq\left(\frac{n_{i,o}+\nu_i\xi}{\sum_{i\in L}n_{i,o}+\xi\sum_{i\in L}\nu_i}\right)^{\nu_i}\ \forall i\in L \tag{A.5.10}$$

Then, the above equilibrium relation becomes:

$$\left\{\prod_{i\in G}\left(\frac{n_{i,o}+\nu_i\xi}{\sum_{i\in G}n_{i,o}+\xi\sum_{i\in G}\nu_i}\right)^{\nu_i}\prod_{i\in L}\left(\frac{n_{i,o}+\nu_i\xi}{\sum_{i\in L}n_{i,o}+\xi\sum_{i\in L}\nu_i}\right)^{\nu_i}=\left(\frac{P}{P^o}\right)^{-\left(\sum_{i\in G}\nu_i\right)}\exp\left[\frac{-\Delta G^o(T)}{RT}\right]\right\}\Leftrightarrow \tag{A.5.11}$$

$$\boxed{\left\{\prod_{i\in G}f_i(\xi)\prod_{i\in L}g_i(\xi)=\left(\frac{P}{P^o}\right)^{-\left(\sum_{i\in G}\nu_i\right)}\exp\left[\frac{-\Delta G^o(T)}{RT}\right]\right\}} \tag{A.5.12}$$

Further, it also holds:

$$\frac{df_i(\xi)}{d\xi} = \nu_i \left(\frac{n_{i,o} + \nu_i \xi}{\sum_{i \in G} n_{i,o} + \xi \sum_{i \in G} \nu_i} \right)^{\nu_i - 1} \left(\frac{\nu_i \left(\sum_{i \in G} n_{i,o} + \xi \sum_{i \in G} \nu_i \right) - \left(\sum_{i \in G} \nu_i \right) \left(n_{i,o} + \nu_i \xi \right)}{\left(\sum_{i \in G} n_{i,o} + \xi \sum_{i \in G} \nu_i \right)^2} \right) \forall i \in G \Rightarrow$$

(A.5.13)

$$\frac{df_i(\xi)}{d\xi} = \nu_i \left(\frac{n_{i,o} + \nu_i \xi}{\sum_{i \in G} n_{i,o} + \xi \sum_{i \in G} \nu_i} \right)^{\nu_i - 1} \left(\frac{\nu_i \left(\sum_{i \in G} n_{i,o} \right) - \left(\sum_{i \in G} \nu_i \right) \left(n_{i,o} \right)}{\left(\sum_{i \in G} n_{i,o} + \xi \sum_{i \in G} \nu_i \right)^2} \right) \forall i \in G \Rightarrow \qquad \text{(A.5.14)}$$

$$\frac{df_i(\xi)}{d\xi} = \nu_i f_i(\xi) \left(\frac{\nu_i \left(\sum_{i \in G} n_{i,o} \right) - \left(\sum_{i \in G} \nu_i \right) \left(n_{i,o} \right)}{\left(n_{i,o} + \nu_i \xi \right) \left(\sum_{i \in G} n_{i,o} + \xi \sum_{i \in G} \nu_i \right)} \right) \forall i \in G \qquad \text{(A.5.15)}$$

$$\frac{dg_i(\xi)}{d\xi} = \nu_i \left(\frac{n_{i,o} + \nu_i \xi}{\sum_{i \in L} n_{i,o} + \xi \sum_{i \in L} \nu_i} \right)^{\nu_i - 1} \left(\frac{\nu_i \left(\sum_{i \in L} n_{i,o} + \xi \sum_{i \in L} \nu_i \right) - \left(\sum_{i \in L} \nu_i \right) \left(n_{i,o} + \nu_i \xi \right)}{\left(\sum_{i \in L} n_{i,o} + \xi \sum_{i \in L} \nu_i \right)^2} \right) \forall i \in L \Rightarrow$$

(A.5.16)

$$\frac{dg_i(\xi)}{d\xi} = \nu_i \left(\frac{n_{i,o} + \nu_i \xi}{\sum_{i \in L} n_{i,o} + \xi \sum_{i \in L} \nu_i} \right)^{\nu_i - 1} \left(\frac{\nu_i \left(\sum_{i \in L} n_{i,o} \right) - \left(\sum_{i \in L} \nu_i \right) \left(n_{i,o} \right)}{\left(\sum_{i \in L} n_{i,o} + \xi \sum_{i \in L} \nu_i \right)^2} \right) \forall i \in L \qquad \text{(A.5.17)}$$

$$\frac{dg_i(\xi)}{d\xi} = \nu_i g_i(\xi) \left(\frac{\nu_i \left(\sum_{i \in L} n_{i,o} \right) - \left(\sum_{i \in L} \nu_i \right) \left(n_{i,o} \right)}{\left(n_{i,o} + \nu_i \xi \right) \left(\sum_{i \in L} n_{i,o} + \xi \sum_{i \in L} \nu_i \right)} \right) \forall i \in L \qquad \text{(A.5.18)}$$

It then holds:

$$\left\{\begin{array}{l} \nu_i < 0 \ \ \forall i \in R, \nu_i > 0 \ \ \forall i \in P \\ n_{i,o} \geq 0 \ \ \forall i \in P \cup R = \{1, \cdots, NC\} \\ 0 \leq \xi \leq \dfrac{n_{i,o}}{-\nu_i} \ \ \forall i \in R \end{array}\right\} \Rightarrow \left\{\begin{array}{l} 0 \leq \xi \leq \min\limits_{i \in R}\left(\dfrac{n_{i,o}}{-\nu_i}\right) \\ 0 \leq n_{i,o} + \nu_i \xi \ \ \forall i \in \{1, \cdots, NC\} = G \cup L \cup S \end{array}\right\} \Rightarrow$$

$$\left\{\begin{array}{l} 0 \leq \xi \leq \min\limits_{i \in R}\left(\dfrac{n_{i,o}}{-\nu_i}\right) \\ 0 \leq n_{i,o} + \nu_i \xi \ \ \forall i \in G \\ 0 \leq n_{i,o} + \nu_i \xi \ \ \forall i \in L \end{array}\right\} \Rightarrow .$$

$$\left\{\begin{array}{l} 0 \leq \xi \leq \min\limits_{i \in R}\left(\dfrac{n_{i,o}}{-\nu_i}\right) \\ 0 \leq n_{i,o} + \nu_i \xi \ \ \forall i \in G \\ 0 \leq \sum\limits_{i \in G} n_{i,o} + \xi \sum\limits_{i \in G} \nu_i \\ 0 \leq n_{i,o} + \nu_i \xi \ \ \forall i \in L \\ 0 \leq \sum\limits_{i \in L} n_{i,o} + \xi \sum\limits_{i \in L} \nu_i \end{array}\right\} \Rightarrow \left\{\begin{array}{ll} 0 \leq \xi \leq \min\limits_{i \in R}\left(\dfrac{n_{i,o}}{-\nu_i}\right) & \\ 0 \leq n_{i,o} + \nu_i \xi \ \ \forall i \in G & \\ 0 \leq f_i(\xi) \triangleq \left(\dfrac{n_{i,o} + \nu_i \xi}{\sum\limits_{i \in G} n_{i,o} + \xi \sum\limits_{i \in G} \nu_i}\right)^{\nu_i} & \forall i \in G \\ 0 \leq n_{i,o} + \nu_i \xi \ \ \forall i \in L & \\ 0 \leq g_i(\xi) \triangleq \left(\dfrac{n_{i,o} + \nu_i \xi}{\sum\limits_{i \in L} n_{i,o} + \xi \sum\limits_{i \in L} \nu_i}\right)^{\nu_i} & \forall i \in L \end{array}\right\}$$

Given that

$$\left\{\begin{array}{l}
\xi \in \left[0, \min\limits_{i\in R}\left(\dfrac{n_{i,o}}{-\nu_i}\right)\right] \\
0 \le n_{i,o} + \nu_i \xi \ \ \forall i \in G,\ 0 \le n_{i,o} + \nu_i \xi \ \ \forall i \in L \\
0 \le f_i(\xi) \triangleq \left(\dfrac{n_{i,o} + \nu_i \xi}{\sum\limits_{i\in G} n_{i,o} + \xi \sum\limits_{i\in G} \nu_i}\right)^{\nu_i} \quad \forall i \in G \\
0 \le g_i(\xi) \triangleq \left(\dfrac{n_{i,o} + \nu_i \xi}{\sum\limits_{i\in L} n_{i,o} + \xi \sum\limits_{i\in L} \nu_i}\right)^{\nu_i} \quad \forall i \in L \\
\dfrac{df_i(\xi)}{d\xi} = \nu_i f_i(\xi)\left(\dfrac{\nu_i\left(\sum\limits_{i\in G} n_{i,o}\right) - \left(\sum\limits_{i\in G} \nu_i\right)\left(n_{i,o}\right)}{\left(n_{i,o} + \nu_i \xi\right)\left(\sum\limits_{i\in G} n_{i,o} + \xi \sum\limits_{i\in G} \nu_i\right)}\right) \forall i \in G \\
\dfrac{dg_i(\xi)}{d\xi} = \nu_i g_i(\xi)\left(\dfrac{\nu_i\left(\sum\limits_{i\in L} n_{i,o}\right) - \left(\sum\limits_{i\in L} \nu_i\right)\left(n_{i,o}\right)}{\left(n_{i,o} + \nu_i \xi\right)\left(\sum\limits_{i\in L} n_{i,o} + \xi \sum\limits_{i\in L} \nu_i\right)}\right) \forall i \in L
\end{array}\right\} \qquad \text{(A.5.19)}$$

it then holds

$$\left\{0 \le \frac{df_i(\xi)}{d\xi} \ \ \forall \xi \in \left[0, \min_{i\in R}\left(\frac{n_{i,o}}{-\nu_i}\right)\right] \ \ i \in G\right\} \Leftrightarrow \left\{0 \le \nu_i\left(\nu_i\left(\sum_{i\in G} n_{i,o}\right) - \left(\sum_{i\in G} \nu_i\right)\left(n_{i,o}\right)\right) \ \ i \in G\right\} \Leftrightarrow$$

$$\left\{0 \le \nu_i^2\left(\sum_{j\in G} n_{j,o}\right) - \nu_i\left(\sum_{j\in G} \nu_j\right)\left(n_{i,o}\right) \ \ i \in G\right\} \Leftrightarrow \left\{\frac{\left(\sum\limits_{j\in G} \nu_j\right)\left(n_{i,o}\right)}{\nu_i} \le \left(\sum_{j\in G} n_{j,o}\right) \ \ i \in G\right\}$$

and

$$\left\{0 \le \frac{dg_i(\xi)}{d\xi} \ \ \forall \xi \in \left[0, \min_{i\in R}\left(\frac{n_{i,o}}{-\nu_i}\right)\right] \ \ i \in L\right\} \Leftrightarrow \left\{0 \le \nu_i\left(\nu_i\left(\sum_{i\in L} n_{i,o}\right) - \left(\sum_{i\in L} \nu_i\right)\left(n_{i,o}\right)\right) \ \ i \in L\right\} \Leftrightarrow$$

$$\left\{0 \le \nu_i^2\left(\sum_{j\in L} n_{j,o}\right) - \nu_i\left(\sum_{j\in L}\nu_j\right)\left(n_{i,o}\right) \;\; i \in L\right\} \Leftrightarrow \left\{\frac{\left(\sum_{j\in L}\nu_j\right)\left(n_{i,o}\right)}{\nu_i} \le \left(\sum_{j\in L} n_{j,o}\right) \;\; i \in L\right\}$$

Consider that the feed is stoichiometric for the reactants and contains no products.

Then the relation $\left\{\frac{\left(\sum_{j\in G}\nu_j\right)\left(n_{i,o}\right)}{\nu_i} \le \left(\sum_{j\in G} n_{j,o}\right) \;\; i \in G\right\}$ becomes:

$$\left\{\begin{array}{c}\left\{\frac{\left(\sum_{j\in G}\nu_j\right)\left(-\nu_i\right)}{\nu_i} \le \left(\sum_{j\in G\cap R}\left(-\nu_j\right)\right) \;\; i \in G\cap R\right\} \\ \vee \\ \left\{\frac{\left(\sum_{j\in G}\nu_j\right)(0)}{\nu_i} \le \left(\sum_{j\in G\cap R}\left(-\nu_j\right)\right) \;\; i \in G\cap P\right\}\end{array}\right\} \Leftrightarrow \left\{\begin{array}{c}\left\{-\sum_{j\in G}\nu_j \le -\sum_{j\in G\cap R}\nu_j \;\; i \in G\cap R\right\} \\ \vee \\ \left\{0 \le -\sum_{j\in G\cap R}\nu_j \;\; i \in G\cap P\right\}\end{array}\right\} \Leftrightarrow$$

$$\left\{\begin{array}{c}\left\{0 \le \sum_{j\in G\cap P}\nu_j \;\; i \in G\cap R\right\} \\ \vee \\ \left\{\sum_{j\in G\cap R}\nu_j \le 0 \;\; i \in G\cap P\right\}\end{array}\right\}$$ which is always true.

Similarly, the relation $\left\{\frac{\left(\sum_{j\in L}\nu_j\right)\left(n_{i,o}\right)}{\nu_i} \le \left(\sum_{j\in L} n_{j,o}\right) \;\; i \in L\right\}$ becomes:

$$\left\{\begin{array}{c}\left\{0 \le \sum_{j\in L\cap P} \nu_j \quad i \in L\cap R\right\} \\ \vee \\ \left\{\sum_{j\in L\cap R} \nu_j \le 0 \quad i \in L\cap P\right\}\end{array}\right\} \text{ which is always true.}$$

Appendix A.6 –Theorem 2

A function $f(x)$ that is Lipschitz continuous satisfies the following inequality[83]:

$$\left\| f(x_1) - f(x_2) \right\| \le L\left\| x_1 - x_2 \right\| \; \forall x_1, x_2 \in \Re^n, L \in \Re < \infty \tag{A.6.1}$$

A function is said to be Lipschitz continuous on a domain $\mathrm{T} \subset \Re^n$ if[84]:

$$\forall T_1, T_2 \in \mathrm{T} \; \exists L \in \Re,\; L < \infty \;\; s.t. \; \left\| f(T_1) - f(T_2) \right\| \le L\left\| T_1 - T_2 \right\| \tag{A.6.2}$$

The equation for $\dfrac{\Delta G^o(T)}{RT}$ can be reduced to general form of:

$$\left\{\frac{\Delta G^o(T)}{RT} = \begin{pmatrix} x_1 T^4 + x_2 T^3 + x_3 T^2 + x_4 T \\ + x_5 \ln(T) + x_6 \dfrac{\ln T}{T} + x_7 T^{-1} + x_8 T^{-2} + x_9 \end{pmatrix} \;\; \forall x_i \in \mathbb{R},\; i = 1,....9\right\} \tag{A.6.3}$$

where the coefficients $x_1, x_2, x_3, x_4, x_5, x_6, x_7, x_8, x_9 \in \Re$ represent appropriate addition/subtraction of the original formulation in A.1.10 for all species present in a reaction. Additionally, $\dfrac{d\left(\dfrac{\Delta G^o(T)}{RT}\right)}{dT}$ is given by:

$$\left\{\frac{d\left(\frac{\Delta G^o(T)}{RT}\right)}{dT} = \begin{pmatrix} \frac{x_1}{4} T^3 + \frac{x_2}{3} T^2 + \frac{x_3}{2} T + x_4 \\ + \frac{x_5}{T} + \frac{x_6 \ln(T)}{T^2} - \frac{(x_7 + x_6)}{T^2} - \frac{2x_8}{T^3} \end{pmatrix} \;\; \forall x_i \in \mathbb{R}, \forall T \in \mathbb{R}^+ \setminus \{0\},\; i = 1,....9\right\} \Rightarrow$$

(A.6.4)

which implies that:

$$\left\{ \exists T_c \in \left[T_1, T_2\right] \; st \; \frac{\frac{\Delta G^o\left(T_1\right)}{RT_1} - \frac{\Delta G^o\left(T_2\right)}{RT_2}}{T_1 - T_2} = \frac{d\left(\frac{\Delta G_i^o\left(T_c\right)}{RT_c}\right)}{dT} \;\; \forall x_i \in \mathbb{R}, \forall T \in \mathbb{R}^+ \setminus \{0\}, \; i = 1,....9 \right\}$$

(A.6.5)

by the Mean Value Theorem. In order to prove that $\Delta G^o\left(T\right)$ is Lipschitz continuous on the interval $T \in \left[T_{\min}, T_{\max}\right], T_{\min} > \sqrt{e}$, $T_{\max} < \infty$, it is sufficient to show that $\frac{d\Delta G^o\left(T\right)}{dT}$ can bounded by a real number L for all values $T_1, T_2 \in T$:

$$\left\{ \exists L \in \mathbb{R}^+ \; st \; \frac{\frac{\Delta G^o\left(T_1\right)}{RT_1} - \frac{\Delta G^o\left(T_2\right)}{RT_2}}{T_1 - T_2} = \frac{d\left(\frac{\Delta G_i^o\left(T_c\right)}{RT_c}\right)}{dT} \leq L \;\; \forall x_i \in \mathbb{R}, \forall T_1, T_2, T_c \in \left[T_{\min}, T_{\max}\right], \; i = 1,....9 \right\}$$

(A.6.6)

We begin by noting that if each of the individual terms on the RHS of A.2.21 can be bounded, then the whole function is bounded by the summation of each component:

$$\left\{ \begin{array}{l} \sup\left(\sum_{i=1}^{N}\left\{A_i\right\}\right) = \left\{\sum_{i=1}^{N}\sup\left(\left\{A_i\right\}\right)\right\} \\ \inf\left(\sum_{i=1}^{N}\left\{A_i\right\}\right) = \left\{\sum_{i=1}^{N}\inf\left(\left\{A_i\right\}\right)\right\} \end{array} \right\} \qquad \text{(A.6.7)}$$

The first three terms are continuous and monotonic on the given interval as their derivative with respect to T have no real roots. They are therefore bounded and achieve their maximum/minimum at one of the endpoints, depending on the sign and magnitude of the coefficient. The fourth term is a constant real number and obviously bounded. The fifth, seventh, and last term can all be shown to be monotonic on the given interval as well, with their derivatives with respect to T also having no real roots implying their maximum/minimum value

is achieved at the end points. The sixth term can be shown to be monotonic for all values of $T > \sqrt{e}$, with its derivative with respect to T have one real root.

$$\left\{\begin{array}{l}\sup\limits_{T\in[T_{\min},T_{\max}]}\left(\frac{x_1}{4}T^3\right)\\ \inf\limits_{T\in[T_{\min},T_{\max}]}\left(\frac{x_1}{4}T^3\right)\\ \left(\frac{d}{dT}\left(\frac{x_1}{4}T^3\right)\right)=\frac{x_1}{12}T^2\end{array}\right\}\Rightarrow\left\{\begin{array}{l}\sup\limits_{T\in[T_{\min},T_{\max}]}\left(\frac{x_1}{4}T^3\right)=\frac{x_1}{4}T_{\min}^3,\ x_1<0\ \vee\ \frac{x_1}{4}T_{\max}^3,\ x_1>0\\ \inf\limits_{T\in[T_{\min},T_{\max}]}\left(\frac{x_1}{4}T^3\right)=\frac{x_1}{4}T_{\min}^3,\ x_1>0\ \vee\ \frac{x_1}{4}T_{\max}^3,\ x_1<0\end{array}\right\} \quad \text{(A.6.8)}$$

$$\left\{\begin{array}{l}\sup\limits_{T\in[T_{\min},T_{\max}]}\left(\frac{x_2}{3}T^2\right)\\ \inf\limits_{T\in[T_{\min},T_{\max}]}\left(\frac{x_2}{3}T^2\right)\\ \frac{d}{dT}\left(\frac{x_2}{3}T^2\right)=\frac{x_2}{6}T\end{array}\right\}\Rightarrow\left\{\begin{array}{l}\sup\limits_{T\in[T_{\min},T_{\max}]}\left(\frac{x_2}{3}T^2\right)=\frac{x_2}{3}T_{\min}^2,\ x_1<0\ \vee\ \frac{x_2}{3}T_{\max}^2,\ x_1>0\\ \inf\limits_{T\in[T_{\min},T_{\max}]}\left(\frac{x_2}{3}T^2\right)=\frac{x_2}{3}T_{\min}^2,\ x_1>0\ \vee\ \frac{x_2}{3}T_{\max}^2,\ x_1<0\end{array}\right\} \quad \text{(A.6.9)}$$

$$\left\{\begin{array}{l}\sup\limits_{T\in[T_{\min},T_{\max}]}\left(\frac{x_3}{2}T\right)\\ \inf\limits_{T\in[T_{\min},T_{\max}]}\left(\frac{x_3}{2}T\right)\\ \frac{d}{dT}\left(\frac{x_3}{2}T\right)=\frac{x_3}{2}\end{array}\right\}\Rightarrow\left\{\begin{array}{l}\sup\limits_{T\in[T_{\min},T_{\max}]}\left(\frac{x_3}{2}T\right)=\frac{x_3}{2}T_{\max}\ ,\ x_3>0\vee\frac{x_3}{2}T_{\min}\ ,\ x_3<0\\ \inf\limits_{T\in[T_{\min},T_{\max}]}\left(\frac{x_3}{2}T\right)=\frac{x_3}{2}T_{\max}\ ,\ x_3<0\vee\frac{x_3}{2}T_{\min}\ ,\ x_3>0\end{array}\right\} \quad \text{(A.6.10)}$$

$$\left\{\begin{array}{l}\sup\limits_{T\in[T_{\min},T_{\max}]}\left(x_4\right)\\ \inf\limits_{T\in[T_{\min},T_{\max}]}\left(x_4\right)\end{array}\right\}=x_4 \quad \text{(A.6.11)}$$

$$\left\{\begin{array}{l}\sup\limits_{T\in[T_{\min},T_{\max}]}\left(\frac{x_5}{T}\right)\\ \inf\limits_{T\in[T_{\min},T_{\max}]}\left(\frac{x_5}{T}\right)\\ \frac{d}{dT}\left(\frac{x_5}{T}\right)=-\frac{x_5}{T^2}\end{array}\right\}\Rightarrow\left\{\begin{array}{l}\sup\limits_{T\in[T_{\min},T_{\max}]}\frac{x_5}{T}=\frac{x_5}{T_{\max}},\ x_5<0\vee\ \frac{x_5}{T_{\min}},\ x_5>0\\ \inf\limits_{T\in[T_{\min},T_{\max}]}\frac{x_5}{T}=\frac{x_5}{T_{\max}},\ x_5>0\vee\ \frac{x_5}{T_{\min}},\ x_5<0\end{array}\right\} \quad \text{(A.6.12)}$$

$$\left\{\begin{array}{l}\sup\limits_{T\in[T_{\min},T_{\max}]}\left(\dfrac{x_6\ln(T)}{T^2}\right)\\ \inf\limits_{T\in[T_{\min},T_{\max}]}\left(\dfrac{x_6\ln(T)}{T^2}\right)\\ \dfrac{d}{dT}\left(\dfrac{x_6\ln(T)}{T^2}\right)=x_6\dfrac{1-2\ln(T)}{T^3}\\ x_6\left(\dfrac{1-2\ln(T)}{T^3}\right)\Big|_{T=\sqrt{e}}=0\end{array}\right\}\Rightarrow\left\{\begin{array}{l}\sup\limits_{T\in[T_{\min},T_{\max}]}\dfrac{x_6\ln(T)}{T^2}=\dfrac{x_6\ln(T_{\min})}{T_{\min}^2}\ ,\ x_6>0\vee\dfrac{x_6\ln(T_{\max})}{T_{\max}^2}\ ,\ x_6<0\\ \inf\limits_{T\in[T_{\min},T_{\max}]}\dfrac{x_6\ln(T)}{T^2}=\dfrac{x_6\ln(T_{\min})}{T_{\min}^2}\ ,\ x_6<0\vee\dfrac{x_6\ln(T_{\max})}{T_{\max}^2}\ ,\ x_6>0\end{array}\right\}$$

(A.6.13)

$$\left\{\begin{array}{l}\sup\limits_{T\in[T_{\min},T_{\max}]}-\dfrac{x_7+x_6}{T^2}\\ \inf\limits_{T\in[T_{\min},T_{\max}]}-\dfrac{x_7+x_6}{T^2}\\ \dfrac{d}{dT}\left(\dfrac{-(x_7+x_6)}{T^2}\right)=\dfrac{2(x_7+x_6)}{T^3}\end{array}\right\}\Rightarrow\left\{\begin{array}{l}\sup\limits_{T\in[T_{\min},T_{\max}]}-\dfrac{x_7+x_6}{T^2}=\dfrac{x_7+x_6}{T_{\max}^2},x_7+x_6>0\vee\dfrac{x_7+x_6}{T_{\min}^2},x_7+x_6<0\\ \inf\limits_{T\in[T_{\min},T_{\max}]}-\dfrac{x_7+x_6}{T^2}=\dfrac{x_7+x_6}{T_{\max}^2},x_7+x_6<0\vee\dfrac{x_7+x_6}{T_{\min}^2},x_7+x_6>0\end{array}\right\}$$

(A.6.14)

$$\left\{\begin{array}{l}\sup\limits_{T\in[T_{\min},T_{\max}]}-\left(\dfrac{2x_8}{T^3}\right)\\ \inf\limits_{T\in[T_{\min},T_{\max}]}-\left(\dfrac{2x_8}{T^3}\right)\\ \dfrac{d}{dT}\left(-\dfrac{2x_8}{T^3}\right)=\dfrac{6x_8}{T^3}\end{array}\right\}\Rightarrow\left\{\begin{array}{l}\sup\limits_{T\in[T_{\min},T_{\max}]}-\left(\dfrac{2x_8}{T^3}\right)=\dfrac{2x_8}{T_{\max}^3}\ ,\ x_8>0\ \vee\dfrac{2x_8}{T_{\min}^3}\ ,\ x_8<0\\ \inf\limits_{T\in[T_{\min},T_{\max}]}-\left(\dfrac{2x_8}{T^3}\right)=\dfrac{2x_8}{T_{\max}^3}\ ,\ x_8<0\ \vee\dfrac{2x_8}{T_{\min}^3}\ ,\ x_8>0\end{array}\right\}\qquad\text{(A.6.15)}$$

It then follows that for any fixed values of $x_1,x_2,x_3,x_4,x_5,x_6,x_7,x_8,x_9$, each term on the RHS of A.2.23 achieves a finite real value for its minimum or maximum, and therefore from the property of real numbers their summation does as well.

$$\left\{\begin{array}{l}\left(\begin{array}{l}\sup\limits_{T\in[T_{\min},T_{\max}]}\left(\frac{x_1}{4}T^3\right)+\sup\limits_{T\in[T_{\min},T_{\max}]}\left(\frac{x_2}{3}T^2\right)+\sup\limits_{T\in[T_{\min},T_{\max}]}\left(\frac{x_3}{2}T\right)+\sup\limits_{T\in[T_{\min},T_{\max}]}\left(x_4\right)\\ +\sup\limits_{T\in[T_{\min},T_{\max}]}\frac{x_5}{T}+\sup\limits_{T\in[T_{\min},T_{\max}]}\frac{x_6\ln(T)}{T^2}+\sup\limits_{T\in[T_{\min},T_{\max}]}-\frac{x_7+x_6}{T^2}+\sup\limits_{T\in[T_{\min},T_{\max}]}-\left(\frac{2x_8}{T^3}\right)\end{array}\right)=L_+,\ -\infty<L_+<\infty\\ \left(\begin{array}{l}\inf\limits_{T\in[T_{\min},T_{\max}]}\left(\frac{x_1}{4}T^3\right)+\inf\limits_{T\in[T_{\min},T_{\max}]}\left(\frac{x_2}{3}T^2\right)+\inf\limits_{T\in[T_{\min},T_{\max}]}\left(\frac{x_3}{2}T\right)+\inf\limits_{T\in[T_{\min},T_{\max}]}\left(x_4\right)\\ +\sup\limits_{T\in[T_{\min},T_{\max}]}\frac{x_5}{T}+\inf\limits_{T\in[T_{\min},T_{\max}]}\frac{x_6\ln(T)}{T^2}+\inf\limits_{T\in[T_{\min},T_{\max}]}-\frac{x_7+x_6}{T^2}+\inf\limits_{T\in[T_{\min},T_{\max}]}-\left(\frac{2x_8}{T^3}\right)\end{array}\right)=L_-,\ -\infty<L_-<\infty\end{array}\right\}$$

$$\forall\left\{\begin{array}{l}x_1,x_2\\ ,x_3,x_4\\ ,x_5,x_6\\ ,x_7,x_8,x_9\end{array}\right\}\in\Re\ ,\ \forall T\in\left[T_{\min},T_{\max}\right]$$

(A.6.16)

From this it can be concluded that:

$$\exists L\in\Re,\ -\infty<L<\infty\ \ st\ L\geq\left|L_+\right|+\left|L_-\right| \qquad \text{(A.6.17)}$$

Appendix A.7 – Theorem 3

Define the following 3 sets:

$$(1)\,LR_1\triangleq\left\{\{l_1,r_1\}:g\left(\left(L\setminus R\right)\times R\right)\forall l_1\in L,r_1\in R\right\}$$

$$(2)\,LR_2\triangleq\left\{\{l_1,r_1\}:g\left(\left(L\bigcap R\right)\times\left(R\setminus L\right)\right)\forall l_1\in L,r_1\in R\right\}$$

$$(3)\,LR_3\triangleq\left\{\{l_1,r_1\}:g\left(\left\{\left\{\begin{pmatrix}L\bigcap R\\ 2\end{pmatrix}\right\}\right\}\right)\forall l_1\in L,r_1\in R\right\}$$

Then LR_1, LR_2, and LR_3 are disjoint.

Proof by contradiction:

Assume: $\left(\exists x\ st\ x\in LR_1\wedge x\in LR_2\ \right)\Rightarrow$

$$\begin{pmatrix} x \in LR_1 \Leftrightarrow \exists \{a_1, a_2\} \, st \; a_1 \in \{\alpha : \alpha \in L \wedge \alpha \notin R\} \vee a_1 \in \{\alpha : \alpha \in R\} \\ x \in LR_2 \Leftrightarrow \exists \{a_1, a_2\} \, st \; a_1 \in \{\beta : \beta \in L \wedge \beta \in R\} \vee a_1 \in \{\beta : \beta \notin L \wedge \beta \in R\} \end{pmatrix}$$

$$\left(if \; \exists \{a_1, a_2\} \in LR_1 \, st \; a_1 \in \{\alpha : \alpha \in L \wedge \alpha \notin R\}\right) \Rightarrow$$

$$\left(\exists a_1 \; st \; a_1 \in R \wedge a_1 \notin R\right) \vee \left(\exists a_1 \; st \; a_1 \in L \wedge a_1 \notin L\right)$$

$$\left(if \; \exists \{a_1, a_2\} \in LR_1 \, st \; a_1 \in \{\alpha : \alpha \in R\}\right) \Rightarrow$$

$$\left(\exists a_2 \; st \; a_2 \in R \wedge a_2 \notin R\right) \vee \left(\exists a_2 \; st \; a_2 \in L \wedge a_2 \notin L\right)$$

$$\left(if \; \exists \{a_1, a_2\} \in LR_2 \, st \; a_1 \in \{\beta : \beta \in L \wedge \beta \in R\}\right) \Rightarrow$$

$$\left(\exists a_2 \; st \; a_2 \in \left(L \setminus R\right) \wedge a_2 \in \left(R \setminus L\right)\right)$$

$$\left(if \; \exists \{a_1, a_2\} \in LR_2 \, st \; a_1 \in \{\beta : \beta \notin L \wedge \beta \in R\}\right) \Rightarrow$$

$$\left(\exists a_2 \; st \; a_2 \in R \wedge a_2 \notin R\right) \vee \left(\exists a_1 \; st \; a_1 \in L \wedge a_1 \notin L\right)$$

Assume $\left(\exists x \, st \, x \in LR_1 \wedge x \in LR_3\right) \Rightarrow$

$$\begin{pmatrix} x \in LR_1 \Leftrightarrow \exists \{a_1, a_2\} \, st \; a_1 \in \{\alpha : \alpha \in L \wedge \alpha \notin R\} \vee a_1 \in \{\alpha : \alpha \in R\} \\ x \in LR_3 \Leftrightarrow \exists \left(a_1, a_2\right) st \; a_1, a_2 \in \{\beta : \beta \in L \wedge \beta \in R\} \end{pmatrix}$$

$$\left(if \; \exists \{a_1, a_2\} \in LR_1 \, st \; a_1 \in \{\alpha : \alpha \in L \wedge \alpha \notin R\}\right) \Rightarrow$$

$$\left(\exists a_1 \; st \; a_1 \in R \wedge a_1 \notin R\right)$$

$$\left(if \; \exists \{a_1, a_2\} \in LR_1 \, st \; a_1 \in \{\alpha : \alpha \in R\}\right) \Rightarrow$$

$$\left(\exists a_2 \; st \; a_2 \in R \wedge a_2 \notin R\right)$$

$$\left(if \; \exists \left(a_1, a_2\right) \in LR_3 \, st \; a_1, a_2 \in \{\beta : \beta \in L \wedge \beta \in R\}\right) \Rightarrow$$

$$\left(\exists a_1 \; st \; a_1 \in R \wedge a_1 \notin R\right)$$

Assume $\exists x \, st \, x \in LR_2 \wedge x \in LR_3$

$$\begin{pmatrix} x \in LR_2 \Leftrightarrow \exists\{a_1,a_2\}\, st\ a_1 \in \{\beta : \beta \in L \wedge \beta \in R\} \vee a_1 \in \{\beta : \beta \notin L \wedge \beta \in R\} \\ x \in LR_3 \Leftrightarrow \exists(a_1,a_2)\, st\ a_1,a_2 \in \{\beta : \beta \in L \wedge \beta \in R\} \end{pmatrix}$$

$$\left(if\ \exists\{a_1,a_2\} \in LR_2\ st\ a_1 \in \{\beta : \beta \in L \wedge \beta \in R\}\right) \Rightarrow$$

$$\left(\exists a_2\ st\ a_2 \in L \wedge a_2 \notin L\right)$$

$$\left(if\ \exists\{a_1,a_2\} \in LR_2\ st\ a_1 \in \{\beta : \beta \notin L \wedge \beta \in R\}\right) \Rightarrow$$

$$\left(\exists a_1\ st\ a_1 \in L \wedge a_1 \notin L\right)$$

$$\left(if\ \exists(a_1,a_2) \in LR_3\ st\ a_1,a_2 \in \{\beta : \beta \in L \wedge \beta \in R\}\right) \Rightarrow$$

$$\left(\exists a_2\ st\ a_2 \in L \wedge a_2 \notin L\right)$$

Since all possible cases lead to contradictions the three defined sets are disjoint and share no members.

Appendix A.8- Theorem4

Theorem 3: *The complexity of* $HR_{\max}$ *is of order* $\Theta\left(\#(N_S)^{S_{sp}}\right)$

$$c_1 \#(N_S)^{S_{sp}} \le \sum_{i=1}^{S_{sp}} \left(\frac{\left(\nu^{\max}\right)^i}{i!} \cdot \prod_{k=0}^{i-1} \left[\#(N_S) - k \right] \right) \le c_2 \#(N_S)^{S_{sp}}$$

$$c_1 \le \frac{1}{\#(N_S)^{S_{sp}}} \sum_{i=1}^{S_{sp}} \left(\frac{\left(\nu^{\max}\right)^i}{i!} \cdot \prod_{k=0}^{i-1} \left[\#(N_S) - k \right] \right) \le c_2$$

$$c_1 \le \sum_{i=1}^{S_{sp}} \left(\frac{1}{\#(N_S)^{S_{sp}}} \frac{\left(\nu^{\max}\right)^i}{i!} \cdot \prod_{k=0}^{i-1} \left[\#(N_S) - k \right] \right) \le c_2$$

Sufficient to show that the limit of:

$$\lim_{\#(N_S)\to\infty}\left(\sum_{i=1}^{S_{sp}}\left(\frac{\left(\nu^{\max}\right)^i}{i!}\cdot\frac{1}{\#\left(N_S\right)^{S_{sp}}}\prod_{k=0}^{i-1}\left[\#\left(N_S\right)-k\right]\right)\right)$$

is bounded and in fact equal to $\frac{\left(\nu^{\max}\right)^{S_{sp}}}{\left(S_{sp}\right)!}$ for there to exists positive constants c_1 and c_2.

Induct on S_{sp}, base case $S_{sp}=1$:

$$\lim_{\#(N_S)\to\infty}\left(\sum_{i=1}^{1}\left(\frac{\left(\nu^{\max}\right)^i}{i!}\cdot\frac{1}{\#\left(N_s\right)^1}\prod_{k=0}^{i-1}\left[\#\left(N_S\right)-k\right]\right)\right)=\lim_{N_S\to\infty}\left(\frac{\left(\nu^{\max}\right)^1}{1!}\frac{\#\left(N_S\right)}{\#\left(N_s\right)^1}\right)=\frac{\left(\nu^{\max}\right)^1}{1!}$$

Assume $S_{sp}=2$, prove $S_{sp}=3$

$$\lim_{\#(N_S)\to\infty}\left(\sum_{i=1}^{3}\left(\frac{\left(\nu^{\max}\right)^i}{i!}\cdot\frac{1}{\#\left(N_s\right)^3}\prod_{k=0}^{i-1}\left[\#\left(N_S\right)-k\right]\right)\right)=$$

$$\lim_{\#(N_S)\to\infty}\left(\begin{array}{l}\frac{\left(\nu^{\max}\right)^1}{1!}\frac{1}{\#\left(N_s\right)^3}\cdot\prod_{k=0}^{1-1}\left[\#\left(N_S\right)-k\right]+\frac{\left(\nu^{\max}\right)^2}{2!}\frac{1}{\#\left(N_s\right)^3}\cdot\prod_{k=0}^{2-1}\left[\#\left(N_S\right)-k\right]\\ +\frac{\left(\nu^{\max}\right)^3}{3!}\frac{1}{\#\left(N_s\right)^3}\cdot\prod_{k=0}^{3-1}\left[\#\left(N_S\right)-k\right]\end{array}\right)=$$

$$\lim_{\#(N_S)\to\infty}\left(\frac{1}{\#\left(N_s\right)}\left(\begin{array}{l}\frac{\left(\nu^{\max}\right)^1}{1!}\frac{1}{\#\left(N_s\right)^2}\cdot\prod_{k=0}^{1-1}\left[\#\left(N_S\right)-k\right]\\ +\frac{\left(\nu^{\max}\right)^2}{2!}\frac{1}{\#\left(N_s\right)^2}\cdot\prod_{k=0}^{2-1}\left[\#\left(N_S\right)-k\right]\end{array}\right)+\frac{\left(\nu^{\max}\right)^3}{3!}\frac{1}{\#\left(N_s\right)^3}\cdot\prod_{k=0}^{3-1}\left[\#\left(N_S\right)-k\right]\right)=$$

$$\lim_{\#(N_S)\to\infty}\left(\frac{1}{\#\left(N_s\right)}\left(\frac{\left(\nu^{\max}\right)^2}{2!}\right)+\frac{\left(\nu^{\max}\right)^3}{3!}\frac{1}{\#\left(N_s\right)^3}\left(\#\left(N_S\right)\right)\left(\#\left(N_S\right)-1\right)\left(\#\left(N_S\right)-2\right)\right)=$$

$$\lim_{\#(N_S)\to\infty}\left(\frac{1}{\#\left(N_s\right)}\left(\frac{\left(\nu^{\max}\right)^2}{2!}\right)+\frac{\left(\nu^{\max}\right)^3}{3!}\frac{1}{\#\left(N_s\right)^3}\left(\#\left(N_S\right)^3-3\#\left(N_S\right)^2+2\#\left(N_S\right)\right)\right)=\frac{\left(\nu^{\max}\right)^3}{3!}$$

Appendix A.9 Selected ΔG_i^o References Comparisons

Table A.1 – Selected ΔG_i^o compared against values obtained by Refs [85],[86],[87],[88], *or* [89] . *Units for ΔG_i^o are $\left(kJ/mol\right)$*

Species: CO_2				**Species: CO**				**Species: H_2O**			
Temperature (K)	Ref	Our Work	% Difference	Temperature (K)	Ref	Our Work	% Difference	Temperature (K)	Ref	Our Work	% Difference
300	-394.394	-394.357	0.00938532	300	-137.328	-137.332	0.0030082	300	-236.839	-236.822	0.00731895
400	-394.675	-394.637	0.00955062	400	-146.338	-146.342	0.0026322	400	-223.937	-223.837	0.04466349
500	-394.939	-394.901	0.009614319	500	-155.414	-155.418	0.0027589	500	-219.069	-218.984	0.03894987
600	-395.182	-395.143	0.009805164	600	-164.486	-164.49	0.002599	600	-214.018	-213.938	0.03740534
700	-395.398	-395.359	0.009844139	700	-173.518	-173.523	0.00294	700	-208.819	-208.741	0.03733483
800	-395.586	-395.547	0.0098367	800	-182.497	-182.502	0.0025162	800	-203.501	-203.423	0.03818979
900	-395.748	-395.708	0.009996066	900	-191.416	-191.42	0.0023253	900	-198.086	-198.008	0.03928007
1000	-395.886	-395.845	0.010236137	1000	-200.275	-200.279	0.0020425	1000	-192.593	-192.515	0.04073405
1100	-396.001	-395.961	0.010190718	1100	-209.075	-209.079	0.0019293	1100	-187.035	-186.957	0.04154914
1200	-396.098	-396.056	0.01055574	1200	-217.819	-217.823	0.0016723	1200	-181.426	-181.349	0.04271663
1300	-396.177	-396.134	0.010824214	1300	-226.509	-226.513	0.0015835	1300	-175.775	-175.698	0.04375549
1400	-396.24	-396.196	0.011089553	1400	-235.149	-235.151	0.0010615	1400	-170.09	-170.014	0.04462692
1500	-396.288	-396.243	0.011292179	1500	-243.74	-243.742	0.0007392	1500	-164.376	-164.303	0.04438972
Species: CH_4				**Species: CaCl**				**Species: HCl**			
Temperature (K)	Ref	Our Work	% Difference	Temperature (K)	Ref	Our Work	% Difference	Temperature (K)	Ref	Our Work	% Difference
300	-50.618	-50.3792	0.471674327	300	-131.129	-131.248	0.0907312	300	-95.318	-95.31073	0.0076321
400	-42.054	-41.8285	0.536221219	400	-139.856	-139.934	0.0559348	400	-96.28	-96.27247	0.00781975
500	-32.741	-32.5322	0.63782769	500	-148.379	-148.405	0.0174101	500	-97.166	-97.15827	0.0079567
600	-22.887	-22.7003	0.815779194	600	-156.709	-156.666	0.0272274	600	-97.985	-97.97709	0.00807648
700	-12.643	-12.4853	1.246962372	700	-164.847	-164.721	0.0767264	700	-98.747	-98.73994	0.00714526
800	-2.115	-1.99834	5.515714429	800	-172.689	-172.475	0.1241626	800	-99.465	-99.4574	0.00764504
900	8.616	8.67878	0.728638881	900	-180.324	-180.053	0.1500685	900	-100.146	-100.1388	0.0071663

1000	19.492	19.48508	0.035492859	1000	-187.761	-187.486	0.1462049	1000	-100.799	-100.7921	0.00682871
1100	30.472	30.37567	0.316138139	1100	-194.992	-194.774	0.1115604	1100	-101.43	-101.4236	0.0063419
1200	41.524	41.31724	0.49793662	1200	-201.384	-201.254	0.0643126	1200	-102.044	-102.0382	0.00570573
1300	52.626	52.28517	0.647654298	1300	-207.526	-207.456	0.0336258	1300	-102.644	-102.6395	0.00436353
1400	63.761	63.26124	0.783800414	1400	-213.546	-213.508	0.0178552	1400	-103.234	-103.2302	0.00366765
1500	74.918	74.23192	0.915774586	1500	-219.452	-219.421	0.0141056	1500	-103.815	-103.8123	0.00263757
Species: SO_2				**Species: SO_3**				**Species: H_2SO_4**			
Temperature (K)	Ref	Our Work	% Difference	Temperature (K)	Ref	Our Work	% Difference	Temperature (K)	Ref	Our Work	% Difference
300	-300.145	-300.145	5.84E-05	300	-370.862	-370.903	0.0110391	300	-689.149	-689.16	0.00157765
400	-300.971	-300.967	0.001312479	400	-362.242	-362.258	0.0044506	400	-647.968	-648.007	0.00598189
500	-300.871	-300.86	0.003695039	500	-352.668	-352.658	0.0028659	500	-607.248	-607.341	0.01532612
600	-300.305	-300.285	0.006815823	600	-342.647	-342.609	0.0111447	600	-567.476	-567.677	0.03537004
700	-299.444	-299.411	0.011134497	700	-332.365	-332.299	0.0199185	700	-537.062	-537.047	0.00286914
800	-298.37	-298.323	0.015848407	800	-321.912	-321.819	0.0288128	800	-507.364	-507.344	0.00402658
900	-296.051	-296.007	0.015029043	900	-310.258	-310.158	0.0322372	900	-476.548	-476.541	0.00139189
1000	-288.725	-288.661	0.022300024	1000	-293.639	-293.513	0.0427901	1000	-440.854	-440.843	0.00239071
1100	-281.409	-281.32	0.03176417	1100	-277.069	-276.919	0.0542755	1100	-405.301	-405.285	0.00393601
1200	-274.102	-274.098	0.00132269	1200	-260.548	-260.372	0.0676004	1200	-369.888	-369.864	0.00636355
1300	-266.806	-266.803	0.001105217	1300	-244.073	-243.871	0.0829486	1300	-334.61	-334.578	0.00948587
1400	-259.518	-259.517	0.000471656	1400	-227.64	-227.412	0.1002719	1400	-299.464	-299.422	0.01410489
1500	-252.239	-252.239	0.000123338	1500	-211.247	-210.992	0.1205399	1500	-264.444	-264.389	0.02061948
Species: LiCl				**Species: Li_2Cl_2**				**Species: $Cu(OH)_2$**			
Temperature (K)	Ref	Our Work	% Difference	Temperature (K)	Ref	Our Work	% Difference	Temperature (K)	Ref	Our Work	% Difference
300	-383.869	-384.099	0.059969311	300	-600.802	-600.803	0.0001093	300	-372.178	-372.213	0.00936159
400	-375.837	-376.062	0.059916906	400	-601.374	-601.379	0.0008536	400	-346.323	-346.339	0.00476286
500	-367.643	-367.874	0.06278974	500	-600.983	-600.992	0.0014615	500	-320.841	-320.838	0.00096728
600	-359.202	-359.453	0.069922927	600	-599.538	-599.553	0.0024656	600	-295.709	-295.682	0.00898269
700	-350.891	-351.174	0.080554378	700	-597.832	-597.853	0.0034341	700	-270.913	-270.861	0.0192911
800	-342.726	-343.049	0.094162953	800	-595.923	-595.946	0.0038288	800	-246.442	-246.36	0.0330783

900	-335.098	-335.467	0.110089959	900	-593.844	-593.869	0.004138	900	-222.279	-222.165	0.05123423
1000	-329.511	-329.91	0.121116077	1000	-591.617	-591.646	0.0048354	1000	-198.401	-198.254	0.07433411
1100	-324.088	-324.51	0.130337525	1100	-589.258	-589.295	0.0062698	1100	-174.782	-174.601	0.10370323
1200	-318.806	-319.253	0.140286078	1200	-586.782	-586.83	0.0082616	1200	-151.395	-151.18	0.14215484
1300	-313.644	-314.126	0.153579578	1300	-584.199	-584.263	0.0109726	1300	-128.209	-127.963	0.19189354
1400	-308.586	-309.116	0.171873818	1400	-581.519	-581.603	0.0144057	1400	-104.79	-104.517	0.26090574
1500	-303.618	-304.215	0.196697516	1500	-578.748	-578.86	0.0193735	1500	-80.96	-80.6646	0.36487177
Species: Cu_2				**Species: $K_2O_2H_2$**				**Species: K_2O**			
Temperature (K)	Ref	Our Work	% Difference	Temperature (K)	Ref	Our Work	% Difference	Temperature (K)	Ref	Our Work	% Difference
300	432.726	432.6863	0.009183933	300	-613.644	-613.635	0.001524	300	-321.839	-321.837	0.00054568
400	415.387	415.3449	0.010129902	400	-598.462	-598.458	0.0007088	400	-307.331	-307.326	0.00156893
500	398.39	398.345	0.011285458	500	-581.907	-581.91	0.0005579	500	-292.638	-292.634	0.00131035
600	381.683	381.6371	0.012024205	600	-564.786	-564.799	0.0022994	600	-278.292	-278.288	0.00147128
700	365.233	365.1862	0.012821557	700	-547.275	-547.298	0.004137	700	-264.299	-264.293	0.00220549
800	349.016	348.967	0.014041539	800	-529.481	-529.511	0.0055733	800	-250.665	-250.655	0.00394903
900	333.014	332.9615	0.015771707	900	-511.469	-511.502	0.0063907	900	-237.394	-237.375	0.007968
1000	317.214	317.1573	0.017875328	1000	-493.279	-493.31	0.0062727	1000	-224.482	-224.449	0.01470269
1100	301.607	301.5471	0.019872442	1100	-465.717	-465.724	0.0015362	1100	-202.704	-202.635	0.03420352
1200	286.19	286.1278	0.021724053	1200	-432.135	-432.14	0.0010944	1200	-175.39	-175.304	0.04908504
1300	270.963	270.9007	0.022985382	1300	-398.606	-398.605	0.0002291	1300	-148.594	-148.487	0.07215214
1400	256.749	256.6831	0.025683526	1400	-365.13	-365.124	0.0017028	1400	-122.306	-122.173	0.10912533
1500	243.852	243.7817	0.028847127	1500	-331.711	-331.698	0.0039784	1500	-96.519	-96.352	0.17299035
Species: GeO_2				**Species: CH_3OH**				**Species: CH_3COOH**			
Temperature (K)	Ref	Our Work	% Difference	Temperature (K)	Ref	Our Work	% Difference	Temperature (K)	Ref	Our Work	% Difference
300	-521.242	-521.2091673	0.006298932	300	-162.057	-161.97166	0.052658893	300	-373.893	-373.8738752	0.005115033
400	-501.61	-501.578371	0.006305501	400	-148.509	-148.42006	0.059887628	400	-353.84	-353.8264166	0.003838854
500	-482.134	-482.1034358	0.006339359	500	-134.109	-134.01693	0.068651408	500	-332.95	-332.9485462	0.000436634
600	-462.859	-462.8295192	0.006369273	600	-119.125	-119.02692	0.082325666	600	-311.554	-311.5628624	0.002844574
700	-443.776	-443.7475037	0.006421325	700	-103.737	-103.62696	0.106068701	700	-289.856	-289.8682631	0.004230753

800	-424.866	-424.8387751	0.006407871	800	-88.063	-87.937666	0.142322604	800	-267.985	-267.9943413	0.00348576
900	-406.113	-406.0861624	0.006608413	900	-72.188	-72.043839	0.199701485	900	-246.026	-246.0285886	0.001052179
1000	-387.502	-387.4761862	0.006661595	1000	-56.17	-56.00648	0.291207139	1000	-224.034	-224.0304552	0.001582272
1100	-369.024	-368.9988306	0.006820537	1100	-40.05	-39.8689276	0.452115694	1100	-202.046	-202.0388783	0.003524815
1200	-350.671	-350.6470754	0.006822516	1200	-23.861	-23.6627225	0.830968604	1200	-180.086	-180.0787936	0.00400163
1300	-329.732	-329.708724	0.007059058	1300	-7.624	-7.41055262	2.799677011	1300	-158.167	-158.1648839	0.001337864
1400	-310.228	-310.205498	0.007253363	1400	8.644	8.871206394	2.628486741	1400	-136.299	-136.3048782	0.004312753
1500	-292.057	-292.0353433	0.007415226	1500	24.93	25.1707862	0.965849502	1500	-114.486	-114.5019971	0.013972977
Species: HCOOH				**Species: Na2CO3**				**Species: Na2O2**			
Temperature (K)	Ref	Our Work	% Difference	Temperature (K)	Ref	Our Work	% Difference	Temperature (K)	Ref	Our Work	% Difference
300	-350.83	-350.7759463	0.015407386	300	-1047.496	-1047.49416	0.000175644	300	-449.233	-449.2253069	0.001712489
400	-341.16	-341.2102008	0.014714731	400	-1019.37	-1019.358297	0.001148015	400	-427.56	-427.5589815	0.000238214
500	-331.29	-331.2198227	0.021183042	500	-990.4	-990.3771602	0.002306122	500	-405.02	-405.0253733	0.00132668
600	-321.05	-320.9777692	0.022498314	600	-961.826	-961.7883688	0.003912477	600	-382.706	-382.7145683	0.002238879
700	-310.66	-310.5923414	0.021778977	700	-933.897	-933.8395425	0.006152447	700	-360.668	-360.6780199	0.002778161
800	-300.21	-300.1346158	0.025110494	800	-906.701	-906.6960055	0.000550845	800	-339.036	-338.9930233	0.012676135
900	-289.73	-289.6522598	0.02683194	900	-879.857	-879.852989	0.000455866	900	-318.303	-318.2798918	0.007259806
1000	-279.24	-279.1768355	0.022620133	1000	-853.412	-853.4129479	0.00011107	1000	-297.81	-297.8080278	0.000662231
1100	-268.85	-268.7279652	0.045391402	1100	-827.441	-827.4490577	0.000973812	1100	-277.525	-277.5481447	0.00833968
1200	-258.41	-258.3170989	0.035951059	1200	-799.127	-799.1386571	0.001458731	1200	-252.54	-252.5659214	0.010264264
1300	-248.05	-247.9496181	0.040468411	1300	-760.294	-760.302277	0.001088662	1300	-216.13	-216.149757	0.009141268
1400	-237.69	-237.6269575	0.026523006	1400	-722.007	-722.0111105	0.000569316	1400	-179.997	-180.0118085	0.008227083
1500	-227.43	-227.3481544	0.035987175	1500	-684.221	-684.2201665	0.000121817	1500	-144.121	-144.1300459	0.006276577
Species: NaOH				**Species: $CuCl_2$**				**Species: Cu_3Cl_3**			
Temperature (K)	Ref	Our Work	% Difference	Temperature (K)	Ref	Our Work	% Difference	Temperature (K)	Ref	Our Work	% Difference
300	-379.454	-379.341171	0.029734562	300	-161.405	-161.4057932	0.000491456	300	-257.196	-257.1923308	0.001426636
400	-363.802	-363.7042385	0.026872182	400	-146.806	-146.8054883	0.000348579	400	-256.737	-256.7381197	0.000436141
500	-347.767	-347.6775208	0.025729647	500	-132.569	-132.5690055	4.16948E-06	500	-256.257	-256.2634321	0.002510009
600	-332.417	-332.3689146	0.014465373	600	-118.638	-118.6378128	0.000157786	600	-255.737	-255.7461315	0.003570668

700	-319.446	-319.2268292	0.06860965	700	-104.971	-104.9701208	0.000837611	700	-255.159	-255.1713607	0.004844327
800	-306.834	-306.4419204	0.12778232	800	-91.535	-91.5334423	0.001701758	800	-254.511	-254.5281088	0.006722205
900	-294.526	-293.9607013	0.191935064	900	-78.302	-78.30115716	0.001076396	900	-253.783	-253.8065545	0.009281356
1000	-282.478	-281.7399424	0.261279685	1000	-65.251	-65.25068883	0.000476876	1000	-252.965	-252.996308	0.012376401
1100	-270.653	-269.7441683	0.335792203	1100	-52.362	-52.3624882	0.00093235	1100	-252.048	-252.0855546	0.01489978
1200	-256.579	-255.492633	0.423404476	1200	-39.619	-39.61912304	0.000310565	1200	-251.018	-251.0602563	0.016833988
1300	-236.877	-235.6189713	0.531089438	1300	-27.004	-27.0037096	0.001075401	1300	-249.857	-249.9024795	0.018202211
1400	-217.387	-215.9702418	0.651721666	1400	-14.093	-14.09346174	0.003276407	1400	-247.32	-247.3722458	0.021124789
1500	-198.087	-196.5276546	0.787202285	1500	-0.721	-0.722461112	0.202650817	1500	-242.937	-242.9974784	0.024894694
Species: C_2H_2				**Species: C_2H_4**				**Species: C_2H_6**			
Temperature (K)	Ref?	Our Work	% Difference	Temperature (K)	Ref*2*	Our Work	% Difference	Temperature (K)	Ref*2*	Our Work	% Difference
300	209.092	210.5568929	0.700597318	300	68.457	68.5482562	0.133304411	300	-31.692	-31.56233585	0.409138435
400	203.242	204.7118298	0.723191966	400	74.302	74.38721691	0.114689927	400	-13.473	-13.35519925	0.874346834
500	197.452	198.9304687	0.748773723	500	80.887	80.96081291	0.091254352	500	5.912	6.012045449	1.692243729
600	191.735	193.2242867	0.776742233	600	87.982	88.04593608	0.072669495	600	26.086	26.17078956	0.325038572
700	186.097	187.599521	0.807385923	700	95.434	95.4952585	0.064189392	700	46.8	46.87657544	0.163622741
800	180.534	182.0544313	0.842185564	800	103.142	103.2073446	0.063354012	800	67.887	67.96170019	0.110036071
900	175.041	176.5821558	0.880454192	900	111.036	111.1093272	0.06603912	900	89.231	89.30736207	0.085577964
1000	169.607	171.1737934	0.923778751	1000	119.067	119.1476844	0.06776385	1000	110.75	110.8280058	0.07043417
1100	164.226	165.8206647	0.971018412	1100	127.198	127.2837554	0.067418854	1100	132.385	132.4627973	0.05876592
1200	158.888	160.5149107	1.023935521	1200	135.402	135.4893376	0.064502475	1200	154.096	154.1681913	0.046848253
1300	153.588	155.2498225	1.082000193	1300	143.66	143.7439488	0.058435767	1300	175.85	175.9132999	0.035996552
1400	148.319	150.0198919	1.146779494	1400	151.955	152.0328462	0.051229802	1400	197.625	197.6764214	0.02601969
1500	143.078	144.8206557	1.217975988	1500	160.275	160.3454309	0.043943782	1500	219.404	219.4423764	0.017491202
Species: C_3H_6O				**Species: C_2H_5OH**				**Species: C_6H_5OH**			
Temperature (K)	Ref	Our Work	% Difference	Temperature (K)	Ref	Our Work	% Difference	Temperature (K)	Ref	Our Work	% Difference
300	-152.339	-152.2919002	0.030917782	300	-167.458	-167.2915368	0.099405926	300	-32.23	-32.26228163	0.100160188
400	-129.913	-129.8781748	0.026806528	400	-144.216	-143.9491956	0.185003352	400	-10.18	-10.17403733	0.058572397
500	-106.315	-106.2833177	0.029800439	500	-119.82	-119.4616026	0.299113196	500	12.97	12.88364522	0.665803974

600	-81.923	-81.88948737	0.04090747	600	-94.672	-94.22771646	0.469287162	600	36.65	36.53481619	0.314280519
700	-56.986	-56.94703454	0.068377248	700	-69.023	-68.49732029	0.761600784	700	60.75	60.56663592	0.301833882
800	-31.673	-31.62653522	0.146701551	800	-43.038	-42.43369969	1.404108721	800	85.02	84.84694985	0.20354052
900	-6.109	-6.048330581	0.993115394	900	-16.825	-16.14883455	4.018813945	900	109.59	109.2866307	0.276822088
1000	19.707	19.70116864	0.02959031	1000	9.539	10.2781378	7.748587939	1000	134.28	133.8226723	0.340577677
1100	45.396	45.56081547	0.363061651	1100	36	36.79205312	2.200147568	1100	158.62	158.4116787	0.13133359
1200	71.463	71.48709782	0.033720696	1200	62.52	63.35401031	1.333989618	1200	183.35	183.0234346	0.178110403
1300	97.362	97.44930529	0.089670803	1300	89.07	89.93663137	0.972977854	1300	208.07	207.6370755	0.208066735
1400	123.47	123.4260558	0.035590969	1400	115.63	116.520946	0.77051461	1400	233.05	232.2387161	0.348115792
1500	149.369	149.4026153	0.022504873	1500	142.185	143.0939657	0.639283819	1500	257.54	256.8194605	0.27977772
Species: HI				**Species: CaOH**				**Species: CaO**			
Temperature (K)	Ref	Our Work	% Difference	Temperature (K)	Ref	Our Work	% Difference	Temperature (K)	Ref	Our Work	% Difference
300	1.406	1.404361679	0.116523564	300	-201.668	-201.7788992	0.054990998	300	-603.305	-602.7796765	0.087074285
400	-6.428	-6.430649995	0.041225817	400	-204.115	-204.1875278	0.035532811	400	-592.755	-592.1285513	0.105684258
500	-10.088	-10.08703458	0.009570025	500	-206.345	-206.3669398	0.010632603	500	-582.316	-581.5952206	0.123778044
600	-10.948	-10.94755665	0.004049569	600	-208.4	-208.3564618	0.020891632	600	-571.975	-571.1580064	0.142837292
700	-11.756	-11.75572223	0.002362801	700	-210.291	-210.1669215	0.059003231	700	-561.701	-560.7784707	0.164238493
800	-12.528	-12.52746696	0.004254806	800	-211.914	-211.7067092	0.097818371	800	-551.362	-550.3278968	0.187554305
900	-13.275	-13.27469923	0.002265673	900	-213.359	-213.0996518	0.121554831	900	-541.024	-539.9016145	0.20745577
1000	-14.006	-14.00593941	0.000432565	1000	-214.633	-214.3738674	0.12073286	1000	-530.677	-529.5054388	0.22076728
1100	-14.727	-14.72698155	0.000125258	1100	-215.727	-215.5284251	0.092049147	1100	-520.297	-519.1208398	0.226055548
1200	-15.441	-15.44167205	0.004352393	1200	-216.008	-215.8991387	0.050396861	1200	-509.239	-508.0695613	0.229644371
1300	-16.151	-16.15253741	0.009518953	1300	-216.065	-216.0149992	0.023141559	1300	-498.082	-496.8693627	0.243461371
1400	-16.858	-16.86103952	0.018030138	1400	-216.024	-216.0038087	0.009346767	1400	-486.943	-485.6390961	0.267773424
1500	-17.562	-17.56784483	0.033281103	1500	-215.891	-215.8768185	0.006568836	1500	-475.823	-474.3829201	0.302650333
Species: $FeCl_2$				**Species: $FeCl_3$**				**Species: Fe_3O_4**			
Temperature (K)	Ref	Our Work	% Difference	Temperature (K)	Ref	Our Work	% Difference	Temperature (K)	Ref	Our Work	% Difference
300	-302.097	-302.0778339	0.006344365	300	-333.524	-333.5229724	0.000308092	300	-1016.797	-1014.486567	0.227226555
400	-289.125	-289.1071611	0.006169948	400	-311.913	-311.911914	0.000348176	400	-982.386	-980.2374793	0.218704324

500	-276.581	-276.5654529	0.005621185	500	-290.964	-290.9661058	0.000723743	500	-948.681	-946.7992767	0.198351528
600	-264.358	-264.3435076	0.005482093	600	-272.414	-272.3866005	0.010058025	600	-915.794	-914.1893068	0.175224252
700	-252.378	-252.3649009	0.005190276	700	-260.33	-260.3164865	0.005190905	700	-883.776	-882.3835927	0.157552056
800	-240.583	-240.5708851	0.005035659	800	-248.877	-248.8778058	0.000323787	800	-852.657	-851.4417959	0.142519685
900	-228.919	-228.905329	0.005971987	900	-237.929	-237.9422906	0.005585962	900	-822.428	-821.5547851	0.106175234
1000	-219.603	-219.5944105	0.003911393	1000	-227.367	-227.3994554	0.014274476	1000	-792.602	-792.0587633	0.068538402
1100	-212.637	-212.6100625	0.012668309	1100	-217.041	-217.0714641	0.014036107	1100	-762.463	-762.2503632	0.02788814
1200	-205.802	-205.7342698	0.032910356	1200	-206.965	-206.9707788	0.002792178	1200	-732.139	-732.1810487	0.005743266
1300	-199.13	-199.034605	0.047905879	1300	-197.159	-197.1541304	0.002469872	1300	-701.771	-702.0663258	0.042082932
1400	-192.686	-192.5637564	0.063441875	1400	-187.679	-187.6652294	0.007337309	1400	-671.59	-672.094894	0.07517891
1500	-186.447	-186.2978351	0.080003937	1500	-178.496	-178.4727585	0.013020729	1500	-641.562	-642.2343068	0.104792185
Species: $Fe(CO)_5$				**Species: $Fe(OH)_2$**				**Species: K_2Cl_2**			
Temperature (K)	Ref	Our Work	% Difference	Temperature (K)	Ref	Our Work	% Difference	Temperature (K)	Ref	Our Work	% Difference
300	-696.547	-696.5122033	0.0049956	300	-491.46	-491.4286895	0.006370921	300	-617.775	-617.7653206	0.001566814
400	-674.716	-674.6839369	0.004752081	400	-464.155	-464.1253666	0.006384386	400	-616.696	-616.6954682	8.62368E-05
500	-654.729	-654.6985004	0.00465836	500	-437.238	-437.2087089	0.006699115	500	-614.699	-614.7029679	0.000645499
600	-635.831	-635.8026305	0.0044618	600	-410.656	-410.6280815	0.006798521	600	-612.395	-612.4031335	0.001328142
700	-617.569	-617.5425366	0.004285099	700	-384.373	-384.3451748	0.007239104	700	-609.851	-609.8635506	0.002057983
800	-631.034	-631.0126822	0.003378233	800	-358.353	-358.3249866	0.007817262	800	-607.109	-607.1251717	0.002663727
900	-619.996	-619.9743707	0.003488624	900	-332.552	-332.5221763	0.008968143	900	-604.194	-604.211664	0.002923558
1000	-608.9	-608.8842556	0.002585718	1000	-306.906	-306.8803603	0.008354245	1000	-601.119	-601.1348629	0.002638895
1100	-597.633	-597.5994523	0.005613424	1100	-281.301	-281.2567844	0.015718256	1100	-588.672	-588.6657695	0.001058398
1200	-586.239	-586.1634249	0.012891511	1200	-255.773	-255.6862999	0.033897302	1200	-570.192	-570.1877659	0.000742568
1300	-574.766	-574.6610783	0.018254678	1300	-230.357	-230.2408744	0.050411137	1300	-551.745	-551.7403805	0.000837252
1400	-563.293	-563.1604838	0.023525275	1400	-205.119	-204.974514	0.070440066	1400	-533.325	-533.3208305	0.000781798
1500	-551.811	-551.6509019	0.029013215	1500	-180.036	-179.8632972	0.095926827	1500	-514.931	-514.9268216	0.000811453
Species: GeO_2				**Species: $GeCl_4$**				**Species: $Fe(OH)_3$**			
Temperature (K)	Ref	Our Work	% Difference	Temperature (K)	Ref	Our Work	% Difference	Temperature (K)	Ref	Our Work	% Difference
300	-521.242	-521.20673	0.006298932	300	-461.343	-461.3165	0.0057	300	-704.678	-704.6327	0.0064

400	-501.610	-501.5371	0.006305501	400	-448.540	-448.5144	0.0057	400	-661.93	-661.8865	0.0066
500	-482.134	-482.10358	0.006339359	500	-435.882	-435.8579	0.0055	500	-619.202	-619.1593	0.0069
600	-462.859	-462.82992	0.006369273	600	-423.347	-423.3240	0.0054	600	-576.661	-576.6229	0.0066
700	-443.776	-443.74757	0.006421325	700	-410.914	-410.8917	0.0054	700	-534.385	-534.3480	0.0069
800	-424.866	-424.8381	0.006407871	800	-398.565	-398.5439	0.0053	800	-492.393	-492.3556	0.0076
900	-406.113	-406.0864	0.006608413	900	-386.287	-386.2667	0.0052	900	-450.671	-450.6330	0.0084
1000	-387.502	-387.4761	0.006661595	1000	-374.068	-374.0489	0.0051	1000	-409.177	-409.1452	0.0078
1100	-369.024	-368.9988	0.006820537	1100	-361.899	-361.8814	0.0049	1100	-367.813	-367.7637	0.0134
1200	-350.671	-350.6470	0.006822516	1200	-349.772	-349.7572	0.0042	1200	-326.624	-326.5338	0.0276
1300	-329.732	-329.708	0.007059058	1300	-334.973	-334.9612	0.0035	1300	-285.654	-285.5342	0.0419
1400	-310.228	-310.205	0.007253363	1400	-319.857	-319.8486	0.0026	1400	-244.97	-244.8223	0.0603
1500	-292.057	-292.03534	0.007415226	1500	-304.771	-304.7645	0.0021	1500	-204.549	-204.3741	0.0855

Appendix A.10 Species Thermodynamic Data

Species	Phase	T_L	T_u	a1	a2	a3	a4	a5	a6	a7	b1	b2
B	b	200	600	259825.934	-4770.7730	34.6412448	-0.1287342	0.00028978	-3.31E-07	1.50E-10	21469.4684	-183.082472
B	b	600	2350	-869.770022	-805.040596	4.07971288	-0.00064233	4.85E-07	-1.25E-10	1.34E-14	3397.91993	-25.05906587
B(OH)2	g	200	1000	1491.659222	364.818484	-2.90600638	0.04136834	-5.78E-05	4.07E-08	-1.13E-11	-53754.8366	38.8853518
B(OH)2	g	1000	6000	1557023.406	-5784.71076	14.87391235	-0.0001821	-3.80E-08	1.03E-11	-6.69E-16	-18068.10301	-65.902689
B2(OH)4	g	200	1000	-17287.17249	849.591348	-8.71595957	0.093623626	-0.00012787	8.81E-08	-2.40E-11	-156433.7133	71.2016931
B2(OH)4	g	1000	6000	2983925.656	-12074.69577	31.6261057	-0.000516368	-4.23E-08	1.67E-11	-1.16E-15	-82809.7697	-165.3010498
B2F4	g	200	1000	-59716.9564	818.942544	-0.643767129	0.038589661	-4.31E-05	2.40E-08	-5.39E-12	-179004.1225	35.5217997
B2F4	g	1000	6000	38558.6589	-2928.842655	17.92063736	-0.0009524	1.61E-07	-1.43E-11	5.22E-16	-161305.1924	-71.8480325
BF(OH)2	g	200	1000	13818.00676	252.9637004	-3.84455204	0.052551409	-7.19E-05	4.95E-08	-1.35E-11	-128312.3258	42.9365937
BF(OH)2	g	1000	6000	1422037.64	-6257.29757	18.22460686	-0.00032214	-7.13E-09	6.76E-12	-5.04E-16	-91862.5419	-85.2789505
BHF	g	200	1000	-49083.6226	961.076021	-2.919850316	0.021491566	-2.60E-05	1.69E-08	-4.55E-12	-14669.25195	41.6070931
BHF	g	1000	6000	1184821.3	-4677.43518	10.67328148	-0.001606367	3.70E-07	-3.80E-11	1.43E-15	18026.40937	-42.8593117
Br2	cr	200	265	-5550117.11	161095.3162	-1913.542203	12.01711944	-0.041706215	7.62E-05	-5.69E-08	-656541.592	9135.571

Br2	L	265	332	5661619.72	-60027.8872	39.635728	2.194289283	-0.012096161	2.61E-05	-2.07E-08	316720.453	-683.259616
Br2	g	332	1000	7497.04754	-235.0884557	5.49193432	-0.002227573	2.93E-06	-1.95E-09	5.31E-13	3521.47505	-1.96415157
Br2	g	1000	6000	-4311698.57	11112.68634	-5.55577561	0.003630517	-2.75E-07	-6.22E-11	7.38E-15	-70365.8416	78.7847802
C	cr	200	600	113285.676	-1980.421677	13.65384188	-0.046360964	0.000102133	-1.08E-07	4.47E-11	8943.85976	-72.9582474
C	cr	600	2000	335600.441	-2596.528368	6.94884191	-0.003484836	1.84E-06	-5.06E-10	5.75E-14	13984.12456	-44.7718304
CH3I	g	200	1000	-45164.6274	1086.208429	-5.66317627	0.036831717	-4.32E-05	2.83E-08	-7.68E-12	-4303.83065	56.8856269
CH3I	g	1000	6000	2511915.982	-9960.28999	18.56907132	-0.001768191	3.24E-07	-3.19E-11	1.31E-15	60669.2995	-95.9077704
CH4	g	200	1000	-176685.0998	2786.18102	-12.0257785	0.039176193	-3.62E-05	2.03E-08	-4.98E-12	-23313.1436	89.0432275
CH4	g	1000	6000	3730042.76	-13835.01485	20.49107091	-0.001961975	4.73E-07	-3.73E-11	1.62E-15	75320.6691	-121.9124889
CO	g	200	1000	14890.45326	-292.2285939	5.72452717	-0.008176235	1.46E-05	-1.09E-08	3.03E-12	-13031.31878	-7.85924135
CO	g	1000	6000	461919.725	-1944.704863	5.91671418	-0.000566428	1.40E-07	-1.79E-11	9.62E-16	-2466.261084	-13.87413108
CO2	g	200	1000	49436.5054	-626.411601	5.30172524	0.002503814	-2.13E-07	-7.69E-10	2.85E-13	-45281.9846	-7.04827944
CO2	g	1000	6000	117696.2419	-1788.791477	8.29152319	-9.22E-05	4.86E-09	-1.89E-12	6.33E-16	-39083.5059	-26.52669281
Ca	a	200	298	22092.14594	0	-2.387095323	0.046748334	-0.000148169	1.69E-07	0	-316.0902334	9.9989079
Ca	a	298	716	8959.6321	0	2.440591375	0.001722094	4.74E-07	0	0	-778.344084	-9.27370805
Ca	b	716	1115	0	0	5.701117685	-0.005810565	4.02E-06	0	0	-1516.788311	-26.0758823
Ca	L	1115	1774	0	0	4.570323447	0	0	0	0	-982.26801	-21.19893317
Ca(OH)2	cr	100	500	-205883.8935	6172.55449	-74.9975099	0.50121824	-0.001423349	1.99E-06	-1.10E-09	-145202.6205	355.244504
Ca(OH)2	cr	500	1023	-124541.3139	0	10.73593032	0.003982436	0	0	0	-122370.7243	-53.0239539
Ca(OH)2	L	1023	6000	0	0	18.40156546	0	0	0	0	-124519.1822	-98.60760364
CaBr	g	200	2500	-13553.62502	-49.30397672	5.156710478	-0.002208523	2.43E-06	-1.04E-09	1.55E-13	-7187.773462	1.435444732
CaBr2	cr	298	1014	-1012936.884	11490.40613	-47.07122446	0.146424105	-0.000206225	1.50E-07	-4.25E-11	-141981.4494	281.0096843
CaBr2	L	1015	2500	-11298862.48	63782.20868	-116.6376357	0.129938863	-6.85E-05	1.84E-08	-1.97E-12	-453582.6744	793.165632
CaCO3	cr	200	500	-13298624.25	250051.7168	-1907.177167	7.61666627	-0.016558709	1.88E-05	-8.72E-09	-1271058.215	9957.49756
CaCO3	cr	500	1603	-258355.5736	0	11.97256363	0.003263812	0	0	0	-149700.9803	-59.61133653
CaCl	g	200	1000	6395.33526	-224.9042269	5.28327839	-0.001447983	1.64E-06	-9.43E-10	2.24E-13	-12701.69	-1.391964289
CaCl	g	1000	6000	1629182.545	-4766.22302	9.65892977	-0.002523044	5.83E-07	-4.10E-11	8.81E-17	16625.99241	-33.98731174
CaCl2	cr	100	500	6000.20601	-446.615217	8.1999886	0.023749176	-0.000100234	1.78E-07	-1.14E-10	-96060.5778	-39.1215957

CaCl2	cr	500	1048	-30188.18908	0	8.644766799	0.001529735	0	0	0	-98458.8075	-36.84266549
CaCl2	L	1048	6000	2661491.778	0	10.7835579	0	0	0	0	-93918.1861	-45.66953897
CaH	g	200	1000	-45137.8223	762.942921	-1.280874223	0.013187747	-1.48E-05	8.54E-09	-1.99E-12	23003.78814	30.53421525
CaH	g	1000	6000	-2696952.529	8607.05975	-7.02745482	0.007467916	-2.32E-06	3.42E-10	-1.89E-14	-27738.19107	78.4582201
CaH2	a	298	1053	0	0	3.599731073	0.004465567	0	0	0	-22559.82511	-16.86197756
CaH2	b	1053	1273	0	0	8.298745206	0	0	0	0	-24226.33646	-44.09678633
CaH2	L	1273	6000	0	0	9.020375224	0	0	0	0	-22498.99474	-47.17727797
CaI	g	200	1000	-826.179018	-85.089759	4.86417169	-0.000786317	1.10E-06	-7.35E-10	2.01E-13	523.675344	3.58539168
CaI	g	1000	6000	1771071.309	-5683.64373	11.53857476	-0.00419402	1.29E-06	-1.73E-10	8.38E-15	35832.932	-44.0591757
CaI2	cr	200	500	-1811328.452	31274.51814	-213.6599007	0.832870588	-0.001721726	1.88E-06	-8.44E-10	-210197.7983	1142.802698
CaI2	cr	500	1056	-6638.996165	0	8.652825001	0.00228456	0	0	0	-67217.3678	-32.54333551
CaI2	L	1056	6000	0	0	12.38798197	0	0	0	0	-64854.2531	-51.37218163
CaO	cr	200	500	-4775526.94	90377.1142	-694.432081	2.802477174	-0.006129403	6.98E-06	-3.25E-09	-482941.143	3619.04632
CaO	cr	500	3172	-145937.644	0	7.174205094	-0.001959947	1.29E-06	-2.08E-10	0	-78915.2508	-36.58562837
CaOH	g	200	2500	75345.78889	-1397.889335	11.11701186	-0.00836637	7.35E-06	-2.76E-09	3.79E-13	-18131.24685	-37.02370714
CaSO4	II	200	500	-13619774.72	258492.9291	-1984.800641	7.96944817	-0.017368052	1.97E-05	-9.17E-09	-1334631.522	10351.3935
CaSO4	II	500	1473	-298394.0124	0	13.59671225	0.00585723	0	0	0	-177784.6313	-68.02481458
CaSO4	I	1473	1733	0	0	19.84482549	0	0	0	0	-179829.8668	-104.5004358
Cl2	g	200	1000	34628.1517	-554.712652	6.20758937	-0.002989632	3.17E-06	-1.79E-09	4.26E-13	1534.069331	-9.438331107
Cl2	g	1000	6000	6092569.42	-19496.27662	28.54535795	-0.014499688	4.46E-06	-6.36E-10	3.33E-14	121211.7724	-169.0778824
Co	a	200	500	-865183.451	14621.35206	-99.7108911	0.37943386	-0.000780011	8.55E-07	-3.89E-10	-67959.6346	530.655021
Co	a	500	700	-987756.074	6820.6022	-15.21637485	0.022345417	-9.02E-06	0	0	-38528.3904	101.4399403
Co	b	700	800	0	0	2.125113886	0.002218475	0	0	0	-619.770942	-8.94454699
Co	b	800	1394	-1576349295	9154318.17	-21979.67504	27.93356668	-0.019803104	7.43E-06	-1.15E-09	-51821984.1	139984.6247
Co	b	1394	1400	0	0	307.0872109	-0.21554872	0	0	0	-213929.295	-1913.104819
Co	b	1400	1768	1648338062	-4036220.19	3722.6857	-1.526326566	0.000235467	0	0	26490102.62	-27514.66647
Co3O4	cr	200	2100	972093.0163	-15760.93361	90.65286147	-0.162664385	0.000192275	-1.01E-07	2.06E-11	-37700.47851	-509.3409508
CoCl2	cr	200	1012	404311.9402	-6537.016008	45.71206789	-0.097141518	0.000141083	-1.02E-07	2.91E-11	-9362.336283	-243.4272624

CoCl2	L	1013	2100	-2161578.149	8948.72024	-3.332283263	0.013708026	-6.84E-06	1.80E-09	-1.95E-13	-90694.20645	50.69765536
CoO	cr	200	3000	-444739.341	3603.547425	-3.700662352	0.01281295	-7.87E-06	2.72E-09	-3.48E-13	-50036.48773	33.4989814
Cu	cr	200	1358	-24557.75109	164.8069205	2.080947143	0.002639078	-2.71E-06	1.40E-09	-9.72E-14	-1737.850969	-8.1331668
Cu	L	1358	6000	0	0	3.944910764	0	0	0	0	-211.1013775	-18.36065775
Cu(OH)2	cr	298	2000	-890385.4622	8861.152448	-23.68682569	0.066000625	-5.39E-05	2.13E-08	-3.29E-12	-103089.9726	155.21307
Cu2	g	200	1000	-852.918348	-97.2004493	4.8822337	-0.000737137	1.00E-06	-6.39E-10	1.67E-13	57493.0702	1.105391325
Cu2	g	1000	6000	-86993.995	320.910387	3.97380288	0.000508081	-1.71E-07	3.22E-11	-1.96E-15	55060.9019	6.91450217
Cu2O	cr	200	600	694309.394	-11072.06812	70.0760082	-0.169301074	0.000229694	-1.19E-07	0	29719.95795	-380.060357
Cu2O	cr	600	1516	4899293.25	-32267.6771	92.4291324	-0.113305351	8.89E-05	-3.91E-08	8.17E-12	156236.4374	-566.828545
Cu2S	a	298	376	121994.4245	0	2.442685885	0.018229333	0	0	0	-10237.57104	-4.69653316
Cu2S	b	376	720	-1211638.496	12562.3353	-36.8330481	0.095472441	-9.86E-05	3.95E-08	0	-76980.513	235.2740334
Cu2S	c	720	1400	15859834.58	-94202.4229	239.8981626	-0.294386539	0.000208437	-7.76E-08	1.18E-11	520307.464	-1502.163502
Cu2S	L	1400	6000	0	0	10.78393315	0	0	0	0	-10752.59326	-45.51698813
Cu3Cl3	g	200	1000	4487.88532	-873.664444	19.36189091	-0.007137448	8.56E-06	-5.42E-09	1.41E-12	-31626.8996	-59.76797945
Cu3Cl3	g	1000	6000	-91885.5968	-15.7193643	16.0129417	-5.57E-06	1.30E-09	-1.56E-13	7.48E-18	-36087.6074	-40.13211395
CuBr	a	298	657	92829739.4	-1403844.53	8783.22347	-29.05323712	0.053733934	-5.27E-05	2.14E-08	6589039.38	-47521.1549
CuBr	b	657	741	20301.34717	0	8.68089931	0.00011927	0	0	0	-14948.45171	-37.8492054
CuBr	c	741	759	0	0	6.99654999	-2.48E-06	0	0	0	-13437.68009	-26.30094995
CuBr	L	759	1500	5249558.1	-27570.8129	71.0303666	-0.073683899	4.26E-05	-1.22E-08	1.49E-12	144286.3364	-436.636559
CuBr2	cr	298	800	-23147.96663	0	9.183704151	0.000623989	0	0	0	-19499.96594	-37.14221219
CuCl	a	298	685	-36581260.5	462246.075	-2297.616527	5.65646511	-0.006837763	3.26E-06	0	-2287516.266	13034.69843
CuCl	b	685	696	0	0	9.57358974	-1.82E-05	0	0	0	-21770.33413	-45.0341269
CuCl	L	696	1700	21363699.78	-112384.2012	257.6303311	-0.296752137	0.000193714	-6.60E-08	9.22E-12	626396.047	-1640.361694
CuCl2	cr	298	675	-21194.56576	-799.603725	12.93400534	-0.006531312	7.39E-06	-2.98E-09	0	-25358.22405	-61.850525
CuCl2	L	675	6000	0	0	9.913368316	0	0	0	0	-29297.00009	-43.86870689
CuF	cr	298	1300	89701.9163	-850.746108	7.49788956	0.00274156	-2.99E-06	1.37E-09	-2.45E-13	-22346.32002	-37.9652378
CuF	g	1300	6000	509415.483	-1415.00987	5.63234938	-0.000162913	-1.16E-07	5.07E-11	-4.15E-15	6305.5066	-7.40777361
CuF2	cr	298	1109	21737.03718	-493.71803	7.14031488	0.009517087	-7.46E-06	1.90E-09	4.47E-13	-64529.0647	-35.3550107
CuF2	L	1109	6000	0	0	12.07719998	0	0	0	0	-63511.335	-56.54007188

F2	g	200	1000	10181.76308	22.74241183	1.97135304	0.008151604	-1.15E-05	7.96E-09	-2.17E-12	-958.6943	11.30600296
F2	g	1000	6000	-2941167.79	9456.5977	-7.73861615	0.007644713	-2.24E-06	2.92E-10	-1.43E-14	-60710.0561	84.2383508
FCO	g	200	1000	11326.62744	-53.979185	2.966927601	0.007559959	-6.21E-06	2.40E-09	-3.37E-13	-22403.69579	10.92652142
FCO	g	1000	6000	-60858.5158	-1022.397533	7.52732256	-0.000105794	-1.37E-09	2.48E-12	-1.00E-16	-18050.98416	-16.30331278
Fe	a	200	500	13504.90931	-780.380625	9.44017147	-0.025217677	5.35E-05	-5.10E-08	1.99E-11	2416.521408	-47.4900285
Fe	a	500	800	3543032.74	-24471.50531	65.6102093	-0.070439297	3.18E-05	0	0	134505.9978	-413.378869
Fe	a	800	1042	2661026334	-7846827.97	-728.921228	26.13888297	-0.034947421	1.76E-05	-2.91E-09	52348684.7	-15290.522
Fe	a	1042	1184	248192305.2	0	-559.434909	0.327170494	0	0	0	646750.343	3669.16872
Fe	c	1184	1665	1442428576	-5335491.34	8052.828	-6.30308963	0.002677273	-5.75E-07	4.72E-11	32642642.5	-55088.5217
Fe(CO)5	L	253	6000	0	0	28.11771229	0	0	0	0	-100522.2674	-119.6624513
Fe(OH)2	cr	298	800	424092.604	-5246.0135	35.6407814	-0.057772854	8.33E-05	-5.35E-08	1.18E-11	-46423.859	-193.7387923
Fe(OH)2	cr	800	1500	8260012.74	-35848.4862	66.3148213	-0.029478932	4.57E-06	1.32E-09	-2.98E-13	142965.2898	-436.461628
Fe(OH)2	g	1500	6000	1612519.19	-6533.24199	18.42922816	-0.00207325	4.27E-07	-4.56E-11	1.99E-15	-2992.568633	-84.4594059
Fe(OH)3	cr	298	1500	-74182.8469	49.1536151	6.3516127	0.027302991	-2.01E-05	7.51E-09	-1.26E-12	-103613.2609	-31.17351481
Fe2(SO4)3	cr	298	700	-3987499.8	44715.8441	-187.1627045	0.520384327	-0.000525517	2.05E-07	0	-541897.628	1097.303717
Fe2(SO4)3	cr	700	2000	-17494751.74	73083.2078	-93.9295136	0.146805141	-7.96E-05	2.31E-08	-2.74E-12	-760714.651	686.533029
Fe3O4	cr	200	298	-51826712.3	1293463.453	-13411.21962	74.0184244	-0.228572589	0.000375288	-2.56E-07	-5570751.24	65756.8971
Fe3O4	cr	298	800	-4407671.38	53517.6027	-261.3667759	0.743193149	-0.000976784	5.86E-07	-8.78E-11	-401807.545	1478.276107
Fe3O4	cr	800	850	0	0	-107.0116148	0.173843671	0	0	0	-92310.226	616.926572
Fe3O4	cr	850	1870	57316919.8	-181610.5186	277.7813396	-0.184983032	6.15E-05	-3.66E-09	-1.38E-12	990699.285	-1868.855147
FeBr2	cr	298	649	1826952.838	2755.331947	-206.8271955	1.383719184	-0.003764823	4.81E-06	-2.36E-09	-14474.61311	931.8244065
FeBr2	cr	650	963	-18458659.3	38136.67353	-130.9064775	0.721938501	-0.001442692	1.20E-06	-3.58E-10	-282430.4623	650.9898947
FeBr2	L	964	2001	-68745.23512	-14700.47148	65.86368475	-0.074810008	5.19E-05	-1.77E-08	2.38E-12	43342.7883	-379.5780748
FeCl2	cr	200	950	-37575.2724	5.93207022	8.82276028	0.003742344	-4.62E-06	4.04E-09	-1.45E-12	-44035.9579	-37.2174735
FeCl2	L	950	6000	0	0	12.2885173	0	0	0	0	-41108.4253	-53.19067642
FeCl3	cr	200	576	1083084.258	-24100.75519	226.7237836	-1.029271661	0.002750292	-3.82E-06	2.18E-09	53283.02815	-1135.31735
FeCl3	L	577	1500	-12211213.72	79334.95983	-193.9681791	0.290116223	-0.000220418	8.74E-08	-1.42E-11	-489197.6449	1251.246286
Ga	cr	100	302	1665.524651	-166.7535996	3.86087638	-0.001325442	2.41E-06	0	0	-157.7791876	-17.3017803
Ga	L	302	6000	28468.30421	0	3.135362156	-3.62E-05	2.90E-08	0	0	-171.6496723	-10.5371728

Ga2Br2	g	200	1000	-11171.83241	-74.7147162	10.30246084	-0.000665793	8.20E-07	-5.30E-10	1.39E-13	-19132.97856	-13.17110316
Ga2Br2	g	1000	6000	-18853.73131	-1.263621802	10.00108034	-4.77E-07	1.14E-10	-1.38E-14	6.69E-19	-19510.53843	-11.41667594
Ga2Br4	g	200	1000	-13155.45939	-413.655302	17.62849229	-0.003514652	4.27E-06	-2.73E-09	7.12E-13	-52831.0181	-44.2752069
Ga2Br4	g	1000	6000	-57421.6721	-7.16013737	16.00598947	-2.61E-06	6.15E-10	-7.41E-14	3.57E-18	-54933.8976	-34.7927166
Ga2Br6	g	200	1000	-6725.11689	-806.752655	25.11671424	-0.006636515	7.98E-06	-5.06E-09	1.31E-12	-83706.352	-75.8527872
Ga2Br6	g	1000	6000	-95261.73	-14.4468188	22.01192546	-5.15E-06	1.20E-09	-1.44E-13	6.93E-18	-87822.233	-57.6589512
Ga2Cl2	g	200	1000	-9246.1337	-259.2159934	11.02847129	-0.002231984	2.72E-06	-1.74E-09	4.56E-13	-28340.59821	-20.67773272
Ga2Cl2	g	1000	6000	-36689.542	-4.43458068	10.00373051	-1.63E-06	3.85E-10	-4.65E-14	2.24E-18	-29656.33085	-14.69535817
Ga2Cl4	g	200	1000	16373.43702	-1140.637354	20.30139827	-0.008997746	1.07E-05	-6.70E-09	1.73E-12	-71623.8501	-66.663619
Ga2Cl4	g	1000	6000	-112711.0409	-21.38517542	16.01738077	-7.42E-06	1.72E-09	-2.05E-13	9.80E-18	-77468.5338	-41.4728087
Ga2Cl6	g	200	1000	60894.6984	-2104.456302	29.59653878	-0.015378098	1.78E-05	-1.10E-08	2.78E-12	-111840.0535	-112.1945814
Ga2Cl6	g	1000	6000	-189844.5426	-44.1365524	22.03505047	-1.47E-05	3.37E-09	-3.98E-13	1.88E-17	-122696.9998	-67.45332883
Ga2F2	g	200	1000	29781.3065	-1013.97552	13.74933053	-0.007728051	9.06E-06	-5.64E-09	1.44E-12	-70860.8337	-41.0983395
Ga2F2	g	1000	6000	-87732.3493	-19.8377587	10.0159403	-6.74E-06	1.56E-09	-1.85E-13	8.78E-18	-76073.6863	-19.08325521
Ga2F4	g	200	1000	142207.9998	-2798.829941	23.95904235	-0.012939048	1.22E-05	-6.25E-09	1.33E-12	-149601.371	-97.3415364
Ga2F4	g	1000	6000	-270436.609	-104.9957196	16.07903965	-3.18E-05	7.05E-09	-8.10E-13	3.76E-17	-164416.9589	-48.9659173
Ga2F6	g	200	1000	240904.5572	-4142.3798	31.9577372	-0.012979143	8.96E-06	-2.73E-09	1.55E-13	-227278.524	-139.8403732
Ga2F6	g	1000	6000	-436866.48	-212.8208368	22.15886373	-6.35E-05	1.40E-08	-1.60E-12	7.41E-17	-249429.8707	-77.8763583
Ga2I2	g	200	1000	-8960.25267	-31.7205721	10.12930491	-0.000286019	3.54E-07	-2.29E-10	6.04E-14	-1233.174068	-9.80196838
Ga2I2	g	1000	6000	-12190.56501	-0.528755447	10.00045392	-2.01E-07	4.80E-11	-5.83E-15	2.83E-19	-1393.258606	-9.05261491
Ga2I4	g	200	1000	-17694.95991	-135.4871509	16.54625333	-0.001199015	1.47E-06	-9.50E-10	2.50E-13	-23334.05795	-33.2571289
Ga2I4	g	1000	6000	-31712.9976	-2.287068836	16.00194812	-8.59E-07	2.04E-10	-2.48E-14	1.20E-18	-24019.40505	-30.08672521
Ga2I6	g	200	1000	-21108.91458	-369.540416	23.46811836	-0.003189178	3.89E-06	-2.49E-09	6.53E-13	-43011.8809	-60.148115
Ga2I6	g	1000	6000	-60156.9815	-6.32920923	22.0053304	-2.33E-06	5.51E-10	-6.66E-14	3.21E-18	-44886.9938	-51.6100875
Ga2O	g	200	1000	56971.9718	-807.408599	7.73306154	0.001478451	-4.10E-06	3.58E-09	-1.11E-12	-9512.21682	-12.56149299
Ga2O	g	1000	6000	-119387.4986	-87.1934161	7.0646782	-2.57E-05	5.65E-09	-6.45E-13	2.98E-17	-13936.94796	-6.9428013
Ge	cr	200	400	-239650.6145	3150.57215	-13.33941357	0.036479978	-2.94E-05	0	0	-16138.82957	79.392116

Ge	cr	400	1211	-18882.41797	0	2.89817307	0.000359166	0	0	0	-943.386408	-12.98669726
Ge	L	1211	6000	0	0	3.319498082	0	0	0	0	3278.99664	-11.85992953
GeO	g	200	1000	-6781.22563	279.1946972	0.619895286	0.01111378	-1.50E-05	1.01E-08	-2.69E-12	-6711.84743	21.56441027
GeO	g	1000	6000	-1044508.485	2734.866048	1.298071298	0.001832639	-5.06E-07	6.37E-11	-2.17E-15	-23621.04658	23.50906051
GeO2	II	100	298	-13620.6101	0	1.390091028	0.016088149	0	0	0	-70956.8274	-8.0174837
GeO2	II	298	1308	-276312.1338	0	9.404643208	-0.001212218	1.11E-06	0	0	-73468.3007	-50.04997052
GeO2	I	1308	1388	-153526.7863	0	7.481860025	0.001711466	0	0	0	-69946.5297	-37.1133196
GeO2	L	1388	6000	0	0	9.441326067	0	0	0	0	-68838.3787	-47.38551165
H2	g	200	1000	40783.2321	-800.918604	8.21470201	-0.012697145	1.75E-05	-1.20E-08	3.37E-12	2682.484665	-30.43788844
H2	g	1000	6000	560812.801	-837.150474	2.975364532	0.001252249	-3.74E-07	5.94E-11	-3.61E-15	5339.82441	-2.202774769
H2O	cr	200	273	-402677.748	2747.887946	57.3833663	-0.826791524	0.004413088	-1.05E-05	9.69E-09	-55303.1499	-190.2572063
H2O	L	273	373	1326371304	-24482953.88	187942.8776	-767.899505	1.761556813	-0.002151167	1.09E-06	110176047.6	-977970.097
H2O	g	373	1000	-39479.6083	575.573102	0.931782653	0.007222713	-7.34E-06	4.96E-09	-1.34E-12	-33039.7431	17.24205775
H2O	g	1000	6000	1034972.096	-2412.698562	4.64611078	0.002291998	-6.84E-07	9.43E-11	-4.82E-15	-13842.86509	-7.97814851
H2SO4	L	298	609	3251892.012	6225.222926	-388.5093749	2.542961544	-0.006832079	8.70E-06	-4.26E-09	-74477.79491	1748.660831
H2SO4	g	610	2500	-3199954.217	13634.97828	-15.09790931	0.034521976	-1.84E-05	5.05E-09	-5.63E-13	-173254.5687	141.4807919
HBr	g	200	1000	25272.22498	-406.511027	6.04311661	-0.007717883	1.15E-05	-7.29E-09	1.75E-12	-3510.41455	-9.90318629
HBr	g	1000	6000	1170033.949	-3786.52101	7.50314805	-0.001284964	3.21E-07	-3.44E-11	1.13E-15	18564.13349	-25.62712911
HCl	g	200	1000	20625.88287	-309.3368855	5.27541885	-0.004828874	6.20E-06	-3.04E-09	4.92E-13	-10677.82299	-7.309305408
HCl	g	1000	6000	915774.951	-2770.550211	5.97353979	-0.000362981	4.74E-08	2.81E-12	-6.66E-16	5674.95805	-16.42825822
HI	g	200	1000	18728.8173	-343.178884	5.95671243	-0.00854344	1.45E-05	-1.05E-08	2.84E-12	3682.95072	-8.14975609
HI	g	1000	6000	472492.145	-1923.465741	5.75804897	-0.000406627	9.47E-08	-1.03E-11	4.61E-16	13948.57037	-11.82487652
I2	cr	200	386	-3901269.14	91432.0233	-890.04575	4.67127016	-0.013571618	2.07E-05	-1.29E-08	-391263.263	4422.60365
I2	L	386	457	0	0	9.568212679	0	0	0	0	-1204.453805	-36.37326088
I2	g	457	1000	-5087.96877	-12.4958521	4.50421909	0.000137096	-1.39E-07	1.17E-10	-2.34E-14	6213.46981	5.58383694
I2	g	1000	6000	-5632594.16	17939.6156	-17.23055169	0.012442141	-3.33E-06	4.13E-10	-1.96E-14	-106850.5292	160.0531883
K	cr	200	336	-102203.1747	0	13.33752016	-0.055809908	9.01E-05	0	0	-2635.06243	-56.1537652
K	L	336	1039	-3935.72203	-45.4727811	4.845244	-0.003083547	2.02E-06	-3.71E-11	5.03E-15	-807.560968	-18.36641748

K	g	1039	6000	-3566422.36	10852.89825	-10.54134898	0.008009801	-2.70E-06	4.72E-10	-2.98E-14	-58753.3701	97.3855124
K2Br2	g	200	1000	-10930.40504	-48.5665148	10.19754923	-0.000436316	5.39E-07	-3.49E-10	9.19E-14	-67580.7324	-12.94944706
K2Br2	g	1000	6000	-15892.29976	-0.810137946	10.00069442	-3.07E-07	7.33E-11	-8.91E-15	4.32E-19	-67825.9544	-11.80425726
K2C2N2	g	200	1000	4627.78948	-972.981062	19.9666591	-0.019530151	3.28E-05	-2.39E-08	6.60E-12	-777.441126	-67.55613632
K2C2N2	g	1000	6000	726959.95	-3492.10868	18.35676822	-0.000878548	1.85E-07	-2.04E-11	9.19E-16	15826.00773	-67.28484052
K2CO3	a	200	693	-363282.643	5957.56784	-30.80710797	0.149455871	-0.000237716	2.23E-07	-8.47E-11	-169413.6603	176.3682121
K2CO3	b	693	1173	0	0	13.1002308	0.008280945	0	0	0	-142406.5852	-58.05609552
K2CO3	L	1173	6000	0	0	24.71582811	0	0	0	0	-146666.3988	-127.30642
K2Cl2	g	200	1000	-13285.26456	-124.1832429	10.5003573	-0.001097776	1.35E-06	-8.70E-10	2.29E-13	-76443.6315	-17.90150052
K2Cl2	g	1000	6000	-26146.11331	-2.096229095	10.00178456	-7.86E-07	1.87E-10	-2.27E-14	1.10E-18	-77071.8933	-14.99720802
K2F2	g	200	1000	-1611.833856	-513.564489	11.99922511	-0.00428011	5.17E-06	-3.29E-09	8.55E-13	-103924.8602	-30.39925079
K2F2	g	1000	6000	-57408.9253	-9.04618211	10.00750685	-3.25E-06	7.63E-10	-9.17E-14	4.41E-18	-106541.3546	-18.7403762
K2I2	g	200	1000	-8977.75244	-27.76460169	10.11331014	-0.000250842	3.10E-07	-2.01E-10	5.30E-14	-53262.0839	-10.32092509
K2I2	g	1000	6000	-11796.34729	-0.472476155	10.00040695	-1.81E-07	4.32E-11	-5.26E-15	2.55E-19	-53402.1023	-9.6644405
K2O	cr	298	2000	-1925745.978	15186.20356	-36.27481065	0.070589709	-5.03E-05	1.93E-08	-2.94E-12	-128588.9257	239.1010865
K2O2	cr	298	818	0	0	9.1512308	0.006015267	0	0	0	-56276.148	-39.86168914
K2O2	L	818	6000	0	0	16.11640373	0	0	0	0	-57495.6103	-78.6415132
K2O2H2	g	200	6000	147183.5354	-1608.75989	12.77519157	0.002747938	-8.70E-07	1.25E-10	-6.84E-15	-73031.32927	-38.71932162
KBF4	cr	298	555	53599714.87	-231572.0473	-2509.638107	22.62862711	-0.070278974	9.87E-05	-5.29E-08	1465529.174	9449.325414
KBF4	cr	556	842	38060485.21	-160278.9963	0.993207796	1.150067822	-0.002455418	2.14E-06	-6.93E-10	779171.9991	-569.5661487
KBF4	L	843	1500	-45532755.96	307264.9295	-794.4420051	1.1042533	-0.000815253	3.13E-07	-4.89E-11	-1933111.987	5026.057887
KCN	II	168	400	47892.2666	-686.939942	11.89656301	-0.009957932	9.25E-06	0	0	-12758.80363	-51.8904736
KCN	II	400	895	-85507.2608	711.510918	5.64244236	0.003733592	-2.88E-06	8.85E-10	0	-19811.54134	-15.8646147
KCN	L	895	6000	0	0	9.057899984	0	0	0	0	-15226.66331	-35.45330543
KCl	cr	200	500	1179895.024	-22178.24961	173.093063	-0.654543415	0.001415898	-1.60E-06	7.39E-10	45607.8273	-899.152715
KCl	cr	500	1044	288.8789664	0	5.28708855	0.004004092	-4.34E-06	2.75E-09	0	-54217.8564	-21.21648362
KCl	L	1044	6000	0	0	8.659560215	0	0	0	0	-53221.1323	-38.76839685
KNO2	II	200	314	-12282974.84	0	1182.559906	-6.07684232	0.008778425	0	0	-245242.4942	-5366.9059

KNO2	I	314	711	0	0	9.827879214	0.002012867	0	0	0	-46877.7497	-37.82318671
KNO2	L	711	6000	0	0	12.2677103	0	0	0	0	-46095.1596	-49.58866367
KNO3	a	200	402	3565624.07	-62913.1938	439.259994	-1.436497824	0.002380418	-1.52E-06	0	225850.5778	-2341.795728
KNO3	b	402	607	3211975.21	0	-50.32659772	0.146207053	-8.16E-05	0	0	-39348.4662	280.712374
KNO3	L	607	6000	0	0	16.95830542	0	0	0	0	-63451.0635	-79.18784042
KOH	a	100	298	-438006.462	11254.72885	-102.3623342	0.437563044	-0.000592035	0	0	-100215.5756	524.130828
KOH	b	298	517	-2814.35707	0	6.478313214	0.006183768	0	0	0	-53138.8216	-28.99826328
KOH	c	517	679	0	0	9.621733572	0	0	0	0	-53258.5783	-44.13346659
KOH	L	679	6000	0	0	10.46363526	0	0	0	0	-52880.0834	-48.22385687
Li	cr	200	298	-9860.65235	0	2.30432385	0.002671664	0	0	0	-838.853612	-10.47881686
Li	cr	298	453	72388.2496	0	0.157031447	0.006770404	0	0	0	-104.9497436	0.996176314
Li	L	453	6000	24655.69228	0	3.755723428	-0.00063323	3.16E-07	0	0	-729.911669	-17.01274654
Li2Br2	g	200	1000	27863.12863	-1005.641437	13.70963066	-0.007633663	8.94E-06	-5.56E-09	1.42E-12	-57628.4584	-41.2184376
Li2Br2	g	1000	6000	-89009.8336	-19.88916335	10.01596418	-6.75E-06	1.56E-09	-1.84E-13	8.77E-18	-62799.8996	-19.43063525
Li2CO3	cr	200	500	19895943.37	-363170.677	2691.242782	-10.3310902	0.022014008	-2.45E-05	1.12E-08	1495415.902	-14132.51128
Li2CO3	cr	500	1005	-52765.0228	0	7.02505154	0.018094794	0	0	0	-149097.7245	-34.878714
Li2CO3	L	1005	6000	0	0	22.25025888	0	0	0	0	-150229.2112	-116.9607936
Li2Cl2	g	200	1000	53133.9861	-1427.266759	15.12410161	-0.010328249	1.19E-05	-7.31E-09	1.85E-12	-67698.604	-52.85131549
Li2Cl2	g	1000	6000	-117957.1272	-30.27126342	10.02397711	-1.00E-05	2.30E-09	-2.71E-13	1.28E-17	-75068.2259	-22.6497023
Li2F2	g	200	1000	144316.6185	-2466.874678	17.0286329	-0.011455412	1.09E-05	-5.57E-09	1.19E-12	-102607.0133	-70.0038661
Li2F2	g	1000	6000	-218893.1683	-92.5981453	10.06970757	-2.80E-05	6.22E-09	-7.15E-13	3.32E-17	-115661.1527	-27.29853181
Li2I2	g	200	1000	10148.72266	-712.042101	12.7039296	-0.005685537	6.77E-06	-4.26E-09	1.10E-12	-43130.6386	-33.0395098
Li2I2	g	1000	6000	-69735.8706	-13.16825508	10.01074855	-4.60E-06	1.07E-09	-1.28E-13	6.11E-18	-46774.7005	-17.21894034
Li2O2	cr	298	1000	0	0	6.874488094	0.007197297	0	0	0	-78441.3559	-34.33817812
Li2O2	g	1000	6000	-293923.2153	-235.9107937	10.17463402	-6.93E-05	1.52E-08	-1.73E-12	7.99E-17	-36184.8191	-29.04221044
LiCl	cr	200	500	-2180497.685	39713.2078	-291.8258028	1.160079971	-0.002482284	2.79E-06	-1.28E-09	-230242.7379	1533.139994
LiCl	cr	500	883	-35956.0933	0	5.4807705	0.002332209	0	0	0	-50994.1173	-24.99631307
LiCl	L	883	6000	0	0	7.601169522	0	0	0	0	-49541.1449	-34.60716245
LiH	cr	200	965	-7983.39954	-413.516742	3.84267241	0.003568428	3.56E-07	9.30E-10	-5.47E-13	-9882.37451	-21.93513588

LiH	L	965	6000	0	0	6.614941831	0	0	0	0	-10890.8882	-34.06734782
LiOH	cr	200	746	-1219596.094	20883.15832	-146.3475951	0.561159282	-0.00108438	1.07E-06	-4.22E-10	-155353.5026	774.413168
LiOH	L	746	6000	0	0	10.49971676	0	0	0	0	-60502.8071	-54.0738796
Mg	cr	100	298	-5412.225134	0	1.458173723	0.013302047	-4.10E-05	4.75E-08	0	-775.947201	-6.989702348
Mg	cr	298	923	-28600.60304	0	3.398877384	-0.000724396	1.41E-06	0	0	-1089.519906	-15.45973664
Mg	L	923	1366	0	0	4.125318269	0	0	0	0	-658.991948	-19.37828582
Mg	g	1366	6000	0	0	2.5	0	0	0	0	16946.58761	3.63433014
Mg(OH)2	cr	200	500	-640145.184	8358.13999	-39.711454	0.123192722	-9.65E-05	0	0	-153724.6903	225.8495398
Mg(OH)2	cr	500	1000	-5543828.43	37008.6861	-90.8862334	0.143168919	-9.51E-05	2.53E-08	0	-318945.089	580.163827
Mg(OH)2	L	1000	6000	-303758.1289	0	12.03462381	0.002202655	0	0	0	-115877.5486	-63.33852645
MgCl	g	200	1000	20439.9528	-407.215516	5.8803723	-0.002594175	2.95E-06	-1.75E-09	4.34E-13	-5851.44495	-6.02354575
MgCl	g	1000	6000	1041328.453	-3380.15833	8.63777547	-0.00244779	7.84E-07	-1.13E-10	5.81E-15	13271.88977	-27.03802395
MgCl2	cr	200	987	203561.3802	-3336.129578	24.96114136	-0.03774926	5.28E-05	-3.78E-08	1.12E-11	-63641.79277	-132.275296
MgCl2	L	987	2500	-99916.5633	-221.7185473	12.19962681	-0.00134223	6.72E-07	-1.48E-10	1.13E-14	-75485.30939	-55.9758817
MgO	cr	200	3100	-388.7191491	-765.3619981	7.055458897	-1.96E-05	-2.12E-07	1.60E-10	-2.53E-14	-70054.68751	-39.52570769
MgSO4	cr	200	1400	-65371.50585	-560.0274958	10.82870546	0.014364799	-1.31E-05	9.57E-09	-2.84E-12	-152562.2485	-56.74781107
MgSO4	L	1400	2500	100260370.3	-30718.08561	-315.2556516	0.490355257	-0.000289226	7.95E-08	-8.43E-12	320864.2667	1856.496536
N2	g	200	1000	22103.71497	-381.846182	6.08273836	-0.008530914	1.38E-05	-9.63E-09	2.52E-12	710.846086	-10.76003744
N2	g	1000	6000	587712.406	-2239.249073	6.06694922	-0.000613969	1.49E-07	-1.92E-11	1.06E-15	12832.10415	-15.86640027
NH4I	cr	298	2000	1412445.443	-13848.55837	59.45867719	-0.087184358	8.90E-05	-3.87E-08	5.83E-12	44771.28372	-341.3141015
Na	cr	200	371	-35844.5801	0	6.47941469	-0.018986973	3.35E-05	0	0	-1504.31974	-26.77783039
Na	L	371	1170	26948.1867	-231.900078	5.16243569	-0.003058572	1.70E-06	-1.52E-10	1.96E-14	284.2114288	-22.2576398
Na	g	1170	60000	952572.338	-2623.807254	5.16259662	-0.001210219	2.31E-07	-1.25E-11	7.23E-16	29129.63564	-15.19717061
Na2CO3	cr	200	723	6729717.889	-111653.7356	743.5793548	-2.449285149	0.004454026	-4.13E-06	1.55E-09	377958.3647	-3990.917634
Na2CO3	cr	723	1123	4626.537542	-31269.76656	121.405768	-0.115864101	1.37E-05	6.13E-08	-2.78E-11	15159.46481	-736.3211564
Na2CO3	L	1123	2500	-861453.6285	-79337.45675	260.3962856	-0.276281339	0.000157465	-4.41E-08	4.86E-12	263080.9603	-1626.188675
NaCl	cr	200	500	2725695.501	-51609.5875	398.458231	-1.547496756	0.003352172	-3.79E-06	1.75E-09	180753.0763	-2076.949046
NaCl	cr	500	1074	2657.827371	0	5.66571869	0.00087089	1.34E-06	0	0	-51193.8472	-23.90773149

NaCl	L	1074	6000	0	0	8.166446369	0	0	0	0	-49434.5901	-36.49536621
NaOH	a	100	298	20083.29119	-771.467716	8.69417109	0.003850883	-3.61E-06	0	0	-49480.2345	-45.2489957
NaOH	a	298	514	1048215.71	0	-95.92892425	0.618956499	-0.001367212	1.07E-06	0	-36635.4104	427.0051072
NaOH	b	514	568	0	0	9.621733572	0	0	0	0	-54425.5895	-47.99292559
NaOH	c	568	594	0	0	10.34336359	0	0	0	0	-54070.5475	-51.22288687
NaOH	L	594	1000	0	0	10.77790513	-0.000711166	0	0	0	-53438.2748	-52.28806116
NaOH	L	1000	6000	0	0	10.06673875	0	0	0	0	-53082.6916	-48.08666421
O2	g	200	1000	-34255.6342	484.700097	1.119010961	0.004293889	-6.84E-07	-2.02E-09	1.04E-12	-3391.45487	18.4969947
O2	g	1000	6000	-1037939.022	2344.830282	1.819732036	0.001267848	-2.19E-07	2.05E-11	-8.19E-16	-16890.10929	17.38716506
S	a	200	368	-10357.10779	0	1.866766938	0.00425614	-3.27E-06	0	0	-751.638958	-7.96106698
S	b	368	388	0	0	2.080514131	0.00244088	0	0	0	-685.271473	-8.60784675
S	L	388	428	-63665507.65	0	2376.860693	-7.888076026	0.007376077	0	0	-635659.492	-11869.29589
S	L	428	432	0	0	6928.522306	-32.54655981	0.038244482	0	0	-983222.268	-31548.06751
S	L	432	453	0	0	164.9945697	-0.684353498	0.000731591	0	0	-26388.46929	-768.1730097
S	L	453	717	1972984.578	0	-24.41009753	0.060903529	-3.74E-05	0	0	11130.1344	136.3174183
S	L	717	882	0	0	3.848693429	0	0	0	0	-828.458983	-17.36128237
S	g	882	6000	-110799.965	656.920447	0.817114236	0.001201911	-3.76E-07	5.57E-11	-3.03E-15	3285.66945	10.2118207
SO2	g	200	1100	-53638.6455	909.5836352	-2.332521169	0.021914097	-2.48E-05	1.41E-08	-3.24E-12	-41152.86137	40.34144856
SO2	g	1100	3000	562150.4576	-3047.540636	10.5830952	-0.002233769	8.42E-07	-1.63E-10	1.30E-14	-19654.66117	-37.22937942
SO3	g	200	1000	-39528.5529	620.857257	-1.437731716	0.027641265	-3.14E-05	1.79E-08	-4.13E-12	-51841.0617	33.91331216
SO3	g	1000	6000	-216692.3781	-1301.022399	10.96287985	-0.00038371	8.47E-08	-9.71E-12	4.50E-16	-43982.8399	-36.55217314

Chapter 7 - References

[1] M. S. Mannan, O. Reyes-Valdes, P. Jain, N. Tamim, and M. Ahammad, “The Evolution of Process Safety: Current Status and Future Direction,” *Annual Review of Chemical and Biomolecular Engineering*, vol. 7, no. 1, pp. 135–162, 2016, doi: 10.1146/annurev-chembioeng-080615-033640.

[2] A. Stankiewicz and J. A. Moulijn, *Re-Engineering the Chemical Processing Plant: Process Intensification*. CRC Press, 2003.

[3] M. Baldea, “From process integration to process intensification,” *Computers & Chemical Engineering*, vol. 81, pp. 104–114, Oct. 2015, doi: 10.1016/j.compchemeng.2015.03.011.

[4] A. Basile *et al.*, “Methane steam reforming in a Pd–Ag membrane reformer: An experimental study on reaction pressure influence at middle temperature,” *International Journal of Hydrogen Energy*, vol. 36, no. 2, pp. 1531–1539, Jan. 2011, doi: 10.1016/j.ijhydene.2010.10.101.

[5] N. Asprion and G. Kaibel, “Dividing wall columns: Fundamentals and recent advances,” *Chemical Engineering and Processing: Process Intensification*, vol. 49, no. 2, pp. 139–146, Feb. 2010, doi: 10.1016/j.cep.2010.01.013.

[6] S. LeViness, S. R. Deshmukh, L. A. Richard, and H. J. Robota, “Velocys Fischer–Tropsch Synthesis Technology—New Advances on State-of-the-Art,” *Top Catal*, vol. 57, no. 6, pp. 518–525, Apr. 2014, doi: 10.1007/s11244-013-0208-x.

[7] J. M. Ponce-Ortega, M. M. Al-Thubaiti, and M. M. El-Halwagi, “Process intensification: New understanding and systematic approach,” *Chemical Engineering and Processing: Process Intensification*, vol. 53, pp. 63–75, Mar. 2012, doi: 10.1016/j.cep.2011.12.010.

[8] S. Sharma and G. P. Rangaiah, “An improved multi-objective differential evolution with a termination criterion for optimizing chemical processes,” *Computers & Chemical Engineering*, vol. 56, pp. 155–173, Sep. 2013, doi: 10.1016/j.compchemeng.2013.05.004.

[9] A. Carvalho, H. A. Matos, and R. Gani, “SustainPro—A tool for systematic process analysis, generation and evaluation of sustainable design alternatives,” *Computers & Chemical Engineering*, vol. 50, pp. 8–27, Mar. 2013, doi: 10.1016/j.compchemeng.2012.11.007.

[10] C.-L. Wei, Y.-C. Chen, C.-C. Cheng, K.-S. Kao, D.-L. Cheng, and C.-J. Chung, “Highly Sensitive UV Sensors Based on SMR Oscillators,” *Procedia Engineering*, vol. 36, pp. 468–475, 2012, doi: 10.1016/j.proeng.2012.03.068.

[11] S. Dabir, W. Deng, M. Sahimi, and T. Tsotsis, “Fabrication of silicon carbide membranes on highly permeable supports,” *Journal of Membrane Science*, vol. 537, pp. 239–247, Sep. 2017, doi: 10.1016/j.memsci.2017.05.038.

[12] R. Carapellucci and A. Milazzo, “Membrane systems for CO2 capture and their integration with gas turbine plants,” *Proceedings of the Institution of Mechanical Engineers, Part A: Journal of Power and Energy*, vol. 217, no. 5, pp. 505–517, Jan. 2003, doi: 10.1243/095765003322407557.

[13] K. Kusakabe, M. Yamamoto, and S. Morooka, “Gas permeation and micropore structure of carbon molecular sieving membranes modified by oxidation,” *Journal of Membrane Science*, vol. 149, no. 1, pp. 59–67, Oct. 1998, doi: 10.1016/S0376-7388(98)00156-2.

[14] M. Conesa, J. F. Sánchez Pérez, I. Alhama, and F. Alhama, “On the nondimensionalization of coupled, nonlinear ordinary differential equations,” *Nonlinear Dynamics*, vol. 84, no. 1, pp. 91–105, Apr. 2016, doi: 10.1007/s11071-015-2233-8.

[15] J. F. Sánchez Pérez, M. Conesa, I. Alhama, F. Alhama, and M. Cánovas, “Searching fundamental information in ordinary differential equations. Nondimensionalization technique,” *PLOS ONE*, vol. 12, no. 10, p. e0185477, Oct. 2017, doi: 10.1371/journal.pone.0185477.

[16] I. Alhama Manteca, M. Alcaraz, E. Trigueros, and F. Alhama, “Dimensionless characterization of salt intrusion benchmark scenarios in anisotropic media,” *Applied Mathematics and Computation*, vol. 247, pp. 1173–1182, Nov. 2014, doi: 10.1016/j.amc.2014.09.033.

[17] M. M. Y. Motamedhashemi, F. Egolfopoulos, and T. Tsotsis, “Application of a flow-through catalytic membrane reactor (FTCMR) for the destruction of a chemical warfare simulant,” *Journal of Membrane Science*, vol. 376, no. 1, pp. 119–131, Jul. 2011, doi: 10.1016/j.memsci.2011.04.013.

[18] M. Alavi, R. Eslamloueyan, and M. R. Rahimpour, “Multi Objective Optimization of a Methane Steam Reforming Reaction in a Membrane Reactor: Considering the Potential Catalyst Deactivation due to the Hydrogen Removal,” *International Journal of Chemical Reactor Engineering*, vol. 16, no. 2, Feb. 2018, doi: 10.1515/ijcre-2017-0066.

[19] T. Tsuru, K. Yamaguchi, T. Yoshioka, and M. Asaeda, “Methane steam reforming by microporous catalytic membrane reactors,” *AIChE Journal*, vol. 50, no. 11, pp. 2794–2805, Nov. 2004, doi: 10.1002/aic.10215.

[20] S. H. Israni, B. K. R. Nair, and M. P. Harold, “Hydrogen generation and purification in a composite Pd hollow fiber membrane reactor: Experiments and modeling,” *Catalysis Today*, vol. 139, no. 4, pp. 299–311, Jan. 2009, doi: 10.1016/j.cattod.2008.02.020.

[21] Y. V. Gokhale, R. D. Noble, and J. L. Falconer, “Effects of reactant loss and membrane selectivity on a dehydrogenation reaction in a membrane-enclosed catalytic reactor,” *Journal of Membrane Science*, vol. 103, no. 3, pp. 235–242, Jul. 1995, doi: 10.1016/0376-7388(95)00006-X.

[22] K. Mohan and R. Govind, “Analysis of a cocurrent membrane reactor,” *AIChE Journal*, vol. 32, no. 12, pp. 2083–2086, 1986, doi: 10.1002/aic.690321219.

[23] J. Xu and G. F. Froment, “Methane steam reforming, methanation and water-gas shift: I. Intrinsic kinetics,” *AIChE Journal*, vol. 35, no. 1, pp. 88–96, 1989, doi: 10.1002/aic.690350109.

[24] C. R. H. de Smet, M. H. J. M. de Croon, R. J. Berger, G. B. Marin, and J. C. Schouten, “Design of adiabatic fixed-bed reactors for the partial oxidation of methane to synthesis gas. Application to production of methanol and hydrogen-for-fuel-cells,” *Chemical Engineering Science*, vol. 56, no. 16, pp. 4849–4861, Aug. 2001, doi: 10.1016/S0009-2509(01)00130-0.

[25] J. R. Rostrup-Nielsen, “Catalytic Steam Reforming,” in *Catalysis: Science and Technology Volume 5*, J. R. Anderson and M. Boudart, Eds. Berlin, Heidelberg: Springer Berlin Heidelberg, 1984, pp. 1–117. doi: 10.1007/978-3-642-93247-2_1.

[26] W. Zhou and V. I. Manousiouthakis, “On dimensionality of attainable region construction for isothermal reactor networks,” *Computers & Chemical Engineering*, vol. 32, no. 3, pp. 439–450, Mar. 2008, doi: 10.1016/j.compchemeng.2007.02.013.

[27] G. Di Marcoberardino, F. Sosio, G. Manzolini, and S. Campanari, “Fixed bed membrane reactor for hydrogen production from steam methane reforming: Experimental and modeling approach,” *International Journal of Hydrogen Energy*, vol. 40, no. 24, pp. 7559–7567, Jun. 2015, doi: 10.1016/j.ijhydene.2014.11.045.

[28] S. A. M. Said, D. S. A. Simakov, M. Waseeuddin, and Y. Román-Leshkov, “Solar molten salt heated membrane reformer for natural gas upgrading and hydrogen generation: A CFD model,” *Solar Energy*, vol. 124, pp. 163–176, Feb. 2016, doi: 10.1016/j.solener.2015.11.038.

[29] W. Deng, X. Yu, M. Sahimi, and T. T. Tsotsis, “Highly permeable porous silicon carbide support tubes for the preparation of nanoporous inorganic membranes,” *Journal of Membrane Science*, vol. 451, pp. 192–204, Feb. 2014, doi: 10.1016/j.memsci.2013.09.059.

[30] M. Huysmans and A. Dassargues, “Review of the use of Péclet numbers to determine the relative importance of advection and diffusion in low permeability environments,” *Hydrogeol J*, vol. 13, no. 5, pp. 895–904, Oct. 2005, doi: 10.1007/s10040-004-0387-4.

[31] S. T. Horseman, J. J. W. Higgo, J. Alexander, and J. F. Harrington, *Water, gas and solute movement through argillaceous media*. Nuclear Energy Agency of the OECD (NEA): Organisation for Economic Co-Operation and Development, 1996.

[32] S. Chapman and T. G. Cowling, *The Mathematical Theory of Non-uniform Gases: An Account of the Kinetic Theory of Viscosity, Thermal Conduction and Diffusion in Gases*. Cambridge University Press, 1990.

[33] L. A. Bromley and C. R. Wilke, “Viscosity Behavior of Gases,” *Ind. Eng. Chem.*, vol. 43, no. 7, pp. 1641–1648, Jul. 1951, doi: 10.1021/ie50499a046.

[34] J. W. Buddenberg and C. R. Wilke, “Viscosities of Some Mixed Gases.,” *J. Phys. Chem.*, vol. 55, no. 9, pp. 1491–1498, Sep. 1951, doi: 10.1021/j150492a008.

[35] D. Roy and G. Thodos, “Thermal Conductivity of Gases. Organic Compounds at Atmospheric Pressure,” *Ind. Eng. Chem. Fund.*, vol. 9, no. 1, pp. 71–79, Feb. 1970, doi: 10.1021/i160033a011.

[36] W. Su, L. Zhao, and S. Deng, “Group contribution methods in thermodynamic cycles: Physical properties estimation of pure working fluids,” *Renewable and Sustainable Energy Reviews*, vol. 79, pp. 984–1001, Nov. 2017, doi: 10.1016/j.rser.2017.05.164.

[37] E. A. Mason and S. C. Saxena, “Approximate Formula for the Thermal Conductivity of Gas Mixtures,” *The Physics of Fluids*, vol. 1, no. 5, pp. 361–369, Sep. 1958, doi: 10.1063/1.1724352.

[38] B. E. Poling, J. M. Prausnitz, and J. P. O’Connell, *The Properties of Gases and Liquids 5E*. McGraw Hill Professional, 2000.

[39] S. W. Benson, “Thermochemical kinetics,” Wiley, 1976. Accessed: Feb. 28, 2022. [Online]. Available: https://scholar.google.com/scholar_lookup?title=Thermochemical+kinetics&author=Benson%2C+Sidney+William.&publication_year=1976

[40] T. H. Cormen, C. E. Leiserson, R. L. Rivest, and C. Stein, *Introduction to Algorithms*. MIT Press, 2009.

[41] B. J. McBride, M. J. Zehe, and S. Gordon, “NASA Glenn Coefficients for Calculating Thermodynamic Properties of Individual Species.” Sep. 01, 2002. Accessed: Mar. 01, 2022. [Online]. Available: https://ntrs.nasa.gov/citations/20020085330

[42] R. Horst, P. M. Pardalos, and N. V. Thoai, *Introduction to Global Optimization*. Springer Science & Business Media, 2000.

[43] R. Paulavičius and J. Žilinskas, “Simplicial Lipschitz Optimization Without Lipschitz Constant,” in *Simplicial Global Optimization*, R. Paulavičius and J. Žilinskas, Eds. New York, NY: Springer, 2014, pp. 61–86. doi: 10.1007/978-1-4614-9093-7_3.

[44] S. C. Endres, C. Sandrock, and W. W. Focke, “A simplicial homology algorithm for Lipschitz optimisation,” *J Glob Optim*, vol. 72, no. 2, pp. 181–217, Oct. 2018, doi: 10.1007/s10898-018-0645-y.

[45] J. M. Gablonsky and C. T. Kelley, “A Locally-Biased form of the DIRECT Algorithm,” *Journal of Global Optimization*, vol. 21, no. 1, pp. 27–37, Sep. 2001, doi: 10.1023/A:1017930332101.

[46] D. J. Wales and J. P. K. Doye, “Global Optimization by Basin-Hopping and the Lowest Energy Structures of Lennard-Jones Clusters Containing up to 110 Atoms,” *J. Phys. Chem. A*, vol. 101, no. 28, pp. 5111–5116, Jul. 1997, doi: 10.1021/jp970984n.

[47] R. Storn and K. Price, “Differential Evolution – A Simple and Efficient Heuristic for global Optimization over Continuous Spaces,” *Journal of Global Optimization*, vol. 11, no. 4, pp. 341–359, Dec. 1997, doi: 10.1023/A:1008202821328.

[48] “Total Energy Monthly Data - U.S. Energy Information Administration (EIA).” https://www.eia.gov/totalenergy/data/monthly/index.php (accessed Sep. 22, 2022).

[49] R. R. Bhosale, “A novel three-step GeO2/GeO thermochemical water splitting cycle for solar hydrogen production,” *International Journal of Hydrogen Energy*, vol. 45, no. 10, pp. 5816–5828, Feb. 2020, doi: 10.1016/j.ijhydene.2019.05.190.

[50] K.-S. Kang, C.-H. Kim, W.-C. Cho, K.-K. Bae, S.-H. Kim, and C.-S. Park, “Novel two-step thermochemical cycle for hydrogen production from water using germanium oxide: KIER 4 thermochemical cycle,” *International Journal of Hydrogen Energy*, vol. 34, no. 10, pp. 4283–4290, May 2009, doi: 10.1016/j.ijhydene.2009.03.017.

[51] L. Mochalov *et al.*, “Synthesis of gallium oxide via interaction of gallium with iodide pentoxide in plasma,” *Opt Quant Electron*, vol. 52, no. 12, p. 510, Nov. 2020, doi: 10.1007/s11082-020-02625-w.

[52] S. Abanades, P. Charvin, G. Flamant, and P. Neveu, “Screening of water-splitting thermochemical cycles potentially attractive for hydrogen production by concentrated solar energy,” *Energy*, vol. 31, no. 14, pp. 2805–2822, Nov. 2006, doi: 10.1016/j.energy.2005.11.002.

[53] O. Oruc and I. Dincer, “Assessing the potential of thermo-chemical water splitting cycles: A bridge towards clean and sustainable hydrogen generation,” *Fuel*, vol. 286, p. 119325, Feb. 2021, doi: 10.1016/j.fuel.2020.119325.

[54] M. Dokiya and Y. Kotera, “Hybrid cycle with electrolysis using Cu□Cl system,” *International Journal of Hydrogen Energy*, vol. 1, no. 2, pp. 117–121, Jan. 1976, doi: 10.1016/0360-3199(76)90064-1.

[55] I. Dincer and G. F. Naterer, “Overview of hydrogen production research in the Clean Energy Research Laboratory (CERL) at UOIT,” *International Journal of Hydrogen Energy*, vol. 39, no. 35, pp. 20592–20613, Dec. 2014, doi: 10.1016/j.ijhydene.2014.06.074.

[56] R. R. Bhosale, “H2 generation via solar assisted CaO/Ca thermochemical H2O splitting cycle,” *International Journal of Hydrogen Energy*, vol. 46, no. 22, pp. 12095–12104, Mar. 2021, doi: 10.1016/j.ijhydene.2020.03.189.

[57] K. E. N’Tsoukpoe *et al.*, “A review on the use of calcium chloride in applied thermal engineering,” *Applied Thermal Engineering*, vol. 75, pp. 513–531, Jan. 2015, doi: 10.1016/j.applthermaleng.2014.09.047.

[58] V. C. Y. Kong, D. W. Kirk, F. R. Foulkes, and J. T. Hinatsu, “Development of hydrogen storage for fuel cell generators II: utilization of calcium hydride and lithium hydride,” *International Journal of Hydrogen Energy*, vol. 28, no. 2, pp. 205–214, Feb. 2003, doi: 10.1016/S0360-3199(02)00039-3.

[59] R. Junginger and B. D. Struck, “Separators for the electrolytic cell of the sulphuric acid hybrid cycle,” *International Journal of Hydrogen Energy*, vol. 7, no. 4, pp. 331–340, Jan. 1982, doi: 10.1016/0360-3199(82)90126-4.

[60] B. D. Struck, R. Junginger, D. Boltersdorf, and J. Gehrmann, “The anodic oxidation of sulfur dioxide in the sulfuric acid hybrid cycle,” *International Journal of Hydrogen Energy*, vol. 5, no. 5, pp. 487–497, Jan. 1980, doi: 10.1016/0360-3199(80)90055-5.

[61] G. Li, D. Zhu, X. Wang, Z. Su, and M. R. Bryce, “Dinuclear metal complexes: multifunctional properties and applications,” *Chemical Society Reviews*, vol. 49, no. 3, pp. 765–838, 2020, doi: 10.1039/C8CS00660A.

[62] W. Uhl, A. El-Hamdan, M. Prött, P. Spuhler, and G. Frenking, “Ga 2 I 2 [C(SiMe 3) 3] 2 – an organogallium(ii) halide containing a Ga–Ga single bond,” *Dalton Transactions*, vol. 0, no. 7, pp. 1360–1364, 2003, doi: 10.1039/B212144C.

[63] W. Uhl, “Tetrahedral homonuclear organoelement clusters and subhalides of aluminium, gallium and indium,” *Naturwissenschaften*, vol. 91, no. 7, pp. 305–319, Jul. 2004, doi: 10.1007/s00114-004-0534-8.

[64] H. Wulfmeier, R. Feder, L. Zhao, and H. Fritze, “Epitaxial Piezoelectric Langasite Thin Films for High-Temperature Application,” *MRS Advances*, vol. 4, no. 9, pp. 523–529, ed 2019, doi: 10.1557/adv.2019.90.

[65] “Chlorination - an overview | ScienceDirect Topics.” https://www.sciencedirect.com/topics/biochemistry-genetics-and-molecular-biology/chlorination (accessed Oct. 31, 2022).

[66] M. Deborde and U. von Gunten, “Reactions of chlorine with inorganic and organic compounds during water treatment—Kinetics and mechanisms: A critical review,” *Water Research*, vol. 42, no. 1, pp. 13–51, Jan. 2008, doi: 10.1016/j.watres.2007.07.025.

[67] Reportlinker, “Global Acetic Acid Market - Segmented by Application, and Geography - Trends and Forecasts (2015-2020) - Reportlinker Review.” https://www.prnewswire.com/news-releases/global-acetic-acid-market---segmented-by-application-and-geography---trends-and-forecasts-2015-2020---reportlinker-review-300145381.html (accessed Sep. 22, 2022).

[68] "Acetic Acid Market Size & Share | Industry Report, 2020-2027." https://www.grandviewresearch.com/industry-analysis/acetic-acid-market (accessed Sep. 22, 2022).

[69] "Dimethyl Ether Market Size and share | Industry Statistics - 2027," *Global Market Insights Inc.* https://www.gminsights.com/industry-analysis/dimethyl-ether-dme-market (accessed Sep. 22, 2022).

[70] "Dimethyl Ether Market Size And Forecast," *Verified Market Research*. https://www.verifiedmarketresearch.com/product/dimethyl-ether-market/ (accessed Sep. 22, 2022).

[71] K. J. Ptasinski, *Efficiency of Biomass Energy: An Exergy Approach to Biofuels, Power, and Biorefineries*. John Wiley & Sons, 2016.

[72] Z. Azizi, M. Rezaeimanesh, T. Tohidian, and M. R. Rahimpour, "Dimethyl ether: A review of technologies and production challenges," *Chemical Engineering and Processing: Process Intensification*, vol. 82, pp. 150–172, Aug. 2014, doi: 10.1016/j.cep.2014.06.007.

[73] R. Ladera, E. Finocchio, S. Rojas, J. L. G. Fierro, and M. Ojeda, "Supported niobium catalysts for methanol dehydration to dimethyl ether: FTIR studies of acid properties," *Catalysis Today*, vol. 192, no. 1, pp. 136–143, Sep. 2012, doi: 10.1016/j.cattod.2012.01.025.

[74] E. D. Larson and H. Yang, "Dimethyl ether (DME) from coal as a household cooking fuel in China," *Energy for Sustainable Development*, vol. 8, no. 3, pp. 115–126, Sep. 2004, doi: 10.1016/S0973-0826(08)60473-1.

[75] R. R. Ratnakar, B. Dindoruk, and L. Wilson, "Experimental investigation of DME–water–crude oil phase behavior and PVT modeling for the application of DME-enhanced waterflooding," *Fuel*, vol. 182, pp. 188–197, Oct. 2016, doi: 10.1016/j.fuel.2016.05.096.

[76] R. R. Ratnakar, B. Dindoruk, and L. C. Wilson, "Development of empirical correlation for DME-partitioning between brine and crudes for enhanced waterflooding applications," *Journal of Petroleum Science and Engineering*, vol. 157, pp. 264–272, Aug. 2017, doi: 10.1016/j.petrol.2017.07.029.

[77] J. Greeley and M. Mavrikakis, “Competitive Paths for Methanol Decomposition on Pt(111),” *J. Am. Chem. Soc.*, vol. 126, no. 12, pp. 3910–3919, Mar. 2004, doi: 10.1021/ja037700z.

[78] L. V. Gurvich, I. V. Veyts, and C. B. Alcock, *Thermodynamic properties of individual substances*. New York: Begell House, 1996.

[79] F. Olmos, B. P. Hennessy, I. V. Manousiouthakis, I. Somiari, and V. I. Manousiouthakis, “Thermodynamic feasibility analysis of a water-splitting thermochemical cycle based on sodium carbonate decomposition,” *International Journal of Hydrogen Energy*, vol. 44, no. 8, pp. 4041–4061, Feb. 2019, doi: 10.1016/j.ijhydene.2018.11.153.

[80] F. E. da Cruz, S. Karagöz, and V. I. Manousiouthakis, “Parametric Studies of Steam Methane Reforming Using a Multiscale Reactor Model,” Nov. 14, 2017. https://pubs.acs.org/doi/abs/10.1021/acs.iecr.7b03253 (accessed Mar. 13, 2019).

[81] S. Karagöz, T. T. Tsotsis, and V. I. Manousiouthakis, “Multi-scale model based design of membrane reactor/separator processes for intensified hydrogen production through the water gas shift reaction,” *International Journal of Hydrogen Energy*, vol. 45, no. 12, pp. 7339–7353, Mar. 2020, doi: 10.1016/j.ijhydene.2019.05.118.

[82] *Introduction to Chemical Engineering Thermodynamics*. 2021. Accessed: Jun. 20, 2022. [Online]. Available: https://www.mheducation.com/highered/product/introduction-chemical-engineering-thermodynamics-smith-van-ness/M9781260721478.html

[83] W. Rudin, *Real and Complex Analysis*. McGraw-Hill, 1987.

[84] H. K. Khalil, *Nonlinear Systems*. Prentice Hall, 2002.

[85] Thomas C. Allison, “NIST-JANAF Thermochemical Tables - SRD 13.” National Institute of Standards and Technology, Jan. 01, 2013. doi: 10.18434/T42S31.

[86] “CRC Handbook of Chemistry and Physics 54th Edition,” *Soil Science Society of America Journal*, vol. 38, no. 3, pp. vi–vi, 1974, doi: 10.2136/sssaj1974.03615995003800030005x.

[87] M. W. Chase, J. L. Curnutt, J. R. Downey, R. A. McDonald, A. N. Syverud, and E. A. Valenzuela, "JANAF Thermochemical Tables, 1982 Supplement," *Journal of Physical and Chemical Reference Data*, vol. 11, no. 3, pp. 695–940, Jul. 1982, doi: 10.1063/1.555666.

[88] R. C. Wilhoit, J. Chao, and K. R. Hall, "Thermodynamic Properties of Key Organic Oxygen Compounds in the Carbon Range C_1 to C_4. Part 1. Properties of Condensed Phases," *Journal of Physical and Chemical Reference Data*, vol. 14, no. 1, pp. 1–175, Jan. 1985, doi: 10.1063/1.555747.

[89] J. Chao, K. R. Hall, K. N. Marsh, and R. C. Wilhoit, "Thermodynamic Properties of Key Organic Oxygen Compounds in the Carbon Range C_1 to C_4. Part 2. Ideal Gas Properties," *Journal of Physical and Chemical Reference Data*, vol. 15, no. 4, pp. 1369–1436, Oct. 1986, doi: 10.1063/1.555769.